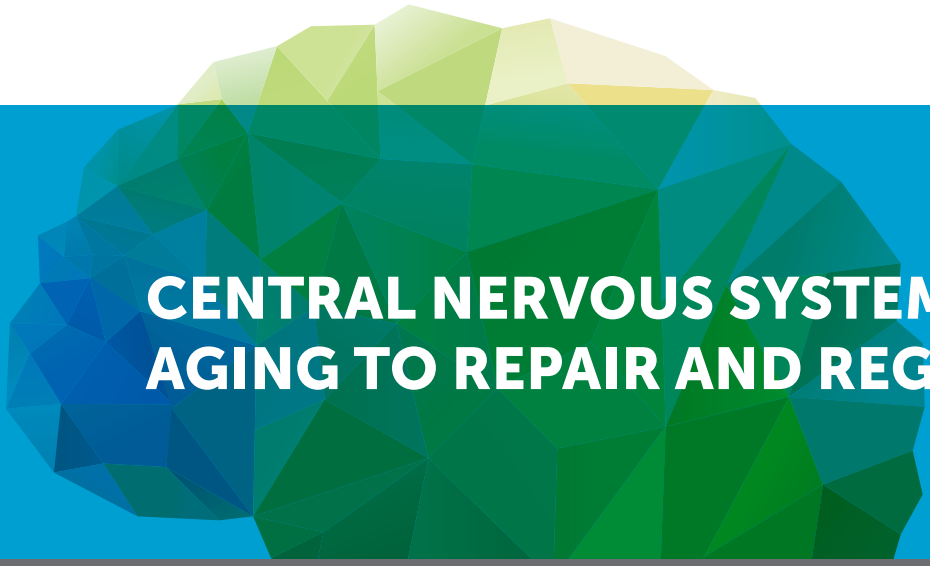

CENTRAL NERVOUS SYSTEM: FROM AGING TO REPAIR AND REGENERATION

EDITED BY: Homaira Nawabi, Karl J. L. Fernandes and Benoit Laurent
PUBLISHED IN: Frontiers in Aging Neuroscience

frontiers Research Topics

ISSN 1664-8714
ISBN 978-2-88976-893-6
DOI 10.3389/978-2-88976-893-6

About Frontiers

Frontiers is more than just an open-access publisher of scholarly articles: it is a pioneering approach to the world of academia, radically improving the way scholarly research is managed. The grand vision of Frontiers is a world where all people have an equal opportunity to seek, share and generate knowledge. Frontiers provides immediate and permanent online open access to all its publications, but this alone is not enough to realize our grand goals.

Frontiers Journal Series

The Frontiers Journal Series is a multi-tier and interdisciplinary set of open-access, online journals, promising a paradigm shift from the current review, selection and dissemination processes in academic publishing. All Frontiers journals are driven by researchers for researchers; therefore, they constitute a service to the scholarly community. At the same time, the Frontiers Journal Series operates on a revolutionary invention, the tiered publishing system, initially addressing specific communities of scholars, and gradually climbing up to broader public understanding, thus serving the interests of the lay society, too.

Dedication to Quality

Each Frontiers article is a landmark of the highest quality, thanks to genuinely collaborative interactions between authors and review editors, who include some of the world's best academicians. Research must be certified by peers before entering a stream of knowledge that may eventually reach the public - and shape society; therefore, Frontiers only applies the most rigorous and unbiased reviews.
Frontiers revolutionizes research publishing by freely delivering the most outstanding research, evaluated with no bias from both the academic and social point of view. By applying the most advanced information technologies, Frontiers is catapulting scholarly publishing into a new generation.

What are Frontiers Research Topics?

Frontiers Research Topics are very popular trademarks of the Frontiers Journals Series: they are collections of at least ten articles, all centered on a particular subject. With their unique mix of varied contributions from Original Research to Review Articles, Frontiers Research Topics unify the most influential researchers, the latest key findings and historical advances in a hot research area! Find out more on how to host your own Frontiers Research Topic or contribute to one as an author by contacting the Frontiers Editorial Office: frontiersin.org/about/contact

CENTRAL NERVOUS SYSTEM: FROM AGING TO REPAIR AND REGENERATION

Topic Editors:
Homaira Nawabi, Institut National de la Santé et de la Recherche Médicale (INSERM), France
Karl J. L. Fernandes, Université de Sherbrooke, Canada
Benoit Laurent, Université de Sherbrooke, Canada

Citation: Nawabi, H., Fernandes, K. J. L., Laurent, B., eds. (2022). Central Nervous System: From Aging to Repair and Regeneration. Lausanne: Frontiers Media SA. doi: 10.3389/978-2-88976-893-6

Table of Contents

frontiers in Aging Neuroscience

REVIEW
published: 08 March 2021
doi: 10.3389/fnagi.2021.650038

Mitochondrial Behavior in Axon Degeneration and Regeneration

Biyao Wang[1†], *Minghao Huang*[2†], *Dehao Shang*[2], *Xu Yan*[1], *Baohong Zhao*[2*] and *Xinwen Zhang*[2*]

[1] The VIP Department, School and Hospital of Stomatology, China Medical University, Liaoning Provincial Key Laboratory of Oral Diseases, Shenyang, China, [2] Center of Implant Dentistry, School and Hospital of Stomatology, China Medical University, Liaoning Provincial Key Laboratory of Oral Diseases, Shenyang, China

Mitochondria are organelles responsible for bioenergetic metabolism, calcium homeostasis, and signal transmission essential for neurons due to their high energy consumption. Accumulating evidence has demonstrated that mitochondria play a key role in axon degeneration and regeneration under physiological and pathological conditions. Mitochondrial dysfunction occurs at an early stage of axon degeneration and involves oxidative stress, energy deficiency, imbalance of mitochondrial dynamics, defects in mitochondrial transport, and mitophagy dysregulation. The restoration of these defective mitochondria by enhancing mitochondrial transport, clearance of reactive oxidative species (ROS), and improving bioenergetic can greatly contribute to axon regeneration. In this paper, we focus on the biological behavior of axonal mitochondria in aging, injury (e.g., traumatic brain and spinal cord injury), and neurodegenerative diseases (Alzheimer's disease, AD; Parkinson's disease, PD; Amyotrophic lateral sclerosis, ALS) and consider the role of mitochondria in axon regeneration. We also compare the behavior of mitochondria in different diseases and outline novel therapeutic strategies for addressing abnormal mitochondrial biological behavior to promote axonal regeneration in neurological diseases and injuries.

Keywords: mitochondria, axon regeneration, aging, traumatic brain injury, spinal cord injury, Alzheimer's disease, Parkinson's disease, Amyotrophic lateral sclerosis

OPEN ACCESS

Edited by:
Homaira Nawabi, Institut National de la Santé et de la Recherche Médicale (INSERM), France

Reviewed by:
Janelle Drouin-Ouellet, Université de Montréal, Canada
Marina Boido, University of Turin, Italy

***Correspondence:**
Baohong Zhao
bhzhao@cmu.edu.cn
Xinwen Zhang
zhangxinwen@cmu.edu.cn

† These authors have contributed equally to this work and share first authorship

Received: *06 January 2021*
Accepted: *18 February 2021*
Published: *08 March 2021*

Citation:
Wang B, Huang M, Shang D, Yan X, Zhao B and Zhang X (2021) Mitochondrial Behavior in Axon Degeneration and Regeneration. Front. Aging Neurosci. 13:650038. doi: 10.3389/fnagi.2021.650038

INTRODUCTION

Mitochondria are dynamic organelles playing a pivotal role in energy generation, signaling, and calcium homeostasis (Han et al., 2016). Axonal mitochondria exhibit a linearly interspersed distribution. Approximately 87% of mitochondria are stationary, and the number of motile mitochondria decreases from the proximal to distal axon (Cheng and Sheng, 2020). Mitochondria are transported to specific sites in axons where high energy is in demand, such as in growth cones and axonal branches (Morris and Hollenbeck, 1993; Tao et al., 2014). These distribution events are stabilized when presynaptic structures and mature neurons are formed. Moreover, mitochondria will rapidly redistribute in response to physiological or pathological stress in order to maintain energy homeostasis. The vigorous response of axonal mitochondria redistribution is predominantly conducted by the cooperation of microtubule-based transport and anchoring substrates, including anchors, adaptors, and motors (Sheng, 2014, 2017; Misgeld and Schwarz, 2017; Guedes-Dias and Holzbaur, 2019). Impairment of these substrates and process will result in the inhibition of axonal mitochondrial transport and ultimately induce local energy depletion and axon degeneration (Sheng and Cai, 2012).

Axon degeneration has been observed during normal neuronal aging, injury (e.g., traumatic brain injury, TBI; spinal cord injury, SCI; Maxwell, 2015; Wang et al., 2019b) and neurodegenerative diseases (e.g., Alzheimer's disease, AD; Parkinson's disease, PD; Amyotrophic lateral sclerosis, ALS; Guo et al., 2020). Axon degeneration usually occurs before the neuronal soma's death at the early stage of the diseases. In most conditions above, there are two different processes of axon degeneration. The distal axons won't connect to soma undergoing Wallerian degeneration while the proximal axons will die back toward soma (Adalbert and Coleman, 2013; Gerdts et al., 2016). Axon degeneration has an intimate association with mitochondrial dysfunction, including energy deficits, oxidative stress, disequilibrium of mitochondrial fission and fusion, impaired axonal mitochondrial transport, and aberrant mitophagy (Court and Coleman, 2012; Sheng and Cai, 2012; Geden and Deshmukh, 2016). Therefore, analysis of the mitochondrial behavior in axons may be considered a novel target for therapeutic strategies.

The intrinsic capacity and process of axon regeneration are different between the peripheral and central nervous systems (PNS and CNS, respectively), and the capacity of the former is superior to that of the latter (Fawcett and Verhaagen, 2018; Mahar and Cavalli, 2018). Axon regeneration in PNS initiates a vigorous regenerative response via the permissive Schwann cell environment and form a new growth cone. This process is supported by a regenerative program through expression of the Regeneration-associated gene (Attwell et al., 2018; Mahar and Cavalli, 2018). Nevertheless, axotomy at the central branch has a minimal regenerative response and the Regeneration-associated gene response also seems to make no difference on axon regeneration (Chandran et al., 2016; Cartoni et al., 2017). While in the CNS, the ability of axon regeneration is dependent on the maturity of the neurons. Moreover, the environment of the injured neuron is full of molecules and structures which may suppress axon regeneration in CNS (Fawcett and Verhaagen, 2018). CNS axons cut from embryos exhibits a potential to grow for long distance after transplanted into an adult CNS via expressing a series of molecules inducing axon growth (Reier et al., 1986; Lu et al., 2012). Nevertheless, axons from the adult CNS respond to axotomy with a minimal regenerative response and a poor change of gene expression despite being in a permissive environment. These diverse response to injury in PNS and CNS (mature and immature) form the concept of intrinsic regenerative capacity of axon regeneration (Fawcett and Verhaagen, 2018). Because this process consumes a large amount of energy and molecules or substrates during restoration, alteration of mitochondria behavior may represent one of the prominent intrinsic regenerative capacities in axon regeneration; however, the mechanisms underlying this process have just begun to be elucidated.

In this review, we summarize the normal mechanism of mitochondrial quality control in axons. We also describe the behavior of mitochondria in axon degeneration under different conditions (i.e., aging, nerve trauma, and neurodegenerative diseases) and their role in axon regeneration and the treatment methods derived from these effects.

NORMAL MITOCHONDRIAL BEHAVIOR IN AXONS

Mitochondrial transport is indispensable for mitochondrial quality control. Anterograde transport contributes to the energy supply and neuronal survival, and retrograde transport helps with damaged mitochondrial clearance (Chen et al., 2016). Only a small proportion of axonal mitochondria (30–40%) is motile *in vivo* and *in vitro*; most mitochondria are stalled and do not move for long periods (Zheng et al., 2019). Mitochondrial transport depends on interactions between microtubules, microtubule motor proteins, adaptor complexes that bind the motor proteins to mitochondria, and their anchors.

Mitochondria are transported along the microtubule filament by the motor proteins kinesin and dynein to the plus and minus ends, respectively (Lin and Sheng, 2015). Kinesin-1 (KIF5) is the major motor protein involved in anterograde transport, the other member of kinesin family such as KIF1Ba and KLP are also participants (Zheng et al., 2019). Mitochondria interact with motor proteins via the adaptor complex formed by Miro, a GTPase located in the outer mitochondrial membrane (OMM), and Milton/TRAK (TRAK 1 and 2 in mammals). TRAK1 binds both the heavy chain of KIF5 and dynein; however, TRAK2 preferentially binds dynein (Smith and Gallo, 2018). Compared to the preference for dynein in dendrites, axonal mitochondria bind either kinesin or dynein via the Miro-TRAK1 complex.

The axon-specific mitochondrial outer membrane protein syntaphilin (SNPH) is a representative cytoskeletal tether (i.e., anchor), which opposes motility by increasing the force between the mitochondria and microtubules and inhibiting ATPase activity (Chen and Sheng, 2013). Microtubule-associated protein, such as myosin V or myosin VI (Pathak et al., 2010), and actin filament-based mechanisms may also regulate stalling and transport in axons (Henderson et al., 2017). Cytosolic calcium is another key regulator of mitochondrial transport. There are two main mechanisms for calcium resulting in the stalling of mitochondria (Zheng et al., 2019). For one thing, SNPH can bind kinesin I and sequester motor protein in the context of calcium signaling. For another, Miro has two EF calcium binding domains and Miro will directly bind KIF5 when binding of calcium (Liu and Hajnóczky, 2009), which will prevent motor activity. Therefore, increased intracellular calcium levels are sufficient to inhibit this process (Woolums et al., 2020).

A dynamic process in mitochondria (i.e., mitochondrial fission and fusion) continuously occurs to maintain a steady mitochondrial morphology and population (Yan et al., 2020b). Mitochondrial fission helps a damaged mitochondrion segregate from the healthy one while mitochondrial fusion facilitates the interaction and fusion of two mitochondria, which repairs each other, demonstrating that the equilibrium of fission and fusion acts a pivotal part in axonal mitochondria (Yu et al., 2016; Pickles et al., 2018). Mitochondrial fission is mediated by the GTPase dynamin-related protein 1 (Drp1), which is recruited to the OMM and forms a contractile ring around the mitochondrion, dividing one mitochondrion into two separate mitochondria

(Otera et al., 2013). GTPase dynamin-related protein 1 (Drp1)-independent mitochondrial fission can also occur (Rival et al., 2011; Stavru et al., 2013; Roy et al., 2016). Mitochondrial fusion involves two separate processes, the fusion of the OMM, which is regulated by mitofusins (Mfns), and the fusion of the inner mitochondrial membrane that is mediated by optic atrophy 1. The fusion of the OMM is regulated by mitofusins 1 and 2 (Mfn1 and Mfn2). Both mitochondrial fission and fusion take place along the axon (Yan et al., 2020b).

Mitophagy plays a key role in relieving oxidative stress and preventing axonal and cytosolic defects and subsequent cell death (Wang et al., 2018). To maintain mitochondrial quality control in axons and cells, mitophagy degrade and recycle damaged mitochondria undergoing physiological or pathological processes, such as mitochondria depolarization and oxidative stress (Martinez-Vicente, 2017). The PINK1/Parkin pathway is a canonical mechanism of mitophagy. In addition to the PINK1/PARKIN pathway, other OMM proteins directly interact with LC3 and promote mitophagy in mammals, including FUNDC1, NIX/BNIP3L, and Bcl2-L-13 (Di Rita et al., 2018).

AGING

Mitochondrial Behavior in Axon Degeneration in Aging

Aging is a normal physiological phenomenon, and glaucoma and many neurodegenerative diseases (e.g., Alzheimer's disease, Parkinson's disease) are related to aging. Mitochondrial behavior plays a key role in axon degeneration. First, aging has been shown to be associated with mitochondrial transport. Glaucoma is a chronic and progressive neurodegenerative disease. Degeneration of ganglion cells and their axons has been shown to be related to aging (Liu et al., 2018). In ganglion cell neurons, with age the cross-section axon area enlarges characterized by axoplasm disorganization and accumulation of hyperphosphorylated neurofilaments which is indicative of axonopathy (Cooper et al., 2016). Further, there are more mitochondria-free regions and decreased lengths of mitochondrial transport in degenerative axons (Mao et al., 2016). The changes in these mitochondria with age are related to changes in the expression of Mfn2. Among the healthy mice in the control group, the level of Mfn2 in retina was slightly elevated in aged mice (Nivison et al., 2017). Considering the function of Mfn2 in maintaining mitochondrial morphology and participating in mitochondrial transport (Misko et al., 2010), this increase indicates the demand of mitochondrial fusion and transport. The increase was more pronounced in retina of DBA mice (a murine glaucoma model), which explained the mitochondria in glaucoma neurons were elongated or fused. However, Mfn2 is either damaged or cannot be transported to optic nerve, resulting in a decrease in the level of this protein in optic nerve, indicating that Mfn2 protein is not transported down axons to function in mitochondrial transport and repair, which leads to disease progression. Moreover, given that phosphorylated Mfn2 is a receptor for Parkin on depolarized mitochondria, the amount of phosphorylated Mfn2 in young mice are also higher than the aged control indicating that the mitochondria transport is altered (Nivison et al., 2017).

Pathological morphology of mitochondria has been reported in degenerative axons with age. The average diameter of axonal mitochondria increases, with few or no cristae observed in the aging axonal mitochondria (Cao et al., 2017). This phenomenon is attributed to reduced optic atrophy 1 and Mfn2 expression (Rebelo et al., 2018) and even the absence of expression at the aging axon terminal. This morphological change is also relevant to neuronal apoptosis, P53-dependent neuronal cell death is associated with increased mitochondrial length mediated by reduced Drp1 and Parkin expression during aging (Wang D. B. et al., 2013).

Different phenomena are observed for mitophagy in axons *in vivo* and *in vitro*. *In vitro*, Sung et al. (2016) demonstrated that autophagosomes co-localized with mitochondria in axons when neurons were treated with drugs to induce mitochondrial damage. However, evidence from *in vivo* imaging suggests that either PINK1/Parkin or Parkin-dependent or mitophagy is indispensable for mitochondria turnover and axon integrity (Cao et al., 2017). Further research is needed to determine whether the mitochondria in axons need to undergo mitophagy or are transported back to the soma.

Finally, all of the described changes in mitochondrial behavior may affect bioenergetics by influencing oxidative phosphorylation and producing excessive reactive oxidative species (ROS). The molecular mechanisms regulating this process in aging include increases in the levels of proteins related to mitochondria and oxidative phosphorylation, more specifically, Complex I (Kline et al., 2019).

Mitochondrial Behavior in Axon Regeneration in Aging

The relationship between aging and axon regeneration is complex and affected by multiple factors. Both endogenous (Geoffroy et al., 2017) and exogenous factors (Sutherland and Geoffroy, 2020) of neurons play an important role in the ability of axons to regenerate after damage and this process is declining with aging (Geoffroy et al., 2016). Although young neurons have a strong ability for axon growth, mature neurons can usually not regenerate after injury because mature CNS axons lose their ability to regenerate due to most mitochondria being stationary, which is associated with high SNPH expression (Lewis et al., 2016). Therefore, without enough local mitochondria, sufficient ATP cannot be provided, and the process of axon regeneration, including re-sealing cell membranes, rearranging cytoskeletal structures, and reforming active growth cones, will be hindered (Bradke et al., 2012). However, mitochondrial transport can be enhanced by stimulating the cAMP/Protein Kinase A (PKA) pathway to upregulate kinesin-1 expression to counteract its decrease during aging (Vagnoni and Bullock, 2018). Interestingly, the effects of cAMP or PKA on increasing mitochondrial transport were more pronounced in the aging group than in the younger group.

The internal components of the mitochondria also affect axonal regeneration by modifying the biological behavior of

mitochondria and oxidizing the respiratory chain. In addition to acting as a transcription factor for axon regeneration in the nucleus, STAT3 can also reach the inner mitochondrial membrane following the activation of mitogen-activated protein kinase (MAPK), which improves axon regeneration by enhancing cell bioenergetics in the spinal cord (Luo et al., 2016) in mature mice with a reduced regenerative capacity. The mitochondrial signature phospholipid cardiolipin present in the inner leaflet of the inner mitochondrial membrane is essential for mitochondrial dynamics, mitochondrial biogenesis, and energy metabolism in the mitochondria (Mårtensson et al., 2017).

INJURY

Traumatic Brain Injury

Traumatic brain injury (TBI) leads to the dynamic deformation of the parenchyma, resulting in shear and stretch injuries to axons, commonly known as diffuse axonal injury. Diffuse axonal injury is demonstrated to result from the mechanical deformation of the axonal cell membranes via calpain-mediated proteolysis of sidearms or phosphorylation, triggering neurofilament compaction, calcium changes, microtubules destabilization, and metabolic dysfunction (Barkhoudarian et al., 2016). Subsequently, axoplasmic transport mechanisms are defective, which leads to the accumulation of transport products that cause axonal swelling, secondary disconnection, and Wallerian degeneration (Frati et al., 2017).

Mitochondrial Behavior in Axon Degeneration Following TBI

Transmembrane sodium channels are damaged in TBI, leading to an abnormal influx of calcium into the axonal plasma (Maxwell, 2015). Calcium is also released from mitochondria and the axoplasmic reticulum (Springer et al., 2018), leading to axonal mitochondria dysfunction. Under Transmission electron microscopy, the axoplasm contains damaged or lucent mitochondria and a disorganized cytoskeleton within injured nerve fibers (Maxwell, 2015). The axonal swellings of TBI are characterized by the aggregation of membranous organelles, especially mitochondria, resulted from the injury and loss of axonal microtubules, which interact with dynein and kinesin (Maxwell, 2015). It is reported that the loss of axonal microtubules in TBI results in the lack of neuronal mitochondria delivery, failing to replace those damaged by the destroyed calcium homeostasis and to provide vesicular profiles (Maxwell et al., 1997; Tuck and Cavalli, 2010). Within an injured mouse optic nerve fiber, which is far away from the secondary axotomy site, accumulating evidence demonstrated the dieback or withdrawal of the proximal and distal terminal swellings (Staal et al., 2010; Wang et al., 2011). In the latter study, the proximal swellings contained intact mitochondria while the distal swellings exhibited defected mitochondria short of cristae, which appeared consistent with an ongoing degenerative process (Wang et al., 2011). In addition, the distal swelling exhibits three types of mitochondria, including mitochondria aggregating pyroantimonate crystals, those unremarkable or intact, and those containing electron lucent spaces in the mitochondrial matrix (Wang et al., 2011).

Damaged mitochondria fail to generate adequate ATP and cannot support the essential physiological and biochemical processes and disturb the transmembrane transporter function (Maxwell, 2015). Furthermore, oxidative stress in TBI results from the uncontrolled influx of Ca^{2+}, leading to calcium accumulation in the mitochondria. The subsequent activation of caspases and calpains correlates with the initiation of apoptosis (Frati et al., 2017). Calpain-mediated spectrin proteolysis reaction product, which is reported to be correlated with damaged mitochondria, spread widely in the axoplasm at foci of neurofilament compaction (Büki et al., 1999), suggesting the defection of neurofilaments (Dewar et al., 2003). Moreover, the release of cytochrome c in the damaged axons triggers retrograde signaling by "apoptosis-inducing factor," resulting in the programmed cell death and apoptosis of injured neurons (Büki et al., 2000).

Mitochondrial Behavior in Axon Regeneration Following TBI

Mitochondrial transport and bioenergetics are enhanced to facilitate axon regeneration following TBI (Misgeld et al., 2007). Within axon regeneration in TBI, it is beneficial to elevate the density of mitochondria while decreasing the density is disadvantageous. Mitochondria are transported into the injured zone in order to elevate the average mitochondria density. Regenerating axons have a higher density of mitochondria than non-regenerating axons in *Caenorhabditis elegans* (Han et al., 2016). Accumulating evidence in the SNPH knockout mice demonstrates that mitochondrial transport is strengthened to clear impaired mitochondria, replenish healthy mitochondria in injured axons, and ultimately reverse the energy deficits in axon regeneration (Zhou et al., 2016; Cheng and Sheng, 2020). In contrast, the Armadillo Repeat Containing X-Linked 1 protein, responsible for connecting the Miro adaptor protein with the mitochondrial membrane, is overexpressed, leading to the acceleration of optic nerve regeneration following TBI (Cartoni et al., 2016). Moreover, the dual leucine zipper kinase 1 microtubule-associated protein kinase pathway in *C. elegans* can promote adequate mitochondrial transport into the regeneration zone independent of Miro to increase the mitochondria density in injured axons (Han et al., 2016). Overall, axon regeneration following TBI can be achieved by increasing the density of mitochondria by enhancing the transport of healthy mitochondria, which provide sufficient energy for axonal regrowth.

Spinal Cord Injury

The damage caused by SCI is mainly divided into two stages. The initial trauma is mainly caused by a contusion or direct compression. The secondary injury is caused by disruption of blood vessels, microcirculation failure, ion homeostasis disorder, excessive production of free radicals, and inflammation (Wang S. et al., 2019).

Mitochondrial Behavior in Axon Degeneration Following SCI

After acute SCI and the accompanying depolarization of neurons, mitochondrial permeability transition pores are opened by calcium influx, which impairs ATP synthesis, destroys the mitochondrial outer membrane, and releases ROS and pro-apoptotic proteins into the cytoplasm (Pivovarova and Andrews, 2010). In an SCI rat model, swollen and disrupted mitochondria with disorganized cristae can be observed in both pre-apoptotic neurons and astrocytes (Xu et al., 2017).

Immunofluorescence staining of post-mortem tissue from *Thy1YFP+* transgenic mice showed that a significant increase in TOMM20 signal reflected the density of mitochondria in the axonal spheroids and endbulbs (Rajaee et al., 2020). The accumulation of mitochondria and tubulin polyglutamylation indicates the disruption of axonal transport, an important characteristic of axonal degeneration. Moreover, the failure of mitochondria to migrate to the remote ends of axons indicates abnormal mitochondrial axonal localization that contributes to axon retraction.

In the early stage of SCI, mitochondria fuse to restore the respiratory chain and inhibit mitochondrial apoptosis. In contrast, mitochondrial fission resulting from mitochondrial dysfunction further inhibits microtubule stabilization and axonal regeneration and is associated with apoptosis (Csordás et al., 2018). The dysfunction of mitochondrial fission and fusion caused by SCI is associated with the upregulation of Drp1, which reduces mitochondrial membrane potential, releases cytochrome C and caspase3, and induces neuronal apoptosis (Jia et al., 2016).

Mitochondrial Behavior in Axon Regeneration Following SCI

Within a few days to a few weeks after a person suffers axon damage, the damaged spinal cord begins to recover. To solve the functional defect caused by the separation of the white matter tracts between the rostral and caudal spinal cords, axonal regeneration is required to reconnect the caudal/rostral neurons and form new neural circuits to restore signal conduction (O'Shea et al., 2017). However, observations in mice showed that the reduced growth capacity of mature neurons and scar tissue caused by reactive astrocytes form a physical barrier, and the upregulation of axon growth-inhibitory factors inhibit axon regeneration (Yiu and He, 2006). However, intravital imaging of murine spinal cord showed that the number of axons increases significantly from 7 to 14 days after injury compared to 3 days post-injury, indicating that a certain number of injured axons undergo endogenous repair (Rajaee et al., 2020), demonstrating that while the regeneration of axons is limited after SCI injury, it can still be improved.

Given the important role of axonal mitochondria in growth cone migration, mitochondrial transport is required for axonal regeneration after SCI. Spinal cord injury (SCI) itself does not directly affect mitochondrial transport in axons; however, enhancing the transport of mitochondria after SCI is helpful for this process. *In vitro* data showed that fibroblast growth factor-13 co-localizes with mitochondria, and its increased activity and density in axons may, in part, explain why fibroblast growth factor-13 promotes axon regeneration in SCI models (Li et al., 2018).

Changing mitochondrial dynamics after SCI, specifically by promoting mitochondrial fusion and inhibiting its fission, positively affects axon regeneration. In an SCI model, Loureirin B significantly increased both bcl-2 and Mfn1 and doubled the size of the mitochondria, which promoted fusion and facilitated axon regeneration (Wang et al., 2019a). Considering the adverse effects of Drp1 upregulation after SCI injury, mitochondrial division inhibitor-1, an inhibitor of Drp1, promotes animal recovery and reduces apoptosis (Jia et al., 2016).

Peripheral Nerve Injury

Once the peripheral nerve is injured, the axon is divided into two segments; the proximal axon segment and the distal segment. The distal axon undergoes Wallerian degeneration, while the proximal axon possibly regenerates via a growth cone, triggering axon extension (Neukomm et al., 2017).

Mitochondrial Behavior During Axon Degeneration Following Peripheral Nerve Injury

In the injured peripheral neuronal axon of *C. elegans* and ric-7 (resistant to inhibitors of cholinesterase) mutants, the density of healthy mitochondria is decreased while the density of defected mitochondria is elevated, leading to energetic failure and oxidative stress (Rawson et al., 2014). Furthermore, mitochondrial transport is similarly inhibited in the Thy1-mitoCFP transgenic mouse (Thy1-MitoCFP mice expressing CFP fused to the human cytochrome c oxidase mitochondrial targeting sequence were from Jackson Laboratories; Misgeld et al., 2007).

In response to injury, multiple proteins are inhibited or activated during distal axon degeneration. Together with increased calcium influx, decreased nicotinamide mononucleotide adenyltransferase (NMNAT) and NAD1 activates SARM1 (Sterile Alpha and TIR Motif Containing 1), which are key initiating factors in Wallerian degeneration (Osterloh et al., 2012). Sterile Alpha and TIR Motif Containing 1 (SARM1) activation results in mitochondrial dysfunction, calpain-dependent defects in the cytoskeleton, and subsequent axon degeneration (Adalbert et al., 2012; Ma et al., 2013; Yang et al., 2015). Wallerian degeneration slow fusion protein (WldS), comprising full NMNAT1, has been shown to alleviate degeneration in Zebrafish and Drosophila (Coleman et al., 1998; Conforti et al., 2000). NMNAT1 has a pivotal role in maintaining axon integrity (O'Donnell et al., 2013; Wang Y. et al., 2015), the activity of which is greatly inhibited by defects in healthy mitochondria, decreases in mitochondrial transport, and ROS accumulation during axon degeneration (Yahata et al., 2009; Avery et al., 2012; Fang et al., 2012; O'Donnell et al., 2013). The dual leucine zipper kinase (DLK) is a mitogen activated protein kinase (MAP3K), and contributes to axon degeneration by reducing energy production. Dual leucine zipper kinase (DLK) is an axonal integrity sensor and interacts with NMNAT and activated SARM1 (Cavalli et al., 2005; Xiong et al., 2012; Yang et al., 2015; Gerdts et al., 2016); subsequently, SARM1 interacts with Axundead to consume NAD1 (Essuman et al., 2017;

Neukomm et al., 2017). Decreased NAD1 production reduces energy generation and ATP levels, causing defects in Na^+/Ca^{2+} exchangers and Ca^{2+} channels, and the loss of mitochondrial membrane potential (Gerdts et al., 2015; Loreto et al., 2015). Thus collectively, these proteins damage axon integrity.

Mitochondrial Behavior During Axon Regeneration Following Peripheral Nerve Injury

In contrast to the central nerve, after peripheral nerves are injured, axons have a strong regenerative ability to restore function. At the proximal segment of peripheral nerve injury, Golgi-derived vesicles transport anterogradely to aggregate near the axon end to repair the ruptured membrane, while increasing intracellular Ca^{2+} levels activate kinases and phosphatases assemble microtubules to support the formation of new growth cones, and drive axon elongation (Girouard et al., 2018). This process is relevant to Schwann cells (Jessen et al., 2015; Nocera and Jacob, 2020) and intrinsic signaling events induced by injury, such as growth-associated protein-43 (GAP-43) (Chung et al., 2020).

Mitochondria are essential for axon regeneration. Increased mitochondrial density in *C. elegans* effectively promotes axon regeneration (Han et al., 2016). Reduced oxidative stress and enhanced axon regeneration are observed in a sciatic nerve crush injury model when mitochondria are injected into injured nerves (Kuo et al., 2017). Thus, increasing mitochondrial density at the site of injured axons can be achieved, mainly by increasing mitochondrial transport in axons, and increasing mitochondrial fission. Miro overexpression enhances mitochondrial transport in proximal segments, whereas axon regeneration is significantly inhibited in individuals where Miro is suppressed (Han et al., 2016). In addition, by imaging axonal mitochondrial transport *in vivo*, and when the intercostal nerve is damaged, mitochondrial anterograde transport is increased (Misgeld et al., 2007), which may be associated with tyrosinated tubulin, and upregulated molecular motors (Yang et al., 2021). An *in vivo* sciatic nerve compression study indicates that enhanced mitochondrial transport, via SNPH knockout in mice, accelerates axon regeneration in the peripheral nervous system (Zhou et al., 2016). The early fission of mitochondria after axon damage is also associated with axon regeneration. For example, in mice, sciatic nerve transection generates significantly increased mitochondrial division in damaged axons (Kiryu-Seo et al., 2016). This is further confirmed by the inhibition of axon regeneration in individuals with mutations in the mitochondrial fusion gene, OPA1 (Knowlton et al., 2017).

Mitochondrial regeneration after peripheral nerve injury highlights the importance of axon transport, to not only provide structural components of cells such as lipid vesicles and microtubules, but to meet the high energy requirements of regenerating axons (Prior et al., 2017; Mahar and Cavalli, 2018). In an *in vitro* sciatic nerve injury study, Hwang et al. found that after sciatic nerve injury, axon CDK5 levels increased, they were translocated into the mitochondria and phosphorylated mitochondrial STAT3, thereby regulating mitochondrial activity (Hwang and Namgung, 2021). STAT3 phosphorylation affects microtubule assembly and energy production in axons (Selvaraj et al., 2012). When translocated to the mitochondria, STAT3 interacts with electron transport chain proteins, regulating ROS production and the release of cytochrome C (Szczepanek et al., 2011), and contributing to ATP energy supply to promote axon regeneration.

Treatment

Mitochondria in the injured axon have pivotal roles in axon degeneration and regeneration. Therefore, mitochondria may be specific therapeutic targets for inhibiting axon degeneration and enhancing axon regeneration. Oxidative stress caused by dysfunctional mitochondria results in a variety of adverse effects. Thus, a potential therapeutic strategy would be to decrease this stress. In a TBI animal model, cyclosporin, an anti-oxidative drug, can decrease cytochrome c release from mitochondria and inhibit Ca^{2+} influx into mitochondria, ultimately alleviating mitochondrial dysfunction and axon damage (Kelsen et al., 2019). Additionally, ROS-mediated axonal degeneration in TBI caused by the aberrant axonal calcium homeostasis is reported to be alleviated via the application of calcium channel blocker (McAllister, 2011; Namjoshi et al., 2014). Moreover, Metformin can stabilize the microstructure in injured axons of SCI by activating the PI3K/Akt signaling pathway. Furthermore, activation of Akt/Nrf2 signaling could be a potential approach for axon regeneration treatment by inhibiting excessive oxidative stress and restoring mitochondrial function (Wang et al., 2020).

Enhancing mitochondrial transport and recruitment aids axon regeneration in injured axons and facilitates the removal of damaged mitochondria and replenishment of healthy ones to provide adequate ATP (Kaasik, 2016; Sheng, 2017; Smith and Gallo, 2018). Inhibiting the microtubule-severing protein Fidgetin (Matamoros et al., 2019) or non-muscle myosin II (Hur et al., 2011) promotes axon regeneration after SCI by facilitating the reorganization of microtubule and actin cytoskeletal proteins. Moreover, Loureirin B promotes mitochondrial fusion and suppresses ER stress by activating the Akt/GSK-3β pathway, facilitating axon regeneration (Wang et al., 2019a). In summary, combined approaches targeting mitochondria may provide a novel therapeutic strategy for alleviating axon degeneration and enhancing axon regeneration in TBI and SCI.

NEURODEGENERATIVE DISEASE

Alzheimer's Disease

Alzheimer's disease is an age-related neurodegenerative disease characterized by progressive cognitive impairment, mobility disorder, and memory loss. Hallmarks of AD include aberrant amyloid-β (Aβ) metabolism and neurofibrillary tangles of hyperphosphorylated Tau protein, which are particularly significant in axon degeneration (Wang et al., 2017). β-site amyloid precursor protein (APP) cleaving enzyme 1 (BACE1) is the major neuronal Aβ-secretase for Aβ generation. Axon degeneration in AD involves a complicated mechanism, including glucose metabolism defects, mitochondrial dysfunction, aberrant calcium homeostasis, oxidative stress, and imbalances in energy homeostasis (Cieri et al., 2018; Mata, 2018; Swerdlow, 2018; Albensi, 2019).

Accumulating evidence has demonstrated that aggregation of pathological Tau and Aβ impairs mitochondria transport (anterograde and retrograde) in axons (Wang Z. X. et al., 2015; Sadleir et al., 2016; Cai and Tammineni, 2017; Zhang et al., 2018). One of the first researches in this area was carried out in primary neurons from *Tg2576* mice with mutant human APP protein (Calkins et al., 2011). Compared to wild-type neurons, primary neurons from *Tg2576* mice exhibited inhibited anterograde mitochondrial transport as well as promoted mitochondrial fission and inhibited mitochondrial fusion (Calkins et al., 2011). Mitochondria transport in axons requires a variety of substrates and molecular support, whose dysfunction can lead to negative impact on mitochondria transport. The defected transport results in the reduction of mitochondria density at the distal axons and the depletion of axonal NMAT protein 2 (NMAT2), which is continually supplemented in axons via fast axonal transport (Ljungberg et al., 2012; Ali et al., 2016). Following axotomy, the transport of NMNAT2 toward axons is inhibited, meanwhile, it has a rapid decline in axons before Wallerian degeneration occurs (Gilley and Coleman, 2010; Gerdts et al., 2016). Since the damaged mitochondria inhibited anterograde and promoted retrograde transport, the quantity of SNPH cargo vesicles is significant elevated in AD axons, similar to ALS. The SNPH-mediated response in axonal mitochondrial transport of AD-related cortical neurons from mutant human APP-expressing transgenic mice is summarized in the ALS section (Lin et al., 2017a,b; Cheng and Sheng, 2020). Ultimately, the impairment of mitochondrial axonal transport in AD inhibits OXPHOS complex activity, causing significant energy deficiency (Spires-Jones and Hyman, 2014).

These two AD hallmarks contribute to mitochondrial transport pathology in axons. Defects in axon transport can be initiated by soluble low molecular weight Aβ species in the plasma membrane in mice (Zhang et al., 2018). Moreover, inhibited axon transport does not promote mitochondrial dysfunction or ATP depletion at once (Zhang et al., 2018), suggesting that reconstruction of mitochondrial axon transport may be advantageous at early AD stages. The restoration of KIF5A, an isoform of kinesin-1, abrogates the impairment of mitochondria axonal transport by Aβ, particularly anterograde transport in 5 × FAD mice (Wang et al., 2019b). Additionally, it is reported that axon degeneration has an intimate correlation with mitochondrial dysfunction and mPTP (Barrientos et al., 2011). The deficiency of cyclophilin D (CypD), a mPTP regulator, inhibited Aβ-mediated permeability transition and mitochondrial swelling, and alleviated oxidative stress both in mice model and brain samples of AD. Notably, knockout of *CypD* gene appears to suppress the mPTP, which may improve cognitive and synaptic function in mouse model (Du et al., 2008, 2011). Moreover, the defection of mitochondrial axon transport triggered by Aβ is dependent on the activation of mPTP, which is mediated by *CypD*. Knockout of *CypD* inhibit the induction of the p38/MAPK signaling pathway mediated by Aβ, restore the dysfunction of axonal mitochondria and synapses (Guo et al., 2013). Furthermore, the defective dynein-snapin coupling mediated by Aβ seriously inhibits retrograde transport, resulting in the aggregation of amphisomes at axonal terminals, which can greatly contribute to mitophagy (Tammineni et al., 2017). Therefore, it seems that there is an intimate relationship between the impaired axonal transport and mitophagy, together consist of the complicated mechanism of mitochondrial dysfunction in axons of AD.

Overexpression or hyperphosphorylation of Tau not only causes defects in mitochondrial transport but also disrupts mitochondrial distribution and localization in mouse and cellular AD models (Cheng and Bai, 2018). It is reported that in tauopathies and AD, the integrity of microtubules is damaged via hyperphosphorylation and binding with protein Tau (Misko et al., 2010). Moreover, mitochondrial transport motor proteins and Tau (Ser199, Ser202, Thr205) are phosphorylated, which can lead to the dysfunction of mitochondrial transport in AD, mediated by a serine/threonine protein kinase, Glycogen synthase kinase 3 (Shahpasand et al., 2012). The aberrant aggregation of Tau is also demonstrated to induce microtubule instability, aggravating the impaired transport.

Amyloid-β (Aβ) oligomers and neurofibrillary tangles also elicit mitochondria dysfunction and oxidative stress (Butterfield and Boyd-Kimball, 2018; Mata, 2018), which may, in turn, impair axonal transport. It is demonstrated that oxidative stress is one of the typical event correlated with axon degeneration at the early stage of AD (Alavi Naini and Soussi-Yanicostas, 2015). Oxidative stress triggered by breaking the equilibrium between antioxidants and pro-oxidants may induce the excessive hyperphosphorylation of Tau. The aggregation of Tau is reported to inhibit microtubule transport, resulting in the decrease of peroxisome, which increase the incidence of oxidative stress (Stamer et al., 2002). Oxidative stress may in turn impair axon transport, which will aggravate tau phosphorylation in animal models and neuronal cultures of AD (Melov et al., 2007; Su et al., 2010). Interestingly, antioxidative treatment conducted in 3xTg-AD mice is found to alleviate oxidative stress, Tau hyperphosphorylation (Clausen et al., 2012). Therefore, the interconnection between oxidative stress and tau hyperphosphorylation seems to act a key role in axon degeneration of AD. Accumulating damaged mechanisms summarized above lead to the damage of axon homeostasis and finally, axonal degeneration in AD, which seems to provide some novel mitochondria-targeted therapeutic strategies in future.

Parkinson's Disease

Parkinson's disease is a common late-onset neurodegenerative disease characterized by the degenerative death of dopamine (DA) neurons in the substantia nigra region and the formation of Lewy bodies, cytoplasmic inclusion bodies that contain α-synuclein (α-Syn) (Gao et al., 2018). Mitochondrial dysfunction is an early event in PD. Indeed, some familial PD cases are caused by mutations in genes encoding mitochondria proteins (e.g., Pink, Parkin, and DJ-1) (Cheng et al., 2010).

The degeneration of DA neurons in PD originates from the distal axons of fragile neurons which is long and highly branched (Surmeier et al., 2017). The increased size of axonal arborization which resulted in elevated mitochondrial bioenergetics is considered of the reason for the vulnerability for DA neurons in the substantia nigra (Pacelli et al., 2015; Giguere et al., 2019).

Highly branched axons needs increased energy to deal with protein delivery, oxidative stress and mitochondrial dysfunction (Bhaskar et al., 2020).

Dysfunction of mitochondrial biogenesis plays a key role in the pathogenesis of PD. For instance, the inactivation of Parkin, which plays an important role in the pathological changes of familial PD, suppresses PCG-1α, a key regulator of mitochondrial biogenesis, ultimately causing the loss of DA neurons (Lee et al., 2017). In contrast, neurodegeneration caused by α-Syn overexpression in zebrafish can be partially relieved by PCG-1α upregulation (O'Donnell et al., 2014). Given that the dopaminergic axons loss precedes the cell death in both PD patient and PD model constructed by exposure to rotenone, a complex I inhibitor linked to PD (Tagliaferro and Burke, 2016), mitochondrial homeostasis in distal axon may participate in initial changes resulting in later neuron death. The limited early increase in mitochondrial density induced by rotenone in distal axons is due to upregulated distal axonal mitochondrial biogenesis (Van Laar et al., 2018), which is likely a compensatory process to mitochondrial disruption in PD.

Analysis of the post-mortem brains of PD patients showed that the distance between the synaptic terminal and mitochondria in DA neurons increased with a decreased volume and number of mitochondria, suggesting that mitochondrial synaptic availability and biomass contribute to degenerative neurons (Mallach et al., 2019). Mutations in Parkin impair Complex I activity, mitochondrial fusion, and the plasticity of synapses (Goldberg et al., 2003). Another example of how dysfunction mitochondria act in PD by disrupting synaptic plasticity comes from DJ-1, which is located in mitochondria and plays a role in synaptic transmission (Wang et al., 2008; Yan et al., 2020b).

Aberrant axonal transport contributes to neurodegeneration in PD (Lamberts et al., 2015). PD can be induced in mice by treatment with 6-hydroxydopamine (6-OHDA), which leads to axonal degeneration in dopaminergic neurons by inducing dysfunction of mitochondrial transport and microtubule disruption (Fuku, 2016). Significant alterations in mitochondria motility were observed in neurons induced from pluripotent stem cells (iPSCs) derived from an *LRRK2* mutant PD patient (Cooper et al., 2012). Prots et al. (2018) discovered that this alteration was associated with α-Syn oligomerization resulting from an increased α-Syn dosage, which resulted in reduced Miro and kinesin light chain-1 levels in axons and increased levels of Tau in neuronal soma.

PINK1 and Parkin are two proteins that can selectively remove damaged mitochondria. Mutations in these proteins can lead to PD and link mitophagy with this disease. Knockout of *Atg5* or *Atg7* causes loss of autophagy, resulting in swelling at the axon terminals and eventually cell death (Maday, 2016). Thus, autophagy plays an indispensable role in axon homeostasis. The accumulation of α-Syn and LRKK2 results from the loss of autophagy (Friedman et al., 2012), providing further proof that defects in autophagy cause the accumulation of abnormal organelles in axons (e.g., mitochondria), leading to oxidative damage and apoptotic cascades. In addition to PINK1/Parkin, LRRK2 is involved in initiating mitophagy by forming a complex with Miro. In pathologic *LRRK2G2019S* neurons, this function is disrupted but can be rescued by reducing Miro levels (Hsieh et al., 2016). While mitophagy has a protective effect on neurons, determining whether increased autophagy levels are the cause or effect of PD requires further study.

Amyotrophic Lateral Sclerosis

Amyotrophic lateral sclerosis (ALS) is the most common adult motor neuron disease with characteristic progressive motor neuron degeneration, leading to muscle atrophy, paralysis, and ultimately death (Taylor et al., 2016). Approximately 90% of cases are sporadic (sALS), while the remaining 10% are familial (fALS) (Turner et al., 2017). fALS is largely associated with gene mutations, particularly in TAR DNA Binding Protein 43 (TDP-43) and Cu/Zn superoxide dismutase (SOD1) (Chia et al., 2018). Accumulating evidence suggests that axon degeneration in fALS is significantly correlated with mitochondrial damage, impairment of mitochondria transport, and autophagy-lysosomal dysfunction. Within an early stage in *SOD1G93A* mice, distal axonal transport is reported to be impaired, meanwhile, the expression of kinesin and dynein is also inhibited (Warita et al., 1999). In both *SOD1* patients (Boillée et al., 2006; De Vos et al., 2007) and *SOD1G93A* mice (Fischer et al., 2004; Damiano et al., 2006; Tallon et al., 2016), damaged mitochondria accumulate at distal sites, causing ATP deficiencies and aberrant calcium homeostasis at neuromuscular junctions, ultimately resulting in distal axon degeneration.

Enhancing mitochondria motility can remove the dysfunctional mitochondria from distal synapses meanwhile deliver the healthy ones to distal axons. Nevertheless, in motor neurons from *hSOD1G93A* mice, axonal mitochondria transport is damaged, and the defective mitochondria aberrantly accumulate in distal axons (De Vos et al., 2007; Magrané and Manfredi, 2009; Bilsland et al., 2010; Cozzolino et al., 2013). In order to address this defection, a research designed to cross *hSOD1G93A* and $SNPH^{-/-}$ mice, aiming to examine whether enhancing mitochondria transport could make effect on the *hSOD1G93A* mice (Zhu and Sheng, 2011). Although the total mitochondrial transport is increased in the crossed mice, it seems to have no differences in the disease course. Moreover, this study reveals that deficits in mitochondrial transport appears to be insufficient to cause axon degeneration in the fALS-linked motor neurons (Zhu and Sheng, 2011), supported by an *in vitro* study in mutant *hSOD1* models (Marinkovic et al., 2012). In the motor neuron of fALS-linked *SOD1G93A* mice and the axons of AD-related cortical neurons from mutant human APP-expressing transgenic mice, impaired mitochondria are removed via the bulk release of SNPH cargo vesicles, which are mitochondria-derived and Parkin-independent, promoting mitochondria transport (Lin et al., 2017a). Recently, a study demonstrated that as the disease progresses in fALS-linked *SOD1G93A* and AD-linked mice, the quantity of SNPH cargo vesicles is also altered (Cheng and Sheng, 2020). It is interesting that at asymptomatic stages of fALS and AD, the number of SNPH cargo vesicles is greatly elevated in the axons of motor neurons (Lin et al., 2017a). Nevertheless, at the onset and late stages of the disease, SNPH is significantly depleted via mitochondrial impairment in these axons (Lin et al., 2017a).

Furthermore, the study revealed that in response to these chronic pathological stresses, the quantity of SNPH cargo vesicles changes in distal axons. The defective mitochondria anchored by SNPH are transported to the soma for recovery or degeneration (Cheng and Sheng, 2020). The SNPH-mediated pathway acts as a protective mechanism during the early asymptomatic stages of fALS and AD and is independent of and acts before PINK1/Parkin mediated mitophagy (Lin et al., 2017b). Thus, it is regarded as a significant hallmark of diagnosis and an early target for treatment. However, simply increasing mitochondrial transport by turning off SNPH-mediated anchoring (Lin et al., 2017a) or eliminating SNPH (Zhu and Sheng, 2011) fails to replenish ATP deficiency in *hSOD1G93A* mutant mice. The autophagy-lysosomal function is also defective in fALS-linked mice at an early stage of disease both *ex vivo* and *in vivo*, preventing the elimination of damaged mitochondria from distal axons (Xie et al., 2015). Thus, the combination of enhanced mitochondria transport and increased defective mitochondria elimination may be an effective therapeutic strategy for fALS.

A study has reported that anterograde and retrograde transport of mitochondria in primary motor neurons axons are greatly defected via overexpression of wild-type *TDP-43*. Interestingly, the study demonstrated that the loss of *TDP-43* also inhibits axonal transport of mitochondria, revealing that damaged mitochondria axonal transport may involve various pathways mediated by *TDP-43* (Wang W. et al., 2013). Moreover, a recent study showed that specific protein synthesis is inhibited (i.e., transcripts involved in mitochondrial energy metabolism, cytoskeletal components, and translational machinery) within the axons of motor neurons in *TDP-43*-knockout mice (Briese et al., 2020). Thus, axonal transport and mitochondria function are significantly defected in *TDP-43*-knockout mice, leading to the impairment of axon growth as well as revealing that depletion of *TDP-43* may act a predominant role in axon degeneration of ALS (Briese et al., 2020).

Treatment

In neurodegenerative diseases, the degeneration of axons often occurs at early disease stages. This degeneration is often accompanied by the accumulation of damaged or fragmented mitochondria. Therefore, maintaining mitochondrial dynamics in axons is a common treatment strategy.

Amyloid-β (Aβ) toxicity and Tau dysfunction in AD, often accompanied by impaired axonal mitochondrial transport, jointly lead to disease progression. Wang et al. (2019b) demonstrated that mitochondrial transport defects can be corrected in Aβ-treated neurons by protecting KIF5A, suggesting that maintaining normal mitochondrial axon transport is a valuable treatment strategy in AD. There are many targeted treatments for reducing the mitochondrial content caused by defective mitochondrial trafficking, as represented by increased retrograde transport rates in axons (Schwab et al., 2017). In addition, glycolytic defects in oligodendrocytes induce axon degeneration in both AD mice and patients via the Drp1-hexokinase 1-NLRP3 (NLR family pyrin domain containing 3) signaling axis, which is considered to be a therapeutic target (Yan et al., 2020a; Zhang et al., 2020). Mdivi-1, Dynasore, and P110 are promising agents that maintain axonal mitochondrial turnover by inhibiting dynamin to prevent the production of fragmented mitochondria, maintain normal mitochondria morphology, and restore ATP levels in a PD model (Elfawy and Das, 2019). Additionally, deep brain stimulation (DBS) is a very effective intervention to treat patients with advanced PD and its mechanism is related to the restoration of the number and volume of mitochondria (Mallach et al., 2019). The selective peptide inhibitor, P110 inhibits the Drp1-Fis1 interaction and improves the structure and function of mitochondria in *G93A SOD1* mutant mice, indicating an attractive target for ALS patients (Joshi et al., 2018). Nicotinamide mononucleotide adenylyl transferase1 (Nmnat1), an enzyme involved in nicotinamide adenine dinucleotide (NAD^+) synthesis, has a protective effect on mitochondrial dynamics and morphology following vincristine-induced axon degeneration (Berbusse et al., 2016).

Reactive oxidative species (ROS) production caused by mitochondrial dysfunction leads to oxidative stress, an important factor in axonal degeneration. Therefore, many treatment strategies focus on mitigating local ROS production using novel antioxidants that directly target mitochondria. Some mitochondria-targeted compounds (e.g., latrepirdine, methylene blue, triterpenoids, and the mitochondrial-targeted coenzyme Q10 derivative MitoQ) have been extensively evaluated in *in vivo* and *in vitro* AD and PD models (Elfawy and Das, 2019). In addition, a significant reduction in ROS levels results from treatment with the selective peptide inhibitor P110 and improves motor capacity and survival rates in G93A SOD1 mutant mice (Joshi et al., 2018).

Axon regeneration is an attractive target in neurodegenerative diseases. Because growth cone formation requires a large ATP supply, targeted mitochondrial therapy is key to axonal regeneration. While mature CNS neurons almost lose their intrinsic capacity for axon regeneration, upregulation of axon cytoskeleton proteins was observed in the 6-OHDA-hemiparkinsonian rat model, indicating a high plasticity and regeneration potential in adult animals (Lessner et al., 2010).

The *G2019S* mutation in the conserved serine kinase MAPK kinase domain contained in LRRK2 is the cause of familial PD (Cookson, 2010). Therefore, reduced neurite outgrowth and increased growth cone size were observed in neurons of *LRRK2 G2019S* mutant mice and the level of F-actin in growth cone also increases (Parisiadou et al., 2009), suggesting that growth cone formation, an essential step for axon regeneration is seriously impacted in PD. However, in the 6-OHDA-induced PD animal model, there are many compensatory responses in early-stage PD, including the upregulation of some proteins related to axon regeneration. Dihydropyrimidinase-related protein 2 (DPYSL2), which is important for axon outgrowth and regeneration (Sun and Cavalli, 2010), first decreased and then gradually recovered in this model. Moreover, axon growth and mitochondrial transport-related proteins (e.g., dynein, dynamin, and myosin) were also overexpressed (Kuter et al., 2016). Thus, a potential therapy to promote axon regeneration would be to enhance the expression of mitochondrial transport-related proteins.

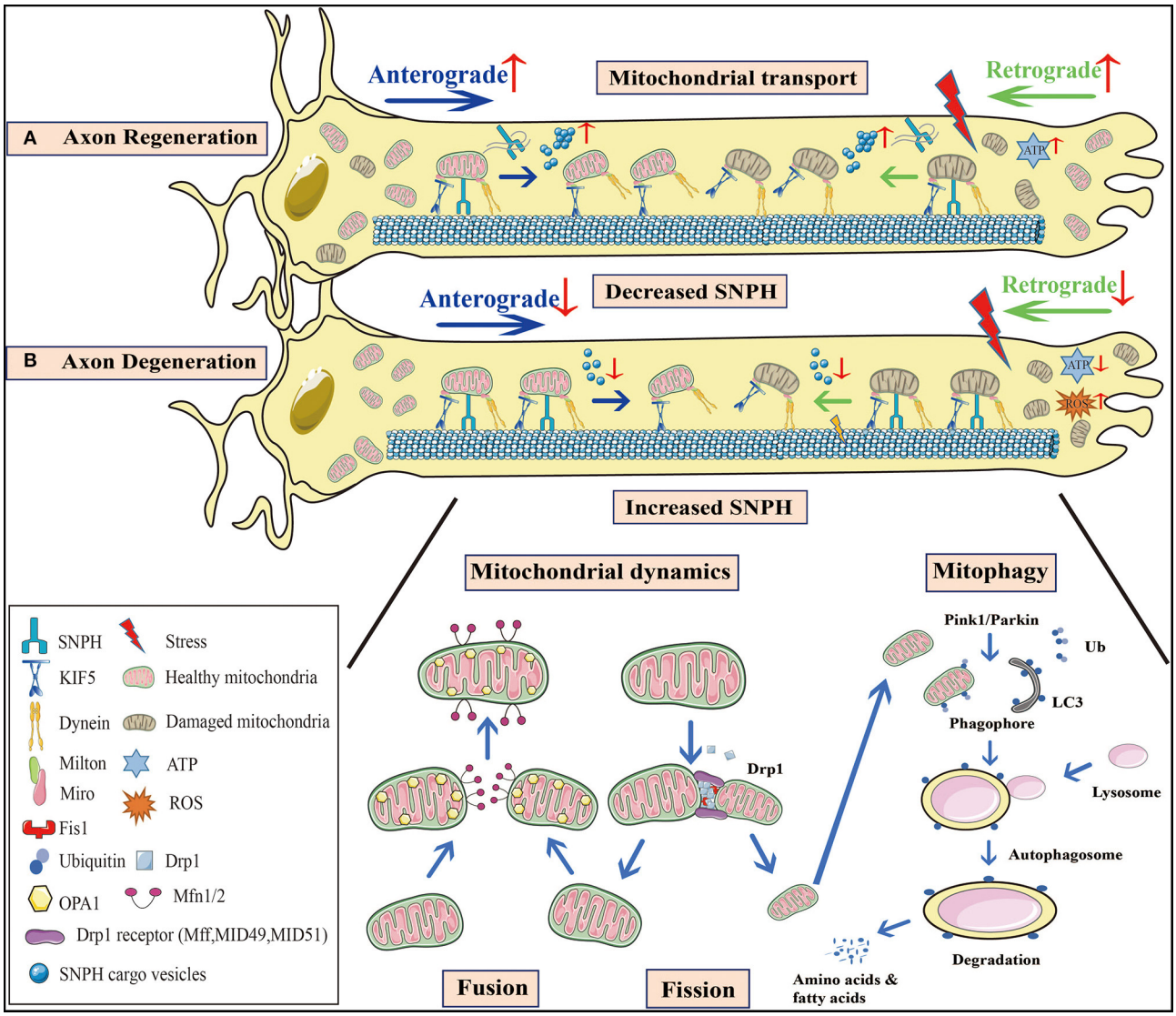

FIGURE 1 | Mitochondrial behavior in axon degeneration and regeneration. **(A)** Axon regeneration: Since this process requires considerable energy, mitochondrial density at distal axons is elevated to provide sufficient ATP. Not only is anterograde transport of healthy mitochondria promoted, but so too is retrograde transport of damaged mitochondria, to increase mitochondrial density at regenerative zones. SNPH knockout in TBI models, or the bulk release of SNPH cargo vesicles at AD and fALS early stages, both enhance axonal mitochondrial transport. **(B)** Axon degeneration: Mitochondrial dysfunction and oxidative stress occur in injured axons. When axonal mitochondrial transport is seriously impaired, damaged mitochondria aggregate at distal zones and the healthy ones fail to transport from the proximal zones to replenish ATP insufficiency. A decrease in SNPH cargo vesicle release at later stages of AD and fALS, as well as increased SNPH expression in SCI models inhibit mitochondrial transport. Moreover, axonal microtubule loss contributes to impaired axonal transport in TBI. Mitochondrial dynamics are also defective during axon degeneration. Due to increased Drp1-mediated fission in SCI, mitochondrial fragmentation is aggravated, causing mitochondrial damage. These organelle fuse with healthy mitochondria, however, most undergo mitophagy. In PD, Pink1-Parkin dependent mitophagy is defective, facilitating damaged mitochondrial accumulation and apoptotic cascades. These processes are interconnected in response to stress, and collectively lead to axon degeneration. SNPH, syntaphilin; TBI, traumatic brain injury; AD, Alzheimer's disease; fALS, familial amyotrophic lateral sclerosis; SCI, spinal cord injury; PD, Parkinson's disease.

A new promising therapeutic method involving exogenous mitochondrial transplant effectively attenuates the progression of neurologic disorders, including experimental Parkinson's disease (Shi et al., 2017). Supportive mitochondrial-targeting therapy is a promising approach for future therapeutic intervention in the CNS to promote axon regeneration. However, it should be noted that there are currently very limited ways to treat neurodegenerative diseases by promoting axon regeneration because of the diminishing intrinsic axonal regeneration in mature CNS neurons compared to PNS neurons, and there are no optimal treatments for these neurodegenerative diseases. Thus, researchers have focused on stopping the degeneration of

these nerves. With the deepening understanding of the treatment of mitochondria to prevent neural degeneration, we believe that axonal mitochondria regeneration will become a better therapeutic target for treating neurodegenerative diseases.

DISCUSSION

Axon degeneration and regeneration are essential parts of CNS neuronal death and restoration of CNS neurons, respectively, in aging, injury, and neurodegenerative diseases. However, the decline in the intrinsic regrowth capacity of mature CNS axons leads to a failure to regenerate after neuronal impairment (Fawcett and Verhaagen, 2018). Accumulating evidence demonstrates that mitochondrial dysfunction is intimately correlated with the initiation of axon degeneration and inhibition of axon regeneration (Qian and Zhou, 2020). Despite the mechanism underlying is still elusive, it suggests that mitochondrial quality control is an important intrinsic capacity of axon regeneration. For axon degeneration, mitochondrial dysfunction not only causes energy deficits and oxidative stress but also comprises mitochondrial dynamics, axonal transport, and mitophagy (Court and Coleman, 2012; Vasic et al., 2019). In contrast, restoring and enhancing these processes during axon regeneration increases the capacity of intrinsic regrowth (**Figure 1**). It comes to a consensus that axon regeneration requires adequate energy production and mitochondrial transport both in aging and in diseases (Zhou et al., 2016; Sheng, 2017; Zheng et al., 2019). Defected mitochondria can be replaced via mitochondria injection, which is demonstrated to decrease oxidative stress and trigger axon regeneration both *in vitro* and *in vivo* (Kuo et al., 2017). Thus, further study of axonal mitochondrial behavior under these conditions is important, not only for the alleviation and treatment of axon degeneration but also for identifying potential targets to enhance axon regeneration.

It is generally accepted that diminished intrinsic regeneration is a major barrier for axon regeneration in mature CNS neurons. Analysis of intrinsic axon degeneration and regeneration pathways and signaling networks can bring new insights for potential mitochondria-targeted therapeutic strategies. For example, a novel therapeutic strategy for enhancing the intrinsic capacity of axon regeneration may include genetic reprogramming through epigenome modifications and the transcriptome (Qian and Zhou, 2020). Mitochondrial damage-associated molecular patterns (mtDAMPs) released by injured axonal mitochondria can activate Schwann cell processes mediated by formylpeptide receptor 2 (FPR2) and toll-like receptor 9 (TLR9), which have a pivotal role in axon regeneration and cell migration (Korimová et al., 2018). Therefore, regulation of these mitochondria-targeted genetic reprogramming can be considered to be a promising molecular strategy for activating axon regeneration. At the cellular level, enhancing mitochondrial transport could greatly contribute to axon regeneration by removing defective mitochondria and replenishing healthy mitochondria at injured axon sites (Zheng et al., 2019). In addition, glial cells (astrocytes, oligodendrocytes, and microglia) contribute to mitochondrial dysfunction during axon growth inhibition and regeneration failure in the adult CNS (Brosius Lutz and Barres, 2014; Cregg et al., 2014; Silver and Silver, 2014). Astrocytes inhibit axonal mitochondrial energy metabolism by increasing nitric oxide production, glutamate levels, and intracellular calcium influx during Multiple Sclerosis (MS) (Correale and Farez, 2015). Similarly, astrocytes can release mitochondria containing particles, and transport them to defective axons following stroke (Babenko et al., 2015; Hayakawa et al., 2016). *In vitro* astrocyte-to-neuron mitochondrial delivery and *in vivo* astrocyte-derived mitochondrial transport improves neuronal survival, plasticity, and behavior outcomes (Hayakawa et al., 2016). Reactive oxygen and nitrogen species generated by microglia directly damage neurons by inhibiting cytochrome C oxidase and mitochondrial respiratory chain complex IV, causing axonal mitochondrial dysfunction in MS (Nikić et al., 2011). Furthermore, oligodendrocytes and astrocytes provide axonal mitochondria with pyruvate or lactate, which are imported into the mitochondria for energy metabolism during MS and AD (Fünfschilling et al., 2012; Correale et al., 2019; Zhang et al., 2020). Clearance of damaged mitochondria not only relies on mitophagy at the injury sites but also depends on mitochondrial retrograde transport, which involves SNPH and dual leucine zipper kinase 1 (Han et al., 2016; Cheng and Sheng, 2020). However, many molecules and substrates engaged in mitochondrial transport or dynamics need to be clarified. Moreover, to strengthen the intrinsic capacity for regrowth, improving the extrinsic inhibiting environment could make a critical difference in axon regeneration. Drugs targeted at oxidative stress via the clearance of ROS (Geden and Deshmukh, 2016) or directed at the restoration of calcium homeostasis by inhibiting calcium channels and calcium-activated enzymes (Mu et al., 2015) will aid axon regeneration. Furthermore, remodeling the neuronal cytoskeleton may be a novel mechanism to alleviate the extrinsic inhibitory cues (Qian and Zhou, 2020). In conclusion, combined approaches that target mitochondria, which increase the intrinsic capacity and decrease the extrinsic inhibiting environment, may provide an effective therapeutic strategy to enhance axon regeneration in aging, injury, and neurodegenerative diseases.

AUTHOR CONTRIBUTIONS

BW, MH, BZ, and XZ made substantial contributions to the conception and design of the study. BW, MH, DS, XY, BZ, and XZ participated in drafting the article. BW and MH created the figure. All authors contributed to the article and approved the submitted version.

FUNDING

This work was supported by the National Natural Science Foundation of China (no. 81700977 to XY, no. 82071151 to BZ, and no. 81500858 to XZ).

REFERENCES

Adalbert, R., and Coleman, M. P. (2013). Review: axon pathology in age-related neurodegenerative disorders. *Neuropathol. Appl. Neurobiol.* 39, 90–108. doi: 10.1111/j.1365-2990.2012.01308.x

Adalbert, R., Morreale, G., Paizs, M., Conforti, L., Walker, S. A., Roderick, H. L., et al. (2012). Intra-axonal calcium changes after axotomy in wild-type and slow Wallerian degeneration axons. *Neuroscience* 225, 44–54. doi: 10.1016/j.neuroscience.2012.08.056

Alavi Naini, S. M., and Soussi-Yanicostas, N. (2015). Tau hyperphosphorylation and oxidative stress, a critical vicious circle in neurodegenerative tauopathies? *Oxid. Med. Cell. Longev.* 2015:151979. doi: 10.1155/2015/151979

Albensi, B. C. (2019). Dysfunction of mitochondria: implications for Alzheimer's disease. *Int. Rev. Neurobiol.* 145, 13–27. doi: 10.1016/bs.irn.2019.03.001

Ali, Y. O., Allen, H. M., Yu, L., Li-Kroeger, D., Bakhshizadehmahmoudi, D., Hatcher, A., et al. (2016). NMNAT2:HSP90 complex mediates proteostasis in proteinopathies. *PLoS Biol.* 14:e1002472. doi: 10.1371/journal.pbio.1002472

Attwell, C. L., van Zwieten, M., Verhaagen, J., and Mason, M. R. J. (2018). The dorsal column lesion model of spinal cord injury and its use in deciphering the neuron-intrinsic injury response. *Dev. Neurobiol.* 78, 926–951. doi: 10.1002/dneu.22601

Avery, M. A., Rooney, T. M., Pandya, J. D., Wishart, T. M., Gillingwater, T. H., Geddes, J. W., et al. (2012). Wld^S prevents axon degeneration through increased mitochondrial flux and enhanced mitochondrial Ca^{2+} buffering. *Curr. Biol.* 22, 596–600. doi: 10.1016/j.cub.2012.02.043

Babenko, V. A., Silachev, D. N., Zorova, L. D., Pevzner, I. B., Khutornenko, A. A., Plotnikov, E. Y., et al. (2015). Improving the post-stroke therapeutic potency of mesenchymal multipotent stromal cells by cocultivation with cortical neurons: the role of crosstalk between cells. *Stem Cells Transl. Med.* 4, 1011–1020. doi: 10.5966/sctm.2015-0010

Barkhoudarian, G., Hovda, D. A., and Giza, C. C. (2016). The molecular pathophysiology of concussive brain injury - an update. *Phys. Med. Rehabil. Clin. N. Am.* 27, 373–393. doi: 10.1016/j.pmr.2016.01.003

Barrientos, S. A., Martinez, N. W., Yoo, S., Jara, J. S., Zamorano, S., Hetz, C., et al. (2011). Axonal degeneration is mediated by the mitochondrial permeability transition pore. *J. Neurosci.* 31, 966–978. doi: 10.1523/jneurosci.4065-10.2011

Berbusse, G. W., Woods, L. C., Vohra, B. P. S., and Naylor, K. (2016). Mitochondrial dynamics decrease prior to axon degeneration induced by vincristine and are partially rescued by overexpressed cytNmnat1. *Front. Cell. Neurosci.* 10:179. doi: 10.3389/fncel.2016.00179

Bhaskar, S., Gowda, J., Prasanna, J., and Kumar, A. (2020). Does altering proteasomal activity and trafficking reduce the arborization mediated specific vulnerability of SNpc dopaminergic neurons of Parkinson's disease? *Med. Hypotheses* 143:110062. doi: 10.1016/j.mehy.2020.110062

Bilsland, L. G., Sahai, E., Kelly, G., Golding, M., Greensmith, L., and Schiavo, G. (2010). Deficits in axonal transport precede ALS symptoms *in vivo*. *Proc. Natl. Acad. Sci. U.S.A.* 107, 20523–20528. doi: 10.1073/pnas.1006869107

Boillée, S., Vande Velde, C., and Cleveland, D. W. (2006). ALS: a disease of motor neurons and their nonneuronal neighbors. *Neuron* 52, 39–59. doi: 10.1016/j.neuron.2006.09.018

Bradke, F., Fawcett, J. W., and Spira, M. E. (2012). Assembly of a new growth cone after axotomy: the precursor to axon regeneration. *Nat. Rev. Neurosci.* 13, 183–193. doi: 10.1038/nrn3176

Briese, M., Saal-Bauernschubert, L., Lüningschrör, P., Moradi, M., Dombert, B., Surrey, V., et al. (2020). Loss of Tdp-43 disrupts the axonal transcriptome of motoneurons accompanied by impaired axonal translation and mitochondria function. *Acta Neuropathol. Commun.* 8:116. doi: 10.1186/s40478-020-00987-6

Brosius Lutz, A., and Barres, B. A. (2014). Contrasting the glial response to axon injury in the central and peripheral nervous systems. *Dev. Cell* 28, 7–17. doi: 10.1016/j.devcel.2013.12.002

Büki, A., Okonkwo, D. O., Wang, K. K., and Povlishock, J. T. (2000). Cytochrome c release and caspase activation in traumatic axonal injury. *J. Neurosci.* 20, 2825–2834. doi: 10.1523/jneurosci.20-08-02825.2000

Büki, A., Siman, R., Trojanowski, J. Q., and Povlishock, J. T. (1999). The role of calpain-mediated spectrin proteolysis in traumatically induced axonal injury. *J. Neuropathol. Exp. Neurol.* 58, 365–375. doi: 10.1097/00005072-199904000-00007

Butterfield, D. A., and Boyd-Kimball, D. (2018). Oxidative stress, amyloid-β peptide, and altered key molecular pathways in the pathogenesis and progression of Alzheimer's disease. *J. Alzheimers. Dis.* 62, 1345–1367. doi: 10.3233/jad-170543

Cai, Q., and Tammineni, P. (2017). Mitochondrial aspects of synaptic dysfunction in Alzheimer's disease. *J. Alzheimers. Dis.* 57, 1087–1103. doi: 10.3233/jad-160726

Calkins, M. J., Manczak, M., Mao, P., Shirendeb, U., and Reddy, P. H. (2011). Impaired mitochondrial biogenesis, defective axonal transport of mitochondria, abnormal mitochondrial dynamics and synaptic degeneration in a mouse model of Alzheimer's disease. *Hum. Mol. Genet.* 20, 4515–4529. doi: 10.1093/hmg/ddr381

Cao, X., Wang, H., Wang, Z., Wang, Q., Zhang, S., Deng, Y., et al. (2017). *In vivo* imaging reveals mitophagy independence in the maintenance of axonal mitochondria during normal aging. *Aging Cell* 16, 1180–1190. doi: 10.1111/acel.12654

Cartoni, R., Norsworthy, M. W., Bei, F., Wang, C., Li, S., Zhang, Y., et al. (2016). The mammalian-specific protein Armcx1 regulates mitochondrial transport during axon regeneration. *Neuron* 92, 1294–1307. doi: 10.1016/j.neuron.2016.10.060

Cartoni, R., Norsworthy, M. W., Bei, F., Wang, C., Li, S., Zhang, Y., et al. (2017). The mammalian-specific protein Armcx1 regulates mitochondrial transport during axon regeneration. *Neuron* 94:689. doi: 10.1016/j.neuron.2017.04.028

Cavalli, V., Kujala, P., Klumperman, J., and Goldstein, L. S. (2005). Sunday driver links axonal transport to damage signaling. *J. Cell Biol.* 168, 775–787. doi: 10.1083/jcb.200410136

Chandran, V., Coppola, G., Nawabi, H., Omura, T., Versano, R., Huebner, E. A., et al. (2016). A systems-level analysis of the peripheral nerve intrinsic axonal growth program. *Neuron* 89, 956–970. doi: 10.1016/j.neuron.2016.01.034

Chen, M., Li, Y., Yang, M., Chen, X., Chen, Y., Yang, F., et al. (2016). A new method for quantifying mitochondrial axonal transport. *Protein Cell* 7, 804–819. doi: 10.1007/s13238-016-0268-3

Chen, Y., and Sheng, Z.-H. (2013). Kinesin-1-syntaphilin coupling mediates activity-dependent regulation of axonal mitochondrial transport. *J. Cell Biol.* 202, 351–364. doi: 10.1083/jcb.201302040

Cheng, A., Hou, Y., and Mattson, M. P. (2010). Mitochondria and neuroplasticity. *ASN Neuro.* 2:e00045. doi: 10.1042/an20100019

Cheng, X. T., and Sheng, Z. H. (2020). Developmental regulation of microtubule-based trafficking and anchoring of axonal mitochondria in health and diseases. *Dev. Neurobiol.* doi: 10.1002/dneu.22748. [Epub ahead of print].

Cheng, Y., and Bai, F. (2018). The association of tau with mitochondrial dysfunction in Alzheimer's disease. *Front. Neurosci.* 12:163. doi: 10.3389/fnins.2018.00163

Chia, R., Chiò, A., and Traynor, B. J. (2018). Novel genes associated with amyotrophic lateral sclerosis: diagnostic and clinical implications. *Lancet Neurol.* 17, 94–102. doi: 10.1016/s1474-4422(17)30401-5

Chung, D., Shum, A., and Caraveo, G. (2020). GAP-43 and BASP1 in axon regeneration: implications for the treatment of neurodegenerative diseases. *Front. Cell Dev. Biol.* 8:567537. doi: 10.3389/fcell.2020.567537

Cieri, D., Vicario, M., Vallese, F., D'Orsi, B., Berto, P., Grinzato, A., et al. (2018). Tau localises within mitochondrial sub-compartments and its caspase cleavage affects ER-mitochondria interactions and cellular Ca(2+) handling. *Biochim. Biophys. Acta Mol. Basis Dis.* 1864, 3247–3256. doi: 10.1016/j.bbadis.2018.07.011

Clausen, A., Xu, X., Bi, X., and Baudry, M. (2012). Effects of the superoxide dismutase/catalase mimetic EUK-207 in a mouse model of Alzheimer's disease: protection against and interruption of progression of amyloid and tau pathology and cognitive decline. *J. Alzheimers. Dis.* 30, 183–208. doi: 10.3233/jad-2012-111298

Coleman, M. P., Conforti, L., Buckmaster, E. A., Tarlton, A., Ewing, R. M., Brown, M. C., et al. (1998). An 85-kb tandem triplication in the slow Wallerian degeneration (Wlds) mouse. *Proc. Natl. Acad. Sci. U.S.A.* 95, 9985–9990. doi: 10.1073/pnas.95.17.9985

Conforti, L., Tarlton, A., Mack, T. G., Mi, W., Buckmaster, E. A., Wagner, D., et al. (2000). A Ufd2/D4Cole1e chimeric protein and overexpression of Rbp7 in the slow Wallerian degeneration (WldS) mouse. *Proc. Natl. Acad. Sci. U.S.A.* 97, 11377–11382. doi: 10.1073/pnas.97.21.11377

Cookson, M. R. (2010). The role of leucine-rich repeat kinase 2 (LRRK2) in Parkinson's disease. *Nat. Rev. Neurosci.* 11, 791–797. doi: 10.1038/nrn2935

Cooper, M. L., Crish, S. D., Inman, D. M., Horner, P. J., and Calkins, D. J. (2016). Early astrocyte redistribution in the optic nerve precedes axonopathy in the DBA/2J mouse model of glaucoma. *Exp. Eye Res.* 150, 22–33. doi: 10.1016/j.exer.2015.11.016

Cooper, O., Seo, H., Andrabi, S., Guardia-Laguarta, C., Graziotto, J., Sundberg, M., et al. (2012). Pharmacological rescue of mitochondrial deficits in iPSC-derived neural cells from patients with familial Parkinson's disease. *Sci. Transl. Med.* 4:141ra190. doi: 10.1126/scitranslmed.3003985

Correale, J., and Farez, M. F. (2015). The role of astrocytes in multiple sclerosis progression. *Front. Neurol.* 6:180. doi: 10.3389/fneur.2015.00180

Correale, J., Marrodan, M., and Ysrraelit, M. C. (2019). Mechanisms of neurodegeneration and axonal dysfunction in progressive multiple sclerosis. *Biomedicines* 7:14. doi: 10.3390/biomedicines7010014

Court, F. A., and Coleman, M. P. (2012). Mitochondria as a central sensor for axonal degenerative stimuli. *Trends Neurosci.* 35, 364–372. doi: 10.1016/j.tins.2012.04.001

Cozzolino, M., Ferri, A., Valle, C., and Carrì, M. T. (2013). Mitochondria and ALS: implications from novel genes and pathways. *Mol. Cell. Neurosci.* 55, 44–49. doi: 10.1016/j.mcn.2012.06.001

Cregg, J. M., DePaul, M. A., Filous, A. R., Lang, B. T., Tran, A., and Silver, J. (2014). Functional regeneration beyond the glial scar. *Exp. Neurol.* 253, 197–207. doi: 10.1016/j.expneurol.2013.12.024

Csordás, G., Weaver, D., and Hajnóczky, G. (2018). Endoplasmic reticulum–mitochondrial contactology: structure and signaling functions. *Trends Cell Biol.* 28, 523–540. doi: 10.1016/j.tcb.2018.02.009

Damiano, M., Starkov, A. A., Petri, S., Kipiani, K., Kiaei, M., Mattiazzi, M., et al. (2006). Neural mitochondrial Ca^{2+} capacity impairment precedes the onset of motor symptoms in G93A Cu/Zn-superoxide dismutase mutant mice. *J. Neurochem.* 96, 1349–1361. doi: 10.1111/j.1471-4159.2006.03619.x

De Vos, K. J., Chapman, A. L., Tennant, M. E., Manser, C., Tudor, E. L., Lau, K. F., et al. (2007). Familial amyotrophic lateral sclerosis-linked SOD1 mutants perturb fast axonal transport to reduce axonal mitochondria content. *Hum. Mol. Genet.* 16, 2720–2728. doi: 10.1093/hmg/ddm226

Dewar, D., Underhill, S. M., and Goldberg, M. P. (2003). Oligodendrocytes and ischemic brain injury. *J. Cereb. Blood Flow Metab.* 23, 263–274. doi: 10.1097/01.wcb.0000053472.41007.f9

Di Rita, A., Peschiaroli, A., D′Acunzo, P., Strobbe, D., Hu, Z., Gruber, J., et al. (2018). HUWE1 E3 ligase promotes PINK1/PARKIN-independent mitophagy by regulating AMBRA1 activation via IKKα. *Nat. Commun.* 9:3755. doi: 10.1038/s41467-018-05722-3

Du, H., Guo, L., Fang, F., Chen, D., Sosunov, A. A., McKhann, G. M., et al. (2008). Cyclophilin D deficiency attenuates mitochondrial and neuronal perturbation and ameliorates learning and memory in Alzheimer's disease. *Nat. Med.* 14, 1097–1105. doi: 10.1038/nm.1868

Du, H., Guo, L., Zhang, W., Rydzewska, M., and Yan, S. (2011). Cyclophilin D deficiency improves mitochondrial function and learning/memory in aging Alzheimer disease mouse model. *Neurobiol. Aging* 32, 398–406. doi: 10.1016/j.neurobiolaging.2009.03.003

Elfawy, H. A., and Das, B. (2019). Crosstalk between mitochondrial dysfunction, oxidative stress, and age related neurodegenerative disease: etiologies and therapeutic strategies. *Life Sci.* 218, 165–184. doi: 10.1016/j.lfs.2018.12.029

Essuman, K., Summers, D. W., Sasaki, Y., Mao, X., DiAntonio, A., and Milbrandt, J. (2017). The SARM1 Toll/Interleukin-1 receptor domain possesses intrinsic NAD(+) cleavage activity that promotes pathological axonal degeneration. *Neuron* 93, 1334.e1335–1343.e1335. doi: 10.1016/j.neuron.2017.02.022

Fang, Y., Soares, L., Teng, X., Geary, M., and Bonini, N. M. (2012). A novel Drosophila model of nerve injury reveals an essential role of Nmnat in maintaining axonal integrity. *Curr. Biol.* 22, 590–595. doi: 10.1016/j.cub.2012.01.065

Fawcett, J. W., and Verhaagen, J. (2018). Intrinsic determinants of axon regeneration. *Dev. Neurobiol.* 78, 890–897. doi: 10.1002/dneu.22637

Fischer, L. R., Culver, D. G., Tennant, P., Davis, A. A., Wang, M., Castellano-Sanchez, A., et al. (2004). Amyotrophic lateral sclerosis is a distal axonopathy: evidence in mice and man. *Exp. Neurol.* 185, 232–240. doi: 10.1016/j.expneurol.2003.10.004

Frati, A., Cerretani, D., Fiaschi, A. I., Frati, P., Gatto, V., La Russa, R., et al. (2017). Diffuse axonal injury and oxidative stress: a comprehensive review. *Int. J. Mol. Sci.* 18:2600. doi: 10.3390/ijms18122600

Friedman, L. G., Lachenmayer, M. L., Wang, J., He, L., Poulose, S. M., Komatsu, M., et al. (2012). Disrupted autophagy leads to dopaminergic axon and dendrite degeneration and promotes presynaptic accumulation of α-synuclein and LRRK2 in the brain. *J. Neurosci.* 32, 7585–7593. doi: 10.1523/JNEUROSCI.5809-11.2012

Fuku, K. (2016). Reactive oxygen species induce neurite degeneration before induction of cell death. *J. Clin. Biochem. Nutr.* 59, 155–159. doi: 10.3164/jcbn.16-34

Fünfschilling, U., Supplie, L. M., Mahad, D., Boretius, S., Saab, A. S., Edgar, J., et al. (2012). Glycolytic oligodendrocytes maintain myelin and long-term axonal integrity. *Nature* 485, 517–521. doi: 10.1038/nature11007

Gao, Y., Wilson, G. R., Stephenson, S. E. M., Bozaoglu, K., Farrer, M. J., and Lockhart, P. J. (2018). The emerging role of Rab GTPases in the pathogenesis of Parkinson's disease. *Mov. Disord.* 33, 196–207. doi: 10.1002/mds.27270

Geden, M. J., and Deshmukh, M. (2016). Axon degeneration: context defines distinct pathways. *Curr. Opin. Neurobiol.* 39, 108–115. doi: 10.1016/j.conb.2016.05.002

Geoffroy, C. G., Hilton, B. J., Tetzlaff, W., and Zheng, B. (2016). Evidence for an age-dependent decline in axon regeneration in the adult mammalian central nervous system. *Cell Rep.* 15, 238–246. doi: 10.1016/j.celrep.2016.03.028

Geoffroy, C. G., Meves, J. M., and Zheng, B. (2017). The age factor in axonal repair after spinal cord injury: a focus on neuron-intrinsic mechanisms. *Neurosci. Lett.* 652, 41–49. doi: 10.1016/j.neulet.2016.11.003

Gerdts, J., Brace, E. J., Sasaki, Y., DiAntonio, A., and Milbrandt, J. (2015). SARM1 activation triggers axon degeneration locally via NAD^+ destruction. *Science* 348, 453–457. doi: 10.1126/science.1258366

Gerdts, J., Summers, D. W., Milbrandt, J., and DiAntonio, A. (2016). Axon self-destruction: new links among SARM1, MAPKs, and NAD+ metabolism. *Neuron* 89, 449–460. doi: 10.1016/j.neuron.2015.12.023

Giguere, N., Delignat-Lavaud, B., Herborg, F., Voisin, A., Li, Y., Jacquemet, V., et al. (2019). Increased vulnerability of nigral dopamine neurons after expansion of their axonal arborization size through D2 dopamine receptor conditional knockout. *PLoS Genet.* 15:e1008352. doi: 10.1371/journal.pgen.1008352

Gilley, J., and Coleman, M. P. (2010). Endogenous Nmnat2 is an essential survival factor for maintenance of healthy axons. *PLoS Biol.* 8:e1000300. doi: 10.1371/journal.pbio.1000300

Girouard, M. P., Bueno, M., Julian, V., Drake, S., Byrne, A. B., and Fournier, A. E. (2018). The molecular interplay between axon degeneration and regeneration. *Dev. Neurobiol.* 78, 978–990. doi: 10.1002/dneu.22627

Goldberg, M. S., Fleming, S. M., Palacino, J. J., Cepeda, C., Lam, H. A., Bhatnagar, A., et al. (2003). Parkin-deficient mice exhibit nigrostriatal deficits but not loss of dopaminergic neurons. *J. Biol. Chem.* 278, 43628–43635. doi: 10.1074/jbc.M308947200

Guedes-Dias, P., and Holzbaur, E. L. F. (2019). Axonal transport: driving synaptic function. *Science* 366:eaaw9997. doi: 10.1126/science.aaw9997

Guo, L., Du, H., Yan, S., Wu, X., McKhann, G. M., Chen, J. X., et al. (2013). Cyclophilin D deficiency rescues axonal mitochondrial transport in Alzheimer's neurons. *PLoS ONE* 8:e54914. doi: 10.1371/journal.pone.0054914

Guo, W., Stoklund Dittlau, K., and Van Den Bosch, L. (2020). Axonal transport defects and neurodegeneration: molecular mechanisms and therapeutic implications. *Semin. Cell Dev. Biol.* 99, 133–150. doi: 10.1016/j.semcdb.2019.07.010

Han, S. M., Baig, H. S., and Hammarlund, M. (2016). Mitochondria localize to injured axons to support regeneration. *Neuron* 92, 1308–1323. doi: 10.1016/j.neuron.2016.11.025

Hayakawa, K., Esposito, E., Wang, X., Terasaki, Y., Liu, Y., Xing, C., et al. (2016). Transfer of mitochondria from astrocytes to neurons after stroke. *Nature* 535, 551–555. doi: 10.1038/nature18928

Henderson, C. A., Gomez, C. G., Novak, S. M., Mi-Mi, L., and Gregorio, C. C. (2017). Overview of the muscle cytoskeleton. *Compr. Physiol.* 7, 891–944. doi: 10.1002/cphy.c160033

Hsieh, C. H., Shaltouki, A., Gonzalez, A. E., Bettencourt da Cruz, A., Burbulla, L. F., St Lawrence, E., et al. (2016). Functional impairment in miro degradation

and mitophagy is a shared feature in familial and sporadic Parkinson's disease. *Cell Stem Cell* 19, 709–724. doi: 10.1016/j.stem.2016.08.002

Hur, E. M., Yang, I. H., Kim, D. H., Byun, J., Saijilafu, Xu, W. L., et al. (2011). Engineering neuronal growth cones to promote axon regeneration over inhibitory molecules. *Proc. Natl. Acad. Sci. U.S.A.* 108, 5057–5062. doi: 10.1073/pnas.1011258108

Hwang, J., and Namgung, U. (2021). Phosphorylation of STAT3 by axonal Cdk5 promotes axonal regeneration by modulating mitochondrial activity. *Exp. Neurol.* 335:113511. doi: 10.1016/j.expneurol.2020.113511

Jessen, K. R., Mirsky, R., and Lloyd, A. C. (2015). Schwann cells: development and role in nerve repair. *Cold Spring Harb. Perspect. Biol.* 7:a020487. doi: 10.1101/cshperspect.a020487

Jia, Z.-Q., Li, G., Zhang, Z.-Y., Li, H.-T., Wang, J.-Q., Fan, Z.-K., et al. (2016). Time representation of mitochondrial morphology and function after acute spinal cord injury. *Neural Regen. Res.* 11, 137–143. doi: 10.4103/1673-5374.175061

Joshi, A. U., Saw, N. L., Vogel, H., Cunnigham, A. D., Shamloo, M., and Mochly-Rosen, D. (2018). Inhibition of Drp1/Fis1 interaction slows progression of amyotrophic lateral sclerosis. *EMBO Mol. Med.* 10:e8166. doi: 10.15252/emmm.201708166

Kaasik, A. (2016). Mitochondrial mobility and neuronal recovery. *N. Engl. J. Med.* 375, 1295–1296. doi: 10.1056/NEJMcibr1607955

Kelsen, J., Karlsson, M., Hansson, M. J., Yang, Z., Fischer, W., Hugerth, M., et al. (2019). Copenhagen head injury ciclosporin study: a phase IIa safety, pharmacokinetics, and biomarker study of ciclosporin in severe traumatic brain injury patients. *J. Neurotrauma* 36, 3253–3263. doi: 10.1089/neu.2018.6369

Kiryu-Seo, S., Tamada, H., Kato, Y., Yasuda, K., Ishihara, N., Nomura, M., et al. (2016). Mitochondrial fission is an acute and adaptive response in injured motor neurons. *Sci. Rep.* 6:28331. doi: 10.1038/srep28331

Kline, R. A., Dissanayake, K. N., Hurtado, M. L., Martínez, N. W., Ahl, A., Mole, A. J., et al. (2019). Altered mitochondrial bioenergetics are responsible for the delay in Wallerian degeneration observed in neonatal mice. *Neurobiol. Dis.* 130:104496. doi: 10.1016/j.nbd.2019.104496

Knowlton, W. M., Hubert, T., Wu, Z., Chisholm, A. D., and Jin, Y. (2017). A select subset of electron transport chain genes associated with optic atrophy link mitochondria to axon regeneration in *Caenorhabditis elegans*. *Front. Neurosci.* 11:263. doi: 10.3389/fnins.2017.00263

Korimová, A., Klusáková, I., Hradilová-SvíŽenská, I., Kohoutková, M., Joukal, M., and Dubový, P. (2018). Mitochondrial damage-associated molecular patterns of injured axons induce outgrowth of schwann cell processes. *Front. Cell. Neurosci.* 12:457. doi: 10.3389/fncel.2018.00457

Kuo, C. C., Su, H. L., Chang, T. L., Chiang, C. Y., Sheu, M. L., Cheng, F. C., et al. (2017). Prevention of axonal degeneration by perineurium injection of mitochondria in a sciatic nerve crush injury model. *Neurosurgery* 80, 475–488. doi: 10.1093/neuros/nyw090

Kuter, K., Kratochwil, M., Marx, S.-H., Hartwig, S., Lehr, S., Sugawa, M. D., et al. (2016). Native DIGE proteomic analysis of mitochondria from substantia nigra and striatum during neuronal degeneration and its compensation in an animal model of early Parkinson's disease. *Arch. Physiol. Biochem.* 122, 238–256. doi: 10.1080/13813455.2016.1197948

Lamberts, J. T., Hildebrandt, E. N., and Brundin, P. (2015). Spreading of α-synuclein in the face of axonal transport deficits in Parkinson's disease: a speculative synthesis. *Neurobiol. Dis.* 77, 276–283. doi: 10.1016/j.nbd.2014.07.002

Lee, Y., Stevens, D. A., Kang, S.-U., Jiang, H., Lee, Y.-I., Ko, H. S., et al. (2017). PINK1 primes Parkin-mediated ubiquitination of PARIS in dopaminergic neuronal survival. *Cell Rep.* 18, 918–932. doi: 10.1016/j.celrep.2016.12.090

Lessner, G., Schmitt, O., Haas, S. J.-P., Mikkat, S., Kreutzer, M., Wree, A., et al. (2010). Differential proteome of the striatum from hemiparkinsonian rats displays vivid structural remodeling processes. *J. Proteome Res.* 2010, 9, 4671–4687. doi: 10.1021/pr100389u

Lewis, T. L., Turi, G. F., Kwon, S.-K., Losonczy, A., and Polleux, F. (2016). Progressive decrease of mitochondrial motility during maturation of cortical axons *in vitro* and *in vivo*. *Curr. Biol.* 26, 2602–2608. doi: 10.1016/j.cub.2016.07.064

Li, J., Wang, Q., Wang, H., Wu, Y., Yin, J., Chen, J., et al. (2018). Lentivirus mediating FGF13 enhances axon regeneration after spinal cord injury by stabilizing microtubule and improving mitochondrial function. *J. Neurotrauma* 35, 548–559. doi: 10.1089/neu.2017.5205

Lin, M.-Y., and Sheng, Z.-H. (2015). Regulation of mitochondrial transport in neurons. *Exp. Cell Res.* 334, 35–44. doi: 10.1016/j.yexcr.2015.01.004

Lin, M. Y., Cheng, X. T., Tammineni, P., Xie, Y., Zhou, B., Cai, Q., et al. (2017a). Releasing syntaphilin removes stressed mitochondria from axons independent of mitophagy under pathophysiological conditions. *Neuron* 94, 595.e596–610.e596. doi: 10.1016/j.neuron.2017.04.004

Lin, M. Y., Cheng, X. T., Xie, Y., Cai, Q., and Sheng, Z. H. (2017b). Removing dysfunctional mitochondria from axons independent of mitophagy under pathophysiological conditions. *Autophagy* 13, 1792–1794. doi: 10.1080/15548627.2017.1356552

Liu, B., McNally, S., Kilpatrick, J. I., Jarvis, S. P., and O'Brien, C. J. (2018). Aging and ocular tissue stiffness in glaucoma. *Surv. Ophthalmol.* 63, 56–74. doi: 10.1016/j.survophthal.2017.06.007

Liu, X., and Hajnóczky, G. (2009). Ca^{2+}-dependent regulation of mitochondrial dynamics by the Miro-Milton complex. *Int. J. Biochem. Cell Biol.* 41, 1972–1976. doi: 10.1016/j.biocel.2009.05.013

Ljungberg, M. C., Ali, Y. O., Zhu, J., Wu, C. S., Oka, K., Zhai, R. G., et al. (2012). CREB-activity and nmnat2 transcription are down-regulated prior to neurodegeneration, while NMNAT2 over-expression is neuroprotective, in a mouse model of human tauopathy. *Hum. Mol. Genet.* 21, 251–267. doi: 10.1093/hmg/ddr492

Loreto, A., Di Stefano, M., Gering, M., and Conforti, L. (2015). Wallerian degeneration is executed by an NMN-SARM1-dependent late Ca(2+) influx but only modestly influenced by mitochondria. *Cell Rep.* 13, 2539–2552. doi: 10.1016/j.celrep.2015.11.032

Lu, P., Wang, Y., Graham, L., McHale, K., Gao, M., Wu, D., et al. (2012). Long-distance growth and connectivity of neural stem cells after severe spinal cord injury. *Cell* 150, 1264–1273. doi: 10.1016/j.cell.2012.08.020

Luo, X., Ribeiro, M., Bray, E. R., Lee, D. H., Yungher, B. J., Mehta, S. T., et al. (2016). Enhanced transcriptional activity and mitochondrial localization of STAT3 co-induce axon regrowth in the adult central nervous system. *Cell Rep.* 15, 398–410. doi: 10.1016/j.celrep.2016.03.029

Mårtensson, C. U., Doan, K. N., and Becker, T. (2017). Effects of lipids on mitochondrial functions. *Biochim. Biophys. Acta. Mol. Cell Biol. Lipids* 1862, 102–113. doi: 10.1016/j.bbalip.2016.06.015

Ma, M., Ferguson, T. A., Schoch, K. M., Li, J., Qian, Y., Shofer, F. S., et al. (2013). Calpains mediate axonal cytoskeleton disintegration during Wallerian degeneration. *Neurobiol. Dis.* 56, 34–46. doi: 10.1016/j.nbd.2013.03.009

Maday, S. (2016). Mechanisms of neuronal homeostasis: autophagy in the axon. *Brain Res.* 1649(Pt B), 143–150. doi: 10.1016/j.brainres.2016.03.047

Magrané, J., and Manfredi, G. (2009). Mitochondrial function, morphology, and axonal transport in amyotrophic lateral sclerosis. *Antioxid. Redox Signal.* 11, 1615–1626. doi: 10.1089/ars.2009.2604

Mahar, M., and Cavalli, V. (2018). Intrinsic mechanisms of neuronal axon regeneration. *Nat. Rev. Neurosci.* 19, 323–337. doi: 10.1038/s41583-018-0001-8

Mallach, A., Weinert, M., Arthur, J., Gveric, D., Tierney, T. S., and Alavian, K. N. (2019). Post mortem examination of Parkinson's disease brains suggests decline in mitochondrial biomass, reversed by deep brain stimulation of subthalamic nucleus. *FASEB J.* 33, 6957–6961. doi: 10.1096/fj.201802628R

Mao, X. R., Kaufman, D. M., and Crowder, C. M. (2016). Nicotinamide mononucleotide adenylyltransferase promotes hypoxic survival by activating the mitochondrial unfolded protein response. *Cell Death Dis.* 7:e2113. doi: 10.1038/cddis.2016.5

Marinkovic, P., Reuter, M. S., Brill, M. S., Godinho, L., Kerschensteiner, M., and Misgeld, T. (2012). Axonal transport deficits and degeneration can evolve independently in mouse models of amyotrophic lateral sclerosis. *Proc. Natl. Acad. Sci. U.S.A.* 109, 4296–4301. doi: 10.1073/pnas.1200658109

Martinez-Vicente, M. (2017). Neuronal mitophagy in neurodegenerative diseases. *Front. Mol. Neurosci.* 10:64. doi: 10.3389/fnmol.2017.00064

Mata, A. M. (2018). Functional interplay between plasma membrane Ca(2+)-ATPase, amyloid β-peptide and tau. *Neurosci. Lett.* 663, 55–59. doi: 10.1016/j.neulet.2017.08.004

Matamoros, A. J., Tom, V. J., Wu, D., Rao, Y., Sharp, D. J., and Baas, P. W. (2019). Knockdown of fidgetin improves regeneration of injured axons by a microtubule-based mechanism. *J. Neurosci.* 39, 2011–2024. doi: 10.1523/JNEUROSCI.1888-18.2018

Maxwell, W. L. (2015). "Development of concepts in the pathology of traumatic axonal and traumatic brain injury," in *Brain Neurotrauma: Molecular,*

Neuropsychological, and Rehabilitation Aspects, ed F. H. Kobeissy (Boca Raton, FL: CRC Press/Taylor and Francis).

Maxwell, W. L., Povlishock, J. T., and Graham, D. L. (1997). A mechanistic analysis of nondisruptive axonal injury: a review. *J. Neurotrauma* 14, 419–440. doi: 10.1089/neu.1997.14.419

McAllister, T. W. (2011). Neurobiological consequences of traumatic brain injury. *Dialogues Clin. Neurosci.* 13, 287–300. doi: 10.31887/DCNS.2011.13.2/tmcallister

Melov, S., Adlard, P. A., Morten, K., Johnson, F., Golden, T. R., Hinerfeld, D., et al. (2007). Mitochondrial oxidative stress causes hyperphosphorylation of tau. *PLoS ONE* 2:e536. doi: 10.1371/journal.pone.0000536

Misgeld, T., Kerschensteiner, M., Bareyre, F. M., Burgess, R. W., and Lichtman, J. W. (2007). Imaging axonal transport of mitochondria *in vivo*. *Nat. Methods* 4, 559–561. doi: 10.1038/nmeth1055

Misgeld, T., and Schwarz, T. L. (2017). Mitostasis in neurons: maintaining mitochondria in an extended cellular architecture. *Neuron* 96, 651–666. doi: 10.1016/j.neuron.2017.09.055

Misko, A., Jiang, S., Wegorzewska, I., Milbrandt, J., and Baloh, R. H. (2010). Mitofusin 2 is necessary for transport of axonal mitochondria and interacts with the Miro/Milton complex. *J. Neurosci.* 30, 4232–4240. doi: 10.1523/jneurosci.6248-09.2010

Morris, R. L., and Hollenbeck, P. J. (1993). The regulation of bidirectional mitochondrial transport is coordinated with axonal outgrowth. *J Cell Sci.* 104 (Pt 3), 917–927.

Mu, J., Song, Y., Zhang, J., Lin, W., and Dong, H. (2015). Calcium signaling is implicated in the diffuse axonal injury of brain stem. *Int. J. Clin. Exp. Pathol.* 8, 4388–4397.

Namjoshi, D. R., Cheng, W. H., McInnes, K. A., Martens, K. M., Carr, M., Wilkinson, A., et al. (2014). Merging pathology with biomechanics using CHIMERA (Closed-Head Impact Model of Engineered Rotational Acceleration): a novel, surgery-free model of traumatic brain injury. *Mol. Neurodegener.* 9:55. doi: 10.1186/1750-1326-9-55

Neukomm, L. J., Burdett, T. C., Seeds, A. M., Hampel, S., Coutinho-Budd, J. C., Farley, J. E., et al. (2017). Axon death pathways converge on axundead to promote functional and structural axon disassembly. *Neuron* 95, 78.e75–91.e75. doi: 10.1016/j.neuron.2017.06.031

Nikić, I., Merkler, D., Sorbara, C., Brinkoetter, M., Kreutzfeldt, M., Bareyre, F. M., et al. (2011). A reversible form of axon damage in experimental autoimmune encephalomyelitis and multiple sclerosis. *Nat. Med.* 17, 495–499. doi: 10.1038/nm.2324

Nivison, M. P., Ericson, N. G., Green, V. M., Bielas, J. H., Campbell, J. S., and Horner, P. J. (2017). Age-related accumulation of phosphorylated mitofusin 2 protein in retinal ganglion cells correlates with glaucoma progression. *Exp. Neurol.* 296, 49–61. doi: 10.1016/j.expneurol.2017.07.001

Nocera, G., and Jacob, C. (2020). Mechanisms of Schwann cell plasticity involved in peripheral nerve repair after injury. *Cell. Mol. Life Sci.* 77, 3977–3989. doi: 10.1007/s00018-020-03516-9

O'Donnell, K. C., Lulla, A., Stahl, M. C., Wheat, N. D., Bronstein, J. M., and Sagasti, A. (2014). Axon degeneration and PGC-1α-mediated protection in a zebrafish model of alpha-synuclein toxicity. *Dis. Model. Mech.* 7, 571–582. doi: 10.1242/dmm.013185

O'Donnell, K. C., Vargas, M. E., and Sagasti, A. (2013). WldS and PGC-1α regulate mitochondrial transport and oxidation state after axonal injury. *J. Neurosci.* 33, 14778–14790. doi: 10.1523/jneurosci.1331-13.2013

O'Shea, T. M., Burda, J. E., and Sofroniew, M. V. (2017). Cell biology of spinal cord injury and repair. *J. Clin. Invest.* 127, 3259–3270. doi: 10.1172/JCI90608

Osterloh, J. M., Yang, J., Rooney, T. M., Fox, A. N., Adalbert, R., Powell, E. H., et al. (2012). dSarm/Sarm1 is required for activation of an injury-induced axon death pathway. *Science* 337, 481–484. doi: 10.1126/science.1223899

Otera, H., Ishihara, N., and Mihara, K. (2013). New insights into the function and regulation of mitochondrial fission. *Biochim. Biophys. Acta* 1833, 1256–1268. doi: 10.1016/j.bbamcr.2013.02.002

Pacelli, C., Giguère, N., Bourque, M.-J., Lévesque, M., Slack, R. S., and Trudeau, L.-É. (2015). Elevated mitochondrial bioenergetics and axonal arborization size are key contributors to the vulnerability of dopamine neurons. *Curr. Biol.* 25, 2349–2360. doi: 10.1016/j.cub.2015.07.050

Parisiadou, L., Xie, C., Cho, H. J., Lin, X., Gu, X.-L., Long, C.-X., et al. (2009). Phosphorylation of ezrin/radixin/moesin proteins by LRRK2 promotes the rearrangement of actin cytoskeleton in neuronal morphogenesis. *J. Neurosci.* 29, 13971–13980. doi: 10.1523/JNEUROSCI.3799-09.2009

Pathak, D., Sepp, K. J., and Hollenbeck, P. J. (2010). Evidence that myosin activity opposes microtubule-based axonal transport of mitochondria. *J. Neurosci.* 30, 8984–8992. doi: 10.1523/JNEUROSCI.1621-10.2010

Pickles, S., Vigie, P., and Youle, R. J. (2018). Mitophagy and quality control mechanisms in mitochondrial maintenance. *Curr. Biol.* 28, R170–R185. doi: 10.1016/j.cub.2018.01.004

Pivovarova, N. B., and Andrews, S. B. (2010). Calcium-dependent mitochondrial function and dysfunction in neurons. *FEBS J.* 277, 3622–3636. doi: 10.1111/j.1742-4658.2010.07754.x

Prior, R., Van Helleputte, L., Benoy, V., and Van Den Bosch, L. (2017). Defective axonal transport: a common pathological mechanism in inherited and acquired peripheral neuropathies. *Neurobiol. Dis.* 105, 300–320. doi: 10.1016/j.nbd.2017.02.009

Prots, I., Grosch, J., Brazdis, R. M., Simmnacher, K., Veber, V., Havlicek, S., et al. (2018). α-Synuclein oligomers induce early axonal dysfunction in human iPSC-based models of synucleinopathies. *Proc. Natl. Acad. Sci. U.S.A.* 115, 7813–7818. doi: 10.1073/pnas.1713129115

Qian, C., and Zhou, F. Q. (2020). Updates and challenges of axon regeneration in the mammalian central nervous system. *J. Mol. Cell Biol.* 12, 798–806. doi: 10.1093/jmcb/mjaa026

Rajaee, A., Geisen, M. E., Sellers, A. K., and Stirling, D. P. (2020). Repeat intravital imaging of the murine spinal cord reveals degenerative and reparative responses of spinal axons in real-time following a contusive SCI. *Exp. Neurol.* 327:113258. doi: 10.1016/j.expneurol.2020.113258

Rawson, R. L., Yam, L., Weimer, R. M., Bend, E. G., Hartwieg, E., Horvitz, H. R., et al. (2014). Axons degenerate in the absence of mitochondria in *C. elegans*. *Curr. Biol.* 24, 760–765. doi: 10.1016/j.cub.2014.02.025

Rebelo, P., Giacomello, M., and Scorrano, L. (2018). Shipping calpastatin to the rescue: prevention of neuromuscular degeneration through Mitofusin 2. *Cell Metab.* 28, 536–538. doi: 10.1016/j.cmet.2018.09.017

Reier, P. J., Bregman, B. S., and Wujek, J. R. (1986). Intraspinal transplantation of embryonic spinal cord tissue in neonatal and adult rats. *J. Comp. Neurol.* 247, 275–296. doi: 10.1002/cne.902470302

Rival, T., Macchi, M., Arnauné-Pelloquin, L., Poidevin, M., Maillet, F., Richard, F., et al. (2011). Inner-membrane proteins PMI/TMEM11 regulate mitochondrial morphogenesis independently of the DRP1/MFN fission/fusion pathways. *EMBO Rep.* 12, 223–230. doi: 10.1038/embor.2010.214

Roy, M., Itoh, K., Iijima, M., and Sesaki, H. (2016). Parkin suppresses Drp1-independent mitochondrial division. *Biochem. Biophys. Res. Commun.* 475, 283–288. doi: 10.1016/j.bbrc.2016.05.038

Sadleir, K. R., Kandalepas, P. C., Buggia-Prévot, V., Nicholson, D. A., Thinakaran, G., and Vassar, R. (2016). Presynaptic dystrophic neurites surrounding amyloid plaques are sites of microtubule disruption, BACE1 elevation, and increased Aβ generation in Alzheimer's disease. *Acta Neuropathol.* 132, 235–256. doi: 10.1007/s00401-016-1558-9

Schwab, A. J., Sison, S. L., Meade, M. R., Broniowska, K. A., Corbett, J. A., and Ebert, A. D. (2017). Decreased sirtuin deacetylase activity in LRRK2 G2019S iPSC-derived dopaminergic neurons. *Stem Cell Rep.* 9, 1839–1852. doi: 10.1016/j.stemcr.2017.10.010

Selvaraj, B. T., Frank, N., Bender, F. L. P., Asan, E., and Sendtner, M. (2012). Local axonal function of STAT3 rescues axon degeneration in the pmn model of motoneuron disease. *J. Cell Biol.* 199, 437–451. doi: 10.1083/jcb.201203109

Shahpasand, K., Uemura, I., Saito, T., Asano, T., Hata, K., Shibata, K., et al. (2012). Regulation of mitochondrial transport and inter-microtubule spacing by tau phosphorylation at the sites hyperphosphorylated in Alzheimer's disease. *J. Neurosci.* 32, 2430–2441. doi: 10.1523/jneurosci.5927-11.2012

Sheng, Z. H. (2014). Mitochondrial trafficking and anchoring in neurons: new insight and implications. *J. Cell Biol.* 204, 1087–1098. doi: 10.1083/jcb.201312123

Sheng, Z. H. (2017). the interplay of axonal energy homeostasis and mitochondrial trafficking and anchoring. *Trends Cell Biol.* 27, 403–416. doi: 10.1016/j.tcb.2017.01.005

Sheng, Z. H., and Cai, Q. (2012). Mitochondrial transport in neurons: impact on synaptic homeostasis and neurodegeneration. *Nat. Rev. Neurosci.* 13, 77–93. doi: 10.1038/nrn3156

Shi, X., Zhao, M., Fu, C., and Fu, A. (2017). Intravenous administration of mitochondria for treating experimental Parkinson's disease. *Mitochondrion* 34, 91–100. doi: 10.1016/j.mito.2017.02.005

Silver, D. J., and Silver, J. (2014). Contributions of chondroitin sulfate proteoglycans to neurodevelopment, injury, and cancer. *Curr. Opin. Neurobiol.* 27, 171–178. doi: 10.1016/j.conb.2014.03.016

Smith, G. M., and Gallo, G. (2018). The role of mitochondria in axon development and regeneration. *Dev. Neurobiol.* 78, 221–237. doi: 10.1002/dneu.22546

Spires-Jones, T. L., and Hyman, B. T. (2014). The intersection of amyloid beta and tau at synapses in Alzheimer's disease. *Neuron* 82, 756–771. doi: 10.1016/j.neuron.2014.05.004

Springer, J. E., Prajapati, P., and Sullivan, P. G. (2018). Targeting the mitochondrial permeability transition pore in traumatic central nervous system injury. *Neural Regen. Res.* 13, 1338–1341. doi: 10.4103/1673-5374.235218

Staal, J. A., Dickson, T. C., Gasperini, R., Liu, Y., Foa, L., and Vickers, J. C. (2010). Initial calcium release from intracellular stores followed by calcium dysregulation is linked to secondary axotomy following transient axonal stretch injury. *J. Neurochem.* 112, 1147–1155. doi: 10.1111/j.1471-4159.2009.06531.x

Stamer, K., Vogel, R., Thies, E., Mandelkow, E., and Mandelkow, E. M. (2002). Tau blocks traffic of organelles, neurofilaments, and APP vesicles in neurons and enhances oxidative stress. *J. Cell Biol.* 156, 1051–1063. doi: 10.1083/jcb.200108057

Stavru, F., Palmer, A. E., Wang, C., Youle, R. J., and Cossart, P. (2013). Atypical mitochondrial fission upon bacterial infection. *Proc. Natl. Acad. Sci. U.S.A.* 110, 16003–16008. doi: 10.1073/pnas.1315784110

Su, B., Wang, X., Lee, H. G., Tabaton, M., Perry, G., Smith, M. A., et al. (2010). Chronic oxidative stress causes increased tau phosphorylation in M17 neuroblastoma cells. *Neurosci. Lett.* 468, 267–271. doi: 10.1016/j.neulet.2009.11.010

Sun, F., and Cavalli, V. (2010). Neuroproteomics approaches to decipher neuronal regeneration and degeneration. *Mol. Cell. Proteomics* 9, 963–975. doi: 10.1074/mcp.R900003-MCP200

Sung, H., Tandarich, L. C., Nguyen, K., and Hollenbeck, P. J. (2016). Compartmentalized regulation of Parkin-mediated mitochondrial quality control in the Drosophila nervous system *in vivo*. *J. Neurosci.* 36, 7375–7391. doi: 10.1523/JNEUROSCI.0633-16.2016

Surmeier, D. J., Obeso, J. A., and Halliday, G. M. (2017). Selective neuronal vulnerability in Parkinson disease. *Nat. Rev. Neurosci.* 18, 101–113. doi: 10.1038/nrn.2016.178

Sutherland, T. C., and Geoffroy, C. G. (2020). The influence of neuron-extrinsic factors and aging on injury progression and axonal repair in the central nervous system. *Front. Cell Dev. Biol.* 8:190. doi: 10.3389/fcell.2020.00190

Swerdlow, R. H. (2018). Mitochondria and mitochondrial cascades in Alzheimer's disease. *J. Alzheimers. Dis.* 62, 1403–1416. doi: 10.3233/jad-170585

Szczepanek, K., Chen, Q., Derecka, M., Salloum, F. N., Zhang, Q., Szelag, M., et al. (2011). Mitochondrial-targeted signal transducer and activator of transcription 3 (STAT3) protects against ischemia-induced changes in the electron transport chain and the generation of reactive oxygen species. *J. Biol. Chem.* 286, 29610–29620. doi: 10.1074/jbc.M111.226209

Tagliaferro, P., and Burke, R. E. (2016). Retrograde axonal degeneration in Parkinson disease. *J. Parkin. Dis.* 6, 1–15. doi: 10.3233/JPD-150769

Tallon, C., Russell, K. A., Sakhalkar, S., Andrapallayal, N., and Farah, M. H. (2016). Length-dependent axo-terminal degeneration at the neuromuscular synapses of type II muscle in SOD1 mice. *Neuroscience* 312, 179–189. doi: 10.1016/j.neuroscience.2015.11.018

Tammineni, P., Ye, X., Feng, T., Aikal, D., and Cai, Q. (2017). Impaired retrograde transport of axonal autophagosomes contributes to autophagic stress in Alzheimer's disease neurons. *Elife* 6: e21776. doi: 10.7554/eLife.21776

Tao, K., Matsuki, N., and Koyama, R. (2014). AMP-activated protein kinase mediates activity-dependent axon branching by recruiting mitochondria to axon. *Dev. Neurobiol.* 74, 557–573. doi: 10.1002/dneu.22149

Taylor, J. P., Brown, R. H. Jr., and Cleveland, D. W. (2016). Decoding ALS: from genes to mechanism. *Nature* 539, 197–206. doi: 10.1038/nature20413

Tuck, E., and Cavalli, V. (2010). Roles of membrane trafficking in nerve repair and regeneration. *Commun. Integr. Biol.* 3, 209–214. doi: 10.4161/cib.3.3.11555

Turner, M. R., Al-Chalabi, A., Chio, A., Hardiman, O., Kiernan, M. C., Rohrer, J. D., et al. (2017). Genetic screening in sporadic ALS and FTD. *J. Neurol. Neurosurg. Psychiatry* 88, 1042–1044. doi: 10.1136/jnnp-2017-315995

Vagnoni, A., and Bullock, S. L. (2018). A cAMP/PKA/kinesin-1 axis promotes the axonal transport of mitochondria in aging Drosophila neurons. *Curr. Biol.* 28, 1265-1272 e1264. doi: 10.1016/j.cub.2018.02.048

Van Laar, V. S., Arnold, B., Howlett, E. H., Calderon, M. J., St. Croix, C. M., Greenamyre, J. T., et al. (2018). Evidence for compartmentalized axonal mitochondrial biogenesis: mitochondrial DNA replication increases in distal axons as an early response to Parkinson's disease-relevant stress. *J. Neurosci.* 38, 7505–7515. doi: 10.1523/jneurosci.0541-18.2018

Vasic, V., Barth, K., and Schmidt, M. H. H. (2019). Neurodegeneration and neuroregeneration-Alzheimer's disease and stem cell therapy. *Int. J. Mol. Sci.* 20:4272. doi: 10.3390/ijms20174272

Wang, D. B., Garden, G. A., Kinoshita, C., Wyles, C., Babazadeh, N., Sopher, B., et al. (2013). Declines in Drp1 and Parkin expression underlie DNA damage-induced changes in mitochondrial length and neuronal death. *J. Neurosci.* 33, 1357–1365. doi: 10.1523/JNEUROSCI.3365-12.2013

Wang, H., Zheng, Z., Han, W., Yuan, Y., Li, Y., Zhou, K., et al. (2020). Metformin promotes axon regeneration after spinal cord injury through inhibiting oxidative stress and stabilizing microtubule. *Oxid. Med. Cell Longev.* 2020:9741369. doi: 10.1155/2020/9741369

Wang, J., Gu, B. J., Masters, C. L., and Wang, Y. J. (2017). A systemic view of Alzheimer disease - insights from amyloid-beta metabolism beyond the brain. *Nat. Rev. Neurol.* 13, 612–623. doi: 10.1038/nrneurol.2017.111

Wang, J., Hamm, R. J., and Povlishock, J. T. (2011). Traumatic axonal injury in the optic nerve: evidence for axonal swelling, disconnection, dieback, and reorganization. *J. Neurotrauma* 28, 1185–1198. doi: 10.1089/neu.2011.1756

Wang, Q., Cai, H., Hu, Z., Wu, Y., Guo, X., Li, J., et al. (2019a). Loureirin B promotes axon regeneration by inhibiting endoplasmic reticulum stress: induced mitochondrial dysfunction and regulating the Akt/GSK-3β pathway after spinal cord injury. *J. Neurotrauma* 36, 1949–1964. doi: 10.1089/neu.2018.5966

Wang, Q., Tian, J., Chen, H., Du, H., and Guo, L. (2019b). Amyloid beta-mediated KIF5A deficiency disrupts anterograde axonal mitochondrial movement. *Neurobiol. Dis.* 127, 410–418. doi: 10.1016/j.nbd.2019.03.021

Wang, S., Smith, G. M., Selzer, M. E., and Li, S. (2019). Emerging molecular therapeutic targets for spinal cord injury. *Expert Opin Ther Targets* 23, 787–803. doi: 10.1080/14728222.2019.1661381

Wang, W., Li, L., Lin, W. L., Dickson, D. W., Petrucelli, L., Zhang, T., et al. (2013). The ALS disease-associated mutant TDP-43 impairs mitochondrial dynamics and function in motor neurons. *Hum Mol Genet.* 22, 4706–4719. doi: 10.1093/hmg/ddt319

Wang, Y., Chandran, J. S., Cai, H., and Mattson, M. P. (2008). DJ-1 is essential for long-term depression at hippocampal CA1 synapses. *Neuromol. Med.* 10, 40–45. doi: 10.1007/s12017-008-8023-4

Wang, Y., Song, M., and Song, F. (2018). Neuronal autophagy and axon degeneration. *Cell Mol Life Sci.* 75, 2389–2406. doi: 10.1007/s00018-018-2812-1

Wang, Y., Zhao, D., Pan, B., Song, Z., Shah, S. Z. A., Yin, X., et al. (2015). Death receptor 6 and caspase-6 regulate prion peptide-induced axonal degeneration in rat spinal neurons. *J. Mol. Neurosci.* 56, 966–976. doi: 10.1007/s12031-015-0562-1

Wang, Z. X., Tan, L., and Yu, J. T. (2015). Axonal transport defects in Alzheimer's disease. *Mol. Neurobiol.* 51, 1309–1321. doi: 10.1007/s12035-014-8810-x

Warita, H., Itoyama, Y., and Abe, K. (1999). Selective impairment of fast anterograde axonal transport in the peripheral nerves of asymptomatic transgenic mice with a G93A mutant SOD1 gene. *Brain Res.* 819, 120–131. doi: 10.1016/s0006-8993(98)01351-1

Woolums, B. M., McCray, B. A., Sung, H., Tabuchi, M., Sullivan, J. M., Ruppell, K. T., et al. (2020). TRPV4 disrupts mitochondrial transport and causes axonal degeneration via a CaMKII-dependent elevation of intracellular Ca(2). *Nat. Commun.* 11:2679. doi: 10.1038/s41467-020-16411-5

Xie, Y., Zhou, B., Lin, M. Y., and Sheng, Z. H. (2015). Progressive endolysosomal deficits impair autophagic clearance beginning at early asymptomatic stages in fALS mice. *Autophagy* 11, 1934–1936. doi: 10.1080/15548627.2015.1084460

Xiong, T., Tang, J., Zhao, J., Chen, H., Zhao, F., Li, J., et al. (2012). Involvement of the Akt/GSK-3β/CRMP-2 pathway in axonal injury after hypoxic-ischemic brain damage in neonatal rat. *Neuroscience* 216, 123–132. doi: 10.1016/j.neuroscience.2012.04.052

Xu, J., Long, H., Chen, W., Cheng, X., Yu, H., Huang, Y., et al. (2017). Ultrastructural features of neurovascular units in a rat model of

chronic compressive spinal cord injury. *Front. Neuroanat.* 11:136. doi: 10.3389/fnana.2017.00136

Yahata, N., Yuasa, S., and Araki, T. (2009). Nicotinamide mononucleotide adenylyltransferase expression in mitochondrial matrix delays Wallerian degeneration. *J. Neurosci.* 29, 6276–6284. doi: 10.1523/jneurosci.4304-08.2009

Yan, X., Hu, Y., Wang, B., Wang, S., and Zhang, X. (2020a). Metabolic dysregulation contributes to the progression of Alzheimer's disease. *Front. Neurosci.* 14:530219. doi: 10.3389/fnins.2020.530219

Yan, X., Wang, B., Hu, Y., Wang, S., and Zhang, X. (2020b). Abnormal mitochondrial quality control in neurodegenerative diseases. *Front. Cell. Neurosci.* 14:138. doi: 10.3389/fncel.2020.00138

Yang, J., Wu, Z., Renier, N., Simon, D. J., Uryu, K., Park, D. S., et al. (2015). Pathological axonal death through a MAPK cascade that triggers a local energy deficit. *Cell* 160, 161–176. doi: 10.1016/j.cell.2014.11.053

Yang, X., Liu, R., Xu, Y., Ma, X., and Zhou, B. (2021). The mechanisms of peripheral nerve preconditioning injury on promoting axonal regeneration. *Neural Plast.* 2021:6648004. doi: 10.1155/2021/6648004

Yiu, G., and He, Z. (2006). Glial inhibition of CNS axon regeneration. *Nat. Rev. Neurosci.* 7, 617–627. doi: 10.1038/nrn1956

Yu, Y., Lee, H. C., Chen, K. C., Suhan, J., Qiu, M., Ba, Q., et al. (2016). Inner membrane fusion mediates spatial distribution of axonal mitochondria. *Sci Rep* 6:18981. doi: 10.1038/srep18981

Zhang, L., Trushin, S., Christensen, T. A., Tripathi, U., Hong, C., Geroux, R. E., et al. (2018). Differential effect of amyloid beta peptides on mitochondrial axonal trafficking depends on their state of aggregation and binding to the plasma membrane. *Neurobiol. Dis.* 114, 1–16. doi: 10.1016/j.nbd.2018.02.003

Zhang, X., Wang, R., Hu, D., Sun, X., Fujioka, H., Lundberg, K., et al. (2020). Oligodendroglial glycolytic stress triggers inflammasome activation and neuropathology in Alzheimer's disease. *Sci. Adv.* 6:eabb8680. doi: 10.1126/sciadv.abb8680

Zheng, Y. R., Zhang, X. N., and Chen, Z. (2019). Mitochondrial transport serves as a mitochondrial quality control strategy in axons: Implications for central nervous system disorders. *CNS Neurosci. Ther.* 25, 876–886. doi: 10.1111/cns.13122

Zhou, B., Yu, P., Lin, M.-Y., Sun, T., Chen, Y., and Sheng, Z.-H. (2016). Facilitation of axon regeneration by enhancing mitochondrial transport and rescuing energy deficits. *J. Cell Biol.* 214, 103–119. doi: 10.1083/jcb.201605101

Zhu, Y. B., and Sheng, Z. H. (2011). Increased axonal mitochondrial mobility does not slow amyotrophic lateral sclerosis (ALS)-like disease in mutant SOD1 mice. *J. Biol. Chem.* 286, 23432–23440. doi: 10.1074/jbc.M111.237818

Conflict of Interest: The authors declare that the research was conducted in the absence of any commercial or financial relationships that could be construed as a potential conflict of interest.

frontiers in Aging Neuroscience

ORIGINAL RESEARCH
published: 08 June 2021
doi: 10.3389/fnagi.2021.651638

Map2k5-Deficient Mice Manifest Phenotypes and Pathological Changes of Dopamine Deficiency in the Central Nervous System

Yumeng Huang[1†], Pei Wang[1†], Rodrigo Morales[2,3], Qi Luo[1] and Jianfang Ma[1]*

[1] Department of Neurology, Institute of Neurology, Shanghai Jiao Tong University Medical School Affiliated Ruijin Hospital, Shanghai, China, [2] Department of Neurology, McGovern Medical School, The University of Texas Health Science Center at Houston, Houston, TX, United States, [3] Centro Integrativo de Biologia y Quimica Aplicada (CIBQA), Universidad Bernardo O'Higgins, Santiago, Chile

MAP2K5, a member of the MAPK family, is associated with central nervous system disorders. However, neural functional of Map2k5 from animal models were not well examined so far. Here, we established a Map2k5-targeted knockout mouse model to investigate the behavior phenotypes and its underlying molecular mechanism. Our results showed that female Map2k5 mutant mice manifested decreased circadian-dependent ambulatory locomotion, coordination, and fatigue. Male Map2k5 mutant mice displayed impairment in open field exploration and prepulse inhibition of acoustic startle response (ASR) when compared with wild-type controls. Furthermore, Map2k5 mutant mice showed a decreased dopaminergic cell survival and tyrosine hydroxylase levels in nigrostriatal pathway, indicating a crucial role of MAP2K5 in regulating dopamine system in the central nervous system. In conclusion, this is the first study demonstrating that Map2k5 mutant mice displayed phenotypes by disturbing the dopamine system in the central nervous system, implicating Map2k5 mutant mouse as a promising model for many dopamine related disorders.

Keywords: MAP2K5, mouse model, dopamine, sensorimotor phenotypes, restless legs syndrome, Parkinson's disease

OPEN ACCESS

Edited by:
Benoit Laurent,
Université de Sherbrooke, Canada

Reviewed by:
Cathy Tournier,
The University of Manchester, United Kingdom
Sebastien Carnicella,
INSERM U1216 Grenoble Institut des Neurosciences (GIN), France

***Correspondence:**
Jianfang Ma
mjf10924@rjh.com.cn

†These authors share first authorship

Received: *10 January 2021*
Accepted: *03 May 2021*
Published: *08 June 2021*

Citation:
Huang Y, Wang P, Morales R, Luo Q and Ma J (2021) Map2k5-Deficient Mice Manifest Phenotypes and Pathological Changes of Dopamine Deficiency in the Central Nervous System. Front. Aging Neurosci. 13:651638. doi: 10.3389/fnagi.2021.651638

INTRODUCTION

MAP2K5 (mitogen-activated protein kinase kinase 5, also known as MEK5) has been associated with various diseases including cardiovascular diseases, cancers, and central nervous system disorders (Appari et al., 2017; Liu et al., 2017; Castro et al., 2019). In the central nervous system, some polymorphisms of MAP2K5 have been associated with restless legs syndrome/William–Ekbom disease (RLS/WED) and neuropsychologic disorders (Winkelmann et al., 2007; Yang et al., 2011; Li et al., 2017). In addition, studies also suggested

Abbreviations: ACh, acetylcholine; AMB, ambulatory activity; ASR, acoustic startle response; DA, dopamine; Epi, epinephrine; GAPDH, glyceraldehyde-3-phosphate dehydrogenase; Gln, glutamine; HCG, human chorionic gonadotropin; HPLC, high-performance liquid chromatography; KO, knockout; MAP2K5, mitogen-activated protein kinase kinase 5; P18d, postnatal 18 days; PBS, phosphate-buffered saline; PFA, paraformaldehyde; Phe, phenylalanine; PLMS, periodic limb movements; PPI, prepulse inhibition; qRT-PCR, semi-quantitative reverse transcriptase-PCR; RLS/WED, restless legs syndrome/Willis–Ekbom disease; SNc, substantia nigra pars compacta; SNP, single-nucleotide polymorphism; TH, tyrosine hydroxylase; TOT, total activity; Tyr, tyrosine; WT, wild type.

its etiologic or therapeutic role in amyotrophic lateral sclerosis, Parkinson's disease (PD), schizophrenia, suicidal behavior, and others (Gan-Or et al., 2015; Jo et al., 2017; Kang et al., 2018; Cabrera-Mendoza et al., 2020). Although the role of Map2k5-Erk5 in cardiovascular diseases and cancer has been mostly clarified, the molecular mechanism of Map2k5 in the central nervous system remained largely unknown.

MAP2K5 is a member of the MAP kinase family, and it is involved in growth factor-induced cell proliferation, survival, and differentiation (Dinev et al., 2001; Liu et al., 2006). It specifically activates ERK5 by phosphorylation on threonine and tyrosine residues (Johnson and Lapadat, 2002). The MAP2K5–ERK5 pathway regulates many transcription factors including MEF2, c-MYC, and NF-κB (English et al., 1998; Kato et al., 2000; Simões et al., 2015), which were identified as essential in cells' survival and development. Moreover, the role of the MAP2K5–ERK5 pathway in neurons' proliferation, differentiation, and apoptosis were demonstrated in many studies, and included activity in cortical, dopaminergic, and GABAergic neurons (Liu et al., 2006; Zou et al., 2012; Parmar et al., 2015; Ding et al., 2020). Target deletion of MAP2K5 in animals may help us to discover its role in biochemical processes and gross functions. However, there are few studies using animal models focused on the role of MAP2K5 in the central nervous system. This is probably due to the fact that fully knockout Map2k5 mice died at early embryonic periods from heart deficits (Wang et al., 2005).

Based on the finding that polymorphisms (rs12593813, rs11635424, and rs868036) in MAP2K5 were associated with a reduced risk of RLS/WED, a neurological disorder characterized by dopamine and iron dysfunction, we established a targeted deletion of Map2k5 in mice. Specifically, we focused on the deletion of exons 18–22, which harbor three risky SNPs. This model was hypothesized to be useful in exploring the role of this protein in the central nervous system *in vivo*. We found that the homozygous Map2k5-deficient mouse died at mid gestation, similarly, as previously reported (Wang et al., 2005). Heterozygous female Map2k5-deficient mouse manifested decreased locomotion, impaired coordination, and was prone to fatigue. Interestingly, these phenotypes are contrary to RLS/WED and, in some aspects, similar to PD (another movement disorder involving dopamine system disturbance). Furthermore, we found reduced dopaminergic neurons and decreased tyrosine hydroxylase (TH) levels in female Map2k5-deficient mice compared with wild-type (WT) mice in nigrostriatal dopaminergic pathway, which may explain the motor dysfunction in female Map2k5-deficient mice. To our knowledge, this is the first *in vivo* study that demonstrated the relationship of dopaminergic system disturbance with the Map2k5–Erk5 pathway.

MATERIALS AND METHODS

Map2k5^{em41}Cd71454 Mice

Animal experiments were performed in accordance with the guidelines and policies of the Association for Assessment and Accreditation of Laboratory Animal Care International (AAALAC International), China National Accreditation Service for Conformity Assessment (CNAS), and Laboratory Animal Resource Center of Shanghai Jiao Tong University School of Medicine. Map2k5^{em41}Cd71454 mice were created in Nanjing, China (GemPharmmatech Co., Ltd.) via CRISPR/Cas9 technique on a C57B6/JGpt (GemPharmmatech Co., Ltd.) background. In this strain, based on the findings that most reported SNPs in MAP2k5 of RLS/WED [rs12593813 (A/G), rs11635424 (A/G), and rs868036 (T/A)] were located in the intron area of gene Map2k5 between exons 17–18 and exons 19–20 (RefSeq: NM_011840), transgenic mice with Map2k5 exons 18–22 deletion were constructed. Two sgRNAs on both sides of the targeted region were designed specifically (**Figure 1A**) (sgRNA1: GGCTCCGTAAGTGTCCACATGGG; sgRNA3: TGCAGGCACGGGCCTTTGACTGG) and constructed by using MEGAshortscript^{TM} Kit (Thermo Fisher Scientific, Waltham, MA, United States). In order to microinject Cas9 protein and sgRNA into fertilized eggs, male C57BL6/J mice were individually caged for 1 week before mating. Female C57BL6/J mice were given 5 IU of serum gonadotropin and 5 IU of human chorionic gonadotropin (HCG) to pregnant horses for superovulation. After C57BL6/J male and female mice were injected with HCG, the fertilized eggs of male and female mice were taken for mating. SgRNA (40 ng/μl) and Cas9 protein (40 ng/μl) were injected into the cytoplasm of the fertilized egg at the single-cell stage using continuous flow injection microinjection. The surviving two-cell embryos were implanted into the fallopian tube of a pseudo-pregnant female. The generated mice (F0) were analyzed in the born pups. F0 mice were mated with C57BL6/J wild-type mice to gain the obtained F1 mice. Their Map2k5 with exons 18–22 deletion sequencing were examined by Sanger Sequencing (**Supplementary Material 1**). To exclude the off-target effect, genetic sequencing of high frequent loci of each sgRNA (sgRNA1 and sgRNA3) were predicted by CRISPOR (Concordet and Haeussler, 2018)[1] and confirmed by Sanger sequencing (**Supplementary Material 2**).

All offspring were identified by genotyping tail DNA (Accili et al., 1996). KO (knockout) primers (5′ GATGAA GCAAAGGGTGACGATAG 3′ and 5′ CTTGGGAAGGCAAGC ACTACTC 3′, 940 bp) and WT primers (5′ ACATTCCA TCCTACCTCAGCCTAG 3′ and 5′ CCTACTTGCTTGGCTTCA GTCTG 3′, 461 bp) were used for this purpose (**Figure 1B**). F1 mice were interbred to obtain F2 homozygous, while homozygous mutants were examined dead prenatally after. Large quantities of F3 experiment's mice were interbred with F2 heterozygous mice (some PCR genetic identification results are shown in **Figure 1C**). In all experiments, heterozygous Map2k5$^{+/-}$ mice and their WT littermates were used, as homozygotes were embryonic lethal.

mRNA Prepared and Semiquantitative Reverse Transcriptase -PCR

Total RNA was extracted from homogenized frozen brain, heart, and spleen tissue followed by TRIzol^{TM} Reagent (Invitrogen, Carlsbad, CA, United States) extraction protocols. Reverse

[1]http://crispor.tefor.net

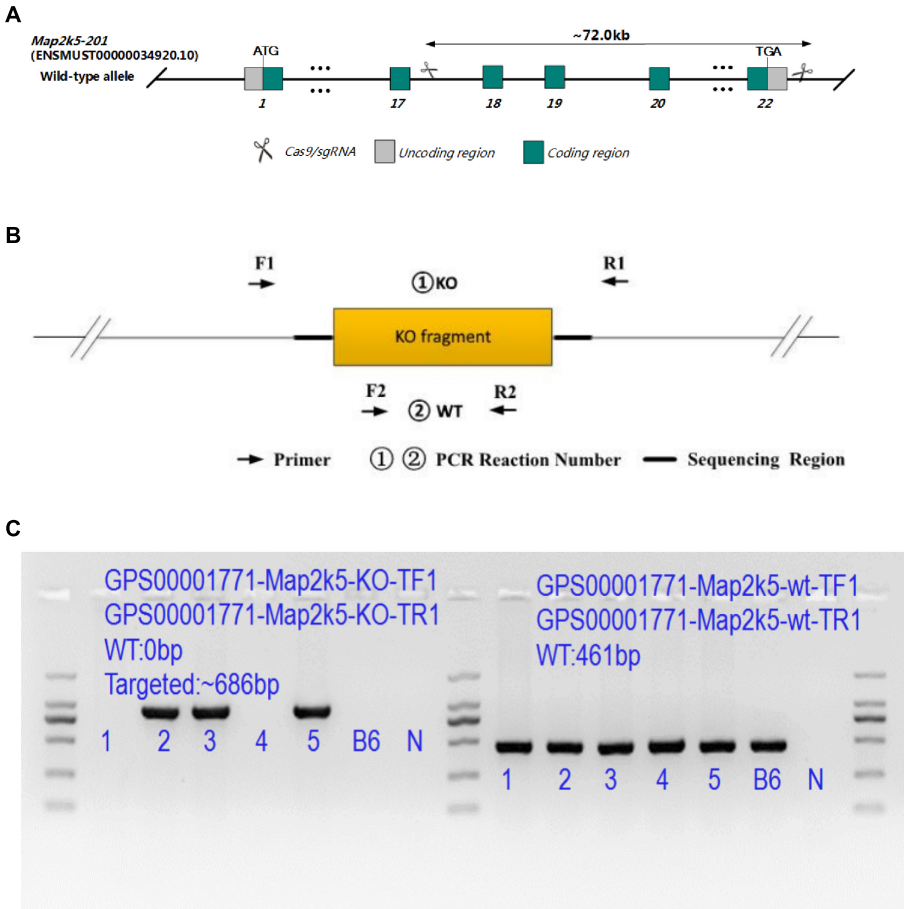

FIGURE 1 | (A) Targeting strategy of Map2k5-targeted allele. Green boxes represent coding regions, gray boxes represent noncoding exon regions, and scissors represent the targeted area of Map2k5 between exons 18 and 22. **(B)** Primers designed for genotype identification of Map2k5$^{+/-}$ heterozygous and wild-type (WT) mice. **(C)** PCR results of some Map2k5^{em41}Cd71454 mice.

transcription was performed using PrimeScript^{TM} RT reagent Kit with gDNA Eraser [TAKARA Biomedical Technology (Beijing) Co., Ltd., China] and qRT-PCR using TB Green® Premix Ex Taq^{TM} II [TAKARA Biomedical Technology (Beijing) Co., Ltd., China] with the SYBR Green Method (Applied Biosystems, Foster City, CA, United States). Oligonucleotides_Map2k5 (5′ AAG CGA TGA AGA GAT GAA G 3′ and 5′ ATG TAT GTT CCG TTC CCC A 3′) targeted the dominant Map2k5 mRNA. The primers of the glyceraldehyde-3-phosphate dehydrogenase (Gapdh) gene (5′ AAA TGG TGA AGG TCG GTG TG 3′ and 5′ AGG TCA ATG AAG GGG TCG TT 3′) were used as the reference gene—glyceraldehyde-3-phosphate dehydrogenase (Gapdh). Run method: (a) 30 s at 95°C; (b): 40 cycles of 5 s at 95°C, 34 s at 64°C; (c)15 s at 95°C at 1.6°C/s, 1 min at 65°C at 20°C/s, 15 s at 95°C at 0.05°C/s.

Behavioral Studies

Map2k5$^{+/-}$ mutant mice and WT littermates were grouped by genotype and gender. Behavior studies were carried out from 9 to 25 weeks, and their body weights were tracked by an electronic weigher (NV621ZH, OHAUS, Parsippany NJ, United States) from 6 to 27 weeks.

Rotarod

Rotarod (ZH-600B, Anhui Zhenghua Co., Huaibei, China) was used to measure the motor coordination, learning ability, and fatigability of the mice. A rotarod device was placed in an SPF experiment room. Each mouse was placed in the room for 30 min for adaptation before running the experiments. Both WT and Map2k5$^{+/-}$ mutant mice aged 9 weeks were tested in the rotarod. During the learning period, both groups of mice were trained three times per day for continuous 3 days at a speed of 1 rpm for 30 s and then at an accelerating speed from 1 to 10 rpm by 1 rpm/30 s for 300 s. On the day 4, all mice were tested on the rotarod at an accelerating speed of from 4 to 30 rpm for 500 s and 30-min resting interval between each trial. The latency to fall off the rotarod was recorded.

Open Field

Open field device (XR-XZ301, Shanghai Xinruan Co., Shanghai, China) was placed in an SPF experiment room. It had infrared

sensors, and the center was exposed to bright illumination (90–120 lx). All experimental mice were aged 12 weeks. Each mouse was placed in the middle of one edge of the open field box and recorded for 20 min. The activity of each mouse from 0 to 5 min was used for analysis. TopScan Lite Analysis Software (TopScan Lite, CleverSys) was used to collect and analyze data.

Limbs' Strength

Fore and four limbs strength were tested by the ability to hold on to a grip sensor (Bioseb G3, Chaville). Mice aged 13 weeks were tested. Each mouse was placed on a wire screen with their fore limbs or four limbs grasping to the grip. The grip sensor recorded the force of a metal grate being pulled in grams. We conducted three trials per mouse. The average strength of three trials was analyzed.

Acoustic Startle Response (ASR) and Prepulse Inhibition (PPI)

ASR and PPI apparatus Startle Response System (SR-LAB, San Diego, CA, United States) were used. We followed the standard protocols published by the International Mouse Phenotyping Consortium (IMPC) on the website[2]. Mice aged 17 weeks were tested. Each experiment was carried out at the late active phase from 7:00 to 8:00 a.m. The session was initiated with a 5-min acclimation period (only background noise was used). In addition, it had an option to acclimate to the startle pulse in which 110–120 dB/40–60 ms of white noise was presented alone, five times. These were excluded from the statistical analysis. Different prepulse trials of 20-ms duration of white noise stimuli were presented alone (PP1 = 72 dB, PP2 = 78 dB, PP3 = 84 dB, or PP4 = 90 dB) and preceded the pulse by 70 ms (PP1 + pulse, PP2 + pulse, PP3 + pulse, or PP4 + pulse) to derive the pre-pulse inhibition response. Startle pulse trials were started where 120 dB/50 ms of white noise was presented alone. No stimulus trials in which only background noise was presented were used to measure baseline movement of the animal in the chamber. Background noise was 65–70 dB. Startle responses were recorded and analyzed.

Homecage Locomotor Activity

Individual mice aged 25 weeks were placed in the Laboratory Animal Monitoring System (CLAMS, Columbus Instruments) for 24-h adapting followed by 48-h test. Data were collected and analyzed every 20 min in the system and resulted in 63 readings per individual a day. Total activity (TOT) and ambulatory activity (AMB) were measured based on the infrared beam breaks.

Immunofluorescence Staining

The cohorts included three female mice of each group aged postnatal 18 days (P18d), 21 weeks, 28 weeks, and 38 weeks. Mice were perfused with 4% paraformaldehyde (PFA) in phosphate-buffered saline (PBS) and sacrificed. Mouse brains were isolated on ice and fixed in 4% PFA for at least 24 h. Brain tissues were embedded with paraffin and serially cut into 5-μm-thick coronal sections. Brain sections of SNc and striatum were dewaxed by dimethylbenzene and gradient ethanol solutions. Citrate antigen retrieval solution was used, heated for 6 min at 65°C, with 1-min interval, and reheated for 6 min at 65°C for antigen retrieval. Every four continuous sections of SNc and striatum regions were stained in each mouse. The sections of mouse brains were immunostained at 4°C overnight with primary anti-tyrosine hydroxylase antibody (1:500, MAB318, Millipore Co., Massachusetts, United States), MAP2K5 (Concordet and Haeussler, 2018). Antibody (1:200, sc-135986, Santa Cruz Biotechnology, Inc., Northern California, United States), followed by Alexa Fluor 594-conjugated secondary antibodies and 488-conjugated secondary antibodies (1:200, YEASEN Biotech Co., Ltd., Shanghai, China). Each section was incubated by 4′,6-diamidino-2-phenylindole dihydrochloride (1:1,000, DAPI, Sigma-Aldrich, St. Louis, United States) for 20 min and treated with Antifade Mounting Medium (Beyotime Biotechnology, Shanghai, China). Images of each section were captured via fluorescence microscopy (Nikon Eclipse C1, Nikon, Tokyo, Japan). For each brain, three sections of substantia nigra pars compacta (SNc) and striatum were analyzed. The TH^+ stained cell counts and mean immunofluorescence intensity per section were measured using ImageJ (NIH).

Western Blot

$Map2k5^{+/-}$ mutant mice and WT littermates (female, aged 21 weeks, $n = 4$ per group) were perfused with PBS and sacrificed. Brains were then dissected quickly within 10 min and snap frozen in liquid nitrogen. Proteins were prepared from the ventral midbrain (Yun et al., 2018) including nigrostriatal dopaminergic neurons. Cytoplasmic proteins were extracted by RIPA Lysis Buffer (Strong) (Beyotime Biotechnology, Shanghai, China) supplemented with Complete Protease Inhibitor Cocktail (10×) and PhosSTOP™ Cocktail (10×) (Roche Ltd., Basel, Switzerland). Western blots were performed using sodium dodecyl sulfate polyacrylamide gel electrophoresis and nitrocellulose membranes. Primary antibodies included anti-tyrosine hydroxylase Ab (1:1,000, MAB318, Millipore Co., Massachusetts, United States), Erk5 Antibody (1:1,000, #3372, CST Ltd., Boston, United States), Phospho-Erk5 (1:1,000, Thr218/Tyr220), Antibody (1:1,000, #3371, CST), MAP2K5 (Concordet and Haeussler, 2018). Antibody (1:200, sc-135986, Santa Cruz Biotechnology, Inc., Northern California, United States), and GAPDH (D16H11) XP® Rabbit mAb (1:1,000, #5174, CST). Signals were detected with an ECL agent (Millipore). Blotting images were acquired and quantitatively analyzed by Image Lab Software (Bio-Rad, CA, United States).

High-Performance Liquid Chromatography (HPLC)

Striatal samples of 21-week-aged female mice were prepared for neurochemical measurements via HPLC analysis (Bionovogene Co., Ltd., Suzhou, China). The tissue was homogenized in 10% methanol formic solution–ddH2O (1:1) (200 μ) and centrifuged at a speed of 12,000 rpm at 4°C for 5 min. One hundred microliters of supernatant and 100 ppb of double isotopes of L-valine (C13) L-phenylalanine (C13) internal standards (100 μl) were mixed and passed through a 0.22-μm filter membrane.

[2]https://www.mousephenotype.org/impress/index

Samples were injected in an ACQUITY UPLC® BEH C18 HPLC column (2.1 × 100 mm, 1.7 μm, Waters Co.) at 40°C. The mobile phase consisted of A-50% methanol with 0.1% formic acid and B-10% methanol with 0.1% formic acid. Compounds were measured with Analyst Software (AB SCIEX). The neurotransmitter metabolite peak areas were integrated and quantified against standard samples. The standard curves $r > 0.99$, and the relative standard deviation (RSD) of the samples was < 9%. Phenylalanine (Phe), tyrosine (Tyr), DOPA, dopamine (DA), epinephrine (Epi), glutamine (Gln), acetylcholine (ACh), serotonin, and 5-HIAA were measured. Results were normalized to the weight of each tissue and reported in μg/g.

Statistics

Analyses of mouse data were conducted via SPSS 26 (IBM). The test for genotype and gender-independent factor interactions of behavior studies were tested by two-way ANOVA followed by Tukey's *post hoc* tests for multiple comparisons in our behavior tests. Test for genotype effect of biochemical studies was conducted via Student's *t*-test, two-tailed analysis. A *p*-value of 0.05 was set as statistically significant.

RESULTS

Characterization of Homozygous Map2k5$^{-/-}$ Mutant Embryos That Died at Mid-Gestation

Map2k5^{em41}Cd71454 heterozygous Map2k5$^{+/-}$ mice were viable and fertile. By tracking the body weight of Map2k5$^{+/-}$ and WT mice through 6–27 weeks, it was found that different genotypes exert no influence on body weight of mice, except for male mice at 11 weeks (**Figure 1** in **Supplementary Material 3**).

However, Map2k5^{em41}Cd71454 homozygous Map2k5$^{-/-}$ mice died at mid-gestation with gross development retardation. At E9.5 (gestation day 9.5), homozygous Map2k5$^{-/-}$ mutant embryos showed normal phenotype. However, 9 out of 56 (16.67%) homozygous Map2k5$^{-/-}$ embryos displayed developmental retardation at E10.5. Moreover, three homozygous Map2k5$^{-/-}$ out 32 embryos at E11.5 (10.71%) were found dead, 0/11 live embryos were found at E12.5, and 0/32 were found at E13.5. We deduced that Map2k5^{em41}Cd71454 strain's homozygous Map2k5$^{-/-}$ mutant embryos with exons 18–22 depletion died at approximately E11.5. This outcome was similar to the one found in a previous study reporting that Map2k5$^{-/-}$ mutant homozygous mice die at E10.5 due to a defect in fetal cardiogenesis (Wang et al., 2005). Thus, Map2k5$^{+/-}$ heterozygous mice and their WT littermates were used in the postnatal experiments.

Map2k5$^{+/-}$ Heterozygous Mice Expressed Decreased Levels of Map2k5 mRNA in Different Organs

To assess how effective the Map2k5 exons 18–20 gene deletion was on terminating transcription, the mRNA expression level of Map2k5$^{+/-}$ mutant mice was detected in different organs including the brain, heart, and spleen via qRT-PCR. We found a significant decreased expression levels of Map2k5 mRNA in all three different tissues (brain, heart, and spleen). Specifically, 20–30% relative quantitative levels of Map2k5 mRNA were expressed in Map2k5$^{+/-}$ mutant mice compared with WT mice in the brain, heart, and spleen (referred to GAPDH) ($P = 0.009$, 0.007, 0.007, respectively, **Figure 2A**). Western blots of corresponding tissues were examined, which displayed a significant decrease in Map2k5 expression in the brain, and a less decrease in the heart and spleen (**Figure 2B**).

Map2k5$^{+/-}$ Mice Displayed Sex-Dependent and Circadian-Related Motor Dysfunction

Many movement disorders are circadian related. Based on the fact that RLS/WED is a disease usually presenting clinical signs in the evening and that women have higher risk than men[1], we explored the profile of motor function in Map2k5$^{+/-}$ mutant mice by performing a series of behavioral tests including open field test, rotarod test, and 12 h–12 h cycle infrared locomotor activity pattern. All these tests were done considering animal sex to assess for potential differences at this level. To exclude the

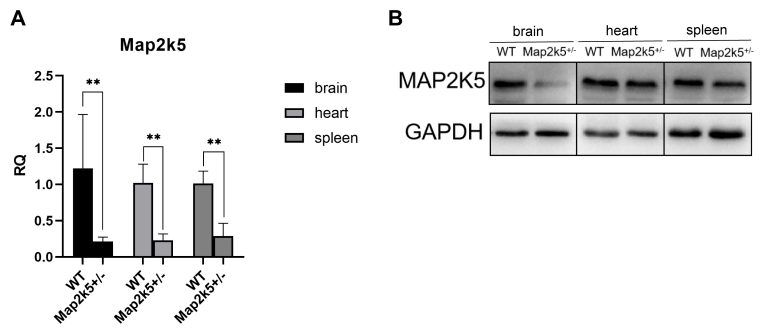

FIGURE 2 | (A) Map2k5$^{+/-}$ heterozygous mice expressed 20–30% relative quantitative (RQ) levels of intact Map2k5 mRNA in the brain, heart, and spleen (*t*-test, $n = 6$). Bars represent means with standard errors of the mean (SEM). **(B)** Western blot of Map2k5 expressions in different tissues (brain, heart, and spleen) in WT and Map2k5$^{+/-}$ mice. $^{**}P < 0.01$.

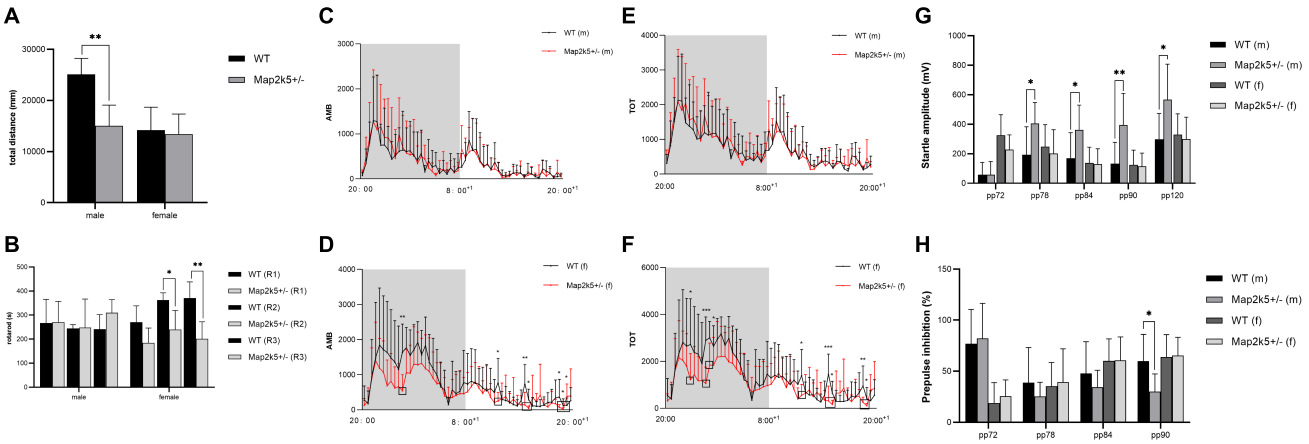

FIGURE 3 | (A) Open field test to measure volitional locomotion. Male Map2k5$^{+/-}$ mice displayed a decreased total distance compared with WT mice in traveled in open field test (P = 0.004, n = 4). **(B)** Rotarod test. Female Map2k5$^{+/-}$ mice have impaired coordination ability in rounds 2 and 3 (P_1 = 0.157, P_2 = 0.036, P_3 = 0.003, n = 4). **(C–F)** Total activity (TOT) and ambulatory activity (AMB) with 12 h (light)–12 h (dark) cycle in both male **(C,E)** and female mice **(D,F)**. AMB and TOT were decreased significantly in female Map2k5$^{+/-}$ mice during their light phase (rest phase) (n = 8). **(G,H)** Acoustic startle response (ASR) and prepulse inhibition (PPI) of WT and Map2k5$^{+/-}$ mutant mice. **(G)** ASR increased in male Map2k5$^{+/-}$ mutant mice at 78, 84, 90, and 120 dB (P = 0.035, 0.029, 0.006, and 0.019, respectively). **(H)** Prepulse inhibition (PPI) was decreased in male Map2k5$^{+/-}$ mutant mice at 90 dB (P = 0.024, n = 6). Results are plotted as mean with SEM. Bars represent means with SEM. *P < 0.05, **P < 0.01.

effect of muscle strengths in the motor test results, we examined the force of four and fore limbs in Map2k5$^{+/-}$ and WT mice.

Male Map2k5$^{+/-}$ mice manifested a decreased total distance traveled in the open field test (P = 0.004) when compared with WT mice, while female Map2k5$^{+/-}$ mice displayed no differences compared with the WT controls (**Figure 3A**). There was also a trend, but not a statistically significant difference, between different genotypes in which male Map2k5$^{+/-}$ mice exhibited decreased central zone duration (P = 0.075, figure not shown). These results indicated a different motor response to the new environment of Map2k5 mutant male mice. Previous studies showed that mice exploration behaviors could be influenced by hormones considering the open field cage as a new environment (Lalonde and Strazielle, 2017). Our results implied that male Map2k5+/- mice might display less motivation to explore and locomotion in the open field test.

As a measurement of motor coordination, learning, and fatigability, we evaluated the latency to fall from an accelerating rotarod three times on the test day following a 3-day learning period. It is important to consider that the three times repetition used in this test implies fatigue levels in each mouse. Female Map2k5$^{+/-}$ mutant mice displayed decreased latency to fall at the second and third rounds at the test day, and spared the first round of tests (P_1 = 0.157, P_2 = 0.036, P_3 = 0.003, **Figure 3B**), suggesting increased fatigue propensity, impaired coordination and learning abilities, while male Map2k5$^{+/-}$ mice displayed no differences compared with WT mice. This indicated that Map2k5 deficiency in female mice may induce fatigue and poor coordination, similar to some motor symptoms presented in PD.

To analyze potential differences of volitional locomotion of Map2k5$^{+/-}$ mutant mice subjected to a circadian variation, we collected motor data per 20 min in a cage equipped with infrared beams (divided a whole day into 63 equal periods). Total activity (TOT, which includes when animals scratches themselves and move their limbs without locomotion) and ambulatory activity (AMB, which only includes their body movement) were recorded with a 12 h (light)–12 h (dark) cycle for a day. Through this method, we found that there was interaction between genders and genotypes (p = 0.043); the main effect of genotype on both AMB and TOT in female mice was significant. Specifically, AMB and TOT of female Map2k5$^{+/-}$ mutant mice decreased significantly during their sleeping time (light-on phase, **Figures 3D,F**), implying a hypokinetic and bradykinetic phenotype (Kim et al., 2016; Langley et al., 2017). However, male Map2k5$^{+/-}$ mutant mice did not display any differences compared with their WT littermates (**Figures 3C,E**). This provided us with a gender-dependent, circadian-related movement dysfunction profile, contrary to RLS/WED symptoms to some extent (Allen et al., 2014).

When considering the gender-dependent different results of 12 h–12 h locomotor activity trace [significant decreased sleeping body movements (AMB and TOT) only in female mice] and open field tests (only male mice showed a significant reduction in total distance in open field), we thought that as a novel environment exposure, mice were also experienced in the open filed apparatus, the behavior found in male mice indicated stress-based movement in these mice (Lalonde and Strazielle, 2017; Zhang et al., 2019), whereas 12 h–12 h locomotor activity trace data were more similar to the nature pattern of movement, including circadian-distinctive manners. Therefore, male Map2k5-deficient mice motor dysfunction can be interpreted into a stress-based alteration, while female Map2k5 deficient mice movement phenotypes are basal changes due to motor-control pathway dysfunctions.

To discard the effect of limbs' strength on the behavioral performance, each mouse's fore and four limbs' strengths were

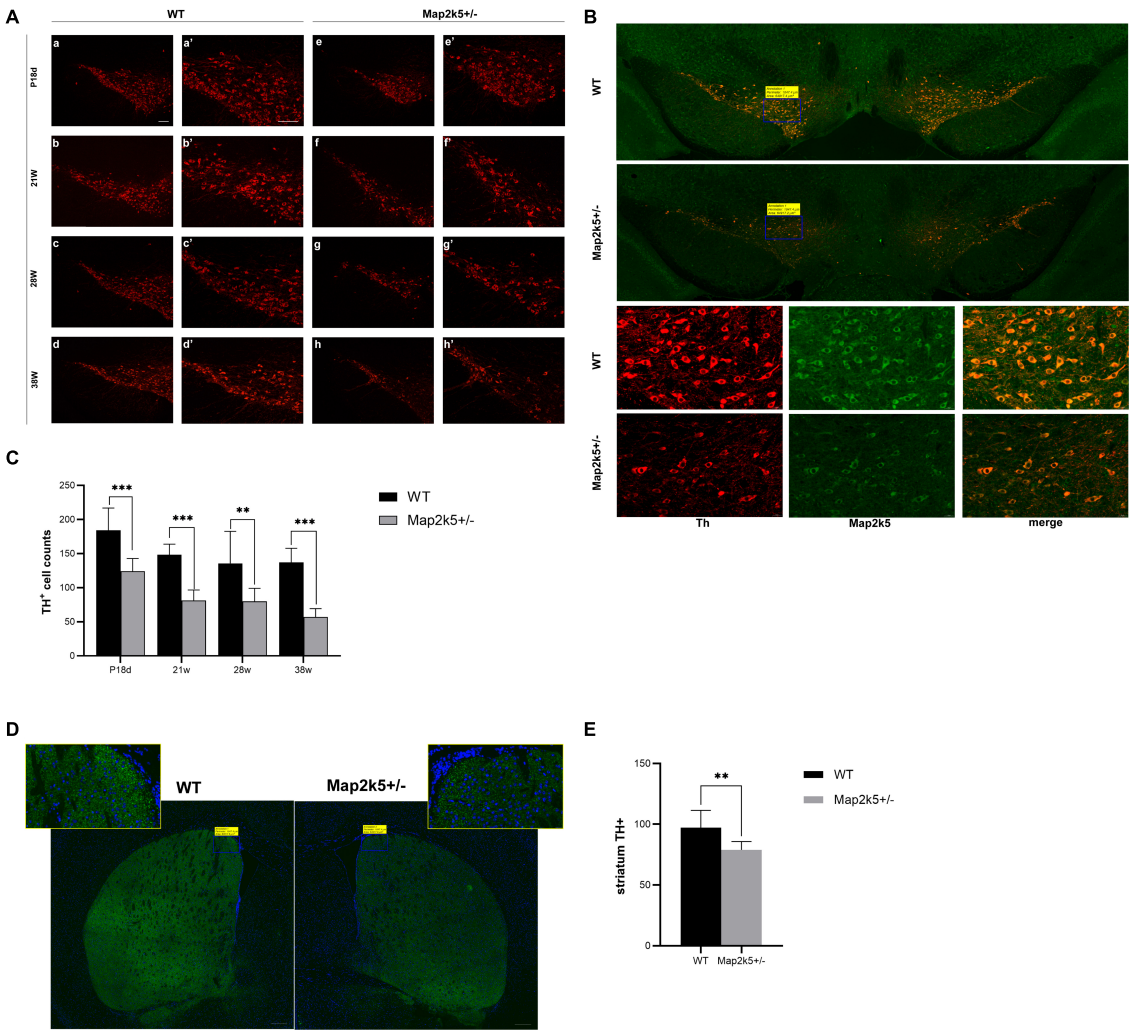

FIGURE 4 | (A) Coronal sections of substantia nigra pars compacta (SNc) were prepared from P18d, 21, 28, and 38 weeks and immunostained with an anti-TH antibody. Map2k5$^{+/-}$ mutant mice had decreased TH^{+} cell number in SNc at P18d, 21, 28, and 32 weeks. (a–d) Immunostained TH^{+} cells in SNc of Map2k5$^{+/+}$ WT mice (100x). (e–h) TH^{+} cells in SNc of Map2k5$^{+/-}$ mutant mice (100×). (a'–h') High-magnification images (200 ×) of the corresponding section in (a–h). Scale bar, 100 μm. **(B)** TH^{+} and Map2k5^{+}-stained cells, and merged pictures of Map2k5$^{+/-}$ mutant and WT mice in SNc of at 38 weeks. Low-magnification images (50×) and high-magnification images (400×). 200 μm (50×), 20 μm (400×). **(C)** TH+ cell counts in SNc were reduced in female Map2k5$^{+/-}$ mutant mice compared with WT mice at P18d, 21, 28, and 38 weeks ($P_{18d} < 0.001$, $P_{21w} < 0.001$, $P_{28w} = 0.005$, $P_{38w} < 0.001$). **(D)** Coronal sections of striatum immunostained with anti-TH antibody. We found decrease immunofluorescence in Map2k5$^{+/-}$ mutant mice compared with WT mice. Low-magnification images (50 ×) and high-magnification images (630×). Scale bar, 200 μm (50×), 20 μm (630×). **(E)** Mean immunofluorescence intensity of each slice was analyzed. There was decreased TH density in Map2k5$^{+/-}$ mutant mice ($P = 0.006$). Results are plotted as mean with SEM. Bars represent means with SEM. $^{**}P < 0.01$, $^{***}P < 0.001$.

tested. The results showed that the limbs' force has no difference between WT and Map2k5$^{+/-}$ mutant mice in both male and female subjects (**Figure 2** in **Supplementary Material 3**).

Male Map2k5$^{+/-}$ Mutant Mice Display Sensorimotor Gating Deficits

The main complaint of+oldd unpleasant feelings displayed by RLS/WED patients is hard to evaluate in mice. In order to measure this phenotype, we tested the sensorimotor gating levels on each group of mice. The sensory response adaptation was recorded by acoustic startle response (ASR) and prepulse inhibition (PPI) tests. Male Map2k5$^{+/-}$ mutant mice represented a decreased ASR at 78, 84, 90, and 120 dB (P = 0.035, 0.029, 0.006, and 0.019, respectively, **Figure 3G**), and PPI results implied sensorimotor gating deficits at 9 0dB (p = 0.024, **Figure 3H**). This implied that male Map2k5$^{+/-}$ mutant mice displayed deficits on sensory stimulus, but not female mutant mice. ASR and PPI tests examined the intact function of the vestibular system, auditory system, ventrolateral tegmental nucleus, pontine reticular formation, and their interactions (Yeomans et al., 2002). In addition, there is also evidence showing that the amygdala, accumbens nuclei, and other limbic systems contribute to the performance of ASR

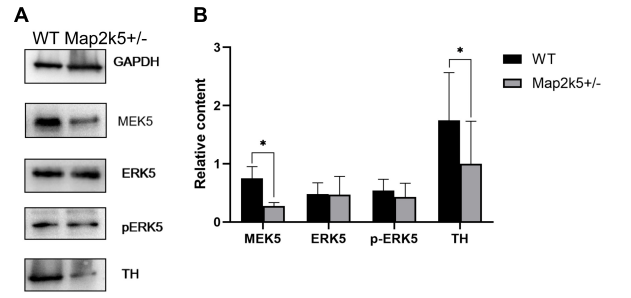

FIGURE 5 | (A) Representative Western blots images of MAP2K5, ERK5, phosphorylated ERK5 (active), TH protein, and GAPDH are depicted. **(B)** Data from male WT and Map2k5$^{+/-}$ mutant mice were pooled for this analysis. Bar graph is hemi-quantitative analysis of the Western blot, showing a significant decrease in MAP2K5 and TH (P_{Map2k5} = 0.023, P_{TH} = 0.013, respectively) in the Map2k5$^{+/-}$ mutant mice. Results are plotted as mean with SEM (paired *t*-test, n = 4). Results are plotted as mean with SEM. Bars represent means with SEM. *P < 0.05.

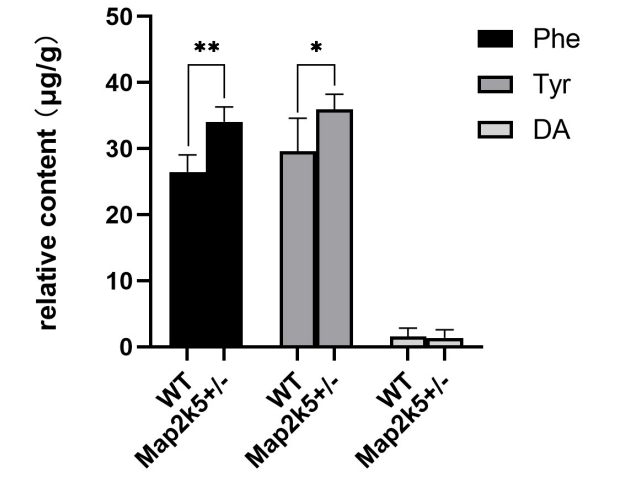

FIGURE 6 | The values of neurochemicals in dopamine synthesis pathway are represented. Phe and Tyr are accumulated significantly in Map2k5$^{+/-}$ mutant mice (P = 0.001, 0.033, respectively, n = 5). Results are plotted as mean with SEM. Bars represent means with SEM. *P < 0.05, **P < 0.01.

and PPI (Frau et al., 2019). Considering the results we got from open field and PPI, where only male mutant mice displayed stress-related sensorimotor deficits, and taking in account that both tests involve the accumbens nucleus, amygdala nucleus, and mesolimbic dopamine system (that participate in many psychiatric disorders, such as schizophrenia, depression, obsessive–compulsive disorder, psychological substance-induced behavior, and so on), we hypothesized that sex hormone levels might affect the behaviors of Map2k5$^{+/-}$ mutant mice where male mice was prone to manifest stress-related responses (Pittenger et al., 2016; Khan and Powell, 2018; Liu et al., 2018; Bilel et al., 2019; Tapias-Espinosa et al., 2019).

The Quantity of SNc and Striatum TH^{+} Cells Were Reduced in Map2k5$^{+/-}$ Mutant Mice

Based on the behavior tests' results found in female mice, we thought that the phenotype of bradykinesia, poor coordination, and fatigue was similar to the motor dysfunction caused by nigrostriatal pathway deficits. Dopaminergic neurons are crucial for the nigrostriatal pathway, so we assessed the levels of dopaminergic neurons by immunostaining of TH protein (the rate-limiting enzyme in the dopamine synthesis pathway) in SNc. We assessed the TH^{+} cell counts in the SNc region of the mice brain. TH^{+} cells were stained and captured by florescence microscopy (**Figure 4A**), and a montaged image of Map2k5-stained section was captured, which indicated a synchronous declination of Map2k5 and TH protein (**Figure 4B**). Results showed a decreased SNc TH^{+} cell number in female Map2k5$^{+/-}$ mutant mice at P18d, 21 weeks, 28 weeks, and 38 weeks compared with WT mice (P_{18d} < 0.001, P_{21w} < 0.001, P_{28w} = 0.005, P_{38w} < 0.001, **Figure 4C**). The reduction of TH^{+} cells in SNc suggested that MAP2K5 might be involved in the survival of dopaminergic cells in SNc early in life. At P18d, the TH^{+} cells of Map2k5$^{+/-}$ mutant mice were 70% of their WT littermates, 50–60% at 21 and 28 weeks, while this number declined to about 40% at age by 38 weeks. Thus, Map2k5$^{+/-}$ deficiency might disturb the dopamine system in SNc, and the effect of Map2k5$^{+/-}$ deficiency on losing dopaminergic neurons increased with aging.

SNc dopaminergic neurons project to the striatum forming the nigrostriatal pathway and facilitate movement via direct and indirect pathways. We conducted immunostaining of TH+ protein in the striatum of 21-week female mice to evaluate the dopaminergic neural fibers' density in this area, where DA is released and acts on the postsynaptic membrane. Immunofluorescence images of the striatum displayed a reduction in TH intensity (**Figure 4D**). Mean immunofluorescence intensity was calculated for each tissue slice, showing a significant decrease in dopaminergic neuron fibers' density in female Map2k5$^{+/-}$ mutant mice compared with WT mice (p = 0.006, **Figure 4E**). These results confirmed the decreased dopaminergic neurons in Map2k5$^{+/-}$ mutant mice, consistent with the movement phenotypes displayed in behavior tests.

Decreased Quantities of Map2k5 and TH Protein, but Not pErk5 in Map2k5$^{+/-}$ Mutant Mice

To explore the mechanism of reduced dopaminergic neurons in Map2k5$^{+/-}$ mutant mice, we measured the level of Map2k5–Erk5 pathway molecules and TH protein in ventral midbrain including dopaminergic neurons in the nigrostriatal pathway. Four female mice aged 21 weeks for each genotype were used. Proteins of MAP2K5 (MEK5), ERK5, phosphorylated ERK5 (active), TH, and GAPDH were stained (**Figure 5A**). The ratio of each protein was calculated by its relative quantity referred to the GAPDH band. The results implied a synchronized decrease in Map2k5 and TH proteins in the ventral midbrain

TABLE 1 | Levels of phenylalanine (Phe), tyrosine (Tyr), dopamine (DA), epinephrine (Epi), serotonin, and its metabolite 5-HIAA in the striatum.

Neurochemicals	WT	Map2k5$^{+/-}$	*P*-value
Phe	26.46 ± 1.17	34.04 ± 1.01	0.001**
Tyr	29.62 ± 2.24	35.95 ± 1.01	0.033*
DA	1.55 ± 0.59	1.34 ± 0.63	0.815
Epi	1.50 ± 0.62	1.07 ± 0.46	0.621
Gln	675.43 ± 189.03	574.01 ± 163.44	0.695
ACh	0.58 ± 0.17	0.22 ± 0.07	0.094
Serotonin	0.04 ± 0.00	0.03 ± 0.02	0.743
5-HIAA	0.35 ± 0.11	0.26 ± 0.05	0.478

*The values of neurochemicals are represented in means ± SEM (μg/g) of the tissue (t-test, n = 5). *P < 0.05, **P < 0.01.*

(P_{Map2k5} = 0.023, P_{TH} = 0.013, respectively), while Erk5 was not reduced, and phosphorylated Erk5 was reduced without a statistical significance (P = 0.324, **Figure 5B**). It is possible that MAP2K5 deficiency decreases TH expression in an ERK5-independent manner. However, more studies are needed to clarify the molecular mechanism of this phenomenon.

Dopamine Levels Were Not Altered in Striatum, but Its Substrates Were Accumulated

As TH is the key enzyme of dopamine synthesis and Map2k5-deficient mice showed dopaminergic neuron deficiency in the nigrostriatal pathway, we tried to investigate whether Map2k5 deficiency-induced TH reduction had an effect on neurotransmitters and their metabolites (Obara et al., 2016). We used HPLC to examine monoamine neurochemical systems in the striatum on five female 21-week-old mice per group. The substrates of DA in its synthesis pathway (Phe and Tyr) were accumulated significantly (P = 0.001, 0.033, respectively, **Figure 6**) in Map2k5$^{+/-}$ female mutant mice compared with WT female mice, while the gross DA content decreased but without significant difference between WT and Map2k5$^{+/-}$ mutant mice. Other neurotransmitters, such as Gln, ACh, serotonin, and its metabolite 5-HIAA were not altered in Map2k5$^{+/-}$ mutant mice (**Table 1**). The accumulation of substrates of phenylalanine and tyrosine is consistent with the result of decreased TH enzyme in the nigrostriatal pathway. However, there was no statistical difference on the dopamine levels between Map2k5$^{+/-}$ mutant and WT mice. This inconsistent finding may be due to two reasons. First, the dopamine level in the striatum was very low to be detected, beyond the linear dynamic range of the HPLC standard curve. This problem may be solved by other techniques like fluorometric detection (Ghani et al., 2021). Second, TH reduction in Map2k5-deficient mouse model was not strong enough to create a significant reduction in dopamine in the nigrostriatal pathway in Map2k5 mutant mice. Interestingly, previous studies showed that DA was not significantly reduced when TH protein level decreased significantly at 3 weeks in Th mutant mice. However, at 1 year old, when TH content reduced at 3% of WT mice, DA reduced to a significant level ($P < 0.001$) (Korner et al., 2015). Therefore, there may be a threshold of TH reduction when DA decreased into a significant level.

DISCUSSION

In this study, we described for the first time the movement phenotypes and underlying dopaminergic disturbance in a Map2k5-deficient mouse model. These behavioral changes were contrary to RLS/WED symptoms, but similar to PD in some aspects, including reduced circadian-dependent ambulatory locomotion, coordination, and balance ability. Similarly, reduced dopaminergic neurons and TH protein in the nigrostriatal pathway resembled some pathological aspects of PD. Actually, both diseases share many common features, such as high prevalence of comorbidity of RLS/WED with PD, dopaminergic dysregulation in the pathogenesis of both diseases, and good response to dopamine agonists (Splinter, 2007). This suggests similar mechanisms that might be shared by both disorders (Alonso-Navarro et al., 2019). In addition, SNPs of MAP2K5 have been shown to be associated with the reduced risk of RLS/WED (Winkelmann et al., 2007; Yang et al., 2011; Moore et al., 2014; Li et al., 2017), but increased the risk of tremor in PD (rs12593813, 61.0% vs. 46.5%, p = 0.001) (Gan-Or et al., 2015). This further indicates a close relationship, but probably opposite, effect of MAP2K5 in RLS/WED and PD. Also, PD patients usually present with odor problems, and previous studies reported deficits in odor discrimination in the conditional deletion of Erk5 mouse (Zou et al., 2012). Therefore, we hypothesized that the Map2k5–Erk5 pathway might be involved in the pathophysiology of both RLS/WED and PD.

Several *in vitro* studies found that the MAP2K5–ERK5 pathway was crucial in dopaminergic neuron survival. It protected dopaminergic neurons under both basal conditions and in response to oxidative stress (Cavanaugh et al., 2006). MAP2K5–ERK5 was also involved in Mn-induced cytotoxicity, altering neurons' survival and DA production in MN9D cells (Ding et al., 2020). ERK5 was reported to induce ankrd1 for catecholamines biosynthesis and homeostasis in adrenal gland medullary cells (Obara et al., 2016). Thus, it is reasonable to hypothesize that reduced dopaminergic neurons and TH protein in our Map2k5-deficient mouse model might be due to decreased Map2k5–Erk5 pathway. However, p-Erk5 level remained unchanged in our Map2k5-deficient mouse. Based on the fact that the level of p-ERK5 dropped greatly after birth (Parmar et al., 2015) and Erk5 is the only present known substrate of Map2k5, the regulation of the Map2k5–Erk5 pathway on dopaminergic neuron probably occurred in the early developmental stage. Actually, Map2k5–Erk5 seems to be involved in protecting embryonic, but not mature, cortical neurons in an *in vitro* study (Liu et al., 2003, 2006). Also, conditional deletion of Erk5 in the nervous system was once reported for impaired neuron migration into the olfactory bulb during nervous system development at prenatal stages (Li et al., 2013). Since the heterozygous Map2k5 mutant mice already displayed reduction in TH^{+} dopaminergic cells significantly on postnatal 18 days in our study, it is plausible to think that the Map2k5–Erk5 pathway regulates the dopaminergic development in an earlier period and contributes to central nervous system disorders such as RLS/WED and PD. Actually, we aim to explore the Map2k5-deficient

effect on dopaminergic neuron development of early neurogenesis in our future research.

Additionally, our results of behavioral tests displayed sexual distinctions. Here, we uncovered the nigrostriatal dopaminergic system disturbance in female Map2k5-deficient mice, while the underlying mechanism of stress-related alterations in sensorimotor response of male Map2k5-deficient mice, involving amygdala, hippocampus, and accumbens nuclei in the limbic system (Lalonde and Strazielle, 2017; Frau et al., 2019) is worth to be further studied.

There are limitations of our study. The dopamine level in the striatum was very low to be detected. As a matter of fact, several heterozygous samples' DA concentrations were beyond the linear dynamic range of the HPLC standard curve. It could indeed account to difficulties to detect any difference in DA between groups. This problem may be solved by other techniques like fluorometric detection (Ghani et al., 2021). What is more, our results showed significant accumulation of substrates (Phe and Tyr) of dopamine before the step mediated by TH accompanied by insignificant reduction in DA, so we hypothesized that a threshold may exist where the reduction in TH induces DA decrease into a significant level.

CONCLUSION

In conclusion, Map2k5-deficient mice manifest movement impairments, consistent with reductions in dopaminergic neurons and TH protein in the nigrostriatal dopaminergic system. These features confirmed that dopaminergic disturbance by the Map2k5–Erk5 pathway was involved in the pathogenesis of movement disorders like RLS/WED and PD. In addition, our Map2k5-deficient mouse model provides a unique tool to further investigate the role of the Map2k5–Erk5 pathway in other central nervous system disorders with dopamine deficits, such as schizophrenia.

DATA AVAILABILITY STATEMENT

The raw data supporting the conclusions of this article will be made available by the authors, without undue reservation.

ETHICS STATEMENT

The animal study was reviewed and approved by the Ruijin Hospital, Shanghai Jiao Tong University School of Medicine.

AUTHOR CONTRIBUTIONS

YH contributed to the project configuration, experiment investigation, data analysis, and original manuscript description. JM contributed to the project supervision, data analysis manuscript modification, and funding acquisition. RM contributed to the manuscript modification and data curation. PW and QL participated in the experiment investigation, data analysis, and methodology support. All authors contributed to the article and approved the submitted version.

FUNDING

This work was supported by the National Natural Science Foundation of China (81571103) and the National Key R&D Program of China (2016YFC1306000).

ACKNOWLEDGMENTS

We thank Minghan Tong (Shanghai Institute of Biochemistry and Cell Biology, Chinese Academy of Sciences) for technical assistance and manuscript modifications. We thank GemPharmmatech Co., Ltd. for technical assistance and cooperation.

SUPPLEMENTARY MATERIAL

The Supplementary Material for this article can be found online at: https://www.frontiersin.org/articles/10.3389/fnagi.2021.651638/full#supplementary-material

REFERENCES

Accili, D., Fishburn, C. S., Drago, J., Steiner, H., Lachowicz, J. E., Park, B. H., et al. (1996). A targeted mutation of the D3 dopamine receptor gene is associated with hyperactivity in mice. *Proc. Natl. Acad. Sci. U.S.A.* 93, 1945–1949. doi: 10.1073/pnas.93.5.1945

Allen, R. P., Picchietti, D. L., Garcia-Borreguero, D., Ondo, W. G., Walters, A. S., Winkelman, J. W., et al. (2014). Restless legs syndrome/Willis-Ekbom disease diagnostic criteria: updated International Restless Legs Syndrome Study Group (IRLSSG) consensus criteria–history, rationale, description, and significance. *Sleep Med.* 15, 860–873. doi: 10.1016/j.sleep.2014.03.025

Alonso-Navarro, H., García-Martín, E., Agúndez, J. A. G., and Jiménez-Jiménez, F. J. (2019). Association between restless legs syndrome and other movement disorders. *Neurology* 92, 948–964. doi: 10.1212/wnl.0000000000007500

Appari, M., Breitbart, A., Brandes, F., Szaroszyk, M., Froese, N., Korf-Klingebiel, M., et al. (2017). C1q-TNF-Related Protein-9 promotes cardiac hypertrophy and failure. *Circ. Res.* 120, 66–77. doi: 10.1161/circresaha.116.309398

Bilel, S., Tirri, M., Arfè, R., Stopponi, S., Soverchia, L., Ciccocioppo, R., et al. (2019). Pharmacological and behavioral effects of the synthetic cannabinoid AKB48 in Rats. *Front. Neurosci.* 13:1163. doi: 10.3389/fnins.2019.01163

Cabrera-Mendoza, B., Martínez-Magaña, J. J., Genis-Mendoza, A. D., Sarmiento, E., Ruíz-Ramos, D., Tovilla-Zárate, C. A., et al. (2020). High polygenic burden is associated with blood DNA methylation changes in individuals with suicidal behavior. *J. Psychiatr. Res.* 123, 62–71. doi: 10.1016/j.jpsychires.2020.01.008

Castro, M., Laviña, B., Ando, K., Álvarez-Aznar, A., Abu Taha, A., Brakebusch, C., et al. (2019). CDC42 deletion elicits cerebral vascular malformations via

increased MEKK3-dependent KLF4 expression. *Circ. Res.* 124, 1240–1252. doi: 10.1161/circresaha.118.314300

Cavanaugh, J. E., Jaumotte, J. D., Lakoski, J. M., and Zigmond, M. J. (2006). Neuroprotective role of ERK1/2 and ERK5 in a dopaminergic cell line under basal conditions and in response to oxidative stress. *J. Neurosci. Res.* 84, 1367–1375. doi: 10.1002/jnr.21024

Concordet, J. P., and Haeussler, M. (2018). CRISPOR: intuitive guide selection for CRISPR/Cas9 genome editing experiments and screens. *Nucleic Acids Res.* 46(W1), W242–W245. doi: 10.1093/nar/gky354

Dinev, D., Jordan, B. W., Neufeld, B., Lee, J. D., Lindemann, D., Rapp, U. R., et al. (2001). Extracellular signal regulated kinase 5 (ERK5) is required for the differentiation of muscle cells. *EMBO Rep.* 2, 829–834. doi: 10.1093/embo-reports/kve177

Ding, H., Wang, F., Su, L., Zhao, L., Hu, B., Zheng, W., et al. (2020). Involvement of MEK5/ERK5 signaling pathway in manganese-induced cell injury in dopaminergic MN9D cells. *J. Trace Elem. Med. Biol.* 61:126546. doi: 10.1016/j.jtemb.2020.126546

English, J. M., Pearson, G., Baer, R., and Cobb, M. H. (1998). Identification of substrates and regulators of the mitogen-activated protein kinase ERK5 using chimeric protein kinases. *J. Biol. Chem.* 273, 3854–3860. doi: 10.1074/jbc.273.7.3854

Frau, R., Miczán, V., Traccis, F., Aroni, S., Pongor, C. I., Saba, P., et al. (2019). Prenatal THC exposure produces a hyperdopaminergic phenotype rescued by pregnenolone. *Nat. Neurosci.* 22, 1975–1985. doi: 10.1038/s41593-019-0512-2

Gan-Or, Z., Alcalay, R. N., Bar-Shira, A., Leblond, C. S., Postuma, R. B., Ben-Shachar, S., et al. (2015). Genetic markers of restless legs syndrome in Parkinson disease. *Parkinsonism Relat. Disord.* 21, 582–585. doi: 10.1016/j.parkreldis.2015.03.010

Ghani, S. M., Rezaei, B., Jamei, H. R., and Ensafi, A. A. (2021). Novel synthesis of a dual fluorimetric sensor for the simultaneous analysis of levodopa and pyridoxine. *Anal. Bioanal. Chem.* 413, 377–387. doi: 10.1007/s00216-020-03005-9

Jo, M., Chung, A. Y., Yachie, N., Seo, M., Jeon, H., Nam, Y., et al. (2017). Yeast genetic interaction screen of human genes associated with amyotrophic lateral sclerosis: identification of MAP2K5 kinase as a potential drug target. *Genome Res.* 27, 1487–1500. doi: 10.1101/gr.211649.116

Johnson, G. L., and Lapadat, R. (2002). Mitogen-activated protein kinase pathways mediated by ERK, JNK, and p38 protein kinases. *Science* 298, 1911–1912. doi: 10.1126/science.1072682

Kang, S. G., Lee, Y. J., Park, Y. M., Kim, L., and Lee, H. J. (2018). Haplotype association of the MAP2K5 gene with antipsychotics-induced symptoms of restless legs syndrome among patients with schizophrenia. *Psychiatry Investig.* 15, 84–89. doi: 10.4306/pi.2018.15.1.84

Kato, Y., Zhao, M., Morikawa, A., Sugiyama, T., Chakravortty, D., Koide, N., et al. (2000). Big mitogen-activated kinase regulates multiple members of the MEF2 protein family. *J. Biol. Chem.* 275, 18534–18540. doi: 10.1074/jbc.M001573200

Khan, A., and Powell, S. B. (2018). Sensorimotor gating deficits in "two-hit" models of schizophrenia risk factors. *Schizophr. Res.* 198, 68–83. doi: 10.1016/j.schres.2017.10.009

Kim, B. W., Jeong, K. H., Kim, J. H., Jin, M., Kim, J. H., Lee, M. G., et al. (2016). Pathogenic upregulation of glial lipocalin-2 in the Parkinsonian dopaminergic system. *J. Neurosci.* 36, 5608–5622. doi: 10.1523/jneurosci.4261-15.2016

Korner, G., Noain, D., Ying, M., Hole, M., Flydal, M. I., Scherer, T., et al. (2015). Brain catecholamine depletion and motor impairment in a Th knock-in mouse with type B tyrosine hydroxylase deficiency. *Brain* 138(Pt 10), 2948–2963. doi: 10.1093/brain/awv224

Lalonde, R., and Strazielle, C. (2017). Neuroanatomical pathways underlying the effects of hypothalamo-hypophysial-adrenal hormones on exploratory activity. *Rev. Neurosci.* 28, 617–648. doi: 10.1515/revneuro-2016-0075

Langley, M., Ghosh, A., Charli, A., Sarkar, S., Ay, M., Luo, J., et al. (2017). Mito-Apocynin prevents mitochondrial dysfunction, microglial activation, oxidative damage, and progressive Neurodegeneration in MitoPark transgenic mice. *Antioxid Redox Signal.* 27, 1048–1066. doi: 10.1089/ars.2016.6905

Li, G., Tang, H., Wang, C., Qi, X., Chen, J., Chen, S., et al. (2017). Association of BTBD9 and MAP2K5/SKOR1 with restless legs syndrome in Chinese population. *Sleep* 40:zsx028. doi: 10.1093/sleep/zsx028

Li, T., Pan, Y. W., Wang, W., Abel, G., Zou, J., Xu, L., et al. (2013). Targeted deletion of the ERK5 MAP kinase impairs neuronal differentiation, migration, and survival during adult neurogenesis in the olfactory bulb. *PLoS One* 8:e61948. doi: 10.1371/journal.pone.0061948

Liu, F., Zhang, H., and Song, H. (2017). Upregulation of MEK5 by Stat3 promotes breast cancer cell invasion and metastasis. *Oncol. Rep.* 37, 83–90. doi: 10.3892/or.2016.5256

Liu, L., Cavanaugh, J. E., Wang, Y., Sakagami, H., Mao, Z., and Xia, Z. (2003). ERK5 activation of MEF2-mediated gene expression plays a critical role in BDNF-promoted survival of developing but not mature cortical neurons. *Proc. Natl. Acad. Sci. U.S.A.* 100, 8532–8537. doi: 10.1073/pnas.1332804100

Liu, L., Cundiff, P., Abel, G., Wang, Y., Faigle, R., Sakagami, H., et al. (2006). Extracellular signal-regulated kinase (ERK) 5 is necessary and sufficient to specify cortical neuronal fate. *Proc. Natl. Acad. Sci. U.S.A.* 103, 9697–9702. doi: 10.1073/pnas.0603373103

Liu, Y. P., Yang, Y. Y., Wan, F. J., and Tung, C. S. (2018). Importance of intervention timing in the effectiveness of antipsychotics. *Prog. Neuropsychopharmacol. Biol. Psychiatry* 81, 493–500. doi: 10.1016/j.pnpbp.2017.02.003

Moore, Ht, Winkelmann, J., Lin, L., Finn, L., Peppard, P., and Mignot, E. (2014). Periodic leg movements during sleep are associated with polymorphisms in BTBD9, TOX3/BC034767, MEIS1, MAP2K5/SKOR1, and PTPRD. *Sleep* 37, 1535–1542. doi: 10.5665/sleep.4006

Obara, Y., Nagasawa, R., Nemoto, W., Pellegrino, M. J., Takahashi, M., Habecker, B. A., et al. (2016). ERK5 induces ankrd1 for catecholamine biosynthesis and homeostasis in adrenal medullary cells. *Cell Signal.* 28, 177–189. doi: 10.1016/j.cellsig.2015.12.016

Parmar, M. S., Jaumotte, J. D., Zigmond, M. J., and Cavanaugh, J. E. (2015). ERK1, 2, and 5 expression and activation in dopaminergic brain regions during postnatal development. *Int. J. Dev. Neurosci.* 46, 44–50. doi: 10.1016/j.ijdevneu.2015.06.009

Pittenger, C., Adams, T. G. Jr., Gallezot, J. D., Crowley, M. J., Nabulsi, N., James, R., et al. (2016). OCD is associated with an altered association between sensorimotor gating and cortical and subcortical 5-HT1b receptor binding. *J. Affect. Disord.* 196, 87–96. doi: 10.1016/j.jad.2016.02.021

Simões, A. E., Pereira, D. M., Gomes, S. E., Brito, H., Carvalho, T., French, A., et al. (2015). Aberrant MEK5/ERK5 signalling contributes to human colon cancer progression via NF-κB activation. *Cell Death Dis.* 6:e1718. doi: 10.1038/cddis.2015.83

Splinter, M. Y. (2007). Rotigotine: transdermal dopamine agonist treatment of Parkinson's disease and restless legs syndrome. *Ann. Pharmacother.* 41, 285–295. doi: 10.1345/aph.1H113

Tapias-Espinosa, C., Río-Álamos, C., Sánchez-González, A., Oliveras, I., Sampedro-Viana, D., Castillo-Ruiz, M. D. M., et al. (2019). Schizophrenia-like reduced sensorimotor gating in intact inbred and outbred rats is associated with decreased medial prefrontal cortex activity and volume. *Neuropsychopharmacology* 44, 1975–1984. doi: 10.1038/s41386-019-0392-x

Wang, X., Merritt, A. J., Seyfried, J., Guo, C., Papadakis, E. S., Finegan, K. G., et al. (2005). Targeted deletion of mek5 causes early embryonic death and defects in the extracellular signal-regulated kinase 5/myocyte enhancer factor 2 cell survival pathway. *Mol. Cell Biol.* 25, 336–345. doi: 10.1128/mcb.25.1.336-345.2005

Winkelmann, J., Schormair, B., Lichtner, P., Ripke, S., Xiong, L., Jalilzadeh, S., et al. (2007). Genome-wide association study of restless legs syndrome identifies common variants in three genomic regions. *Nat. Genet.* 39, 1000–1006. doi: 10.1038/ng2099

Yang, Q., Li, L., Chen, Q., Foldvary-Schaefer, N., Ondo, W. G., and Wang, Q. K. (2011). Association studies of variants in MEIS1, BTBD9, and MAP2K5/SKOR1 with restless legs syndrome in a US population. *Sleep Med.* 12, 800–804. doi: 10.1016/j.sleep.2011.06.006

Yeomans, J. S., Li, L., Scott, B. W., and Frankland, P. W. (2002). Tactile, acoustic and vestibular systems sum to elicit the startle reflex. *Neurosci. Biobehav. Rev.* 26, 1–11. doi: 10.1016/s0149-7634(01)00057-4

Yun, S. P., Kim, D., Kim, S., Kim, S., Karuppagounder, S. S., Kwon, S. H., et al. (2018). α-Synuclein accumulation and GBA deficiency due to L444P GBA

mutation contributes to MPTP-induced parkinsonism. *Mol. Neurodegener.* 13:1. doi: 10.1186/s13024-017-0233-5

Zhang, J. Y., Liu, T. H., He, Y., Pan, H. Q., Zhang, W. H., Yin, X. P., et al. (2019). Chronic stress remodels synapses in an amygdala circuit-specific manner. *Biol. Psychiatry* 85, 189–201. doi: 10.1016/j.biopsych.2018.06.019

Zou, J., Pan, Y. W., Wang, Z., Chang, S. Y., Wang, W., Wang, X., et al. (2012). Targeted deletion of ERK5 MAP kinase in the developing nervous system impairs development of GABAergic interneurons in the main olfactory bulb and behavioral discrimination between structurally similar odorants. *J. Neurosci.* 32, 4118–4132. doi: 10.1523/jneurosci.6260-11.2012

Conflict of Interest: The authors declare that the research was conducted in the absence of any commercial or financial relationships that could be construed as a potential conflict of interest.

frontiers in Aging Neuroscience

ORIGINAL RESEARCH
published: 13 July 2021
doi: 10.3389/fnagi.2021.684171

Acute TBK1/IKK-ε Inhibition Enhances the Generation of Disease-Associated Microglia-Like Phenotype Upon Cortical Stab-Wound Injury

Rida Rehman[1†], Lilla Tar[1,2†], Adeyemi Jubril Olamide[1,3], Zhenghui Li[1,4], Jan Kassubek[1], Tobias Böckers[5,6], Jochen Weishaupt[1,6], Albert Ludolph[1,2,6], Diana Wiesner[1,2,6‡] and Francesco Roselli[1,2,6‡]*

[1] Department of Neurology, Ulm University, Ulm, Germany, [2] German Center for Neurodegenerative Diseases (DZNE)-Ulm, Ulm, Germany, [3] Master in Translational and Molecular Neuroscience, Ulm University, Ulm, Germany, [4] Department of Neurosurgery, Kaifeng Central Hospital, Kaifeng, China, [5] Institute of Anatomy and Cell Biology, Ulm University, Ulm, Germany, [6] Neurozentrum Ulm, Ulm, Germany

OPEN ACCESS

Edited by:
Karl J. L. Fernandes, Université de Montréal, Canada

Reviewed by:
Marie-Ève Tremblay, University of Victoria, Canada
Angeliki Maria Nikolakopoulou, University of Southern California, Los Angeles, United States
Audrey Lafrenaye, Virginia Commonwealth University, United States

***Correspondence:**
Francesco Roselli
francesco.roselli@uni-ulm.de

[†] These authors have contributed equally to this work

[‡] These authors share senior authorship

Received: *22 March 2021*
Accepted: *21 June 2021*
Published: *13 July 2021*

Citation:
Rehman R, Tar L, Olamide AJ, Li Z, Kassubek J, Böckers T, Weishaupt J, Ludolph A, Wiesner D and Roselli F (2021) Acute TBK1/IKK-ε Inhibition Enhances the Generation of Disease-Associated Microglia-Like Phenotype Upon Cortical Stab-Wound Injury. Front. Aging Neurosci. 13:684171. doi: 10.3389/fnagi.2021.684171

Traumatic brain injury has a poorer prognosis in elderly patients, possibly because of the enhanced inflammatory response characteristic of advanced age, known as "inflammaging." Recently, reduced activation of the TANK-Binding-Kinase 1 (Tbk1) pathway has been linked to age-associated neurodegeneration and neuroinflammation. Here we investigated how the blockade of Tbk1 and of the closely related IKK-ε by the small molecule Amlexanox could modify the microglial and immune response to cortical stab-wound injury in mice. We demonstrated that Tbk1/IKK-ε inhibition resulted in a massive expansion of microglial cells characterized by the $TMEM119^{+}/CD11c^{+}$ phenotype, expressing high levels of CD68 and CD317, and with the upregulation of Cst7a, Prgn and Ccl4 and the decrease in the expression levels of Tmem119 itself and P2yr12, thus a profile close to Disease-Associated Microglia (DAM, a subset of reactive microglia abundant in Alzheimer's Disease and other neurodegenerative conditions). Furthermore, Tbk1/IKK-ε inhibition increased the infiltration of $CD3^{+}$ lymphocytes, $CD169^{+}$ macrophages and $CD11c^{+}/CD169^{+}$ cells. The enhanced immune response was associated with increased expression of Il-33, Ifn-g, Il-17, and Il-19. This upsurge in the response to the stab wound was associated with the expanded astroglial scars and increased deposition of chondroitin-sulfate proteoglycans at 7 days post injury. Thus, Tbk1/IKK-ε blockade results in a massive expansion of microglial cells with a phenotype resembling DAM and with the substantial enhancement of neuroinflammatory responses. In this context, the induction of DAM is associated with a detrimental outcome such as larger injury-related glial scars. Thus, the Tbk1/IKK-ε pathway is critical to repress neuroinflammation upon stab-wound injury and Tbk1/IKK-ε inhibitors may provide an innovative approach to investigate the consequences of DAM induction.

Keywords: TBK1, microglia, traumatic brain injury, amlexanox, neuroinflammation, stab wound injury

INTRODUCTION

Traumatic Brain Injury (TBI) is a major worldwide cause of morbidity and mortality (Bruns and Hauser, 2003; Jiang et al., 2019). The incidence of TBI is not homogeneously distributed throughout ages. At least, two peaks have been recognized in epidemiological datasets, the first attributed to the adolescent-young adult population (15–24 years) and the second occurring in the geriatric population (Kraus et al., 1984; Tiret et al., 1990; Bruns and Hauser, 2003; Peeters et al., 2015). These two subgroups are often conflated when clinical trials are performed, under the assumption that, although age may be a risk factor for TBI, the unfolding of TBI-associated cascades may be similar. This notion is challenged by the worse prognosis observed in older patients with TBI (Thompson et al., 2006) and by experimental evidence of distinct microglial phenotypes and heightened neuroinflammation in aged mice (Ritzel et al., 2019; Early et al., 2020).

Aging *per se* is characterized by an enhanced inflammatory response at systemic (Salminen et al., 2012; Franceschi and Campisi, 2014; Mogilenko et al., 2021) as well as at brain level (Cheng H. et al., 2018; Mejias et al., 2018). According to the "inflammaging" concept, a low-grade inflammatory state is characteristic of advanced age and this primed inflammatory response contributes to a heightened response upon stimuli. Notably, microglial transcriptomes are substantially different in the advanced age (Galatro et al., 2017; Hammond et al., 2019) and recently a microglial phenotype resembling Disease-Associated Microglia (DAM) has been identified in the white matter upon aging (Keren-Shaul et al., 2017; Raj et al., 2017; Safaiyan et al., 2021), where it appears to be involved in the disposal of degenerated myelin. Interestingly, DAM also characterizes several age-related neurodegenerative conditions, such as Alzheimer Disease and Amyotrophic Lateral Sclerosis (Ofengeim et al., 2017; Dols-Icardo et al., 2020; Mifflin et al., 2021) and it is characterized by a distinctive transcriptional profile including the upregulation of *Cst7, Clec7a, CSFR1,* and *ApoE* genes (Krasemann et al., 2017; Keren-Shaul et al., 2017; Rangaraju et al., 2018) and it is believed to be relevant for the phagocytosis of apoptotic cells and for the formation of amyloid plaques (Anderson et al., 2019; Muth et al., 2019; Srinivasan et al., 2019; Sobue et al., 2021). Additional aging-associated subpopulations of microglia have been reported, in particular interferon-driven and inflammatory subpopulations (Hammond et al., 2019) which appear to be related to cognitive impairment (Deczkowska et al., 2018). Irrespective of subpopulation phenotypes, microglia from aging brains secretes higher levels of IL-6 and IL1b (Rawji et al., 2016), expresses a higher level of Toll Like Receptor (TLR) and Major Histocompatibility Complex (MHC) proteins (Letiembre et al., 2009), but display reduced motility and impaired phagocytic capacity (Koellhoffer et al., 2017; Gabandé-Rodríguez et al., 2020). In line with these findings, older mice display a more abundant microglial proliferation and peripheral leukocytes infiltration (in particular neutrophils) upon TBI, larger production of reactive oxygen species, and higher levels of TNF-alpha secretion (Ritzel et al., 2019).

The investigation of the molecular mechanisms involved in the age-related enhanced microglial reactivity has recently identified the TANK1-binding kinase 1 (Tbk1) a player in the inflammaging phenotype. In Tbk1 ± mice, the transcriptional profile characteristic of age-associated pro-inflammatory state appears earlier and progresses faster than in wild-type littermates (Bruno et al., 2020), without overt neurodegeneration. Likewise, blood-brain-barrier permeability is disrupted in Tbk1 ± mice (Alami et al., 2020) and conditional myeloid loss of Tbk1 results in a pro-inflammatory state and cellular infiltrate in the spinal cord and other organs (Duan et al., 2021). Moreover, loss of Tbk1 has been shown to synergize with TAK1 downregulation in bringing about the age-associated activation of Receptor-interacting serine/threonine-protein kinase-1 (RIPK1) and related inflammaging phenotype (Xu et al., 2018). Thus, chronic decrease in Tbk1 activity is hypothesized to be associated with increased inflammatory responses.

The anti-inflammatory agent Amlexanox (AMX; Reilly et al., 2013) is an inhibitor of Tbk1 and of the closely related IKK-ε (Cheng H. et al., 2018). AMX has been shown to reduce canonical signaling through NF-kB (Cheng C. et al., 2018; Möser et al., 2019) by inhibiting IKK-ε and Tbk1, while, through inhibition of Tbk1, causing the de-repression of non-canonical signaling through NIK/NF-kB (Jin et al., 2012). Furthermore, AMX-induced inhibition of Tbk1 has been linked to the decrease in phosphorylation of IRF3 and IRF7 (Mori et al., 2015; Quan et al., 2019; Zhou et al., 2020), implying the downregulation of Tbk1-mediated Interferon signaling. AMX was originally approved for human use in dermatological conditions (Abbasi et al., 2016), and, because of its effects on reducing NF-kB and IRF3/7 activation (through the double targeting of Tbk1 and IKK-ε) AMX has been proposed as a therapeutic agent in autoimmune neuroinflammatory disorders (Quan et al., 2019), neoplastic progression (Wilcz-Villega et al., 2020) and diabetes-associated macrophage-driven inflammation (Oral et al., 2017).

Here, we have investigated the effect of acute Tbk1/IKK-ε blockade by AMX administration in a model of focal traumatic (stab wound) brain injury. We conceptualized two possible outcomes: a predominant anti-inflammatory effect, as seen in the context of other inflammatory conditions, or a predominant pro-inflammatory effect, in agreement to the enhanced reactivity observed upon Tbk1 deletion and in aging. We found that AMX treatment caused the increase in microglial and lymphocytic infiltration in the injury site, associated with the upregulation of a subset of inflammatory cytokines such as IL-17 and IFN-gamma, and that, most notably, microglial cells assumed a phenotype similar to DAM (Keren-Shaul et al., 2017). AMX treatment was ultimately found to lead to a larger astrocytic scar after injury.

MATERIALS AND METHODS

Animals

Male mice originated from the breeding of wild-type male and female B6SJL/F1 mice (from Jackson labs[1]) were used

[1]https://www.jax.org/strain/100012

for the present study at the age of 55–65 days. Mice were maintained at 22°C with a 12/12 h light/dark cycle and had food and water *ad libitum* as previously reported (Alami et al., 2020). The present study has been authorized by Ulm University Animal Experimentation oversight service and by the Regierungspräsidium Tübingen under the permit no. 1379; the study has been performed in agreement with the national animal welfare legislation. In order to minimize confounding factors deriving from oestrus cycle and fluctuating levels of hormones, we employed only male mice for this study.

Stab Wound Injury

The stab wound injury (SWI) was performed as previously reported (Frik et al., 2018; Wiesner et al., 2018). Briefly, 60 days old mice were anesthetized with an intraperitoneal injection of midazolam, medetomidine, and fentanyl (5 mg/kg; 0.5 mg/kg; 0.05 mg/kg). A unilateral craniotomy was performed 1 mm above bregma and 1 mm ventral the cranial sutures ($x = +1.0$, $y = +1.0$). The blade was inserted into the primary motor cortex up to a depth of 0.8 mm ($z = -0.8$) and moved 1 mm in the dorsal direction. Three parallel stab-injuries were performed with a gap of 0.2 mm; this gap was chosen so that the three injuries would actually form a single lesion area. Afterward the craniotomy was covered and anesthesia was antagonized with atipamezole-flumazenil-buprenorphine-injection (2.5 mg/kg; 0.5 mg/kg; 0.1 mg/kg). Animals were monitored daily for the appearance of motor impairment, but no mouse displayed disturbances requiring humane euthanization. The health status of the animals was monitored twice daily after the procedure and until the end of the experiment. If any animal had shown severe weight loss (>20%), motor impairment, hunched posture, apathy or other signs of permanent impairment related to the procedure, it would have been removed from the experiment and killed painlessly; no animal was actually euthanized because of discomfort. Starting from the day of injury, mice were treated with 100 mg/kg Amlexanox or vehicle (5% PEG400; 5% Tween20; 90% NaCl 0.9%) administered by oral gavage for 7 consecutive days, once daily. The first treatment with Amlexanox (AMX) or vehicle by oral gavage was given 2 h after surgery and then daily (every 24 h). Mice were either sacrificed 7 or 40 days after the trauma.

For the biochemical analysis, animals were sacrificed by cervical dislocation, the brain was extracted and 1.5 mm-diameter cortex biopsies from the injured region (or from the control primary motor cortex) were obtained, sealed in 1.5 ml eppendorf tubes, and frozen in liquid nitrogen. For histological analysis, animals were deeply anesthetized with 1 mg/kg body weight ketamine chlorhydrate and 0.5 mg/kg body weight xylazine, and transcardially perfused with 1.5 ml/g of ice-cold PBS and then with 1.5 ml/g of 4% paraformaldehyde in 0.1M pH 7.4 phosphate buffer. Brains were thereafter dissected out, post-fixed for 24 h in 4% paraformaldehyde, and cryoprotected for 48 h with 30% sucrose in PBS before being embedded in Optimum Cutting Temperature (OCT) sectioning medium. Upon cryostat sectioning (40 μm thickness), sections were collected from 0.75 mm caudally to the bregma until 1.75 mm rostrally to the bregma, spanning the injury site. Only sections corresponding to the middle part of the injury site were considered, once those with obvious artifacts had been discarded.

Real Time (RT)- Quantitative Polymerase Chain Reaction (qPCR)

RNA was isolated from the ipsilateral and contralateral cortical samples using the ISOLATE II RNA/DNA/Protein Kit (Bioline) according to the manufacturer's instruction. Reverse transcription was performed with 0.75μg RNA using reverse transcriptase (Promega), RNase Inhibitor (RiboLock, Thermo Scientific), dNTPs (Genaxxon), and random hexamers (Biomers). qPCR was performed on the LightCycler 480II (Roche) with the Power PCR SYBR green PCR master mix (Takara). 2 μl of cDNA was used in a total volume of 10 μl (3 μl primer mix and 5 μl of SYBR green) in a 96-well plate. The following parameters were used for the amplification: Holding stage :95°C (30 s).

$$\text{Cycling stage (40 cyles)}: \ 95^{\circ}\text{C (5 s)} \rightarrow 60^{\circ}\text{C (20 s)};$$

$$\text{melt curve stage}: \ 95^{\circ}\text{C (10 s)} \rightarrow 60^{\circ}\text{C (60 s)};$$

clooldown:hold 4°C. Samples were duplicated and the housekeeping gene GAPDH was used as a control (for the cytokine primer sequences see **Supplementary Table 1**). Data were analyzed using the Cycler software and normalized to the normalization factor according to the following equation: 2-ΔCt (ΔCt = Cttarget gene—CtGapdh) = relative mRNA.

Western Blotting

Protein lysates were prepared using Radioimmunoprecipitation assay (RIPA) buffer (150 mM NaCl, 10 mM Tris pH 7,6, 0,1% SDS, 1% Triton X-100, 5 mM EDTA). Protease (Roche) and phosphatase inhibitors (Sigma Aldrich) were added to the buffer. Protein concentrations in the samples were determined using the BiCinchoninic Acid (BCA) assay kit (Thermo Fisher Scientific). The Protein samples (30 μg) were then run on an 10% gel for 2 h at 60V and transferred to a nitrocellulose membrane using semidry blotting method (Ouali-Alami et al., 2020). The membranes were blocked for 1 h at room temperature with 5% skim milk powder or 5% BSA dissolved in Tris-Buffered Saline-Tween (TBS-T), followed by an overnight incubation of primary antibodies at 4°C: rabbit anti NAK/TBK1, 1:2,000 (Abcam); rabbit anti NAK/TBK1 (Ser 172), 1:2,000 (Abcam); mouse anti-β-Actin, 1:5,000 (CST); rabbit anti SQSTM1/p62, 1:2,000 (Abcam); rabbit anti phospho-SQSTM1/p62 (Ser403), 1:1,000 (GeneTex); rabbit anti STING, 1:1,000 (Cell signaling); rabbit anti phospho-STING (Ser365), 1:1,000 (Cell signaling), mouse anti PSD95, 1:1,200 (abcam) rabbit anti NR1, 1:1,000 (Sigma). The blots were then incubated in a secondary goat conjugated IgG-HRP antibody (rabbit, mouse, or rat; depending on the primary host) for 1 h at RT. The blots were visualized (Enhanced chemiluminescence; ECL-immunodetection) using BIORAD ImageLab (duration of exposure time 1–20 s). Samples were corrected for background and quantified using BIORAD Image Lab Software®5.0, following manufacturer's procedures. All values were normalized first to the housekeeping genes

(β-actin) and then to their respective total protein. The list of material used has been summarized in **Supplementary Table 2**.

Immunohistochemistry

Free-floating sections were blocked for 2 h at RT in 3% BSA and 0.3% Triton in Phosphate-buffered saline (PBS) and incubated with primary antibodies [rabbit anti-TMEM119; 1:100 (Abcam), mouse anti-CD11c; 1:100 (Abcam), rat anti-CD169; 1:200 (BioLegend) rabbit anti-CD3; 1:100 (Abcam), mouse anti-CD45; 1:500 (BD biosciences), mouse anti-CD68; 1:500 (Abcam), mouse anti-CD317; 1:100 (R&D Systems), mouse anti-CS-56; 1:200 (Abcam), rat anti-GFAP; 1:200 (Thermo Fisher Scientific)], mouse anti-NeuN; 1:100 (Millipore), for 48 h at 4°C. Sections were washed for 3 × 30 min in PBS and incubated for 2 h at RT with secondary antibodies [Donkey anti-mouse 568, 1:500 (Invitrogen); Donkey anti-rat 488, 1:500 (Invitrogen); Donkey anti-rabbit 568, 1:500 (Invitrogen)]; Donkey anti-mouse 647, 1:1,000 (Invitrogen) together with DAPI (1:1,000). After a second round of washing (3 × 30 min in PBS), sections were mounted with Fluorogold prolong antifade mounting medium (Invitrogen). The list of material used has been summarized in **Supplementary Table 2**.

Image Analysis

The images (2 × 2 tile) were acquired in 1024 × 1024 pixel 12-bit format, using a Leica DMi8 microscope, equipped with an ACS APO 40x oil objective. Imaging parameters were set to obtain signals from the stained antibody while avoiding saturation. To avoid fluorescence cross-bleed, all fluorescent channels were acquired independently. All experiments included 3 animals per group with 4 brain sections each, sampling the stab injury site, were imaged. Confocal stacks (20 optical sections each) were collapsed in maximum intensity projection pictures. For quantification of $TMEM119^+$, $CD11c^+$, $CD3^+$, $CD45^+$, $CD68^+$, $CD317^+$, $CD169^+$, and $NeuN^+$ cells, images were subjected to thresholding (based on the histogram of the images, with a value cutting off the lower 20% of pixels) with the sole purpose of objectively identifying "positive" from "negative" cells, and a region of interest of 2×10^4 μm^2 located at the injury site was selected. The ROI was positioned on the axis of the injury stab at a constant distance from the pial surface, chosen so that the ROI is located within layer II–III.

In the region of interest, the absolute number of cells (each cell identified by the presence of a DAPI-positive nucleus) was manually counted and recorded for statistical analysis; we defined as "cell density" the number of cells per area unit. For quantification of CS-56 and GFAP images were subjected to thresholding but, in contrast to the counts of microglial cells, the cumulative positive area above the threshold was calculated (this considering the scar area as the ultimate readout, irrespective of the number of astrocytes composing it).

Statistical Procedures

All datasets were tested for normality by the Shapiro-Wilk test. Outliers were screened by the ROUT algorythm with Q set at 1%. No outlier was identified or eliminated during the data analysis. For statistical analysis, one-way ANOVA was used for comparing mean values that were considered significantly different. For analysis of TMEM 119, CD169, and CD11c cells, one-way ANOVA was used when the factors treatment (vehicle, AMX) vs. injury (sham, TBI) were compared. Tukey's *post hoc* comparison was applied to take into account the multiple comparisons. Data are presented either as the standard error of the mean (SEM) or mean standard deviation (SD). Graph Prism software (GraphPad Software Inc.) was used to perform statistical analysis. Detailed statistics for each experiment are reported in **Supplementary Tables 2–10**. The evaluation of the images and of expression data was performed by two experiments (RR and LT), whereas the treatment was performed by an independent experiment (DW). The experiments involved in the analysis were blind to the treatment group but were not blind to the presence/absence of injury, since the lesion is obvious in the microscopy images.

RESULTS

Amlexanox Inhibits the Phosphorylation of Tbk1 Substrates in the Brain

We set out to demonstrate target engagement by AMX, by verifying that downstream substrates of Tbk1/IKK-ε were down-phosphorylated upon inhibitor treatment (**Figure 1**). Tbk1/IKK-ε sport a very large set of substrates (Kim et al., 2013), many of which relevant to inflammation and aging. We consider only a small subset of them to confirm that AMX was penetrating the brain parenchyma in concentrations sufficient to significantly block Tbk1/IKK-ε activity. First, we considered the total levels of Stimulator of Interferon Genes (STING) protein and of STING phosphorylated on Ser366 (pSTING), a site specifically targeted by Tbk1 (Liu et al., 2015). pSTING (S366) showed a trend toward reduced levels in AMX treated mice (subject to sham surgery or Stab Wound Injury; SWI) (**Figures 1A,B**). Importantly, total levels of STING were substantially increased by the AMX treatment (irrespective of the injury status; **Figures 1A,C**; VH Sham vs. AMX Sham: $p = 0.0017$, VH Sham vs. AMX SWI: $p = 0.0008$, VH SWI vs. AMX Sham: $p = 0.0293$, VH SWI vs. AMX SWI: $p = 0.0122$), in agreement with the role of Tbk1 in stimulating STING degradation (Prabakaran et al., 2018). Overall, the fraction of phosphorylated STING was decreased to less than 50% of baseline (vehicle-treated, sham surgery mice) upon AMX treatment (**Figure 1D**; VH Sham vs. AMX Sham: $p = 0.0028$, VH SWI vs. AMX SWI: $p = 0.0090$). Second, we monitored the total levels of p62 and the levels of p62 phosphorylated on S403 (phospho-p62), which is another typical phosphorylation target of Tbk1 (Matsumoto et al., 2015). We observed in AMX treated mice a significant decrease in phospho-p62 levels (**Figures 1E,F**) while observing at the same an increase in total p62 levels (**Figures 1E,G**), corresponding to the substantial decrease in the fraction of the total pool of p62 phosphorylated on S403, confirming the effective blockade of p62 phosphorylation and its degradation upon AMX treatment (**Figures 1E,H**; VH Sham vs. VH SWI: $p = 0.0178$, VH Sham vs. AMX Sham: $p < 0.0001$, VH Sham vs. AMX SWI: $p < 0.0001$, VH SWI vs. AMX Sham: $p < 0.0001$, VH SWI vs. AMX SWI: $p < 0.0001$).

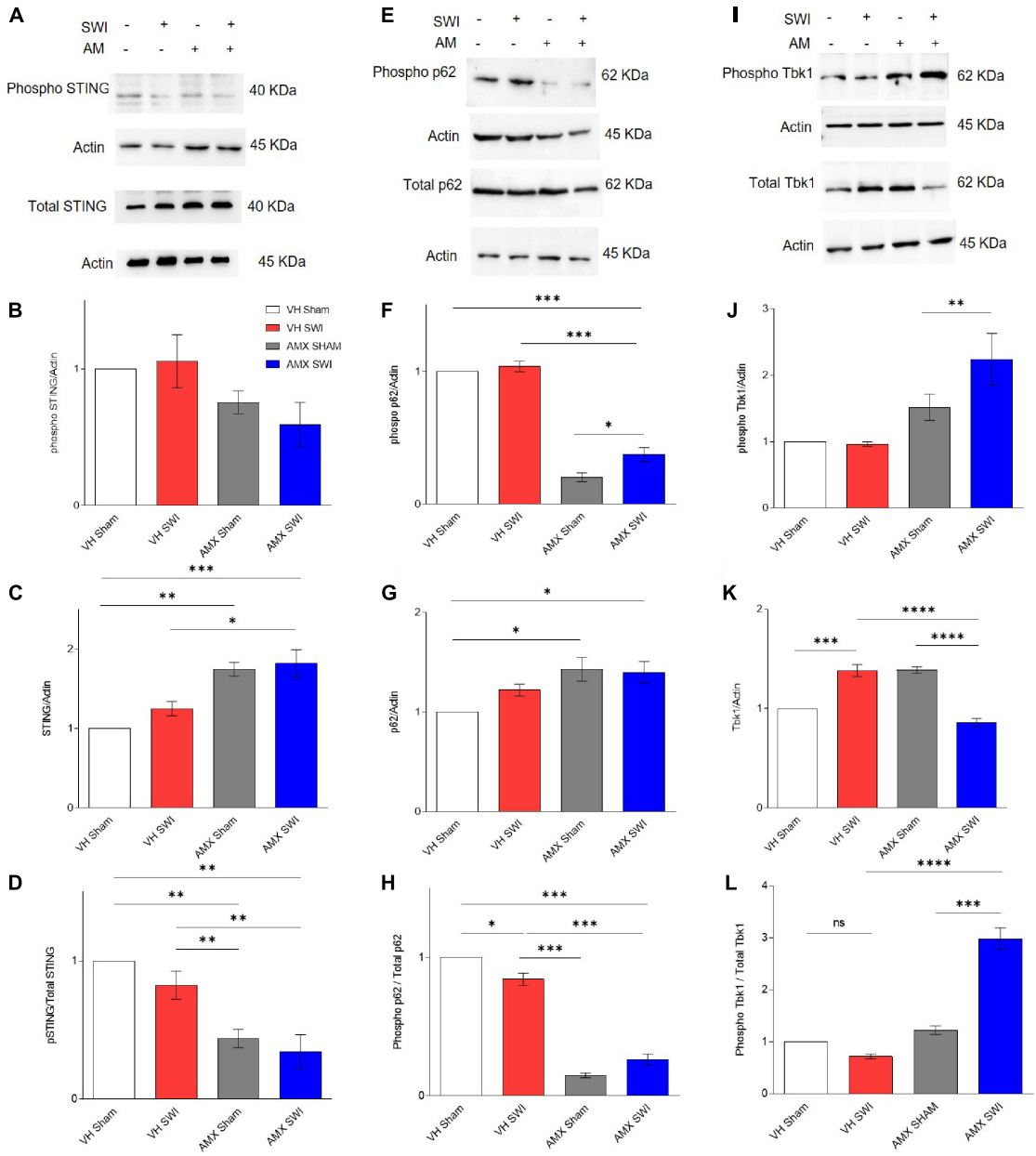

FIGURE 1 | Amlexanox (AMX) reduces the phosphorylation of Tbk1 targets STING and p62 upon Stab Wound Injury (SWI). Western blots of cortical biopsies (at 7 dpi) homogenates show trend toward decreased levels of phospho STING **(A,B)** but an increase in total STING levels **(A,C)**, resulting in a significant decrease in the fraction of phosphorylated STING **(D)**. Likewise, levels of phospho p62 **(E,F)** were significantly decreased the AMX treatment (irrespective of SWI) whereas the total amount of p62 was slightly increased **(E,G)**, resulting in a substantial decrease in the fraction of phosphorylated p62 in the overall p62 pool **(H)**. Levels of phosphorylated Tbk1 were strongly increased in AMX-SWI samples **(I,J)** whereas total levels of Tbk1 were reduced in these samples (but slightly increased by AMX or SWI alone) **(K)**, resulting in a massive increase in the fraction of phosphorylated Tbk1 in the Tbk1 pool in AMX-SWI samples **(L)**. $n = 3$ animals/group. Average ± SEM; one-way ANOVA ns: not significant, $^{*}p < 0.05$, $^{**}p < 0.01$, $^{***}p < 0.001$, $^{****}p < 0.0001$; full statistical report in **Supplementary Table 3**; original full uncropped WB in **Supplementary File 1**.

Levels of phosphorylated Tbk1 were not upregulated upon SWI in vehicle-treated mice (**Figures 1I,J**) but were significantly increased by AMX treatment, and even further in AMX-SWI samples (**Figures 1I,J**). Interesting, total Tbk1 levels were upregulated by SWI in vehicle-treated mice as well as in AMX-treated sham animals, but were downregulated in SWI-AMX samples (**Figures 1I,K**; VH Sham vs. VH SWI: $p = 0.0006$, VH Sham vs. AMX Sham: $p = 0.0006$, VH SWI vs. AMX SWI: $p < 0.0001$, AMX Sham vs. AMX SWI: $p < 0.0001$). However, the ratio of phospho Tbk1/total Tbk1 was actually increased in presence of AMX (indicating that a larger fraction of Tbk1 was actually phosphorylated

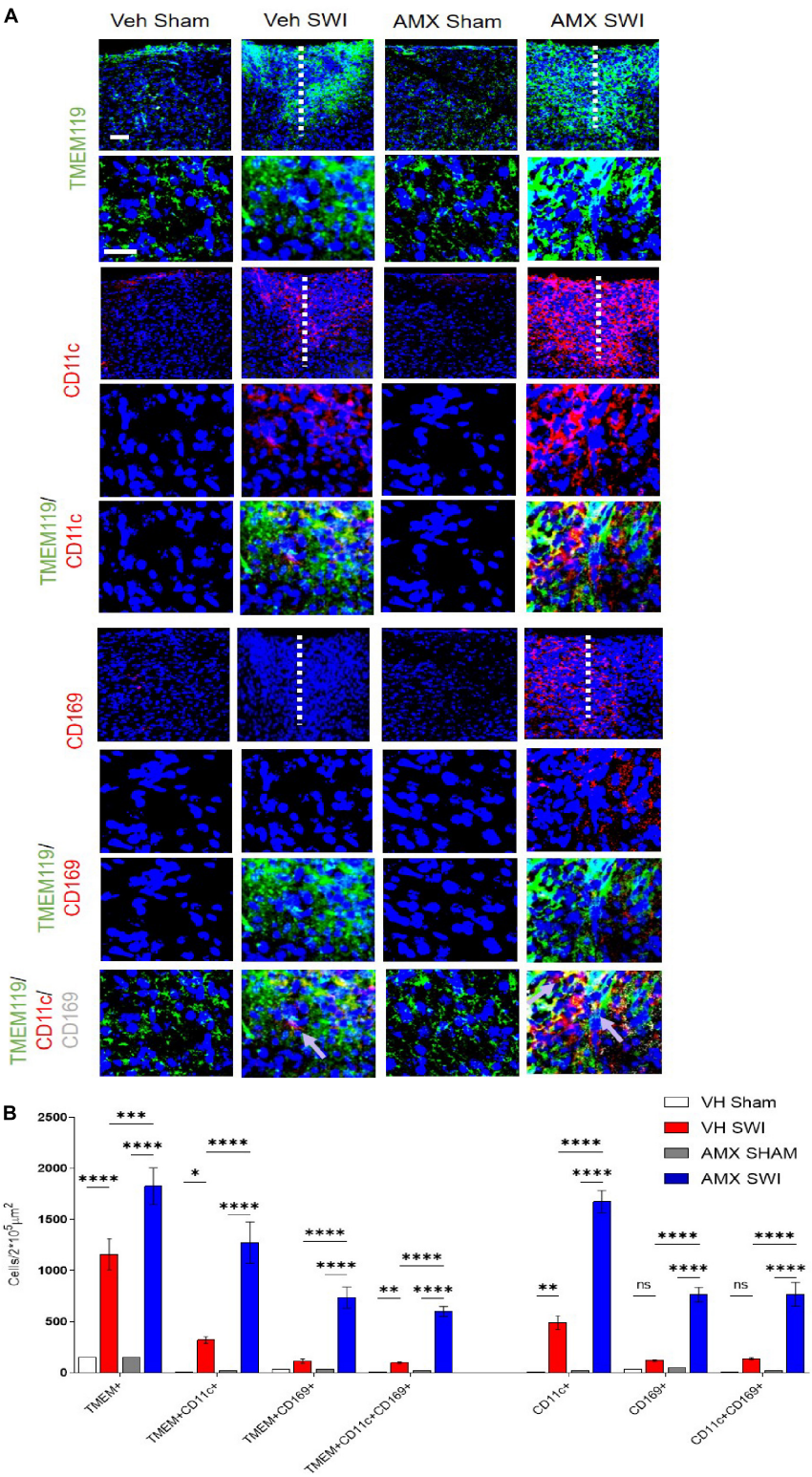

FIGURE 2 | Tbk1 blockade enhances the induction of CD11c$^+$ and CD169$^+$ microglia upon Stab Wound Injury (SWI). **(A,B)** AMX treatment caused the significant elevation in TMEM119$^+$ microglial cells in the SWI injury site at 7 dpi. Co-immunostaining with makers of microglial subsets CD11c and CD169 revealed the massive expansion of CD11c$^+$ microglia (disease associated microglia; DAM) as well as reactive CD11c$^+$/CD169$^+$ microglia. ($n = 3$ animals/group with 4 sections/animal. Average ± SD; one-way ANOVA with Tukey's post hoc; ns: not significant, *$p < 0.05$, **$p < 0.01$, ***$p < 0.001$, ****$p < 0.0001$; full statistical analysis in **Supplementary Table 4**). Upper panel, low magnification; lower panel, high magnification. Scale bars (equal for both sets of panels) 200 µm.

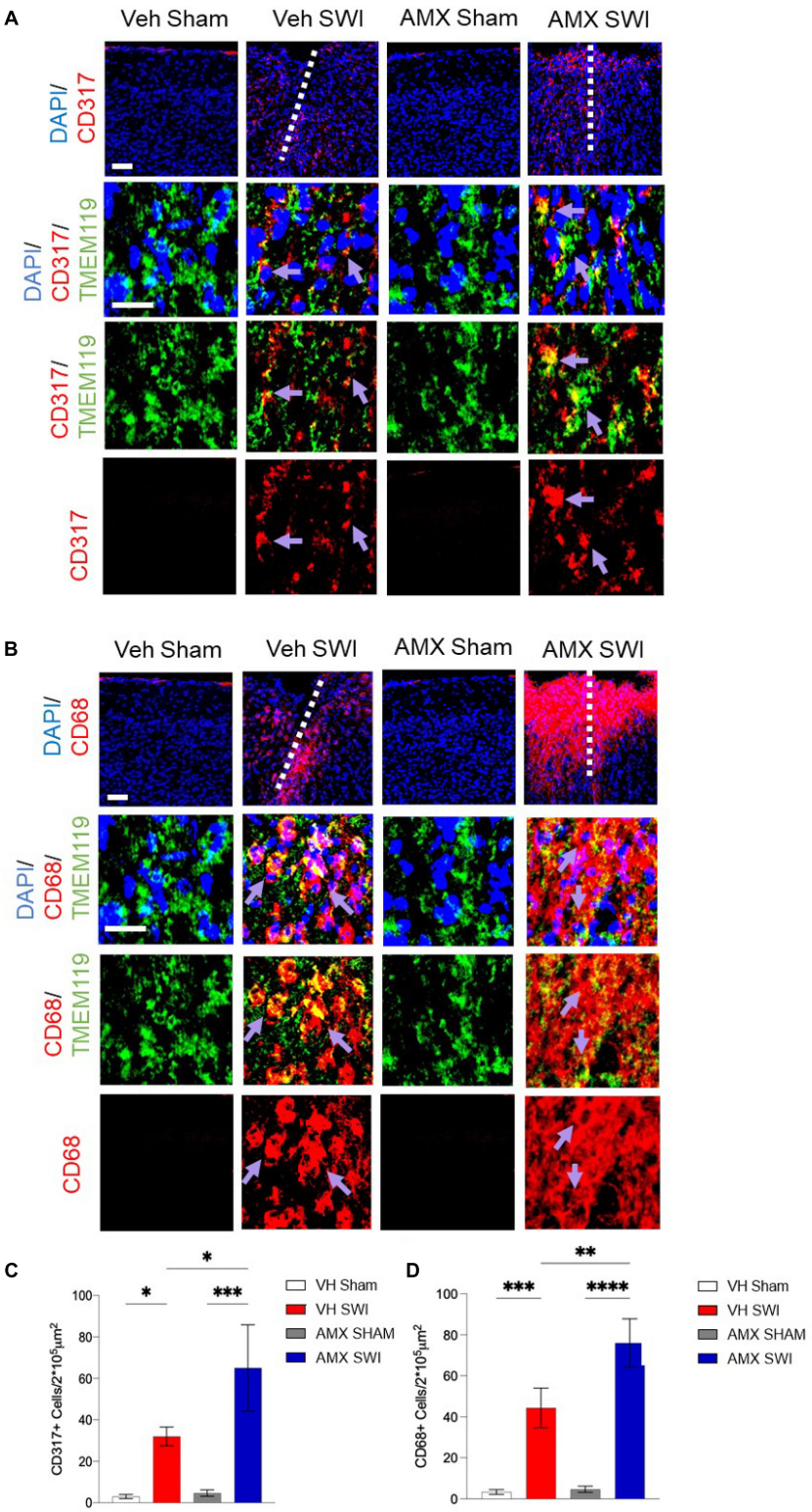

FIGURE 3 | Tbk1 blockade enhances the induction of CD317^{+} interferon-stimulated microglia and CD68^{+} phagocytic microglia. **(A,C)** AMX treatment substantially increased the number of microglia TMEM119^{+} that expressed the interferon-induced CD317 marker upon SWI (at 7 dpi). **(B,D)** AMX upregulated the expression of the phagocytosis marker CD68 in TMEM119^{+} microglia upon SWI. ($n = 3$ animals/group with 4 sections/animal. Average ± SD; two-way ANOVA with Tukey's *post hoc*; *$p < 0.05$, **$p < 0.01$ ***$p < 0.001$, ****$P < 0.0001$; full statistical report in **Supplementary Table 5**). Upper panel, low magnification; lower panels, insets at high magnification. Scale bars (equal for both sets of panels) 200 µm.

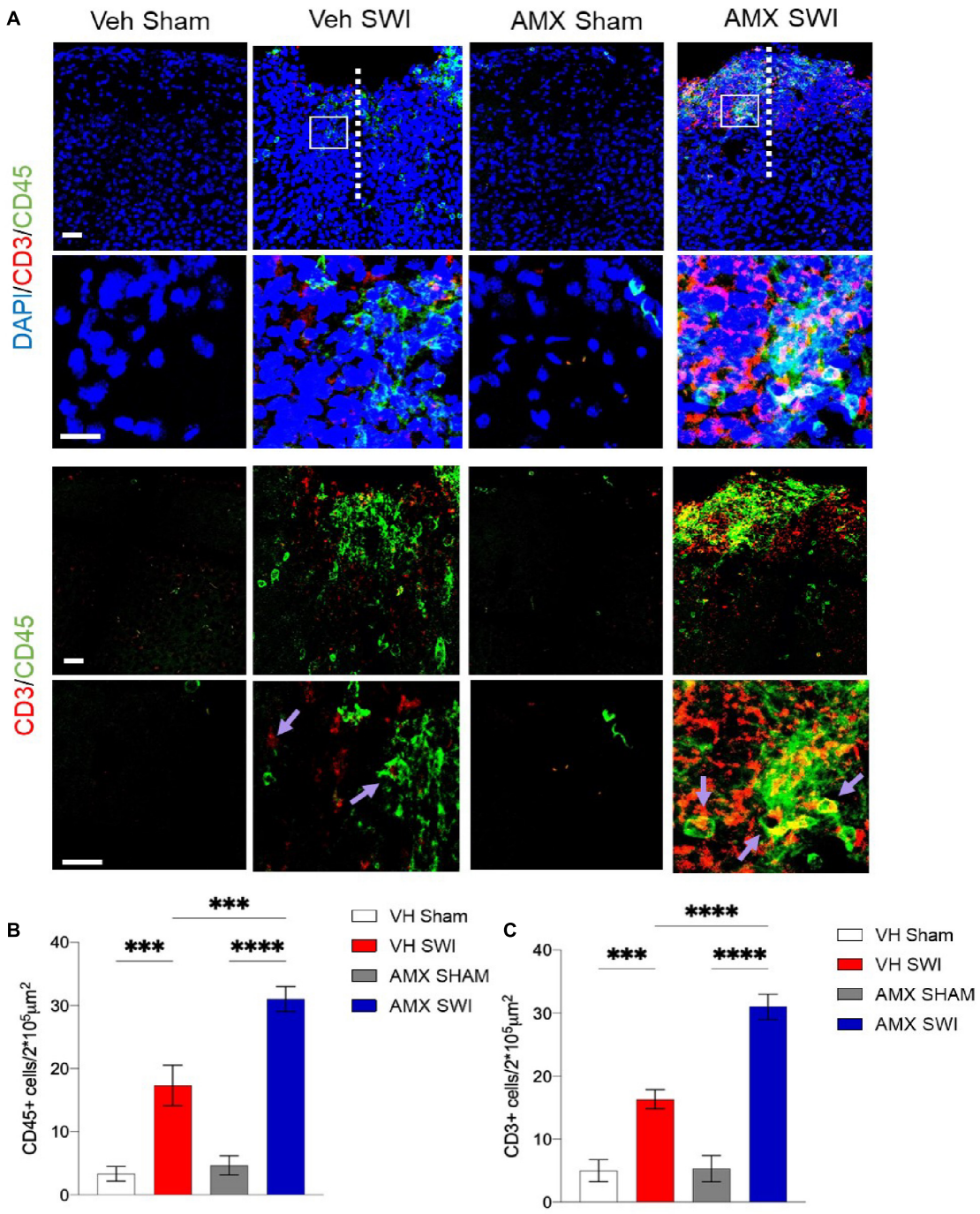

FIGURE 4 | Tbk1 blockade enhances infiltration of the Stab Wound Injury (SWI) by peripheral immune cells. **(A)** In AMX-treated animals (at 7 dpi), the SWI site displayed a substantial increase in the density of CD45-bright cells including peripheral leukocytes; quantified in **(B)** and lymphocytes $CD3^+$ cells; quantified in **(C)**; average ± SD; two-way ANOVA with Tukey's *post hoc* ($n = 3$ animals/group with 4 sections/animal. $^{***}p < 0.001$, $^{****}p < 0.0001$; full statistical report in **Supplementary Table 6**). Upper panel, low magnification; insets at high magnification. Scale bars (both sets of panels) 200 µm.

despite the decrease in total protein level) and in particular in AMX-SWI samples (**Figures 1I,L**; VH SWI vs. AMX Sham: $p < 0.0001$, VH SWI vs. AMX SWI: $p < 0.0001$, AMX SHAM vs. AMX SWI: $p < 0.0001$), suggesting that even if the autophosphorylation ability of Tbk1 dimers is suppressed, other upstream kinases can still phosphorylate Tbk1 (Clark et al., 2009) and that although reduced in total quantity, remaining Tbk1 is heavily phosphorylated. Taken together, these data show that a substantial inhibition of the Tbk1 pathway takes place in the brain upon systemic AMX treatment,indicating a substantial

penetration of the brain by the drug and providing proof of target engagement.

Tbk1 Inhibition Drives the Massive Expansion of CD11c$^+$ Disease-Associated Microglia and the Infiltration of Peripheral Immune Cells Upon SWI

Next, we set out to evaluate the effect of Tbk1/IKK-ε inhibition by AMX on the microglial response triggered by SW injury (SWI). This injury model was chosen because of its very high reproducibility in terms of injury severity and location, and because of its established role for the study of microglial and astroglial responses to injury. Mice subject to SWI were treated with either vehicle or AMX (100 mg/kg) daily and were sacrificed at 7 dpi. Microglial cells were identified by TMEM119 immunostaining (Bennett et al., 2016). We also took into consideration two subpopulations of microglia: TMEM 119$^+$/CD11c$^+$ cells (compatible with disease-associated microglia, DAM; Keren-Shaul et al., 2017) and TMEM119$^+$/CD169$^+$ cells (reactive microglia; Bogie et al., 2018). In sham-operated animals, the density of microglial cells and their subpopulations were comparable in vehicle- and AMX-treated mice. When compared to sham mice, SWI caused in vehicle-treated mice a strong increase in the number of TMEM119$^+$ microglial cells in the region surrounding the injury site. Remarkably, in SWI mice treated with AMX, the microglial density was substantially larger than in vehicle-treated mice (**Figure 2**; VH Sham vs. VH SWI, VH Sham vs. AMX SWI, AMX Sham vs. VH SWI, AMX Sham vs. AMX SWI: $p < 0.0001$, VH SWI vs. AMX SWI: $p = 0.0006$). Remarkably, TMEM 119$^+$/CD11c$^+$ microglia (almost undetectable in sham animals), represented only a small fraction of total microglial cells in SWI-injured mice but were more than fourfold more abundant in SWI mice treated with AMX (**Figure 2**; VH Sham vs. VH SWI: $p = 0.0216$, VH Sham vs. AMX SWI: $p < 0.0001$, AMX Sham vs. VH SWI: $p = 0.0287$, AMX Sham vs. AMX SWI: $p < 0.0001$, VH SWI vs. AMX SWI: $p < 0.0001$).

Furthermore, we detected a massive (almost eightfold) increase in the number of TMEM119$^+$/CD169$^+$ cells in mice subject to SWI and treated with AMX (compared to SWI mice treated with vehicle; **Figure 2**; VH Sham vs. AMX SWI: $p < 0.0001$, AMX Sham vs. AMX SWI: $p < 0.0001$, VH SWI vs. AMX SWI: $p < 0.0001$). Interestingly, almost all TMEM119$^+$/CD169$^+$ cells (representing about one-third of the total TMEM119$^+$ population) were also CD11c$^+$ (although the opposite was not true, and almost one-half of TMEM119$^+$/CD11c$^+$ cells were CD169-), suggesting that a distinct TMEM119$^+$ /CD11c$^+$/CD169$^+$ phenotype was induced by AMX treatment.

We further explored the diversity of the microglial response triggered by SWI injury under AMX treatment by taking into consideration the activation marker (Ajami et al., 2018; Olde Heuvel et al., 2019) and interferon-activated (Polyak et al., 2013) gene CD317. CD317 is expressed at a very low level (as detected by immunohistological techniques) in microglia in sham-treated mice or even in vehicle-treated SWI mice (**Figure 3A**; VH Sham vs. VH SWI: $p = 0.0421$, VH Sham vs. AMX SWI: $p = 0.0005$, VH SWI vs. AMX SWI: $p = 0.0223$, AMX Sham vs. AMX SWI: $p = 0.0006$). However, the density of TMEM119$^+$CD317$^+$ cells was substantially increased in AMX-SWI mice, indicating the interferon-driven massive activation of microglial cells (**Figure 3C**). Moreover, a minor fraction of microglial cells in the injury site in vehicle-treated mice were positive for the DAM marker CD68, but their number was significantly larger in AMX-treated SWI mice, representing the majority of TMEM119$^+$ cells (**Figures 3B,D**; VH Sham vs. VH SWI: $p = 0.0008$, VH Sham vs. AMX SWI: $p < 0.0001$, VH SWI vs. AMX Sham: $p = 0.001$, VH SWI vs. AMX SWI: $p = 0.0044$, AMX Sham vs. AMX SWI: $p < 0.0001$).

Finally, AMX treatment upon SWI also resulted in a significant increase (compared to SWI followed by vehicle administration) in TMEM119-/CD11c$^+$ or TMEM119-/CD169$^+$ cells, indicating that, besides the massive expansion of DAM-like microglia and triple-positive microglia, AMX treatment also resulted in a substantial increase in recruitment of peripheral immune cells such as dendritic cells and monocytes/macrophages (**Figure 2**). We further explored this aspect by assessing the number of peripheral leukocytes and the number of lymphocytes infiltrating the site of injury. In line with the CD169 and CD11c data, we found that the SWI contained very few CD45$^+$ bright cells at 7 dpi (**Figures 4A,B**; VH Sham vs. VH SWI, $p = 0.0002$, VH Sham vs. AMX SWI: $p < 0.0001$, VH SWI vs. AMX Sham: $p = 0.0004$, VH SWI vs. AMX SWI: $p = 0.0002$, AMX Sham vs. AMX SWI: $p < 0.0001$), and almost no CD3$^+$ lymphocyte in vehicle-treated mice (**Figures 4A,C**; VH Sham vs. VH SWI, $p = 0.0003$, VH Sham vs. AMX SWI: $p < 0.0001$, VH SWI vs. AMX Sham: $p = 0.0004$, VH SW vs. AMX SWI: $p < 0.0001$, AMX Sham vs. AMX SWI: $p < 0.0001$) (sham mice displayed almost no CD45$^+$ or CD3$^+$ cell, irrespective of treatment), but their number was substantially higher in the injury site of AMX-treated mice (**Figure 4**).

Tbk1 Inhibition by AMX Induces a Disease-Associated Microglia-Like Transcriptional Profile Upon SWI

To confirm and expand the characterization of the microglia phenotype observed upon SWI and AMX treatment, we performed targeted transcriptional profiling of the cortical samples at 7 dpi. First, we considered a set of genes characteristically upregulated (Cst7; Lpl; Clec7a; Ccl3; Ccl4; Prgn; Csf1; Tlr4; Il13; Trem2) or downregulated (Tmem119; P2ry12; Cx3cl1; Csf1r) in DAM (Keren-Shaul et al., 2017; Krasemann et al., 2017). Notably, the expression of the DAM-associated genes Cst7 (**Figure 5A**; VH Sham vs. VH SWI: $p = 0.0026$), Clec7a (**Figure 5B**; VH Sham vs. VH SWI: $p = 0.0003$), Ccl4 (**Figure 5C**; VH Sham vs. VH SWI: $p < 0.0001$), Prgn (**Figure 5D**; VH Sham vs. VH SWI: $p = 0.023$), and Ccl3 (**Figure 5E**; VH Sham vs. VH SWI: $p < 0.0001$) was modestly upregulated by SWI in vehicle-treated mice (compared to sham controls). In AMX treated mice, expression of Cst7 (**Figure 5A**; VH SWI vs. AMX SWI: $p = 0.0026$), Lpl (**Figure 5F**; AMX

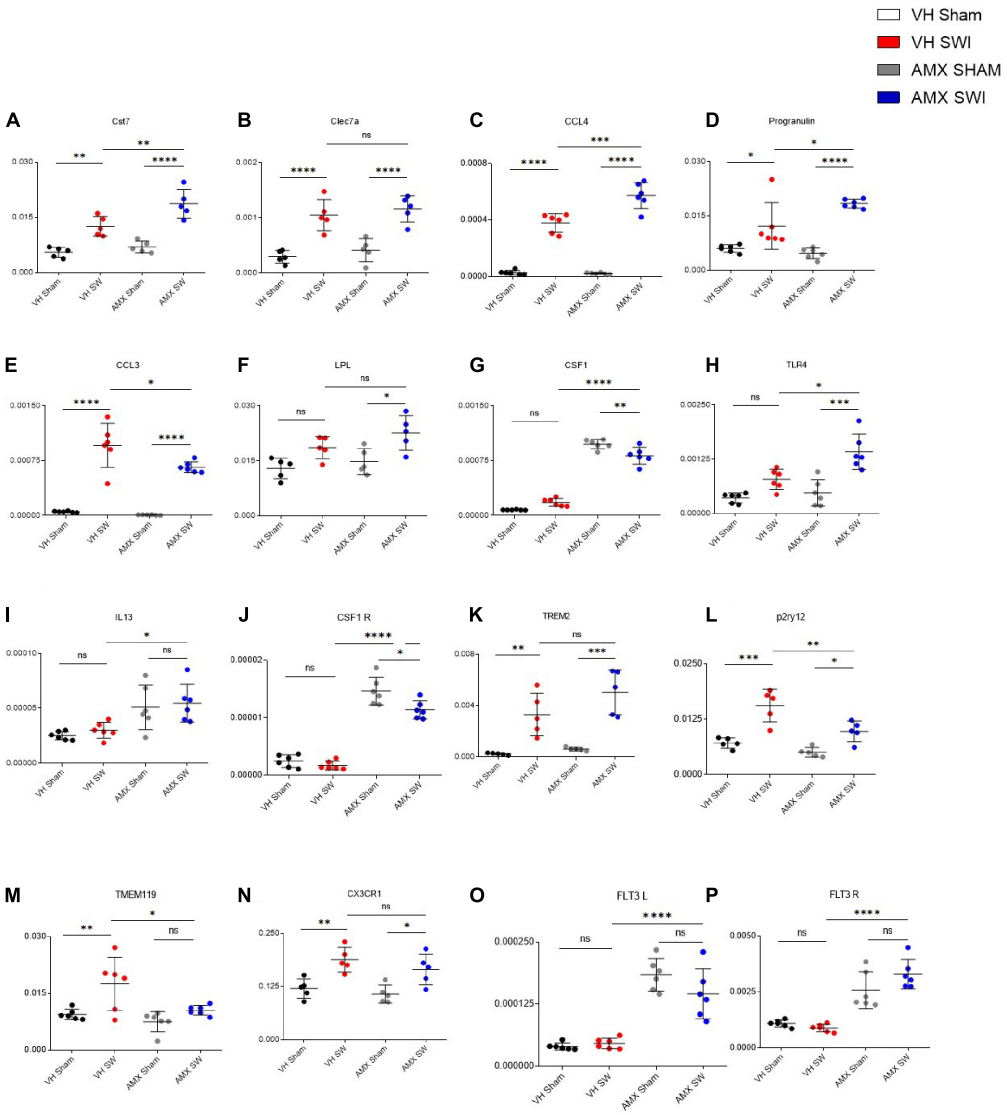

FIGURE 5 | Tbk1 blockade enhances the expression of genes associated with the Disease Associated Microglia (DAM) microglial phenotype after SWI. qPCR from whole-biopsy homogenates were obtained from the injury site (or the corresponding anatomical location in sham mice) from animals treated with either vehicle or AMX at 7 dpi. Among the DAM signature genes, upon SWI, AMX upregulated the expression of Cst7 **(A)**, CCL4 **(C)**, Progranulin **(D)**, CCL3 **(E)**, CSF1 **(G)**, TLR4 **(H)**, and IL-13 **(I)**. Among the genes characteristically downregulated in DAM, AMX substantially reduced the expression of P2ry12 **(L)** and TMEM119 **(M)**. Notably, AMX alone, with or without SWI, upregulated the expression of CSF1 **(G)**, CSF1R **(J)**, Flt3 **(O)** and Flt3R **(P)**. No difference in expression levels was observed upon SWI with or without inhibitor treatment in Clec7a **(B)**, LPL **(F)**, TREM2 **(K)**, and CX3CR1 **(N)**. ($n = 3$ animals/group with 4 sections/animal. Average ± SD, plus individual data points indicated; one-way ANOVA with Tukey post hoc; ns: not significant, $^{*}p < 0.05$, $^{**}p < 0.01$, $^{***}p < 0.001$, $^{****}p < 0.0001$; full statistical report in **Supplementary Table 7**).

SWI vs. AMX SWI: $p = 0.0164$), Ccl4 (**Figure 5C**; AMX SWI vs. AMX SWI: $p = 0.0003$), Prgn (**Figure 5D**; VH SWI vs. AMX SWI: $p = 0.0232$), Csf1 (**Figure 5G**; VH SWI vs. AMX SWI: $p < 0.0001$), Tlr4 (**Figure 5H**; VH SWI vs. AMX SWI: $p = 0.0049$), Il13 (**Figure 5I**; VH SWI vs. AMX SWI: $p = 0.0283$), and Csf1r (**Figure 5J**; VH SWI vs. AMX SWI: $p < 0.0001$) was substantially upregulated, and trends toward upregulation were seen for Trem2 (**Figure 5K**; AMX SWI vs. AMX SWI: $p = 0.0001$) (whereas Clec7a was not affected by AMX). Conversely, P2ry12 (**Figure 5L**; VH SWI vs. AMX SWI: $p = 0.0056$) and Tmem119 (**Figure 5M**; VH SWI vs. AMX SWI: $p = 0.0421$) were significantly downregulated and Cx3cr1 (**Figure 5N**; AMX SWI vs. AMX SWI: $p = 0.0217$) showed a trend toward downregulation (whereas Csf1r was upregulated). Thus, the genes up- and down-regulated by AMX treatment showed a strong resemblance with the expression fingerprint of DAM microglia, supporting the hypothesis that AMX enhances the induction of DAM-like cells upon SWI (since the transcriptional profile is not completely matching the DAM genome-wide characterization, we opt for the "DAM-like" definition). Of note, TMEM119 mRNA was downregulated in AMX-treated SWI mice but immunoreactivity for TMEM119 was still readily detectable

(**Figure 2**), in agreement with previous observations of persisting TMEM119 proteins when mRNA levels are reduced (Satoh et al., 2016; Krasemann et al., 2017).

Upon closer inspection, we noticed that a subset of genes (Il13, Csf1, Csf1r) was upregulated by AMX alone (in AMX-treated sham-operated mice, compared to vehicle-treated mice subject to either sham or SWI); actually, expression of Csf1r (**Figure 5J**) and Csf1 (**Figure 5G**) (inducers of $CD11c^+$ microglia; Wlodarczyk et al., 2019) was slightly decreased by AMX (while still being substantially higher than in vehicle controls). We further explored this apparent "priming" effect of AMX alone by assessing the expression of Flt3 (**Figure 5O**) and Flt3r (**Figure 5P**) (characteristic of $CD11c^+$ microglia (Immig et al., 2015). Most notably, AMX increased the expression of both Flt3 and Flt3r both in sham and SWI mice (compared to vehicle control), with the little additional effect of the injury.

Thus, Tbk1/IKK-ε blockade in SWI is associated with the upregulation of DAM-like transcriptional profiles (in agreement with the histological findings). Furthermore, Tbk1 blockade alone is sufficient to upregulate a few, but not all, genes associated with $CD11c^+$ microglia.

Tbk1/IKK-ε Inhibition Upregulates Inflammatory Cytokines but Downregulates Chemokines in the Cortex Subject to SWI

Having observed the massive upregulation of $CD11c^+$ microglia density and its gene expression profile, as well as the enhanced leukocytes and lymphocytes infiltration, in the injured cortex of mice treated with AMX, we further explored if these corresponded to a distinct neuroimmunological profile. To this aim, we assessed the expression of 12 inflammatory and immunomodulatory cytokines (Il-1b, Tnf-a, Il-33, Ifn-b, Il-6, Il-17, Il-12, Ifn-g, Il-18, Il-10, Il-19, Il-25) in cortical samples obtained at 7 dpi from mice treated with vehicle or AMX and subject to sham surgery or SWI (as above). Interestingly, AMX treated significantly upregulated Il-33 (**Figure 6A**; AMX Sham vs. AMX SWI: $p = 0.0034$) expression, whereas Il-1b (**Figure 6B**), Il-6 (**Figure 6C**), Il-18 (**Figure 6D**), and Il-25 (**Figure 6E**) were downregulated. Meanwhile, Tnf-a (**Figure 6F**; VH Sham vs. VH SWI: $p = 0.0119$), Il-6 (**Figure 6C**; VH Sham vs. VH SWI: $p = 0.0134$) (and, as trend only, Ifn-b; **Figure 6G**) were upregulated by SWI but unaffected by AMX. Most notably, when AMX was administered to SWI mice, it caused the massive elevation in lymphocyte-specific cytokines, such as Ifn-g (**Figure 6H**; VH SWI vs. AMX SWI: $p = 0.0005$), Il-17 (**Figure 6I**; VH SWI vs. AMX SWI: $p < 0.0001$), and Il-19 (**Figure 6J**; VH SWI vs. AMX SWI: $p = 0.0102$) (only trends were observed for Il-10; **Figure 6K**). Upon closer inspection, once again we detected a significant effect of AMX alone in elevating Il-17 (**Figure 6I**) and Il-12 (**Figure 6L**) expressions already in absence of SWI (Il-12 was then actually downregulated by SWI).

Finally, we explored if the altered cytokine profile, including pro- and anti-inflammatory changes, would affect the landscape of chemokines involved in regulating inflammation and chemotaxis. We assessed the expression of the C-C chemokines Ccl2 (**Figure 7A**), Ccl5 (**Figure 7B**), Ccl7 (**Figure 7C**), Ccl3 (**Figure 7D**), Ccl9 (**Figure 7E**), Ccl12 (**Figure 7F**) as well as the C-X-C chemokine Cxcl1 (**Figure 7G**) and the complement factor C3 (**Figure 7H**). Whereas all these mediators were upregulated by SWI (in vehicle-treated mice), AMX treatment exerted a mainly suppressive effect, resulting in the downregulation of Ccl3 (**Figure 7D**; VH SWI vs. AMX SWI: $p = 0.0162$), Ccl7 (**Figure 7C**; VH SWI vs. AMX SWI: $p = 0.0014$), Ccl12 (**Figure 7F**), and Ccl5 (**Figure 7B**; VH SWI vs. AMX SWI: $p < 0.0001$) (as a trend, also for Ccl9 and Ccl2; **Figure 7**). Surprisingly, Cxcl1 was strongly upregulated by AMX in SWI mice (**Figure 7G**) (C3 expression remained unaffected by AMX; **Figure 7H**). Thus, despite a substantial increase in inflammatory cells and microglia and the upregulation of inflammatory cytokines, AMX largely suppresses chemokine induction with the notable exception of Cxcl1 (which rather corresponds to the upregulation of Il-17).

The Expansion of $CD11c^+$ Microglia Is Reversed by AMX Withdrawal

Next, we explored if the AMX-induced altered expansion of $CD11c^+$ and $CD169^+$ microglial subpopulations would result in a persistent modification of the microglial populations. To this aim, we subjected mice to SWI (or sham), treated them with AMX or vehicle for 7 days but we sacrificed the mice at 40 days, after 33 days of AMX wash-out. We observed that microglial density was still significantly higher in the injury site of AMX-treated mice compared to vehicle-treated ones (**Figure 8A**; VH SWI vs. AMX SWI: $p = 0.0025$). However, the density of $TMEM119^+$ /$Cd11c^+$ cells and $TMEM119^+$/$CD11c^+$/$CD169^+$ cells was still higher than in vehicle treated mice, but showed a lower absolute value than at the 7 days timepoint (**Figure 8B**; TMEM119/CD11c: VH SWI vs. AMX SWI: $p = 0.0003$, TMEM119/CD169: VH SWI vs. AMX SWI: $p < 0.0001$). A similar situation was observed when the AMX treatment was prolonged for 21 days and the mice were sacrificed 20 days after the last dose. Thus, although the expansion of the microglial population caused by the AMX treatment may be persistent, the $CD11c^+$ and CD11c/$CD169^+$ phenotype may slowly vanish upon AMX withdrawal.

Treatment With Tbk1/IKK-ε Inhibitor Results in Increased Astrogliosis, Chondroitin-Sulfate Proteoglycans Deposition and Loss of Post-synaptic Proteins After SWI

Finally, we explored the consequences of the strongly enhanced DAM-like phenotype and lymphocyte infiltration caused by AMX in mice subject to SWI. First, we considered the extent of astroglial scarring (Förstner et al., 2018; Frik et al., 2018). We found that SWI induced a substantial increase in $GFAP^+$ astrocytes in and around the lesion site (Frik et al., 2018) at 7dpi, but also that astrogliosis was significantly increased in AMX-treated mice (**Figures 9A,D**; VH SWI vs. AMX SWI: $p = 0.0007$). Likewise, the deposition of glycosaminoglycans such

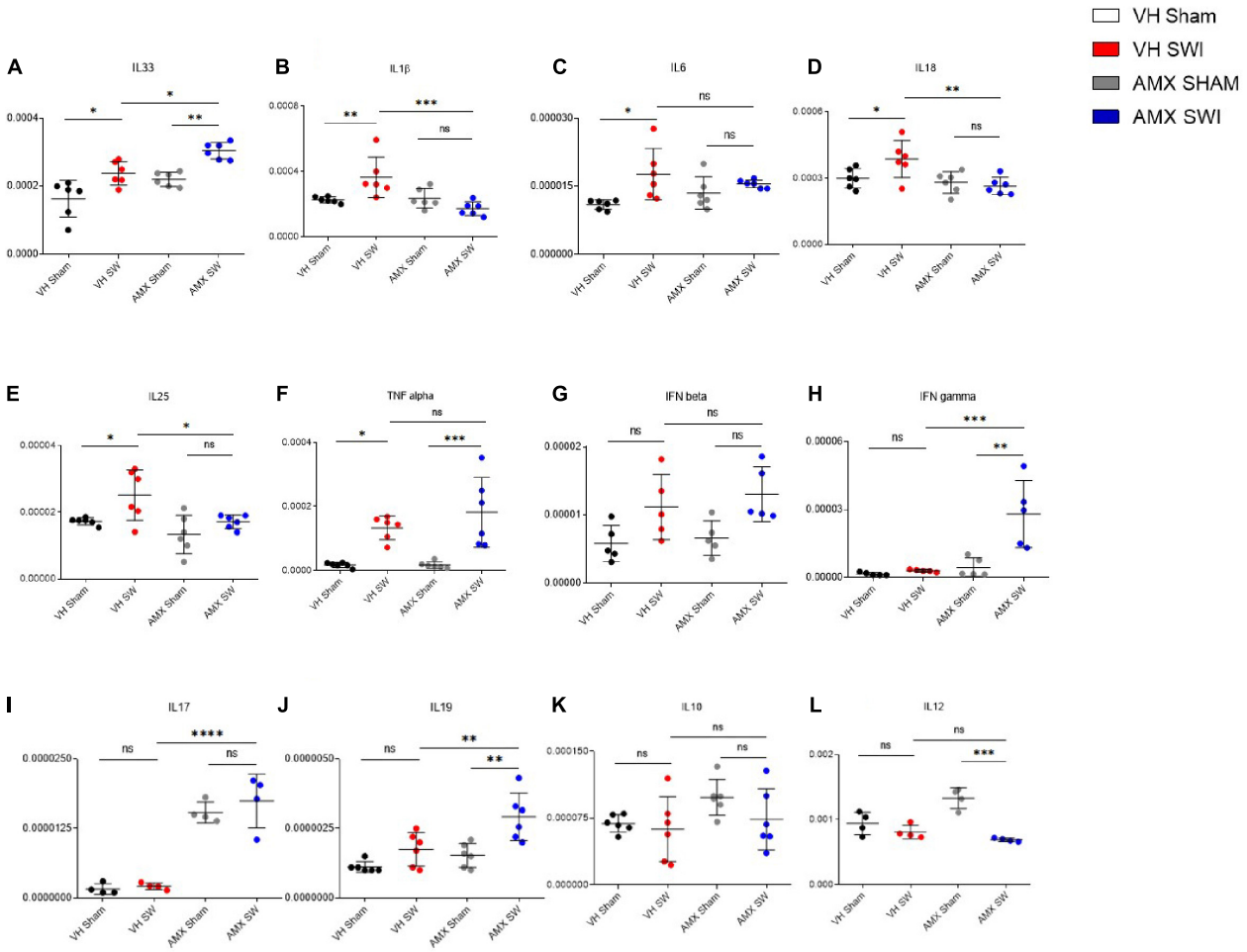

FIGURE 6 | Tbk1 blockade induces a distinct inflammatory cytokines profile upon Stab Wound Injury (SWI). qPCR from whole-biopsy homogenates were obtained from the injury site (or the corresponding anatomical location in sham mice) from animals treated with either vehicle or AMX at 7 dpi. AMX treatment after SWI significantly upregulated the expression of IL-33 **(A)**, IFN-γ **(H)**, IL-17 **(I)** and IL-19 **(J)**. Interestingly, AMX after SWI (7 dpi) also significantly reduced the expression of IL-1β **(B)**, IL-18 **(D)**, IL-25 **(E)**. Notably, AMX alone, irrespective of concomitant SWI, substantially increased the levels of IL-17 mRNA **(I)**. No difference in expression levels was observed upon SWI with or without inhibitor treatment in IL6 **(C)**, TNF alpha **(F)**, IFN beta **(G)**, IL10 **(K)**, and IL12 **(L)**. ($n = 3$ animals/group with 4 sections/animal. Average ± SD, plus individual data points indicated; two-way ANOVA with Tukey post hoc; ns: not significant, $^{*}p < 0.05$, $^{**}p < 0.01$, $^{***}p < 0.001$, $^{****}p < 0.0001$; full statistical report in **Supplementary Table 8**).

as in chondroitin sulfate proteoglycans (CSPG; as detected the immunostaining with CS56 antibody) was massively expanded in the lesion site of AMX-treated mice (**Figures 9B,E**; VH SWI vs. AMX SWI: $p = 0.0041$). Second, we considered the consequences of the DAM-like induction on neuronal and synaptic phenotypes. The number of $NeuN^{+}$ (neurons) cells per area unit was not significantly affected by the SWI, either in vehicle or in AMX-treated mice (**Figures 9C,F**). On the contrary, the amount of the marker of excitatory postsynaptic structures PSD-95 (assessed by WD in whole-cortical biopsy protein extract) decrease in AMX-sham but showed a trend toward being further decreased in AMX SWI samples (**Figures 9G,H**; VH Sham vs. AMX Sham: $p = 0.0018$, VH SWI vs. AMX SWI: $p = 0.0086$). Likewise, the NMDAR glutamate receptor subunit NR1 was reduced by AMX alone as well as in AMX-SWI samples (**Figures 9I,J**; VH Sham vs. AMX Sham: $p = 0.0028$, VH SWI vs. AMX SWI: $p = 0.0052$).

Thus, AMX treatment results in a substantial expansion of astroglial and CSPG scar and a significant loss of synaptic proteins, indicating an ultimately detrimental consequence of the enhanced microglial inflammation and leukocyte infiltration.

DISCUSSION

Our findings show that acute blockade of Tbk1/IKK-ε using the small molecule AMX determines a substantial shift in the neuroinflammation associated with SWI. We detected a massive enhancement in the number and reactivity of microglial cells with the appearance of large numbers of microglial cells with phenotype (defined DAM-like) strongly resembling the DAM described in Alzheimer's disease and other aging-associated neurodegenerative conditions. Furthermore, we observed a substantial increase in the infiltration of peripheral lymphocytes

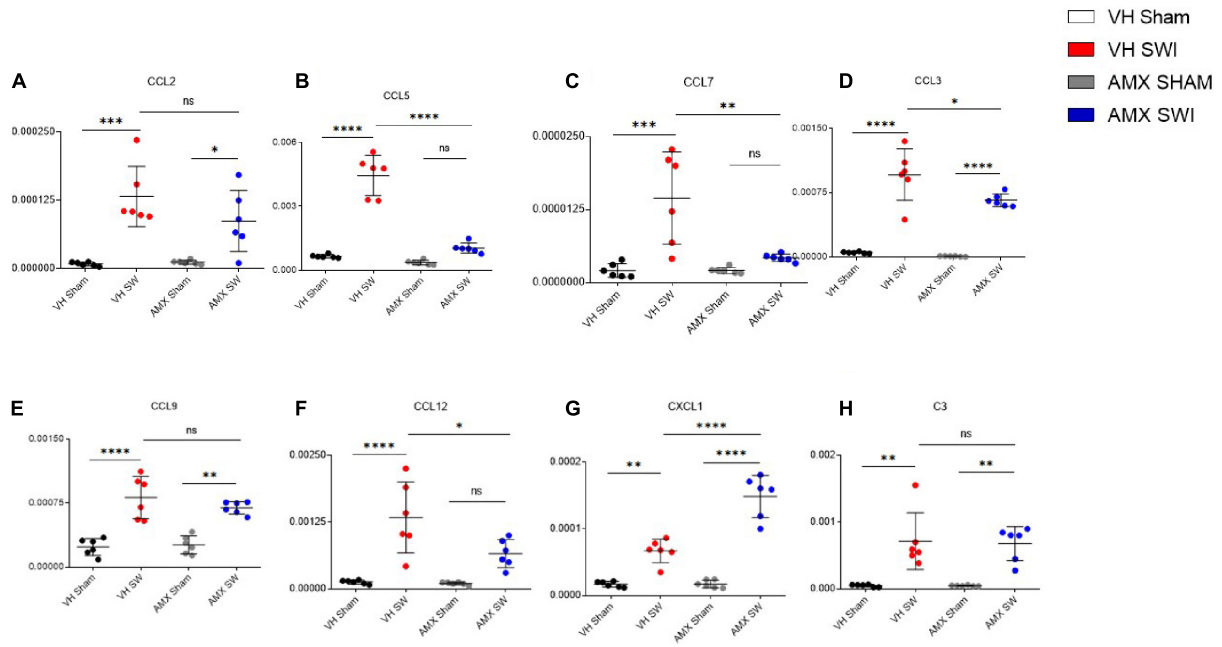

FIGURE 7 | Tbk1 blockade modifies the chemokine profile after Stab Wound Injury (SWI) injury. qPCR from whole-biopsy homogenates were obtained from the injury site (or the corresponding anatomical location in sham mice) from animals treated with either vehicle or AMX at 7 dpi. AMX strongly downregulated the expression of CCL-5 **(B)**, CCL-7 **(C)**, CCL-3 **(D)**, CCL-3 **(E)**, CCL-12 **(F)** but not of CCL-2 **(A)**, and strongly upregulated the expression of CXCL1 **(G)**. Expression of the complement factor C3 was unchanged **(H)**. ($n = 3$ animals/group with 4 sections/animal. Average ± SD, plus individual data points indicated; two-way ANOVA with Tukey post hoc; ns: not significant, $^{*}p < 0.05$, $^{**}p < 0.01$, $^{***}p < 0.001$, $^{****}p < 0.0001$; full statistical report in **Supplementary Table 9**).

and leukocytes, associated with a cytokine and chemokine profile dominated by the upregulation of IL-17, IFN-gamma, and CXCL1. Interestingly, AMX alone, without the application of SWI, appeared to prime the immune response toward increased reactivity, upregulating the levels of IL-13, IL-17, CSF1/CSF1R, and Flt3/Flt3R. The ultimate impact of this increased activation of microglia with DAM-like phenotype and lymphocyte infiltration appears to be detrimental since it corresponded to a substantial expansion of astrocytic and G scar. Thus, Tbk1/IKK-ε inhibition appears to lead to an increased inflammatory response with enlarged astroglial scarring. It must be underscored that the SWI model is especially suited to study glial responses to injury and does not recapitulate the complexity of other TBI conditions, such as blunt trauma with or without hematoma and skull fracture.

In terms of molecular mechanisms, the dual inhibition Tbk1 and IKK-ε by AMX makes it not possible to disentangle the contribution of either kinase. Nevertheless, both kinases display a certain degree of convergence in terms of signaling cascades: AMX treatment has been shown to result in a decrease in canonical NF-kB signaling (Cheng C. et al., 2018; Möser et al., 2019) as well as STING-dependent NF-kB activation (Balka et al., 2020). Furthermore, Tbk1 and IKK-ε are critical components of the Interferon signaling cascade (Fitzgerald et al., 2003) as well as in limiting the phosphorylation and the signaling through RIPK1 signaling (Lafont et al., 2018). Elucidation of any non-redundant role of each kinase in the phenotype evoked by AMX is the object of active investigation.

In terms of cellular mechanisms and interactions, AMX displayed at least two remarkable effects in the SWI model which may be implicated, possibly in cooperation, in this overall detrimental effect: increased lymphocytes and monocytes infiltration and, most notably, the induction of a DAM-like ($Tmem119^{+}CD11c^{+}$ as well as the $Tmem119^{+}CD11c^{+}CD169^{+}$) phenotype in local microglia. Both effects seem to point toward an enhancement of the reaction to the injury, in contrast to the anticipated anti-inflammatory effects of AMX and of the inhibition of Tbk1 and IKK-ε (**Figure 10A**).

Which mechanisms may link the blockade of Tbk1 and IKK-ε to the increased infiltration of lymphocytes in the injury site? Loss of Tbk1 alone has been previously associated with a reduced threshold for lymphocytes activation, the generation of Th1 and Th17 subpopulations, and with the substantial enhancement of IFN-gamma secretion (Yu et al., 2015), although, at the same time, retention of lymphocytes in lymph nodes and reduced brain inflammation was observed upon EAE induction in mice lacking Tbk1 in lymphocytes (Yu et al., 2015). Notably, AMX administration in the context of EAE also results in a decreased activation of Th1 and Th17 and in the reduction of their infiltration of the brain (Quan et al., 2019). In contrast, we do observe an increase in lymphocyte trafficking in the CNS upon AMX treatment, suggesting that the outcome of Tbk1/IKK-ε inhibition may be dependent on the type of injury and the timing of administration (e.g., before injury or after). In fact, partial deletion of Tbk1 alone is associated with enhanced inflammatory profile in aging (Bruno et al., 2020) but reduces the microglial

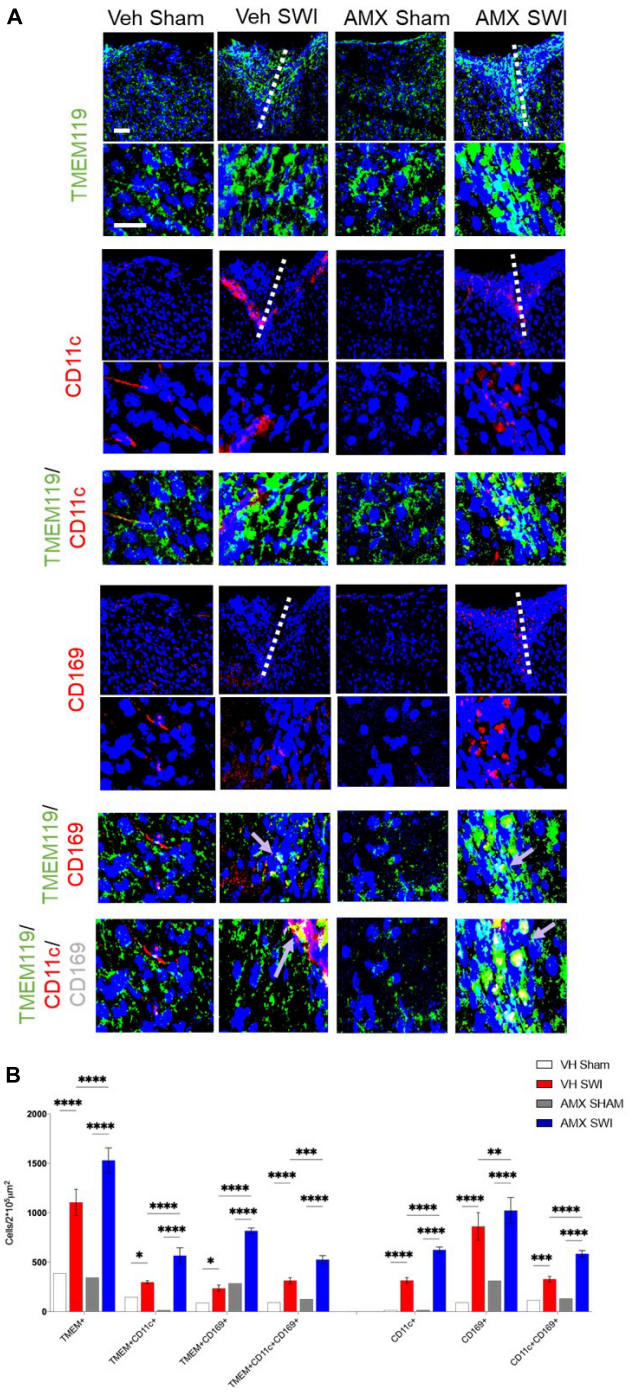

FIGURE 8 | Persistent effect of 7-days Tbk1 blockade on microglial DAM-like phenotype after 33 days of washout. **(A,B)** Mice were subject to cortical SWI injury and treated with AMX for 7 days; AMX was then withdrawn and mice were sacrificed 43 days later (40 days after injury). In AMX-treated mice, even after long wash-out, the density of $CD11c^+$ and $CD169^+$ microglia ($TMEM119^+$) remained significantly higher than in vehicle-treated animals. ($n = 3$ animals/group with 4 sections/animal. Average ± SD, plus individual data points indicated; two-way ANOVA with Tukey *post hoc*; ns: not significant, $^*p < 0.05$, $^{**}p < 0.01$, $^{***}p < 0.001$, $^{****}P < 0.0001$; full statistical report in **Supplementary Table 10**). Length of scale bars for both low-magnification and high-magnification insets is 200 µm.

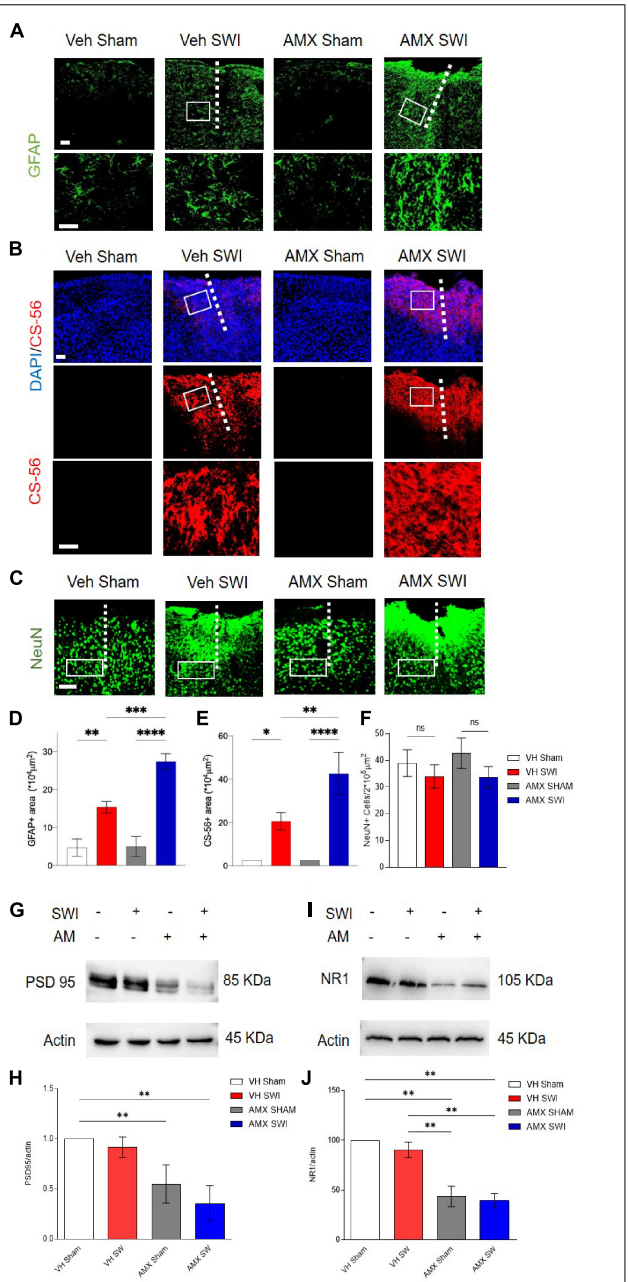

FIGURE 9 | Tbk1 blockade enlarges the gliotic scar and amplifies the deposition of CPSG at 7dpi after Stab Wound Injury (SWI). **(A,D)** The density of reactive astrocytes ($GFAP^+$) is substantially larger at 7 dpi in mice treated with AMX for 7 days after SWI compared to vehicle-treated controls. **(B,E)** The extent of the CSPG scar deposition (as revealed by immunostaining with the CS-56 antibody) is substantially increased by the treatment with AMX for 7 days after SWI injury. **(C,F)** The density of $NeuN^+$ cells is unaffected by either vehicle or AMX treatment. Western blots of cortical biopsies (at 7 dpi) homogenates show decreased levels of **(G,H)** PSD-95 and **(I,J)** NR1. ($n = 3$ animals/group with 4 sections/animal. $n = 4$ animals for the vehicle treated group and $n = 6$ animals for the amlexanox treated group. Average ± SD; one-way ANOVA with Tukey *post hoc*; ns: not significant, $^*p < 0.05$, $^{**}p < 0.01$, $^{***}p < 0.001$, $^{****}P < 0.0001$; original uncropped blots in **Supplementary File 2**; full statistical report in **Supplementary Table 11**). Length of scale bars for both low-magnification and high-magnification insets is 200 µm.

activation associated with neurodegeneration (Brenner et al., 2019). Furthermore, several of the cytokines upregulated upon AMX treatment may be involved in the increased leukocytes and lymphocytes infiltration. In fact, the induction of IL-17 may critically contribute to the recruitment of other leukocytes through the elevation of the chemokine Cxcl1 (Wojkowska et al., 2017). Additional cytokines upregulated by AMX, such as IL-13 and IFN-γ appear to be able to enhance the secretion of IL-6 and TNF-α as well as the release of Nitric Oxide from microglia (Quarta et al., 2021). We also identified a distinctive elevation in IL-19 mRNA. This cytokine is known to be predominantly secreted by microglia subject to inflammatory stimuli (such as LPS), and to act back on microglia itself to reduce the induction of inflammatory cytokines such as suppress IL-6 and TNF-α; it is therefore thought to be induced by inflammation as part of a negative feedback loop (Horiuchi et al., 2015).

One of the most striking effects of AMX treatment in SWI is the enhancement of microglial ($TMEM119^+$) subpopulations highly expressing CD11c ($TMEM119^+CD11c^+$), or CD169 ($TMEM119^+CD169^+$) and the double-positive $TMEM119^+CD11c^+CD169^+$ subpopulation. These subpopulations were barely detected in vehicle-treated SWI samples but were substantially represented in the AMX treated mice. $TMEM119^+$ $CD11c^+$ microglia (which may encompass more than one subset) has been recently identified as DAM, a subpopulation characteristically associated with neurodegenerative diseases (Keren-Shaul et al., 2017; Krasemann et al., 2017; Cao et al., 2021) and white matter aging (Sato-Hashimoto et al., 2019; Safaiyan et al., 2021). Expression profiling of DAM has revealed the upregulation of genes involved in lipid metabolism (most notably, ApoE) and apparently reduced capacity for engulfment, phagocytosis and degradation (Krasemann et al., 2017; Ulland et al., 2017). Although often associated with degenerative processes (Deczkowska et al., 2018), it has been reported to be involved in either protective processes (such as amyloid plaque compaction in AD, debris clearing in stroke or myelin damage; Cignarella et al., 2020; Meilandt et al., 2020; Lee et al., 2021) or detrimental processes (Götzl et al., 2019) depending on the pathological condition. On the other hand, CD169 expression characterizes actively phagocytosing cells (O'Neill et al., 2013); CD169 is normally not expressed in microglia but a distinct population of $CD169^+$ microglia has been associated with active phagocytosis of myelin and it is highly pathogenic in EAE models (Bogie et al., 2018; Ostendorf et al., 2021). Together the $TMEM119^+$ $CD169^+$ and the currently uncharacterized population of $TMEM119^+$ $CD11c^+$ $CD169^+$ are anticipated to be associated with massive phagocytosis of neurons and myelin in the site of injury (**Figures 10A,B**).

How does the inhibition of Tbk1 and IKK-ε lead to induction of a DAM-like phenotype in microglia? Several non-mutually exclusive molecular pathways may be involved. Recent evidence suggests a model in which Tbk1 may suppress or limit the appearance of a DAM-like phenotype in microglia in a cell-autonomous way (i.e., independently of the increased leukocytes infiltration). The DAM-like phenotype is dependent on the activity of the RIPK1, and genetic or pharmacological inhibition of RIPK1 prevents the upregulation of the DAM marker Cst7 and reverses the compromised phagocytic/autophagic degradation pathway (Ofengeim et al., 2017). Indeed, Tbk1 is one of the most important upstream inhibitors of RIPK1, and phosphorylation of RIPK1 by Tbk1 on T189/T190 prevents RIPK1 activation and genetic or pharmacological inhibition of Tbk1 results in an enhanced RIPK1 pathway activation and microglial reactivity (Xu et al., 2018). Moreover, both Tbk1 and IKK-ε are able to phosphorylate Ik-B (leading to its degradation) and contribute to the activation of NF-kB-dependent transcriptional responses so that blockade of the two kinases would result in a decrease in canonical activation of NF-kB in immune cells (Carr et al., 2020); at the same time, upregulation of non-canonical NF-kB signaling has been reported upon the Tbk1 blockade (Jin et al., 2012). Interestingly, loss of the p50 subunit of NF-kB is associated with increased reactive microglial morphology and enhanced secretion of TNF-α upon LPS challenge in aged mice (Taetzsch et al., 2019), suggesting that reduced canonical activation of NF-kB (like in case of AMX treatment) may also translate into increased microglial reactivity. Third, a subset of microglia in AMX-treated SWI mice display high levels of CD317, a well-known type-I IFN-induced gene (Polyak et al., 2013) suggesting the possibility that AMX may drive the induction of an interferon-response microglial phenotype (Sala Frigerio et al., 2019); however, these cells are relatively low in absolute number and the levels of IFNb mRNA were not actually modified. On the other hand, Tbk1 phosphorylates STING and Tbk1 and IKK-ε are essential for its signaling through IRF3 and NF-kB (Balka et al., 2020; Yum et al., 2021); in our experimental conditions, we verified that AMX treatment reduced the levels of STING phosphorylation. Recently it has been shown that activation of STING signaling pathway in microglia is actually responsible for a decrease in microglial reactivity (Mathur et al., 2017); furthermore, microglia can undergo STING-dependent apoptosis to limit IFN production during viral infections (Reinert et al., 2021). Therefore, loss of Tbk1/IKK-ε-STING may actually contribute to the enhanced microglial reactivity and increased accumulation seen upon AMX treatment. Finally, contributions to the induction of the DAM-like phenotype may be provided by infiltrating lymphocytes'cytokines: IL-17 is well-known to induce microglial activation (Chen et al., 2020), although the specific role in the DAM phenotype is not yet clear.

Interestingly, some of the cytokines related to the pro-inflammatory environment due to AMX appear to be elevated already in sham-operated mice, independently of SWI. It is, thus, conceivable that AMX alone may prime the inflammatory state of microglia, with SWI triggering the DAM-like phenotype, in a multi-step process reminiscent of what has been formerly hypothesized in other conditions (Keren-Shaul et al., 2017). Furthermore, the AMX-induced phenotype closely resembles the one observed upon aging in white matter microglia. This effect is also compatible with a role for the Tbk1 pathway in inflammaging (Franceschi et al., 2018) i.e., in driving low-grade baseline inflammatory activation and in amplifying responses upon injury (Xu et al., 2018; Bruno et al., 2020; Gerbino et al., 2020). Although downregulation of TBK1 signaling takes place in aging (Xu et al., 2018), it remains to be seen if acute TBK1 inhibition faithfully mimics the long-term decline

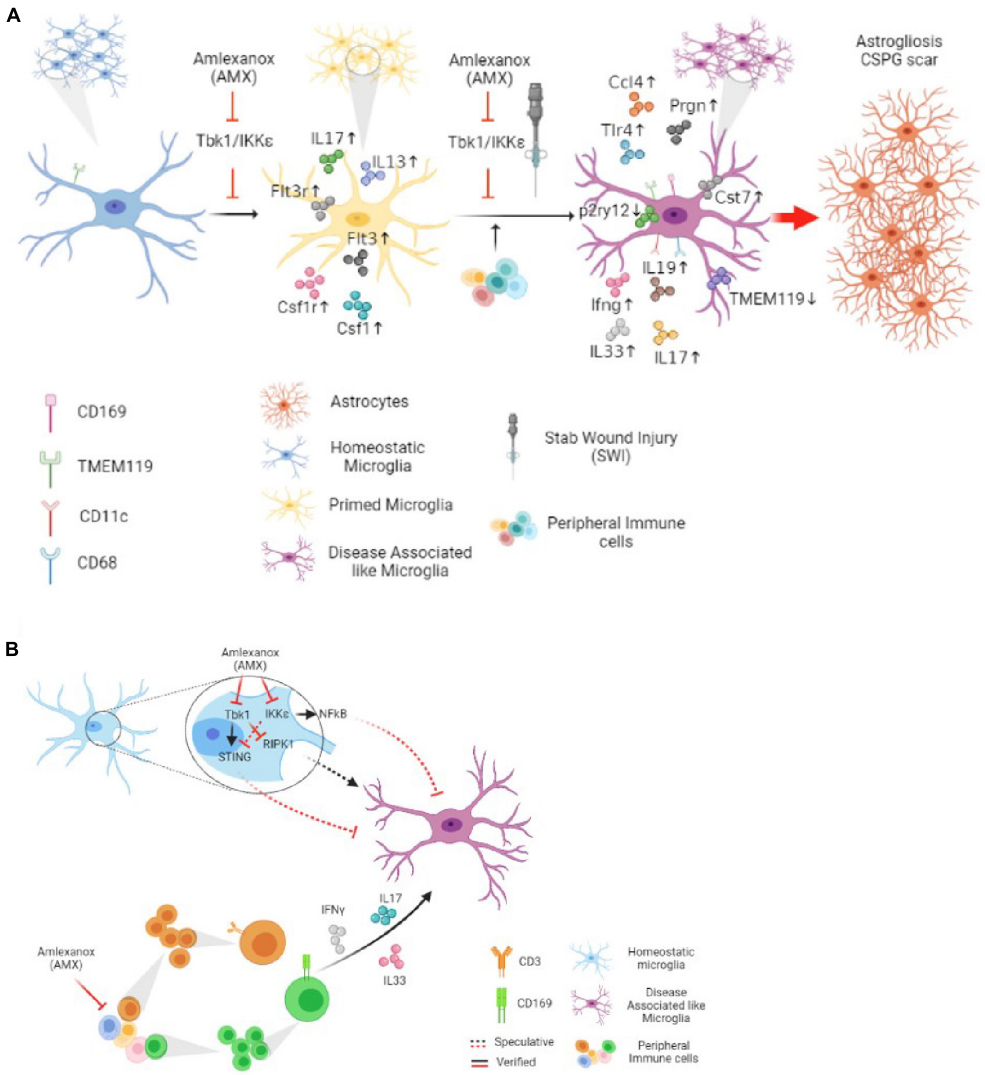

FIGURE 10 | Tbk1 inhibition by Amlexanox modifiedy the microglial and immune response in cortical Stab Wound Injury (SWI) injury. **(A)** Blockade of Tbk1 alone by Amlexanox (AMX), in absence of additional damage, is sufficient to increase the expression of IL-17, CSF1, CSF1R, Flt3, Flt3R, and IL-13, indicating an initial baseline pro-inflammatory state; upon SWI injury, AMX administration causes the substantial expansion of reactive microglia with immunohistochemical and expression profile similar to the Disease-Associated Microglia described in neurodegenerative conditions as well as the significant increase in the infiltration by lymphocytes and monocytes/macrophages. The ultimate effect appears to be increased astrogliosis and extensive deposition of CSPG scar. **(B)** At least two molecular mechanisms are proposed for AMX effect on microglial phenotype: the de-repression of the RIPK1 pathway and the de-activation of the STING pathway. The concomitant upregulation of inflammatory cytokines, some of lymphocytic origin such as IL-17 and IFN-γ, is likely to contribute to the peculiar microglial phenotype.

in TBK1 activity in aging, and their associated inflammaging phenotypes.

The ultimate role of DAM is currently the object of an ongoing debate: when first identified, DAM was judged to be a beneficial component of the response to AD-associated amyloid plaques, and enhancement of DAM generation was hypothesized to be a viable therapeutic strategy (Keren-Shaul et al., 2017; Deczkowska et al., 2018; Ewers et al., 2020). On the other hand, the kinetics of DAM appearance suggested that it may be a detrimental component of neurodegeneration (Rangaraju et al., 2018). DAM was shown to be involved in the removal of apoptotic neurons (Krasemann et al., 2017), and therefore it would have a beneficial role in tissue injury by removing debris. In the context of acute injury, deletion of TREM2, which is normally involved in the induction of reactive microglia and whose deletion is anticipated to prevent such reactive phenotype (Nugent et al., 2020), has been reported to be beneficial in traumatic brain injury (Saber et al., 2017), implying a detrimental role. A similar effect was reported in stroke models (Wu et al., 2017; Chen et al., 2020). Our data seems to point to a similar detrimental role of DAM-like microglia in SWI since the blockade of Tbk1 and the massive expansion of the $CD11c^{+}$ microglia is associated with increased deposition of CSPG and increased astrogliosis. To date, individual immune peripheral and microglial contributions

to this ultimate effect are to be investigated, since one of the limitations of the present study is the use of a systemic inhibitor of Tbk1/IKK-ε.

Although the induction of a DAM-like phenotype by AMX in the context of SWI appears detrimental, as measured by the larger astrocytic scar, the induction of a DAM phenotype as been hypothesized to be beneficial in the context of Alzheimer Disease (AD; Lewcock et al., 2020). In AD, genetic variants reducing TREM2 signaling causes the reduced induction of DAM, which normally surround amyloid plaques and display active phagocytosis and lipid metabolism, with beneficial consequences on synaptic loss, amyloid peptides burden and dystrophic dendrites (Meilandt et al., 2020; Lee et al., 2021). Since TREM2 with reduced signaling appear to be risk factors for AD and are associated with incomplete DAM induction, strategies have been developed to upregulate TREM2 signaling using genetic (e.g., Lee et al., 2018) or antibody (Cignarella et al., 2020; Lewcock et al., 2020) approaches. In this context, our findings suggest that AMX (and more broadly, the Tbk1/IKK-ε inhibition) may contribute to enhancing the induction of DAM. However, increased number of DAM is actually associated with neurodegeneration upon progranulin loss (Götzl et al., 2019), implying that the effect of AMX may be difficult to extrapolate, due to the beneficial or detrimental effects of reactive microglia (Aguzzi et al., 2013) and may be worth exploring in different disease models. It must be noted that the conditions of acute damage with substantial immune cells infiltration are not similar to those of chronic, slowly progressive neurodegenerative conditions: thus, the actual phenotype of microglial cells and their impact on the ongoing pathogenic process may be highly disease- and stage-dependent (e.g., Ouali Alami et al., 2018).

DATA AVAILABILITY STATEMENT

The raw data supporting the conclusions of this article will be made available by the authors, without undue reservation.

ETHICS STATEMENT

The animal study was reviewed and approved by the Regierungspraesidium Tubingen, no. 1379.

AUTHOR CONTRIBUTIONS

FR conceived the study, supervised the project, and planned the experiments. RR collected samples, performed analyses, prepared figures, and worked on the manuscript. LT performed staining, western blot, and PCR experiments. AO performed preliminary analysis for GFAP and CS56 immunostainings. ZL performed expression analysis. DW performed SWI injury and western blot experiments. TB and JK provided critical reagents and resources. FR, JW, TB, JK, and AL contributed reagents and participated in the drafting of the manuscript. FR and RR contributed to the final version of the manuscript. All authors read and approved the manuscript.

FUNDING

This work was supported by the Deutsche Forschungsgemeinschaft in the context of the SFB1149 (FR; no. 251293561) and by BMBF (FKZ 01EW1705A) as part of the ERANET-Micronet consortium (FR). FR was also supported by the Thierry Latran Foundation (projects "Trials" and "Hypothals"), by the Radala Foundation, by the Deutsche Forschungsgemeinschaft (DFG) as part of the SFB1149 and with the individual grant nos. 431995586, 446067541, and 443642953, by the Cellular and Molecular Mechanisms in Aging (CEMMA) Research Training Group and by BMBF (FKZ 01EW1705A, as member of the ERANET-NEURON consortium "MICRONET"). RR is a member of the MICRONET consortium and is also independently funded by the Hannelore Kohl Foundation Award.

ACKNOWLEDGMENTS

We thank Prof. Anita Ignatius for the access to the histology laboratory, to Prof. Frank Kirchoff for the use of the LSM710 confocal microscope, and to Prof. Thomas Wirth for the use of the LightCycler qPCR apparatus. We thank Thomas Lenk and Tanja Wipp for their dedicated technical support.

SUPPLEMENTARY MATERIAL

The Supplementary Material for this article can be found online at: https://www.frontiersin.org/articles/10.3389/fnagi.2021.684171/full#supplementary-material

Supplementary Table 1 | Sequences of the primers used in the qPCR experiments.

Supplementary Table 2 | List of materials used in the study.

Supplementary Table 3 | Detailed statistics for the experiments depicted in **Figure 1**.

Supplementary Table 4 | Detailed statistics for the experiments depicted in **Figure 2**.

Supplementary Table 5 | Detailed statistics for the experiments depicted in **Figure 3**.

Supplementary Table 6 | Detailed statistics for the experiments depicted in **Figure 4**.

Supplementary Table 7 | Detailed statistics for the experiments depicted in **Figure 5**.

Supplementary Table 8 | Detailed statistics for the experiments depicted in **Figure 6**.

Supplementary Table 9 | Detailed statistics for the experiments depicted in **Figure 7**.

Supplementary Table 10 | Detailed statistics for the experiments depicted in **Figure 8**.

Supplementary Table 11 | Detailed statistics for the experiments depicted in **Figure 9**.

Supplementary File 1 | Uncropped Western Blot from **Figure 1**.

Supplementary File 2 | Uncropped Western Blot from **Figure 9**.

REFERENCES

Abbasi, F., Raoof, M., Khatami, R., Shadman, N., Borjian-Boroojeni, F., and Nazari, F. (2016). Effectiveness of Amlexanox and Adcortyl for the treatment of recurrent aphthous ulcers. *J. Clin. Exp. Dent.* 18, 368–372. doi: 10.4317/jced.52540

Aguzzi, A., Barres, B. A., and Bennett, M. L. (2013). Microglia: scapegoat, saboteur, or something else? *Science* 339, 156–161. doi: 10.1126/science.1227901

Ajami, B., Samusik, N., Wieghofer, P., Ho, P. P., Crotti, A., Bjornson, Z., et al. (2018). Single-cell mass cytometry reveals distinct populations of brain myeloid cells in mouse neuroinflammation and neurodegeneration models. *Nat. Neurosci.* 21, 541–551. doi: 10.1038/s41593-018-0100-x

Alami, N. O., Tang, L., Wiesner, D., Commisso, B., Bayer, D., Weishaupt, J., et al. (2020). Multiplexed chemogenetics in astrocytes and motoneurons restore blood-spinal cord barrier in ALS. *Life Sci. Alliance* 3:e201900571. doi: 10.26508/LSA.201900571

Anderson, S. R., Roberts, J. M., Zhang, J., Steele, M. R., Romero, C. O., Bosco, A., et al. (2019). Developmental apoptosis promotes a disease-related gene signature and independence from CSF1R signaling in retinal microglia. *Cell Rep.* 27, 2002–2013. doi: 10.1016/j.celrep.2019.04.062

Balka, K. R., Louis, C., Saunders, T. L., Smith, A. M., Calleja, D. J., D'Silva, D. B., et al. (2020). TBK1 and IKKε act redundantly to mediate STING-induced NF-κB responses in myeloid cells. *Cell Rep.* 31:107492. doi: 10.1016/j.celrep.2020.03.056

Bennett, M. L., Bennett, F. C., Liddelow, S. A., Ajami, B., Zamanian, J. L., Fernhoff, N. B., et al. (2016). New tools for studying microglia in the mouse and human CNS. *Proc. Natl. Acad. Sci. U.S.A.* 113, E1738–E1746. doi: 10.1073/pnas.1525528113

Bogie, J. F., Boelen, E., Louagie, E., Delputte, P., Elewaut, D., van Horssen, J., et al. (2018). CD169 is a marker for highly pathogenic phagocytes in multiple sclerosis. *Mult. Scler. J.* 24, 290–300. doi: 10.1177/1352458517698759

Brenner, D., Sieverding, K., Bruno, C., Lüningschrör, P., Buck, E., Mungwa, S., et al. (2019). Heterozygous *Tbk1* loss has opposing effects in early and late stages of ALS in mice. *J. Exp. Med.* 216, 267–278. doi: 10.1084/jem.20180729

Bruno, C., Sieverding, K., Freischmidt, A., Satoh, T., Walther, P., Mayer, B., et al. (2020). Haploinsufficiency of TANK-binding kinase 1 prepones age-associated neuroinflammatory changes without causing motor neuron degeneration in aged mice. *Brain Commun.* 2:fcaa133. doi: 10.1093/braincomms/fcaa133

Bruns, J., and Hauser, W. A. (2003). The epidemiology of traumatic brain injury: a review. *Epilepsia* 44, 2–10. doi: 10.1046/j.1528-1157.44.s10.3.x

Cao, Z., Harvey, S. S., Chiang, T., Foltz, A. G., Lee, A. G., Cheng, M. Y., et al. (2021). Unique subtype of microglia in degenerative thalamus after cortical stroke. *Stroke* 52, 687–698. doi: 10.1161/strokeaha.120.032402

Carr, M., Mamand, S., Chapman, K. L., Perrior, T., and Wagner, S. D. (2020). IKKε and TBK1 in diffuse large B-cell lymphoma: a possible mechanism of action of an IKKε/TBK1 inhibitor to repress NF-κB and IL-10 signalling. *J. Cell. Mol. Med.* 24, 11573–11582. doi: 10.1111/jcmm.15774

Chen, J., Liu, X., and Zhong, Y. (2020). Interleukin-17A: the key cytokine in neurodegenerative diseases. *Front. Aging Neurosci.* 12:566922. doi: 10.3389/fnagi.2020.566922

Chen, S., Peng, J., Sherchan, P., Ma, Y., Xiang, S., Yan, F., et al. (2020). TREM2 activation attenuates neuroinflammation and neuronal apoptosis via PI3K/Akt pathway after intracerebral hemorrhage in mice. *J. Neuroinflammation* 17:168. doi: 10.1186/s12974-020-01853-x

Cheng, C., Ji, Z., Sheng, Y., Wang, J., Sun, Y., Zhao, H., et al. (2018). Aphthous ulcer drug inhibits prostate tumor metastasis by targeting IKKε/TBK1/NF-κB signaling. *Theranostics* 8, 4633–4648. doi: 10.7150/thno.26687

Cheng, H., Xuan, H., Green, C. D., Han, Y., Sun, N., Shen, H., et al. (2018). Repression of human and mouse brain inflammaging transcriptome by broad gene-body histone hyperacetylation. *Proc. Natl. Acad. Sci. U.S.A.* 115, 7611–7616. doi: 10.1073/pnas.1800656115

Cignarella, F., Filipello, F., Bollman, B., Cantoni, C., Locca, A., Mikesell, R., et al. (2020). TREM2 activation on microglia promotes myelin debris clearance and remyelination in a model of multiple sclerosis. *Acta Neuropathol.* 140, 513–534. doi: 10.1007/s00401-020-02193-z

Clark, K., Plater, L., Peggie, M., and Cohen, P. (2009). Use of the pharmacological inhibitor BX795 to study the regulation and physiological roles of TBK1 and IκB Kinase ∈: a distinct upstream kinase mediates ser-172 phosphorylation and activation. *J. Biol. Chem.* 284, 14136–14146. doi: 10.1074/jbc.M109.000414

Deczkowska, A., Keren-Shaul, H., Weiner, A., Colonna, M., Schwartz, M., and Amit, I. (2018). Disease-associated microglia: a universal immune sensor of neurodegeneration. *Cell* 173, 1073–1081. doi: 10.1016/j.cell.2018.05.003

Dols-Icardo, O., Montal, V., Sirisi, S., López-Pernas, G., Cervera-Carles, L., Querol-Vilaseca, M., et al. (2020). Motor cortex transcriptome reveals microglial key events in amyotrophic lateral sclerosis. *Neurol. Neuroimmunol. Neuroinflamm.* 7:e829. doi: 10.1212/nxi.0000000000000829

Duan, W., Yi, L., Tian, Y., Huang, H. P., Li, Z., Bi, Y., et al. (2021). Myeloid TBK1 deficiency induces motor deficits and axon degeneration through inflammatory cell infiltration. *Mol. Neurobiol.* 58, 2435–2446. doi: 10.1007/s12035-020-02235-3

Early, A. N., Gorman, A. A., Van Eldik, L. J., Bachstetter, A. D., and Morganti, J. M. (2020). Effects of advanced age upon astrocyte-specific responses to acute traumatic brain injury in mice. *J. Neuroinflammation* 17:115. doi: 10.1186/s12974-020-01800-w

Ewers, M., Biechele, G., Suárez-Calvet, M., Sacher, C., Blume, T., Morenas-Rodriguez, E., et al. (2020). Higher CSF sTREM2 and microglia activation are associated with slower rates of beta-amyloid accumulation. *EMBO Mol. Med.* 12:e12308. doi: 10.15252/emmm.202012308

Fitzgerald, K. A., McWhirter, S. M., Faia, K. L., Rowe, D. C., Latz, E., Golenbock, D. T., et al. (2003). IKKε and TBK1 are essential components of the IRF3 signaling pathway. *Nat. Immunol.* 4, 491–496. doi: 10.1038/ni921

Förstner, P., Rehman, R., Anastasiadou, S., Haffner-Luntzer, M., Sinske, D., Ignatius, A., et al. (2018). Neuroinflammation after traumatic brain injury is enhanced in activating transcription factor 3 mutant mice. *J. Neurotrauma* 35, 2317–2329. doi: 10.1089/neu.2017.5593

Franceschi, C., and Campisi, J. (2014). Chronic inflammation (Inflammaging) and its potential contribution to age-associated diseases. *J. Gerontol. Ser. A Biol. Sci. Med. Sci.* 69, S4–S9. doi: 10.1093/gerona/glu057

Franceschi, C., Garagnani, P., Parini, P., Giuliani, C., and Santoro, A. (2018). Inflammaging: a new immune–metabolic viewpoint for age-related diseases. *Nat. Rev. Endocrinol.* 14, 576–590. doi: 10.1038/s41574-018-0059-4

Frik, J., Merl-Pham, J., Plesnila, N., Mattugini, N., Kjell, J., Kraska, J., et al. (2018). Cross-talk between monocyte invasion and astrocyte proliferation regulates scarring in brain injury. *EMBO reports* 19:e45294. doi: 10.15252/embr.201745294

Gabandé-Rodríguez, E., Keane, L., and Capasso, M. (2020). Microglial phagocytosis in aging and Alzheimer's disease. *J. Neurosci. Res.* 98, 284–298. doi: 10.1002/jnr.24419

Galatro, T., Holtman, I., and Lerario, A. (2017). Transcriptomic analysis of purified human cortical microglia reveals age-associated changes. *Nat. Neurosci.* 20, 1162–1171. doi: 10.1038/nn.4597

Gerbino, V., Kaunga, E., Ye, J., Canzio, D., O'Keeffe, S., Rudnick, N. D., et al. (2020). The loss of TBK1 kinase activity in motor neurons or in all cell types differentially impacts ALS disease progression in SOD1 mice. *Neuron* 106, 789–805.e5. doi: 10.1016/j.neuron.2020.03.005

Götzl, J. K., Brendel, M., Werner, G., Parhizkar, S., Sebastian Monasor, L., Kleinberger, G., et al. (2019). Opposite microglial activation stages upon loss of PGRN or TREM 2 result in reduced cerebral glucose metabolism. *EMBO Mol. Med.* 11:e9711.

Hammond, T. R., Dufort, C., Dissing-Olesen, L., Giera, S., Young, A., Wysoker, A., et al. (2019). Single-cell RNA sequencing of microglia throughout the mouse lifespan and in the injured brain reveals complex cell-state changes. *Immunity* 50, 253–271.e6. doi: 10.1016/j.immuni.2018.11.004

Horiuchi, H., Parajuli, B., Wang, Y., Azuma, Y.-T., Mizuno, T., Takeuchi, H., et al. (2015). Interleukin-19 acts as a negative autocrine regulator of activated microglia. *PLoS One* 10:e0118640. doi: 10.1371/journal.pone.0118640

Immig, K., Gericke, M., Menzel, F., Merz, F., Krueger, M., Schiefenhövel, F., et al. (2015). CD11c-positive cells from brain, spleen, lung, and liver exhibit site-specific immune phenotypes and plastically adapt to new environments. *Glia* 63, 611–625. doi: 10.1002/glia.22771

Jiang, J. Y., Gao, G. Y., Feng, J. F., Mao, Q., Chen, L. G., Yang, X. F., et al. (2019). Traumatic brain injury in China. *Lancet Neurol.* 18, 286–295. doi: 10.1016/S1474-4422(18)30469-1

Jin, J., Xiao, Y., Chang, J. H., Yu, J., Hu, H., Starr, R., et al. (2012). The kinase TBK1 controls IgA class switching by negatively regulating noncanonical NF-κB signaling. *Nat. Immunol.* 13, 1101–1109. doi: 10.1038/ni.2423

Keren-Shaul, H., Spinrad, A., Weiner, A., Matcovitch-Natan, O., Dvir-Szternfeld, R., Ulland, T. K., et al. (2017). A unique microglia type associated with restricting development of Alzheimer's disease. *Cell* 169, 1276–1290.e17. doi: 10.1016/j.cell.2017.05.018

Kim, J. Y., Welsh, E. A., Oguz, U., Fang, B., Bai, Y., Kinose, F., et al. (2013). Dissection of TBK1 signaling via phosphoproteomics in lung cancer cells. *Proc. Natl. Acad. Sci. U.S.A.* 110, 12414–12419. doi: 10.1073/pnas.1220674110

Koellhoffer, E., McCullough, L., and Ritzel, R. (2017). Old Maids: aging and its impact on microglia function. *Int. J. Mol. Sci.* 18:769. doi: 10.3390/ijms18040769

Krasemann, S., Madore, C., Cialic, R., Baufeld, C., Calcagno, N., El Fatimy, R., et al. (2017). The TREM2-APOE pathway drives the transcriptional phenotype of dysfunctional microglia in neurodegenerative diseases. *Immunity* 47, 566–581.e9. doi: 10.1016/j.immuni.2017.08.008

Kraus, J. F., Black, M. A., Hessol, N., Ley, P., Rokaw, W., Sullivan, C., et al. (1984). The incidence of acute brain injury and serious impairment in a defined population. *Am. J. Epidemiol.* 119, 186–201. doi: 10.1093/oxfordjournals.aje.a113737

Lafont, E., Draber, P., Rieser, E., Reichert, M., Kupka, S., de Miguel, D., et al. (2018). TBK1 and IKKε prevent TNF-induced cell death by RIPK1 phosphorylation. *Nat. Cell Biol.* 20, 1389–1399. doi: 10.1038/s41556-018-0229-6

Lee, C. D., Daggett, A., Gu, X., Jiang, L. L., Langfelder, P., Li, X., et al. (2018). Elevated TREM2 gene dosage reprograms microglia responsivity and ameliorates pathological phenotypes in Alzheimer's disease models. *Neuron* 97, 1032–1048. doi: 10.1016/j.neuron.2018.02.002

Lee, S. H., Meilandt, W. J., Xie, L., Gandham, V. D., Ngu, H., Barck, K. H., et al. (2021). Trem2 restrains the enhancement of tau accumulation and neurodegeneration by β-amyloid pathology. *Neuron* 109, 1283–1301. doi: 10.1016/j.neuron.2021.02.010

Letiembre, M., Liu, Y., Walter, S., Hao, W., Pfander, T., Wrede, A., et al. (2009). Screening of innate immune receptors in neurodegenerative diseases: a similar pattern. *Neurobiol. Aging* 30, 759–768. doi: 10.1016/j.neurobiolaging.2007.08.018

Lewcock, J. W., Schlepckow, K., Di Paolo, G., Tahirovic, S., Monroe, K. M., and Haass, C. (2020). Emerging microglia biology defines novel therapeutic approaches for Alzheimer's disease. *Neuron* 108, 801–821. doi: 10.1016/j.neuron.2020.09.029

Liu, S., Cai, X., Wu, J., Cong, Q., Chen, X., Li, T., et al. (2015). Phosphorylation of innate immune adaptor proteins MAVS, STING, and TRIF induces IRF3 activation. *Science* 347:aaa2630. doi: 10.1126/science.aaa2630

Mathur, V., Burai, R., Vest, R. T., Bonanno, L. N., Lehallier, B., Zardeneta, M. E., et al. (2017). Activation of the STING-dependent type I interferon response reduces microglial reactivity and neuroinflammation. *Neuron* 96, 1290–1302. doi: 10.1016/j.neuron.2017.11.032

Matsumoto, G., Shimogori, T., Hattori, N., and Nukina, N. (2015). TBK1 controls autophagosomal engulfment of polyubiquitinated mitochondria through p62/SQSTM1 phosphorylation. *Hum. Mol. Genet.* 24, 4429–4442. doi: 10.1093/hmg/ddv179

Meilandt, W. J., Ngu, H., Gogineni, A., Lalehzadeh, G., Lee, S. H., Srinivasan, K., et al. (2020). Trem2 deletion reduces late-stage amyloid plaque accumulation, elevates the Aβ42: Aβ40 ratio, and exacerbates axonal dystrophy and dendritic spine loss in the PS2APP Alzheimer's mouse model. *J. Neurosci.* 40, 1956–1974. doi: 10.1523/jneurosci.1871-19.2019

Mejias, N. H., Martinez, C. C., Stephens, M. E., and De Rivero Vaccari, J. P. (2018). Contribution of the inflammasome to inflammaging. *J. Inflamm.* 15:23. doi: 10.1186/s12950-018-0198-3

Mifflin, L., Hu, Z., Dufort, C., Hession, C. C., Walker, A. J., Niu, K., et al. (2021). A RIPK1-regulated inflammatory microglial state in amyotrophic lateral sclerosis. *Proc. Natl. Acad. Sci. U.S.A.* 118:e2025102118. doi: 10.1073/pnas.2025102118

Mogilenko, D. A., Shpynov, O., Andhey, P. S., Arthur, L., Swain, A., Esaulova, E., et al. (2021). Comprehensive profiling of an aging immune system reveals clonal GZMK+ CD8+ T cells as conserved hallmark of inflammaging. *Immunity* 54, 99–115.e12. doi: 10.1016/j.immuni.2020.11.005

Mori, D., Koide, N., Tsolmongyn, B., Nagata, H., Sano, T., Nonami, T., et al. (2015). Poly I: C enhances production of nitric oxide in response to interferon-γ via upregulation of interferon regulatory factor 7 in vascular endothelial cells. *Microvasc. Res.* 98, 68–73. doi: 10.1016/j.mvr.2015.01.003

Möser, C. V., Möller, M., Fleck, S. C., Thomas, D., Geisslinger, G., and Niederberger, E. (2019). Inhibition of the protein kinase IKKepsilon attenuates neuropathic pain in mice. *Neuropharmacology* 146, 198–211. doi: 10.1016/j.neuropharm.2018.12.004

Muth, C., Hartmann, A., Sepulveda-Falla, D., Glatzel, M., and Krasemann, S. (2019). Phagocytosis of apoptotic cells is specifically upregulated in ApoE4 expressing microglia in vitro. *Front. Cell. Neurosci.* 13:181. doi: 10.3389/fncel.2019.00181

Nugent, A. A., Lin, K., van Lengerich, B., Lianoglou, S., Przybyla, L., Davis, S. S., et al. (2020). TREM2 regulates microglial cholesterol metabolism upon chronic phagocytic challenge. *Neuron* 105, 837–854.e9. doi: 10.1016/j.neuron.2019.12.007

O'Neill, A. S., van den Berg, T. K., and Mullen, G. E. (2013). Sialoadhesin–a macrophage-restricted marker of immunoregulation and inflammation. *Immunology* 138, 198–207. doi: 10.1111/imm.12042

Ofengeim, D., Mazzitelli, S., Ito, Y., DeWitt, J. P., Mifflin, L., Zou, C., et al. (2017). RIPK1 mediates a disease-associated microglial response in Alzheimer's disease. *Proc. Natl. Acad. Sci. U.S.A.* 114, E8788–E8797. doi: 10.1073/pnas.1714175114

Olde Heuvel, F., Holl, S., Chandrasekar, A., Li, Z., Wang, Y., Rehman, R., et al. (2019). STAT6 mediates the effect of ethanol on neuroinflammatory response in TBI. *Brain Behav. Immun.* 81, 228–246. doi: 10.1016/j.bbi.2019.06.019

Oral, E. A., Reilly, S. M., Gomez, A. V., Meral, R., Butz, L., Ajluni, N., et al. (2017). Inhibition of IKKε and TBK1 improves glucose control in a subset of patients with type 2 diabetes. *Cell Metab.* 26, 157–170.e7. doi: 10.1016/j.cmet.2017.06.006

Ostendorf, L., Dittert, P., Biesen, R., Duchow, A., Stiglbauer, V., Ruprecht, K., et al. (2021). SIGLEC1 (CD169): a marker of active neuroinflammation in the brain but not in the blood of multiple sclerosis patients. *Sci. Rep.* 11:10299.

Ouali Alami, N., Schurr, C., Olde Heuvel, F., Tang, L., Li, Q., Tasdogan, A., et al. (2018). NF-κB activation in astrocytes drives a stage-specific beneficial neuroimmunological response in ALS. *EMBO J.* 37:e98697. doi: 10.15252/embj.201798697

Peeters, W., van den Brande, R., Polinder, S., Brazinova, A., Steyerberg, E. W., Lingsma, H. F., et al. (2015). Epidemiology of traumatic brain injury in Europe. *Acta Neurochir.* 157, 1683–1696. doi: 10.1007/s00701-015-2512-7

Polyak, M. J., Vivithanaporn, P., Maingat, F. G., Walsh, J. G., Branton, W., Cohen, E. A., et al. (2013). Differential type 1 interferon-regulated gene expression in the brain during AIDS: interactions with viral diversity and neurovirulence. *FASEB J.* 27, 2829–2844. doi: 10.1096/fj.13-227868

Prabakaran, T., Bodda, C., Krapp, C., Zhang, B., Christensen, M. H., Sun, C., et al. (2018). Attenuation of cGAS-STING signaling is mediated by a p62/ SQSTM1-dependent autophagy pathway activated by TBK1. *EMBO J.* 37:e97858. doi: 10.15252/embj.201797858

Quan, M. Y., Song, X. J., Liu, H. J., Deng, X. H., Hou, H. Q., Chen, L. P., et al. (2019). Amlexanox attenuates experimental autoimmune encephalomyelitis by inhibiting dendritic cell maturation and reprogramming effector and regulatory T cell responses. *J. Neuroinflammation* 16:52. doi: 10.1186/s12974-019-1438-z

Quarta, A., Meese, T., Pieters, Z., Van Breedam, E., Le Blon, D., Van Broeckhoven, J., et al. (2021). Murine induced pluripotent stem cell-derived neuroimmune cell culture models emphasize opposite immune-effector functions of interleukin 13-primed microglia and macrophages in terms of neuroimmune toxicity. *Glia* 69, 326–345. doi: 10.1002/glia.23899

Raj, D., Yin, Z., Breur, M., Doorduin, J., Holtman, I. R., Olah, M., et al. (2017). Increased white matter inflammation in aging-and Alzheimer's disease brain. *Front. Mol. Neurosci.* 10:206. doi: 10.3389/fnmol.2017.00206

Rangaraju, S., Dammer, E. B., Raza, S. A., Rathakrishnan, P., Xiao, H., Gao, T., et al. (2018). Identification and therapeutic modulation of a pro-inflammatory subset of disease-associated-microglia in Alzheimer's disease. *Mol. Neurodegener.* 13:24. doi: 10.1186/s13024-018-0254-8

Rawji, K. S., Mishra, M. K., Michaels, N. J., Rivest, S., Stys, P. K., and Yong, V. W. (2016). Immunosenescence of microglia and macrophages: impact on the ageing central nervous system. *Brain* 139, 653–661. doi: 10.1093/brain/awv395

Reilly, S. M., Chiang, S.-H., Decker, S. J., Chang, L., Uhm, M., Larsen, M. J., et al. (2013). An inhibitor of the protein kinases TBK1 and IKK- & improves obesity-related metabolic dysfunctions in mice. *Nat. Med.* 19, 313–321. doi: 10.1038/nm.3082

Reinert, L. S., Rashidi, A. S., Tran, D. N., Katzilieris-Petras, G., Hvidt, A. K., Gohr, M., et al. (2021). Brain immune cells undergo cGAS/STING-dependent apoptosis during herpes simplex virus type 1 infection to limit type I IFN production. *J. Clin. Invest.* 131:e136824. doi: 10.1172/JCI136824

Ritzel, R. M., Doran, S. J., Glaser, E. P., Meadows, V. E., Faden, A. I., Stoica, B. A., et al. (2019). Old age increases microglial senescence, exacerbates secondary neuroinflammation, and worsens neurological outcomes after acute traumatic brain injury in mice. *Neurobiol. Aging* 77, 194–206. doi: 10.1016/j.neurobiolaging.2019.02.010

Saber, M., Kokiko-Cochran, O., Puntambekar, S. S., Lathia, J. D., and Lamb, B. T. (2017). Triggering receptor expressed on myeloid cells 2 deficiency alters acute macrophage distribution and improves recovery after traumatic brain injury. *J. Neurotrauma* 34, 423–435. doi: 10.1089/neu.2016.4401

Safaiyan, S., Besson-Girard, S., Kaya, T., Cantuti-Castelvetri, L., Liu, L., Ji, H., et al. (2021). White matter aging drives microglial diversity. *Neuron* 109, 1100–1117.e10. doi: 10.1016/j.neuron.2021.01.027

Sala Frigerio, C., Wolfs, L., Fattorelli, N., Thrupp, N., Voytyuk, I., Schmidt, I., et al. (2019). The major risk factors for Alzheimer's disease: age, sex, and genes modulate the microglia response to Aβ plaques. *Cell Rep.* 27, 1293–1306.e6. doi: 10.1016/j.celrep.2019.03.099

Salminen, A., Kaarniranta, K., and Kauppinen, A. (2012). Inflammaging: disturbed interplay between autophagy and inflammasomes. *Aging* 4, 166–175. doi: 10.18632/aging.100444

Sato-Hashimoto, M., Nozu, T., Toriba, R., Horikoshi, A., Akaike, M., Kawamoto, K., et al. (2019). Microglial SIRPα regulates the emergence of CD11c+ microglia and demyelination damage in white matter. *Elife* 8:e42025.

Satoh, J.-i, Kino, Y., Asahina, N., Takitani, M., Miyoshi, J., Ishida, T., et al. (2016). TMEM119 marks a subset of microglia in the human brain. *Neuropathology* 36, 39–49. doi: 10.1111/neup.12235

Sobue, A., Komine, O., Hara, Y., Endo, F., Mizoguchi, H., Watanabe, S., et al. (2021). Microglial gene signature reveals loss of homeostatic microglia associated with neurodegeneration of Alzheimer's disease. *Acta Neuropathol. Commun.* 9:1. doi: 10.1097/00002093-199903000-00001

Srinivasan, K., Friedman, B. A., Etxeberria, A., Huntley, M. A., van der Brug, M. P., Foreman, O., et al. (2019). Alzheimer's patient brain myeloid cells exhibit enhanced aging and unique transcriptional activation. *bioRxiv* [Preprint] 610345. doi: 10.1101/610345

Taetzsch, T., Benusa, S., Levesque, S., Mumaw, C. L., and Block, M. L. (2019). Loss of NF-κB p50 function synergistically augments microglial priming in the middle-aged brain. *J. Neuroinflammation* 16:60.

Thompson, H. J., McCormick, W. C., and Kagan, S. H. (2006). Traumatic brain injury in older adults: epidemiology, outcomes, and future implications. *J. Am. Geriatr. Soc.* 54, 1590–1595. doi: 10.1111/j.1532-5415.2006.00894.x

Tiret, L., Hausherr, E., Thicoipe, M., Garros, B., Maurette, P., Castel, J. P., et al. (1990). The epidemiology of head trauma in aquitaine (France), 1986: a community-based study of hospital admissions and deaths. *Int. J. Epidemiol.* 19, 133–140. doi: 10.1093/ije/19.1.133

Ulland, T. K., Song, W. M., Huang, S. C. C., Ulrich, J. D., Sergushichev, A., Beatty, W. L., et al. (2017). TREM2 maintains microglial metabolic fitness in Alzheimer's disease. *Cell* 170, 649–663. doi: 10.1016/j.cell.2017.07.023

Wiesner, D., Tar, L., Linkus, B., Chandrasekar, A., Olde Heuvel, F., Dupuis, L., et al. (2018). Reversible induction of TDP-43 granules in cortical neurons after traumatic injury. *Exp. Neurol.* 299, 15–25. doi: 10.1016/j.expneurol.2017.09.011

Wilcz-Villega, E., Carter, E., Ironside, A., Xu, R., Mataloni, I., Holdsworth, J., et al. (2020). Macrophages induce malignant traits in mammary epithelium via IKKε/TBK1 kinases and the serine biosynthesis pathway. *EMBO Mol. Med.* 12:e10491. doi: 10.15252/emmm.201910491

Wlodarczyk, A., Benmamar-Badel, A., Cédile, O., Jensen, K. N., Kramer, I., Elsborg, N. B., et al. (2019). CSF1R stimulation promotes increased neuroprotection by CD11c+ microglia in EAE. *Front. Cell. Neurosci.* 12:523. doi: 10.3389/fncel.2018.00523

Wojkowska, D., Szpakowski, P., and Glabinski, A. (2017). Interleukin 17A promotes lymphocytes adhesion and induces CCL2 and CXCL1 release from brain endothelial cells. *Int. J. Mol. Sci.* 18:1000. doi: 10.3390/ijms18051000

Wu, R., Li, X., Xu, P., Huang, L., Cheng, J., Huang, X., et al. (2017). TREM2 protects against cerebral ischemia/reperfusion injury. *Mol. Brain* 10:20. doi: 10.1186/s13041-017-0296-9

Xu, D., Jin, T., Zhu, H., Chen, H., Ofengeim, D., Zou, C., et al. (2018). TBK1 suppresses RIPK1-driven apoptosis and inflammation during development and in aging. *Cell* 174, 1477–1491.e19. doi: 10.1016/j.cell.2018.07.041

Yu, J., Zhou, X., Chang, M., Nakaya, M., Chang, J. H., Xiao, Y., et al. (2015). Regulation of T-cell activation and migration by the kinase TBK1 during neuroinflammation. *Nat. Commun.* 6:6074. doi: 10.1038/ncomms7074

Yum, S., Li, M., Fang, Y., and Chen, Z. J. (2021). TBK1 recruitment to STING activates both IRF3 and NF-κB that mediate immune defense against tumors and viral infections. *Proc. Natl. Acad. Sci. U.S.A.* 118:e2100225118. doi: 10.1073/pnas.2100225118

Zhou, Z., Qi, J., Lim, C. W., Kim, J. W., and Kim, B. (2020). Dual TBK1/IKKε inhibitor amlexanox mitigates palmitic acid-induced hepatotoxicity and lipoapoptosis in vitro. *Toxicology* 444:152579. doi: 10.1016/j.tox.2020.152579

Conflict of Interest: The authors declare that the research was conducted in the absence of any commercial or financial relationships that could be construed as a potential conflict of interest.

frontiers in Aging Neuroscience

ORIGINAL RESEARCH
published: 30 July 2021
doi: 10.3389/fnagi.2021.709620

A Shift in Tissue Stiffness During Hippocampal Maturation Correlates to the Pattern of Neurogenesis and Composition of the Extracellular Matrix

*Youngjae Ryu[1†], Misato Iwashita[1], Wonyoung Lee[1], Kenji Uchimura[2] and Yoichi Kosodo[1]**

[1]Neural Regeneration Lab, Korea Brain Research Institute, Daegu, South Korea, [2]Unit of Glycobiology Structure and Functions, CNRS—UMR 8576/University of Lille, Lille, France

OPEN ACCESS

Edited by:
Karl J. L. Fernandes,
Université de Montréal, Canada

Reviewed by:
Chase Matthew Carver,
The University of Texas Health Science Center at San Antonio, United States
Angeliki Maria Nikolakopoulou,
University of Southern California, United States

***Correspondence:**
Yoichi Kosodo
kosodo@kbri.re.kr

†Present address:
Youngjae Ryu,
Molecular Regeneration and Neuroimaging Laboratory, Burke Neurological Institute, Weill Cornell Medicine, White Plains, NY, United States

Received: 14 May 2021
Accepted: 14 July 2021
Published: 30 July 2021

Citation:
Ryu Y, Iwashita M, Lee W, Uchimura K and Kosodo Y (2021) A Shift in Tissue Stiffness During Hippocampal Maturation Correlates to the Pattern of Neurogenesis and Composition of the Extracellular Matrix. Front. Aging Neurosci. 13:709620. doi: 10.3389/fnagi.2021.709620

Aging changes the mechanical properties of brain tissue, such as stiffness. It has been proposed that the maintenance and differentiation of neural stem cells (NSCs) are regulated in accordance with extracellular stiffness. Neurogenesis is observed in restricted niches, including the dentate gyrus (DG) of the hippocampus, throughout mammalian lifetimes. However, profiles of tissue stiffness in the DG in comparison with the activity of NSCs from the neonatal to the matured brain have rarely been addressed so far. Here, we first applied ultrasound-based shear-wave elasticity imaging (SWEI) in living animals to assess shear modulus as *in vivo* brain stiffness. To complement the assay, atomic force microscopy (AFM) was utilized to determine the Young's modulus in the hippocampus as region-specific stiffness in the brain slice. The results revealed that stiffness in the granule cell layer (GCL) and the hilus, including the subgranular zone (SGZ), increased during hippocampal maturation. We then quantified NSCs and immature neural cells in the DG with differentiation markers, and verified an overall decrease of NSCs and proliferative/immature neural cells along stages, showing that a specific profile is dependent on the subregion. Subsequently, we evaluated the amount of chondroitin sulfate proteoglycans (CSPGs), the major extracellular matrix (ECM) components in the premature brain by CS-56 immunoreactivity. We observed differential signal levels of CSPGs by hippocampal subregions, which became weaker during maturation. To address the contribution of the ECM in determining tissue stiffness, we manipulated the function of CSPGs by enzymatic digestion or supplementation with chondroitin sulfate, which resulted in an increase or decrease of stiffness in the DG, respectively. Our results illustrate that stiffness in the hippocampus shifts due to the composition of ECM, which may affect postnatal neurogenesis by altering the mechanical environment of the NSC niche.

Keywords: mechanical property, dentate gyrus, adult neurogenesis, atomic force microscopy, ultrasound microscopy, shear wave elasticity imaging, extracellular matrix, chondroitin sulfate proteoglycans

INTRODUCTION

Mechanical properties in the brain, including stiffness, are defined by various heterogeneous components, such as neurons, glial cells, vessels, the extracellular matrix (ECM), and interstitial fluids (Franze et al., 2013; Javier-Torrent et al., 2021). Several *in vitro* studies have shown that the proliferation, differentiation, and migration of neural stem cells (NSCs), progenitor cells, and post-mitotic neurons can be regulated depending on the stiffness of the surrounding environment (Saha et al., 2008; Leipzig and Shoichet, 2009; Rammensee et al., 2017). This has been considered as one of the fundamental cell fate-determining factors in neural development and neurological disorders (Barnes et al., 2017; Abuwarda and Pathak, 2020; Hall et al., 2021; Javier-Torrent et al., 2021).

NSCs are observed in specific areas in the mammalian brain, such as the subventricular zone (SVZ) and the dentate gyrus (DG) of the hippocampus, even in grown adults (Fuentealba et al., 2012; Bond et al., 2015). Among the NSCs observed in the adult brain, some are in an active state, while most are in a quiescent state (Urban et al., 2019). In the case of the DG, neurogenesis occurs from glia-like NSCs, which are located in the subgranular zone (SGZ). NSCs transform into neural progenitor cells, which subsequently differentiate into granule cells (Toni and Schinder, 2015; Toda et al., 2019). Previous studies have reported on heterogeneous tissue stiffness in the rodent hippocampus at the neonatal, juvenile, and adult stages (Elkin et al., 2010; Antonovaite et al., 2021). Based on such findings, it is deduced that the stiffness may be related to the niche of NSCs and their activity, including the maintenance and regulation of NSCs (Urban et al., 2019; Kobayashi and Kageyama, 2021). Indeed, it is reported that the mechanical stiffness of the stem cell niche in the SVZ can regulate NSC activity (Kjell et al., 2020). However, the following major questions remain to be addressed: (1) Does a shift in hippocampal stiffness correlate to the differentiation status of NSCs *in vivo*?; and (2) What is the principal component that determines tissue stiffness in the hippocampus?

As a technical aspect, atomic force microscopy (AFM) is generally employed to determine the Young's modulus as the stiffness in local brain regions at both the embryonic (Iwashita et al., 2014; Nagasaka et al., 2016) and adult (Elkin et al., 2007; Luque et al., 2016; Antonovaite et al., 2018) stages. However, tissue slices are required to measure stiffness using AFM, which is a limitation for live animals. Recently, a method using ultrasound (US) has emerged to assess the shear modulus as stiffness in living animals. An acoustic radiation force (ARF) generated by a focused US beam induces shear waves inside the body, which allows for the measurement of the shear modulus *in vivo* (Doherty et al., 2013; Kuo et al., 2017). Using shear-wave elasticity imaging (SWEI), researchers showed that the shear modulus of a rodent brain is different depending on the brain region (Mace et al., 2011) and the age [4 vs. 11 months (M); Lay et al., 2019].

The hippocampus shows more abundant ECM expression levels than other regions (Dauth et al., 2016). It is reported that ECMs, such as hyaluronan and proteoglycan link protein 1 (Hapln1) and proteoglycans, are progressively upregulated over the aging process in rodents (Elkin et al., 2010; Vegh et al., 2014). Among those ECMs, particularly, chondroitin sulfate proteoglycans (CSPGs) are known to be abundant ECM components in developing nervous tissue and have been shown to be related to tissue stiffness in *Xenopus* brains (Koser et al., 2016). Moreover, CSPGs are highly expressed in neurogenic niches and promote hippocampal neurogenesis (Yamada et al., 2018). However, the role of CSPGs associated with hippocampal tissue stiffness has not been investigated so far.

Therefore, in this study, we examined the stiffness of the mouse brain at various time courses during maturation and observed the differentiation status of NSCs as well as immature neural cells. To suggest a correlation between the mechanical properties and pattern of neurogenesis, we observed subregions of the DG separately. Furthermore, we explored the transition and function of CSPGs in the hippocampus to find out their relevance for maturation-dependent changes in brain-tissue stiffness.

MATERIALS AND METHODS

Experimental Animals

All the experiments were performed according to the guidelines of the Korea Brain Research Institute (KBRI) animal care and use committee. Animal experiments and related activities were approved by this committee (IACUC-20-00052). A total of 79 C57BL/6 mice were used in this experiment (purchased from OrientBio, South Korea, or bred at the KBRI). We used 38 male mice for AFM experiments, while both male and female mice were mixed randomly for other analyses. The day of birth was defined as postnatal day 0 (P0). We prepared the following time points for mice in this study: P1, P8, P15, P22, P31, 2–4 M, and 9–10 M. The animals were housed in a 12-h light/12-h dark cycle under controlled temperature (23–25°C). Food and water were supplied *ad libitum*.

US-Based SWEI

Mice were anesthetized using sodium pentobarbital (50 mg/kg dose, intraperitoneal injection; Entobar, Hanlim Pharm., Seoul, South Korea). With the mouse in the prone position, the head of the animal was shaved appropriately, then the skull was gently opened from the Lambda to the Bregma suture point to expose the hippocampal region. After surgery, ultrasound gel (Aquasonic 100, Parker laboratories Inc., Fairfield, NJ, USA) was sufficiently placed onto the opened skull. For US imaging, we used PROSPECT T1 high-frequency US micro-imaging system (S-Sharp Corporation, Taiwan). First, we checked the correct position and the hippocampus area with B-mode imaging. Then, we attached an external radiation force transducer with an independent pulse generator and changed to the ARF mode to obtain the shear modulus. Information detailing the calculation of US-based elasticity can be found in the study of Mace et al. (2011) and the manufacturer[1]. US-SWEI was repeated four times using the same conditions for each animal.

[1]https://www.s-sharp.com

The parameters for the US navigation using the transducer probe were a broadband of 40.0 MHz, a 20-Hz frame rate, 30-μm resolution, and a dynamic range at 50 dB. For the ARF mode, we set the parameters at a 20.0-MHz push frequency, a 40.0-MHz detect frequency, and a 4,000 push cycle with a 200 μm duration and 190 μm intervals. After the US images were taken, mice were sacrificed by cervical dislocation.

Acute Brain Slice Preparation and AFM Measurement

Mice were deeply anesthetized with intraperitoneal injections of sodium pentobarbital. Immediately after the brain was dissected out, we performed vibratome sectioning. The mouse brains were cut into 300-μm-thick whole coronal sections in ice-cold slicing artificial cerebrospinal fluid (aCSF; sucrose 175 mM, glucose 11 mM, NaCl 20 mM, KCl 3.5 mM, NaH_2PO_4 1.25 mM, $NaHCO_3$ 26 mM, and $MgCl_2$ 1.3 mM) using a vibratome (VT1200S, Leica Biosystems, Richmond, IL, USA). Acute slices were incubated in slicing aCSF for 45 min on ice, then transferred to measuring-aCSF buffer (glucose 11 mM, NaCl 120 mM, KCl 3.5 mM, NaH_2PO_4 1.25 mM, $NaHCO_3$ 26 mM, $MgCl_2$ 1.3 mM, and $CaCl_2$ 2 mM) on a 35-mm poly-D-lysine-coated dish prior to indentation. The measurement of brain tissue stiffness was performed as previously described (Iwashita et al., 2020). Briefly, we used an AFM (Bioscope Resolve, NanoScope 9.4, Bruker, Billerica, MA, USA) mounted on an inverted microscope (ECLIPSE Ti2, Nikon, Japan). A tipless silicon cantilever with a 20-μm borosilicate bead (Novascan, Ames, IA, USA) was attached. The spring constant of the cantilever was calibrated using the thermal noise method in air. We chose cantilevers with the same spring constant (nominal value: 0.03 N/m; actual value: 0.07 N/m). The applied force was 10 nN. The specific parameters for the AFM measurement were a ramp size of 10 μm, a ramp rate of 1.0 Hz, a forward and reverse velocity of 20.0 μm/s, a sample Poisson's ratio of 0.5, and a bead radius of 10.0 μm. The measurement was made under physiological conditions (37°C) for the acute slices. The force curves were acquired using the contact mode. To determine the right positions and region of interests (ROIs), bright field images were acquired by a CMOS camera (ORCA-Flash4.0, C13440-20CU, Hamamatsu, Japan).

Manipulation of CSPGs

To induce the degradation of CSPGs, chondroitinase ABC (chABC; Sigma C3667) was used. Acute brain slices obtained from P8 were incubated with 2.5 unit/ml of chABC in measuring-aCSF buffer for 3 h at 25°C (Miller et al., 1997), then washed out with measuring-aCSF buffer to remove enzyme. Chondroitin sulfate (CS; Sigma C4384) was applied to acute brain slices in measuring-aCSF buffer (5 and 15 mg/ml) for 3 h at 25°C (Walz et al., 2002), then washed out with measuring-aCSF buffer to remove the CS that remained in the buffer. For the AFM measurement, the chABC or CS-treated slice was placed on 35-mm poly-D-lysine coated dish and kept in measuring-aCSF buffer prior to indentation. Brain slices untreated with either chABC or CS were used as a control for each experiment.

Immunohistochemistry and Tissue Imaging

The P22, P31, and adult mice were deeply anesthetized with sodium pentobarbital and transcardially fixed with a 4% paraformaldehyde (PFA) solution. In the P1, P8, and P15 mice, the brain tissues were directly collected and immediately immersed in the PFA solution. The brain tissues were post-fixed in a 4% PFA solution for an additional 24 h at 4°C and soaked in a 20%-sucrose solution overnight. The tissues were cryosectioned into 30-μm-thick slices (Leica CM1520 cryostat, Leica Biosystems, Richmond, IL, USA). The tissue sections were incubated in a 2% BSA/0.1% Triton-X 100 solution for the blocking procedure, followed by incubation with diluted primary antibodies overnight. We used the following primary antibodies for immunostaining: anti-glial fibrillary acidic protein antibody (GFAP; mouse, 1:500, G3893, Merck Millipore, USA), anti-Sox2 antibody (rabbit, 1:300, AB5603, Merck Millipore, USA), anti-doublecortin antibody (DCX; rabbit, 1:500, #4604, Cell Signaling Technology, MA, USA), anti-Ki-67 antibody (Ki67; mouse, 1:500, #550609, BD Bioscience, USA), and anti-CSPG (CS-56; mouse, 1:300, ab11570). On the following day, the sections were incubated with secondary antibodies (Alexa Fluor 488 and 568 for each species-matched type, 1:500, Thermo Fisher Scientific, USA) and 4′,6-diamidino-2-phenylindole (DAPI; 1:1,000, Merck Millipore, USA) for 2 h. All tissue images were acquired using a confocal laser scanning microscope (TCS-SP8, Leica Biosystems, Richmond, IL, USA) and an upright confocal laser microscope (A1R-MP, Nikon, Japan). *Z*-stacked images were used for further analysis using five *z*-planes in 3–4 μm intervals.

Data and Image Analysis

For US image analysis, we manually drew an ROI, and the shear modulus was calculated using PROSPECT software (S-Sharp Corporation, Taiwan). The targeted ROI areas were one of left or right hippocampus and the paired side of cortical region.

The AFM data were calculated using Nanoscope Analysis 1.9 software (Bruker, Billerica, MA, USA). The obtained force curves were adjusted to the baseline of each sample and analyzed to calculate Young's modulus fit with the Hertzian model.

The brain tissue image analysis for cell counting and immunoreactivity of CS-56 was done using ImageJ (NIH, MD, USA) and Leica application suite X software (LAS X; Leica Biosystems, Richmond, IL, USA). The ROI area of the stained tissue was the DG in the hippocampus, and each sample of ROIs was analyzed using consequential tissue sections (mouse Bregma −1.70 mm to −2.20 mm).

Statistical Analysis

All statistical analyses were performed using GraphPad Prism software (Version 9, GraphPad Software, San Diego, CA, USA). Statistically significant differences were determined by the student's two-tailed *t*-test and a one-way or two-way analysis of variance (ANOVA) with *post hoc* Bonferroni test for correction of multiple comparisons. Results with $p < 0.05$ were considered

to be statistically significant. The error bars in the figures denotes the standard error of the mean (SEM).

RESULTS

Mechanical Properties of the Mouse Hippocampus and Cortex During Maturation as Evaluated by SWEI and AFM

To assess the mechanical properties of the brain tissue in live animals, we first applied US-based SWEI to mice of various ages, from P8 to grown adults (2–4 M and 9–10 M). The shear wave propagation generated by the ARF using a focused US beam shows reliable and consistent results to quantify the shear modulus as *in vivo* stiffness of the brain tissue, including humans and rodents (Mace et al., 2011; Tzschatzsch et al., 2018). From B-mode imaging, we identified the hippocampal and cortical (somatosensory) regions. Then, the ROIs were manually determined to calculate the shear modulus (**Figure 1A**). The shear modulus of the hippocampi and cortices in the adult mice (2–4 M) were 16.0 ± 0.6 kPa and 13.9 ± 0.7 kPa, respectively, which were in the comparable range of previously reported rodent brains (Mace et al., 2011; Lay et al., 2019). Notably, we found that the shear modulus of the P8 hippocampus (9.3 ± 0.5 kPa) and the cortex (9.2 ± 0.4 kPa) was significantly lower than at other ages ($n = 4$ for each group, two-way ANOVA; **Figure 1B**). Compared to 2–4 M mice, we observed a decreased shear modulus of the hippocampus in older mice (9–10 M; 11.8 ± 1.1 kPa) while a similar level in the cortex (14.1 ± 0.7 kPa), which was consistent with previous reporting (Lay et al., 2019). However, we did not observe significant differences between the shear modulus of the hippocampal and cortical regions in any groups.

To determine the subregional stiffness of the hippocampus, an AFM measurement was performed along the maturation course. AFM analysis is widely used for measuring the Young's modulus for stiffness in biological samples, including brain tissue, and is considered a current gold standard method (see "Introduction" section). Since AFM-based stiffness measurement is hardly applicable to live animals, we prepared *ex vivo* acute brain slices to acquire the Young's modulus from the neonatal (P1) to adult stages (2–4 M and 9–10 M). For indentation, we determined ROIs in the DG of the hippocampus where newborn neurons are observed in adult mice (**Figure 2A**), and then subdivided the DG regions into the granule cell layer (GCL), the hilus including the SGZ (SGZ+HL), and the crest (Amaral, 1978; MacLennan et al., 1998). The Young's modulus of the somatosensory region in the cortex was measured as a reference. We found that the stiffness in all subregions of the hippocampi and cortices tested here increased during maturation ($n = 3$ for P1, P31, 2–4 M, and 9–10 M, $n = 4$ for P8, P15, and P22, one-way ANOVA; **Figure 2B** and **Table 1**). A slight decrease in Young's modulus was observed in the cortex in older mice (9–10 M). Notably, we recognized that the stages when stiffness reached a plateau differed among subregions in the hippocampus. In the case of the GCL, the stiffness increased gradually from P1 (140 ± 22 Pa) to P22 (386 ± 12 Pa) with significant differences. There were no significant changes from P22 to 9–10 M. Similarly, in the SGZ+HL and crest, stiffness started around 140 Pa at P1, significantly increased along with age, and reached its peak at P31 (418 ± 58 Pa) for SGZ+HL or 2–4 M (442 ± 37 Pa) for the crest (**Figure 2B**). Taking the result of the US-based SWEI and AFM analysis together, it can be commonly indicated that the stiffness of hippocampal tissue increases from the neonatal to the early adult stage. Furthermore, time courses of the shift in mechanical environments have specific profiles among subregions in the DG along the maturation course.

Cell Type Populations in the Specific Neural Differentiation Phase at Various Postnatal Stages in the DG of the Hippocampus

Next, we analyzed the activity of NSCs using neurogenesis markers to address the relationship with mechanical characteristics of the hippocampus. Using PFA-fixed brain sections, we examined the expression of Ki-67, a proliferative cell marker, and doublecortin (DCX) for defining immature neuronal cells (**Figure 3A**; Rao and Shetty, 2004). The number of Ki-67-positive cells in the DG was higher at neonatal stages (P1 and P8), then decreased during maturation. The Ki-67-labeled cells were mostly downregulated by the P31 stage, showing a similar level to adult brains ($n = 3$ for each group, left graph: one-way ANOVA, right graph: two-way ANOVA; **Figure 3B**). The number of Ki-67/DCX-double-positive cells peaked at P8, then decreased in later stages (left graph: one-way ANOVA, right graph: two-way ANOVA; **Figure 3C**). It is noteworthy that the Ki-67-positive cells and Ki-67/DCX-double-positive cells were located significantly more in the SGZ+HL than in the GCL at P1, but the population densities reversed at P8. After the P8 stage, the Ki-67-positive and Ki-67/DCX-double-positive cells were located more in the SGZ+HL than the GCL, or were similar between the two regions.

In order to assess the population of NSCs in the DG, we counted GFAP and Sox2 in each postnatal group (**Figure 4A**). Sox2 is a transcription factor expressed in multipotent NSCs (Ellis et al., 2004), while primitive radial glia-like NSCs are double positive for GFAP and Sox2 (Sachewsky et al., 2014). As expected, the total population of Sox2-labeled cells in the DG gradually decreased after P1. At the P1 and P8 stages, the number of Sox2-positive cells in the GCL was significantly higher than the SGZ+HL. Notably, it was observed that the number of Sox2-positive cells in the GCL became fewer than in the SGZ+HL at P15 and P22 ($n = 3$ for each group, left graph: one-way ANOVA, right graph: two-way ANOVA; **Figure 4B**). We found that the number of Sox2/GFAP-double-positive cells in the DG was lowest at P8 among the early postnatal stages (P1 to P22). Similar to the pattern of Ki67/DCX-double-positive cell populations, the Sox2/GFAP-double-positive cells were significantly increased in the SGZ+HL compared to the GCL after P8 ($n = 3$ for each group, left graph: one-way ANOVA, right graph: two-way ANOVA; **Figure 4C**).

Regarding the adult stages tested in this study (2–4 M and 9–10 M), neither the staining patterns nor the quantification

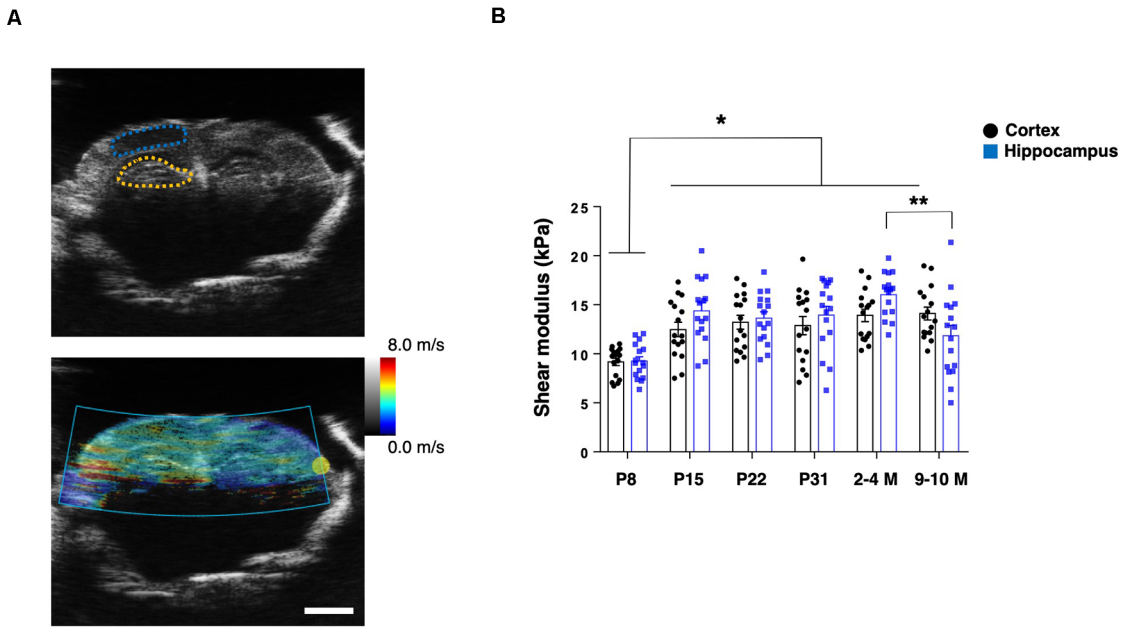

FIGURE 1 | US-based shear-wave elasticity imaging (SWEI) to living post-natal mouse brain during maturation. **(A)** Top: representative B-mode image and regions of interest (ROIs; adult stage; blue-dotted line: somatosensory cortex; yellow-dotted line: hippocampus), bottom: shear wave propagation visualized by acoustic radiation force (ARF) mode. Scale bar: 2 mm. **(B)** Comparison of shear modulus obtained at various postnatal stages (black-round plots: cortex; blue-square plots: hippocampus). *$p < 0.05$, **$p < 0.01$.

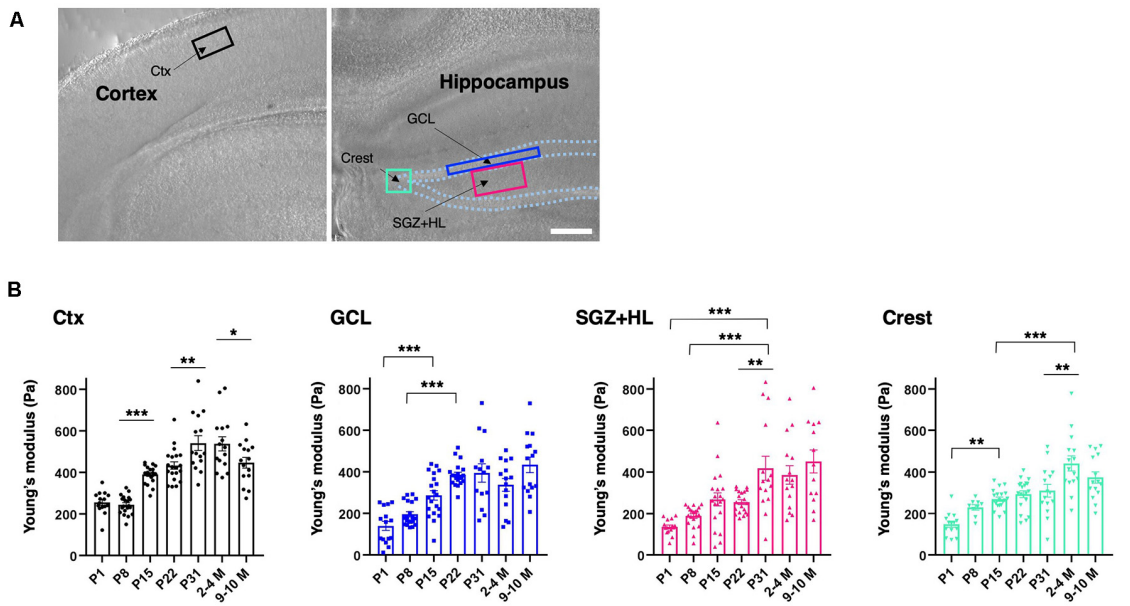

FIGURE 2 | Spatiotemporal shift in stiffness in the dentate gyrus (DG) as examined by atomic force microscopy (AFM). **(A)** The representative cortical and hippocampal areas under a bright field microscope (P8 stage). Rectangles indicate the ROIs for AFM measurement. Ctx, cortex; GCL, granule cell layer; SGZ, subgranular zone; HL, hilus. Scale bar: 200 μm. **(B)** The bar graph with plots presenting Young's modulus in various subregions (black-round plots: cortex; blue-square plots: GCL; magenta-triangle plots: SGZ+HL; green-inverted triangle plots: crest of the DG). *$p < 0.05$, **$p < 0.01$, ***$p < 0.001$.

of used markers (Ki-67/DCX or Sox2/GFAP) were different between the groups (only data for 2–4 M is shown). Our quantitative analysis indicates that postnatal neurogenesis in the DG occurs differently among the hippocampal subregions during brain maturation, especially in the stages between P1 and P22.

TABLE 1 | Summary of the atomic force microscopy (AFM) measurements.

	P1 (*n* = 3)	P8 (*n* = 4)	P15 (*n* = 4)	P22 (*n* = 4)	P31 (*n* = 3)	2–4 M (*n* = 3)	9–10 M (*n* = 3)
Cortex	255 ± 14 Pa (*15*)	244 ± 10 Pa (*20*)	390 ± 9 Pa (*20*)	433 ± 18 Pa (*20*)	541 ± 35 Pa (*15*)	537 ± 34 Pa (*15*)	447 ± 26 Pa (*15*)
GCL	140 ± 22 Pa (*15*)	196 ± 12 Pa (*20*)	287 ± 23 Pa (*20*)	386 ± 12 Pa (*20*)	394 ± 44 Pa (*14*)	337 ± 31 Pa (*15*)	434 ± 37 Pa (*15*)
SGZ+HL	136 ± 9 Pa (*15*)	188 ± 11 Pa (*20*)	268 ± 31 Pa (*20*)	255 ± 12 Pa (*20*)	418 ± 58 Pa (*15*)	386 ± 45 Pa (*15*)	451 ± 55 Pa (*13*)
Crest	149 ± 15 Pa (*14*)	230 ± 13 Pa (*9*)	269 ± 10 Pa (*20*)	293 ± 16 Pa (*20*)	310 ± 30 Pa (*15*)	442 ± 37 Pa (*15*)	374 ± 27 Pa (*15*)

**The "n" indicates the number of animals as well as the number of measured slices (one slice from each animal). **Italicized figures: number of measured points*

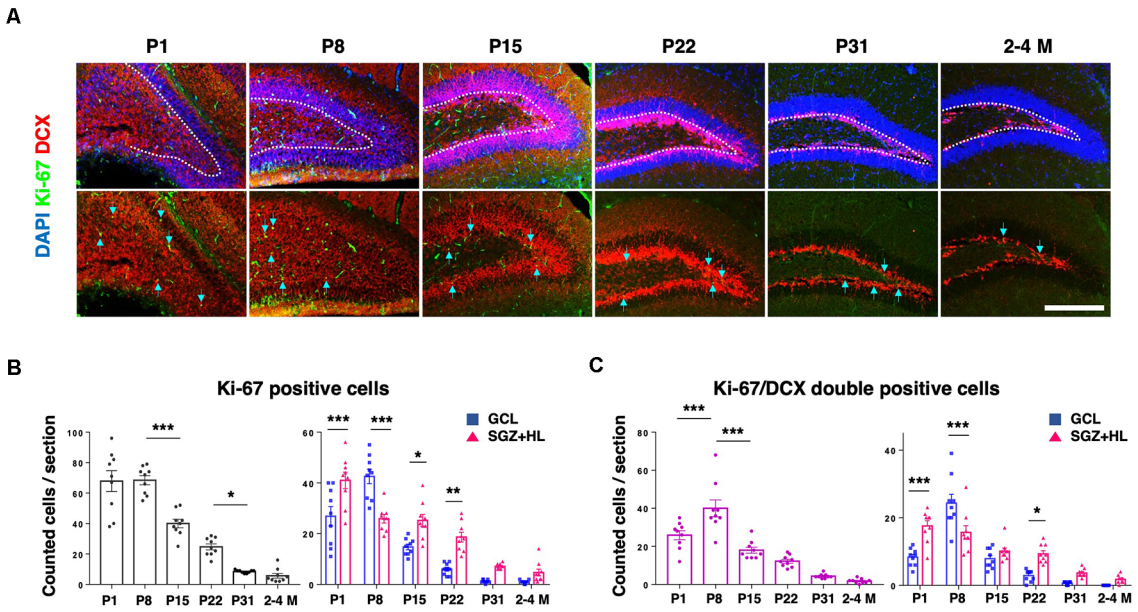

FIGURE 3 | The expression of Ki-67 and DCX in the DG. **(A)** Representative immunostaining images for Ki-67 (green), DCX (red), and DAPI (blue) at various postnatal stages. Arrows indicate Ki-67/DCX-double-positive cells. Scale bar: 200 μm. **(B)** Left: the number of Ki-67-positive cells in the DG in each section. Right: comparison of Ki-67-positive cells in the GCL and SGZ+HL area. **(C)** Left: the number of Ki-67/DCX-double-positive cells in the DG in each section. Right: comparison of the double-positive cells in the GCL and SGZ+HL area (blue-square plots: GCL; magenta-triangle plots: SGZ+HL). *$p < 0.05$, **$p < 0.01$, ***$p < 0.001$.

The Role of CSPGs in Determining Tissue Stiffness in the DG During Hippocampal Maturation

To explore the factors accounting for the shift in brain tissue stiffness during maturation, we examined the immunoreactivity of CS-56 antibody, which recognizes the specific oligosaccharide structure containing both C6-sulfation and C4-sulfation in CSPGs (Miyata and Kitagawa, 2016; **Figure 5A**). We found that CS-56 immunoreactivity was significantly higher in the SGZ+HL than the GCL at the P1 and P8 stages (n = 3 for each group, two-way ANOVA; **Figure 5B**), exhibiting a gradual decrease during maturation toward the adult stages (only data for 2–4 M is shown). The result implies that CS-56-positive CSPGs are enriched in the early postnatal stages when the hippocampal tissue shows softer stiffness and has more NSC population in the DG.

For further investigation of the link between CSPGs and stiffness in the DG, we manipulated the molecular functions of CSPGs in tissue combined with the stiffness measurement by AFM. First, we applied chABC to enzymatically degrade CSPGs in the slice of P8 brain at the stage when a higher level of CS-56 immunoreactivity was observed. Subsequent AFM measurement revealed that stiffness in both the GCL and SGZ+HL was significantly increased in chABC-treated brain slices (n = 3 for each group, unpaired t-test; **Figure 5C** and **Table 2A**). Next, we treated the P8 brain slices with excessive CS, as performed in the developing *Xenopus* brain to decrease tissue stiffness (Koser et al., 2016). We observed that stiffness in both the GCL and SGZ+HL was decreased in CS-treated brain slices in a concentration-dependent manner (n = 3 for control and 15 mg/ml of CS and n = 2 for 5 mg/ml of CS, one-way ANOVA; **Figure 5D** and **Table 2B**). These results imply that CSPGs serve a critical role in determining tissue stiffness in the DG during hippocampal maturation.

DISCUSSION

In the present study, we focused on the mechanical properties of the hippocampus, especially stiffness in the DG along with the time course of tissue maturation at various postnatal stages.

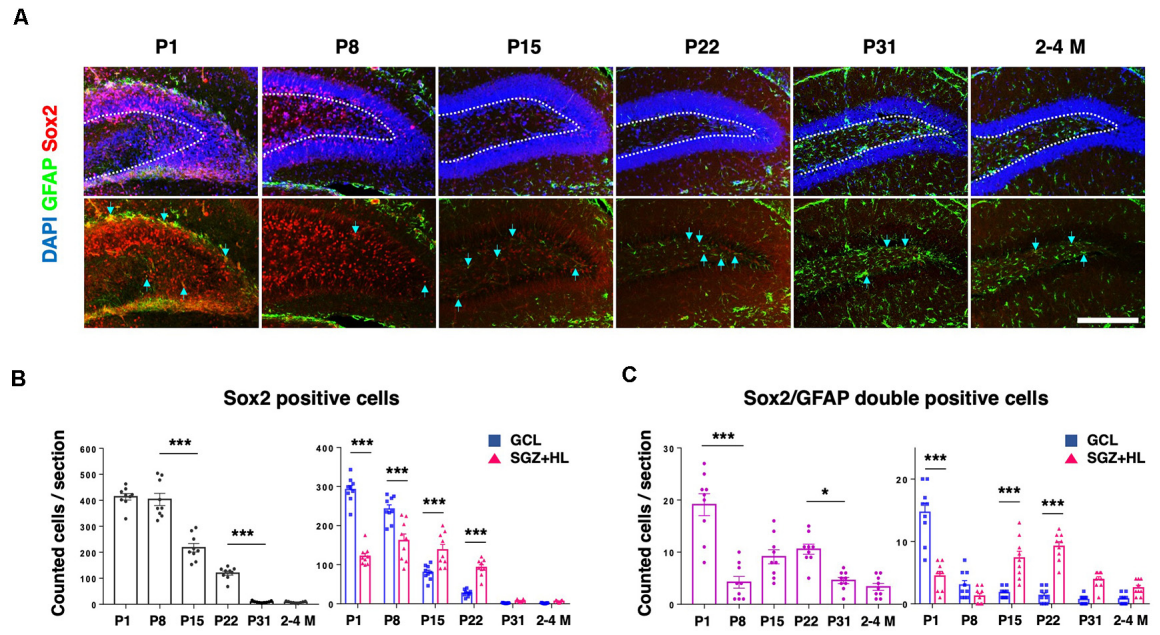

FIGURE 4 | The Sox2- and GFAP-positive cells in the DG. **(A)** Representative immunostaining images for Sox2 (red), GFAP (green), and DAPI (blue) at various postnatal stages. Arrows indicate Sox2/GFAP-double-positive cells. Scale bar: 200 μm. **(B)** Left: the number of Sox2-positive cells in the DG in each section. Right: Comparison of Sox2-positive cells in the GCL and SGZ+HL area. **(C)** Left: the number of Sox2/GFAP-double-positive cells in the DG in each section. Right: comparison of the double-positive cells in the GCL and SGZ+HL area (blue-square plots: GCL; magenta-triangle plots: SGZ+HL). $^{*}p < 0.05$, $^{***}p < 0.001$.

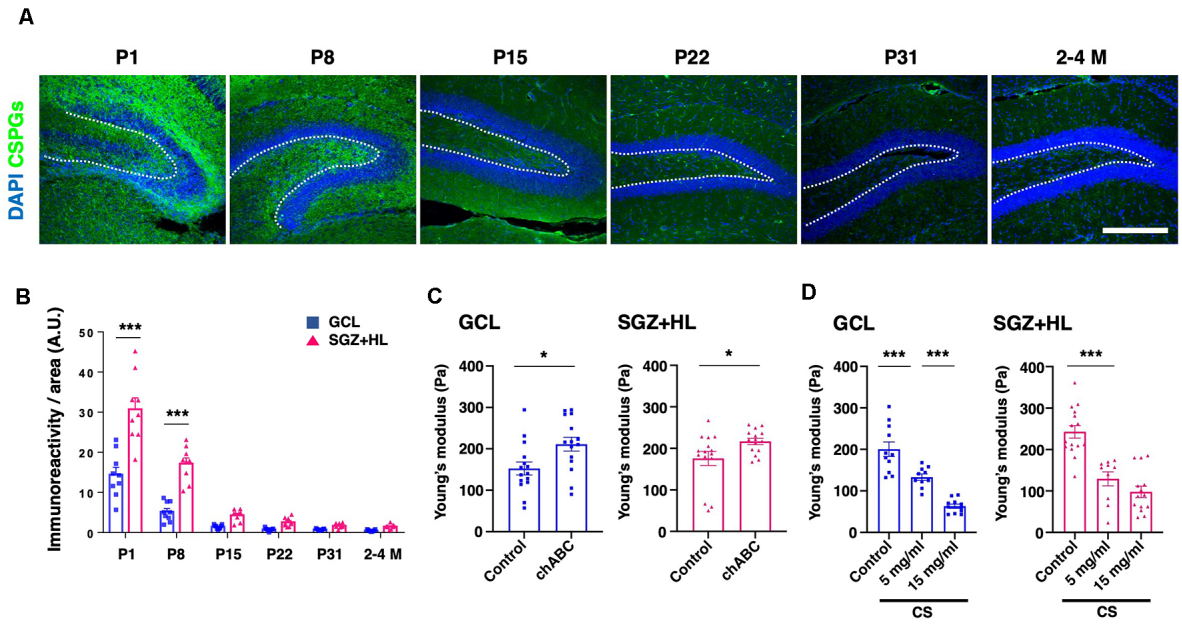

FIGURE 5 | The transition of CSPGs in the DG during maturation and the shift in stiffness by CSPG manipulation. **(A)** Representative immunostaining images for CSPGs using CS-56 antibody (green) and DAPI (blue) at various postnatal stages. The white-dotted lines represent the border between the GCL and SGZ+HL area. Scale bar: 200 μm. **(B)** The bar graph with plots presents a quantitative analysis of the immunoreactivity of the CSPGs in the GCL and SGZ+HL area (blue-square plots: GCL; magenta-triangle plots: SGZ+HL). **(C)** The bar graph with plots presents a quantitative analysis of the stiffness in the GCL and SGZ+HL area treated with chABC (blue-square plots: GCL; magenta-triangle plots: SGZ+HL). **(D)** The bar graph with plots presents a quantitative analysis of the stiffness in the GCL and SGZ+HL area treated with CS. Final concentrations supplied in the buffer are indicated. $^{*}p < 0.05$, $^{***}p < 0.001$.

TABLE 2 | Summary of the AFM measurements with chondroitin sulfate proteoglycan (CSPG) manipulation.

(A) Young's modulus of the chABC-treated tissue

GCL		SGZ+HL	
Control (n = 3)	chABC (n = 3)	Control (n = 3)	chABC (n = 3)
152 ± 16 Pa (*15*)	211 ± 17 Pa (*15*)	176 ± 17 Pa (*15*)	217 ± 7 Pa (*15*)

(B) Young's modulus of CS-treated tissue

GCL			SGZ+HL		
Control (n = 3)	5 mg/ml (n = 2)	15 mg/ml (n = 3)	Control (n = 3)	5 mg/ml (n = 2)	15 mg/ml (n = 3)
200 ± 17 Pa (*11*)	133 ± 8 Pa (*10*)	63 ± 5 Pa (*11*)	243 ± 15 Pa (*15*)	129 ± 17 Pa (*10*)	98 ± 14 Pa (*14*)

**The "n" indicates the number of animals as well as the number of measured slices (one slice from each animal). **Italicized figures: number of measured points*

For this purpose, we used US-based SWEI and AFM to quantify the *in vivo* shear modulus and the *ex vivo* subregional Young's modulus, respectively. Also, we compared the population and differentiation of NSCs in subregions of the hippocampus at the time points when stiffness measurements were taken. Furthermore, we addressed the transition profile and role of CSPGs as the major factor in determining hippocampal tissue stiffness. Together, our work uncovered the relevance between spatiotemporal stiffness and the significant potency of the ECM, which may regulate NSC activity in the hippocampus.

SWEI allows for assessment of the shear modulus as intact tissue stiffness using ARF generated by a push transducer. Recently, SWEI has been widely used for evaluating stiffness *in vivo*, including musculotendinous tissues (Kammoun et al., 2019). Our results pertaining to cortical and hippocampal tissue stiffness are in a comparable range to other studies that used SWEI in adult rodents (within 10 ± 7 kPa; Mace et al., 2011; Lay et al., 2019). However, these results are not of the same order of magnitude as the Young's modulus acquired by AFM-based indentation assessment for the same tissue (ranged within 1 ± 0.5 kPa), which are in agreement with the values of previous reports on post-natal mouse brains (Elkin et al., 2010; Iwashita et al., 2020; Antonovaite et al., 2021). A possible way to account for this difference is that amputation of stiffer tissue components, such as vessels and axons, by slice preparation for AFM measurement may result in decreased stiffness compared to the intact brain. Besides, because of its softness and high deformability for brain tissue, the application of a nonlinear model combined with an inverse analysis might be appropriate for calculating the shear modulus in SWEI measurements (Jiang et al., 2015). In this study, initially, we used SWEI to detect brain tissue stiffness in living animals, although we could not specify subregions of the hippocampus due to insufficient resolution. We then utilized an AFM measurement by preparing *ex vivo* brain slices to evaluate specific regional stiffness. Of note, the SWEI assay indicates that the overall shear modulus in the hippocampus region was significantly decreased in the older brain (9–10 M) compared to the younger brain, while the tendency of the Young's moduli determined by AFM varied dependent on the subregions of the DG (**Figures 1**, **2**). Despite these points, both approaches commonly showed the overall increase of tissue stiffness during hippocampal maturation, which is consistent with previous studies on rodent brains (Elkin et al., 2010; Antonovaite et al., 2021). It is reported that the GCL of adult mice shows lower stiffness relative to the other parts of the hippocampus (Antonovaite et al., 2018). Our data are largely in agreement with this report on the adult brain, although we could not detect statistically significant differences. Notably, we further identified that the stiffness of the GCL was higher (386 ± 12 Pa) than that of the SGZ+HL area (255 ± 12 Pa) at P22 (**Figure 2** and **Table 1**). This result suggests that there is a dynamic conversion in stiffness in particular subregions during brain maturation. We assume that it can be due to: (1) vigorous alteration of neural cell types and populations by cellular differentiation as well as migration with morphological changes (Abuwarda and Pathak, 2020); or (2), production or degradation of specific ECM components (Walma and Yamada, 2020, and this study).

Neurogenesis in the DG of the hippocampus is observed throughout the lifetime of mammals, and the differentiation of NSCs in the hippocampus can be dependent on the tissue environments, including mechanical cues (Urban et al., 2019; Kobayashi and Kageyama, 2021). Indeed, several *in vitro* studies have shown that mechanical stiffness affects the migration and differentiation of NSCs (see "Introduction" section). Here, our data show that the neurogenesis in the DG decreases during maturation; meanwhile, the hippocampal tissue stiffness increases. Particularly, we observed that the populations of NSCs (Sox2/GFAP-double-positive cells; **Figure 4**) and proliferative immature neural cells (Ki-67/DCX-double-positive cells; **Figure 3**) in the SGZ+HL compared to the GCL area show dynamically differential patterns from the neonatal to the adult stage. As described above, the SGZ+HL showed lower stiffness than that of the GCL area especially at P22 (**Figure 2** and **Table 1**). Considering that NSCs are more differentiated into glial cells on a harder substrate than a soft substrate (Saha et al., 2008; Tse and Engler, 2011), the significantly greater populations of Sox2/GFAP- and Ki-67/DCX-double-positive neural cells in the SGZ+HL compared to the GCL area at P22 but not P31 and adult stages (**Figures 3**, **4**) may be well explained by the preference of softer regions for neural cells. Taking the previous results and our study together, we raise a possibility that the differences in stiffness among the hippocampal subregions could be one of the factors determining the pattern of transition/migration of the NSCs and the immature neural-cell population.

Our approach to manipulating the function of CSPGs in brain slices revealed the importance of ECM composition

to determining tissue stiffness. The enzymatic digestion of CSPGs induced the stiffening of tissue, while the addition of CS had the opposite effect. These results fit well into the temporal profiling of the ECM and the shear modulus as well as Young's modulus; that is, a higher level of CS-56-positive CSPGs correlated to lower brain stiffness at early postnatal stages in the hippocampus. Among the subregions of the DG, the CSPG level in the SGZ+HL was higher than that of the GCL in all groups, although the stiffness between the SGZ+HL and GCL was essentially similar during hippocampal maturation except at P22. We consider the possibility that the other ECMs of perineuronal nets, such as hyaluronan and Hapln1, may be involved in determining stiffness in the hippocampus (Vegh et al., 2014; Richter et al., 2018). Alternatively, not only the amount of CSPGs but also the difference in the mode of chondroitin sulfation may affect the mechanical microenvironment in tissue. Indeed, it has been shown that chondroitin C6-sulfation is dominant early in the postnatal period, while the degree of C4-sulfation increases during the maturation of the mouse brain (Miyata et al., 2012). Further systematic analyses to clarify the molecular constituent of ECMs and their origins in tissue, as well as cell-types, are required.

By coupling the measurement of mechanical properties in hippocampal tissue and quantitative cellular characterization at the various postnatal stages, our data suggest a correlation between the tissue's micro-mechanical stiffness and the composition of the ECMs, which may have regulatory effects on the activity of NSCs. It is worth noting that the changes of NSCs/neural immature cell populations and stiffness in the subregions of the DG were observed during the early postnatal period. Whether the same or different principle exists in the case of a much older brain or neurodegenerative disease is still an open question. We expect that further related studies can reveal regulatory mechanisms of *in vivo* neurogenesis associated with the modulation of brain tissue stiffness.

DATA AVAILABILITY STATEMENT

The original contributions presented in the study are included in the article, further inquiries can be directed to the corresponding author.

ETHICS STATEMENT

The animal study was reviewed and approved by Korea Brain Research Institute Animal Care and Use Committee.

AUTHOR CONTRIBUTIONS

YR and YK: study design and conceptualization. YR: manuscript writing. YR, MI, and YK: manuscript editing. Experiments: YR for US-SWEI, AFM, and neural differentiation analyses, MI for AFM and CSPG manipulations, WL for US-SWEI. YR, MI, and KU: resources. YR, MI, and YK: data validation. YK: project administration. All authors contributed to the article and approved the submitted version.

FUNDING

This study was funded by grants from the KBRI Basic Research Program by the Ministry of Science, ICT, and Future Planning (No. 21-BR-02-02; to YK), and the National Research Foundation of Korea 2019R1F1A1061003 (to MI).

ACKNOWLEDGMENTS

We thank Gwanghyun Park (KBRI) for valuable support, and the Research Equipment Core Facility Team (KBRI) for technical assistance. We acknowledge SPIRITS 2020 of Kyoto University for supporting research communications.

REFERENCES

Abuwarda, H., and Pathak, M. M. (2020). Mechanobiology of neural development. *Curr. Opin. Cell. Biol.* 66, 104–111. doi: 10.1016/j.ceb.2020.05.012

Amaral, D. G. (1978). A golgi study of cell types in the hilar region of the hippocampus in the rat. *J. Comp. Neurol.* 182, 851–914. doi: 10.1002/cne.901820508

Antonovaite, N., Beekmans, S. V., Hol, E. M., Wadman, W. J., and Iannuzzi, D. (2018). Regional variations in stiffness in live mouse brain tissue determined by depth-controlled indentation mapping. *Sci. Rep.* 8:12517. doi: 10.1038/s41598-018-31035-y

Antonovaite, N., Hulshof, L. A., Hol, E. M., Wadman, W. J., and Iannuzzi, D. (2021). Viscoelastic mapping of mouse brain tissue: relation to structure and age. *J. Mech. Behav. Biomed. Mater.* 113:104159. doi: 10.1016/j.jmbbm.2020.104159

Barnes, J. M., Przybyla, L., and Weaver, V. M. (2017). Tissue mechanics regulate brain development, homeostasis and disease. *J. Cell. Sci.* 130, 71–82. doi: 10.1242/jcs.191742

Bond, A. M., Ming, G. L., and Song, H. (2015). Adult mammalian neural stem cells and neurogenesis: five decades later. *Cell Stem Cell* 17, 385–395. doi: 10.1016/j.stem.2015.09.003

Dauth, S., Grevesse, T., Pantazopoulos, H., Campbell, P. H., Maoz, B. M., Berretta, S., et al. (2016). Extracellular matrix protein expression is brain region dependent. *J. Comp. Neurol.* 524, 1309–1336. doi: 10.1002/cne.23965

Doherty, J. R., Trahey, G. E., Nightingale, K. R., and Palmeri, M. L. (2013). Acoustic radiation force elasticity imaging in diagnostic ultrasound. *IEEE Trans. Ultrason. Ferroelectr. Freq. Control* 60, 685–701. doi: 10.1109/TUFFC.2013.2617

Elkin, B. S., Azeloglu, E. U., Costa, K. D., and Morrison, B. III. (2007). Mechanical heterogeneity of the rat hippocampus measured by atomic force microscope indentation. *J. Neurotrauma* 24, 812–822. doi: 10.1089/neu.2006.0169

Elkin, B. S., Ilankovan, A., and Morrison, B. III. (2010). Age-dependent regional mechanical properties of the rat hippocampus and cortex. *J. Biomech. Eng.* 132:011010. doi: 10.1115/1.4000164

Ellis, P., Fagan, B. M., Magness, S. T., Hutton, S., Taranova, O., Hayashi, S., et al. (2004). SOX2, a persistent marker for multipotential neural stem cells derived from embryonic stem cells, the embryo or the adult. *Dev. Neurosci.* 26, 148–165. doi: 10.1159/000082134

Franze, K., Janmey, P. A., and Guck, J. (2013). Mechanics in neuronal development and repair. *Annu. Rev. Biomed. Eng.* 15, 227–251. doi: 10.1146/annurev-bioeng-071811-150045

Fuentealba, L. C., Obernier, K., and Alvarez-Buylla, A. (2012). Adult neural stem cells bridge their niche. *Cell Stem Cell* 10, 698–708. doi: 10.1016/j.stem.2012.05.012

Hall, C. M., Moeendarbary, E., and Sheridan, G. K. (2021). Mechanobiology of the brain in ageing and Alzheimer's disease. *Eur. J. Neurosci.* 53, 3851–3878 doi: 10.1111/ejn.14766

Iwashita, M., Kataoka, N., Toida, K., and Kosodo, Y. (2014). Systematic profiling of spatiotemporal tissue and cellular stiffness in the developing brain. *Development* 141, 3793–3798. doi: 10.1242/dev.109637

Iwashita, M., Nomura, T., Suetsugu, T., Matsuzaki, F., Kojima, S., and Kosodo, Y. (2020). Comparative analysis of brain stiffness among amniotes using glyoxal fixation and atomic force microscopy. *Front. Cell. Dev. Biol.* 8:574619. doi: 10.3389/fcell.2020.574619

Javier-Torrent, M., Zimmer-Bensch, G., and Nguyen, L. (2021). Mechanical forces orchestrate brain development. *Trends. Neurosci.* 44, 110–121. doi: 10.1016/j.tins.2020.10.012

Jiang, Y., Li, G., Qian, L. X., Liang, S., Destrade, M., and Cao, Y. (2015). Measuring the linear and nonlinear elastic properties of brain tissue with shear waves and inverse analysis. *Biomech. Model. Mechanobiol.* 14, 1119–1128. doi: 10.1007/s10237-015-0658-0

Kammoun, M., Ternifi, R., Dupres, V., Pouletaut, P., Meme, S., Meme, W., et al. (2019). Development of a novel multiphysical approach for the characterization of mechanical properties of musculotendinous tissues. *Sci. Rep.* 9:7733. doi: 10.1038/s41598-019-44053-1

Kjell, J., Fischer-Sternjak, J., Thompson, A. J., Friess, C., Sticco, M. J., Salinas, F., et al. (2020). Defining the adult neural stem cell niche proteome identifies key regulators of adult neurogenesis. *Cell Stem Cell* 26, 277.e8–293.e8. doi: 10.1016/j.stem.2020.01.002

Kobayashi, T., and Kageyama, R. (2021). Lysosomes and signaling pathways for maintenance of quiescence in adult neural stem cells. *FEBS J.* 288, 3082–3093. doi: 10.1111/febs.15555

Koser, D. E., Thompson, A. J., Foster, S. K., Dwivedy, A., Pillai, E. K., Sheridan, G. K., et al. (2016). Mechanosensing is critical for axon growth in the developing brain. *Nat. Neurosci.* 19, 1592–1598. doi: 10.1038/nn.4394

Kuo, P. L., Charng, C. C., Wu, P. C., and Li, P. C. (2017). Shear-wave elasticity measurements of three-dimensional cell cultures for mechanobiology. *J. Cell. Sci.* 130, 292–302. doi: 10.1242/jcs.186320

Lay, F. Y., Chen, P. Y., Cheng, H. F., Kuo, Y. M., and Huang, C. C. (2019). *Ex Vivo* Evaluation of mouse brain elasticity using high-frequency ultrasound elastography. *IEEE Trans. Biomed. Eng.* 66, 3426–3435. doi: 10.1109/TBME.2019.2905551

Leipzig, N. D., and Shoichet, M. S. (2009). The effect of substrate stiffness on adult neural stem cell behavior. *Biomaterials* 30, 6867–6878. doi: 10.1016/j.biomaterials.2009.09.002

Luque, T., Kang, M. S., Schaffer, D. V., and Kumar, S. (2016). Microelastic mapping of the rat dentate gyrus. *R. Soc. Open Sci.* 3:150702. doi: 10.1098/rsos.150702

Mace, E., Cohen, I., Montaldo, G., Miles, R., Fink, M., and Tanter, M. (2011). *in vivo* Mapping of brain elasticity in small animals using shear wave imaging. *IEEE Trans Med. Imaging* 30, 550–558. doi: 10.1109/TMI.2010.2079940

MacLennan, K. M., Smith, P. F., and Darlington, C. L. (1998). Adrenalectomy-induced neuronal degeneration. *Prog. Neurobiol.* 54, 481–498. doi: 10.1016/s0301-0082(97)00076-2

Miller, B., Sheppard, A. M., and Pearlman, A. L. (1997). Developmental expression of keratan sulfate-like immunoreactivity distinguishes thalamic nuclei and cortical domains. *J. Comp. Neurol.* 380, 533–552. doi: 10.1002/(sici)1096-9861(19970421)380:4<533::aid-cne9>3.0.co;2-2

Miyata, S., and Kitagawa, H. (2016). Chondroitin 6-sulfation regulates perineuronal net formation by controlling the stability of aggrecan. *Neural Plast.* 2016:1305801. doi: 10.1155/2016/1305801

Miyata, S., Komatsu, Y., Yoshimura, Y., Taya, C., and Kitagawa, H. (2012). Persistent cortical plasticity by upregulation of chondroitin 6-sulfation. *Nat. Neurosci.* 15, 414–422, S411–412. doi: 10.1038/nn.3023

Nagasaka, A., Shinoda, T., Kawaue, T., Suzuki, M., Nagayama, K., Matsumoto, T., et al. (2016). Differences in the mechanical properties of the developing cerebral cortical proliferative zone between mice and ferrets at both the tissue and single-cell levels. *Front. Cell. Dev. Biol.* 4:139. doi: 10.3389/fcell.2016.00139

Rammensee, S., Kang, M. S., Georgiou, K., Kumar, S., and Schaffer, D. V. (2017). Dynamics of mechanosensitive neural stem cell differentiation. *Stem Cells* 35, 497–506. doi: 10.1002/stem.2489

Rao, M. S., and Shetty, A. K. (2004). Efficacy of doublecortin as a marker to analyze the absolute number and dendritic growth of newly generated neurons in the adult dentate gyrus. *Eur. J. Neurosci.* 19, 234–246. doi: 10.1111/j.0953-816x.2003.03123.x

Richter, R. P., Baranova, N. S., Day, A. J., and Kwok, J. C. (2018). Glycosaminoglycans in extracellular matrix organization: are concepts from soft matter physics key to understanding the formation of perineuronal nets? *Curr. Opin. Struct. Biol.* 50, 65–74. doi: 10.1016/j.sbi.2017.12.002

Sachewsky, N., Leeder, R., Xu, W., Rose, K. L., Yu, F., Van Der Kooy, D., et al. (2014). Primitive neural stem cells in the adult mammalian brain give rise to GFAP-expressing neural stem cells. *Stem Cell Rep.* 2, 810–824. doi: 10.1016/j.stemcr.2014.04.008

Saha, K., Keung, A. J., Irwin, E. F., Li, Y., Little, L., Schaffer, D. V., et al. (2008). Substrate modulus directs neural stem cell behavior. *Biophys. J.* 95, 4426–4438. doi: 10.1529/biophysj.108.132217

Toda, T., Parylak, S. L., Linker, S. B., and Gage, F. H. (2019). The role of adult hippocampal neurogenesis in brain health and disease. *Mol. Psychiatry.* 24, 67–87. doi: 10.1038/s41380-018-0036-2

Toni, N., and Schinder, A. F. (2015). Maturation and functional integration of new granule cells into the adult hippocampus. *Cold Spring Harb. Perspect. Biol.* 8:a018903. doi: 10.1101/cshperspect.a018903

Tse, J. R., and Engler, A. J. (2011). Stiffness gradients mimicking *in vivo* tissue variation regulate mesenchymal stem cell fate. *PLoS One* 6:e15978. doi: 10.1371/journal.pone.0015978

Tzschatzsch, H., Kreft, B., Schrank, F., Bergs, J., Braun, J., and Sack, I. (2018). *in vivo* Time-harmonic ultrasound elastography of the human brain detects acute cerebral stiffness changes induced by intracranial pressure variations. *Sci. Rep.* 8:17888. doi: 10.1038/s41598-018-36191-9

Urban, N., Blomfield, I. M., and Guillemot, F. (2019). Quiescence of adult mammalian neural stem cells: a highly regulated rest. *Neuron* 104, 834–848. doi: 10.1016/j.neuron.2019.09.026

Vegh, M. J., Rausell, A., Loos, M., Heldring, C. M., Jurkowski, W., Van Nierop, P., et al. (2014). Hippocampal extracellular matrix levels and stochasticity in synaptic protein expression increase with age and are associated with age-dependent cognitive decline. *Mol. Cell. Proteomics.* 13, 2975–2985. doi: 10.1074/mcp.M113.032086

Walma, D. A. C., and Yamada, K. M. (2020). The extracellular matrix in development. *Development* 147:dev175596. doi: 10.1242/dev.175596

Walz, A., Anderson, R. B., Irie, A., Chien, C. B., and Holt, C. E. (2002). Chondroitin sulfate disrupts axon pathfinding in the optic tract and alters growth cone dynamics. *J. Neurobiol.* 53, 330–342. doi: 10.1002/neu.10113

Yamada, J., Nadanaka, S., Kitagawa, H., Takeuchi, K., and Jinno, S. (2018). Increased synthesis of chondroitin sulfate proteoglycan promotes adult hippocampal neurogenesis in response to enriched environment. *J. Neurosci.* 38, 8496–8513. doi: 10.1523/JNEUROSCI.0632-18.2018

Conflict of Interest: The authors declare that the research was conducted in the absence of any commercial or financial relationships that could be construed as a potential conflict of interest.

Publisher's Note: All claims expressed in this article are solely those of the authors and do not necessarily represent those of their affiliated organizations, or those of the publisher, the editors and the reviewers. Any product that may be evaluated in this article, or claim that may be made by its manufacturer, is not guaranteed or endorsed by the publisher.

frontiers in Aging Neuroscience

ORIGINAL RESEARCH
published: 27 September 2021
doi: 10.3389/fnagi.2021.717644

Enriched Environment Attenuates Pyroptosis to Improve Functional Recovery After Cerebral Ischemia/Reperfusion Injury

Jingying Liu[1†], Jun Zheng[1†], Yang Xu[2], Wenyue Cao[1], Jinchen Wang[3], Biru Wang[1], Linyao Zhao[2], Xin Zhang[1] and Weijing Liao[1*]*

[1] Department of Rehabilitation Medicine, Zhongnan Hospital of Wuhan University, Wuhan, China, [2] Department of Neurosurgery, Renmin Hospital of Wuhan University, Wuhan, China, [3] Department of Anesthesiology, Zhujiang Hospital of Southern Medical University, Guangzhou, China

Enriched environment (EE) is a complex containing social, cognitive, and motor stimuli. Exposure to EE can promote functional recovery after ischemia/reperfusion (I/R) injury. However, the underlying mechanisms remained unclear. Pyroptosis has recently been identified and demonstrated a significant role in ischemic stroke. The purpose of this study was to explore the effect of EE on neuronal pyroptosis after cerebral I/R injury. In the current study, middle cerebral artery occlusion/reperfusion (MCAO/R) was applied to establish the cerebral I/R injury model. Behavior tests including the modified Neurological Severity Scores (mNSS) and the Morris Water Maze (MWM) were performed. The infarct volume was evaluated by Nissl staining. To evaluate the levels of pyroptosis-related proteins, the levels of GSDMD-N and nod-like receptor protein 1/3 (NLRP1/3) inflammasome-related proteins were examined. The mRNA levels of IL-1β and IL-18 were detected by Quantitative Real-Time PCR (qPCR). The secretion levels of IL-1β and IL-18 were analyzed by ELISA. Also, the expression of p65 and p-p65 were detected. The results showed that EE treatment improved functional recovery, reduced infarct volume, attenuated neuronal pyroptosis after cerebral I/R injury. EE treatment also suppressed the activities of NLRP1/NLRP3 inflammasomes. These may be affected by inhabiting the NF-κB p65 signaling pathway. Our findings suggested that neuronal pyroptosis was probably the neuroprotective mechanism that EE treatment rescued neurological deficits after I/R injury.

Keywords: cerebral ischemia/reperfusion, inflammasome, ischemic stroke, enriched environment, neuronal pyroptosis

OPEN ACCESS

Edited by:
Homaira Nawabi, Institut National de la Santé et de la Recherche Médicale (INSERM), France

Reviewed by:
Yuanyuan Liu, National Institute of Dental and Craniofacial Research (NIDCR), United States
Julia Schaeffer, Université Grenoble Alpes, France

***Correspondence:**
Xin Zhang
zhangxin0439@163.com
Weijing Liao
weijingliaorehab@163.com

[†] These authors have contributed equally to this work

Received: *31 May 2021*
Accepted: *01 September 2021*
Published: *27 September 2021*

Citation:
Liu J, Zheng J, Xu Y, Cao W, Wang J, Wang B, Zhao L, Zhang X and Liao W (2021) Enriched Environment Attenuates Pyroptosis to Improve Functional Recovery After Cerebral Ischemia/Reperfusion Injury. Front. Aging Neurosci. 13:717644. doi: 10.3389/fnagi.2021.717644

INTRODUCTION

Stroke is a disease with the highest mortality and disability rates in the world. Ischemic stroke is responsible for the majority of strokes (Campbell et al., 2019; Stinear et al., 2020). Despite the increasing improvement in the treatment of stroke, many survivors remain with residual functional deficits (Winstein et al., 2016). Therefore, the need for effective stroke rehabilitation is essential for the patients to deal with life challenges after stroke.

Enriched environment (EE) is a complex containing social, cognitive, and motor stimuli (Kempermann, 2019). EE provides laboratory animals with greater living space, further sensory stimulation, more possibilities for social interaction, and increasing opportunities for learning than the standard environment (Dahlqvist et al., 2003). The benefits of EE in neurological diseases have been extensive studied (Begenisic et al., 2015; Jungling et al., 2017; Song et al., 2017; Shin et al., 2018). In the EE, the ability of learning and memory has been significantly improved while the anxiety behavior was reduced (Benaroya–Milshtein et al., 2004). Meanwhile, exposure to EE enhanced the experience-dependent plasticity of the brain and promoted the recovery of cognitive and motor functions after ischemia/reperfusion (I/R) injury (Livingston-Thomas et al., 2016). EE improved cognitive function via neurogenesis and angiogenesis by regulating the activation of PI3K/AKT/GSK-3/β-catenin signaling pathways and intrinsic axon guidance molecules following I/R (Zhan et al., 2020). Moreover, EE mediated neurogenesis by inhibiting the production and secretion of IL-17A from astrocyte *via* NF-κB/p65 after I/R injury (Zhang et al., 2018). EE also facilitated cognitive recovery through remodeling bilateral synaptic after ischemic stroke (Wang C. et al., 2019). However, there has been little research on the relationship between EE-mediated ischemic stroke recovery and cell death. Evidence has shown that EE reduced spontaneous apoptotic cell death in the rat hippocampus (Young et al., 1999). A recent study has demonstrated that enriched environment-induced neuronal autophagy boosted the post-stroke recovery of neurological function (Deng et al., 2021). Our previous studies have illustrated that EE reduced neuronal apoptosis conducting to the superior recovery after I/R injury (Chen et al., 2017). However, the mechanisms by which EE attenuated cell death following stroke remained unclear.

Pyroptosis is a type of lytic cell death that features cell swelling, rapid rupture of the plasma membrane, and release of proinflammatory intracellular contents as a result of cleaving pore-forming proteins gasdermin D (GSDMD) following by activation of inflammasomes (Shi et al., 2017). Inflammasomes are large multimolecular complexes formed of a cytosolic sensor (nucleotide-binding domain and leucine-rich-repeat-containing [NLR] Pyrin domain containing NLRP1 and NLRP3), an adaptor protein (apoptosis-associated speck-like protein containing a CARD [ASC]), and an effector caspase pro-caspase-1 (Rathinam and Fitzgerald, 2016). After ischemic stroke attacks, the expression of inflammasomes is abundant in the brain (Abulafia et al., 2009). Pro-caspase-1 is activated through NLRP1 and NLRP3 signal cleaving GSDMD into the N-terminal gasdermin-N domain and the C-terminal gasdermin-C domain (Shi et al., 2015; Wang et al., 2020b). Then the pore-forming GSDMD-N domain causes membrane lysis inducing pyroptosis (Ding et al., 2016; Sborgi et al., 2016). Also, activated caspase-1 mediates the maturation of Interleukin-1β (IL-1β) and Interleukin-18 (IL-18) which are released into the extracellular environment subsequently (Brough and Rothwell, 2007). In recent years, increasing evidence indicated that inflammasome-mediated pyroptosis following ischemic stroke performed a crucial role in the course of functional recovery (Xu et al., 2019; Li et al., 2020). In addition, the activation of inflammasome was considered an essential step for neuroinflammation in subsequent brain injury (Walsh et al., 2014). Increasing expression of NLRP1 and NLRP3 inflammasome has been confirmed in neurons, microglia, and astrocytes (Barrington et al., 2017). Particularly, NLRP1 and NLRP3 inflammasome-mediated neuronal pyroptosis performed an increasingly crucial role in the course of ischemic stroke (Yang-Wei Fann et al., 2013; Ito et al., 2015). As a widely studied inflammation-associated transcriptional element, NF-κB regulated numerous genes and signaling pathways associated with inflammation (Afonina et al., 2017). Furthermore, emerging evidence suggested that the elevated expression of NLRP1 and NLRP3 inflammasome proteins could be modulated by the NF-κB signaling pathway in ischemic stroke (Gross et al., 2011; Fann et al., 2018). Although the accumulated evidence has shown that pyroptosis was involved in ischemic stroke injury, the relationship between neuronal pyroptosis and EE-mediated functional recovery following ischemic stroke was still unknown.

Since EE was neuroprotective and pyroptosis was involved in the progress of ischemic stroke. We formulated the hypothesis that post-stroke neurological outcomes could be improved by EE treatment to attenuate neuronal pyroptosis. In the current study, we investigated pyroptosis-related protein expression levels in the penumbra in a rat I/R injury model. Additionally, EE decreased the expression levels of NLRP1, NLRP3, and GSDMD-N. We firstly demonstrated that EE rescued neurological deficits after I/R injury involving the suppressing of neuronal pyroptosis. Generally, our findings indicated EE as a promising therapeutic method for ischemic stroke-mediated inflammasome activity.

MATERIALS AND METHODS

Animals

Male Sprague–Dawley rats (6–7 weeks old, 200–220 g) from Beijing Vital River Laboratory Animal Technology Company were kept in individually ventilated cages (temperature: 20 ± 1°C, relative humidity: 55 ± 5%, lighting period: 8:00 ∼ 20:00) with free access to water and rat feed. Upon arrival, all rats had a 3-day acclimation before receiving the operation. Following acclimation, the animals were numbered and randomly divided into various groups: the sham + standard condition group (SSC), the sham + enriched environment group (SEE), the ischemia/reperfusion + standard condition group (ISC), and the ischemia/reperfusion + enriched environment group (IEE). The schematic representation of the experimental timeline and the setting of EE were shown in **Figure 1**. All animal experimental procedures were approved according to the Animal Care and Use Committee of Wuhan University. All efforts were made to minimize the mortality of animals and their suffering.

Middle Cerebral Artery Occlusion and Reperfusion

Following adapting, male rats were subjected to transient Middle Cerebral Artery Occlusion and Reperfusion (MCAO/R) injury as previously described (Longa et al., 1989). All experimental animals were anesthetized by isoflurane through a face mask (inducing concentration: 4%, maintaining concentration: 2%, respectively, in 2:1 N_2O:O_2). An approximately 2 cm incision

FIGURE 1 | Flow chart of the experimental protocol and enrichment settings. **(A)** Timeline of behavioral testing after stroke. Modified Neurological Severity Scores (mNSS) were tested 3, 7, 14, and 21 days post-stroke (arrows) and compared with baseline performances to evaluate sensorimotor deficits. Morris Water Maze (MWM) test was performed from day 21 to day 26 post-stroke to evaluate spatial learning and memory. **(B)** The setting of an enriched environment.

was made in the middle of the neck. The common carotid artery (CCA), internal carotid artery (ICA), and external carotid artery (ECA) were meticulously separated. And a 5–0 silk thread was used to ligate the left ECA. Then ligating the CCA with 5-0 silk thread, and clamping it at the bifurcation of the ICA with a blood vessel clip. The CCA was cut, and a monofilament nylon filament (Cinontech) was gently inserted into the ICA to approximately 18–20 mm distal to the carotid artery bifurcation. Then the left MCA was occluded. After 90 min, the filament was carefully removed to initiate reperfusion. All surgery procedures except insertion of the nylon filament were performed on rats in the sham-operation group. After recovering from anesthesia, all rats were assessed by a five-point neurological deficit score in a blinded fashion (Longa et al., 1989). Rats with scores of 1–3 points were included in this study, while the rats with scores of 0 or 4 were excluded from the study. N = 18/group in this study. All the experimental procedures *in vivo* were approved by The Animal Care and Use Committee of Wuhan University.

Housing Conditions

Twenty four hour after MCAO/R, the rats were returned to their respective housing conditions. The rats of the SSC, ISC groups were kept in the standard conditions (SC) while the rats in the SEE, IEE groups were kept in the enriched environment. The details of SC and EE were as follows:

Standard Conditions

The rats were kept in individually ventilated cages (length: 44 cm, width: 32 cm, height: 20 cm) with bedding for animals inside. Three rats were kept in one cage.

Enriched Environment

The animals are placed in a stainless-steel net cage (length: 75 cm, width: 90 cm, height: 50 cm) which contained ladders, platforms, swings, colorful balls, different-shaped wooden blocks, plastic tunnels, and a running wheel for sensorimotor stimulations. And 6–10 rats were grouping housed in the EE for social stimulations. The type and location of the items in the cage were changed three times a week to ensure novelty and exploration (**Figure 1B**).

Behavioral Tests

Modified Neurological Severity Scores (mNSS) (Chen et al., 2001), an 18-point scoring system compositing of motor, sensory, reflex, and balance tests, was utilized 1 day before surgery and on day 3, 7, 14, and 21 post-stroke to evaluate sensorimotor deficits (n = 12/group).

For spatial learning and memory testing, Morris Water Maze (MWM) test was performed on days 21–26 following I/R in a blinded situation (Morris, 1984). A round black platform (9 cm diameter, 30 cm height) was concealed in a pool (150 cm diameter, 60 cm deep, water temperature: 20 ± 1°C). On day 1–5, rats were dropped into the water from four different quadrants in turn while the position of the platform was fixed. The mean of escaping tendency to the platform in the four trials was recorded. The rat was required to stay on the platform for 15 s when reaching the platform within 60 s. The rat was guided to the platform for 15 s when reaching the platform exceeding 60 s. On day 6, the rats underwent the probe trial that allowed them to swim freely for 60 s without the platform. Swimming trajectories and the average times to reach the submerged platform were captured using an Animal Video Tracking Analysis System (n = 12/group) (Anilab Scientific Instruments Co., Ltd., China).

Nissl Staining

After being fixed with 4% paraformaldehyde, tissues were embedded in paraffin cut into seriatim 4-μm-thick coronal sections with adjacent sections separated by 400 μm. The sections were placed in xylene, xylene, xylene, 100, 95, and 80% ethanol for 5 min each and rinsed under running water for 5 min. Then the sections were treated with Cresyl Violet Solution (Servicebio, China) for 3min. After washing in running water and drying thoroughly, the sections were coverslipped with neutral resin. The stained sections were scanned and measured with the ImageJ software. The total infarct volume was calculated by the formula as previously described (n = 6/group) (Chen et al., 2017).

Western Blotting

Protein samples were harvested from penumbra. Tissues were ground separately in RIPA buffer comprising protease and phosphatase inhibitors (cocktails and PMSF from Aspen) for 30 min at 4°C. A BCA kit (Aspen) was used to detect the total protein concentration of each sample. Proteins were processed by SDS-PAGE (10–12.5%) and electro-blotted onto a PVDF membrane. And the membrane was then incubated in blocking buffer (5% skim milk) for 1 h at room temperature and incubated with primary antibodies including GSDMD (Abclonal), NLRP1, NLRP3, Caspase-1 (Novus), IL-1β,IL-18 (R&D), total p-65 (Proteintech),phosphorylated p-65 (Abclonal), GAPDH (Proteintech) overnight at 4°C. After washing three times, the membrane was incubated in secondary antibody for 1 h at 24°C. The proteins were scanned with a Bio-Rad system. ImageJ software was used to quantify protein levels which were normalized to GAPDH (n = 6/group).

Immunofluorescence Assays

Brain paraffin sections (4 μm) were hydrated and Tris/EDTA buffer performed heat-mediated antigen retrieval for 20 min. The sections blocked with 5% BSA for 1 h were incubated with Neun (Proteintech) along with primary antibodies Caspase-1 (Novus) overnight at 4°C and subsequently incubated in fluorescent secondary antibodies (Proteintech) for 1 h at 24°C. DAPI (Antgene) was used for nuclei staining. Images were taken with an Olympus BX53 microscope (Olympus). Positive cells were counted using ImageJ software (n = 6/group).

Immunohistochemistry

Brain paraffin sections (4 μm) were hydrated and Tris/EDTA buffer performed heat-mediated antigen retrieval for 20 min. The sections were then processed with 3% H_2O_2 for 10 min. The sections blocked with 5% BSA for 1 h were incubated with primary antibodies GSDMD (Abclonal), phosphorylated p65 (Abclonal) overnight at 4°C, and then incubated in HRP-labeled secondary antibodies (Proteintech). DAB (Servicebio) was utilized for dyeing while hematoxylin was used for nuclei staining. Images were acquired using the Olympus BX53 microscope (Olympus). The distribution and intensity of GSDMD and p-p65 staining was described by a semiquantitative score in a blinded fashion (0-negative, 1-weak, 2-moderate, 3-strong, and 4-strong and widely distributed) (n = 6/group) (Xu et al., 2020).

Enzyme-Linked Immunosorbent Assay (ELISA)

Rat (n = 3/group) penumbra tissues were separated and homogenized with PBS. After being centrifuged at 5000 rpm for 10 min at 4°C, the supernatants were collected. The secretion levels of inflammatory cytokines (IL-1β and IL-18) were analyzed by ELISA (Elabscience). Following the instructions on the ELISA kit, the optical density (OD) at 450 nm was measured by an enzyme-labeled instrument (PerkinElmer Singapore Pte. Ltd).

Quantitative Real-Time PCR

Rat (n = 3/group) penumbra tissues were separated and homogenized with Trizol reagent (Invitrogen, United States). The PrimeScript RT Reagent Kit (RR047A, Takara, Japan) was used for the reverse transcription of RNA. According to the manufacturers' protocol, we performed qPCR to detect the mRNA levels using SYBR Premix Ex Taq II (RR820A, Takara) in a 2.1 Real-Time PCR System (Bio-Rad, United States). The relative Ct method was adopted to compare the data and GAPDH was set as internal control. The primer sequences were listed as follows:

IL-1β (F): TGACTTCACCATGGAACCCG
IL-1β (R): TCCTGGGGAAGGCATTAGGA
IL-18 (F): TGACAAAAGAAAGCCGCCTG
IL-18 (R): ATAGGGTCACAGCCAGTCCT
GAPDH (F): CGCTAACATCAAATGGGGTG
GAPDH (R): TTGCTGACAATCTTGAGGGAG

Statistical Analysis

SPSS 23.0 software and GraphPad Prism 8.0 were used for data analysis. Analysis of mNSS was implemented by a non-parametric Kruskal–Wallis test. Analysis of escape latency in the MWM test was implemented by two-way repeated-measures ANOVA followed by Tukey's *post hoc* test. And differences between groups were compared by two-tailed Student's t-test and one-way ANOVA followed by Tukey's *post hoc* test. All experimental data are expressed as mean ± standard deviation (SD). Statistical significance was determined as $p < 0.05$.

RESULTS

Enriched Environment Improved Long-Term Neurobehavioral Function After Ischemia/Reperfusion Injury

Ischemia/reperfusion injury caused marked Behavioral dysfunction (Yirmiya and Goshen, 2011). To determine whether EE treatment improved functional recovery after I/R injury, a series of behavioral tests were performed. To evaluate the neurological function, mNSS was assessed on day 3, 7, 14, 21 after I/R injury. Rats had persistent sensorimotor defects after MCAO/R operation and EE treatment could effectively reverse the defects (**Figure 2A**; $p < 0.001$). To assess long-term spatial learning and memory functions, MWM was assessed on day 21–26 after I/R injury. In the spatial learning phase, the escape latency of rats in all groups decreased as the training days progressed. And MCAO/R rats spent more time reaching the platform compared with sham-operated rats on days 1–5 of training. However, rats housed in EE demonstrated the superior performance of shorter escape latency than rats housed in standard conditions following I/R injury (**Figure 2B**; $p < 0.001$). Probe trials proceeded 24 h after the final spatial learning trial. Rats of the IEE group spent more time in the correct quadrant and revealed more crossovers compared to rats of the ISC group (**Figures 2C–E**; $p < 0.001$ and $p < 0.01$). To sum up, EE treatment improved long-term neurobehavioral function after I/R injury.

Enriched Environment Decreased Ischemic Infarction and Inhibited Pyroptosis After Ischemia/Reperfusion Injury

As the improvement in functional outcome could be attributed to a reduction in brain damage, Nissl staining was performed to confirm the effects of EE on infarct volume after I/R injury. The schematic diagram of the ischemic border was shown in **Figure 3A**. EE treatment significantly reduced infarct volume in comparison with the ISC group (**Figures 3B,D**; $p < 0.001$). No lesion was found in SSC and SEE groups. Reduced post-stroke ischemic infarction has been reported to be associated with inhibition of pyroptosis (Ye et al., 2020). Next, we explored whether EE could rescue ischemia-induced pyroptosis. GSDMD was downstream of pyroptosis and GSDMD-N fragments transferred to the plasma membrane to form pores that caused

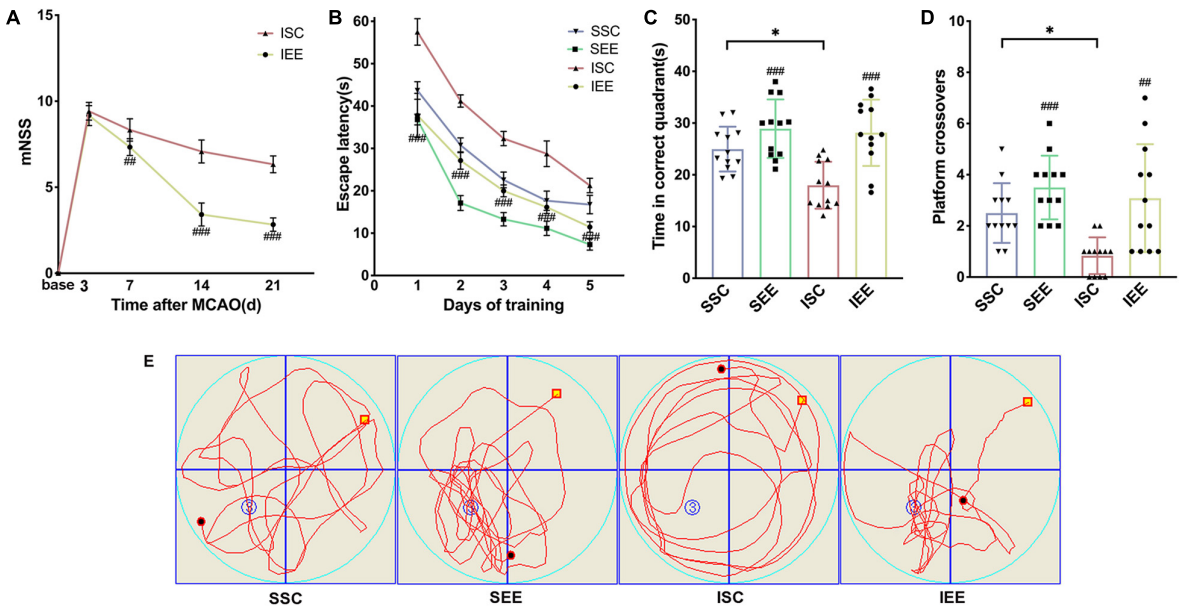

FIGURE 2 | Enriched environment improved long-term neurobehavioral function of MCAO/R rats. **(A)** The mNSS of ISC and IEE group. Rats were tested before MCAO surgery. **(B)** The escape latency in the spatial learning phase. **(C,D)** Time in the correct quadrant and the crossovers in the target quadrant was recorded and analyzed. **(E)** Representative swimming trajectories of SSC, SEE, ISC, and IEE group in the probe trials. $n = 12$. Data are expressed as mean ± SD. $^{*}p < 0.05$ vs. SSC group; $^{\#\#}p < 0.01$, $^{\#\#\#}p < 0.001$ vs. ISC group.

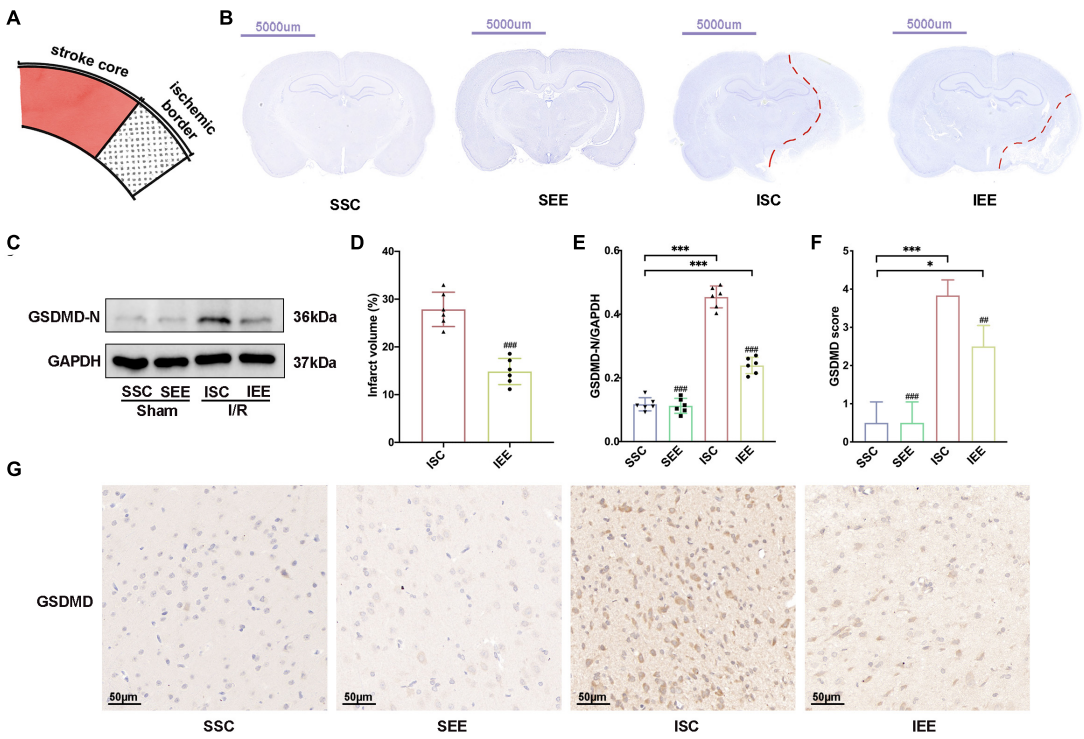

FIGURE 3 | Enriched environment decreased ischemic infarction and inhibited pyroptosis after I/R injury. **(A)** Schematic brain with a highlight of the ischemic border. **(B,D)** Representative cresyl violet stained brain slices and quantification of cerebral infarct volume percentage. Scale bars, 5000 μm. $n = 6$. **(C,E)** Protein levels of GSDMD-N in peri-infarct tissues. $n = 6$. **(G,F)** Representative IHC staining images for GSDMD in the penumbra and IHC score of GSDMD in the penumbra. Scale bars, 50 μm. $n = 6$. Data are expressed as mean ± SD. $^{*}p < 0.05$, $^{***}p < 0.001$ vs. SSC group; $^{\#\#}p < 0.01$, $^{\#\#\#}p < 0.001$ vs. ISC group.

lytic cell death and the secretion of mature IL-1β and mature IL-18 (Kovacs and Miao, 2017). The expression levels of GSDMD-N from the ischemic border were detected. Western blot results demonstrated enhanced expression levels of GSDMD-N in the ISC group. And the expression levels of GSDMD-N were apparently reduced in the IEE group in comparison with the ISC group (**Figures 3C,E**; $p < 0.001$).

Furthermore, we performed immunohistochemistry GSDMD and found that the IEE group expressed an obviously lower level of GSDMD in comparison with the ISC group (**Figures 3F,G**; $p < 0.01$).

Collectively, all of these data suggested that ischemic infarction and pyroptosis after I/R injury were negatively regulated by EE treatment.

Enriched Environment Suppressed the Activities of NLRP1/NLRP3 Inflammasomes

To investigate how EE influenced neuronal pyroptosis after ischemic stroke, the activation of inflammasomes which was regarded as the upstream signal in the early stage of pyroptosis was detected. As neuronal pyroptosis might be mediated by the activation of NLRP1 and NLRP3 inflammasomes in the course of ischemic stroke, western blot was performed to explore whether EE inhibited pyroptosis by suppressing the activities of NLRP1/NLRP3 inflammasomes. The expression levels of NLRP1 and NLRP3 inflammasome proteins, mature IL-1β and mature IL-18 in the ischemic border of MCAO/R rats were measured. It was obvious that the expression levels of NLRP1 and NLRP3 were increased following I/R in comparison with sham controls while EE treatment decreased the expression levels of NLRP1 and NLRP3 in comparison with the ISC group (**Figures 4A–C**; $p < 0.05$ and $p < 0.01$). The elevated levels of cleaved caspases-1, mature IL-1β, and mature IL-18 indicated the activation of NLRP1/NLRP3 inflammasomes. I/R increased the expression levels of cleaved caspases-1, mature IL-1β, and mature IL-18 in comparison with sham controls while rats in the IEE group expressed a lower level (**Figures 4D–G**; $p < 0.01$, $p < 0.001$, and $p < 0.001$). To compare the expression levels of inflammatory factors, ELISAs were performed to detect inflammatory cytokines IL-1β and IL-18. We found that the expression levels of IL-1β and IL-18 were significantly increased following I/R in comparison with sham controls while EE treatment decreased the expression levels of IL-1β and IL-18 in comparison with the ISC group (**Figures 5A,B**; $p < 0.01$ and $p < 0.01$). The IL-1β and IL-18 mRNA expression levels were further examined by q-PCR. The mRNA levels of IL-1β and IL-18 were significantly reduced following I/R when the rats were housed in EE (**Figures 5C,D**; $p < 0.01$ and $p < 0.05$).

In addition, immunofluorescence analysis in the penumbra from the IEE group demonstrated a lower level of caspase-1compared with the ISC group (**Figures 4H,I**, $p < 0.001$). Notably, caspase-1 was highly colocalized with Neun + neurons, suggesting the inflammasome activity in neurons. These results demonstrated EE inhibited neuronal pyroptosis by suppressing the activities of NLRP1/NLRP3 inflammasomes.

Enriched Environment Inhibited p65 Phosphorylation After Ischemia/Reperfusion Injury

As NF-κB was reported to mediate pyroptosis by regulating the transcription of NLRP and then regulated its downstream substrates (Fann et al., 2018), we next explored how EE treatment inhabited pyroptosis through evaluating the NF-κB signaling pathway proteins. First, a western blot was used for the detection of p-65 and p-p65 expression levels in the penumbra following I/R injury. The results suggested that p65 levels were not influenced by EE treatment ($p > 0.05$). However, p-p65 was reduced when the rats after I/R injury were housed in EE (**Figures 6A–C**, $p < 0.01$). Furthermore, we used immunohistochemistry to explore the expression levels of p-p65 in the penumbra and found that rats of the IEE group significantly down-regulated p-p65 expression in comparison with rats of the ISC group (**Figures 6D,E**, $p < 0.05$). As is well known, p65 phosphorylation indicates the activation of the p65 NF-κB signal (Pradère et al., 2016); thus, these results illustrate that EE can inhibit the p65 NF-κB signal activation after cerebral I/R injury.

In general, these data revealed that EE treatment inhibited neuronal pyroptosis by attenuating the expression of NLRP1/NLRP3 inflammasomes following cerebral I/R injury. These may be affected by inhabiting the NF-κB p65 signaling pathway.

DISCUSSION

Despite the high rate of disability associated with stroke worldwide, valid therapeutic methods were restricted (Virani et al., 2020). Residual dysfunction of stroke greatly affected the life quality of the survivors (Stinear et al., 2020). It should not be overlooked to search methods for the recovery of the functional deficit caused by stroke. Abundant evidence showed that EE could effectively promote functional recovery after ischemic stroke (Chen J.Y. et al., 2017; Kubota et al., 2018; Lin et al., 2021, p. 1). However, due to the complexity of transforming EE into clinical practice, EE remained mainly a laboratory stage (Lang et al., 2015). Therefore, exploring the potential mechanism underlying the role of EE in promoting functional recovery may provide precise targets for the recovery of ischemic stroke and expedite its clinical application. Our previous study demonstrated the connections between neuroprotective effects of EE and neuronal cell death (Chen et al., 2017). A variety of pathological stimuli such as heart attacks, obesity, or cancer could trigger pyroptosis (Bergsbaken et al., 2009). Moreover, pyroptosis was closely related to central nervous system diseases (Fricker et al., 2018). In models of multiple sclerosis, pyroptosis inhibition preserved axons in the spinal cord lesions (McKenzie et al., 2018). In models of Alzheimer's disease, pyroptosis relived the behavioral ability (Han et al., 2020). Previous research showed that neuronal pyroptosis affected the prognosis after ischemic stroke, which suggested that anti-pyroptosis was an effective treatment for all functional recovery following

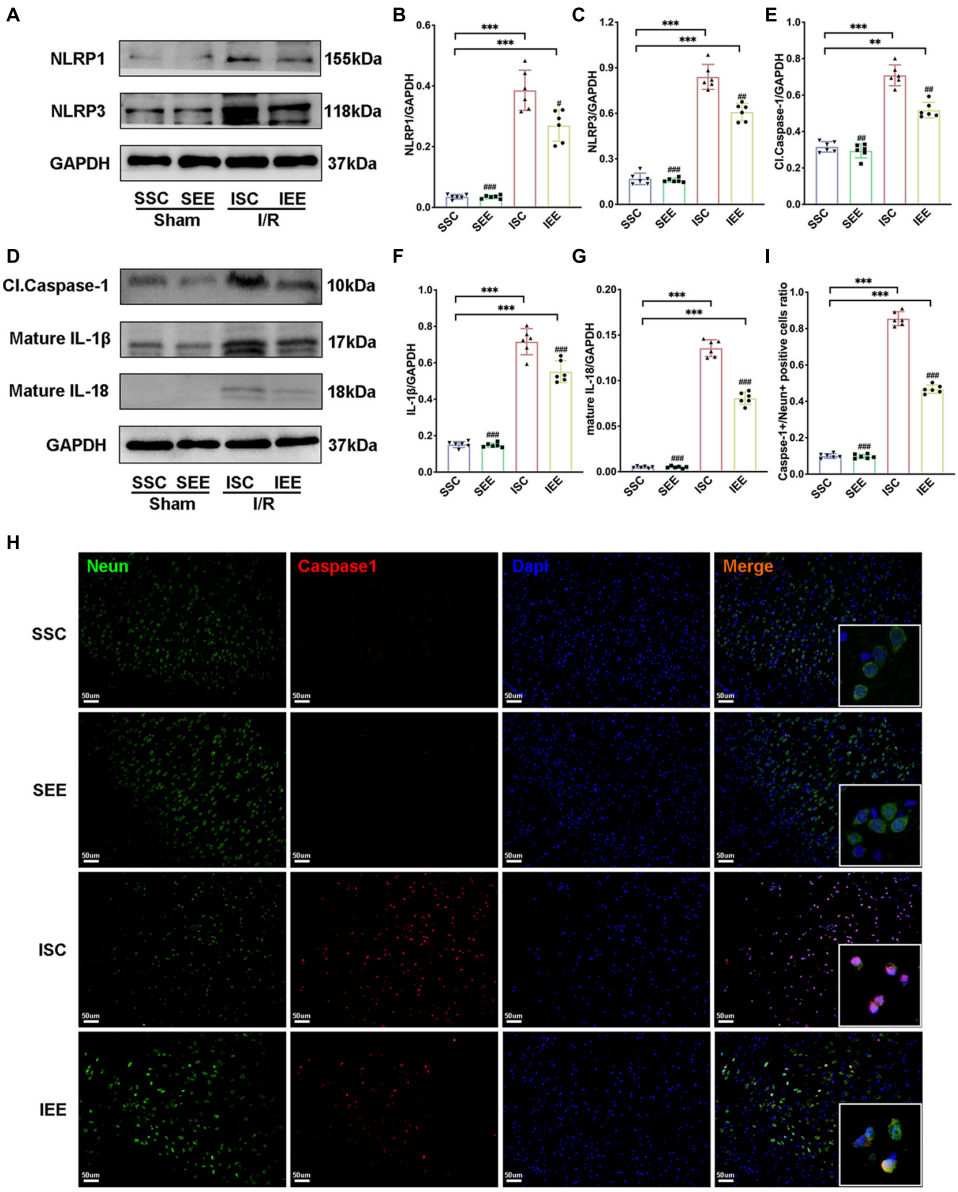

FIGURE 4 | Enriched environment suppressed the activities of NLRP1/NLRP3 inflammasomes of MCAO/R rats. **(A–G)** Western blots and quantification of NLRP1/NLRP3 inflammasomes related proteins including NLRP1, NLRP3, cleaved caspase-1, mature IL-1β, and IL-18 in peri-infarct tissues. $n = 6$. **(H,I)** Double immunostaining of Neun and Caspase-1 revealed a good co-localization of these two makers. Statistical analysis of the positive rate is shown. Treatment with EE reduced Caspase-1 positive neurons in the ischemic penumbra. Scale bars, 50 μm. $n = 6$. Data are expressed as mean ± SD. $^{**}p < 0.01$, $^{***}p < 0.001$ vs. SSC group; $^{\#}p < 0.05$, $^{\#\#}p < 0.01$, $^{\#\#\#}p < 0.001$ vs. ISC group.

I/R injury (Lu et al., 2021). But there remained insufficient evidence that whether pyroptosis was essential for EE-mediated ischemic stroke recovery, and if so, how EE influenced neuronal pyroptosis after the pathological process. A key finding of our research was that EE attenuated pyroptosis and improved functional recovery after cerebral ischemia/reperfusion injury. The schematic mechanism was shown in **Figure 7**.

Being a novel type of cell death, pyroptosis mainly featured plasma-membrane pores formation, rapid plasma membrane rupture, and the release of intracellular inflammatory substances (Kuang et al., 2017). In the present study, we showed compelling evidence that the expression levels of GSDMD-N, the major pore-forming executive in pyroptosis, increased in the MCAO/R group versus the sham-operated group, and this alteration was counteracted in the EE treatment group. Then, to investigate how EE influenced neuronal pyroptosis after ischemic stroke, we detected the activation of inflammasomes which was regarded as the upstream signal in the early stage of pyroptosis. Inflammasomes were a group of the multimolecular complex that identified multiple inflammation-induced stimuli and mediate

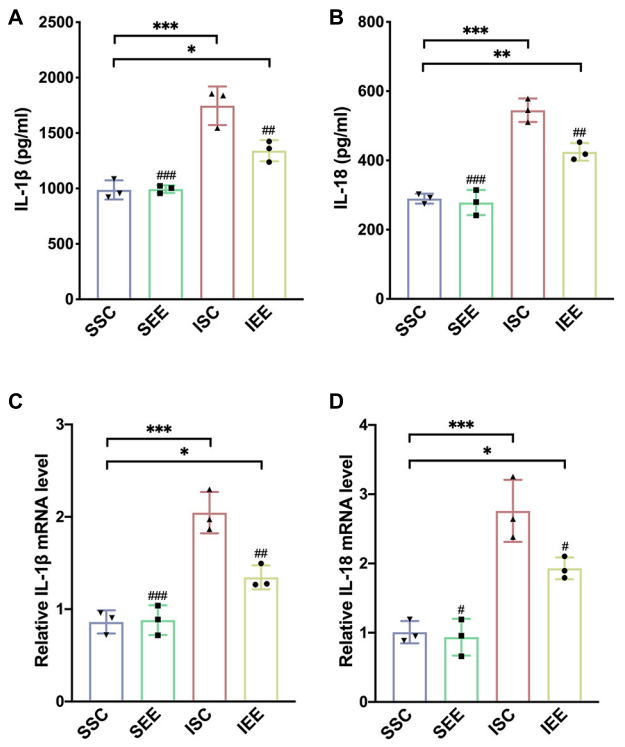

FIGURE 5 | Enriched environment suppressed the expression levels of inflammatory cytokines in the penumbra. **(A,B)** Effects of EE treatment on IL-1β and IL-18 expression in penumbra according to ELISA. $n = 3$. **(C,D)** Quantitative analysis of IL-1β and IL-18 mRNA levels in penumbra. $n = 3$. Data are expressed as mean ± SD. $^{*}p < 0.05$, $^{**}p < 0.01$, $^{***}p < 0.001$ vs. SSC group; $^{\#}p < 0.05$, $^{\#\#}p < 0.01$,$^{\#\#\#}p < 0.001$ vs. ISC group.

the maturation of critical proinflammatory cytokines in the process of pyroptosis (Strowig et al., 2012; Xue et al., 2019). It was worth noting that NLRP1 and NLRP3 inflammasomes were reported to be involved in ischemic stroke (Fann et al., 2014; Yang et al., 2014). However, it is not known whether EE treatment worked in the modulation of NLRP1/NLRP3 inflammasomes activation. The present research provided compelling evidence that EE treatment significantly modulated the activation of NLRP1/NLRP3 inflammasomes. The expression levels of NLRP1, NLRP3, the cleaved caspase-1, and the inflammatory cytokines mature IL-1β, and mature IL-18 were downregulated by EE treatment compared with standard conditions after I/R injury. And we found that the related proteins mainly expressed in the neurons through immunofluorescence double staining to locate its position. In summary, we found that EE treatment inhibited neuronal pyroptosis by affecting the activation of inflammasomes and thereby improved the functional recovery after I/R injury.

Next, we investigated the potential molecular mechanism of EE-reduced NLRP1 and NLRP3 inflammasome expression and activation in neurons. The activation of NLRP1 and NLRP3 inflammasome in the brain following I/R injury may be induced by pattern recognition receptors (PRRs) including toll-like receptors (TLRs), the receptor for advanced glycation end products (RAGE), and the IL-1 receptor 1 (IL-1R1) (Gelderblom et al., 2015). PRRs identified different pathological stimuli including endogenous damage-associated molecular patterns (DAMPs) released from damaged cells in the stroke core such as high mobility group box 1 protein (HMGB1), heat shock proteins, and peroxiredoxin family proteins (Tang et al., 2013; Wang et al., 2020a). DAMPs-activated PRRs further activated the intracellular NF−κB signaling pathway resulting in pyroptosis and the release of inflammatory factors (Schroder and Tschopp, 2010). As a transcription factor, NF-κB played a crucial role in cell death and inflammation (Kondylis et al., 2017; Liu et al., 2017). As a cytosolic sensor, the NF−κB signal activated and facilitated its nuclear translocation and DNA binding (Liu et al., 2017). Phosphorylation of p65 indicated the activation and functional status of the NF-κB signaling pathway (Pradère et al., 2016). Previous studies have indicated that activation of the NF-κB signaling pathway which could be activated by reactive oxygen species (ROS), hypoxia, and several inflammatory mediators occurred in neurons following I/R injury (Ridder and Schwaninger, 2009; Liu et al., 2019; He et al., 2020). The role of the NF-κB signaling pathway in regulating pyroptosis has been extensively studied in various diseases. Evidence has confirmed that NF-κB could regulate the transcription of NLRP by binding to their promoter region and then regulated its downstream substrates (Liu et al., 2017; Matias et al., 2019). The activation of the NF-κB signaling pathway was essential for the up-regulation of the protein synthesis of NLRP3 (Afonina et al., 2017). It has been demonstrated that the elevated expression level of IL-1β was induced by the activation of the NF-κB signaling pathway in ischemic damage (Zhou et al., 2012). Additionally, studies have confirmed that EE treatment was beneficial for the recovery of central nervous system diseases by inhibiting the NF-κB signaling pathway (Wu et al., 2016; Li et al., 2018). Moreover, Zhang et al. (2018) reported that EE mediated neurogenesis and functional recovery by inhibiting the NF-κB/IL-17A signaling pathway in astrocytes after ischemic stroke. In the present study, EE decreased the phosphorylation of p65 and the expression of NLRP1 and NLRP3 inflammasome proteins induced by I/R injury. This was supported by the study that NF-κB signaling promotes NLRP1 and NLRP3 inflammasome activation in neurons following I/R injury (Fann et al., 2018). In brief, our findings suggested that the anti-pyroptosis effect of EE after ischemic stroke was associated with the inhibition of the NF-κB p-65 signaling pathway and the reduced expression levels of NLRP1 and NLRP3 inflammasome-related proteins.

Less perfection was that the upstream regulator of p65 phosphorylation remained to be explored in this study. As the activation of NLRP1 and NLRP3 inflammasome may be induced by PRRs which identified DAMPs released from dying neural cells and stimulated NF-κB translocation during the I/R process, the sources of danger signals that promoted inflammatory response remained to be further investigated (Dong et al., 2018). Downregulation of the HMGB1/TLR4/NF-κB pathway was associated with inhibition of pyroptosis (Sun et al., 2020). HMGB1 activated the NLRP3 inflammasome *via* the NF-κB signaling pathway in acute glaucoma (Chi et al., 2015). The activation of the TLR4/NF-κB signaling pathway could modulate NLRP3 inflammasome activation in inflammatory bowel disease

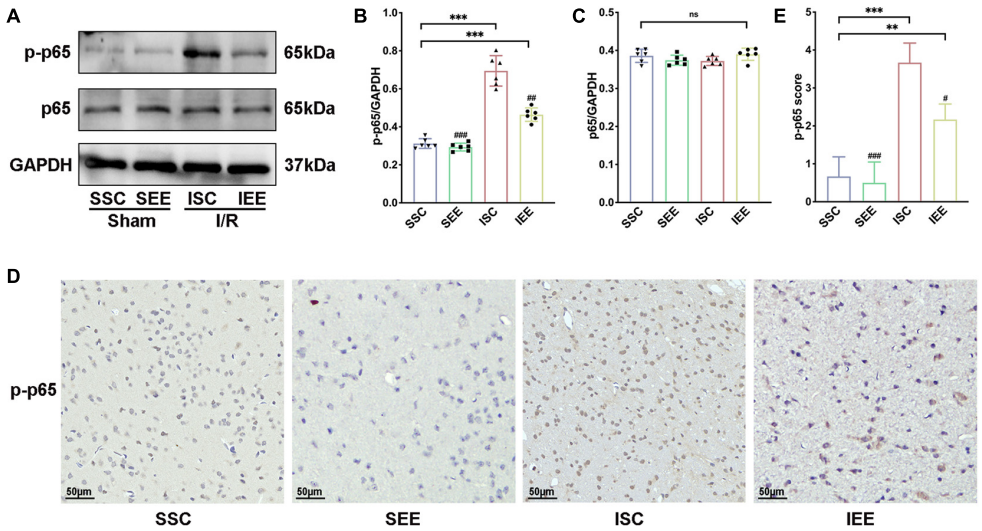

FIGURE 6 | Enriched environment inhibited p65 phosphorylation after I/R injury. **(A–C)** Western blots and quantification illustrating increases in the activation of NF-κB (p-p65) in the penumbra. **(D)** Representative IHC staining images for p-p65 in the penumbra. Scale bars, 50 μm. **(E)** IHC score of p-p65 in penumbra. $n = 6$. Data are expressed as mean ± SD. $^{**}p < 0.01$, $^{***}p < 0.001$ vs. SSC group; $^{\#}p < 0.05$, $^{\#\#}p < 0.01$, $^{\#\#\#}p < 0.001$ vs. ISC group.

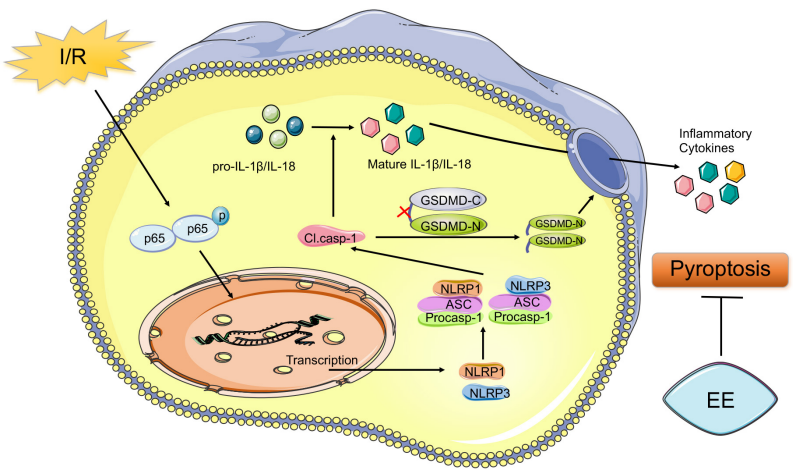

FIGURE 7 | Schematic mechanism of EE treatment regulates post-ischemic pyroptosis. The NF-κB signaling pathway is activated following I/R injury, which stimulates the nucleus to induce transcription of NLRP1 and NLRP3 proteins to form the NLRP1 and NLRP3 inflammasome. Pro-caspase-1 is activated through NLRP1 and NLRP3 signal cleaving GSDMD into GSDMD-N and GSDMD-C. Then the pore-forming GSDMD-N domain causes membrane lysis inducing pyroptosis. Also, cleaved caspase-1 mediates the maturation of IL-1β and IL-18 which are released into the extracellular environment. EE attenuates pyroptosis resulting in ischemic stroke outcomes amelioration.

and induce GSDMD-mediated pyroptosis in tubular cells in diabetic kidney disease (Chen et al., 2019; Wang Y. et al., 2019). Moreover, SYK expression which was downregulated by the activation of miRNA-27a could stimulate the NF-κB signaling pathway and facilitate NLRP3-mediated pyroptosis (Li et al., 2021). The previous study has shown that EE could regulate the expression of HMGB1 and mediate post-stroke angiogenesis (Chen J.Y. et al., 2017). EE was also associated with growth factors (epithelial growth factor, hepatocyte growth factor) and signaling pathways (STAT3, JNK, EKR1/2, NF-κB) expressed in the gastrocnemius muscle (Le Guennec et al., 2020). However, it remained to be explored whether EE regulated the NF-κB signaling pathway by regulating the expression of these growth factors or DAMPs. It was essential to figure out the upstream signaling pathway to reveal the underlying mechanism of the EE-mediated effect on the NF-κB activation. In our future research, we would focus on solving this problem. In another hand, to confirm the exact effect of EE on the NF-κB signaling pathway, the agonist of NF-κB should be included. Our future work would dwell on this. Moreover, NF-κB pathway activation resulted in pyroptosis and the release of inflammatory factors. In turn, these inflammatory factors may act by activating the NF-κB

signaling which would keep the cells in an activated cyclic state (Vallabhapurapu and Karin, 2009).

There was increasing evidence that many cell death pathways including apoptosis, autophagy and pyroptosis were simultaneously present in the ischemic core and penumbral area, which were fine-tuned and had either beneficial, deleterious or dual roles in the progression of post-stroke brain damage (Şekerdağ et al., 2018). However, the relevant research of EE on different types of cell death following ischemic stroke was extremely limited. In our previous studies, EE performed beneficial effects by inhibiting apoptosis of neurons following I/R (Chen et al., 2017). EE treatment increased the levels of anti-apoptotic protein Bcl-2 while decreased the levels of pro-apoptotic protein Bax, cytochrome *c*, caspase-3 in the penumbra after cerebral I/R injury. Caspases, the main drivers of apoptosis, were also involved in the crosstalk between apoptosis and autophagy. Activated caspases could inhibit autophagy by degrading autophagy proteins such as beclin-1, Atg5 and Atg7 (Wu et al., 2014). A recent study also demonstrated that EE promoted autophagy by increasing the expression of beclin-1 and enhancing the lysosomal activities of lysosomal-associated membrane protein 1, cathepsin B, and cathepsin D, which eventually boosted neurological function recovery following ischemic stroke (Deng et al., 2021). This kind of crosstalk in EE regulated cell death pathways after stroke could also be found in autophagy and pyroptosis. The evidence for the role of NLRP1/3 inflammasomes and pyroptosis in stroke pathology was well defined in the previous studies (Yang-Wei Fann et al., 2013; Barrington et al., 2017). Recently, autophagy has been linked to the regulation of inflammatory response. In Beclin1 +/- cells, the levels of NLRP3 and cleaved caspase1 were increased and the number of cells with inflammasome were elevated, indicating that autophagy inhibited inflammasome activation through NLRP3 degradation (Houtman et al., 2019, p. 1). Meanwhile, NLRs have been shown to increase the synthesis of autophagy-related proteins and assist in the localization of autophagy proteins (Deretic, 2012). In the present study, we found that EE inhabited neuronal pyroptosis by suppressing the activities of NLRP1/NLRP3 inflammasomes after I/R injury. The cell death pathways after I/R injury were overlapping each other in several steps of the cascades and shared common features. Keeping on exploring the effect of EE on different cell death types and how these mechanisms worked individually or correlatively might bring us a step closer to a promising approach for stroke treatment. What's more, whether EE affected pyroptosis and the cell types experiencing pyroptosis after I/R injury remained unclear. Evidence showed that pyroptosis occurring in neurons, astrocytes, and microglia was involved in the pathological process in diseases other than ischemic stroke (Jamilloux et al., 2013; Alfonso-Loeches et al., 2014; Tan et al., 2014). In this study, we proved the effect of EE on neuronal pyroptosis after I/R injury. However, it was of great importance to notice that EE might not only influence neuronal pyroptosis but also affect pyroptosis or inflammatory reaction of additional cell types including astrocytes and microglia. Our future work would dwell on revealing the pleiotropic roles of EE-inhibited pyroptosis in other cell types.

CONCLUSION

Our finding showed that EE treatment presented a prospective cerebral-protective effect against I/R injury. EE treatment promoted functional recovery after I/R injury, involving inhibition of pyroptosis by suppressing the activities of NLRP1/NLRP3 inflammasomes. The beneficial effect of EE may result from the inhibition of NF-κB p65 phosphorylation. As a result, the therapeutic application of EE after I/R injury, including several potential therapeutic targets was probably a promising strategy for stroke recovery.

DATA AVAILABILITY STATEMENT

The original contributions presented in the study are included in the article/supplementary material, further inquiries can be directed to the corresponding author/s.

ETHICS STATEMENT

The animal study was reviewed and approved by the experimental animal Ethics Committee of Wuhan University (WP2020-08052).

AUTHOR CONTRIBUTIONS

JL performed the research. XZ, YX, and JL were responsible for experimental design. WC, JW, and BW contributed essential reagents and tools. LZ and JZ helped in collecting and analyzing the data. JL and JZ wrote the manuscript. XZ and WL reviewed and edited the manuscript. All the authors contributed to the article and approved the submitted version.

FUNDING

This work was supported by grants from the National Natural Science Foundation of China (No. 81902304 to XZ).

ACKNOWLEDGMENTS

The authors thank the personnel in the department of rehabilitation medicine at the Zhongnan Hospital of Wuhan University. In particular, JL wants to thank YX for his care, companionship and encouragement over the years. I love you!

REFERENCES

Abulafia, D. P., de Rivero Vaccari, J. P., Lozano, J. D., Lotocki, G., Keane, R. W., and Dietrich, W. D. (2009). Inhibition of the inflammasome complex reduces the inflammatory response after thromboembolic stroke in mice. *J. Cereb. Blood Flow Metab.* 29, 534–544. doi: 10.1038/jcbfm.2008.143

Afonina, I. S., Zhong, Z., Karin, M., and Beyaert, R. (2017). Limiting inflammation-the negative regulation of NF-κB and the NLRP3 inflammasome. *Nat. Immunol.* 18, 861–869. doi: 10.1038/ni.3772

Alfonso-Loeches, S., Ureña-Peralta, J. R., Morillo-Bargues, M. J., Oliver-De La Cruz, J., and Guerri, C. (2014). Role of mitochondria ROS generation in ethanol-induced NLRP3 inflammasome activation and cell death in astroglial cells. *Front. Cell Neurosci.* 8:216. doi: 10.3389/fncel.2014.00216

Barrington, J., Lemarchand, E., and Allan, S. M. (2017). A brain in flame; do inflammasomes and pyroptosis influence stroke pathology? *Brain Pathol.* 27, 205–212. doi: 10.1111/bpa.12476

Begenisic, T., Sansevero, G., Baroncelli, L., Cioni, G., and Sale, A. (2015). Early environmental therapy rescues brain development in a mouse model of Down syndrome. *Neurobiol. Dis.* 82, 409–419. doi: 10.1016/j.nbd.2015.07.014

Benaroya–Milshtein, N., Hollander, N., Apter, A., Kukulansky, T., Raz, N., Wilf, A., et al. (2004). Environmental enrichment in mice decreases anxiety, attenuates stress responses and enhances natural killer cell activity. *Eur. J. Neurosci.* 20, 1341–1347. doi: 10.1111/j.1460-9568.2004.03587.x

Bergsbaken, T., Fink, S. L., and Cookson, B. T. (2009). Pyroptosis: host cell death and inflammation. *Nat. Rev. Microbiol.* 7, 99–109. doi: 10.1038/nrmicro2070

Brough, D., and Rothwell, N. J. (2007). Caspase-1-dependent processing of pro-interleukin-1beta is cytosolic and precedes cell death. *J. Cell Sci.* 120, 772–781. doi: 10.1242/jcs.03377

Campbell, B. C. V., De Silva, D. A., Macleod, M. R., Coutts, S. B., Schwamm, L. H., Davis, S. M., et al. (2019). Ischaemic stroke. *Nat. Rev. Dis. Primers* 5:70. doi: 10.1038/s41572-019-0118-8

Chen, J., Li, Y., Wang, L., Zhang, Z., Lu, D., Lu, M., et al. (2001). Therapeutic benefit of intravenous administration of bone marrow stromal cells after cerebral ischemia in rats. *Stroke* 32, 1005–1011. doi: 10.1161/01.str.32.4.1005

Chen, J.-Y., Yu, Y., Yuan, Y., Zhang, Y.-J., Fan, X.-P., Yuan, S.-Y., et al. (2017). Enriched housing promotes post-stroke functional recovery through astrocytic HMGB1-IL-6-mediated angiogenesis. *Cell Death Discov.* 3:17054. doi: 10.1038/cddiscovery.2017.54

Chen, X., Zhang, X., Xue, L., Hao, C., Liao, W., and Wan, Q. (2017). Treatment with enriched environment reduces neuronal apoptosis in the periinfarct cortex after cerebral ischemia/reperfusion injury. *Cell Physiol. Biochem.* 41, 1445–1456. doi: 10.1159/000468368

Chen, X., Liu, G., Yuan, Y., Wu, G., Wang, S., and Yuan, L. (2019). NEK7 interacts with NLRP3 to modulate the pyroptosis in inflammatory bowel disease *via* NF-κB signaling. *Cell Death Dis.* 10:906. doi: 10.1038/s41419-019-2157-1

Chi, W., Chen, H., Li, F., Zhu, Y., Yin, W., and Zhuo, Y. (2015). HMGB1 promotes the activation of NLRP3 and caspase-8 inflammasomes *via* NF-κB pathway in acute glaucoma. *J. Neuroinflamm.* 12:137. doi: 10.1186/s12974-015-0360-2

Dahlqvist, P., Rönnbäck, A., Risedal, A., Nergårdh, R., Johansson, I.-M., Seckl, J. R., et al. (2003). Effects of postischemic environment on transcription factor and serotonin receptor expression after permanent focal cortical ischemia in rats. *Neuroscience* 119, 643–652. doi: 10.1016/S0306-4522(03)00195-7

Deng, Y.-H., Dong, L.-L., Zhang, Y.-J., Zhao, X.-M., and He, H.-Y. (2021). Enriched environment boosts the post-stroke recovery of neurological function by promoting autophagy. *Neural Regen. Res.* 16, 813–819. doi: 10.4103/1673-5374.297084

Deretic, V. (2012). Autophagy as an innate immunity paradigm: expanding the scope and repertoire of pattern recognition receptors. *Curr. Opin. Immunol.* 24, 21–31. doi: 10.1016/j.coi.2011.10.006

Ding, J., Wang, K., Liu, W., She, Y., Sun, Q., Shi, J., et al. (2016). Pore-forming activity and structural autoinhibition of the gasdermin family. *Nature* 535, 111–116. doi: 10.1038/nature18590

Dong, Z., Pan, K., Pan, J., Peng, Q., and Wang, Y. (2018). The possibility and molecular mechanisms of cell pyroptosis after cerebral ischemia. *Neurosci. Bull.* 34, 1131–1136. doi: 10.1007/s12264-018-0294-7

Fann, D. Y.-W., Lee, S.-Y., Manzanero, S., Chunduri, P., Sobey, C. G., and Arumugam, T. V. (2013). Pathogenesis of acute stroke and the role of inflammasomes. *Ageing Res. Rev.* 12, 941–966. doi: 10.1016/j.arr.2013.09.004

Fann, D. Y.-W., Lim, Y.-A., Cheng, Y.-L., Lok, K.-Z., Chunduri, P., Baik, S.-H., et al. (2018). Evidence that NF-κB and MAPK signaling promotes NLRP inflammasome activation in neurons following ischemic stroke. *Mol. Neurobiol.* 55, 1082–1096. doi: 10.1007/s12035-017-0394-9

Fann, D. Y.-W., Santro, T., Manzanero, S., Widiapradja, A., Cheng, Y.-L., Lee, S.-Y., et al. (2014). Intermittent fasting attenuates inflammasome activity in ischemic stroke. *Exp. Neurol.* 257, 114–119. doi: 10.1016/j.expneurol.2014.04.017

Fricker, M., Tolkovsky, A. M., Borutaite, V., Coleman, M., and Brown, G. C. (2018). Neuronal cell death. *Physiol. Rev.* 98, 813–880. doi: 10.1152/physrev.00011.2017

Gelderblom, M., Sobey, C. G., Kleinschnitz, C., and Magnus, T. (2015). Danger signals in stroke. *Ageing Res. Rev.* 24, 77–82. doi: 10.1016/j.arr.2015.07.004

Gross, O., Thomas, C. J., Guarda, G., and Tschopp, J. (2011). The inflammasome: an integrated view. *Immunol. Rev.* 243, 136–151. doi: 10.1111/j.1600-065X.2011.01046.x

Han, C., Yang, Y., Guan, Q., Zhang, X., Shen, H., Sheng, Y., et al. (2020). New mechanism of nerve injury in Alzheimer's disease: β-amyloid-induced neuronal pyroptosis. *J. Cell Mol. Med.* 24, 8078–8090. doi: 10.1111/jcmm.15439

He, X., Zeng, Y., Li, G., Feng, Y., Wu, C., Liang, F., et al. (2020). Extracellular ASC exacerbated the recurrent ischemic stroke in an NLRP3-dependent manner. *J. Cereb. Blood Flow Metab.* 40, 1048–1060. doi: 10.1177/0271678X19856226

Houtman, J., Freitag, K., Gimber, N., Schmoranzer, J., Heppner, F. L., and Jendrach, M. (2019). Beclin1-driven autophagy modulates the inflammatory response of microglia via NLRP3. *EMBO J.* 38. doi: 10.15252/embj.201899430

Ito, M., Shichita, T., Okada, M., Komine, R., Noguchi, Y., Yoshimura, A., et al. (2015). Bruton's tyrosine kinase is essential for NLRP3 inflammasome activation and contributes to ischaemic brain injury. *Nat. Commun.* 6:7360. doi: 10.1038/ncomms8360

Jamilloux, Y., Pierini, R., Querenet, M., Juruj, C., Fauchais, A.-L., Jauberteau, M.-O., et al. (2013). Inflammasome activation restricts *Legionella pneumophila* replication in primary microglial cells through flagellin detection. *Glia* 61, 539–549. doi: 10.1002/glia.22454

Jungling, A., Reglodi, D., Karadi, Z. N., Horvath, G., Farkas, J., Gaszner, B., et al. (2017). Effects of postnatal enriched environment in a model of Parkinson's disease in adult rats. *Int. J. Mol. Sci.* 18:406. doi: 10.3390/ijms18020406

Kempermann, G. (2019). Environmental enrichment, new neurons and the neurobiology of individuality. *Nat. Rev. Neurosci.* 20, 235–245. doi: 10.1038/s41583-019-0120-x

Kondylis, V., Kumari, S., Vlantis, K., and Pasparakis, M. (2017). The interplay of IKK, NF-κB and RIPK1 signaling in the regulation of cell death, tissue homeostasis and inflammation. *Immunol. Rev.* 277, 113–127. doi: 10.1111/imr.12550

Kovacs, S. B., and Miao, E. A. (2017). Gasdermins: effectors of pyroptosis. *Trends Cell Biol.* 27, 673–684. doi: 10.1016/j.tcb.2017.05.005

Kuang, S., Zheng, J., Yang, H., Li, S., Duan, S., Shen, Y., et al. (2017). Structure insight of GSDMD reveals the basis of GSDMD autoinhibition in cell pyroptosis. *Proc. Natl. Acad. Sci. U.S.A.* 114, 10642–10647. doi: 10.1073/pnas.1708194114

Kubota, K., Nakano, M., Kobayashi, E., Mizue, Y., Chikenji, T., Otani, M., et al. (2018). An enriched environment prevents diabetes-induced cognitive impairment in rats by enhancing exosomal miR-146a secretion from endogenous bone marrow-derived mesenchymal stem cells. *PLoS One* 13:e0204252. doi: 10.1371/journal.pone.0204252

Lang, C. E., Lohse, K. R., and Birkenmeier, R. L. (2015). Dose and timing in neurorehabilitation: prescribing motor therapy after stroke. *Curr. Opin. Neurol.* 28, 549–555. doi: 10.1097/WCO.0000000000000256

Le Guennec, D., Hatte, V., Farges, M.-C., Rougé, S., Goepp, M., Caldefie-Chezet, F., et al. (2020). Modulation of inter-organ signalling in obese mice by spontaneous physical activity during mammary cancer development. *Sci. Rep.* 10:8794. doi: 10.1038/s41598-020-65131-9

Li, B., Xu, P., Wu, S., Jiang, Z., Huang, Z., Li, Q., et al. (2018). Diosgenin attenuates lipopolysaccharide-induced Parkinson's disease by inhibiting the TLR/NF- κB pathway. *J. Alzheimer's Dis.* 64, 943–955. doi: 10.3233/JAD-180330

Li, Q., Cao, Y., Dang, C., Han, B., Han, R., Ma, H., et al. (2020). Inhibition of double-strand DNA-sensing cGAS ameliorates brain injury after ischemic stroke. *EMBO Mol. Med.* 12:e11002. doi: 10.15252/emmm.201911002

Li, Y., Song, W., Tong, Y., Zhang, X., Zhao, J., Gao, X., et al. (2021). Isoliquiritin ameliorates depression by suppressing NLRP3-mediated pyroptosis via

miRNA-27a/SYK/NF-κB axis. *J. Neuroinflamm.* 18:1. doi: 10.1186/s12974-020-02040-8

Lin, Y., Yao, M., Wu, H., Wu, F., Cao, S., Ni, H., et al. (2021). Environmental enrichment implies GAT-1 as a potential therapeutic target for stroke recovery. *Theranostics* 11, 3760–3780. doi: 10.7150/thno.53316

Liu, H., Wu, X., Luo, J., Wang, X., Guo, H., Feng, D., et al. (2019). Pterostilbene attenuates astrocytic inflammation and neuronal oxidative injury after ischemia-reperfusion by inhibiting NF-κB phosphorylation. *Front. Immunol.* 10:2408. doi: 10.3389/fimmu.2019.02408

Liu, Z., Gan, L., Xu, Y., Luo, D., Ren, Q., Wu, S., et al. (2017). Melatonin alleviates inflammasome-induced pyroptosis through inhibiting NF-κB/GSDMD signal in mice adipose tissue. *J. Pineal Res.* 63:e12414. doi: 10.1111/jpi.12414

Livingston-Thomas, J., Nelson, P., Karthikeyan, S., Antonescu, S., Jeffers, M. S., Marzolini, S., et al. (2016). Exercise and environmental enrichment as enablers of task-specific neuroplasticity and stroke recovery. *Neurotherapeutics* 13, 395–402. doi: 10.1007/s13311-016-0423-9

Longa, E. Z., Weinstein, P. R., Carlson, S., and Cummins, R. (1989). Reversible middle cerebral artery occlusion without craniectomy in rats. *Stroke* 20, 84–91. doi: 10.1161/01.str.20.1.84

Lu, L.-Q., Tian, J., Luo, X.-J., and Peng, J. (2021). Targeting the pathways of regulated necrosis: a potential strategy for alleviation of cardio-cerebrovascular injury. *Cell. Mol. Life Sci.* 78, 63–78. doi: 10.1007/s00018-020-03587-8

Matias, M. L., Gomes, V. J., Romao-Veiga, M., Ribeiro, V. R., Nunes, P. R., Romagnoli, G. G., et al. (2019). Silibinin downregulates the NF-κB pathway and NLRP1/NLRP3 inflammasomes in monocytes from pregnant women with preeclampsia. *Molecules* 24:1548. doi: 10.3390/molecules24081548

McKenzie, B. A., Mamik, M. K., Saito, L. B., Boghozian, R., Monaco, M. C., Major, E. O., et al. (2018). Caspase-1 inhibition prevents glial inflammasome activation and pyroptosis in models of multiple sclerosis. *Proc. Natl. Acad. Sci. U.S.A.* 115, E6065–E6074. doi: 10.1073/pnas.1722041115

Morris, R. (1984). Developments of a water-maze procedure for studying spatial learning in the rat. *J. Neurosci. Methods* 11, 47–60. doi: 10.1016/0165-0270(84)90007-4

Pradère, J.-P., Hernandez, C., Koppe, C., Friedman, R. A., Luedde, T., and Schwabe, R. F. (2016). Negative regulation of NF-κB p65 activity by serine 536 phosphorylation. *Sci. Signal.* 9:ra85. doi: 10.1126/scisignal.aab2820

Rathinam, V. A. K., and Fitzgerald, K. A. (2016). Inflammasome complexes: emerging mechanisms and effector functions. *Cell* 165, 792–800. doi: 10.1016/j.cell.2016.03.046

Ridder, D. A., and Schwaninger, M. (2009). NF-kappaB signaling in cerebral ischemia. *Neuroscience* 158, 995–1006. doi: 10.1016/j.neuroscience.2008.07.007

Sborgi, L., Rühl, S., Mulvihill, E., Pipercevic, J., Heilig, R., Stahlberg, H., et al. (2016). GSDMD membrane pore formation constitutes the mechanism of pyroptotic cell death. *EMBO J.* 35, 1766–1778. doi: 10.15252/embj.201694696

Schroder, K., and Tschopp, J. (2010). The inflammasomes. *Cell* 140, 821–832. doi: 10.1016/j.cell.2010.01.040

Şekerdağ, E., Solaroğlu, I., and Gürsoy-Özdemir, Y. (2018). Cell Death Mechanisms in stroke and novel molecular and cellular treatment options. *Curr. Neuropharmacol.* 16:1396. doi: 10.2174/1570159X16666180302115544

Shi, J., Gao, W., and Shao, F. (2017). Pyroptosis: gasdermin-mediated programmed necrotic cell death. *Trends Biochem. Sci.* 42, 245–254. doi: 10.1016/j.tibs.2016.10.004

Shi, J., Zhao, Y., Wang, K., Shi, X., Wang, Y., Huang, H., et al. (2015). Cleavage of GSDMD by inflammatory caspases determines pyroptotic cell death. *Nature* 526, 660–665. doi: 10.1038/nature15514

Shin, S. S., Krishnan, V., Stokes, W., Robertson, C., Celnik, P., Chen, Y., et al. (2018). Transcranial magnetic stimulation and environmental enrichment enhances cortical excitability and functional outcomes after traumatic brain injury. *Brain Stimul.* 11, 1306–1313. doi: 10.1016/j.brs.2018.07.050

Song, Y., Gan, Y., Wang, Q., Meng, Z., Li, G., Shen, Y., et al. (2017). Enriching the housing environment for mice enhances their NK cell antitumor immunity via sympathetic nerve–dependent regulation of NKG2D and CCR5. *Cancer Res.* 77, 1611–1622. doi: 10.1158/0008-5472.CAN-16-2143

Stinear, C. M., Lang, C. E., Zeiler, S., and Byblow, W. D. (2020). Advances and challenges in stroke rehabilitation. *Lancet Neurol.* 19, 348–360. doi: 10.1016/S1474-4422(19)30415-6

Strowig, T., Henao-Mejia, J., Elinav, E., and Flavell, R. (2012). Inflammasomes in health and disease. *Nature* 481, 278–286. doi: 10.1038/nature10759

Sun, Z., Nyanzu, M., Yang, S., Zhu, X., Wang, K., Ru, J., et al. (2020). VX765 attenuates pyroptosis and HMGB1/TLR4/NF-κB pathways to improve functional outcomes in TBI mice. *Oxid. Med. Cell Longev.* 2020:7879629. doi: 10.1155/2020/7879629

Tan, M.-S., Tan, L., Jiang, T., Zhu, X.-C., Wang, H.-F., Jia, C.-D., et al. (2014). Amyloid-β induces NLRP1-dependent neuronal pyroptosis in models of Alzheimer's disease. *Cell Death Dis.* 5:e1382. doi: 10.1038/cddis.2014.348

Tang, S.-C., Wang, Y.-C., Li, Y.-I., Lin, H.-C., Manzanero, S., Hsieh, Y.-H., et al. (2013). Functional role of soluble receptor for advanced glycation end products in stroke. *Arterioscler Thromb Vasc. Biol.* 33, 585–594. doi: 10.1161/ATVBAHA.112.300523

Vallabhapurapu, S., and Karin, M. (2009). Regulation and function of NF-κB transcription factors in the immune system. *Annu. Rev. Immunol.* 27, 693–733. doi: 10.1146/annurev.immunol.021908.132641

Virani, S. S., Alonso, A., Benjamin, E. J., Bittencourt, M. S., Callaway, C. W., Carson, A. P., et al. (2020). Heart disease and stroke statistics-2020 update: a report from the American heart association. *Circulation* 141, e139–e596. doi: 10.1161/CIR.0000000000000757

Walsh, J. G., Muruve, D. A., and Power, C. (2014). Inflammasomes in the CNS. *Nat. Rev. Neurosci.* 15, 84–97. doi: 10.1038/nrn3638

Wang, C., Zhang, Q., Yu, K., Shen, X., Wu, Y., and Wu, J. (2019). Enriched environment promoted cognitive function via bilateral synaptic remodeling after cerebral ischemia. *Front. Neurol.* 10:1189. doi: 10.3389/fneur.2019.01189

Wang, Y., Zhu, X., Yuan, S., Wen, S., Liu, X., Wang, C., et al. (2019). TLR4/NF-κB signaling induces GSDMD-related pyroptosis in tubular cells in diabetic kidney disease. *Front. Endocrinol. (Lausanne)* 10:603. doi: 10.3389/fendo.2019.00603

Wang, K., Ru, J., Zhang, H., Chen, J., Lin, X., Lin, Z., et al. (2020a). Melatonin enhances the therapeutic effect of plasma exosomes against cerebral ischemia-induced pyroptosis through the TLR4/NF-κB pathway. *Front. Neurosci.* 14:848. doi: 10.3389/fnins.2020.00848

Wang, K., Sun, Q., Zhong, X., Zeng, M., Zeng, H., Shi, X., et al. (2020b). Structural mechanism for GSDMD targeting by autoprocessed caspases in pyroptosis. *Cell* 180, 941.e20–955.e20. doi: 10.1016/j.cell.2020.02.002

Winstein, C. J., Stein, J., Arena, R., Bates, B., Cherney, L. R., Cramer, S. C., et al. (2016). Guidelines for adult stroke rehabilitation and recovery: a guideline for healthcare professionals from the American Heart Association/American stroke association. *Stroke* 47, e98–e169. doi: 10.1161/STR.0000000000000098

Wu, H., Che, X., Zheng, Q., Wu, A., Pan, K., Shao, A., et al. (2014). Caspases: a molecular switch node in the crosstalk between autophagy and apoptosis. *Int. J. Biol. Sci.* 10, 1072–1083. doi: 10.7150/ijbs.9719

Wu, J., Bie, B., and Naguib, M. (2016). Epigenetic manipulation of brain-derived neurotrophic factor improves memory deficiency induced by neonatal anesthesia in rats. *Anesthesiology* 124, 624–640. doi: 10.1097/ALN.0000000000000981

Xu, P., Zhang, X., Liu, Q., Xie, Y., Shi, X., Chen, J., et al. (2019). Microglial TREM-1 receptor mediates neuroinflammatory injury via interaction with SYK in experimental ischemic stroke. *Cell Death Dis.* 10, 1–17. doi: 10.1038/s41419-019-1777-9

Xu, Y., Sun, Q., Yuan, F., Dong, H., Zhang, H., Geng, R., et al. (2020). RND2 attenuates apoptosis and autophagy in glioblastoma cells by targeting the p38 MAPK signalling pathway. *J. Exp. Clin. Cancer Res.* 39:174. doi: 10.1186/s13046-020-01671-2

Xue, Y., Enosi Tuipulotu, D., Tan, W. H., Kay, C., and Man, S. M. (2019). Emerging activators and regulators of inflammasomes and pyroptosis. *Trends Immunol.* 40, 1035–1052. doi: 10.1016/j.it.2019.09.005

Yang, F., Wang, Z., Wei, X., Han, H., Meng, X., Zhang, Y., et al. (2014). NLRP3 deficiency ameliorates neurovascular damage in experimental ischemic stroke. *J. Cereb. Blood Flow. Metab.* 34, 660–667. doi: 10.1038/jcbfm.2013.242

Yang-Wei Fann, D., Lee, S.-Y., Manzanero, S., Tang, S.-C., Gelderblom, M., Chunduri, P., et al. (2013). Intravenous immunoglobulin suppresses NLRP1 and NLRP3 inflammasome-mediated neuronal death in ischemic stroke. *Cell Death Dis.* 4:e790. doi: 10.1038/cddis.2013.326

Ye, A., Li, W., Zhou, L., Ao, L., Fang, W., and Li, Y. (2020). Targeting pyroptosis to regulate ischemic stroke injury: molecular mechanisms and preclinical evidences. *Brain Res. Bull.* 165, 146–160. doi: 10.1016/j.brainresbull.2020.10.009

Yirmiya, R., and Goshen, I. (2011). Immune modulation of learning, memory, neural plasticity and neurogenesis. *Brain Behav. Immun.* 25, 181–213. doi: 10.1016/j.bbi.2010.10.015

Young, D., Lawlor, P. A., Leone, P., Dragunow, M., and During, M. J. (1999). Environmental enrichment inhibits spontaneous apoptosis, prevents seizures and is neuroprotective. *Nat. Med.* 5, 448–453. doi: 10.1038/7449

Zhan, Y., Li, M.-Z., Yang, L., Feng, X.-F., Lei, J.-F., Zhang, N., et al. (2020). The three-phase enriched environment paradigm promotes neurovascular restorative and prevents learning impairment after ischemic stroke in rats. *Neurobiol. Dis.* 146:105091. doi: 10.1016/j.nbd.2020.105091

Zhang, Y., Xu, D., Qi, H., Yuan, Y., Liu, H., Yao, S., et al. (2018). Enriched environment promotes post-stroke neurogenesis through NF-κB-mediated secretion of IL-17A from astrocytes. *Brain Res.* 1687, 20–31. doi: 10.1016/j.brainres.2018.02.030

Zhou, H., Chen, S., Wang, W., Wang, Z., Wu, X., and Zhang, Z. (2012). Nanog inhibits lipopolysaccharide-induced expression of pro-inflammatory cytokines by blocking NF-κB transcriptional activity in rat primary microglial cells. *Mol. Med. Rep.* 5, 842–846. doi: 10.3892/mmr.2011.719

Conflict of Interest: The authors declare that the research was conducted in the absence of any commercial or financial relationships that could be construed as a potential conflict of interest.

Publisher's Note: All claims expressed in this article are solely those of the authors and do not necessarily represent those of their affiliated organizations, or those of the publisher, the editors and the reviewers. Any product that may be evaluated in this article, or claim that may be made by its manufacturer, is not guaranteed or endorsed by the publisher.

frontiers in Aging Neuroscience

REVIEW
published: 29 September 2021
doi: 10.3389/fnagi.2021.738529

Current Approaches and Molecular Mechanisms for Directly Reprogramming Fibroblasts Into Neurons and Dopamine Neurons

Fabin Han[1,2,3]†, Yanming Liu[2,3]†, Jin Huang[4], Xiaoping Zhang[5] and Chuanfei Wei[3]*

[1] Innovation Institute for Traditional Chinese Medicine, Shandong University of Traditional Chinese Medicine, Jinan, China, [2] Shenzhen Research Institute of Shandong University, Jinan, China, [3] The Institute for Tissue Engineering and Regenerative Medicine, Liaocheng University/Liaocheng People's Hospital, Liaocheng, China, [4] Laboratory of Basic Medical Research, Medical Centre of PLA Strategic Support Force, Beijing, China, [5] College of Pharmacy, Shandong University of Traditional Chinese Medicine, Jinan, China

Parkinson's disease is mainly caused by specific degeneration of dopaminergic neurons (DA neurons) in the substantia nigra of the middle brain. Over the past two decades, transplantation of neural stem cells (NSCs) from fetal brain-derived neural stem cells (fNSCs), human embryonic stem cells (hESCs), and induced pluripotent stem cells (iPSCs) has been shown to improve the symptoms of motor dysfunction in Parkinson's disease (PD) animal models and PD patients significantly. However, there are ethical concerns with fNSCs and hESCs and there is an issue of rejection by the immune system, and the iPSCs may involve tumorigenicity caused by the integration of the transgenes. Recent studies have shown that somatic fibroblasts can be directly reprogrammed to NSCs, neurons, and specific dopamine neurons. Directly induced neurons (iN) or induced DA neurons (iDANs) from somatic fibroblasts have several advantages over iPSC cells. The neurons produced by direct transdifferentiation do not pass through a pluripotent state. Therefore, direct reprogramming can generate patient-specific cells, and it can overcome the safety problems of rejection by the immune system and teratoma formation related to hESCs and iPSCs. However, there are some critical issues such as the low efficiency of direct reprogramming, biological functions, and risks from the directly converted neurons, which hinder their clinical applications. Here, the recent progress in methods, mechanisms, and future challenges of directly reprogramming somatic fibroblasts into neurons or dopamine neurons were summarized to speed up the clinical translation of these directly converted neural cells to treat PD and other neurodegenerative diseases.

Keywords: Parkinson's disease, fibroblast, direct reprogramming, transcription factor, miRNA, induced dopamine neuron

OPEN ACCESS

Edited by:
Benoit Laurent,
Université de Sherbrooke, Canada

Reviewed by:
Janelle Drouin-Ouellet,
Université de Montréal, Canada
Seungkwon You,
Korea University, South Korea

***Correspondence:**
Fabin Han
fhan2013@126.com

†*These authors share first authorship*

Received: *09 July 2021*
Accepted: *27 August 2021*
Published: *29 September 2021*

Citation:
Han F, Liu Y, Huang J, Zhang X and Wei C (2021) Current Approaches and Molecular Mechanisms for Directly Reprogramming Fibroblasts Into Neurons and Dopamine Neurons. Front. Aging Neurosci. 13:738529. doi: 10.3389/fnagi.2021.738529

Abbreviations: PD, Parkinson's disease; iN, induced neuron; iDAN, induced DA neuron; NSC, neural stem cell; NPC, neural precursor cells; fNSC, fetal brain-derived neural stem cell; mESC, mouse embryonic stem cell; hESC, human embryonic stem cell; iPSC, induced pluripotent stem cell; MEF, mouse embryonic fibroblast; HEF, human embryonic fibroblast; TTF, tail-tip fibroblast; TF, transcription factor; CNV, copy number variation; ncRNA, non-coding RNA; L1, LINE-1; gRNAs, guide-RNAs; cmRNA, chemically modified mRNA.

INTRODUCTION

Parkinson's disease is mainly caused by the degenerative loss of dopamine neurons (DA neurons) in the substantia nigra of the midbrain. Its characteristic biomarker is the formation of the Lewy body, which is composed of aggregated proteins in degenerating dopamine neurons and glial cells. Dopamine replacement drugs only delay the progression of the disease without curing the patients. Therefore, transplanting cells to replace damaged DA neurons has great potential in treating symptoms of Parkinson's disease (PD) (Hu et al., 2015; Waldthaler and Timmermann, 2019; Wu et al., 2020).

Early studies transplanted human fetal brain-derived midbrain tissue or fetal neural stem cells (fNSCs) to PD patients and achieved some therapeutic effects (Lindvall et al., 1990; Freed et al., 2001; Li et al., 2008). Transplanted fNSCs have continuously improved the symptoms of PD patients, and they have survived in the brains of some patients for 16 years or even more than 24 years (Li et al., 2016; Xu et al., 2020). Other stem cells, such as embryonic stem cells (ESC), mesenchymal stem cells (MSC), and dopaminergic precursor cells, have been used to treat PD in preclinical studies (Han et al., 2015a; Cyranoski, 2017; Studer, 2017; Takahashi, 2017). The generation of autologous induced pluripotent stem cells (iPSCs) overcomes the rejection of other stem cells by the immune system, and it has broad clinical application in cell therapy and regenerative medicine (Han et al., 2015a, 2019). However, iPSC-derived neural stem cells and dopamine neurons may contain some residual undifferentiated cells and foreign gene integration, so iPSCs may pose a risk of tumorigenicity (Miura et al., 2009; Zhang et al., 2018; Barker and TRANSEURO Consortium, 2019; Ma, 2019). To overcome these obstacles, recent studies have explored directly reprogramming neurons or dopamine neurons from fibroblasts for transplantation therapy in PD (Fong et al., 2010).

Direct reprogramming, also known as transdifferentiation (Hou and Lu, 2016), uses exogenous genes to transform a mature somatic cell into another type of cell directly without going through the pluripotent stage. This approach is based on the reprogramming technology of iPS cells. In 2006, (Takahashi and Yamanaka, 2006) first reprogrammed mouse skin fibroblasts to iPS cells by retrovirus-mediated expression of four transcription factors, namely, Oct3/4, Sox2, Klf4, and c-Myc. In 2007, Yamanaka lab and Thomson lab reported the successful generation of human iPS cells by retrovirus-mediated transfection of OCT3/4, SOX2, KLF4, and c-MYC or lentiviral-mediated expression of four factors (OCT4, SOX2, NANOG, and LIN28) in human skin fibroblasts (Yu et al., 2007). Later, iPS cell-derived neural stem cells were reported to improve functions in animal models with PD, Alzheimer's disease, and amyotrophic lateral sclerosis (ALS) (Han et al., 2015b, 2019; Bahmad et al., 2017). Furthermore, iPS cell-derived dopaminergic precursor cells or DA neurons were shown to improve the functional deficits of the primate model with PD (Hallett et al., 2015; Kikuchi et al., 2017).

Direct reprogramming of somatic cells mainly changes the expression of lineage-specific genes of the original cells through different epigenetic modifications without changing the genomic sequences of the genes. Mouse embryonic fibroblasts (MEFs) and human fibroblasts are the most commonly used starting cells for direct reprogramming to generate neural stem cells or neurons (Caiazzo et al., 2011).

The adult brain is composed of various neurons that are differentiated from neural precursor cells or neural stem cells. The maturation and differentiation of specific neurons, such as dopaminergic neurons, are involved in a series of complex and orderly gene expression and regulation processes. The developmental process of dopaminergic neurons *in vivo* has four main stages: (1) embryonic stem cells are induced into neural stem cells under the synergistic effect of transcription factor genes such as Ascl1, Lmx1a/b, Ngn2, En1/2, Nurr1, and Pitx3, (2) neural stem cells differentiate to the neurons or dopaminergic neuron lineage leading to the generation of early dopaminergic precursor cells, (3) early immature dopaminergic neurons are produced, and (4) at the same time the transcription factors act on the expression of the dopamine neuron-specific tyrosine hydroxylase (TH) or dopamine active transporter (DAT) genes to promote the maturation of dopamine neurons as shown in **Figure 1** (Ang, 2006; Van Heesbeen et al., 2013; Veenvliet and Smidt, 2014; Arenas et al., 2015; Han et al., 2015b; Chen et al., 2020).

Based on the lineage-determining transcription regulatory networks in neural differentiation, different approaches have been developed to convert the fibroblast cells to neurons or DA neurons directly. They do this through epigenetic modification of genomic DNA, including methylation, histone modification, and nucleosome localization, and by repressing and activating the key regulating genes in determining the neural lineages (Graf, 2011; Xie et al., 2013; Mitchell et al., 2014; De Gregorio et al., 2018; Della Valle et al., 2020).

CURRENT METHODS TO REPROGRAM SOMATIC FIBROBLASTS TO NEURONS AND DOPAMINE NEURONS DIRECTLY

The cell fate is mainly controlled by endogenous lineage pathways and epigenetic modifications. Thus, the exogenous expression of the transcriptional factors to regulate the fate of the cell induces the direct conversion of somatic fibroblasts to neurons or dopamine neurons. Various approaches have been developed to convert fibroblasts to neurons or dopamine neurons. These include overexpression of transcription factors, RNA-based regulation of transcription factors, combining transcription factors with small-molecule compounds or other physical factors, and protein-based and *in vivo* approaches to induce epigenetic modification. These are summarized in **Figure 2**.

Transcription Factor (TF)-Induced Direct Reprogramming of Fibroblasts to Neurons/Dopamine Neurons

Yamanaka et al. used four transcription factors, namely, OCT4, SOX2, c-MYC, and KLF4, to reprogram fibroblasts into iPS cells, showing that one cell type can be transdifferentiated to another type (Takahashi and Yamanaka, 2006). Like iPSC technology,

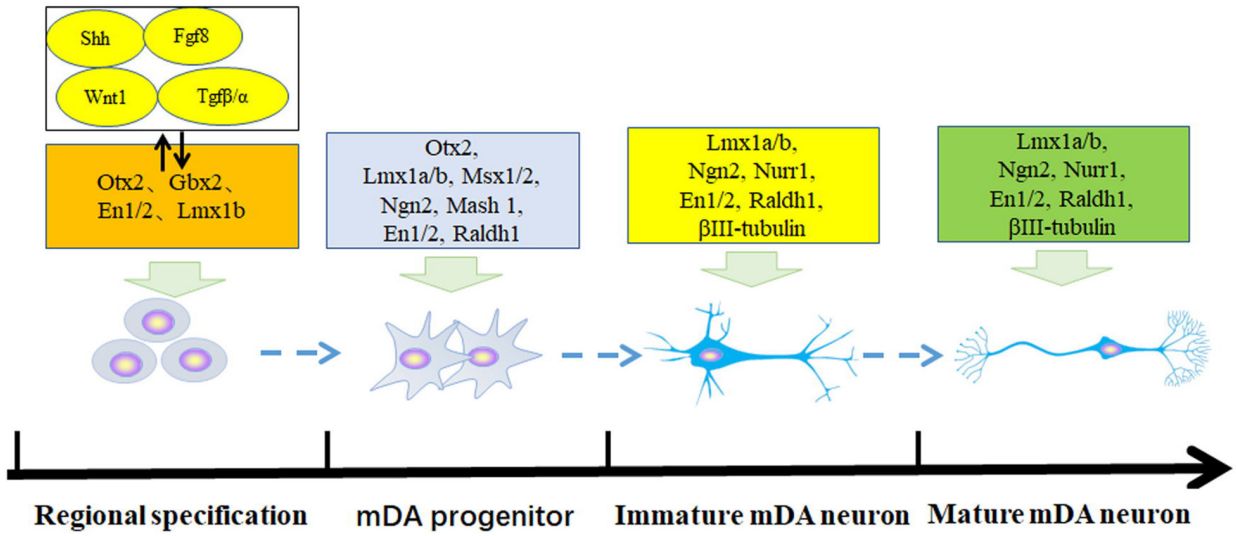

FIGURE 1 | Transcriptional regulation of embryonic stem cells into mesencephalic dopamine progenitor and mature dopamine neurons. The development of dopamine neurons has four stages: regional neural specification, middle brain dopaminergic precursor cells, immature dopamine neurons, and immature dopamine neurons. These are controlled by different transcription factors.

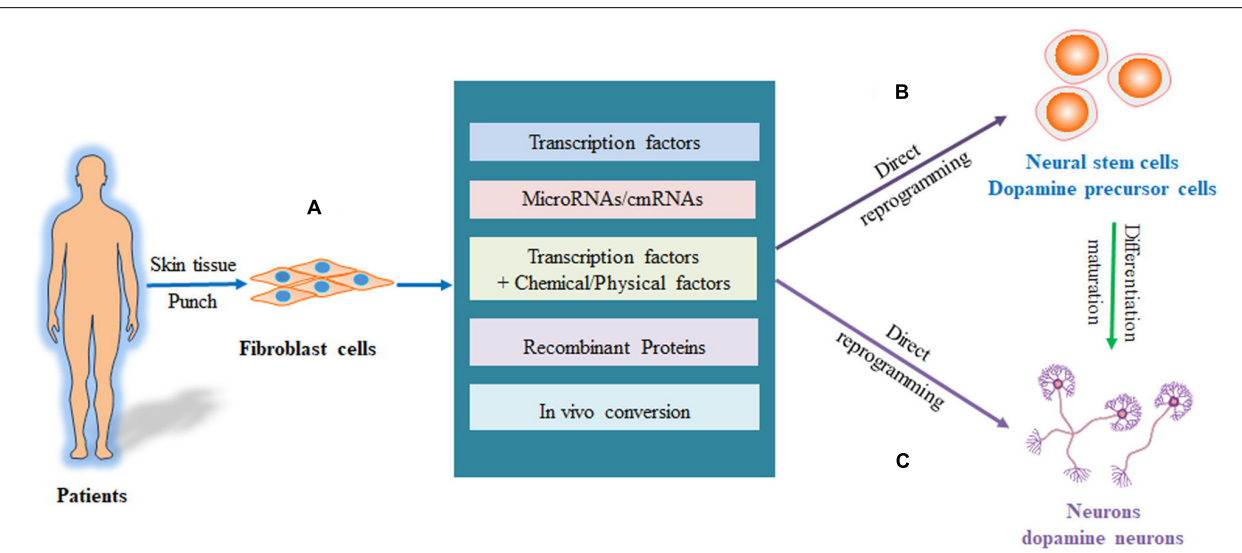

FIGURE 2 | Process of directly reprogramming fibroblasts into neurons and DA neurons. **(A)** The fibroblasts are isolated from patients and reprogrammed to iPS cells, which are then differentiated into neurons or DA neurons. **(B)** The fibroblasts are directly converted to neural stem cells or dopaminergic precursor cells, which are then induced into neurons or DA neurons. **(C)** The fibroblasts can be directly reprogrammed into neurons or DA neurons. DA, dopaminergic neurons; iPS cells, pluripotent stem cells.

most direct reprogramming also forced expression of the defined transcription factors to induce cell-fate conversion. Vierbuchen et al. (2010) first overexpressed transcription factors of Ascl1, Brn2, and Mytl1 to induce MEFs into mature neurons directly. This conversion process jumped over the state of pluripotent stem cells to convert mouse fibroblasts into functional neurons directly (Vierbuchen et al., 2010).

Shortly after that, Pfisterer et al. (2011) showed that the combined expression of the Ascl1, Brn2, and Myt1l with two additional Lmx1a and Foxa2 genes induced fibroblasts to specific iDANs with functional electrophysiological properties. They found that the combination of three factors, Ascl1, Brn2, and Myt1l, could convert fibroblasts to more than 95% of the neurons expressing the neuron marker MAP2 and more than 90% of the converted neurons expressed synaptophysin. This indicated that synapses were forming among the induced neurons (iN) (Pfisterer et al., 2011). In addition, the average resting membrane potential of the induced neurons was approximately −59 mV

(range: −30 to −78 mV) at 30–32 days after transduction of the genes, indicating these converted cells exhibited the similar electrophysiological properties of functional neurons.

To induce specific DA neurons, they initially identified 10 genes involved in the specification of dopamine neurons in the midbrain (En1, Foxa2, Gli1, Lmx1a, Lmx1b, Msx1, Nurr1, Otx2, Pax2, and Pax5). These genes were ever thought to be required for converting the fibroblasts into induced neurons (iNs). Of these converted neurons, some also expressed the dopaminergic marker, TH, indicating that some iN cells were specified to dopamine neurons. They further determined that the minimal required genes are Lmx1a and Foxa2, which are co-expressed with the factors Ascl1, Brn2, and Myt1l, to induce the fibroblasts to dopaminergic neurons. These iDA neurons were found to have morphological and electrophysiological characteristics similar to dopaminergic neurons from fetal brain tissues. These iDAs were shown to co-express TH, Aromatic l-amino acid decarboxylase (AADC), the second enzyme in dopamine synthesis, and Nurr1 expressed by midbrain dopaminergic neurons. In the meantime, Caiazzo et al. (2011) directly reprogrammed human and mouse embryonic fibroblasts to functional dopamine neurons with a conversion efficiency of 18 ± 3%. They did this by combining three transcription factors: Ascl1, Nurr1, and Lmx1a. High-performance liquid chromatography showed that the iDAs released dopamine transmitters into the culture medium even though the iDAs still had some gene expression profiles different from midbrain-derived dopamine neurons (Caiazzo et al., 2011). Jongpil Kim et al. included sonic hedgehog (SHH) and fibroblast growth factor 8 (FGF8) proteins in the induction medium to promote the differentiation and maturation of iDAs. As a result, a combination of Ascl1, Nurr1, Pitx3, Lmx1a, Foxa2, and EN1 with SHH and FGF8 significantly enhanced the efficiency of $EGFP^+$ iDAs from 8% on day 12 to 9.1% by day 18. After transplantation, the iDAs survived in the brain of the PD mouse model and improved the symptoms of dyskinesia in the PD mouse model (Kim et al., 2011; Liu et al., 2012).

Oh et al. (2014) efficiently reprogrammed mouse fibroblasts into a variety of neuronal cells including dopaminergic neurons. They found that after overexpressing the transcription factors Ascl1 and Nurr1 in MEFs, dopaminergic neurons were obtained by culturing the induced cells with growth factors such as SHH and FGF8 (Oh et al., 2014). They reduced the number of transcription factors and promoted the conversion of dopamine neurons from MEFs by modifying the culture conditions. This showed that the required transcription factors can be reduced and the efficiency of converting iDANs can be increased by changing the conditions of the induction culture. The Jialin Zheng team used another combination of transcription factors, namely, Brn2, Sox2, and Foxa2, to reprogram mouse embryonic fibroblasts and human fibroblasts directly into dopaminergic precursor cells. They showed that the dopaminergic precursor cells did not differentiate into astrocytes, and they did not form tumors. These studies suggest that induced dopamine precursor cells derived from direct reprogramming can be used for transplantation treatment of PD (Tian et al., 2015; He et al., 2019). It was also reported that induced noradrenergic (iNA) neurons can be induced from mouse astrocytes and human fibroblast cells by direct reprogramming of seven transcription factors (TFs) (Ascl1, Phox2b, AP-2α, Gata3, Hand2, Nurr1, and Phox2a). These iNA neurons function to release, and re-uptake of noradrenaline and can survive and form synaptic connections after transplantation to mouse model with neurological disorder (Li et al., 2019). The transcription factors used to induce fibroblasts to neurons or dopamine neurons by direct reprogramming are summarized in **Table 1**.

RNA-Mediated Direct Reprogramming

RNA is another approach to mediate reprogramming fibroblasts directly to neurons. This approach can eliminate the risk of mutations from integrating and inserting plasmid-based foreign genes and thus has the good potential use for clinical application of the converted cells (Ambasudhan et al., 2011; Yoo et al., 2011; Liu and Verma, 2015). There are two methods for RNA-based direct reprogramming.

Direct Reprogramming Mediated by MicroRNA (miRNAs)

The ectopic expression of miRNAs (miR-9/9* and miR-124) was shown to promote the direct conversion of human fibroblasts into neurons. To generate more-specific neuronal types, miR-9/9* and miR-124 were co-expressed with the striatum-enriched transcription factors, BCL11B, DLX1, DLX2, and Myt1l to induce human postnatal and adult fibroblasts into neurons that were similar to striatal spiny neurons (MSNs). In addition, after being transplanted into the mouse striatum, these converted neurons displayed functional properties similar to native MSNs. This study suggests that directly reprogrammed neurons might also be used in transplantation therapy of PD (Victor et al., 2014).

To increase the efficiency of converting fibroblasts to iDANs by RNA-based reprogramming, Jiang et al. (2015) combined three transcription factors (Ascl1, Nurr1, and Lmx1a) with miR124 and p53-shRNA to knockdown p53 synergistically and induce human embryonic lung fibroblasts to iDANs. They found that inhibiting p53 can arrest the cell cycle in the G1 phase and significantly increase the conversion of human fibroblasts to dopamine neurons. The efficiency of converting $Tuj1^+$ neurons was increased from 17.9 to 31.1% and the efficiency of converting TH^+ iDANs was increased from 8.3 to 15.4% (Jiang et al., 2015). Pu et al. (2020) used miR124 and p53-shRNA in a combination of transcription factors to reprogram the patient's fibroblasts with Parkin gene mutation to the induced neurons. They found that mutations in the Parkin gene reduced the efficiency of converting somatic fibroblasts to TH + dopamine neurons (8.3 ± 0.6%), but did not affect the conversion efficiency of fibroblasts to total Tuj1 + neurons (18.2 ± 1.2%) (Pu et al., 2020). De Gregorio et al. (2018) used miR-34b/c combined with the transcription factors Ascl1 and NURR1 to reprogram fibroblasts into dopamine neurons directly with an efficiency of 19.5%. They showed that miR-34b/c helped cells to leave the cell cycle by regulating the expression of WNT1, and this greatly improved reprogramming efficiency. The iDANs have also been shown to synthesize dopamine, and they are consistent with the electrophysiological properties of dopaminergic neurons of the human midbrain (De Gregorio et al., 2018).

TABLE 1 | The transdifferentiation of fibroblasts to neurons and dopamine neurons by direct reprogramming.

Source cells	Induced cells	Transcription factors/miRNA/chemicals	Efficiency	Transplantation	Investigators	PMID
Mouse embryonic and postnatal fibroblasts	Functional neurons	Ascl1, Brn2, and Myt1l	19.55% neurons	No	Vierbuchen et al., 2010	20107439
Human fibroblasts	Dopaminergic neurons	Ascl1, Brn2, Myt11, Lmx1a, FoxA2	16% neurons; 4.3% DA neurons	No	Pfisterer et al., 2011	21646515
Mouse and human fibroblasts	Functional dopaminergic neurons	Mash1 (Ascl1), Nurr1 (Nr4a2), and Lmx1a	10% neurons; 5% DA neurons	No	Caiazzo et al., 2011	21725324
Human fetal lung fibroblasts	DA neurons	Mash1, Ngn2, Sox2, Nurr1, and Pitx3	Less than 4% DA neurons	Yes	Liu et al., 2012	22105488
Mouse fibroblasts	Induced neurons and DA neurons	Ascl1 and Nurr1 and neurotrophic factors including SHH and FGF8b	51% Tuj1$^+$ neurons, 33% DA neurons	No	Oh et al., 2014	24991651
Human embryonic fibroblasts	Induced neurons	Ascl1,Brn2,Myt1l, small molecules	MAp2 $^+$ neurons 46%	Yes	Pereira et al., 2014	25208484
Mouse fibroblasts	Dopaminergic precursors	Brn2, Sox2 and Foxa2, SHH, and FGF8	TH$^+$ 90% of the Tuj1$^+$ neurons	Yes	Tian et al., 2015	26224135
Human fetal lung fibroblast	Dopaminergic neurons	Ascl1, Nurr1, Lmx1a and miR124, p53 shRNA	Tuj1$^+$ cells 31.1 ± 1.9%; TH$^+$ cells (15.4 ± 1.1%)	No	Jiang et al., 2015	26639555
Human fibroblasts	Neurons/ dopaminergic neurons	Brn2, Sox2, and Foxa2	96.67 and 86.75% expressing TH$^+$/NeuN$^+$ and TH$^+$/MAP2$^+$	No	He et al., 2019	30664902
Mouse and human Astrocytes and Foreskin fibroblasts	Functional noradrenergic neurons	Ascl1, Phox2b, Ap-2a, Gata3, Hand2, Nurr1, andPhox2a	6.6 ± 1.0%TH$^+$ neuron	Yes	Li et al., 2019	31315047
Human postnatal and adult fibroblasts	Striatal neurons, GABAergic neurons	miR-9/9*-124 with CTIP2 (BCL11B) DLX1, DLX2, MYT1L	90% MAP2$^+$, and 84% NeuN$^+$; 72.3% GABAergic neurons of MAP2$^+$ cells	Yes	Victor et al., 2014	25374357
Human fetal lung fibroblast	Neurons/iDA neurons	miR124, p53 shRNA,Ascl1, Nurr1, and Lmx1a	31.1% Tuj1$^+$ cells, 15.4% TH$^+$ cells	No	Jiang et al., 2015	26639555
Human dermal fibroblasts	Neural precursor cells, GABAergic or glutamatergic neurons	cmRNA SOX2 and cmRNA PAX6	38% TUJ1$^+$ neurons	No	Connor et al., 2018	30450440
Mouse embryonic fibroblasts and adult tail-tip fibroblasts	Neural stem cells, neurons	Valproic acid, Bix01294, RG108, PD0325901, CHIR99021, Vitamin C, and A83-01 treatment	31% neurons expressing MAP2$^+$	Yes	Han et al., 2016	26788068
Mouse fibroblasts	Neuron-like cells	VPA, TD114-2 (CHIR99021), 616452, Tranylcypromine, Forskolin, AM580, EPZ004777	50% of cells expressing tau, Tuj1 and MAP2	Yes	Li et al., 2017	28648365
Human dermal fibroblasts	Neuron-like cells	Ngn2 and Ascl1; LDN-193189, A83-1, CHIR99021, Forskolin, SB-431542, Pyrintegrin, ZM336372, AZ960, and KC7F2	80% of cells expressing Tuj1 and NeuN	No	Herdy et al., 2019	31099332
Fibroblasts	Induced neuronal cells	Fusion protein of 30Kc19 and Ascl1	Not indicated	No	Ryu et al., 2020	32058047
Mouse embryo fibroblasts	Induced neuronal cells	PTB-shRNA	Not indicated	No		23313552
Mouse astrocytes *in vivo*	Induced dopamine neuron	NEUROD1, ASCL1 and LMX1A, and miR218	30.97% neurons and 16% induced dopamine neuron	Yes	Rivetti Di Val Cervo et al., 2017	28398344
Mouse muller glia and astrocytes in striatum mouse	Induced neuron conversion	CasRx gene with two gRNAs 5 and 6 to knockdown Ptbp1	32% TH$^+$ cells	Yes	Zhou et al., 2020	32272060
Astrocytes in the middle brain	Neurons, DA neurons	PTB-shRNA	80% of cells expressing NeuN; 22% of cell expressed TH and GIRK2 (A9 DA neurons)	No	Qian H. et al., 2020	32581380

Direct Reprogramming Mediated by Chemically Modified mRNA (cmRNA)

In 2018, for the first time, Bronwen Connor et al. (2018) developed a method to transiently express the neural transcription factors SOX2 and PAX6 through cmRNA to induce neural stem cells from adult human fibroblasts directly. Transfecting fibroblasts with cmRNA-expressing SOX2 and PAX6 resulted in a higher conversion of fibroblasts to NSCs, and it improved cell survival. Furthermore, the cmRNA-induced NSCs were shown to differentiate to GABAergic and glutamatergic neuronal phenotypes to form in conjunction with astrocytes. The same research team also used cmRNA to reprogram adult fibroblasts into intermediate neural precursor cells (iNPs) and to induce iNPs to dopamine neuron-like cells expressing TUJ1, TH, AADC, DAT, VMAT2, and GIRK2 *via* (Playne et al., 2018). Compared with plasmid transfection, cmRNA has the advantage of being extremely stable and non-immunogenic. This makes it clinically applicable for gene delivery to generate directly induced neurons to treat neurological diseases.

Direct Reprogramming Mediated by the Combination of Transcription Factors and Small-Molecule Compounds

Small molecules were reported to promote the neural conversion of fibroblasts by inhibiting or activating the signal pathways that regulate the neuronal lineage fate. Ladewig et al. (2012) demonstrated that the combination of transcription factors Ascl1 and Ngn2 with the small-molecule compounds, GSK-3β, SB431542, CHIR99021, Noggin, and LDN193189 converted human fibroblasts into functional neuronal cells. By inhibiting the SMAD signaling pathway, small molecules significantly improved the converted efficiency of iNs to 80% compared with the approach mediated by transcription factors (Ladewig et al., 2012). Pereira et al. (2014) co-expressed transcription factors of Ascl1, Brn2, Myt1l, Lmx1a, Lmx1b, Foxa2, and Otx2 in human embryonic fibroblasts (HEF) with small-molecule compounds (CHIR99021, SB431542, Noggin, LDN193189) to convert HEF into specific dopamine neurons efficiently (Pereira et al., 2014). The combination of small molecules with transcription factors reduces the number of required transcription factor genes for direct reprogramming. On the other hand, it can also decrease the potential risk of gene mutation and tumorigenicity caused by integrating foreign genes into the chromosomes of somatic cells (Wang et al., 2016).

Some studies used only chemical compounds for the direct conversion of fibroblasts to neurons without transcription factors. In 2015, Deng et al. reported that using only small molecule compounds could directly reprogram MEFs into functional neurons (Li et al., 2015). In the same year, Wenxiang Hu et al. used seven small molecules of valproic acid (VPA), CHIR99021, Repsox, Forskolin, SP600125 (a JNK inhibitor), GO6983 (a PKC inhibitor), and Y-27632 (ROCK inhibitor) to convert human fibroblasts directly into neuronal cells expressing doublecortin (Dcx), neuron-specific class III ß-tubulin (Tuj1), and microtubule-associated protein 2 (Map2). These chemical-induced human neuronal cells resembled the human iPSC-derived neurons in terms of morphology, gene expression, and electrophysiological properties (Hu et al., 2015). Then, Wang et al. (2016) used small molecule compounds (SB431542, Noggin, RA) and specific growth factors (SHH, bFGF, EGF, GDNF, and FGF8b) to convert MEF cells into dopamine neurons efficiently. Yang et al. (2019) used small-molecule compound combinations to induce human skin fibroblasts into neural cells efficiently. After transplantation, the induced neural cells can form functional connections with host cells in immune-deficient mice (Yang et al., 2019). Of note, by now studies have reported the transdifferentiation of MEF cells into neurons or dopamine neurons using only the small molecules, but no adult fibroblasts have been converted to neurons only by small molecules. Some of the small molecules used indirectly can activate neuronal TFs, so this suggests that they do not do so at expression levels high enough to drive reprogramming. The small molecules, PD0325901, CHIR99021, and A83-01 were first used to start the neural induction of MEFs and mouse tail-tip fibroblasts (TTF) by regulating the fate of stem cells. Then, the small molecules valproic acid, Bix01294, and RG108 were added to the medium to improve the induction of NSC and decrease the apoptosis of cells induced by vitamin C during the induction. These direct induced cells expressed the NSC markers of sex-determining region Y box-2 SRY-Box Transcription Factor 2 (Sox2), glial fibrillary acidic protein (GFAP), and oligodendrocyte transcription factor (Olig2), and they could be differentiated further to 31% neurons expressing Map2 and glial cells including 20% of GFAP-positive cells (astrocytes), 36% of O4-positive cells (oligodendrocytes) (Han et al., 2016). Li et al. reported that a seven-compound cocktail [VPA, TD114-2 (CHIR99021), 616452, Tranylcypromine, Forskolin, AM580, EPZ004777] induced MEFs into extra-embryonic endoderm (XEN)-like cells. Then they used Dorsomorphin, LDN193189, SB431542, and Ch55 to promote XEN-like cells into neurons of which more than 50% expressed neuron-specific genes tau, Tuj1, and MAP2. By day 18, more than 80% of the tau-positive cells were differentiated neurons expressing vGLUT1. This study also showed that the XEN-like cells further differentiate to mature neurons after transplantation into the adult mouse brains (Li et al., 2017).

Physical factors also can be combined with transcription factors to induce direct reprogramming. Junsang Yoo et al. (2015) reprogrammed fibroblasts into dopamine neurons through nanoscale biophysical stimulation. The fibroblasts were cultured on flat microgrooved and nanogrooved substrates. After biophysical stimulation, the expression of DA markers was gradually detected in the induced fibroblasts. These neuron conversions by physical stimulation may be attributed to specific histone modifications and transcriptional changes associated with mesenchymal-to-epithelial transition (Yoo et al., 2015). Another study reported that the same transcription factors (Ascl1, Pitx3, Nurr1, and Lmx1a) with the use of electromagnetic gold nanoparticles can directly reprogram mouse tail fibroblasts and human fibroblasts into dopamine neurons with great efficiency (Yoo et al., 2017). Chang et al. (2018) used mesoporous silica nanoparticles as non-viral vectors to transduce three

plasmids, pAscl1, pBrn2, and pMyt1l, into mouse fibroblasts to produce functional dopaminergic neuron-like cells with function similar to fetal brain-derived dopamine neurons.

Protein-Mediated Reprogramming

In this approach, recombinant proteins are transferred to somatic cells directly to induce their transdifferentiation into neurons. Mirakhori et al. (2015) used *trans*-activator of transcription (TAT)-mediated recombinant proteins of the transcription factors SOX2 and LMX1a, which were transfected into human embryonic fibroblasts in combination with small-molecule compounds, to generate dopaminergic precursor-like cells (iDPCs). Then they directly differentiated them into dopamine neurons (Mirakhori et al., 2015). This was the first report that iDPCs could self-proliferate and were safe and that they might become an option for cell replacement therapy in PD. Ryu et al. (2020) used the fusion partner of 30Kc19 protein and transcription factor Ascl1 to induce fibroblasts directly into neurons. Although its conversion efficiency was lower than that of other methods, protein-based direct reprogramming avoids the potential risk of gene mutation caused by foreign genes, and it also shows good potential for clinical application (Ryu et al., 2020).

Recently, human fibroblasts were converted into DA neuron-like cells by a combination of proteins and small molecules. The fibroblasts were first induced in the neural induction medium with valproic acid (VPA), Repsox, kenpaullone, forskolin, L Y-27632, and purmorphamine for 6–8 days. Then the induction medium was replaced with neuronal maturation medium with forskolin, kenpaullone, L-ascorbic acid, SHH, FGF-8b, bFGF, BDNF, and GDNF for two more weeks. The fibroblasts were converted into the induced DA neuron-like cells that expressed DA markers, exhibited neuronal morphology, and showed electrophysiological properties like that of fetal DA neurons. Further analysis showed that about 87.9% of the cells were converted into $TUJ1^{+}/TH^{+}$ neurons, indicating high yields of DA neuron-like cells were possible after induction by small molecules and proteins (Qin et al., 2020).

In vivo Direct Reprogramming

The exogenous transplantation of directly converted neurons from cultured fibroblasts faces the problem of rejection by the immune system. However, direct reprogramming of glial cells into neurons *in vivo* also has made significant progress for clinical translation. Retroviral vectors infect dividing cells like progenitor cells or reactive glial cells without infecting the neurons. When retroviral vectors expressing transcription factor NeuroD1 were injected directly into the adult mouse cortex, the astrocytes were reprogrammed into functional neurons, such as glutamatergic neurons *in vivo* (Guo et al., 2014). To produce the induced dopamine neurons *in vivo*, the astrocytes of the mouse brain were transfected with NEUROD1, Ascl1, and LMX1A. The miR218 (NeAL218) were converted into iDAs with an efficiency of 16%. Importantly, this combination of NeAL218 successfully converted the striatal astrocytes into iDAs in a mouse model of Parkinson's disease, and it improved some motor deficits *in vivo*. This meant that this approach might be suitable for clinical therapies in PD (Rivetti Di Val Cervo et al., 2017).

TABLE 2 | Comparison of the PROS and CONS of different reprogramming approaches.

Approaches	PROS	CONS
Transcription factors-mediated method	High transdifferentiation efficiency, More precisely control the directions of transdifferentiation	Lenti_viral transfection integrate the foreign genes to the cell genome to induce mutagenesis
Combination of transcription factors and small molecules	Improved the converted efficiency of iNs to 80%, Using the small molecules to regulate the target genes and reduce the number of transcription factors required for direct reprogramming	May have genomic integration of some transcription factor genes, May have the risk of mutagenesis in directly reprogrammed cells
Chemical-mediated method	No foreign gene integration into the genome to reduce the risk of mutagenesis, suitable for clinical application	Has lower reprogramming efficiency and induced neurons are not mature. No adult fibroblasts have been converted to neurons by small molecules only.
mRNA-mediated method	No foreign gene integration into the genome to reduce the risk of mutagenesis, being extremely stable and non-immunogenic, suitable for clinical application	The safety and efficacy of the induced neurons needs further approval
Protein-mediated method	No foreign gene integration into the genome to reduce the risk of mutagenesis, A good potential for clinical application	Has lower reprogramming efficiency

As it was discussed above, different approaches have their advantages and shortages to directly reprogram one cell type to another. Here the pros and cons of direct reprogramming were summarized as **Table 2**.

THE MOLECULAR MECHANISMS OF DIRECT REPROGRAMMING

To increase the efficiency of directly reprogramming fibroblasts into neurons or dopamine neurons, it is necessary to understand the molecular and cellular mechanisms of cell fate conversion. This includes the roles of transcription factors, the regulatory networks of the transcriptome, and epigenetic modification during different stages of cell transitions. These mechanisms are mainly involved in the direct conversion of fibroblasts to neural stem cells, neurons, and dopamine neurons as noted in the following subsections.

Transcription Factors Induce Direct Reprogramming of Fibroblasts to Neurons and Dopamine Neurons

As noted above, most studies used three transcription factors, namely, Ascl1, Brn2, and Myt1l or Ascl1, Nurr1, and Lmx1a to

induce converted neurons and dopamine neurons. Ascl1 seems to play a pivotal role in the direct reprogramming of fibroblasts into neurons. It might be that Ascl1 enters the nuclei of the cells and binds its neuronal target genes across the genome of the fibroblasts. Structural analysis showed that bHLH transcription factors like Ascl1 bind to the two neighboring major groves of target DNA sequences with its α-helical basic domains as a heterodimer to induce the epigenetic modification and neuronal conversion (Ma et al., 1994; Kim et al., 2009). One study investigated this mechanism by characterizing the Ascl1 binding sites in MEF cells. ChIP-seq analysis showed that after Ascl1 was transfected into MEF cells, the Ascl1 binding pattern of MEFs was identical to that for all three transcription factors (Ascl1, Brn2, and Myt1l). This suggests that Ascl1 binds the same critical sites in the promoter regions of the regulatory genes as the other two factors, Brn2 and Myt1l, to start the conversion of fibroblasts to neurons. This showed that exogenous Ascl1 binds to the specific DNA sequence sites in fibroblasts without association with Brn2 or Myt1l (Wapinski et al., 2013). To further characterize the binding sites of Ascl1, a genome-wide analysis found that different binding sites had an affinity comparable to that of Ascl1 in MEFs. Furthermore, the CAGCTG sequence was identified as the key motif in the binding site of Ascl1. Several target genes also were bound by Ascl1. Some of them are members of the notch and JAK/STAT signaling pathways such as Zfp238, *Hes6*, *Dll1*, and *Mfng*. Others are genes such as *NeuroD4* that are associated with neural development.

The binding sites of Brn2 were also analyzed in different cells by ChIP-seq. The results showed that there was little overlap in the binding sites of Brn2 between fibroblasts and neural precursor cells (NPCs). However, an E-box motif was significantly enriched in a large fraction of these binding sites. A comparison of Brn2 and Ascl1 targets in MEFs infected by Ascl1, Brn2, and Myt1l found a high overlap between the target sites of Ascl1 alone and of both Brn2 and Ascl1. This suggests that Ascl1 actively recruits Brn2 to its targets, and it was further confirmed by the co-localization of Brn2 and Ascl1. Ascl1 binding sites are similar in MEFs and NPCs. However, a small fraction of sites was bound by Ascl1 in NPCs that are not bound in MEFs. This suggests that Ascl1 binds to specific sites of MEFs to induce neuronal conversion. That study also explored more than 25 predicted target genes, and it identified the transcription factor Zfp238 as the critical target of Ascl1 to mediate the reprogramming of fibroblasts to iN, together with other unidentified critical downstream factors (Wapinski et al., 2013).

Interestingly, another study reported that ASCL1 alone is able to induce functional iN cells from mouse and human fibroblasts and embryonic stem cells, further indicating that ASCL1 is playing the key role for iN and that MYT1L and BRN2 is primarily to promote the neuronal maturation (Chanda et al., 2014).

To explore the epigenetic methylation in the transdifferentiation of fibroblasts, an epigenetic model of ChromHMM was used to define chromatin methylation and acylation in entire genomes of MEFs (Ernst and Kellis, 2012). That analysis identified a specific MEF chromatin state (ChromHMM state 5) that is enriched at Ascl1 binding sites. ChromHMM state 5 represents the combination of high enrichment values for H3K4me1 and H3K27ac and low-to-intermediate enrichment levels of H3K9me3 in MEFs. Among MEFs, NPCs, human fibroblasts, and keratinocytes, this trivalent chromatin state, composed of H3K4me1, H3K27ac, and H3K9me3, was confirmed to be the key histone modification in the genome. Of all chromatin hidden Markov model (ChromHMM) states, state 5 had the highest enrichment at Ascl1 targets. Sequential immunoprecipitation of mono-nucleosomes isolated from MEFs revealed the co-occurrence of the three chromatin states (H3K27ac, H3K4me1, and H3K9me3) on single nucleosomes. This validated the existence of this trivalent state in the MEFs.

Several studies showed that small-molecule compounds increase transdifferentiation by inhibiting several cell fate signaling pathways. They include TGF-b/SMAD signaling, GSK-3b signaling (Ladewig et al., 2012), adenylyl cyclase activation (Gascon et al., 2016), and the RE1-silencing transcription factor (REST) pathway (Masserdotti et al., 2015). Herdy et al. (2019) have converted the fibroblasts to neurons by expressing the two transcription factors of NGN2 and Ascl1 and including small molecules in the induction medium to get more than 90% induced neurons (iN) over the starting fibroblasts (Wendt et al., 2014).

Transcriptome analysis was performed at different time points of direct iN. It found that more than 500 pathways were significantly modified in the transdifferentiation process. The 10 most important pathways were characterized through 20 small molecules to activate or inhibit each of the pathways during conversion. As a result, four compounds were found to increase the conversion of positive iNs significantly. Each of these compounds promoted the conversion of young and old fibroblasts into iNs through different mechanisms. They were Pyrintegrin as integrin activator, AZ960 as Jak2 inhibitor, ZM336372 as Raf-1 activator, and KC7F2 as HIF1a inhibitor. Importantly, the combination of all four compounds (ZPAK) produced a higher yield of iN than any of the four compounds separately. This helped these compounds act through different pathways to induce conversion of fibroblasts to iN synergistically (Herdy et al., 2019).

The JAK/STAT signaling is involved in the reversible process of cell proliferation and differentiation. Inhibiting JAK2 was shown to force fibroblasts from the cell cycle and promote mesenchymal-to-epithelial transition (MET) and neuronal reprogramming of the fibroblasts. Fibroblasts exiting the cell cycle have been reported to improve the MET process. Moreover, adding AZ960 to inhibit Jak2, significantly decreased STAT3. This induced a more rapid switch to promote the MET in converted neurons (Wendt et al., 2014).

Characterizing the Regulatory Genes and Signaling Pathways in Direct Reprogramming by Transcriptome Analysis (Rna-Seq)

To identify the transcriptional networks during direct conversion of fibroblasts into neurons, Treutlein et al. used single-cell

RNA-seq to analyze multiple time points during the 22 day-process of reprogramming MEFs into induced neurons (iN) (Trapnell et al., 2014). They explored how individual fibroblasts responded to overexpression of Ascl1 during the initial phase of reprogramming and found that an expression threshold is required for Ascl1 to start direct reprogramming. Ascl1 is responsible for starting the expression of target genes to induce direct neural conversion. It was observed that over-expression of Ascl1 in MEFs upregulates neuronal target genes of Zfp238, Hes6, Atoh8 and downregulates cell cycle genes such as Birc5, Ube2c, and Hmga2. Most fibroblasts are found to be partially reprogrammed at the early phase, and later events are responsible for the complete reprogramming. Further analysis of the single MEF cells showed that in the first 5 days forced expression of Ascl1 is associated with increased expression of neuronal genes in reprogrammed MEF cells. Detailed time-lapse track of GFP-labeled single cells showed that some MEF cells with low or no Ascl1 expression in the converting process might never have been started for direct reprogramming (Treutlein et al., 2016).

During the 22-day process of converting MEFs into iN cells, a continuous intermediate process was observed at each time point through Monocle analysis of single converting cells (Trapnell et al., 2014). Principal component analysis (PCA) of all single cells in the early, intermediate, and late stages of neuronal transdifferentiation identified two genetic regulatory events during reprogramming. First, there is an initiation stage where MEFs exit the cell cycle upon Ascl1 induction, and regulating genes such as *Birc5*, *Ube2c*, *Hmga2* involved in mitosis are turned down or off. Concomitantly, the expression of some genes associated with cytoskeletal reorganization (*Sept3/4*, *Coro2b*, *Ank2*, *Mtap1a*, *Homer2*, and *Akap9*), synaptic transmission (*Snca*, *Stxbp1*, *Vamp2*, *Dmpk*, and *Ppp3ca*), and neural projection [*Cadm1*, *Dner*, *Klhl24*, *Tubb3*, and *Mapt (Tau)]* were all up regulated. This showed that Ascl1 induces the expression of genes involved in defining neuronal conversion during early reprogramming. This initiation phase is followed by a maturation stage in which extracellular matrix genes are turned off and the genes involved in synaptic maturation (*Syp*, *Rab3c*, *Gria2*, *Syt4*, *Nrxn3*, *Snap25*, and *Sv2a*) are turned on in converted MEF cells. These findings are consistent with the previous finding that Tuj1 + cells with immature neuron-like morphology could be found as early as the third day after Ascl1 is expressed, while functional synapses are not formed until 2 to 3 weeks after reprogramming begins (Xu et al., 2020).

Retrotransposon-Mediated Conversion of Fibroblasts Into Dopamine Neurons

In mammalian cells, LINE-1 (L1) retrotransposons make up about 15 to 20% of the genomic DNA sequence. The mouse genome contains about a half-million L1 copies, but only 3,000 L1 copies can drive their expansion in the genome with a copy-paste mechanism. In the adult brain, L1 retrotransposons are preferentially expressed in some neural genes. Some L1 copies inserted in these genes induce deletions and replications of large genomic DNA fragments, and this inactivates some neural genes and induces the neural conversion of somatic cells (Upton et al., 2015; Erwin et al., 2016). Recently, Della Valle et al. (2020) reported that L1 reactivation mediated neuronal conversion through a conserved *de novo* insertion site in the expressed gene loci of iDANs. Through RNA-seq and transposase-accessible chromatin sequencing (ATAC-seq), they identified that, near L1 insertion sites, more non-coding RNAs (ncRNAs) are produced. This shows there is a correlation between L1 reactivation and cell lineage conversion (Caiazzo et al., 2011; Della Valle et al., 2020). In the direct conversion of MEF cells to iDANs through overexpression of three specific transcription factors, namely, Nurr1, Ascl1, and Lmx1a, L1 reactivation was confirmed by the production of full-length LINE-1 RNA in iDANs (Caiazzo et al., 2011). At the same time, the L1 copy number variation (CNV) was significantly increased in TH + iDANs. However, other retrotransposable elements, such as active and autonomous intracisternal A-type particle (IAP) elements and non-autonomous SINE B1 and B2 elements, were not induced in iDANs. That study provided evidence for the mechanism of L1 reactivation and CNV increase when mouse embryonic fibroblasts are converted into dopaminergic neurons.

miRna-Mediated Mechanisms to Convert Fibroblasts to Neurons or DA Neurons

miRNAs are important for promoting the conversion of fibroblasts by regulating Wnt signaling and other pathways. Thus, regulating Wnt signaling has promoted the conversion of fibroblasts to mDA neurons *in vitro* (Nouri et al., 2015). Studies have shown that two miRNAs, miR-9/9* and miR-124, can convert fibroblasts into neurons. A further study reported that miR-9* and miR-124 induced the transdifferentiation of mouse fibroblasts to neurons by repressing the BAF53a subunit of the neural-progenitor (np) BAF chromatin-remodeling complex. This means that miR-9/9* and miR-124 (miR-9/9*-124) are involved in regulating neuronal differentiation and miR-9/9*-124 combined with NEUROD2 converted the human fibroblasts into neurons. It also showed that adding transcription factors, Ascl1 and Myt1l, increased the conversion rate and the maturation of the converted neurons, but expression of these transcription factors alone without miR-9/9*-124 was relatively ineffective (Yoo et al., 2011). In addition, without miR-9/9*-124, the same transcription factors hardly induce neuronal conversion. This means that miRNA might initiate neuronal states, and that transcription factors promote the maturation of converted neurons.

Further study showed that co-expression of miR-9/9*-124 with the transcription factors BCL11B, DLX1, DLX2, and Myt1l enriched in the developing striatum, can convert human postnatal and adult fibroblasts into specific neurons analogous to striatal spiny neurons (MSNs) (Victor et al., 2014). Transcriptome analysis of starting fibroblasts and induced neurons showed the loss of fibroblast gene expressions such as S100A4, VIM, and COL13A1, and the gain of a pan-neuronal identity (MAP2, NEFL, SNAP25, and SCN1A) 35 days after the expression of miR-9/9*-124 in fibroblasts. A time-lapse analysis of the transcriptome of cells undergoing a conversion induced by miR-9/9*-124 showed that molecular pathways were potentially

targeted by REST through the transcript regulation of REST (Abernathy et al., 2017).

Systematic analyses of the transcriptome, genome-wide DNA-methylation, and chromatin modification revealed that miR-9/9*-124 can induce extensive modification of the epigenome and activate a neuronal lineage and the reconfiguration of chromatin accessibilities simultaneously. The miR-9/9*-124 were shown to open the genomic loci for multiple subtype-specific genes, including established motor neuron markers. Therefore, it was postulated that specific neuron-enriched transcription factors would cooperate with miR-9/9*-124 to specify a neuron subtype conversion of fibroblasts. To explore how miR-9/9*-124 are involved in controlling REST expression to activate neuronal genes during neuronal reprogramming, it was found that repressing REST-activated chromatin opened regions that contained neuronal genes that encompassed binding sites of REST in the regulatory regions. Moreover, BAF53b was found to be a transcriptional target of REST and EZH2 repression, leading to REST destabilization to induce neuronal conversion. This is a conserved mechanism during neuronal differentiation of neural stem cells and developing mouse brain. This result showed that the activity of miRNAs represses EZH2-REST to promote the neuronal conversion of fibroblasts (Lee et al., 2018).

In a recent study, the miR-34b/c (miR-34b-5p/miR-34c-5p) were found to be involved in regulating the Wnt signaling pathway to increases *in vitro* differentiation of DA neurons significantly (De Gregorio et al., 2018). Thus, miR-34b/c was found to bind the *Wnt1 3'UTR* to reduce *Wnt1* directly in DA-differentiated mouse embryonic stem cells (mESCs). It was clearly shown that co-expression with Ascl1 and NURR1, miR-34b/c significantly increased the transdifferentiation efficiency of fibroblasts to iDANs with upregulated expression of DA markers such as Th, Nurr1, Pitx3, Dmrt5, Foxa2a, and Lmx1a. These iDANs were found to have specific electrophysiological properties as striatum DA neurons. In addition, microarray analysis of the iDANs revealed that five Wnt genes (Wnt1, Wnt5a, Wnt5b, Wnt7a, and Wnt9a) are downregulated in miR-34b/c-induced DA neurons from day 9 and day 14. This further suggests that miR-34b/c induced the transdifferentiation of fibroblasts to DA neurons through Wnt signaling. By transfecting plasmids expressing miR-34b/c and miR-148a-3p with a pmiR-luciferase reporter containing Wnt1 3-UTR, both miR-34b/c and miR-148a-3p could reduce luciferase activity significantly. This effect was repressed after mutation of the predicted binding site for miR-34b/c but not for miR-148a-3p. This suggests that only miR-34b/c effectively binds to its predicted site at 3'-UTR of Wnt1. To validate this result, the MEF cells derived from TH-GFP mice were infected with Ascl1, Nurr1, and miR-34b/c in the presence of CHIR99021, which can inhibit GSK3β to mimic Wnt activation. The result further confirmed that miR-34b/c induced transdifferentiation of fibroblasts to DA neurons by regulating Wnt signaling.

The mechanisms for *in vivo* direct reprogramming to convert glial cells to DA neurons are similar to that for direct conversion of the fibroblast cells to neurons or dopamine neurons *in vitro*. The commonly used cell source for brain repair is the astrocytes for direct reprogramming *in vivo* to generate DA neurons due to their wide distribution throughout the CNS. These mechanisms are mainly involved in the transcription factors, mRNAs, RNA interfere (RNAi) or miRNAs to regulate the specific genes such as for neuronal development and maturation (Rivetti Di Val Cervo et al., 2017; Wang et al., 2021) or to knockdown the specific genes such as the single RNA bing protein (Ptbp1) to directly reprogramming astrocytes to neurons *in vivo* (Zhou et al., 2020). A recent study has also systemically reviewed the progress and mechanisms of direct reprogramming *in vivo* (Qian C. et al., 2020).

CONCLUSION

Direct reprogramming induces somatic cells to convert into functional neurons and dopamine neurons, which has great potential for drug screening and transplantation treatment of neurodegenerative diseases. The directly converted cells do not need to go through the state of pluripotent stem cells, avoiding the formation of tumors after being transplanted to the brain or other organs. Now iNs or iDANs can be easily achieved by forced expression of specific sets of transcription factors, miRNAs, or a combination with chemical compounds to activate or inhibit developmental lineages by regulating the Wnt, Notch, and JAK/STAT signal pathways.

Since the exogenous transcription factor genes may integrate into the host cell genome to induce genomic mutations in the directly reprogrammed cells (Pereira et al., 2019), future direct reprogramming can take advantage of the episomal plasmids to replace the viral vectors to express lineage-specific transcription factors without transgene integration. In addition, the use of RNA, miRNA, proteins, or small-molecule compounds is another safe way to generate clinically applicable neurons or dopamine neurons converted from fibroblasts.

When the induced neurons or dopamine neurons *in vitro* are transplanted to the brains, only a few percentage of these cells can survive for a long term to form synaptic connections with the host cells even though some studies reported that some levels of functional integration of the transplanted cells have been observed in host brains (Kim et al., 2011; Dell'anno et al., 2014). Thus *in vivo* transdifferentiation provides a significant advantage to induce the local glial cells of the brain to convert to the required neurons for treatment of neurodegenerative diseases such as PD or AD. A challenge for *in vivo* direct reprogramming is to know that the converted neurons are derived from local glial cells. One way to resolve this issue is to assess the functional improvement in neurological behavior abnormalities. Most recently, Qian H. et al. (2020) used a chemogenetic approach to improve the chemical-induced motor dysfunction of the mouse model of PD. This provided evidence for restoring neurological function by *in vivo* transdifferentiation. Another approach is to label the converted neuronal cells for *in vivo* tracking genetically (Rivetti Di Val Cervo et al., 2017; Qian H. et al., 2020).

Another problem facing direct reprogramming is the low efficiency of conversion and the poor survival of directly reprogrammed cells after transplantation. With increased understanding of the molecular mechanism and signaling

pathways in the process of direct reprogramming, more efficient direct reprogramming methods will be developed to generate a large scale of induced neurons or dopamine neurons for clinical and research uses. In addition, efficient cell sorting technology will continue to be developed to purify the directly converted cells. In the future, skin fibroblasts will be directly reprogrammed to specific neurons, such as dopamine neurons, that are closer to their natural state, and they will provide sufficient cell sources for the treatment of PD and other neurodegenerative diseases by clinical transplantation.

AUTHOR CONTRIBUTIONS

FH contributed to the design, conceptualization, data collection, formal analysis, methodology, supervision, visualization, and writing the original draft. YL, XZ, JH, and CW contributed to the data collection, preparation of the figures and tables, and writing some of the manuscript. All authors read and approved the final manuscript.

FUNDING

This work was supported by the National Natural Science Foundation of China (NSFC 81571241), Shenzhen Science and Technology Program (Grant No. JCYJ20180305164256295), and the key basic research fund from the Natural Science Foundation of Shandong Province, China (ZR2019ZD39).

ACKNOWLEDGMENTS

We thank Dr. Gangming Zou from the American Journal of Translational Medicine in United States for English proofreading.

REFERENCES

Abernathy, D. G., Kim, W. K., Mccoy, M. J., Lake, A. M., Ouwenga, R., Lee, S. W., et al. (2017). MicroRNAs Induce a Permissive Chromatin Environment that Enables Neuronal Subtype-Specific Reprogramming of Adult Human Fibroblasts. *Cell Stem Cell* 21, 332–348.e9. doi: 10.1016/j.stem.2017.08.002

Ambasudhan, R., Talantova, M., Coleman, R., Yuan, X., Zhu, S., Lipton, S. A., et al. (2011). Direct reprogramming of adult human fibroblasts to functional neurons under defined conditions. *Cell Stem Cell* 9, 113–118. doi: 10.1016/j.stem.2011.07.002

Ang, S. L. (2006). Transcriptional control of midbrain dopaminergic neuron development. *Development* 133, 3499–3506. doi: 10.1242/dev.02501

Arenas, E., Denham, M., and Villaescusa, J. C. (2015). How to make a midbrain dopaminergic neuron. *Development* 142, 1918–1936. doi: 10.1242/dev.097394

Bahmad, H., Hadadeh, O., Chamaa, F., Cheaito, K., Darwish, B., Makkawi, A. K., et al. (2017). Modeling Human Neurological and Neurodegenerative Diseases: from Induced Pluripotent Stem Cells to Neuronal Differentiation and Its Applications in Neurotrauma. *Front. Mol. Neurosci.* 10:50. doi: 10.3389/fnmol.2017.00050

Barker, R. A., and TRANSEURO Consortium (2019). Designing stem-cell-based dopamine cell replacement trials for Parkinson's disease. *Nat. Med.* 25, 1045–1053. doi: 10.1038/s41591-019-0507-2

Caiazzo, M., Dell'anno, M. T., Dvoretskova, E., Lazarevic, D., Taverna, S., Leo, D., et al. (2011). Direct generation of functional dopaminergic neurons from mouse and human fibroblasts. *Nature* 476, 224–227. doi: 10.1038/nature10284

Chanda, S., Ang, C. E., Davila, J., Pak, C., Mall, M., Lee, Q. Y., et al. (2014). Generation of induced neuronal cells by the single reprogramming factor ASCL1. *Stem Cell Rep.* 3, 282–296. doi: 10.1016/j.stemcr.2014.05.020

Chang, J. H., Tsai, P. H., Wang, K. Y., Wei, Y. T., Chiou, S. H., and Mou, C. Y. (2018). Generation of Functional Dopaminergic Neurons from Reprogramming Fibroblasts by Nonviral-based Mesoporous Silica Nanoparticles. *Sci. Rep.* 8:11. doi: 10.1038/s41598-017-18324-8

Chen, Q., Liu, J., Sawada, T., Wei, C., Wu, S., and Han, F. (2020). Possible role of EphA4 and VEGFR2 interactions in neural stem and progenitor cell differentiation. *Exp. Ther. Med.* 19, 1789–1796. doi: 10.3892/etm.2020.8419

Connor, B., Firmin, E., Mccaughey-Chapman, A., Monk, R., Lee, K., Liot, S., et al. (2018). Conversion of adult human fibroblasts into neural precursor cells using chemically modified mRNA. *Heliyon* 4:e00918. doi: 10.1016/j.heliyon.2018.e00918

Cyranoski, D. (2017). Trials of embryonic stem cells to launch in China. *Nature* 54, 15–16. doi: 10.1038/546015a

De Gregorio, R., Pulcrano, S., De Sanctis, C., Volpicelli, F., Guatteo, E., von Oerthel, L., et al. (2018). miR-34b/c Regulates Wnt1 and Enhances Mesencephalic Dopaminergic Neuron Differentiation. *Stem Cell Rep.* 10, 1237–1250. doi: 10.1016/j.stemcr.2018.02.006

Della Valle, F., Thimma, M. P., Caiazzo, M., Pulcrano, S., Celii, M., Adroub, S. A., et al. (2020). Transdifferentiation of Mouse Embryonic Fibroblasts into Dopaminergic Neurons Reactivates LINE-1 Repetitive Elements. *Stem Cell Rep.* 14, 60–74. doi: 10.1016/j.stemcr.2019.12.002

Dell'anno, M. T., Caiazzo, M., Leo, D., Dvoretskova, E., Medrihan, L., Colasante, G., et al. (2014). Remote control of induced dopaminergic neurons in parkinsonian rats. *J. Clin. Invest.* 124, 3215–3229. doi: 10.1172/jci74664

Ernst, J., and Kellis, M. (2012). Chromhmm: automating chromatin-state discovery and characterization. *Nat. Methods* 9, 215–216. doi: 10.1038/nmeth.1906

Erwin, J. A., Paquola, A. C., Singer, T., Gallina, I., Novotny, M., Quayle, C., et al. (2016). L1-associated genomic regions are deleted in somatic cells of the healthy human brain. *Nat. Neurosci.* 19, 1583–1591. doi: 10.1038/nn.4388

Fong, C. Y., Gauthaman, K., and Bongso, A. (2010). Teratomas from pluripotent stem cells: a clinical hurdle. *J. Cell. Biochem.* 111, 769–781. doi: 10.1002/jcb.22775

Freed, C. R., Greene, P. E., Breeze, R. E., Tsai, W. Y., DuMouchel, W., Kao, R., et al. (2001). Transplantation of embryonic dopamine neurons for severe Parkinson's disease. *N. Engl. J. Med.* 344, 710–719. doi: 10.1056/nejm200103083441002

Gascon, S., Murenu, E., Masserdotti, G., Ortega, F., Russo, G. L., Petrik, D., et al. (2016). Identification and Successful Negotiation of a Metabolic Checkpoint in Direct Neuronal Reprogramming. *Cell Stem Cell* 18, 396–409. doi: 10.1016/j.stem.2015.12.003

Graf, T. (2011). Historical origins of transdifferentiation and reprogramming. *Cell Stem Cell* 9, 504–516. doi: 10.1016/j.stem.2011.11.012

Guo, Z., Zhang, L., Wu, Z., Chen, Y., Wang, F., and Chen, G. (2014). In vivo direct reprogramming of reactive glial cells into functional neurons after brain injury and in an Alzheimer's disease model. *Cell Stem Cell* 14, 188–202. doi: 10.1016/j.stem.2013.12.001

Hallett, P. J., Deleidi, M., Astradsson, A., Smith, G. A., Cooper, O., Osborn, T. M., et al. (2015). Successful function of autologous iPSC-derived dopamine neurons following transplantation in a non-human primate model of Parkinson's disease. *Cell Stem Cell* 16, 269–274. doi: 10.1016/j.stem.2015.01.018

Han, F., Baremberg, D., Gao, J., Duan, J., Lu, X., Zhang, N., et al. (2015a). Development of stem cell-based therapy for Parkinson's disease. *Transl. Neurodegener.* 4:16.

Han, F., Liu, C., Huang, J., Chen, J., Wei, C., Geng, X., et al. (2019). The application of patient-derived induced pluripotent stem cells for modeling and treatment of Alzheimer's disease. *Brain Sci. Adv.* 5, 21–40. doi: 10.1177/2096595819896178

Han, F., Wang, W., Chen, B., Chen, C., Li, S., Lu, X., et al. (2015b). Human induced pluripotent stem cell-derived neurons improve motor asymmetry in a 6-hydroxydopamine-induced rat model of Parkinson's disease. *Cytotherapy* 17, 665–679. doi: 10.1016/j.jcyt.2015.02.001

Han, Y. C., Lim, Y., Duffieldl, M. D., Li, H., Liu, J., Abdul Manaph, N. P., et al. (2016). Direct Reprogramming of Mouse Fibroblasts to Neural Stem Cells by Small Molecules. *Stem Cells Int.* 2016:4304916. doi: 10.1155/2016/4304916

He, M., Zhang, H., Li, Y., Tian, C., Tang, B., Huang, Y., et al. (2019). Direct and selective lineage conversion of human fibroblasts to dopaminergic precursors. *Neurosci. Lett.* 699, 16–23. doi: 10.1016/j.neulet.2019.01.033

Herdy, J., Schafer, S., Kim, Y., Ansari, Z., Zangwill, D., Ku, M., et al. (2019). Chemical modulation of transcriptionally enriched signaling pathways to optimize the conversion of fibroblasts into neurons. *Elife* 8:e41356. doi: 10.7554/eLife.41356.036

Hou, S., and Lu, P. (2016). Direct reprogramming of somatic cells into neural stem cells or neurons for neurological disorders. *Neural Regen. Res.* 11, 28–31. doi: 10.4103/1673-5374.169602

Hu, W., Qiu, B., Guan, W., Wang, M., Li, W., Gao, L., et al. (2015). Direct Conversion of Normal and Alzheimer's Disease Human Fibroblasts into Neuronal Cells by Small Molecules. *Cell Stem Cell* 17, 204–212. doi: 10.1016/j.stem.2015.07.006

Jiang, H., Xu, Z., Zhong, P., Ren, Y., Liang, G., Schilling, H. A., et al. (2015). Cell cycle and p53 gate the direct conversion of human fibroblasts to dopaminergic neurons. *Nat. Commun.* 6:10100. doi: 10.1038/ncomms10100

Kikuchi, T., Morizane, A., Doi, D., Magotani, H., Onoe, H., Hayashi, T., et al. (2017). Human iPS cell-derived dopaminergic neurons function in a primate Parkinson's disease model. *Nature* 548, 592–596. doi: 10.1038/nature23664

Kim, H. J., Mcmillan, E., Han, F., and Svendsen, C. N. (2009). Regionally specified human neural progenitor cells derived from the mesencephalon and forebrain undergo increased neurogenesis following overexpression of ASCL1. *Stem Cells* 27, 390–398. doi: 10.1634/stemcells.2007-1047

Kim, J., Su, S. C., Wang, H., Cheng, A. W., Cassady, J. P., Lodato, M. A., et al. (2011). Functional integration of dopaminergic neurons directly converted from mouse fibroblasts. *Cell Stem Cell* 9, 413–419. doi: 10.1016/j.stem.2011.09.011

Ladewig, J., Mertens, J., Kesavan, J., Doerr, J., Poppe, D., Glaue, F., et al. (2012). Small molecules enable highly efficient neuronal conversion of human fibroblasts. *Nat. Methods* 9, 575–578. doi: 10.1038/nmeth.1972

Lee, S. W., Oh, Y. M., Lu, Y. L., Kim, W. K., and Yoo, A. S. (2018). MicroRNAs Overcome Cell Fate Barrier by Reducing EZH2-Controlled Rest Stability during Neuronal Conversion of Human Adult Fibroblasts. *Dev. Cell* 46, 73–84.e7. doi: 10.1016/j.devcel.2018.06.007

Li, J. Y., Englund, E., Holton, J. L., Soulet, D., Hagell, P., Lees, A. J., et al. (2008). Lewy bodies in grafted neurons in subjects with Parkinson's disease suggest host-to-graft disease propagation. *Nat. Med.* 14, 501–503. doi: 10.1038/nm1746

Li, S., Shi, Y., Yao, X., Wang, X., Shen, L., Rao, Z., et al. (2019). Conversion of astrocytes and fibroblasts into functional noradrenergic neurons. *Cell Rep.* 28, 682–697. doi: 10.1016/j.CellRep.2019.06.042

Li, W., Englund, E., Widner, H., Mattsson, B., van Westen, D., Lätt, J., et al. (2016). Extensive graft-derived dopaminergic innervation is maintained 24 years after transplantation in the degenerating parkinsonian brain. *Proc. Natl. Acad. Sci. U. S. A.* 113, 6544–6549. doi: 10.1073/pnas.1605245113

Li, X., Liu, D., Ma, Y., Du, X., Jing, J., Wang, L., et al. (2017). Direct Reprogramming of Fibroblasts via a Chemically Induced XEN-like State. *Cell Stem Cell* 21, 264–273.e7. doi: 10.1016/j.stem.2017.05.019

Li, X., Zuo, X., Jing, J., Ma, Y., Wang, J., Liu, D., et al. (2015). Small-Molecule-Driven Direct Reprogramming of Mouse Fibroblasts into Functional Neurons. *Cell Stem Cell* 17, 195–203. doi: 10.1016/j.stem.2015.06.003

Lindvall, O., Brundin, P., Widner, H., Rehncrona, S., Gustavii, B., Frackowiak, R., et al. (1990). Grafts of fetal dopamine neurons survive and improve motor function in Parkinson's disease. *Science* 247, 574–577. doi: 10.1126/science.2105529

Liu, J., and Verma, P. J. (2015). Synthetic mRNA Reprogramming of Human Fibroblast Cells. *Methods Mol. Biol.* 1330, 17–28. doi: 10.1007/978-1-4939-2848-4_2

Liu, X., Li, F., Stubblefield, E. A., Blanchard, B., Richards, T. L., Larson, G. A., et al. (2012). Direct reprogramming of human fibroblasts into dopaminergic neuron-like cells. *Cell Res.* 22, 321–332. doi: 10.1038/cr.2011.181

Ma, C. (2019). Progress in research into spinal cord injury repair: tissue engineering scaffolds and cell transdifferentiation. *J. Neurorestoratol.* 07, 196–206. doi: 10.26599/jnr.2019.9040024

Ma, P. C. M., Rould, M. A., Weintraub, H., and Pabo, C. O. (1994). Crystal structure of MyoD bHLH domain-DNA complex: perspectives on DNA recognition and implications for transcriptional activation. *Cell* 77:451. doi: 10.1016/0092-8674(94)90159-7

Masserdotti, G., Gillotin, S., Sutor, B., Drechsel, D., Irmler, M., Jørgensen, H. F., et al. (2015). Transcriptional Mechanisms of Proneural Factors and REST in Regulating Neuronal Reprogramming of Astrocytes. *Cell Stem Cell* 17, 74–88. doi: 10.1016/j.stem.2015.05.014

Mirakhori, F., Zeynali, B., Rassouli, H., Salekdeh, G. H., and Baharvand, H. (2015). Direct conversion of human fibroblasts into dopaminergic neural progenitor-like cells using TAT-mediated protein transduction of recombinant factors. *Biochem. Biophys. Res. Commun.* 459, 655–661. doi: 10.1016/j.bbrc.2015.02.166

Mitchell, R., Szabo, E., Shapovalova, Z., Aslostovar, L., Makondo, K., and Bhatia, M. (2014). Molecular evidence for OCT4-induced plasticity in adult human fibroblasts required for direct cell fate conversion to lineage specific progenitors. *Stem Cells* 32, 2178–2187. doi: 10.1002/stem.1721

Miura, K., Okada, Y., Aoi, T., Okada, A., Takahashi, K., Okita, K., et al. (2009). Variation in the safety of induced pluripotent stem cell lines. *Nat. Biotechnol.* 27, 743–745. doi: 10.1038/nbt.1554

Nouri, N., Patel, M. J., Joksimovic, M., Poulin, J. F., Anderegg, A., Taketo, M. M., et al. (2015). Excessive Wnt/beta-catenin signaling promotes midbrain floor plate neurogenesis, but results in vacillating dopamine progenitors. *Mol. Cell Neurosci.* 68, 131–142. doi: 10.1016/j.mcn.2015.07.002

Oh, S. I., Park, H. S., Hwang, I., Park, H.-Y., Choi, K.-A., Jeong, H., et al. (2014). Efficient reprogramming of mouse fibroblasts to neuronal cells including dopaminergic neurons. *ScientificWorldJournal* 2014:957548. doi: 10.1155/2014/957548

Pereira, M., Birtele, M., and Rylander Ottosson, D. (2019). Direct reprogramming into interneurons: potential for brain repair. *Cell Mol. Life Sci.* 76, 3953–3967. doi: 10.1007/s00018-019-03193-3

Pereira, M., Pfisterer, U., Rylander, D., Torper, O., Lau, S., Lundblad, M., et al. (2014). Highly efficient generation of induced neurons from human fibroblasts that survive transplantation into the adult rat brain. *Sci. Rep.* 4:6330. doi: 10.1038/srep06330

Pfisterer, U., Kirkeby, A., Torper, O., Wood, J., Nelander, J., Dufour, A., et al. (2011). Direct conversion of human fibroblasts to dopaminergic neurons. *Proc. Natl. Acad. Sci. U. S. A.* 108, 10343–10348. doi: 10.1073/pnas.1105135108

Playne, R., Jones, K., and Connor, B. (2018). Generation of dopamine neuronal-like cells from induced neural precursors derived from adult human cells by non-viral expression of lineage factors. *J. Stem Cells Regen. Med.* 14, 34–44. doi: 10.46582/jsrm.1401005

Pu, J., Gao, T., Zheng, R., Fang, Y., Ruan, Y., Jin, C., et al. (2020). Parkin mutation decreases neurite complexity and maturation in neurons derived from human fibroblasts. *Brain Res. Bull.* 159, 9–15. doi: 10.1016/j.brainresbull.2020.03.006

Qian, C., Dong, B., Wang, X. Y., and Zhou, F. Q. (2020). In vivo glial trans-differentiation for neuronal replacement and functional recovery in central nervous system. *FEBS J.* 288, 4773–4785. doi: 10.1111/febs.15681

Qian, H., Kang, X., Hu, J., Zhang, D., Liang, Z., Meng, F., et al. (2020). Reversing a model of Parkinson's disease with in situ converted nigral neurons. *Nature* 582, 550–556. doi: 10.1038/s41586-020-2388-4

Qin, H., Zhao, A. D., Sun, M. L., Ma, K., and Fu, X. B. (2020). Direct conversion of human fibroblasts into dopaminergic neuron-like cells using small molecules and protein factors. *Mil. Med. Res.* 7:52. doi: 10.1186/s40779-020-00284-2

Rivetti Di Val Cervo, P., Romanov, R. A., Spigolon, G., Masini, D., Martín-Montañez, E., Toledo, E. M., et al. (2017). Induction of functional dopamine neurons from human astrocytes in vitro and mouse astrocytes in a Parkinson's disease model. *Nat. Biotechnol.* 35, 444–452. doi: 10.1038/nbt.3835

Ryu, J., Hwang, N. S., Park, H. H., and Park, T. H. (2020). Protein-based direct reprogramming of fibroblasts to neuronal cells using 30Kc19 protein and transcription factor Ascl1. *Int. J. Biochem. Cell Biol.* 121:105717. doi: 10.1016/j.biocel.2020.105717

Studer, L. (2017). Strategies for bringing stem cell-derived dopamine neurons to the clinic-The NYSTEM trial. *Prog. Brain Res.* 230, 191–212. doi: 10.1016/bs.pbr.2017.02.008

Takahashi, J. (2017). Strategies for bringing stem cell-derived dopamine neurons to the clinic: the Kyoto trial. *Prog. Brain Res.* 230, 213–226. doi: 10.1016/bs.pbr.2016.11.004

Takahashi, K., and Yamanaka, S. (2006). Induction of pluripotent stem cells from mouse embryonic and adult fibroblast cultures by defined factors. *Cell* 126, 663–676. doi: 10.1016/j.cell.2006.07.024

Tian, C., Li, Y., Huang, Y., Wang, Y., Chen, D., Liu, J., et al. (2015). Selective Generation of Dopaminergic Precursors from Mouse Fibroblasts by Direct Lineage Conversion. *Sci. Rep.* 5:12622. doi: 10.1038/srep12622

Trapnell, C., Cacchiarelli, D., Grimsby, J., Pokharel, P., Li, S., Morse, M., et al. (2014). The dynamics and regulators of cell fate decisions are revealed by pseudotemporal ordering of single cells. *Nat. Biotechnol.* 32, 381–386. doi: 10.1038/nbt.2859

Treutlein, B., Lee, Q. Y., Camp, J. G., Mall, M., Koh, W., Mohammad Shariati, S. A., et al. (2016). Dissecting direct reprogramming from fibroblast to neuron using single-cell RNA-seq. *Nature* 534, 391–395. doi: 10.1038/nature18323

Upton, K. R., Gerhardt, D. J., Jesuadian, J. S., Richardson, S. R., Sánchez-Luque, F. J., Bodea, G. O., et al. (2015). Ubiquitous L1 mosaicism in hippocampal neurons. *Cell* 161, 228–239. doi: 10.1016/j.cell.2015.03.026

Van Heesbeen, H. J., Mesman, S., Veenvliet, J. V., and Smidt, M. P. (2013). Epigenetic mechanisms in the development and maintenance of dopaminergic neurons. *Development* 140, 1159–1169. doi: 10.1242/dev.089359

Veenvliet, J. V., and Smidt, M. P. (2014). Molecular mechanisms of dopaminergic subset specification: fundamental aspects and clinical perspectives. *Cell Mol. Life Sci.* 71, 4703–4727. doi: 10.1007/s00018-014-1681-5

Victor, M. B., Richner, M., Hermanstyne, T. O., Ransdell, J. L., Sobieski, C., Deng, P. Y., et al. (2014). Generation of human striatal neurons by microRNA-dependent direct conversion of fibroblasts. *Neuron* 84, 311–323. doi: 10.1016/j.neuron.2014.10.016

Vierbuchen, T., Ostermeier, A., Pang, Z. P., Kokubu, Y., Südhof, T. C., and Wernig, M. (2010). Direct conversion of fibroblasts to functional neurons by defined factors. *Nature* 463, 1035–1041. doi: 10.1038/nature08797

Waldthaler, J., and Timmermann, L. (2019). [Update on diagnostics and therapy of idiopathic Parkinson's disease]. *Fortschr. Neurol. Psychiatr.* 87, 445–461. doi: 10.1055/a-0952-8075

Wang, F., Cheng, L., and Zhang, X. (2021). Reprogramming Glial Cells into Functional Neurons for Neuro-regeneration: challenges and Promise. *Neurosci. Bull.* doi: 10.1007/s12264-021-00751-3 [Online ahead of print]

Wang, Y., Yang, H., Yang, Q., Yang, J., Wang, H., Xu, H., et al. (2016). Chemical conversion of mouse fibroblasts into functional dopaminergic neurons. *Exp. Cell Res.* 347, 283–292. doi: 10.1016/j.yexcr.2016.07.026

Wapinski, O. L., Vierbuchen, T., Qu, K., Lee, Q. Y., Chanda, S., Fuentes, D. R., et al. (2013). Hierarchical mechanisms for direct reprogramming of fibroblasts to neurons. *Cell* 155, 621–635. doi: 10.1016/j.cell.2013.09.028

Wendt, M. K., Balanis, N., Carlin, C. R., and Schiemann, W. P. (2014). STAT3 and epithelial-mesenchymal transitions in carcinomas. *JAKSTAT* 3:e28975. doi: 10.4161/jkst.28975

Wu, G., Ruben, M. D., Lee, Y., Jiajia, Li, Hughes, M. E., John, B., et al. (2020). Genome-wide studies of time of day in the brain: design and analysis. *Brain Sci. Adv.* 6, 92–105. doi: 10.26599/BSA.2020.9050005

Xie, W., Schultz, M. D., Lister, R., Hou, Z., Rajagopal, N., Ray, P., et al. (2013). Epigenomic analysis of multilineage differentiation of human embryonic stem cells. *Cell* 153, 1134–1148. doi: 10.1016/j.cell.2013.04.022

Xu, J. T., Qian, Y., Wang, W., Chen, X. X., Li, Y., Li, Y., et al. (2020). Effect of stromal cell-derived factor-1/CXCR4 axis in neural stem cell transplantation for Parkinson's disease. *Neural Regen. Res.* 15, 112–119. doi: 10.4103/1673-5374.264470

Yang, Y., Chen, R., Wu, X., Zhao, Y., Fan, Y., Xiao, Z., et al. (2019). Rapid and Efficient Conversion of Human Fibroblasts into Functional Neurons by Small Molecules. *Stem Cell Rep.* 13, 862–876. doi: 10.1016/j.stemcr.2019.09.007

Yoo, A. S., Sun, A. X., Li, L., Shcheglovitov, A., Portmann, T., Li, Y., et al. (2011). MicroRNA-mediated conversion of human fibroblasts to neurons. *Nature* 476, 228–231. doi: 10.1038/nature10323

Yoo, J., Lee, E., Kim, H. Y., Youn, D.-H., Jung, J., Kim, H., et al. (2017). Electromagnetized gold nanoparticles mediate direct lineage reprogramming into induced dopamine neurons in vivo for Parkinson's disease therapy. *Nat. Nanotechnol.* 12, 1006–1014. doi: 10.1038/nnano.2017.133

Yoo, J., Noh, M., Kim, H., Jeon, N. L., Kim, B. S., and Kim, J. (2015). Nanogrooved substrate promotes direct lineage reprogramming of fibroblasts to functional induced dopaminergic neurons. *Biomaterials* 45, 36–45. doi: 10.1016/j.biomaterials.2014.12.049

Yu, J., Vodyanik, M. A., Smuga-Otto, K., Antosiewicz-Bourget, J., Frane, J. L., Tian, S., et al. (2007). Induced pluripotent stem cell lines derived from human somatic cells. *Science* 318, 1917–1920. doi: 10.1126/science.1151526

Zhang, N., Lu, X., Wu, S., Li, X., Duan, J., Chen, C., et al. (2018). Intrastriatal transplantation of stem cells from human exfoliated deciduous teeth reduces motor defects in Parkinsonian rats. *Cytotherapy* 20, 670–686. doi: 10.1016/j.jcyt.2018.02.371

Zhou, H., Su, J., Hu, X., Zhou, C., Li, H., Chen, Z., et al. (2020). Glia-to-Neuron Conversion by CRISPR-CasRx Alleviates Symptoms of Neurological Disease in Mice. *Cell* 181, 590–603.e16. doi: 10.1016/j.cell.2020.03.024

Conflict of Interest: The authors declare that the research was conducted in the absence of any commercial or financial relationships that could be construed as a potential conflict of interest.

Publisher's Note: All claims expressed in this article are solely those of the authors and do not necessarily represent those of their affiliated organizations, or those of the publisher, the editors and the reviewers. Any product that may be evaluated in this article, or claim that may be made by its manufacturer, is not guaranteed or endorsed by the publisher.

frontiers in Aging Neuroscience

ORIGINAL RESEARCH
published: 26 November 2021
doi: 10.3389/fnagi.2021.777404

Impaired Cognitive Function and Hippocampal Changes Following Chronic Diazepam Treatment in Middle-Aged Mice

*Tomonori Furukawa[1], Yoshikazu Nikaido[2,3], Shuji Shimoyama[1,4], Nozomu Masuyama[1], Ayaka Notoya[1] and Shinya Ueno[1,4]**

[1] Department of Neurophysiology, Hirosaki University Graduate School of Medicine, Hirosaki, Japan, [2] Department of Frailty Research and Prevention, Hirosaki University Graduate School of Medicine, Hirosaki, Japan, [3] Department of Anesthesiology, Hirosaki University Graduate School of Medicine, Hirosaki, Japan, [4] Research Center for Child Mental Development, Hirosaki University Graduate School of Medicine, Hirosaki, Japan

Background: Gamma-aminobutyric acid (GABA) type A receptors are positively allosterically modulated by benzodiazepine binding, leading to a potentiated response to GABA. Diazepam (DZP, a benzodiazepine) is widely prescribed for anxiety, epileptic discharge, and insomnia, and is also used as a muscle relaxant and anti-convulsant. However, some adverse effects – such as tolerance, dependence, withdrawal effects, and impairments in cognition and learning – are elicited by the long-term use of DZP. Clinical studies have reported that chronic DZP treatment increases the risk of dementia in older adults. Furthermore, several studies have reported that chronic DZP administration may affect neuronal activity in the hippocampus, dendritic spine structure, and cognitive performance. However, the effects of chronic DZP administration on cognitive function in aged mice is not yet completely understood.

Methods: A behavioral test, immunohistochemical analysis of neurogenic and apoptotic markers, dendritic spine density analysis, and long-term potentiation (LTP) assay of the hippocampal CA1 and CA3 were performed in both young (8 weeks old) and middle-aged (12 months old) mice to investigate the effects of chronic DZP administration on cognitive function. The chronic intraperitoneal administration of DZP was performed by implanting an osmotic minipump. To assess spatial learning and memory ability, the Morris water maze test was performed. Dendritic spines were visualized using Lucifer yellow injection into the soma of hippocampal neurons, and spine density was analyzed. Moreover, the effects of exercise on DZP-induced changes in spine density and LTP in the hippocampus were assessed.

Results: Learning performance was impaired by chronic DZP administration in middle-aged mice but not in young mice. LTP was attenuated by DZP administration in the CA1 of young mice and the CA3 of middle-aged mice. The spine density of hippocampal neurons was decreased by chronic DZP administration in the CA1 of both young and middle-aged mice as well as in the CA3 of middle-aged mice. Neither neurogenesis nor apoptosis in the hippocampus was affected by chronic DZP administration.

OPEN ACCESS

Edited by:
Benoit Laurent, Université de Sherbrooke, Canada

Reviewed by:
Liang Zhang, University of Toronto, Canada
Karl J. L. Fernandes, Université de Sherbrooke, Canada

***Correspondence:**
Shinya Ueno
shinyau@hirosaki-u.ac.jp

Received: *15 September 2021*
Accepted: *04 November 2021*
Published: *26 November 2021*

Citation:
Furukawa T, Nikaido Y, Shimoyama S, Masuyama N, Notoya A and Ueno S (2021) Impaired Cognitive Function and Hippocampal Changes Following Chronic Diazepam Treatment in Middle-Aged Mice. Front. Aging Neurosci. 13:777404. doi: 10.3389/fnagi.2021.777404

Conclusion: The results of this study suggest that the effects of chronic DZP are different between young and middle-aged mice. The chronic DZP-induced memory retrieval performance impairment in middle-aged mice can likely be attributed to decreased LTP and dendritic spine density in hippocampal neurons in the CA3. Notably, prophylactic exercise suppressed the adverse effects of chronic DZP on LTP and spine maintenance in middle-aged mice.

Keywords: benzodiazepine, chronic diazepam, middle-aged, cognitive function, exercise, LTP (long-term potentiation), spine

INTRODUCTION

Benzodiazepines (BZDs) are positive allosteric modulators of gamma-aminobutyric acid type A receptors (GABAA-R) and potentiate GABAA-R activities, which results in the suppression of neural activity in the brain and spinal cord. Because this effect reduces anxiety, seizures, convulsions, muscle tone, and insomnia, BZDs have been widely prescribed as a medicine with high efficacy and low toxicity. However, the long-term use of BZDs is limited because of adverse effects such as tolerance, dependence, and withdrawal effects (Lader, 1991; Michelini et al., 1996; O'Brien, 2005). Additionally, it has been reported that long-term BZD administration induces cognitive decline in older adults, which provides evidence for another type of toxicity (Paterniti et al., 2002; Picton et al., 2018; Liu et al., 2020). Moreover, some clinical studies have reported that long-term BZD exposure increases the risk of incident Alzheimer's disease in older adults (Yaffe and Boustani, 2014; Rosenberg, 2015). However, although guidelines generally recommend that BZDs are limited to short-term use, long-term use still often occurs.

The chronic administration of diazepam (DZP) or other BZDs elicits alterations at the molecular level, such as the downregulation of GABAA-R subunit gene expression (Pratt et al., 1998; Foitzick et al., 2020), internalization of GABAA-R (Ali and Olsen, 2001; Lorenz-Guertin et al., 2019), expression of glutamate receptor subunit genes (Allison and Pratt, 2003; Van Sickle et al., 2004), and expression of proteins associated with synaptic plasticity in the hippocampus (Monti et al., 2010, 2012). These findings are considered a probable mechanism for the tolerance, dependence, and withdrawal effects of BZDs. Additionally, structural changes involving decreased dendritic spine density have been described in the cortical pyramidal cells of chronic DZP-administered mice (Curto et al., 2016). Although the effects of BZDs have been extensively studied (del Cerro et al., 1992; McNamara et al., 1993; Joksimovic et al., 2013), the precise vulnerability of older adults to chronic BZD-induced cognitive decline is not yet fully understood.

In the aging process of mammals, defects in synaptic transmission and plasticity occur in different brain regions that are associated with cognitive function (Foster and Norris, 1997; Barnes, 2003; Disterhoft et al., 2004). The cognitive function involved in learning and memory is affected by several factors, such as neurogenesis, synaptic plasticity, and dendritic spine density (Drapeau et al., 2003; Bruel-Jungerman et al., 2005; Walker and Herskowitz, 2020); these factors decline with aging. For example, in aged rodents, the levels of neurogenesis are lower than in younger rodents (Kuhn et al., 1996; Kempermann et al., 1998; McDonald and Wojtowicz, 2005). In addition, aging-induced attenuation of hippocampal long-term potentiation (LTP) and dendritic spine density has also been observed (Nunzi et al., 1987; Arias-Cavieres et al., 2017). However, the effects of chronic BZD administration on such age-related changes remain unknown.

It has been reported that regular exercise prevents stress-induced neurotoxic effects such as dendritic retraction, spine loss in the hippocampus, and memory consolidation (Leem et al., 2019). In aged animals, exercise enhances brain health and cognitive performance (Larson et al., 2006; Ahlskog et al., 2011), and longitudinal studies have suggested that exercise enhances cognitive function in older adults (Kramer et al., 1999; Laurin et al., 2001; Barnes et al., 2003). In addition, it has been reported that exercise increases synaptic plasticity and LTP (van Praag et al., 1999), reverses dendritic spine loss (Toy et al., 2014), enhances hippocampal neurogenesis (van Praag et al., 2005), and upregulates brain-derived neurotrophic factor (BDNF) expression (Garza et al., 2004). These findings raise the possibility that exercise may have a preventive effect on chronic BZD-induced cognitive decline.

The present study was designed to investigate whether chronic DZP administration induces cognitive decline by modulating synaptic function and neurogenesis in the hippocampus. To examine the specific vulnerability of cognitive function in older adults to chronic DZP administration, both young and middle-aged mice were included. Furthermore, we investigated whether exercise has a protective effect in the hippocampus against the adverse consequences of chronic DZP administration.

MATERIALS AND METHODS

Animals

Adult male C57BL/6J mice were used in this study. Eight-week-old mice were studied as the young group, while 12-month-old mice were used for the middle-aged group. Animals were group housed at 24 ± 2°C under a 12-h light/dark cycle (lights on at 8:00 a.m.), and food and water were available *ad libitum*. All experiments were performed in accordance with the guidelines for animal research issued by the Physiological Society of Japan and the Hirosaki University School of Medicine (approval number M12007), and all efforts were made to minimize the number of animals used and their suffering.

Chronic Administration of Diazepam

Diazepam was chronically administered using ALZET osmotic pumps (Model 2004, 0.25 μL/h, 28-day duration; DURECT Corporation, Cupertino, CA, United States). Under isoflurane anesthesia, the ALZET osmotic pumps filled with either DZP or vehicle were intraperitoneally implanted. DZP was dissolved in 35% dimethyl sulfoxide (DMSO), 55% polyethylene glycol 400 (PEG 400), and 10% alcohol (70% volume/volume) (Vinkers et al., 2012). DZP concentrations were adjusted to deliver 5 mg/kg/day (Allison and Pratt, 2006).

Morris Water Maze

Spatial memory was assessed using the Morris water maze (MWM) task in a circular pool (diameter: 95 cm, depth: 30 cm) filled with water at 23 ± 2°C (Bromley-Brits et al., 2011). During each trial, swimming trajectories of the mice were recorded using the CaptureStar video recording system (CleverSys Inc., Reston, VA, United States). An invisible escape platform (diameter, 10 cm) was placed 1 cm below the water surface. The visible platform task (60 s/trial × 5) was conducted using the flagged platform on Day 10. Mice that did not swim or reach the platform throughout this task were excluded for the following task. From days 11 to 14, the animals were then subjected to the hidden platform task (60 s/trial × 5/day × 4 days) to assess spatial acquisition. The latency to find the platform (escape latency, s), time spent swimming in the quadrant with the platform (target quadrant), and total swimming path length (m) were quantified in each trial using TopScan behavioral analysis software (CleverSys Inc.). On days 15 and 30, a probe test (60 s/test) was performed to estimate short- and long-term spatial memory formation. Escape latency and the percentage time spent in the target quadrant were analyzed. In this study, to define the duration of chronic DZP administration, the mice which was used in MWM were not used in other experiments.

Histology and Immunohistochemistry

Neurogenesis and apoptosis in the hippocampus were studied histologically. The mice (N = 5/group) were transcardially perfused with 4% paraformaldehyde in 0.1 M phosphate buffer (PB), and the brains were then removed and postfixed in the same solution for 48 h. After postfixation, the brains were transferred to 20% sucrose in PB for 3 days. Tissue was cut coronally with a cryostat into 30 μm thick sections and rinsed in phosphate-buffered saline (PBS). To analyze neurogenesis, neurogenic differentiation factor 1 (NeuroD1; a marker of early neuronal differentiation) was stained immunohistochemically (Gao et al., 2009). Briefly, sections were rinsed in PBS-T buffer (0.1 M PBS, 1% Triton X-100) and incubated for 18 h at 4°C with antibodies against NeuroD1 (1:200, ab213725, monoclonal rabbit IgG; Abcam, Cambridge, United Kingdom). After rinsing in PBS, sections were incubated for 1 h with secondary antibodies against rabbit IgG (1:250, anti-rabbit biotinylated BA1000; Vector Laboratories, Burlingame, CA, United States). Visualization was performed using DyLight 488 streptavidin (1:500, SA-5488; Vector Laboratories). Primary and secondary antibodies were diluted in PBS containing 5% normal goat serum albumin and 0.1% Triton X-100. Apoptotic cell death was qualified by terminal deoxynucleotidyl transferase dUTP nick end labeling (TUNEL) staining using an *in situ* cell death detection kit (Sigma-Aldrich, San Diego, CA, United States) as per the manufacturer's instructions. As a positive control, PBS-T-rinsed sections were incubated with DNase I (10 U/mL: Sigma-Aldrich) in PBS for 60 min at 37°C. After immunohistochemical or TUNEL staining, sections were stained with 4′,6-diamidino-2-phenylindole (DAPI), mounted on slides, coverslipped, and observed under a microscope (BZX-700; Keyence, Osaka, Japan). The numbers of stained cells in the hippocampus were counted using ImageJ software (National Institutes of Health, Bethesda, MD, United States) and presented as the density. The area in which positive cells were counted was also measured using ImageJ software.

Electrophysiology

Mice (sedentary groups: N = 6 per group, exercise groups: N = 5 per group) were deeply anesthetized before their brains were rapidly removed and placed in cold (4°C), oxygenated, modified cutting artificial cerebrospinal fluid (ACSF) containing (in mM): 92 NaCl, 2.5 KCl, 1.2 NaH_2PO_4, 10.0 $MgSO_4$, 2.0 $CaCl_2$, 30.0 $NaHCO_3$, 5.0 sodium ascorbate, 2.0 thiourea, 3.0 sodium pyruvate, 20.0 4-(2-hydroxyethyl)-1-piperazineethanesulfonic acid (HEPES), and 25.0 glucose. Transverse 350 μm sections that included the hippocampus were cut using a microslicer (Vibratome 3000; Vibratome, St Louis, MO, United States). Sections were incubated for 12 min in choline chloride-based recovery ACSF containing (in mM): 92 ChCl, 2.5 KCl, 1.2 NaH_2PO_4, 10.0 $MgSO_4$, 2.0 $CaCl_2$, 30.0 $NaHCO_3$, 5.0 sodium ascorbate, 2.0 thiourea, 3.0 sodium pyruvate, 20.0 HEPES, and 25.0 glucose. After the incubation in recovery ACSF at 32°C, sections were maintained in recording ACSF containing (in mM): 126 NaCl, 2.5 KCl, 1.25 NaH_2PO_4, 1.2 $MgSO_4$, 2.0 $CaCl_2$, 26.0 $NaHCO_3$, and 20.0 glucose. All solutions used in the experiment were gassed with 95% O_2/5% CO_2 prior to use. Next, individual sections were transferred to a chamber of the recording system (MED Probe; Alpha MED Scientific, Osaka, Japan), perfused with recording ACSF (2 mL/min), and maintained at 30°C. The field excitatory postsynaptic potentials (fEPSPs) of the CA1 or CA3 region of the hippocampus were recorded using a multi-electrode array system (MED64; Alpha MED Scientific). The fEPSPs were evoked (at 0.05 Hz) using stimulation strengths that were sufficient to elicit fEPSPs that were approximately 30% of the maximal fEPSP slope (10–90%). LTP was induced at 15 min of recording using a theta burst stimulation (TBS) paradigm. Offline analysis was performed using Mobius software (Alpha MED Scientific). LTP magnitude was measured as a percentage of the baseline fEPSP slope during the 15-min period just prior to TBS.

Exercise Protocol

In the current study, forced running wheel (FRW) exercise was used. Before the chronic DZP administration, exercise was performed using a motor-driven running wheel (FWS-1505; Melquest Ltd., Toyama, Japan) for 20–50 min/day, 5 days/week for 12 weeks. As the FWS-1505 is programmable motorized wheel to control wheel speed, running time, and acceleration

speed, the amount of exercise was equal for all exercise group mice. During the first week, the running speed and time were started at 2 m/min for 10 min, and then increased to 5 m/min for 10 min. The exercise was gradually increased for 5 weeks (week 2: 3 m/min for 10 min + increased to 5 m/min for 10 min + 5 m/min for 10 min, week 3: 3 m/min for 10 min + increased to 6 m/min for 10 min + 6 m/min for 10 min, week 4: 4 m/min for 10 min + increased to 7 m/min for 10 min + 7 m/min for 20 min, weeks 5–12: Initially 4 m/min, immediately increased to 7 m/min for 20 min + 7 m/min for 30 min).

Spine Density Analysis

The protocol for spine density analysis was as previously described (Nishijima et al., 2014). Briefly, 4 weeks after the DZP administration, mice ($N = 4$ per group) were deeply anesthetized and intracardially perfused with 4% paraformaldehyde, and their brains were extracted and placed in PB. Coronal sections (250 μm) that included the hippocampus were prepared using a microslicer (VT-1000; Leica, Wetzlar, Germany). Neuronal spines were visualized using Lucifer yellow injection into pyramidal neurons of the CA1/3 by iontophoresis pump (BAB-600; Kation Scientific, Minneapolis, MN, United States) under a fluorescence microscope (BX51; Olympus, Tokyo, Japan). The sections were then mounted onto slides and coverslipped with Permount and SlowFade Gold Antifade Reagent (S36937; Invitrogen, Tokyo, Japan). Images of the Lucifer yellow-injected neurons were acquired using a laser confocal microscope (C1si; Nikon, Tokyo, Japan) with a 60 × oil-immersion lens. We then measured the density of spines on apical branches that were observed to be 100–200 μm from the cell body in the pyramidal cell layer of CA1 or CA3. Images (2–4 images/neuron) were acquired with zoom and were taken at 0.25 μm focal steps. Images were analyzed offline using NIS-Elements software (Nikon). The average number of spines per 20 μm of dendritic length was expressed as the spine density.

Chemicals

The following drugs were used: DZP (FUJIFILM Wako Pure Chemical Industries, Osaka, Japan), PEG 400 (FUJIFILM Wako Pure Chemical), DMSO (Sigma-Aldrich), and Lucifer yellow (Sigma-Aldrich).

Statistics

All values are presented as the mean ± SEM. Chi-squared tests were used to confirm the effects of DZP on MWM exclusion criteria. The unpaired *t*-test, one-way analysis of variance (ANOVA), or two-way ANOVA with repeated measures were performed to compare behavioral data. For the NeuroD1-positive cell counts, one-way ANOVA was performed. Simple comparisons of two groups (TUNEL-positive cell counts, spine density analysis, and LTP analysis) were performed using the Student's *t*-test. For the LTP analysis, fEPSP slopes were constructed using the average of the last 15 min. Differences were considered statistically significant at $P < 0.05$.

RESULTS

Effects of Chronic Diazepam Administration on Cognitive Function

To evaluate the effects of chronic DZP treatment on spatial memory formation, the MWM was performed on four groups of mice: young control (CON, $n = 11$), young DZP-administered (DZP, $n = 8$), middle-aged CON ($n = 14$), and middle-aged DZP ($n = 12$). All mice were implanted with ALZET osmotic pumps filled with DZP or vehicle at day 0 (**Figure 1A**). After the osmotic pump implantation, young mice showed daily body weight gain during the MWM period independently of chronic DZP treatment [two-way ANOVA with repeated measures: "Treatment," $F(1,17) = 0.13$, $P > 0.05$; "Day," $F(6,102) = 54.0$, $P < 0.05$; "Treatment × Day," $F(6,102) = 3.71$, $P < 0.05$; **Figure 1Ba**]. There were no significant effects of DZP on changes in body weight in middle-aged animals during the MWM period [$F(1,24) = 2.87$, $P > 0.05$; "Day," $F(6,144) = 1.02$, $P > 0.05$; "Treatment × Day," $F(6,144) = 1.10$, $P > 0.05$; **Figure 1Bb**]. Ten days after surgery, the visible platform task was performed. Four mice from the young CON group, one mouse from the young DZP group, six mice from the middle-aged CON group, and five mice from the middle-aged DZP group were excluded because they met the exclusion criteria for the visible platform task. Therefore, seven mice in the young CON group, seven in the young DZP group, eight in the middle-aged CON group, and seven in the middle-aged DZP group were included in the following behavioral analysis. The effects of DZP on the escape latency of young and middle-aged mice in the visible platform task were then examined. Chronic DZP treatment did not influence exclusion in either experimental set (young: $\chi^2 = 1.36$, $P > 0.05$; middle-aged: $\chi^2 = 0.004$, $P > 0.05$). There were no significant differences in escape latency and path length in the visible platform task [escape latency: young: $t(12) = 1.36$, $P > 0.05$; middle-aged: $t(13) = 1.29$, $P > 0.05$; path length: young: $t(12) = 1.08$, $P > 0.05$; middle-aged: $t(13) = 0.59$, $P > 0.05$; **Figure 1C**]. From days 11 to 14, the hidden platform task was performed, and the escape latencies and path lengths were plotted (**Figure 1D**). Young CON and DZP animals showed a stable learning performance in the hidden platform task (escape latency: "Treatment," $F(1,12) = 0.26$, $P > 0.05$; "Day," $F(3,36) = 13.0$, $P < 0.05$; "Treatment × Day," $F(3,36) = 0.81$, $P > 0.05$; path length: "Treatment," $F(1,12) = 0.03$, $P > 0.05$; "Day," $F(3,36) = 4.18$, $P < 0.05$; "Treatment × Day," $F(3,36) = 1.91$, $P > 0.05$; **Figures 1Da,b**]. The young mice also showed comparable spatial memory retrieval in the probe tests on days 15 and 30 ($P > 0.05$, CON vs. DZP; **Figures 1Ea–c**). In the middle-aged mice, escape latencies in the hidden platform task were significantly higher in the DZP group than in the CON group ["Treatment," $F(1,13) = 18.6$, $P < 0.05$; "Day," $F(3,39) = 1.34$, $P > 0.05$; "Treatment × Day," $F(3,39) = 4.39$, $P < 0.05$; **Figure 1Dc**]. There were no significant differences in the path lengths between the CON and DZP groups ["Treatment," $F(1,12) = 0.03$, $P > 0.05$; "Day," $F(3,36) = 4.18$, $P < 0.05$; "Treatment × Day," $F(3,36) = 1.91$, $P > 0.05$; **Figure 1Dd**]. In the subsequent probe tests on days 15 and

30, the middle-aged DZP mice showed impairment of spatial memory retrieval ($P < 0.05$, CON vs. DZP; **Figures 1Ed,e**). Their motor performance was reduced on day 15 ($P > 0.05$, CON vs. DZP; **Figure 1Ef**) but not day 30. These results indicate that chronic DZP treatment impairs spatial learning in middle-aged mice but not in young mice. Chronic DZP treatment did not influence motor performance in both age groups except for the short-term probe test. Additionally, to evaluate the effects of aging, behavioral performance was compared between the young and middle-aged groups. There were no significant differences in escape latency in the hidden platform task between the young CON and middle-aged CON groups ["Treatment," $F(1,13) = 2.26$, $P > 0.05$; "Day," $F(3,39) = 10.5$, $P < 0.05$; "Treatment × Day," $F(3,39) = 2.23$, $P > 0.05$; **Figures 1Da,c**]. In the probe tests, there was a slight but significant difference in escape latency on day 15 only ($P < 0.05$), but mice in the CON group of both ages had equivalent memory retrieval performances (**Figures 1Ea,b,d,e**). Unlike the results from the CON groups, the middle-aged DZP group had significantly worse performances in both the hidden platform task ["Treatment," $F(1,12) = 5.18$, $P < 0.05$; "Day," $F(3,36) = 1.43$, $P > 0.05$; "Treatment × Day," $F(3,36) = 6.20$, $P < 0.05$; **Figures 1Da,c**] and the probe test ($P < 0.05$, young DZP vs. middle-aged DZP; **Figures 1Ea,b,d,e**) compared with the young DZP group. These results suggest that the effects of chronic DZP treatment on behavioral performance in the MWM were stronger in middle-aged mice than in young mice.

Effects of Chronic Diazepam Administration on Hippocampal Neurogenesis and Apoptosis

Neurogenesis in the adult dentate gyrus of the hippocampus occurs constitutively throughout postnatal life, and the rate of neurogenesis alters cognitive functions (Ansorg et al., 2012). In addition, apoptosis in the hippocampus is associated with cognitive deficits (Sima and Li, 2005). To examine the effects of chronic DZP administration on neurogenesis and apoptosis, TUNEL and NeuroD1 staining were performed in the hippocampus. There were very few TUNEL-positive cells in the hippocampus (≤5 cells/section) among all groups (**Figure 2A**; young CON: $n = 40$, young DZP: $n = 41$, middle-aged CON: $n = 41$, middle-aged DZP: $n = 39$ sections). NeuroD1-positive cells were detected in the dentate gyrus in all groups (**Figures 2B,C**; young CON: $n = 42$, young DZP: $n = 42$, middle-aged CON: $n = 44$, middle-aged DZP: $n = 40$ sections). There was a significant reduction in the number of NeuroD1-positive cells with age (**Figure 2C** and **Supplementary Figure 1Aa**; young vs. middle-aged: $P < 0.01$, one-way ANOVA, Tukey's test) but no significant differences between the CON and DZP groups (**Figure 2C**; young CON vs. young DZP: $P = 0.97$; middle-aged CON vs. middle-aged DZP: $P = 1.00$; one-way ANOVA, Tukey's test). These results suggest that neurogenesis is reduced with aging, and that the regulation of apoptosis and neurogenesis in the hippocampus is not affected by chronic DZP administration.

Hippocampal Long-Term Potentiation in Chronic Diazepam-Administered Mice

Many studies have suggested that synaptic plasticity of the hippocampus is related to spatial memory abilities (Morris et al., 1982; Baez et al., 2018). LTP was induced in the hippocampal CA1 and CA3 to evaluate synaptic plasticity in chronic DZP-administered mice. The magnitude of LTP was assessed at 45 min after TBS. Hippocampal LTP was impaired by chronic DZP administration in both the CA1 and CA3 in young mice [CA1: CON ($n = 10$) vs. DZP ($n = 9$), $P = 0.01$; CA3: CON ($n = 15$) vs. DZP ($n = 14$), $P < 0.01$; **Figure 3A**]. In middle-aged mice, a significant reduction of LTP was also observed in the CA3 of the DZP-administered group [CA1: CON ($n = 10$) vs. DZP ($n = 9$), $P = 0.70$; CA3: CON ($n = 14$) vs. DZP ($n = 15$), $P = 0.04$; **Figure 3B**]. Additionally, the LTP magnitude was significantly reduced by aging in the CA1 and CA3 (**Supplementary Figure 1Ab**: CA1: young vs. middle-aged CON, $P < 0.01$; CA3: young vs. middle-aged CON, $P < 0.05$). These results indicate that LTP, which is impaired in aging, is further attenuated by chronic DZP administration in the CA3 of middle-aged mice.

Spine Density of Hippocampal Neurons in Chronic Diazepam-Administered Mice

There is wide agreement that the integrity of the hippocampal neural network contributes to spatial memory behavior. To investigate the effects of DZP on synaptic connections in the hippocampal neural network, dendritic spine density was analyzed in both the CA1 and CA3 of the hippocampus (**Figure 4A**). Pyramidal neuron spines in the hippocampus were visualized using intracellular injections of Lucifer yellow into the soma in fixed sections, and spine density was then examined. In young mice, chronic DZP administration reduced spine density in the CA1 but not the CA3 [CA1: CON ($n = 7$) vs. DZP ($n = 6$), $P < 0.01$; CA3: CON ($n = 5$) vs. DZP ($n = 6$), $P = 0.85$; **Figure 4Ba**]. In middle-aged mice, spine density was reduced by DZP in both the CA1 and CA3 [CA1: CON ($n = 10$) vs. DZP ($n = 7$), $P < 0.01$; CA3: CON ($n = 8$) vs. DZP ($n = 8$), $P < 0.01$; **Figure 4Bb**]. In the CA1 of the hippocampus, there was also a significant reduction in spine density with aging (**Supplementary Figure 1Ac**: $P < 0.01$). These results suggest that dendritic spine maintenance is impaired by chronic DZP administration, especially in middle-aged mice.

Exercise Improves Diazepam-Induced Impairments in Spine Density and Long-Term Potentiation in Hippocampal Neurons

The facilitation or improvement of hippocampal LTP has been attempted using various approaches, including exercise. In the present study, we examined whether FRW exercise was able to attenuate the chronic DZP-induced effects on the hippocampus. After 12 weeks of FRW exercise, hippocampal LTP and spine density were investigated in chronic DZP-administered mice. In both the CA1 and CA3 of young mice and the CA3 of

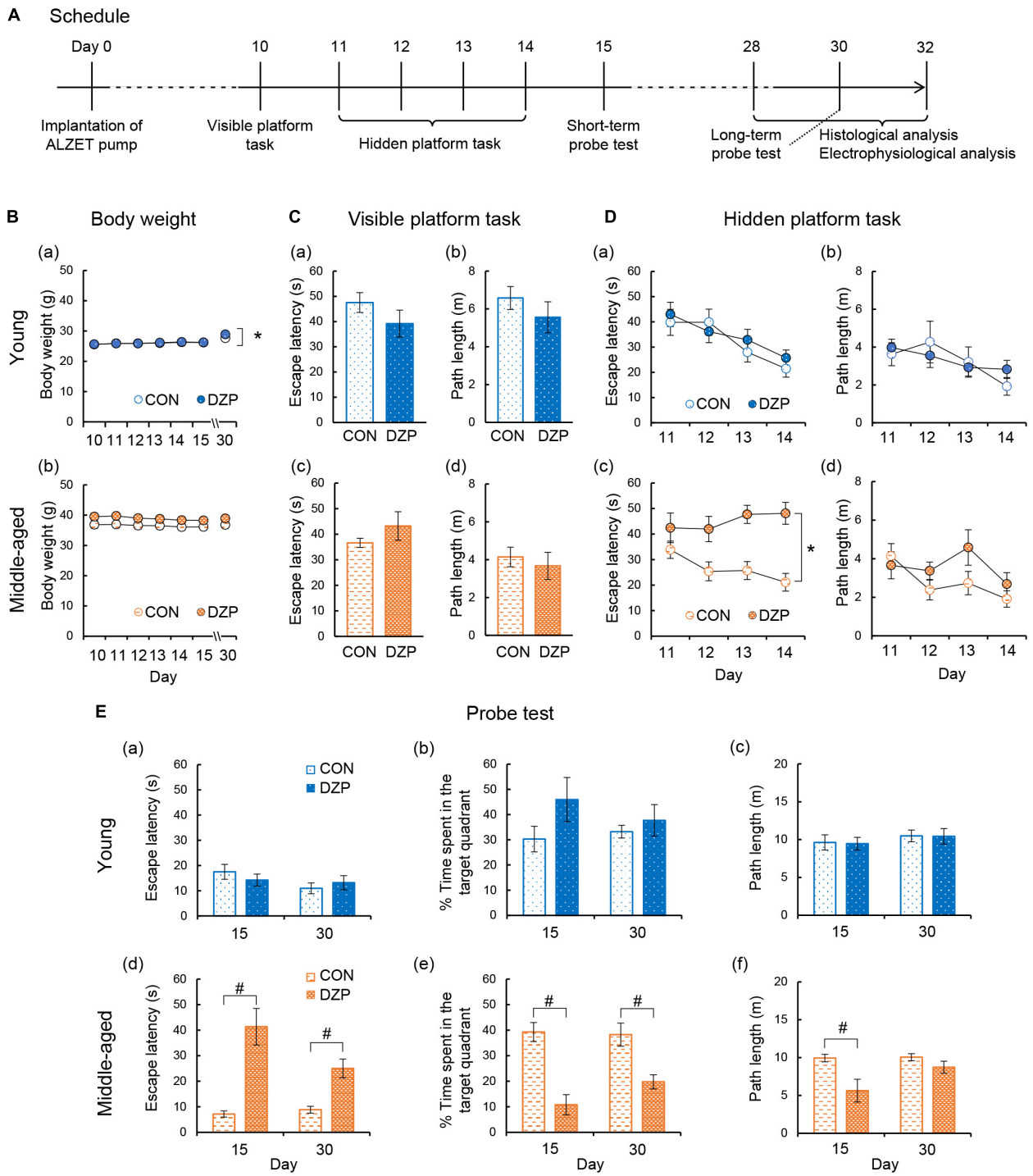

FIGURE 1 | Effects of chronic diazepam administration on spatial memory performance. **(A)** The schedule of this research including Morris water maze, electrophysiological recordings, and histological analysis. **(B)** Changes in the body weight during the Morris water maze period. **(C–E)** Results of the Morris water maze test. **(C)** Escape latency and path length in the visible platform task of young and middle-aged mice. **(D)** Escape latency and path length in the hidden platform task from days 11 to 14. **(E)** Latency to the target quadrant, time spent in the target quadrant, and path length in the probe test on days 15 (short-term) and 30 (long-term). The number of mice that were analyzed in the tasks and probe test was as follows: young CON, $n = 7$; young DZP, $n = 7$; middle-aged CON, $n = 8$; middle-aged DZP, $n = 7$. Error bar: mean ± SEM. $^{*}P < 0.05$, two-way analysis of variance with repeated measures. $^{\#}P < 0.05$, t-test. CON, control group; DZP, diazepam group.

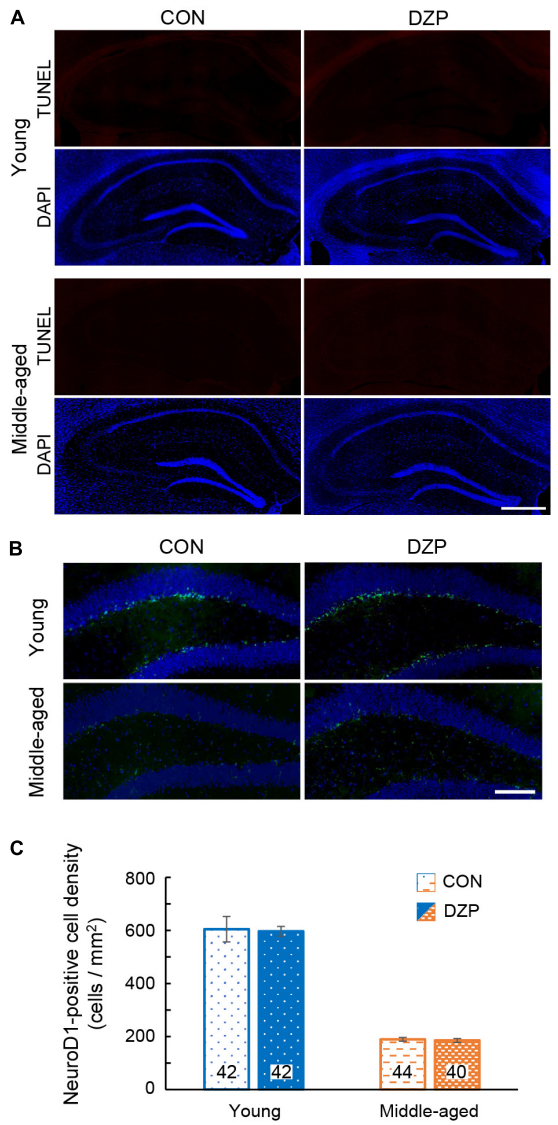

FIGURE 2 | Effects of chronic diazepam administration on apoptosis and neurogenesis in the hippocampus. **(A)** Fluorescence microscopic image of TUNEL (red) and DAPI (blue) staining. Scale bar, 500 μm. **(B)** Immunofluorescence image of NeuroD1 (green) and DAPI (blue) staining in the hippocampus of young and middle-aged mice. Scale bar, 50 μm. **(C)** Density of NeuroD1-positive cells in the dentate gyrus. The number in bar graph indicate the number of sections (*N* = 5 animal, 7–9 sections/animal). Error bar: mean ± SEM. CON, control group; DAPI, 4′,6-diamidino-2-phenylindole; DZP, diazepam group; NeuroD1, neurogenic differentiation factor 1; TUNEL, terminal deoxynucleotidyl transferase dUTP nick end labeling.

middle-aged mice (all of which were significantly affected by DZP administration in sedentary mice; **Figure 3**), there was no significant reduction in LTP magnitude with chronic DZP administration [young CA1: exercise (Ex) (n = 8) vs. Ex + DZP (n = 10), P = 0.69; young CA3: Ex (n = 9) vs. Ex + DZP (n = 12), P = 0.58; middle-aged CA3: Ex (n = 14) vs. Ex + DZP (n = 15), P = 0.12; **Figures 5A,B**]. Likewise, in the analysis of dendritic spine density in middle-aged mice, a significant difference remained in the CA1 but not in the CA3 [CA1: Ex (n = 14) vs. Ex + DZP (n = 15), $P < 0.01$; CA3: Ex (n = 15) vs. Ex + DZP (n = 14), P = 0.20; **Figures 6A,B**]. Furthermore, when comparing between the DZP and Ex + DZP groups, dendritic spine density in the CA1 of the exercise group was significantly higher than that of the sedentary group (**Supplementary Figure 1B**). These results indicate that the chronic DZP-induced reductions in dendritic spine density and LTP magnitude are preventable by FRW exercise before the DZP administration.

DISCUSSION

In the present study, we investigated the effects of chronic DZP administration on hippocampal function in both young and middle-aged mice. In the MWM test, cognitive performance was impaired by chronic DZP administration in middle-aged mice but not in young mice. This result suggests that the cognitive performance of middle-aged mice is more vulnerable to chronic DZP administration than that of young mice. Partially consistent with the results of the behavioral test, both hippocampal LTP in the CA3 and spine density were reduced in middle-aged mice by chronic DZP, although there was no modulation of neurogenesis or apoptosis. Consistent with this finding, previous studies have reported that DZP administration does not alter neurogenesis or apoptosis (Sarnowska et al., 2009; Wu and Castren, 2009; Nochi et al., 2013). In chronic DZP-administered young mice, although a reduction in cognitive performance was not observed in the MWM test, there was reduced hippocampal LTP and spine density in these animals. These results suggest that, regardless of behavioral cognitive performance, chronic DZP administration induces impairments in synaptic plasticity and spine maintenance in hippocampal neurons. In contrast, NeuroD1- and TUNEL-positive signals were not affected by chronic DZP administration in young or middle-aged mice. Together, our results suggest that chronic DZP-induced cognitive decline in middle-aged mice is not caused by changes in neurogenesis or apoptosis. In addition to the effects of DZP, there were aging-related effects on hippocampal neurons. Both LTP magnitude and neurogenesis were significantly lower in middle-aged mice than in young mice (**Supplementary Figures 1Aa,b**). In DZP administered mice, LTP magnitude of young mice was higher than that of aged mice. Especially in CA1, LTP magnitude of DZP treated young mice was higher than middle-aged control mice. Taking these findings into account, the vulnerability of middle-aged mice to chronic DZP administration may be attributed to aging. The effects of aging and chronic DZP administration on hippocampal neurons were similar, and the cognitive impairment that was observed in middle-aged mice in the MWM test might be induced by a synergistic effect of aging and chronic DZP administration. This synergistic effect could explain the fact that there was contrasting data between MWM and LTP with regards to both young and aged mice.

The effects of chronic DZP administration on spine loss and LTP suppression were observed in the hippocampal neurons of both young and middle-aged mice. We have previously reported

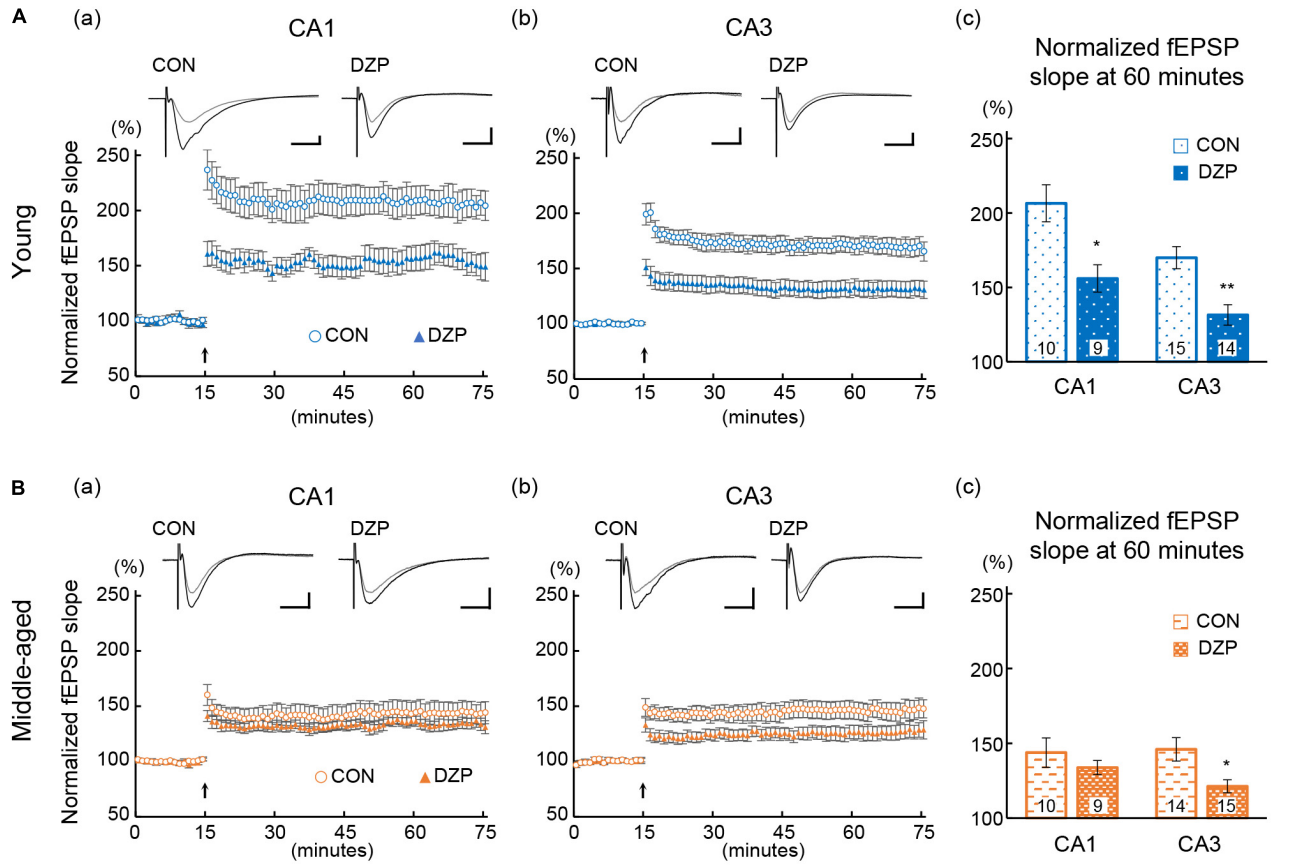

FIGURE 3 | Effects of chronic diazepam administration on long-term potentiation in the hippocampal CA1 and CA3 regions of young **(A)** and middle-aged **(B)** mice. Long-term potentiation was induced by TBS at 15 min of recording. The typical fEPSP responses (upper **a,b**) from 5 min before (gray) and 45 min after (black) the TBS are superimposed. The peak response of 5 min before TBS was normalized to 100%. Scale bar indicates 0.3 mV/10 ms in **(A)** and 0.2 mV/10 ms in **(B)**. The plot shows normalized fEPSP slopes every 1 min. The average normalized fEPSP slopes from the last 15 min were used to compare the magnitude of long-term potentiation between CON and DZP. The number in bar graph indicate the number of recorded slices (N = 6 animal, 1–3 slices/animal). Error bar: mean ± SEM. $^{*}P < 0.05$, Student's t-test; $^{**}P < 0.01$, Student's t-test; vs. CON. CON, control group; DZP, diazepam group; fEPSP, field excitatory postsynaptic potentials.

that chronic DZP administration increases lipocalin 2 expression (Furukawa et al., 2017), and another recent study revealed that chronic BZD administration to aged mice upregulates amyloid beta 42 expression and downregulates neprilysin expression (Jung et al., 2020). The expression of such molecules at normal levels is essential for neural excitability, spine maintenance, and synaptic plasticity (Huang et al., 2006; Lauren et al., 2009; Mucha et al., 2011). Thus, the chronic DZP-induced adverse effects of the present study might be associated with these molecules. Additionally, the chronic DZP-induced adverse effects might trigger activation of those molecules by modulating GABAA-R activity. If so, treatment of flumazenil, a competitive benzodiazepine receptor antagonist, would prevent or attenuate the chronic DZP effects. It was reported that there are both beneficial and adverse effect of flumazenil treatment for cognitive function (Neave et al., 2000; Colas et al., 2017). Further research will be needed to clarify the effect of flumazenil on cognitive impairment induced by chronic DZP.

Meanwhile, numerous studies suggested correlation between spine density and LTP in hippocampus (Zhai et al., 2020). However, our results were not completely consistent between LTP and spine density. In young mice, although LTP of CA3 was significantly reduced, spine density of CA3 were not decreased. Occasionally, it was reported that LTP was impaired without affecting spine density in the hippocampus of drebrin A knock out mice (Kojima et al., 2016). Additionally, the LTP of middle-aged mice were significantly or tend to reduce by chronic DZP, however the magnitude of decrease in LTP was smaller than that of young mice, even though magnitudes of decrease by DZP in spine density were not so remarkable. Our study could not explain these unexpected results, and the maintenance mechanism of spine density in aged animal was not fully elucidated. It was assumed that responses and function of molecules associated with LTP induction and spine maintenance might be modified by aging and different in regions. Further investigation is necessary to clarify the underlying molecular mechanisms.

Age-related declines in cognitive function have been explored in numerous studies. Several reports have revealed that cognitive function in mice aged 18 months or older is lower than that in

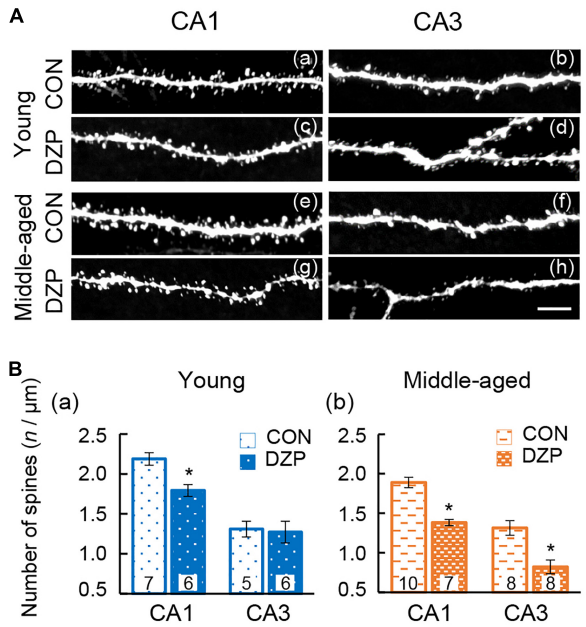

FIGURE 4 | Effects of chronic diazepam administration on the spine density of hippocampal neurons. **(A)** Representative images of visualized spines in the CA1 and CA3 regions of young and middle-aged mice. **(B)** Spines were counted and the results are summarized in bar graphs. The number in bar graph indicate the number of analyzed neurons (N = 4 animals, 1–3 neurons/animal). Scale bar, 5 μm. Error bar: mean ± SEM. *P < 0.01, t-test, vs. CON. CON, control group; DZP, diazepam group.

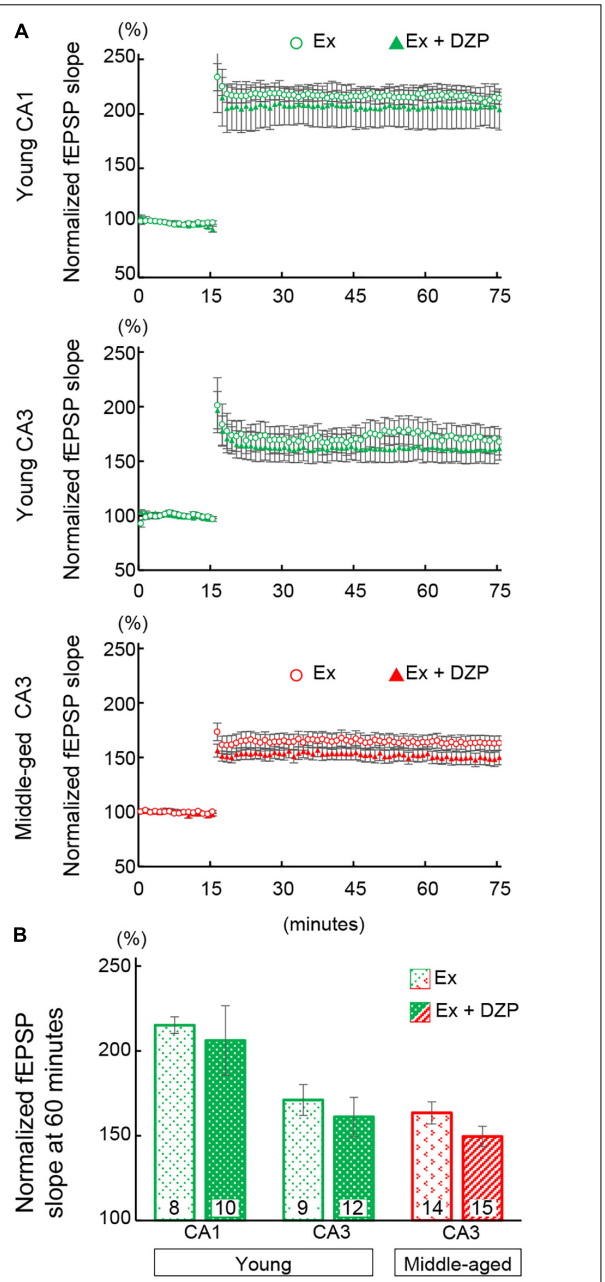

FIGURE 5 | Effects of exercise on hippocampal long-term potentiation in chronic diazepam- or vehicle-administered young and middle-aged mice. **(A)** Averages of every 1 min of normalized fEPSP slopes were plotted. Theta burst stimulation was delivered at 15 min of recording to induce long-term potentiation. **(B)** To compare the magnitudes of long-term potentiation, the normalized fEPSP slopes of 60- to 75-min recordings were averaged and are summarized as a bar graph. The number in bar graph indicate the number of recorded slices (N = 5 animal, 1–3 slices/animal). Error bar: mean ± SEM. Ex, exercise group; Ex + DZP, exercise + diazepam group; fEPSP, field excitatory postsynaptic potentials.

young mice (van Praag et al., 2005; Oliveira et al., 2012). However, our data revealed that the cognitive performance of middle-aged control mice in the MWM test was nearly identical to that of young control mice. This discrepancy might be attributed to the differences in mouse ages. The 12-month-old mice used in the present study might not have been sufficiently old enough to exhibit age-related cognitive decline in this behavioral test (Tsai et al., 2018). However, we did observe age-related reductions in hippocampal LTP and neurogenesis in these mice. Together, these findings suggest that middle-aged mice might be vulnerable to chronic DZP administration even though they do not show cognitive impairment in behavioral tests.

The preventive effects of regular physical exercise against cognitive deterioration and dementia risk have been reported (Paillard, 2015). In the current study, we examined whether the adverse effects of chronic DZP administration were prevented by physical exercise. The chronic DZP-induced reductions in LTP magnitude and spine density were attenuated by FRW exercise for 12 weeks. These results suggest that physical exercise may be a potential treatment to protect against cognitive decline caused by chronic DZP. However, our data were unable to elucidate the molecular mechanisms of these exercise-induced beneficial effects on hippocampal neurons. Previous studies have demonstrated that exercise increases BDNF and tropomyosin receptor kinase B mRNA expression levels in the brains of rodents (Gomez-Pinilla et al., 2002; Garza et al., 2004; Jin et al., 2017). BDNF is a protein that promotes neural survival and the differentiation of new neurons and synapses. BDNF is thought to be a major contributor toward enhancing memory and increasing spine density (Leem et al., 2019). In addition

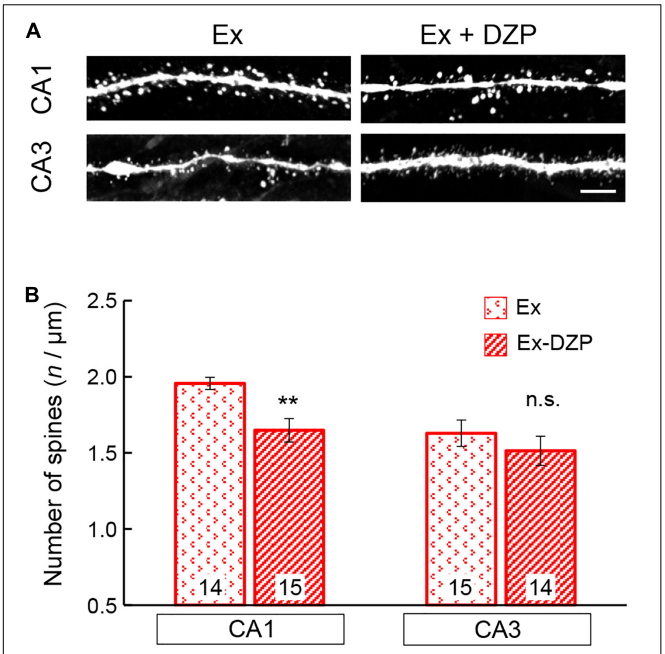

FIGURE 6 | Effects of exercise on the spine density of hippocampal neurons in middle-aged mice. **(A)** Representative images of visualized spines in the CA1 and CA3 regions of middle-aged mice. **(B)** Spine density was measured and is summarized in a bar graph. The number in bar graph indicate the number of analyzed neurons (N = 4 animals, 3–4 neurons/animal). Scale bar, 5 μm. Error bar: mean ± SEM. $^{**}P < 0.01$, t-test, vs. Ex group; n.s., not significant. Ex, exercise group; Ex + DZP, exercise + diazepam group.

to BDNF, the expression of other growth factors – such as fibroblast growth factor (Gomez-Pinilla et al., 1997, 1998), insulin-like growth factor I (Stein et al., 2018), and nerve growth factor (Chae and Kim, 2009) – are elevated by exercise. These factors play an important role in neural function in the adult brain (van Praag, 2008). It is therefore likely that the expression of growth factors was upregulated by exercise even in the hippocampus of chronic DZP-administered mice in the present study, thus leading to the observed beneficial effects in hippocampal neurons. Furthermore, a recent study identified exercise-responsive peripheral molecules that are associated with protective effects against cognitive decline (McGee and Hargreaves, 2020). For example, the peripheral overexpression of fibronectin type III domain-containing protein 5 rescues synaptic plasticity and memory in Alzheimer's disease model mice (Lourenco et al., 2019). In addition, glycosylphosphatidylinositol-specific phospholipase D1 in plasma is increased by exercise, and is related to improved cognitive function in middle-aged mice (Horowitz et al., 2020). Such molecules may have been functional even in our model mice, but further research is needed to reveal the detailed mechanisms of exercise-induced protective effects in chronic DZP-administered mice.

Exercise enhances cognitive function and prevents age-related memory decline (Gomes da Silva et al., 2012). However, in the current study, although we observed age-related reductions in dendritic spine density and impairments in LTP, FRW exercise did not improve the effects of aging in the control group. It is possible that the intensity of FRW exercise that was used in this study was not sufficient to improve these effects of aging. Additionally, our mice may not have been old enough to be able to observe any FRW exercise-induced improvements of age-related effects in the hippocampus.

It is well known that sedation was produced by BZDs. The injection of BZD induces sedative effects after the acute injection. However, tolerance is induced by chronic BZD administrations, and sedation is progressively decreased through 7 days (Griffiths et al., 1992). In this study, MWM experiments were started at 10 days after the osmotic pump implantation. On the day performing visible platform task, body weight and path length, indicating motor performance, were not significantly different between control and DZP groups of both young and middle-aged mice. These results indicated that sedative effects of DZP have disappeared by day 10 in the MWM experiment. Meanwhile, there was a possibility that DZP-induced sedation and home cage behaviors might be affected by aging and/or exercise. However, as our data were confined to chronic DZP effects, the effects of aging and exercise on DZP-induced sedation and home cage behaviors could not be defined. In future, further studies about home cage behaviors and physiological parameters of exercised mice before and following DZP administration would reveal detail mechanism and availability of exercise against to the effect of aging and DZP administration.

In conclusion, we demonstrated that synaptic plasticity and dendritic spine density were reduced in the hippocampus by chronic DZP administration. In middle-aged mice, although no behavioral signs of cognitive decline were observed, there were several age-related alterations in the hippocampus. These alterations were likely contributing factors to the vulnerability of cognitive function to chronic DZP administration in the middle-aged mice. Furthermore, our findings provide evidence that FRW exercise may reduce the effects of chronic DZP administration on the hippocampus; however, further research is needed to identify the underlying molecular mechanisms.

DATA AVAILABILITY STATEMENT

The original contributions presented in the study are included in the article/**Supplementary Material**, further inquiries can be directed to the corresponding author.

ETHICS STATEMENT

The animal study was reviewed and approved by the Hirosaki University School of Medicine.

AUTHOR CONTRIBUTIONS

TF and SU designed the study. YN performed the behavioral experiments. TF, NM, and AN performed the electrophysiological, imaging, and histochemical experiments.

TF, YN, SS, NM, and AN analyzed the data. TF and YN wrote the manuscript with contributions from SU. All authors read and approved the final manuscript.

FUNDING

This work was supported by a Grant-in-Aid for Young Scientists #JP19K18234 (to TF); an Interdisciplinary Collaborative Research Grant for Young Scientists, Hirosaki University (to TF); and a Grant-in-Aid for Scientific Research (C) #JP18K08846 (to SU).

ACKNOWLEDGMENTS

We thank Bronwen Gardner, Ph.D., from Edanz (https://jp.edanz.com/ac) for editing a draft of this manuscript.

SUPPLEMENTARY MATERIAL

The Supplementary Material for this article can be found online at: https://www.frontiersin.org/articles/10.3389/fnagi.2021.777404/full#supplementary-material

REFERENCES

Ahlskog, J. E., Geda, Y. E., Graff-Radford, N. R., and Petersen, R. C. (2011). Physical exercise as a preventive or disease-modifying treatment of dementia and brain aging. *Mayo Clin. Proc.* 86, 876–884.

Ali, N. J., and Olsen, R. W. (2001). Chronic benzodiazepine treatment of cells expressing recombinant GABA(A) receptors uncouples allosteric binding: studies on possible mechanisms. *J. Neurochem.* 79, 1100–1108. doi: 10.1046/j.1471-4159.2001.00664.x

Allison, C., and Pratt, J. A. (2003). Neuroadaptive processes in GABAergic and glutamatergic systems in benzodiazepine dependence. *Pharmacol. Ther.* 98, 171–195. doi: 10.1016/s0163-7258(03)00029-9

Allison, C., and Pratt, J. A. (2006). Differential effects of two chronic diazepam treatment regimes on withdrawal anxiety and AMPA receptor characteristics. *Neuropsychopharmacology* 31, 602–619. doi: 10.1038/sj.npp.1300800

Ansorg, A., Witte, O. W., and Urbach, A. (2012). Age-dependent kinetics of dentate gyrus neurogenesis in the absence of cyclin D2. *BMC Neurosci.* 13:46. doi: 10.1186/1471-2202-13-46

Arias-Cavieres, A., Adasme, T., Sanchez, G., Munoz, P., and Hidalgo, C. (2017). Aging Impairs Hippocampal- Dependent Recognition Memory and LTP and Prevents the Associated RyR Up-regulation. *Front. Aging Neurosci.* 9:111. doi: 10.3389/fnagi.2017.00111

Baez, M. V., Cercato, M. C., and Jerusalinsky, D. A. (2018). NMDA Receptor Subunits Change after Synaptic Plasticity Induction and Learning and Memory Acquisition. *Neural Plast.* 2018:5093048. doi: 10.1155/2018/5093048

Barnes, C. A. (2003). Long-term potentiation and the ageing brain. *Philos. Trans. R. Soc. Lond. B Biol. Sci.* 358, 765–772.

Barnes, D. E., Yaffe, K., Satariano, W. A., and Tager, I. B. (2003). A longitudinal study of cardiorespiratory fitness and cognitive function in healthy older adults. *J. Am. Geriatr. Soc.* 51, 459–465. doi: 10.1046/j.1532-5415.2003.51153.x

Bromley-Brits, K., Deng, Y., and Song, W. (2011). Morris water maze test for learning and memory deficits in Alzheimer's disease model mice. *J. Vis. Exp.* 2011:2920. doi: 10.3791/2920

Bruel-Jungerman, E., Laroche, S., and Rampon, C. (2005). New neurons in the dentate gyrus are involved in the expression of enhanced long-term memory following environmental enrichment. *Eur. J. Neurosci.* 21, 513–521. doi: 10.1111/j.1460-9568.2005.03875.x

Chae, C. H., and Kim, H. T. (2009). Forced, moderate-intensity treadmill exercise suppresses apoptosis by increasing the level of NGF and stimulating phosphatidylinositol 3-kinase signaling in the hippocampus of induced aging rats. *Neurochem. Int.* 55, 208–213. doi: 10.1016/j.neuint.2009.02.024

Colas, D., Chuluun, B., Garner, C. C., and Heller, H. C. (2017). Short-term treatment with flumazenil restores long-term object memory in a mouse model of Down syndrome. *Neurobiol. Learn. Mem.* 140, 11–16. doi: 10.1016/j.nlm.2017.02.006

Curto, Y., Garcia-Mompo, C., Bueno-Fernandez, C., and Nacher, J. (2016). Chronic benzodiazepine treatment decreases spine density in cortical pyramidal neurons. *Neurosci. Lett.* 613, 41–46. doi: 10.1016/j.neulet.2015.12.048

del Cerro, S., Jung, M., and Lynch, G. (1992). Benzodiazepines block long-term potentiation in slices of hippocampus and piriform cortex. *Neuroscience* 49, 1–6. doi: 10.1016/0306-4522(92)90071-9

Disterhoft, J. F., Wu, W. W., and Ohno, M. (2004). Biophysical alterations of hippocampal pyramidal neurons in learning, ageing and Alzheimer's disease. *Ageing Res. Rev.* 3, 383–406. doi: 10.1016/j.arr.2004.07.001

Drapeau, E., Mayo, W., Aurousseau, C., Le Moal, M., Piazza, P. V., and Abrous, D. N. (2003). Spatial memory performances of aged rats in the water maze predict levels of hippocampal neurogenesis. *Proc. Natl. Acad. Sci. U S A.* 100, 14385–14390. doi: 10.1073/pnas.2334169100

Foitzick, M. F., Medina, N. B., Iglesias Garcia, L. C., and Gravielle, M. C. (2020). Benzodiazepine exposure induces transcriptional down-regulation of GABAA receptor alpha1 subunit gene via L-type voltage-gated calcium channel activation in rat cerebrocortical neurons. *Neurosci. Lett.* 721:134801. doi: 10.1016/j.neulet.2020.134801

Foster, T. C., and Norris, C. M. (1997). Age-associated changes in Ca(2+)-dependent processes: relation to hippocampal synaptic plasticity. *Hippocampus* 7, 602–612. doi: 10.1002/(SICI)1098-1063(1997)7:6<602::AID-HIPO3>3.0.CO;2-G

Furukawa, T., Shimoyama, S., Miki, Y., Nikaido, Y., Koga, K., Nakamura, K., et al. (2017). Chronic diazepam administration increases the expression of Lcn2 in the CNS. *Pharmacol. Res. Perspect.* 5:e00283. doi: 10.1002/prp2.283

Gao, Z., Ure, K., Ables, J. L., Lagace, D. C., Nave, K. A., Goebbels, S., et al. (2009). Neurod1 is essential for the survival and maturation of adult-born neurons. *Nat. Neurosci.* 12, 1090–1092.

Garza, A. A., Ha, T. G., Garcia, C., Chen, M. J., and Russo-Neustadt, A. A. (2004). Exercise, antidepressant treatment, and BDNF mRNA expression in the aging brain. *Pharmacol. Biochem. Behav.* 77, 209–220. doi: 10.1016/j.pbb.2003.10.020

Gomes da Silva, S., Unsain, N., Masco, D. H., Toscano-Silva, M., de Amorim, H. A., et al. (2012). Early exercise promotes positive hippocampal plasticity and improves spatial memory in the adult life of rats. *Hippocampus* 22, 347–358. doi: 10.1002/hipo.20903

Gomez-Pinilla, F., Dao, L., and So, V. (1997). Physical exercise induces FGF-2 and its mRNA in the hippocampus. *Brain Res.* 764, 1–8. doi: 10.1016/s0006-8993(97)00375-2

Gomez-Pinilla, F., So, V., and Kesslak, J. P. (1998). Spatial learning and physical activity contribute to the induction of fibroblast growth factor: neural substrates for increased cognition associated with exercise. *Neuroscience* 85, 53–61. doi: 10.1016/s0306-4522(97)00576-9

Gomez-Pinilla, F., Ying, Z., Roy, R. R., Molteni, R., and Edgerton, V. R. (2002). Voluntary exercise induces a BDNF-mediated mechanism that promotes neuroplasticity. *J. Neurophysiol.* 88, 2187–2195. doi: 10.1152/jn.00152.2002

Griffiths, R. R., Sannerud, C. A., Ator, N. A., and Brady, J. V. (1992). Zolpidem behavioral pharmacology in baboons: self-injection, discrimination, tolerance and withdrawal. *J. Pharmacol. Exp. Ther.* 260, 1199–1208.

Horowitz, A. M., Fan, X., Bieri, G., Smith, L. K., Sanchez-Diaz, C. I., Schroer, A. B., et al. (2020). Blood factors transfer beneficial effects of exercise on neurogenesis and cognition to the aged brain. *Science* 369, 167–173. doi: 10.1126/science.aaw2622

Huang, S. M., Mouri, A., Kokubo, H., Nakajima, R., Suemoto, T., Higuchi, M., et al. (2006). Neprilysin-sensitive synapse-associated amyloid-beta peptide oligomers impair neuronal plasticity and cognitive function. *J. Biol. Chem.* 281, 17941–17951. doi: 10.1074/jbc.M601372200

Jin, J. J., Ko, I. G., Kim, S. E., Hwang, L., Lee, M. G., Kim, D. Y., et al. (2017). Age-dependent differences of treadmill exercise on spatial learning ability between

young- and adult-age rats. *J. Exerc. Rehabil.* 13, 381–386. doi: 10.12965/jer.1735070.535

Joksimovic, S., Divljakovic, J., Van Linn, M. L., Varagic, Z., Brajkovic, G., Milinkovic, M. M., et al. (2013). Benzodiazepine-induced spatial learning deficits in rats are regulated by the degree of modulation of alpha1 GABA(A) receptors. *Eur. Neuropsychopharmacol.* 23, 390–399. doi: 10.1016/j.euroneuro.2012.05.003

Jung, M. E., Metzger, D. B., and Hall, J. (2020). The long-term but not short-term use of benzodiazepine impairs motoric function and upregulates amyloid beta in part through the suppression of translocator protein. *Pharmacol. Biochem. Behav.* 191:172873. doi: 10.1016/j.pbb.2020.172873

Kempermann, G., Kuhn, H. G., and Gage, F. H. (1998). Experience-induced neurogenesis in the senescent dentate gyrus. *J. Neurosci.* 18, 3206–3212. doi: 10.1523/JNEUROSCI.18-09-03206.1998

Kojima, N., Yasuda, H., Hanamura, K., Ishizuka, Y., Sekino, Y., and Shirao, T. (2016). Drebrin A regulates hippocampal LTP and hippocampus-dependent fear learning in adult mice. *Neuroscience* 324, 218–226. doi: 10.1016/j.neuroscience.2016.03.015

Kramer, A. F., Hahn, S., Cohen, N. J., Banich, M. T., McAuley, E., Harrison, C. R., et al. (1999). Ageing, fitness and neurocognitive function. *Nature* 400, 418–419. doi: 10.1038/22682

Kuhn, H. G., Dickinson-Anson, H., and Gage, F. H. (1996). Neurogenesis in the dentate gyrus of the adult rat: age-related decrease of neuronal progenitor proliferation. *J. Neurosci.* 16, 2027–2033. doi: 10.1523/jneurosci.16-06-02027.1996

Lader, M. (1991). History of benzodiazepine dependence. *J. Subst. Abuse. Treat.* 8, 53–59. doi: 10.1016/0740-5472(91)90027-8

Larson, E. B., Wang, L., Bowen, J. D., McCormick, W. C., Teri, L., Crane, P., et al. (2006). Exercise is associated with reduced risk for incident dementia among persons 65 years of age and older. *Ann. Intern. Med.* 144, 73–81. doi: 10.7326/0003-4819-144-2-200601170-00004

Lauren, J., Gimbel, D. A., Nygaard, H. B., Gilbert, J. W., and Strittmatter, S. M. (2009). Cellular prion protein mediates impairment of synaptic plasticity by amyloid-beta oligomers. *Nature* 457, 1128–1132. doi: 10.1038/nature07761

Laurin, D., Verreault, R., Lindsay, J., MacPherson, K., and Rockwood, K. (2001). Physical activity and risk of cognitive impairment and dementia in elderly persons. *Arch. Neurol.* 58, 498–504.

Leem, Y. H., Park, J. S., Chang, H., Park, J., and Kim, H. S. (2019). Exercise Prevents Memory Consolidation Defects Via Enhancing Prolactin Responsiveness of CA1 Neurons in Mice Under Chronic Stress. *Mol. Neurobiol.* 56, 6609–6625. doi: 10.1007/s12035-019-1560-z

Liu, L., Jian, P., Zhou, Y., Zhou, J., Jia, L., Tang, M., et al. (2020). Is the Long-Term Use of Benzodiazepines Associated With Worse Cognition Performance in Highly Educated Older Adults? *Front. Psychiatry* 11:595623. doi: 10.3389/fpsyt.2020.595623

Lorenz-Guertin, J. M., Bambino, M. J., Das, S., Weintraub, S. T., and Jacob, T. C. (2019). Diazepam Accelerates GABAAR Synaptic Exchange and Alters Intracellular Trafficking. *Front. Cell Neurosci.* 13:163. doi: 10.3389/fncel.2019.00163

Lourenco, M. V., Frozza, R. L., de Freitas, G. B., Zhang, H., Kincheski, G. C., Ribeiro, F. C., et al. (2019). Exercise-linked FNDC5/irisin rescues synaptic plasticity and memory defects in Alzheimer's models. *Nat. Med.* 25, 165–175.

McDonald, H. Y., and Wojtowicz, J. M. (2005). Dynamics of neurogenesis in the dentate gyrus of adult rats. *Neurosci. Lett.* 385, 70–75.

McGee, S. L., and Hargreaves, M. (2020). Exercise adaptations: molecular mechanisms and potential targets for therapeutic benefit. *Nat. Rev. Endocrinol.* 16, 495–505. doi: 10.1038/s41574-020-0377-1

McNamara, R. K., dePape, G. E., and Skelton, R. W. (1993). Differential effects of benzodiazepine receptor agonists on hippocampal long-term potentiation and spatial learning in the Morris water maze. *Brain. Res.* 626, 63–70. doi: 10.1016/0006-8993(93)90563-3

Michelini, S., Cassano, G. B., Frare, F., and Perugi, G. (1996). Long-term use of benzodiazepines: tolerance, dependence and clinical problems in anxiety and mood disorders. *Pharmacopsychiatry* 29, 127–134. doi: 10.1055/s-2007-979558

Monti, M. C., Almiron, R. S., Bignante, E. A., and Ramirez, O. A. (2010). Changes in hippocampal arc protein expression and synaptic plasticity by the presentation of contextual cues linked to drug experience. *Synapse* 64, 39–46. doi: 10.1002/syn.20700

Monti, M. C., Gabach, L. A., Perez, M. F., and Ramirez, O. A. (2012). Impact of contextual cues in the expression of the memory associated with diazepam withdrawal: involvement of hippocampal PKMzeta in vivo, and Arc expression and LTP in vitro. *Eur. J. Neurosci.* 36, 3118–3125. doi: 10.1111/j.1460-9568.2012.08206.x

Morris, R. G., Garrud, P., Rawlins, J. N., and O'Keefe, J. (1982). Place navigation impaired in rats with hippocampal lesions. *Nature* 297, 681–683. doi: 10.1038/297681a0

Mucha, M., Skrzypiec, A. E., Schiavon, E., Attwood, B. K., Kucerova, E., and Pawlak, R. (2011). Lipocalin-2 controls neuronal excitability and anxiety by regulating dendritic spine formation and maturation. *Proc. Natl. Acad. Sci. U S A.* 108, 18436–18441. doi: 10.1073/pnas.1107936108

Neave, N., Reid, C., Scholey, A. B., Thompson, J. M., Moss, M., Ayre, G., et al. (2000). Dose-dependent effects of flumazenil on cognition, mood, and cardio-respiratory physiology in healthy volunteers. *Br. Dent. J.* 189, 668–674. doi: 10.1038/sj.bdj.4800860

Nishijima, H., Suzuki, S., Kon, T., Funamizu, Y., Ueno, T., Haga, R., et al. (2014). Morphologic changes of dendritic spines of striatal neurons in the levodopa-induced dyskinesia model. *Mov. Disord.* 29, 336–343.

Nochi, R., Kaneko, J., Okada, N., Terazono, Y., Matani, A., and Hisatsune, T. (2013). Diazepam treatment blocks the elevation of hippocampal activity and the accelerated proliferation of hippocampal neural stem cells after focal cerebral ischemia in mice. *J. Neurosci. Res.* 91, 1429–1439. doi: 10.1002/jnr.23264

Nunzi, M. G., Milan, F., Guidolin, D., and Toffano, G. (1987). Dendritic spine loss in hippocampus of aged rats. Effect of brain phosphatidylserine administration. *Neurobiol. Aging* 8, 501–510. doi: 10.1016/0197-4580(87)90124-2

O'Brien, C. P. (2005). Benzodiazepine use, abuse, and dependence. *J. Clin. Psychiatry* 66(Suppl. 2), 28–33.

Oliveira, A. M., Hemstedt, T. J., and Bading, H. (2012). Rescue of aging-associated decline in Dnmt3a2 expression restores cognitive abilities. *Nat. Neurosci.* 15, 1111–1113. doi: 10.1038/nn.3151

Paillard, T. (2015). Preventive effects of regular physical exercise against cognitive decline and the risk of dementia with age advancement. *Sports. Med. Open* 1:20. doi: 10.1186/s40798-015-0016-x

Paterniti, S., Dufouil, C., and Alperovitch, A. (2002). Long-term benzodiazepine use and cognitive decline in the elderly: the Epidemiology of Vascular Aging Study. *J. Clin. Psychopharmacol.* 22, 285–293. doi: 10.1097/00004714-200206000-00009

Picton, J. D., Marino, A. B., and Nealy, K. L. (2018). Benzodiazepine use and cognitive decline in the elderly. *Am. J. Health Syst. Pharm.* 75, e6–e12. doi: 10.2146/ajhp160381

Pratt, J. A., Brett, R. R., and Laurie, D. J. (1998). Benzodiazepine dependence: from neural circuits to gene expression. *Pharmacol. Biochem. Behav.* 59, 925–934. doi: 10.1016/s0091-3057(97)00539-x

Rosenberg, P. B. (2015). Benzodiazepine exposure increases risk of Alzheimer's disease. *Evid. Based. Med.* 20:75. doi: 10.1136/ebmed-2014-110117

Sarnowska, A., Beresewicz, M., Zablocka, B., and Domanska-Janik, K. (2009). Diazepam neuroprotection in excitotoxic and oxidative stress involves a mitochondrial mechanism additional to the GABAAR and hypothermic effects. *Neurochem. Int.* 55, 164–173. doi: 10.1016/j.neuint.2009.01.024

Sima, A. A., and Li, Z. G. (2005). The effect of C-peptide on cognitive dysfunction and hippocampal apoptosis in type 1 diabetic rats. *Diabetes* 54, 1497–1505. doi: 10.2337/diabetes.54.5.1497

Stein, A. M., Silva, T. M. V., Coelho, F. G. M., Arantes, F. J., Costa, J. L. R., Teodoro, E., et al. (2018). Physical exercise, IGF-1 and cognition A systematic review of experimental studies in the elderly. *Dement. Neuropsychol.* 12, 114–122. doi: 10.1590/1980-57642018dn12-020003

Toy, W. A., Petzinger, G. M., Leyshon, B. J., Akopian, G. K., Walsh, J. P., Hoffman, M. V., et al. (2014). Treadmill exercise reverses dendritic spine loss in direct and indirect striatal medium spiny neurons in the 1-methyl-4-phenyl-1,2,3,6-tetrahydropyridine (MPTP) mouse model of Parkinson's disease. *Neurobiol. Dis.* 63, 201–209. doi: 10.1016/j.nbd.2013.11.017

Tsai, S. F., Ku, N. W., Wang, T. F., Yang, Y. H., Shih, Y. H., Wu, S. Y., et al. (2018). Long-Term Moderate Exercise Rescues Age-Related Decline in Hippocampal Neuronal Complexity and Memory. *Gerontology* 64, 551–561. doi: 10.1159/000488589

van Praag, H. (2008). Neurogenesis and exercise: past and future directions. *Neuromolecular. Med.* 10, 128–140. doi: 10.1007/s12017-008-8028-z

van Praag, H., Christie, B. R., Sejnowski, T. J., and Gage, F. H. (1999). Running enhances neurogenesis, learning, and long-term potentiation in mice. *Proc. Natl. Acad. Sci. U S A.* 96, 13427–13431. doi: 10.1073/pnas.96.23.13427

van Praag, H., Shubert, T., Zhao, C., and Gage, F. H. (2005). Exercise enhances learning and hippocampal neurogenesis in aged mice. *J. Neurosci.* 25, 8680–8685. doi: 10.1523/jneurosci.1731-05.2005

Van Sickle, B. J., Xiang, K., and Tietz, E. I. (2004). Transient plasticity of hippocampal CA1 neuron glutamate receptors contributes to benzodiazepine withdrawal-anxiety. *Neuropsychopharmacology* 29, 1994–2006. doi: 10.1038/sj.npp.1300531

Vinkers, C. H., van Oorschot, R., Nielsen, E. O., Cook, J. M., Hansen, H. H., Groenink, L., et al. (2012). GABA(A) receptor alpha subunits differentially contribute to diazepam tolerance after chronic treatment. *PLoS One* 7:e43054. doi: 10.1371/journal.pone.0043054

Walker, C. K., and Herskowitz, J. H. (2020). Dendritic Spines: Mediators of Cognitive Resilience in Aging and Alzheimer's Disease. *Neuroscientist* 27, 487–505. doi: 10.1177/1073858420945964

Wu, X., and Castren, E. (2009). Co-treatment with diazepam prevents the effects of fluoxetine on the proliferation and survival of hippocampal dentate granule cells. *Biol. Psychiatry* 66, 5–8. doi: 10.1016/j.biopsych.2009.01.023

Yaffe, K., and Boustani, M. (2014). Benzodiazepines and risk of Alzheimer's disease. *BMJ* 349:g5312. doi: 10.1136/bmj.g5312

Zhai, B., Fu, J., Xiang, S., Shang, Y., Yan, Y., Yin, T., et al. (2020). Repetitive transcranial magnetic stimulation ameliorates recognition memory impairment induced by hindlimb unloading in mice associated with BDNF/TrkB signaling. *Neurosci. Res.* 153, 40–47. doi: 10.1016/j.neures.2019.04.002

Conflict of Interest: The authors declare that the research was conducted in the absence of any commercial or financial relationships that could be construed as a potential conflict of interest.

Publisher's Note: All claims expressed in this article are solely those of the authors and do not necessarily represent those of their affiliated organizations, or those of the publisher, the editors and the reviewers. Any product that may be evaluated in this article, or claim that may be made by its manufacturer, is not guaranteed or endorsed by the publisher.

frontiers in Aging Neuroscience

REVIEW
published: 17 February 2022
doi: 10.3389/fnagi.2022.814528

Age-Related Hearing Loss: Sensory and Neural Etiology and Their Interdependence

Karen L. Elliott[1], *Bernd Fritzsch*[1]*, *Ebenezer N. Yamoah*[2] *and Azel Zine*[3]

[1]Department of Biology, University of Iowa, Iowa City, IA, United States, [2]Department of Physiology and Cell Biology, School of Medicine, University of Nevada, Reno, NV, United States, [3]LBN, Laboratory of Bioengineering and Nanoscience, University of Montpellier, Montpellier, France

Age-related hearing loss (ARHL) is a common, increasing problem for older adults, affecting about 1 billion people by 2050. We aim to correlate the different reductions of hearing from cochlear hair cells (HCs), spiral ganglion neurons (SGNs), cochlear nuclei (CN), and superior olivary complex (SOC) with the analysis of various reasons for each one on the sensory deficit profiles. Outer HCs show a progressive loss in a basal-to-apical gradient, and inner HCs show a loss in a apex-to-base progression that results in ARHL at high frequencies after 70 years of age. In early neonates, SGNs innervation of cochlear HCs is maintained. Loss of SGNs results in a considerable decrease (~50% or more) of cochlear nuclei in neonates, though the loss is milder in older mice and humans. The dorsal cochlear nuclei (fusiform neurons) project directly to the inferior colliculi while most anterior cochlear nuclei reach the SOC. Reducing the number of neurons in the medial nucleus of the trapezoid body (MNTB) affects the interactions with the lateral superior olive to fine-tune ipsi- and contralateral projections that may remain normal in mice, possibly humans. The inferior colliculi receive direct cochlear fibers and second-order fibers from the superior olivary complex. Loss of the second-order fibers leads to hearing loss in mice and humans. Although ARHL may arise from many complex causes, HC degeneration remains the more significant problem of hearing restoration that would replace the cochlear implant. The review presents recent findings of older humans and mice with hearing loss.

Keywords: OHC, IHC, SGN, cochlear nuclei, SOC

OPEN ACCESS

Edited by:
Benoit Laurent,
Université de Sherbrooke, Canada

Reviewed by:
Togay Muderris,
Izmir Bakircay University, Turkey
Lisheng Yu,
Peking University People's Hospital, China

***Correspondence:**
Bernd Fritzsch
bernd-fritzsch@uiowa.edu

Specialty section:
This article was submitted to Cellular and Molecular Mechanisms of Brain-aging, a section of the journal Frontiers in Aging Neuroscience

Received: *13 November 2021*
Accepted: *03 January 2022*
Published: *17 February 2022*

Citation:
Elliott KL, Fritzsch B, Yamoah EN and Zine A (2022) Age-Related Hearing Loss: Sensory and Neural Etiology and Their Interdependence. Front. Aging Neurosci. 14:814528. doi: 10.3389/fnagi.2022.814528

INTRODUCTION

Age-related hearing loss (ARHL) is a significant issue that leads to a reduced hearing perception in older humans. Half of the adult men over the age of 70 have ARHL (Roccio et al., 2020; Yamoah et al., 2020; Wu et al., 2021), which makes it a significant public health concern. The World Health Organization (WHO) predicts that there will be approximately 1 billion people over the age of 65 by the year 2050. Thus, ARHL is poised to be a substantial problem. ARHL involves a combination of conductive hearing loss (middle ear defects) and/or neurosensory hearing loss (loss of hair cells or neurons). It may also involve second-order neuron functional decline in the cochlear nuclei (CN) and associated superior

olivary complex (SOC) (Makary et al., 2011; Lang, 2016; Caspary and Llano, 2018; Fattal et al., 2018; Dubno, 2019; Syka, 2020). Roughly 30% of women and men older than 65 have a reduced hearing sensitivity (Homans et al., 2017; Eggermont, 2019) affecting approximately 600 million people worldwide who may develop a progressive neurosensory hearing loss. Overall, one can imply that about 90% of people aged 90 years and older will eventually suffer from overt hearing loss unilaterally, affecting at least one ear (Sheffield and Smith, 2019). Aging also decreases sound localization accuracy and the ability to detect weak signals in noise.

Additionally, the repeated noise exposure begets noise-induced hearing loss (NIHL), which may exacerbate ARHL. These deficits may also indirectly affect cognition through decreased social activities and communication (Dubno, 2019; Eckert et al., 2019; Syka, 2020). A better understanding of the aging auditory system mechanisms and eventually replacing lost hair cells and sensory neurons to maintain hearing is required to help those with hearing replacement, including cochlear implants.

Currently, mouse models are the most common model of ARHL. The model appears to have limited transformation of supporting cells into HCs (Walters et al., 2017; Yamashita et al., 2018; Roccio et al., 2020; Li et al., 2020). In contrast, age-related hearing loss is understudied compared to earliest hair cell replacements (Zine et al., 2014, 2021; Devare et al., 2018; Yamoah et al., 2020). Notably, we realize that the stages of mouse development are different compared to humans (Lim and Brichta, 2016; Wang et al., 2018): a 2-year-old mouse is equivalent to a ∼70-year-old human (**Figure 1A**). The corresponding human age to which hair cells are lost, leading to a particularly profound hearing loss in a mouse (Rauch et al., 2001; Kusunoki et al., 2004; Eggermont, 2019; Sheffield and Smith, 2019) depends upon the specific mouse strain (Zheng et al., 1999). Age-related hearing loss and changes in hearing of aged people have been identified at many levels across the entire auditory system, from the cochlear hair cells to the CN to the SOC. Reviews have reported central auditory dysfunction, including the downregulation of synaptic inhibition due to peripheral deafferentation and maladaptive plasticity. Aging-related decreases in synaptic inhibition (Stebbings et al., 2016; Caspary and Llano, 2018) may be triggered by high metabolic demands that lead to inhibitory neurons that being affected, while the relative to the decline of their excitatory counterparts (Kann et al., 2014), yielding an inhibitory-excitatory imbalance. Metabolic demands may be higher in the auditory brainstem, including the SOC, due to having high firing rates of neurons (Sanes and Rubel, 1988; Kujawa and Liberman, 2009), potentially making them more vulnerable to aging-related declines. Recent data suggest that lateral superior olivary neurons (LSON) are more resistant to metabolic stress than SOC overall (Brosel et al., 2018).

Hair cell loss is one of the early signs leading to the progressive worsening of the organ of Corti (Pauley et al., 2008; Taylor et al., 2012; Kersigo and Fritzsch, 2015; Herranen et al., 2020; Wu et al., 2021). The loss of spiral ganglion neurons (SGN), cochlear nuclei (AVCN, PVCN, DCN), and superior olivary complex (SOC) may follow or may occur in tandem. A common consequence of hair-cell loss is a flat epithelium (Shibata et al., 2010), which constitutes a predominated clinical situation of hearing loss that requires a future cure (Yamasoba et al., 2013; Yang et al., 2015; Homans et al., 2017; Revuelta et al., 2017; Dawson and Bowl, 2019; Dubno, 2019; Lopez-Juarez et al., 2019). Several studies have focused on various aspects of age-related hearing loss prevention, while others work toward the therapy (Schilder et al., 2019; Eshraghi et al., 2020; Roccio et al., 2020; Sekiya and Holley, 2021). For instance, cochlear implants (CI) are effectively used to functionally replace hair cells (Gantz et al., 2018, 2005). In addition, current approaches are attempting to define in detail the genetic basis of ARHL (Lewis M. A. et al., 2018). Improved hearing loss measurement (Simpson et al., 2019; Cassarly et al., 2020) will guide the restoration of hair cells to ameliorate hearing loss.

The presented review will describe mouse mutants to endorse a genetic model with a flat auditory epithelium and associated loss of sensory neurons of the ear and the brainstem. We aim through this approach to inspire innovative research and novel interventions by framing the hallmarks of aging (Campisi, 2013; López-Otín et al., 2013; Sekiya and Holley, 2021) to improve the upcoming translatability of present restoration challenges. Developing those leads to novel mouse models to deal with the strengths and weaknesses. It would be helpful to develop restoration strategies that are temporally mountable from postnatal to old age. Age-dependent dysregulation of the cochlear duct endolymph composition is a problem (Dubno, 2019) that aggravates neuronal loss (Lang, 2016; Elliott et al., 2021b) and are other avenues of investigation. Their possible restoration for hearing perfection is being explored (Gantz et al., 2018; Yamoah et al., 2020). We focus on hair cells, sensory neurons, cochlear nuclei, and the MOC innervation as late-age-related restoration targets.

HAIR CELL LOSSES BEGIN IN THE OUTER HAIR CELLS FOLLOWED BY INNER HAIR CELL LOSS

Hair cells and supporting cells form the functional cellular assembly in the organ of Corti in the inner ear (Fritzsch et al., 2006; Groves and Fekete, 2017). In mice, hair-cells exit the cell cycle around embryonic days E12–14 in an apex to base progression (Ruben, 1967; Matei et al., 2005). In humans, this happens around gestational weeks GW12 (Locher et al., 2013). Many transcription factors and other genes are involved in cochlear hair cell development. For instance, *Eya1*/*Six1* early gene expression (Zou et al., 2004; Ahmed et al., 2012; Li et al., 2020; Xu et al., 2021) is followed by *Sox2* (Kiernan et al., 2005; Dvorakova et al., 2016, 2020). Other genes are needed such as *Gata3* (Karis et al., 2001; Duncan and Fritzsch, 2013; Walters et al., 2017), *Pax2* (Bouchard et al., 2010; Kempfle and Edge, 2014), *Shh* (Riccomagno et al., 2005; Muthu et al., 2019), and *miR-183* (Pierce et al., 2008; Kersigo et al., 2011).

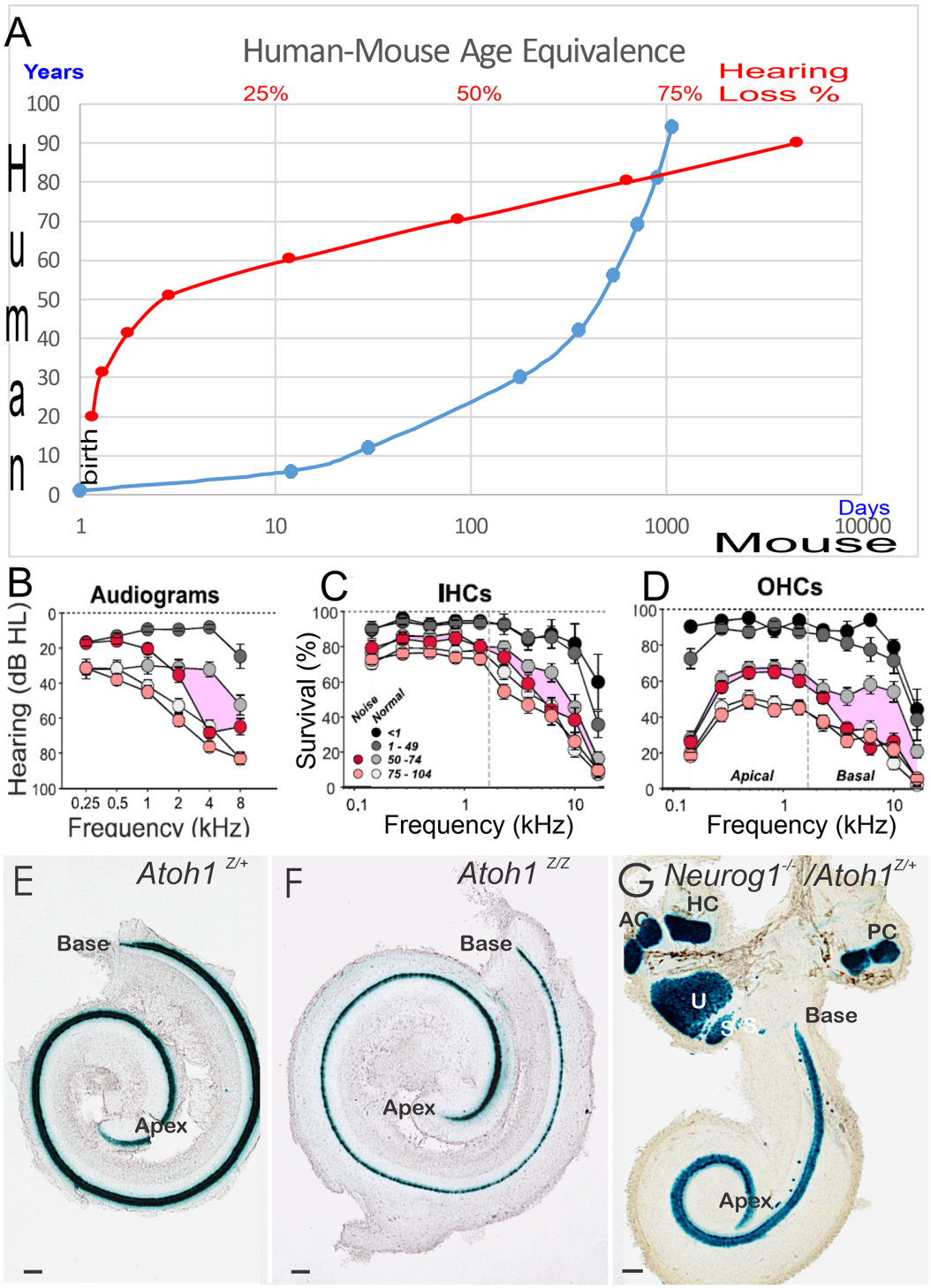

FIGURE 1 | Panel **(A)** provides an overview of a 70-year-old human comparable to a 2-year-old mouse. The age group in humans displays profound hearing decay, shown as percent (%) of hearing loss (**A**, in red) follow-on hearing loss of 90-year-old humans. Limited restoration is attempted that has focused on 2-year or mostly younger mice, that is driven by the cost of keeping animals to old age and is providing a lack of decent models. Audiograms **(B)** and histology **(C,D)** demonstrated the loss of IHC **(C)**, OHC **(D)**, and the progressive threshold reduction in older people shown with the audiogram **(B)**. Note that people exposed to noise have an additional loss in hair cells **(C,D)** and show a threshold reduction in the audiogram **(B)** in the middle age of 50–74 years old. In newborn mice, we demonstrate the phenotype of *Atoh1* LacZ in control mice **(E)** Atoh1LacZ/LacZ null mice **(F)** is comparable (i.e., a single row of undifferentiated IHCs). Compared to *Neurog1* null mice, a shorter cochlea has outliers in the GER area **(G)**. Data were taken from the Jackson lab, WHF, and Fritzsch et al. (2005), Matei et al. (2005), Sheffield and Smith (2019), and Wu et al. (2021). Scale bars: 100 μm **(E–G)**.

In addition, we know of several *Lim* domain factors such as *Isl1* (Huang et al., 2008; Chumak et al., 2016) and *Lhx3* (Hertzano et al., 2007) that are needed for normal development of the cochlear hair cells. A unique loss of *Lmx1a* (Huang et al., 2008, 2018; Nichols et al., 2008, 2020) and its interaction with *Lmx1b* (Chizhikov et al., 2021) regulates the development of all cochlear hair cells, comparable to deletions of either *Pax2* (Bouchard et al., 2010) or *Shh* (Muthu et al., 2019). Another subset of early transcription factors is known for proliferation, such as $p27^{kip}$ (Löwenheim et al., 1999; Zine et al., 2014), n-*Myc* (Kopecky et al., 2011), and *Prox1* (Fritzsch et al., 2010).

Atoh1 expression is an essential early step of all inner ear hair cell differentiation (Bermingham et al., 1999; Fritzsch et al., 2005; Pan et al., 2012; **Figures 1E–G**). It is required for healthy sensory hair cell development in a cyclical sequential fashion (Fritzsch et al., 2006; Kageyama et al., 2019; Tateya et al., 2019). *Atoh1* can induce the naïve epithelial cells into hair cells, but the viability of those cells is limited (Jahan et al., 2018; Atkinson et al., 2019). Beyond neonatal cell conversion (Mantela et al., 2005; Kelly et al., 2012; Koehler et al., 2017; McGovern et al., 2019) using pluripotent stem cells (van der Valk et al., 2021; Zine et al., 2021) to make novel cochlear hair cells that are inner- and outer hair cell-specific is beyond our current ability. Cellular deviations are regularly observed in aged materials and almost all aspects of the cell, including nuclear structure, cellular state, mitochondria, genetic material, and protein function that reduce the outer and inner hair cells with time (Kersigo and Fritzsch, 2015; Chessum et al., 2018; Wiwatpanit et al., 2018; Driver and Kelley, 2020; Filova et al., 2020; Herranen et al., 2020). Notably, several later transcription factors interact to maximize the generation of cochlear hair cells (Chen et al., 2021). Approximately 300 genes are identified and associated with ARHL (Bowl et al., 2017). *TMC1/2* is vital for the normal formation of hearing function (Yoshimura et al., 2019; Erives and Fritzsch, 2020), as well as *Cdh23* and *Pcdh15*, which together form the tip links of stereocilia (Elliott et al., 2018; Qiu and Müller, 2018).

Outer hair cells degenerate before inner hair cells in older humans and mice (Spongr et al., 1997; Kane et al., 2012). Specifically, early loss of OHC is pronounced in specific mutations, such as inactivated *Manf* or loss of *Atg7* (Herranen et al., 2020; Perkins et al., 2020; Zhou et al., 2020). Loss of OHCs occurs at different degrees depending on mouse strains. For example, ∼80% of OHCs are lost by 26 months of age in C57bl6 mice. In contrast, only ∼50% are lost in CBA mice by 26 months. Indeed, in CBA strains, ∼100% of hair cells are intact until 18 months. Among the first early loss that affects IHCs, are specific mutants such as *Srrm3/4* (Nakano et al., 2012, 2020) followed by loss of *Cdc42* (Ueyama et al., 2014) and *Arhgef6* (Zhu et al., 2018). Loss of OHC, followed by IHC using a novel diphtheria toxin, was shown in postnatal mice (Tong et al., 2015).

In humans, a loss of OHCs is followed by IHCs that progresses around 65 years of age (Nadol Jr and Xu, 1992; Rauch et al., 2001; Liu et al., 2021). A most detailed description was recently provided that shows a comparable loss of OHCs and IHCs (Wu et al., 2021) that reduces IHCs ∼50% in the base of ∼75-year-old humans, compared to ∼40% in the same region of OHCs (**Figures 1C,D**). Interestingly enough, in older people with noise-induced hearing loss (NIHL) and/or age-related hearing loss (ARHL), there is a progressive loss of OHC in the base. In contrast, the nearby IHCs remain near normal. Compared to the high-frequency loss, progressive ∼50 dB SPL at about 75-year-old to ∼60 dB SPL affects nearly 85-year-old or older humans (**Figure 1B**). Unfortunately, much of the current biological restorative strategies focus on the earliest induction of new hair cells, knowing well that the delayed loss of cochlear hair cells happens about 60 years later (**Figure 1A**).

Generating vestibular and cochlear hair cells from human pluripotent stem cells have begun the earliest major steps, as mentioned above (Koehler et al., 2017; Lahlou et al., 2018; Patel et al., 2018; Romano et al., 2021; van der Valk et al., 2021; Zine et al., 2021). To date, no one has succeeded in producing both types of the organ of Corti sensory hair cells *in vitro* in the correct proportion and disparity distribution needed for the restoration of hair cells within the organ of Corti. Many issues remain open, but we have no solution at hand, turning the feasibility of producing hair cells with following repopulation of the damaged organ of Corti into a future option (Liu et al., 2021). Restoration of the flat auditory non-sensory epithelium between the lingering patches of hair cells (Pirvola et al., 2002; Kiernan et al., 2005; Soukup et al., 2009; Pan et al., 2012; Duncan and Fritzsch, 2013; Herranen et al., 2020) also requires restoration of innervation to the newly molded hair cells. Concentrating on the proliferation and transdifferentiating of undistinguishable epithelial cells of the flat epithelium requires several steps that need to be taken before precursor cells can respond with genes like *Sox2* and *Atoh1* (Dabdoub et al., 2008; Nyberg et al., 2019; Dvorakova et al., 2020; Yamoah et al., 2020). Appropriate hair cell differentiation in the aging cochlea is the prime objective of hair cell regeneration. Artificial gene governing networks (Ausländer et al., 2012; Sedlmayer et al., 2018; Xie and Fussenegger, 2018; Krawczyk et al., 2020) can be used to drive *Sox2* and *Atoh1* in an oscillatory dynamic manner in BMP4-positive cells. We predict a cargo load of 25 kb is required for this oscillatory gene regulation, well within the choice of the helper-dependent adenovirus (HdAd; 37 kb). It assumes that BMP4 expressing cells can activate and the generation of the LuxR protein will enable the activation of the LuxI, AiiA, and Sox2 proteins. Oscillation will initiate the level of Sox2 gene expression, activating *Atoh1* gene (Neves et al., 2012; Alonso et al., 2018). The expression of the Atoh1 protein can act as positive feedback on its enhancer (Pan et al., 2012) and can provide a negative feedback loop back onto *Sox2* (Dabdoub et al., 2008; Kempfle et al., 2016; Yamoah et al., 2020). Once hair cell differentiation has initiated, *BMP4* expression can be reduced using a negative feedback loop (Lewis R. M. et al., 2018). Eventually, the gene regulation system will shut down after time, leaving feedback loops in the differentiating hair cells to complete the process. Hair cell formation is required to be induced in all age and classes of mice, from young to adult, requiring a scalable expression to

take advantage of using synthetic biology to directly repopulate the flat epithelium from undifferentiated supporting cells into cochlear hair cells.

In summary, the progressive loss of cochlear hair cells depends on a large number of genes (Liu et al., 2021) that results in the flat auditory epithelium and requires a re-establishment of normal hair cells for hearing restoration. Alternative approaches, such as incorporating induced hair cells into the cochlea, are challenging. In this case, the hair cells would die once they are exposed to the endolymphatic fluid containing high potassium levels (∼140 mM). Early development of hair cells is possible, but the induction of novel hair cells to replace lost hair cells in old mice and humans remains a future biological treatment option.

SPIRAL GANGLION NEURONS DEVELOP INDEPENDENT OF HAIR CELLS AND COCHLEAR NUCLEI

The sensory neurons of the cochlea, the spiral ganglion neurons (SGNs), depend on *Neurog1* (Ma et al., 1998, 2000; Elliott et al., 2021b) and are myelinated by Schwann cells (Mao et al., 2014; Kersigo et al., 2021). Neurons begin proliferation in a base-to-apex progression around embryonic days E10–12 in mice (Ruben, 1967; Matei et al., 2005), equivalent to gestational week (GW10) in humans (Locher et al., 2013). Central fibers reach the cochlear nuclei at about E12.5, followed by peripheral innervation of hair cells at E14.5 (Yang et al., 2011; Schmidt and Fritzsch, 2019).

The genes, *Eya1* (Xu et al., 2021), *Sox2* (Dvorakova et al., 2020), *Shh* (Muthu et al., 2019), *Pax2* (Bouchard et al., 2010), *Lmx1a/b* (Chizhikov et al., 2021), *Dicer/miR-183* (Kersigo et al., 2011), *Fgf7/10* (Pauley et al., 2003; Urness et al., 2018), and *Neurog1* (Ma et al., 1998, 2000; Elliott et al., 2021b), among others, are required to induce the formation of spiral ganglion neurons, as well as cochlear nuclei. Downstream of *Neurog1*, a subset of transcription factors are upregulated to promote SGN differentiation, including *Neurod1* (Jahan et al., 2010a; Macova et al., 2019), *Pou4f1* (Huang et al., 2001), *Gfi1* (Matern et al., 2020), *Isl1* (Radde-Gallwitz et al., 2004; Chumak et al., 2016), and others. Additional factors are also required to maintain spiral ganglion neurons as they project to the cochlear nuclei (Brooks et al., 2020). Expression of the neurotrophins, *Bdnf* and *Ntf3*, are needed for maintaining SGNs (Yang et al., 2011; Fritzsch et al., 2016), and in their absence, no SGNs survive. In the absence of SGNS, the ear initially develops near normally; however, after approximately 2 months, cochlear hair cells degenerate (Kersigo and Fritzsch, 2015). In addition, an early loss of SGNs results in a reduced number of cochlear nuclei neurons (**Figures 2B,C**) (Dvorakova et al., 2020; Filova et al., 2020), consistent with an early loss in chicken (Levi-Montalcini, 1949). However, unlike in neonates, loss of the ear has less of an effect on cochlear nuclei survival in older mice, suggesting a critical window (Rubel and Fritzsch, 2002; Harris and Rubel, 2006). Our recent data show that vestibular afferents from transplanted mouse ears can innervate the vestibular nuclei of chickens, thus providing a novel approach to eventually replace ears (Elliott and Fritzsch, 2018). Currently, though, cochlear implants are the only means to restore hearing following a sensorineural hearing loss, so long as enough SGNs survive in humans to transmit the sound stimulation from the ear to the cochlear nucleus (Gantz et al., 2005, 2018). In cats, stimulating the ears will reform the cochlear nuclei and develop large endbulbs of Held (Ryugo et al., 2005) and this likely also happens in humans (Kral et al., 2013). Interestingly enough, a set of miR's show a progressive reduction in cochlear nuclei (Krohs et al., 2021) that acts in parallel to *Dicer* dependent mutations (Kersigo et al., 2011).

The development of SGNs is independent of both cochlear nuclei and cochlear hair cells (Rask-Andersen et al., 2005). Studying the growth and differentiation of SGNs could inform the steps needed to induce otic progenitors to replace lost neurons (Song et al., 2017, 2019; Karlsson et al., 2019). SGN projections follow a simple tonotopic organization (**Figures 2G,H,H'**): basal projection of the cochlea reaches the most dorsal part of the cochlear nuclei, whereas the apex reaches the ventral aspect of the cochlear nuclei (Muniak et al., 2016; Fritzsch et al., 2019). Following the loss of *Neurod1*, there is a reduction in the number of SGNs and a reorganization of these neurons that result in mixed innervation of auditory and vestibular targets and also a loss of tonotopic organization in the cochlear nuclei (Macova et al., 2019; Filova et al., 2020). A somewhat similar reorganization results from the loss of *Nrp2* that shows a disorganized central cochlear projection (Lu et al., 2014; Schmidt and Fritzsch, 2019). Interestingly, SGNs project to the cochlear nuclei in the absence of *Atoh1* (Fritzsch et al., 2005) where they maintain their tonotopic representation of the periphery (Elliott et al., 2017). In addition, SGNs project peripherally in the absence of *Atoh1* and *Pou4f1* (Xiang et al., 2003) to reach the flat epithelium in the absence of cochlear hair cells (Pauley et al., 2008). The latter demonstrates that SGNs form in the absence of hair cells, suggesting long-term retention of the 'de-innervated' neurons (**Figure 2A**) in humans (Nadol Jr, 1990; Nadol Jr and Xu, 1992), cats (Stakhovskaya et al., 2008), and mice (White et al., 2000) whereas neurons of rats degenerate faster within months after the loss of all hair cells (Alam et al., 2007).

Two types of SGNs neurons are known, type I and type II, to innervate the inner hair cells (Petitpré et al., 2018; Shrestha et al., 2018; Sun et al., 2021) and the outer hair cells (Shrestha and Goodrich, 2019; Elliott et al., 2021a), respectively. Innervation of the hair cells occurs in a progression, starting at E18 (Fritzsch et al., 1997) and finishing at about P14 (Petitpré et al., 2018; Shrestha and Goodrich, 2019). In the absence of cochlear hair cells, projecting peripheral neurites of SGNs reach out (Xiang et al., 2003; Fritzsch et al., 2005; Pauley et al., 2008; Pan et al., 2012; Tong et al., 2015), but do not expand beyond the flat auditory epithelium (Shibata et al., 2010). As mentioned above, there is a reduced number of neurons after *Neurod1* deletion and an effect on hair cells in the cochlear apex (Jahan et al., 2010b; Macova et al., 2019). In addition, loss of *Neurod1* results in the conversion of some neurons into hair cells after upregulation of *Atoh1* (Elliott et al., 2021b). Furthermore, in *Neurod1* mutant mice, some OHC are converted into IHC-like

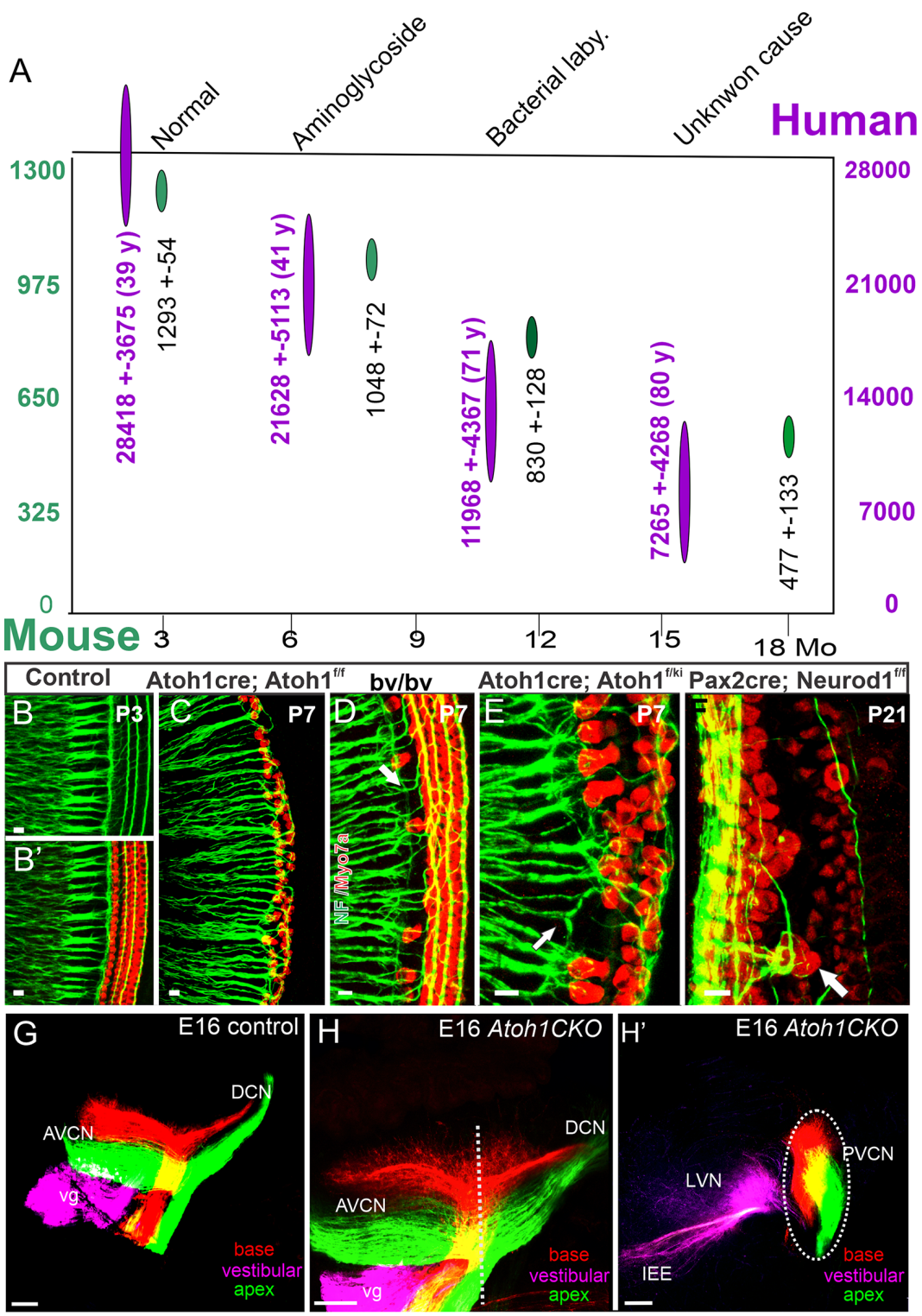

FIGURE 2 | A loss of neurons with time reduces the ~ 28,000 SGNs in ~40-year-old humans to ~25% in 80-year-old humans (**A**, purple). A similar loss is shown for ~1,300 SGNs and reduces to ~40 in 18 month-old mice (**A**, green). Immunoreaction of labeling for neuron markers validates the inner ear afferents in control mice **(B,B')**. This is compared with *Atoh-cre;Atoh1*$^{f/f}$ 'self-termination mice **(C)**, Bronx waltzer (*bv/bv*) **(D)**, *Atoh-cre;Atoh1*$^{ki/f}$ **(E)**, and Pax2-cre;*Neurod1* **(F)**. Central projections reach the anterior (AVCN) and dorsal (DCN) cochlear compared to controls **(G)** and *Atoh*1 *CKO* mice **(H)** that show a tonotopic organization of SGN central projection, despite the absence of cochlear hair cells **(H')**—modified after Nadol Jr (1990), White et al. (2000), Jahan et al. (2018), and Filova et al. (2020). Scale bars: 10 μm **(B–F)** and 100 μm **(G–H)**.

cells (**Figure 2F**) and are innervated by putative type I SGNs (Jahan et al., 2018; Filova et al., 2020). Reorganization of innervation has been shown in *Srrm4* mutant mice. In these mice, IHCs are primarily absent (**Figure 2D**), and type I SGNs innervate the OHCs instead can enforce some of the type I to innervate IHC instead of OHC (**Figures 2B,C**) (Nakano et al., 2012; Jahan et al., 2018). Replacement of one allele of *Atoh1* with *Neurog1*, in which the other *Atoh1* allele is conditionally knocked out, can lead to the formation of near-normal hair cells (**Figure 2E**) that also receive innervation (Jahan et al., 2015). A unique defect of SGNs is observed at a certain reduction level of specific stimulation in mice (Kujawa and Liberman, 2009) that requires additional information in humans (Wu et al., 2021).

In summary, SGNs project centrally to the cochlear nucleus and peripherally to the hair cells. SGNs show a tonotopic organization to the cochlear nuclei even in the absence of hair cells, which is beneficial for cochlear implants. Likewise, in the absence of hair cells, long-term retention of SGNs is demonstrated and ramified within the "flat auditory epithelium" that could possibly be re-connected with novel hair cells in the near future.

COCHLEAR NUCLEI DEPEND ON TRANSCRIPTION FACTORS THAT MAY CHANGE WITH AGE

The cochlear nucleus is the first information processing center for auditory information within the central nervous system and provides output to the superior olivary cells (SOC) and the inferior colliculi (IC) (Malmierca and Ryugo, 2011; Oertel and Cao, 2020). It comprises three subnuclei: anteroventral cochlear nucleus (AVCN) from rhombomere 2 and 3 (r2, 3), posteroventral cochlear nucleus (PVCN; r4), and dorsal cochlear nucleus (DCN, r5). Most cochlear nuclei neurons exit the cell cycle around E10–14 except for the delayed formation of granule cells that finish at E18 in mice (Pierce, 1967). *Atoh1* is a major bHLH gene that defines the cochlear nuclei. It is expressed in regions of the rhombic lip of the hindbrain that contribute cells to the cochlear nucleus. Conditional deletion of *Atoh1* in r3/5 impaired cochlear nucleus formation in those regions (Maricich et al., 2009)., without *Atoh1*, there is no formation of cochlear nuclei (Wang et al., 2005; Fritzsch et al., 2006; Ray and Dymecki, 2009). However, as mentioned earlier, in the absence of *Atoh1*, a near-normal central projection develops (**Figures 3E,F**) of SGNs (Elliott et al., 2017). Notably, a delayed loss of *Atoh1* can be driven by *Pax2* (**Figures 3C,D**). Upstream of *Atoh1* is the expression of *Lmx1a/b* (Chizhikov et al., 2021). Without expression of *Lmx1a/b*, there is a loss of *Gdf7* (Lee et al., 2000), *Atoh1*, and *Wnt3a* expression, and there is no formation of the choroid plexus (Chizhikov et al., 2021; Elliott et al., 2021b). In addition, without *Lmx1a/b*, all aspects of the cochlea are eliminated beyond an undifferentiated sac, including no differentiation of cochlear hair cells or SGNs (**Figures 3A,B**). Additional transcription factors have been identified for cochlear nuclei formation (Milinkeviciute and Cramer, 2020). For instance, *Hoxb1* is expressed in r4 in the PVCN and parts of the DCN (Di Bonito et al., 2017).

The cochlear nuclei have defined numerous cell types based on morphological and physiological criteria (Oertel and Cao, 2020). Synapses from type I SGNs onto bushy cells in the AVCN have structural adaptations that receive the endbulbs of Held; the endbulb of Held permits highly secure signaling between the auditory periphery of SGN and bushy cells (Manis et al., 2012; Caspary and Llano, 2018; Syka, 2020; Wang et al., 2021). Losing proper auditory innervation that leads to a simplification of the endbulb termination (Muniak et al., 2016). Local inhibitory cells in the cochlear nucleus are known as either glycinergic (e.g., D-multipolar, vertical, and cartwheel) or as GABAergic [stellate and Golgi; (Young and Oertel, 1998; Oertel and Cao, 2020)] that receive the SGN projections. Genomically are clustered as miR-183 and miR-96 that reduces the volumes of auditory hindbrain nuclei. Electrophysiological analysis shows that the calyx of Held synapses on the medial nucleus of the trapezoid body (MNTB) demonstrated strongly altered synaptic transmission in young-adult mice (Krohs et al., 2021).

Aging-related changes are known to a certain extent, followed in neuronal morphology and biochemistry in the cochlear nucleus and SOC. The size of the AVCN remains constant with aging, whereas its cell density decreases with age. Moreover, cellular density correlates with aging-related loss of cochlear sensory neuron input. In addition, the cellular density diminishes by about 15% at 7 months of age in certain mice (C57BL/6). Still, it does not show a reduction of cellular density until the 2nd year of life in CBA/CaJ mice (Willott et al., 1987). The reduction of cellular density is complemented by a drop in the size of synaptic terminals by AVCN neurons (Briner and Willott, 1989; Helfert et al., 2003). The volume of the DCN and cell number and size of aging-related decreases have been detected in C57BL/J, suggesting that the losses are related to hearing loss. Changes have been detected in the octopus cell area of the PVCN. Interestingly enough, changes seen in both C57BL/J and CBA/CaJ mice indicate a different aging-related effect (Willott and Bross, 1990; Jalenques et al., 1995). The morphology of the cochlear nucleus in humans with presbycusis suggests an increase in the total cell number and number of multipolar and granule neurons in the cochlear nucleus with aging (Hinojosa and Nelson, 2011), a contradictory result that requires additional work (Syka, 2020).

The calcium-binding proteins parvalbumin, calbindin, and calretinin play a leading role in buffering intracellular calcium during cellular stress in all cochlear nuclei (Lohmann and Friauf, 1996). For example, calretinin-, calbindin-, and parvalbumin-positive cells are perceived in the DCN and PVCN of aged mice; this increase of the three proteins is correlated with hair cell loss (Idrizbegovic et al., 2003; Caspary and Llano, 2018). Recent data suggest the total number of neurons in the DCN and PVCN is decreasing while the proportion of parvalbumin- and calretinin-positive neurons (**Figure 3G**) is increasing (Idrizbegovic et al., 2006; Syka, 2020). Hearing loss goes beyond the three proteins that are the only factor in these increases. Moreover, induced

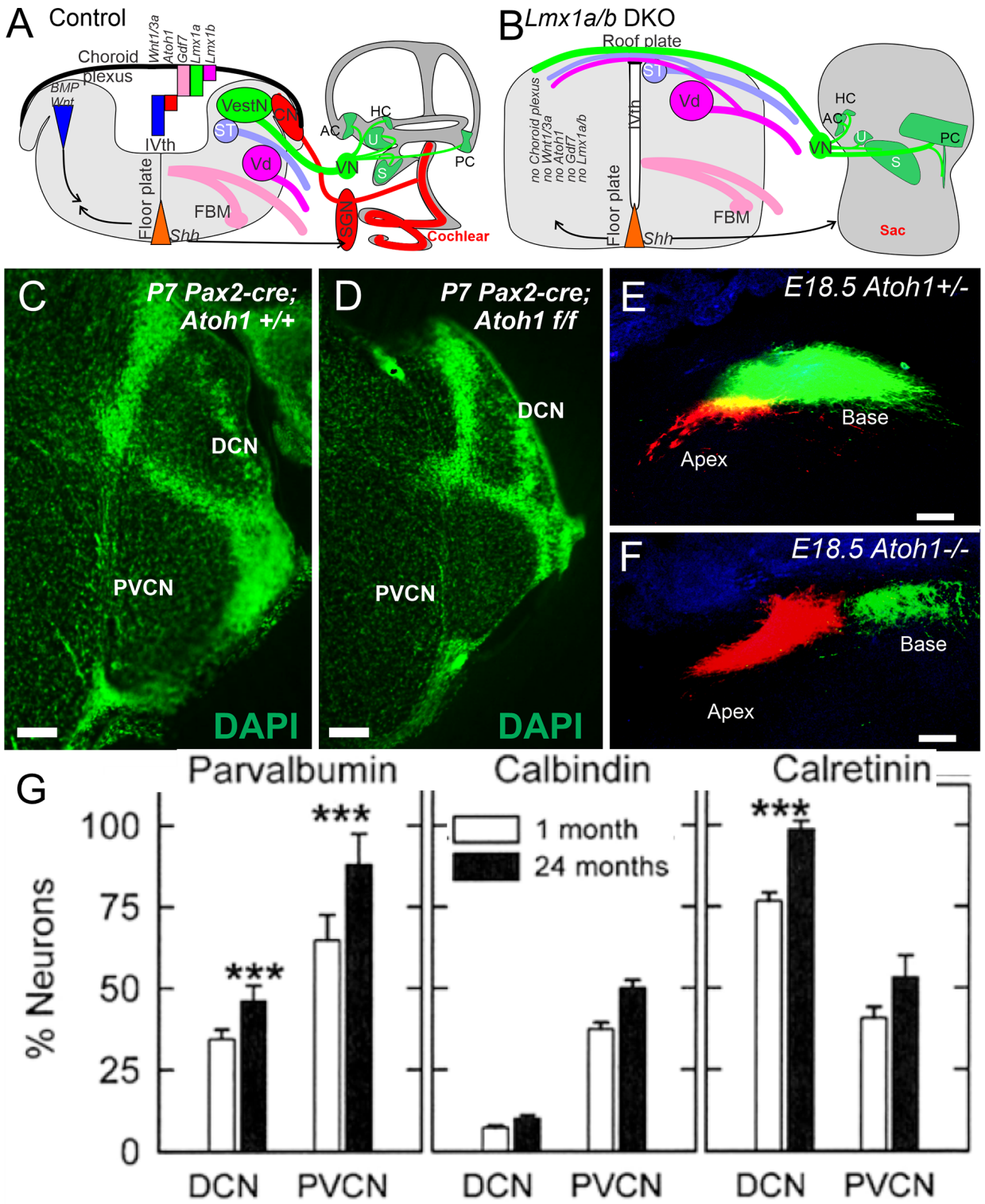

FIGURE 3 | Cochlear nuclei depend on *Lmx1a/b*, upstream of *Gdf7*, *Atoh1*, and *Wnt3a* **(A)**. In the absence of *Lmx1a/b* neither cochlear hair cells, spiral ganglion neurons, nor cochlear nuclei develop **(B)**. The choroid plexus is replaced by a roof plate that allows fibers to cross to the contralateral side **(A,B)**. Cochlear nuclei are smaller in a conditional deletion of *Atoh1* using Pax2-cre **(C,D)**. In *Atoh1*-null mice, there is a normal central projection of SGNs without either peripheral hair cells or cochlear nuclei **(E,F)**. Expression of Parvalbumin, Calbindin and Calretinin showing upregulation in the cochlear nuclei at the level of DCN and PVCN areas that increase in some but not all neurons **(G)**. Modified after Idrizbegovic et al. (2006), Elliott et al. (2017, 2021b), and Chizhikov et al. (2021). Scale bars: 100 μm **(C–F)**. *** indicates significance.

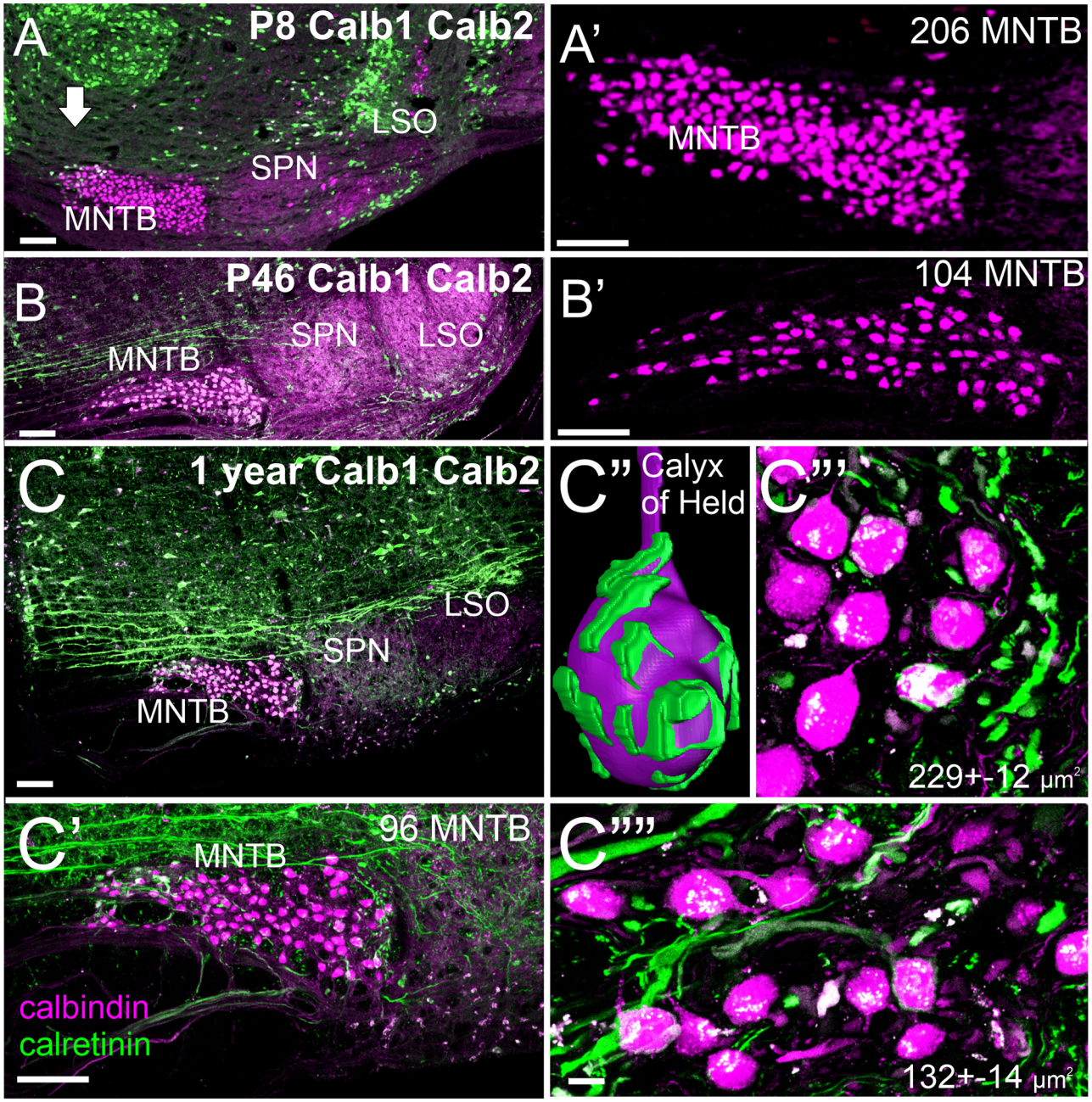

FIGURE 4 | Early expression of *Calbindin* (*Calb1*) and *Calretinin* (*Calb2*) expression in the MNTB at P8 **(A,A')**. *Calb1* expression increases in the LSO by P46 **(B,B')**. At 1 year of age, there is minimal *Calb1* expression in the LSO and SPN. *Calb2*-positive fibers form a calyx of Held in the MNTB **(C–C'''')**. Within the MNTB, there are larger *Calb1*-positive cells close to the cochlear nucleus (~229 μm^2) compared to much smaller cells closer to the midline (~132 μm^2). Our expression shows upregulation of *Calb2* in the MNTB (compare P8 with P46) that progressively upregulates with *Calb1*. Note that fewer MNTB are shown in a single section that likely comes about through lateral distributions. P: postnatal, Bar indicates 100 μm in **(A–C,C')**, 10 μm in **(C''',C'''')**.

hearing loss may cause a *lessened* effect of calretinin-positive neurons in layer III of the aged DCN, innervating the fusiform neurons (Zettel et al., 2003; Syka, 2020) in the human cochlear nucleus. Note that all three calcium-binding proteins decrease progressively from adult to old age (Sharma et al., 2014). The differences in intracellular calcium mobilization may play a role to confirm the differences between the human and mouse data (Ibrahim and Llano, 2019).

Changes with aging in the cochlear nucleus are known to degrade the spiking activity in opposition to temporally patterned impetuses. The Fischer 344 rat showed aging-related decreases in glycine binding sites. In addition, receptor subunits

in the cochlear nucleus are declining (Wang et al., 2009; Caspary and Llano, 2018). Reduction and loss of inhibition are most likely mirrored in cochlear nucleus neurons' firing possessions. Thus, cartwheel and fusiform cells show increased acoustically driven responses in the aging cochlear nucleus. This activity will reflect the loss of inhibition (Caspary et al., 2006; Caspary and Llano, 2018). Physiologically, numerous studies show the temporal fidelity that breaks down at the synapse between cochlear nerve fibers and bushy cells in old mice (Xie, 2016; Xie and Manis, 2017; Wang et al., 2021). These data suggest multiple instruments may be responsible for the aging-related temporal spreading of cochlear nucleus neuronal responses from temporally patterned sounds. Moreover, the first longitudinal investigation of different type Ia is positive for calretinin and innervates the bushy neurons.

In summary, we show that cochlear nuclei depend on *Lmx1a/b* and *Atoh1* and require further studies with heterozygotes to identify the long-term defects in mice. Preliminary data suggest a distinct effect of upregulation of parvalbumin and calretinin that could upregulate the relative calbindin expression and suggest a long-term reduction of calretinin that innervates the bushy cells. No new cochlear nuclei are needed as they survive in the absence of SGNs.

SUPERIOR OLIVE COMPLEX IS AFFECTED BY VARIOUS AUDITORY SYSTEM LOSSES

The superior olivary complex (SOC) is the second major station in the ascending auditory pathway, which consists of the first input at which information from the two ears is combined for binaural information in the central auditory system. The SOC nuclei involved in processing ascending information are the medial superior olive (MSO), lateral superior olive (LSO), and medial nucleus of the trapezoid body (MNTB; Marrs et al., 2013). These three major SOC nuclei play a critical role in sound localization ability, which is known to diminish with age (Caspary and Llano, 2018; Syka, 2020). In mice, neurons are born between embryonic days E9–14 with the latest differentiated neurons in the LSO (Pierce, 1973).

Recent data suggest that the SOC complex is generated in part by dorsal neurons from *Atoh1*-positive cells that identify their contribution to distinct migrating SOC cells (Maricich et al., 2009; Marrs et al., 2013; Di Bonito et al., 2017; Lipovsek and Wingate, 2018). In addition to *Atoh1*, there is a combined expression of *Wnt3a* and *En1* (Jalabi et al., 2013; Altieri et al., 2015; Chizhikov et al., 2021) that are important for the SOC. A noticeable difference is in the SOC of the chicken that generates more caudal nuclei (Lipovsek and Wingate, 2018). A clear progression in Calbindin, Calretinin, and Parvalbumin expression that require a generation of SOCs is demonstrated by tracing and immunological data (Lohmann and Friauf, 1996; Kandler et al., 2020).

Very few studies have investigated variations in the MSO, LSO, and MNTB, particularly with aging. For example, Godfrey et al. found that there were no changes in the dry weight of the superior olive complex, but that was significantly reduced in glutamate, glycine, and GABA (Godfrey et al., 2017). Moreover, there is a reduction of about 25% in the level of neurotransmitters with aging in the auditory system. The size of glycinergic and GABAergic cell size has become smaller in the LSO of gerbils of aging (Gleich et al., 2004). Furthermore, decreases in synaptic terminals have been reduced in MNTB in Sprague-Dawley rat with age (Casey and Feldman, 1982, 1985, 1988). An increase in parvalbumin staining in the MSO, but not LSO or MNTB, is reported in primates with aging (Gray et al., 2013). Changes seem to correlate with deviations in peripheral hearing, implying that parvalbumin upregulation may be a part of the mechanism to compensate for the loss of peripheral input from neurons. Beyond significant changes in the synaptic organization in superior olives that have provided few aging-related physiological changes *in vivo* compared with changes in the ABR threshold (Ibrahim and Llano, 2019; Syka, 2020). Older miR-183/96 require studying in much older mice to study the long-term defects (Krohs et al., 2021).

Our initial set of calretinin and calbindin data suggests a slight reduction in the number of MNTB cells (**Figure 4**) consistent with data in rats (Casey and Feldman, 1988). Using a gene regulation of two distinct nuclei showing a fast up- and down-regulation for three nuclei that are all positive for calbindin (**Figures 4A–C**). Whereas the MNTB is calbindin-positive early and keeps this expression, the SPN and LSO show a strong early up-regulation of calbindin followed by near regular expression of calbindin at 1 year of age. An interesting size of MNTB differs between 1 year-old mice: more significant more lateral neurons are becoming more smaller in the medial MNTB (**Figures 4C,C""**). Individual neurons can be traced by calretinin to form a calyx of Held (**Figure 4C"**) that resembles the endbulb of Held of bushy cells (Wang et al., 2021). While all calyx receives innervation from the contralateral cochlea, the size of innervation suggests that smaller MNTB neurons have fewer calyces (**Figures 4C"',C""**). Further work is needed to detail the loss in mice using calretinin, calbindin, and parvalbumin to investigate the effects in mice 24 months or older.

In summary, we know that the migrated SOC nuclei are derived from the dorsal rhombomere. Our preliminary set of calretinin and calbindin data suggest that different complexity and size of MNTB neurons correlate with the size of neurons with aging.

CONCLUSIONS

Our overview shows the earliest loss of cochlear hair cells, spiral ganglion neurons, cochlear nuclei, and associated superior olivary complex: Nearly all four auditory systems depend on *Lmx1a/b, Atoh1*, and *Neurog1* expression. Later, a progressive loss of hair cells occurs with aging, followed by a spiral ganglion neuron reduction to ∼40% in humans and mice. In contrast, early losses of cochlear nuclei have been well described, showing changes in different proteins for survival. How much of the changes are related to compensation for peripheral hearing loss remains an open question, and the impact of adaptation on sound perception remains a subject for future investigations. Auditory

brainstem neurons may be less vulnerable to oxidative stress, which may have high metabolic demands based on neurons' high firing rates. Thus, different mechanisms may interpret for aging declines, in particular, inhibition that affects the auditory pathway. We suggest that the loss of inhibition may, in part, be responsible for temporal fidelity or may be affected by sound localization or may produce dysregulated plasticity. Future work will be of help to explain the causes of changes of aging that ultimately affect the central auditory system that will lead to novel therapeutic objectives to perfect such changes by adding new hair cells and connecting them with remaining SGNs to connect the cochlear nuclei. How much cochlear nuclei and SOC and IC neurons can plastically revert in sizes and complexity of innervation remains to be seen. Additional investigations to uncover the complex reasons for changes in the central auditory system will contribute to developing new healing targets to alleviate sensory ARHL and associated cognitive decline.

AUTHOR CONTRIBUTIONS

This work was conceived by AZ and BF, final revision was drafted by KE, ENY and BF, reviewed by AZ and ENY. All authors edited the final draft in collaboration and approved the submitted version. All authors contributed to the article and approved the submitted version.

FUNDING

Grants to ENY and BF supported this work from the National Institutes of Health (DC016099, DC015252, DC015135, AG060504, AG051443).

REFERENCES

Ahmed, M., Wong, E. Y., Sun, J., Xu, J., Wang, F., and Xu, P.-X. (2012). Eya1-Six1 interaction is sufficient to induce hair cell fate in the cochlea by activating Atoh1 expression in cooperation with Sox2. *Dev. Cell* 22, 377–390. doi: 10.1016/j.devcel.2011.12.006

Alam, S. A., Robinson, B. K., Huang, J., and Green, S.H. (2007). Prosurvival and proapoptotic intracellular signaling in rat spiral ganglion neurons *in vivo* after the loss of hair cells. *J. Comp. Neurol.* 503, 832–852. doi: 10.1002/cne.21430

Alonso, M. B. D., Hernandez, I. L., de la Fuente, M. A., Garcia-Sancho, J., Giraldez, F., and Schimmang, T. (2018). Transcription factor induced conversion of human fibroblasts towards the hair cell lineage. *PLoS One* 13:e0200210. doi: 10.1371/journal.pone.0200210

Altieri, S. C., Jalabi, W., Zhao, T., Romito-DiGiacomo, R. R., and Maricich, S. M. (2015). En1 directs superior olivary complex neuron positioning, survival and expression of FoxP1. *Dev. Biol.* 408, 99–108. doi: 10.1016/j.ydbio.2015.10.008

Atkinson, P. J., Kim, G. S., and Cheng, A. G. (2019). Direct cellular reprogramming and inner ear regeneration. *Expert Opin. Biol. Ther.* 19, 129–139. doi: 10.1080/14712598.2019.1564035

Ausländer, S., Ausländer, D., Müller, M., Wieland, M., and Fussenegger, M. (2012). Programmable single-cell mammalian biocomputers. *Nature* 487, 123–127. doi: 10.1038/nature11149

Bermingham, N. A., Hassan, B. A., Price, S. D., Vollrath, M. A., Ben-Arie, N., Eatock, R. A., et al. (1999). Math1: an essential gene for the generation of inner ear hair cells. *Science* 284, 1837–1841. doi: 10.1126/science.284.5421.1837

Bouchard, M., de Caprona, D., Busslinger, M., Xu, P., and Fritzsch, B. (2010). Pax2 and Pax8 cooperate in mouse inner ear morphogenesis and innervation. *BMC Dev. Biol.* 10:89. doi: 10.1186/1471-213X-10-89

Bowl, M. R., Simon, M. M., Ingham, N. J., Greenaway, S., Santos, L., Cater, H., et al. (2017). A large scale hearing loss screen reveals an extensive unexplored genetic landscape for auditory dysfunction. *Nat. Commun.* 8:886. doi: 10.1038/s41467-017-00595-4

Briner, W., and Willott, J. F. (1989). Ultrastructural features of neurons in the C57BL/6J mouse anteroventral cochlear nucleus: young mice versus old mice with chronic presbycusis. *Neurobiol. Aging* 10, 295–303. doi: 10.1016/0197-4580(89)90039-0

Brooks, P. M., Rose, K. P., MacRae, M. L., Rangoussis, K. M., Gurjar, M., Hertzano, R., et al. (2020). Pou3f4-expressing otic mesenchyme cells promote spiral ganglion neuron survival in the postnatal mouse cochlea. *J. Comp. Neurol.* 528, 1967–1985. doi: 10.1002/cne.24867

Brosel, S., Grothe, B., and Kunz, L. (2018). An auditory brainstem nucleus as a model system for neuronal metabolic demands. *Eur. J. Neurosci.* 47, 222–235. doi: 10.1111/ejn.13789

Campisi, J. (2013). Aging, cellular senescence and cancer. *Ann. Rev. Physiol.* 75, 685–705. doi: 10.1146/annurev-physiol-030212-183653

Casey, M., and Feldman, M. (1988). Age-related loss of synaptic terminals in the rat medial nucleus of the trapezoid body. *Neuroscience* 24, 189–194. doi: 10.1016/0306-4522(88)90322-3

Casey, M. A., and Feldman, M. L. (1982). Aging in the rat medial nucleus of the trapezoid body I. Light microscopy. *Neurobiol. Aging* 3, 187–195. doi: 10.1016/0197-4580(82)90039-2

Casey, M. A., and Feldman, M. L. (1985). Aging in the rat medial nucleus of the trapezoid body. II. Electron microscopy. *J. Comp. Neurol.* 232, 401–413. doi: 10.1002/cne.902320311

Caspary, D. M., Hughes, L. F., Schatteman, T. A., and Turner, J. G. (2006). Age-related changes in the response properties of cartwheel cells in rat dorsal cochlear nucleus. *Hear. Res.* 216, 207–215. doi: 10.1016/j.heares.2006.03.005

Caspary, D. M., and Llano, D. A. (2018). "Aging processes in the subcortical auditory system," in *The Oxford Handbook of the Auditory Brainstem*, ed K. Kandler (London: Oxford University Press), 639–679. doi: 10.1093/oxfordhb/9780190849061.013.16

Cassarly, C., Matthews, L. J., Simpson, A. N., and Dubno, J. R. (2020). The revised hearing handicap inventory and screening tool based on psychometric reevaluation of the hearing handicap inventories for the elderly and adults. *Ear Hear.* 41, 95–105. doi: 10.1097/AUD.0000000000000746

Chen, Y., Gu, Y., Li, Y., Li, G.-L., Chai, R., Li, W., et al. (2021). Generation of mature and functional hair cells by co-expression of Gfi1, Pou4f3 and Atoh1 in the postnatal mouse cochlea. *Cell Rep.* 35:109016. doi: 10.1016/j.celrep.2021.109016

Chessum, L., Matern, M. S., Kelly, M. C., Johnson, S. L., Ogawa, Y., Milon, B., et al. (2018). Helios is a key transcriptional regulator of outer hair cell maturation. *Nature* 563, 696–700. doi: 10.1038/s41586-018-0728-4

Chizhikov, V. V., Iskusnykh, I. Y., Fattakhov, N., and Fritzsch, B. (2021). Lmx1a and Lmx1b are redundantly required for the development of multiple components of the mammalian auditory system. *Neuroscience* 452, 247–264. doi: 10.1016/j.neuroscience.2020.11.013

Chumak, T., Bohuslavova, R., Macova, I., Dodd, N., Buckiova, D., Fritzsch, B., et al. (2016). Deterioration of the medial olivocochlear efferent system accelerates age-related hearing loss in Pax2-Isl1 transgenic mice. *Mol. Neurobiol.* 53, 2368–2383. doi: 10.1007/s12035-015-9215-1

Dabdoub, A., Puligilla, C., Jones, J. M., Fritzsch, B., Cheah, K. S., Pevny, L. H., et al. (2008). Sox2 signaling in prosensory domain specification and subsequent hair cell differentiation in the developing cochlea. *Proc. Natl. Acad. Sci.* 105, 18396–18401. doi: 10.1073/pnas.0808175105

Dawson, S., and Bowl, M. (2019). Age-related hearing loss. *Cold Spring Harb. Perspect. Med.* 9:a033217. doi: 10.1101/cshperspect.a033217

Devare, J., Gubbels, S., and Raphael, Y. (2018). Outlook and future of inner ear therapy. *Hear. Res.* 368, 127–135. doi: 10.1016/j.heares.2018.05.009

Di Bonito, M., Studer, M., and Puelles, L. (2017). Nuclear derivatives and axonal projections originating from rhombomere 4 in the mouse hindbrain. *Brain Struct. Funct.* 222, 3509–3542. doi: 10.1007/s00429-017-1416-0

Driver, E. C., and Kelley, M. W. (2020). Development of the cochlea. *Development* 147:dev162263. doi: 10.1242/dev.162263

Dubno, J. R. (2019). New insights on age-related hearing loss. *J. South Carolina Acad. Sci.* 17, 3–11.

Duncan, J. S., and Fritzsch, B. (2013). Continued expression of GATA3 is necessary for cochlear neurosensory development. *PLoS One* 8:e62046. doi: 10.1371/journal.pone.0062046

Dvorakova, M., Jahan, I., Macova, I., Chumak, T., Bohuslavova, R., Syka, J., et al. (2016). Incomplete and delayed Sox2 deletion defines residual ear neurosensory development and maintenance. *Sci. Rep.* 6:38253. doi: 10.1038/srep38253

Dvorakova, M., Macova, I., Bohuslavova, R., Anderova, M., Fritzsch, B., and Pavlinkova, G. (2020). Early ear neuronal development, but not olfactory or lens development, can proceed without SOX2. *Dev. Biol.* 457, 43–56. doi: 10.1016/j.ydbio.2019.09.003

Eckert, M. A., Vaden Jr, K. I., and Dubno, J. R. (2019). Age-related hearing loss associations with changes in brain morphology. *Trends Hear.* 23:2331216519857267. doi: 10.1177/2331216519857267

Eggermont, J. J. (2019). *The Auditory Brain and Age-related Hearing Impairment.* London; San Diego: Academic Press, Elsevier. pp. 269.

Elliott, K. L., and Fritzsch, B. (2018). Ear transplantations reveal conservation of inner ear afferent pathfinding cues. *Sci. Rep.* 8:13819. doi: 10.1038/s41598-018-31952-y

Elliott, K. L., Fritzsch, B., and Duncan, J. S. (2018). Evolutionary and developmental biology provide insights into the regeneration of organ of corti hair cells. *Front. Cell. Neurosci.* 12:252. doi: 10.3389/fncel.2018.00252

Elliott, K. L., Kersigo, J., Lee, J. H., Jahan, I., Pavlinkova, G., Fritzsch, B., et al. (2021a). Developmental changes in peripherin-eGFP expression in spiral ganglion neurons. *Front. Cell. Neurosci.* 15:678113. doi: 10.3389/fncel.2021.678113

Elliott, K. L., Pavlínková, G., Chizhikov, V. V., Yamoah, E. N., and Fritzsch, B. (2021b). Development in the mammalian auditory system depends on transcription factors. *Int. J. Mol. Sci.* 22:4189. doi: 10.3390/ijms2208418

Elliott, K. L., Kersigo, J., Pan, N., Jahan, I., and Fritzsch, B. (2017). Spiral ganglion neuron projection development to the hindbrain in mice lacking peripheral and/or central target differentiation. *Front. Neural Circuits* 11:25. doi: 10.3389/fncir.2017.00025

Erives, A., and Fritzsch, B. (2020). A screen for gene paralogies delineating evolutionary branching order of early metazoa. *G3 (Bethesda)* 10, 811–826. doi: 10.1534/g3.119.400951

Eshraghi, A. A., Jung, H. D., and Mittal, R. (2020). Recent advancements in gene and stem cell based treatment modalities: potential implications in noise induced hearing loss. *Anat. Rec. (Hoboken)* 303, 516–526. doi: 10.1002/ar.24107

Fattal, D., Hansen, M., and Fritzsch, B. (2018). "Aging-related balance impairment and hearing Loss," in *The Wiley Handbook on the Aging Mind and Brain*, eds M. Rizzo, S. Anderson, and B. Fritzsch (Hoboken, NJ: John Wiley and Sons), 315–336. doi: 10.1002/9781118772034.ch16

Filova, I., Dvorakova, M., Bohuslavova, R., Pavlinek, A., Elliott, K. L., Vochyanova, S., et al. (2020). Combined Atoh1 and neurod1 deletion reveals autonomous growth of auditory nerve fibers. *Mol. Neurobiol.* 57, 5307–5323. doi: 10.1007/s12035-020-02092-0

Fritzsch, B., Beisel, K. W., and Hansen, L. A. (2006). The molecular basis of neurosensory cell formation in ear development: a blueprint for hair cell and sensory neuron regeneration? *Bioessays* 28, 1181–1193. doi: 10.1002/bies.20502

Fritzsch, B., Dillard, M., Lavado, A., Harvey, N. L., and Jahan, I. (2010). Canal cristae growth and fiber extension to the outer hair cells of the mouse ear require Prox1 activity. *PLoS One* 5:e9377. doi: 10.1371/journal.pone.0009377

Fritzsch, B., Elliott, K. L., and Pavlinkova, G. (2019). Primary sensory map formations reflect unique needs and molecular cues specific to each sensory system. *F1000Res.* 8:F1000. doi: 10.12688/f1000research.17717.1

Fritzsch, B., Fariñas, I., and Reichardt, L. F. (1997). Lack of neurotrophin 3 causes losses of both classes of spiral ganglion neurons in the cochlea in a region-specific fashion. *J. Neurosci.* 17, 6213–6225. doi: 10.1523/JNEUROSCI.17-16-06213.1997

Fritzsch, B., Kersigo, J., Yang, T., Jahan, I., and Pan, N. (2016). "Neurotrophic factor function during ear development: expression changes define critical phases for neuronal viability", in *The Primary Auditory Neurons of the Mammalian Cochlea*, eds A. Dabdoub, B. Fritzsch, A. Popper, and R. Fay (New York, NY: Springer), 49–84. doi: 10.1007/978-1-4939-3031-9_3

Fritzsch, B., Matei, V., Nichols, D., Bermingham, N., Jones, K., Beisel, K., et al. (2005). Atoh1 null mice show directed afferent fiber growth to undifferentiated ear sensory epithelia followed by incomplete fiber retention. *Dev Dyn.* 233, 570–583. doi: 10.1002/dvdy.20370

Gantz, B. J., Dunn, C. C., Oleson, J., and Hansen, M. R. (2018). Acoustic plus electric speech processing: long-term results. *Laryngoscope* 128, 473–481. doi: 10.1002/lary.26669

Gantz, B. J., Turner, C., Gfeller, K. E., and Lowder, M. W. (2005). Preservation of hearing in cochlear implant surgery: advantages of combined electrical and acoustical speech processing. *Laryngoscope* 115, 796–802. doi: 10.1097/01.MLG.0000157695.07536.D2

Gleich, O., Weiss, M., and Strutz, J. (2004). Age-dependent changes in the lateral superior olive of the gerbil (*Meriones unguiculatus*). *Hear. Res.* 194, 47–59. doi: 10.1016/j.heares.2004.03.016

Godfrey, D. A., Chen, K., O'Toole, T. R., and Mustapha, A. I. (2017). Amino acid and acetylcholine chemistry in the central auditory system of young, middle-aged and old rats. *Hear. Res.* 350, 173–188. doi: 10.1016/j.heares.2017.05.002

Gray, D. T., Engle, J. R., and Recanzone, G. H. (2013). Age-related neurochemical changes in the rhesus macaque superior olivary complex. *J. Comp. Neurol.* 522, 573–591. doi: 10.1002/cne.23427

Groves, A. K., and Fekete, D. M. (2017). "New directions in cochlear development," in *Understanding the Cochlea*, eds G. Manley, A. Gummer, A. Popper, and R. Fay (Cham: Springer), 33–73.

Harris, J. A., and Rubel, E. W. (2006). Afferent regulation of neuron number in the cochlear nucleus: cellular and molecular analyses of a critical period. *Hear. Res.* 216, 127–137. doi: 10.1016/j.heares.2006.03.016

Helfert, R. H., Krenning, J., Wilson, T. S., and Hughes, L. F. (2003). Age-related synaptic changes in the anteroventral cochlear nucleus of Fischer-344 rats. *Hear. Res.* 183, 18–28. doi: 10.1016/s0378-5955(03)00194-1

Herranen, A., Ikäheimo, K., Lankinen, T., Pakarinen, E., Fritzsch, B., Saarma, M., et al. (2020). Deficiency of the ER-stress-regulator MANF triggers progressive outer hair cell death and hearing loss. *Cell Death Dis.* 11:100. doi: 10.1038/s41419-020-2286-6

Hertzano, R., Dror, A. A., Montcouquiol, M., Ahmed, Z. M., Ellsworth, B., Camper, S., et al. (2007). Lhx3, a LIM domain transcription factor, is regulated by Pou4f3 in the auditory but not in the vestibular system. *Eur. J. Neurosci.* 25, 999–1005. doi: 10.1111/j.1460-9568.2007.05332.x

Hinojosa, R., and Nelson, E. G. (2011). Cochlear nucleus neuron analysis in individuals with presbycusis. *Laryngoscope* 121, 2641–2648. doi: 10.1002/lary.22383

Homans, N. C., Metselaar, R. M., Dingemanse, J. G., van der Schroeff, M. P., Brocaar, M. P., Wieringa, M. H., et al. (2017). Prevalence of age-related hearing loss, including sex differences, in older adults in a large cohort study. *Laryngoscope* 127, 725–730. doi: 10.1002/lary.26150

Huang, Y., Hill, J., Yatteau, A., Wong, L., Jiang, T., Petrovic, J., et al. (2018). Reciprocal negative regulation between Lmx1a and Lmo4 is required for inner ear formation. *J. Neurosci.* 38, 5429–5440. doi: 10.1523/JNEUROSCI.2484-17.2018

Huang, E. J., Liu, W., Fritzsch, B., Bianchi, L. M., Reichardt, L. F., and Xiang, M. (2001). Brn3a is a transcriptional regulator of soma size, target field innervation and axon pathfinding of inner ear sensory neurons. *Development* 128, 2421–2432. doi: 10.1242/dev.128.13.2421

Huang, M., Sage, C., Li, H., Xiang, M., Heller, S., and Chen, Z. Y. (2008). Diverse expression patterns of LIM-homeodomain transcription factors (LIM-HDs) in mammalian inner ear development. *Dev. Dyn.* 237, 3305–3312. doi: 10.1002/dvdy.21735

Ibrahim, B. A., and Llano, D. A. (2019). Aging and central auditory disinhibition: is it a reflection of homeostatic downregulation or metabolic vulnerability? *Brain Sci.* 9:351. doi: 10.3390/brainsci9120351

Idrizbegovic, E., Bogdanovic, N., Viberg, A., and Canlon, B. (2003). Auditory peripheral influences on calcium binding protein immunoreactivity in the cochlear nucleus during aging in the C57BL/6J mouse. *Hear. Res.* 179, 33–42. doi: 10.1016/s0378-5955(03)00076-5

Idrizbegovic, E., Salman, H., Niu, X., and Canlon, B. (2006). Presbyacusis and calcium-binding protein immunoreactivity in the cochlear nucleus of BALB/c mice. *Hear. Res.* 216–217, 198–206. doi: 10.1016/j.heares.2006.01.009

Jahan, I., Elliott, K. L., and Fritzsch, B. (2018). Understanding molecular evolution and development of the organ of corti can provide clues for hearing restoration. *Integr. Comp. Biol.* 58, 351–365. doi: 10.1093/icb/icy019

Jahan, I., Kersigo, J., Pan, N., and Fritzsch, B. (2010a). Neurod1 regulates survival and formation of connections in mouse ear and brain. *Cell Tissue Res.* 341, 95–110. doi: 10.1007/s00441-010-0984-6

Jahan, I., Pan, N., Kersigo, J., and Fritzsch, B. (2010b). Neurod1 suppresses hair cell differentiation in ear ganglia and regulates hair cell subtype development in the cochlea. *PLoS One* 5:e11661. doi: 10.1371/journal.pone.0011661

Jahan, I., Pan, N., Kersigo, J., and Fritzsch, B. J. D. (2015). Neurog1 can partially substitute for Atoh1 function in hair cell differentiation and maintenance during organ of Corti development. *Development* 142, 2810–2821. doi: 10.1242/dev.123091

Jalabi, W., Kopp-Scheinpflug, C., Allen, P. D., Schiavon, E., DiGiacomo, R. R., Forsythe, I. D., et al. (2013). Sound localization ability and glycinergic innervation of the superior olivary complex persist after genetic deletion of the medial nucleus of the trapezoid body. *J. Neurosci.* 33, 15044–15049. doi: 10.1523/JNEUROSCI.2604-13.2013

Jalenques, I., Albuisson, E., Despres, G., and Romand, R. (1995). Distribution of glial fibrillary acidic protein (GFAP) in the cochlear nucleus of adult and aged rats. *Brain Res.* 686, 223–232. doi: 10.1016/0006-8993(95)00463-z

Kageyama, R., Shimojo, H., and Ohtsuka, T. (2019). Dynamic control of neural stem cells by bHLH factors. *Neurosci. Res.* 138, 12–18. doi: 10.1016/j.neures.2018.09.005

Kandler, K., Lee, J., and Pecka, M. (2020). "2.28 - The superior olivary complex," in *The Senses: A Comprehensive Reference (Second Edition)*, ed B. Fritzsch (Oxford: Elsevier), 533–555.

Kane, K. L., Longo-Guess, C. M., Gagnon, L. H., Ding, D., Salvi, R. J., and Johnson, K. R. (2012). Genetic background effects on age-related hearing loss associated with Cdh23 variants in mice. *Hear. Res.* 283, 80–88. doi: 10.1016/j.heares.2011.11.007

Kann, O., Papageorgiou, I. E., and Draguhn, A. (2014). Highly energized inhibitory interneurons are a central element for information processing in cortical networks. *J. Cereb. Blood Flow Metab.* 34, 1270–1282. doi: 10.1038/jcbfm.2014.104

Karis, A., Pata, I., van Doorninck, J. H., Grosveld, F., de Zeeuw, C. I., de Caprona, D., et al. (2001). Transcription factor GATA-3 alters pathway selection of olivocochlear neurons and affects morphogenesis of the ear. *J. Comp. Neurol.* 429, 615–630. doi: 10.1002/1096-9861(20010122)429:4<615::aid-cne8>3.0.co;2-f

Karlsson, T., Rask-Andersen, M., Pan, G., Höglund, J., Wadelius, C., Ek, W. E., et al. (2019). Contribution of genetics to visceral adiposity and its relation to cardiovascular and metabolic disease. *Nat. Med.* 25, 1390–1395. doi: 10.1038/s41591-019-0563-7

Kelly, M. C., Chang, Q., Pan, A., Lin, X., and Chen, P. (2012). Atoh1 directs the formation of sensory mosaics and induces cell proliferation in the postnatal mammalian cochlea *in vivo*. *J. Neurosci.* 32, 6699–6710. doi: 10.1523/JNEUROSCI.5420-11.2012

Kempfle, J. S., and Edge, A. S. (2014). Pax2 and Sox2 cooperate to promote hair cell fate in inner ear stem cells. *Otolaryngol. Head Neck Surg.* 151, P221–P221. doi: 10.1177/0194599814541629a266

Kempfle, J. S., Turban, J. L., and Edge, A. S. (2016). Sox2 in the differentiation of cochlear progenitor cells. *Sci. Rep.* 6:23293. doi: 10.1038/srep23293

Kersigo, J., D'Angelo, A., Gray, B. D., Soukup, G. A., and Fritzsch, B. (2011). The role of sensory organs and the forebrain for the development of the craniofacial shape as revealed by Foxg1-cre-mediated microRNA loss. *Genesis* 49, 326–341. doi: 10.1002/dvg.20714

Kersigo, J., and Fritzsch, B. (2015). Inner ear hair cells deteriorate in mice engineered to have no or diminished innervation. *Front. Aging Neurosci.* 7:33. doi: 10.3389/fnagi.2015.00033

Kersigo, J., Gu, L., Xu, L., Pan, N., Vijayakuma, S., Jones, T., et al. (2021). Effects of Neurod1 expression on mouse and human schwannoma cells. *Laryngoscope* 131, E259–E270. doi: 10.1002/lary.28671

Kiernan, A. E., Pelling, A. L., Leung, K. K., Tang, A. S., Bell, D. M., Tease, C., et al. (2005). Sox2 is required for sensory organ development in the mammalian inner ear. *Nature* 434, 1031–1035. doi: 10.1038/nature03487

Koehler, K. R., Nie, J., Longworth-Mills, E., Liu, X.-P., Lee, J., Holt, J. R., et al. (2017). Generation of inner ear organoids containing functional hair cells from human pluripotent stem cells. *Nat. Biotechnol.* 35, 583–589. doi: 10.1038/nbt.3840

Kopecky, B., Santi, P., Johnson, S., Schmitz, H., and Fritzsch, B. (2011). Conditional deletion of N-Myc disrupts neurosensory and non-sensory development of the ear. *Dev. Dyn.* 240, 1373–1390. doi: 10.1002/dvdy.22620

Kral, A., Popper, A. N., and Fay, R. R. Eds. (2013). *Deafness*. New York, NY: Springer. doi: 10.1007/978-1-4614-7840-9

Krawczyk, K., Scheller, L., Kim, H., and Fussenegger, M. (2020). Rewiring of endogenous signaling pathways to genomic targets for therapeutic cell reprogramming. *Nat. Commun.* 11:608. doi: 10.1038/s41467-020-14397-8

Krohs, C., Körber, C., Ebbers, L., Altaf, F., Hollje, G., Hoppe, S., et al. (2021). Loss of miR-183/96 alters synaptic strength *via* presynaptic and postsynaptic mechanisms at a central synapse. *J. Neurosci.* 41, 6796–6811. doi: 10.1523/JNEUROSCI.0139-20.2021

Kujawa, S. G., and Liberman, M. C. (2009). Adding insult to injury: cochlear nerve degeneration after "temporary" noise-induced hearing loss. *J. Neurosci.* 29, 14077–14085. doi: 10.1523/JNEUROSCI.2845-09.2009

Kusunoki, T., Cureoglu, S., Schachern, P. A., Baba, K., Kariya, S., and Paparella, M. M. (2004). Age-related histopathologic changes in the human cochlea: a temporal bone study. *Otolaryngol. Head Neck Surg.* 131, 897–903. doi: 10.1016/j.otohns.2004.05.022

Lahlou, H., Nivet, E., Lopez-Juarez, A., Fontbonne, A., Assou, S., and Zine, A. (2018). Enriched differentiation of human otic sensory progenitor cells derived from induced pluripotent stem cells. *Front. Mol. Neurosci.* 11:452. doi: 10.3389/fnmol.2018.00452

Lang, H. (2016). "Loss, degeneration and preservation of the spiral ganglion neurons and their processes," in *The Primary Auditory Neurons of the Mammalian Cochlea*, eds A. Dabdoub, B. Fritzsch, A. N. Popper, and R. R. Fay (New York, NY: Springer New York), 229–262. doi: 10.1007/978-1-4939-3031-9_8

Lee, K. J., Dietrich, P., and Jessell, T. M. (2000). Genetic ablation reveals that the roof plate is essential for dorsal interneuron specification. *Nature* 403, 734–740. doi: 10.1038/35001507

Levi-Montalcini, R. (1949). The development of the acoustico-vestibular centres in the chick embryo in the absence of the afferent root fibers and of descending fiber tracts. *J. Comp. Neurol.* 91, 209–241. doi: 10.1002/cne.900910204

Lewis, M. A., Nolan, L. S., Cadge, B. A., Matthews, L. J., Schulte, B. A., Dubno, J. R., et al. (2018). Whole exome sequencing in adult-onset hearing loss reveals a high load of predicted pathogenic variants in known deafness-associated genes and identifies new candidate genes. *BMC Med. Genomics* 11:77. doi: 10.1186/s12920-018-0395-1

Lewis, R. M., Keller, J. J., Wan, L., and Stone, J. S. (2018). Bone morphogenetic protein 4 antagonizes hair cell regeneration in the avian auditory epithelium. *Hear. Res.* 364, 1–11. doi: 10.1016/j.heares.2018.04.008

Li, J., Zhang, T., Ramakrishnan, A., Fritzsch, B., Xu, J., Wong, E. Y., et al. (2020). Dynamic changes in cis-regulatory occupancy by Six1 and its cooperative interactions with distinct cofactors drive lineage-specific gene expression programs during progressive differentiation of the auditory sensory epithelium. *Nucleic Acids Res.* 48, 2880–2896. doi: 10.1093/nar/gkaa012

Lim, R., and Brichta, A. M. (2016). Anatomical and physiological development of the human inner ear. *Hear. Res.* 338, 9–21. doi: 10.1016/j.heares.2016.02.004

Lipovsek, M., and Wingate, R. J. (2018). Conserved and divergent development of brainstem vestibular and auditory nuclei. *eLife* 7:e40232. doi: 10.7554/eLife.40232

Liu, W., Johansson, Å., Rask-Andersen, H., and Rask-Andersen, M. (2021). A combined genome-wide association and molecular study of age-related hearing loss in H. sapiens. *BMC Med.* 19:302. doi: 10.1186/s12916-021-02169-0

Locher, H., Frijns, J. H., van Iperen, L., de Groot, J. C., Huisman, M. A., and de Sousa Lopes, S. M. C. (2013). Neurosensory development and cell fate determination in the human cochlea. *Neural Dev.* 8:20. doi: 10.1186/1749-8104-8-20

Lohmann, C., and Friauf, E. (1996). Distribution of the calcium-binding proteins parvalbumin and calretinin in the auditory brainstem of adult and developing rats. *J. Comp. Neurol.* 367, 90–109. doi: 10.1002/(SICI)1096-9861(19960325)367:1<90::AID-CNE7>3.0.CO;2-E

Lopez-Juarez, A., Lahlou, H., Ripoll, C., Cazals, Y., Brezun, J. M., Wang, Q., et al. (2019). Engraftment of human stem cell-derived otic progenitors in the damaged cochlea. *Mol. Ther.* 27, 1101–1113. doi: 10.1016/j.ymthe.2019.03.018

López-Otín, C., Blasco, M. A., Partridge, L., Serrano, M., and Kroemer, G. (2013). The hallmarks of aging. *Cell* 153, 1194–1217. doi: 10.1016/j.cell.2013.05.039

Löwenheim, H., Furness, D. N., Kil, J., Zinn, C., Gültig, K., Fero, M. L., et al. (1999). Gene disruption of p27Kip1 allows cell proliferation in the postnatal and adult organ of corti. *Proc. Natl. Acad. Sci. U S A* 96, 4084–4088. doi: 10.1073/pnas.96.7.4084

Lu, C. C., Cao, X.-J., Wright, S., Ma, L., Oertel, D., and Goodrich, L. V. (2014). Mutation of Npr2 leads to blurred tonotopic organization of central auditory circuits in mice. *PLoS Genet.* 10:e1004823. doi: 10.1371/journal.pgen.1004823

Ma, Q., Anderson, D. J., and Fritzsch, B. (2000). Neurogenin 1 null mutant ears develop fewer, morphologically normal hair cells in smaller sensory epithelia devoid of innervation. *J. Assoc. Res. Otolaryngol.* 1, 129–143. doi: 10.1007/s101620010017

Ma, Q., Chen, Z., del Barco Barrantes, I., De La Pompa, J. L., and Anderson, D. J. (1998). neurogenin1 is essential for the determination of neuronal precursors for proximal cranial sensory ganglia. *Neuron* 20, 469–482. doi: 10.1016/s0896-6273(00)80988-5

Macova, I., Pysanenko, K., Chumak, T., Dvorakova, M., Bohuslavova, R., Syka, J., et al. (2019). Neurod1 is essential for the primary tonotopic organization and related auditory information processing in the midbrain. *J. Neurosci.* 39, 984–1004. doi: 10.1523/JNEUROSCI.2557-18.2018

Makary, C. A., Shin, J., Kujawa, S. G., Liberman, M. C., and Merchant, S. N. (2011). Age-related primary cochlear neuronal degeneration in human temporal bones. *J. Assoc. Res. Otolaryngol.* 12, 711–717. doi: 10.1007/s10162-011-0283-2

Malmierca, M. S., and Ryugo, D. K. (2011). "Descending connections of auditory cortex to the midbrain and brain stem," in *The Auditory Cortex*, eds J. A. Winer, and C. E. Schreiner (Boston, MA: Springer), 189–208. doi: 10.1007/978-1-4419-0074-6_9

Manis, P. B., Xie, R., Wang, Y., Marrs, G. S., and Spirou, G. A. (2012). "The endbulbs of held," in *Synaptic Mechanisms in the Auditory System*, eds L. O. Trussell, A. N. Popper, and R. R. Fay (New York, NY: Springer New York), 61–93. doi: 10.1007/978-1-4419-9517-9_4

Mantela, J., Jiang, Z., Ylikoski, J., Fritzsch, B., Zacksenhaus, E., and Pirvola, U. (2005). The retinoblastoma gene pathway regulates the postmitotic state of hair cells of the mouse inner ear. *Development* 132, 2377–2388. doi: 10.1242/dev.01834

Mao, Y., Reiprich, S., Wegner, M., and Fritzsch, B. (2014). Targeted deletion of Sox10 by Wnt1-cre defects neuronal migration and projection in the mouse inner ear. *PLoS One* 9:e94580. doi: 10.1371/journal.pone.0094580

Maricich, S. M., Xia, A., Mathes, E. L., Wang, V. Y., Oghalai, J. S., Fritzsch, B., et al. (2009). Atoh1-lineal neurons are required for hearing and for the survival of neurons in the spiral ganglion and brainstem accessory auditory nuclei. *J. Neurosci.* 29, 11123–11133. doi: 10.1523/JNEUROSCI.2232-09.2009

Marrs, G. S., Morgan, W. J., Howell, D. M., Spirou, G. A., and Mathers, P. H. (2013). Embryonic origins of the mouse superior olivary complex. *Dev. Neurobiol.* 73, 384–398. doi: 10.1002/dneu.22069

Matei, V., Pauley, S., Kaing, S., Rowitch, D., Beisel, K., Morris, K., et al. (2005). Smaller inner ear sensory epithelia in Neurog1 null mice are related to earlier hair cell cycle exit. *Dev. Dyn.* 234, 633–650. doi: 10.1002/dvdy.20551

Matern, M. S., Milon, B., Lipford, E. L., McMurray, M., Ogawa, Y., Tkaczuk, A., et al. (2020). GFI1 functions to repress neuronal gene expression in the developing inner ear hair cells. *Development* 147:dev186015. doi: 10.1242/dev.186015

McGovern, M. M., Randle, M. R., Cuppini, C. L., Graves, K. A., and Cox, B. C. (2019). Multiple supporting cell subtypes are capable of spontaneous hair cell regeneration in the neonatal mouse cochlea. *Development* 146:dev171009. doi: 10.1242/dev.171009

Milinkeviciute, G., and Cramer, K. S. (2020). "2.18 - Development of the ascending auditory pathway," in *The Senses: A Comprehensive Reference (Second Edition)*, ed B. Fritzsch (Oxford: Elsevier), 337–353.

Muniak, M. A., Connelly, C. J., Suthakar, K., Milinkeviciute, G., Ayeni, F. E., and Ryugo, D. K. (2016). "Central projections of spiral ganglion neurons," in *The Primary Auditory Neurons of the Mammalian Cochlea*, eds A. Dabdoub, B. Fritzsch, A. Popper, and R. Fay (New York, NY: Springer), 157–190.

Muthu, V., Rohacek, A. M., Yao, Y., Rakowiecki, S. M., Brown, A. S., Zhao, Y.-T., et al. (2019). Genomic architecture of Shh-dependent cochlear morphogenesis. *Development* 146:dev181339. doi: 10.1242/dev.181339

Nadol Jr, J. B. (1990). Degeneration of cochlear neurons as seen in the spiral ganglion of man. *Hear. Res.* 49, 141–154. doi: 10.1016/0378-5955(90)90101-t

Nadol Jr, J. B., and Xu, W.-Z. (1992). Diameter of the cochlear nerve in deaf humans: implications for cochlear implantation. *Ann. Otol. Rhinol. Laryngol.* 101, 988–993. doi: 10.1177/000348949210101205

Nakano, Y., Jahan, I., Bonde, G., Sun, X., Hildebrand, M. S., Engelhardt, J. F., et al. (2012). A mutation in the Srrm4 gene causes alternative splicing defects and deafness in the Bronx waltzer mouse. *PLoS Genet.* 8:e1002966. doi: 10.1371/journal.pgen.1002966

Nakano, Y., Wiechert, S., Fritzsch, B., and Bánfi, B. (2020). Inhibition of a transcriptional repressor rescues hearing in a splicing factor-deficient mouse. *Life Sci. Alliance* 3:e202000841. doi: 10.26508/lsa.202000841

Neves, J., Uchikawa, M., Bigas, A., and Giraldez, F. (2012). The prosensory function of Sox2 in the chicken inner ear relies on the direct regulation of Atoh1. *PLoS One* 7:e30871. doi: 10.1371/journal.pone.0030871

Nichols, D. H., Bouma, J. E., Kopecky, B. J., Jahan, I., Beisel, K. W., He, D. Z., et al. (2020). Interaction with ectopic cochlear crista sensory epithelium disrupts basal cochlear sensory epithelium development in Lmx1a mutant mice. *Cell Tissue Res.* 380, 435–448. doi: 10.1007/s00441-019-03163-y

Nichols, D. H., Pauley, S., Jahan, I., Beisel, K. W., Millen, K. J., and Fritzsch, B. (2008). Lmx1a is required for segregation of sensory epithelia and normal ear histogenesis and morphogenesis. *Cell Tissue Res.* 334, 339–358. doi: 10.1007/s00441-008-0709-2

Nyberg, S., Abbott, N. J., Shi, X., Steyger, P. S., and Dabdoub, A. (2019). Delivery of therapeutics to the inner ear: the challenge of the blood-labyrinth barrier. *Sci. Transl. Med.* 11:eaao0935. doi: 10.1126/scitranslmed.aao0935

Oertel, D., and Cao, X.-J. (2020). "2.27 - The ventral cochlear nucleus," in *The Senses: A Comprehensive Reference (Second Edition)*, ed B. Fritzsch (Oxford: Elsevier), 517–532.

Pan, N., Jahan, I., Kersigo, J., Duncan, J. S., Kopecky, B., and Fritzsch, B. (2012). A novel Atoh1 "self-terminating" mouse model reveals the necessity of proper Atoh1 level and duration for hair cell differentiation and viability. *PLoS One* 7:e30358. doi: 10.1371/journal.pone.0030358

Patel, D., Shimomura, A., Majumdar, S., Holley, M. C., and Hashino, E. (2018). The histone demethylase LSD1 regulates inner ear progenitor differentiation through interactions with Pax2 and the NuRD repressor complex. *PLoS One* 13:e0191689. doi: 10.1371/journal.pone.0191689

Pauley, S., Kopecky, B., Beisel, K., Soukup, G., and Fritzsch, B. (2008). Stem cells and molecular strategies to restore hearing. *Panminerva Medica* 50, 41–65.

Pauley, S., Wright, T. J., Pirvola, U., Ornitz, D., Beisel, K., and Fritzsch, B. (2003). Expression and function of FGF10 in mammalian inner ear development. *Dev. Dyn.* 227, 203–215. doi: 10.1002/dvdy.10297

Perkins, G., Lee, J. H., Park, S., Kang, M., Perez-Flores, M. C., Ju, S., et al. (2020). Altered outer hair cell mitochondrial and subsurface cisternae connectomics are candidate mechanisms for hearing loss in mice. *J. Neurosci.* 40, 8556–8572. doi: 10.1523/JNEUROSCI.2901-19.2020

Petitpré, C., Wu, H., Sharma, A., Tokarska, A., Fontanet, P., Wang, Y., et al. (2018). Neuronal heterogeneity and stereotyped connectivity in the auditory afferent system. *Nat. Commun.* 9:3691. doi: 10.1038/s41467-018-06033-3

Pierce, E. T. (1967). Histogenesis of the dorsal and ventral cochlear nuclei in the mouse. An autoradiographic study. *J. Comp. Neurol.* 131, 27–54. doi: 10.1002/cne.901310104

Pierce, E. T. (1973). Time of origin of neurons in the brain stem of the mouse. *Prog. Brain Res.* 40, 53–65. doi: 10.1016/S0079-6123(08)60679-2

Pierce, M. L., Weston, M. D., Fritzsch, B., Gabel, H. W., Ruvkun, G., and Soukup, G. A. (2008). MicroRNA-183 family conservation and ciliated neurosensory organ expression. *Evol. Dev.* 10, 106–113. doi: 10.1111/j.1525-142X.2007.00217.x

Pirvola, U., Ylikoski, J., Trokovic, R., Hébert, J. M., McConnell, S. K., and Partanen, J. (2002). FGFR1 is required for the development of the auditory sensory epithelium. *Neuron* 35, 671–680. doi: 10.1016/s0896-6273(02)00824-3

Qiu, X., and Müller, U. (2018). Mechanically gated ion channels in mammalian hair cells. *Front. Cell. Neurosci.* 12:100. doi: 10.3389/fncel.2018.00100

Radde-Gallwitz, K., Pan, L., Gan, L., Lin, X., Segil, N., and Chen, P. (2004). Expression of Islet1 marks the sensory and neuronal lineages in the mammalian inner ear. *J. Comp. Neurol.* 477, 412–421. doi: 10.1002/cne.20257

Rask-Andersen, H., Boström, M., Gerdin, B., Kinnefors, A., Nyberg, G., Engstrand, T., et al. (2005). Regeneration of human auditory nerve. *In vitro*/in video demonstration of neural progenitor cells in adult human and guinea pig spiral ganglion. *Hear. Res.* 203, 180–191. doi: 10.1016/j.heares.2004.12.005

Rauch, S. D., Velazquez-VillaseÑor, L., Dimitri, P. S., and Merchant, S. N. (2001). Decreasing hair cell counts in aging humans. *Ann. N Y Acad. Sci.* 942, 220–227. doi: 10.1111/j.1749-6632.2001.tb03748.x

Ray, R. S., and Dymecki, S. M. (2009). Rautenlippe Redux—toward a unified view of the precerebellar rhombic lip. *Curr. Opin. Cell Biol.* 21, 741–747. doi: 10.1016/j.ceb.2009.10.003

Revuelta, M., Santaolalla, F., Arteaga, O., Alvarez, A., Sanchez-del-Rey, A., and Hilario, E. (2017). Recent advances in cochlear hair cell regeneration—a promising opportunity for the treatment of age-related hearing loss. *Ageing Res. Rev.* 36, 149–155. doi: 10.1016/j.arr.2017.04.002

Riccomagno, M. M., Takada, S., and Epstein, D. J. (2005). Wnt-dependent regulation of inner ear morphogenesis is balanced by the opposing and supporting roles of Shh. *Genes Dev.* 19, 1612–1623. doi: 10.1101/gad.1303905

Roccio, M., Senn, P., and Heller, S. (2020). Novel insights into inner ear development and regeneration for refined hearing loss therapies. *Hear. Res.* 397:107859. doi: 10.1016/j.heares.2019.107859

Romano, D. R., Hashino, E., and Nelson, R. F. (2021). Deafness-in-a-dish: modeling hereditary deafness with inner ear organoids. *Hum. Genet.* doi: 10.1007/s00439-021-02325-9. [Online ahead of print].

Rubel, E. W., and Fritzsch, B. (2002). Auditory system development: primary auditory neurons and their targets. *Ann. Rev. Neurosci.* 25, 51–101. doi: 10.1146/annurev.neuro.25.112701.142849

Ruben, R. J. (1967). Development of the inner ear of the mouse: a radioautographic study of terminal mitoses. *Acta Otolaryngol. (Stockh.)* 220, 1–44.

Ryugo, D., Kretzmer, E., and Niparko, J. (2005). Restoration of auditory nerve synapses in cats by cochlear implants. *Science* 310, 1490–1492. doi: 10.1126/science.1119419

Sanes, D. H., and Rubel, E. (1988). The ontogeny of inhibition and excitation in the gerbil lateral superior olive. *J. Neurosci.* 8, 682–700. doi: 10.1523/JNEUROSCI.08-02-00682.1988

Schilder, A. G., Su, M. P., Blackshaw, H., Lustig, L., Staecker, H., Lenarz, T., et al. (2019). Hearing protection, restoration and regeneration: an overview of emerging therapeutics for inner ear and central hearing disorders. *Otol. Neurotol.* 40, 559–570. doi: 10.1097/MAO.0000000000002194

Schmidt, H., and Fritzsch, B. (2019). Npr2 null mutants show initial overshooting followed by reduction of spiral ganglion axon projections combined with near-normal cochleotopic projection. *Cell Tissue Res.* 378, 15–32. doi: 10.1007/s00441-019-03050-6

Sedlmayer, F., Aubel, D., and Fussenegger, M. (2018). Synthetic gene circuits for the detection, elimination and prevention of disease. *Nat. Biomed. Eng.* 2, 399–415. doi: 10.1038/s41551-018-0215-0

Sekiya, T., and Holley, M. C. (2021). Cell transplantation to restore lost auditory nerve function is a realistic clinical opportunity. *Cell Transplant.* 30:09636897211035076. doi: 10.1177/09636897211035076

Sharma, S., Nag, T. C., Thakar, A., Bhardwaj, D. N., and Roy, T. S. (2014). The aging human cochlear nucleus: changes in the glial fibrillary acidic protein, intracellular calcium regulatory proteins, GABA neurotransmitter and cholinergic receptor. *J. Chem. Neuroanat.* 56, 1–12. doi: 10.1016/j.jchemneu.2013.12.001

Sheffield, A. M., and Smith, R. J. (2019). The epidemiology of deafness. *Cold Spring Harb. Perspect. Med.* 9:a033258. doi: 10.1101/cshperspect.a033258

Shibata, S. B., Cortez, S. R., Beyer, L. A., Wiler, J. A., Di Polo, A., Pfingst, B. E., et al. (2010). Transgenic BDNF induces nerve fiber regrowth into the auditory epithelium in deaf cochleae. *Exp. Neurol.* 223, 464–472. doi: 10.1016/j.expneurol.2010.01.011

Shrestha, B. R., Chia, C., Wu, L., Kujawa, S. G., Liberman, M. C., and Goodrich, L. V. (2018). Sensory neuron diversity in the inner ear is shaped by activity. *Cell* 174, 1229–1246.e17. doi: 10.1016/j.cell.2018.07.007

Shrestha, B. R., and Goodrich, L. V. (2019). *Wiring the Cochlea for Sound Perception*. London: Oxford University Press. pp. 5–25.

Simpson, A. N., Matthews, L. J., Cassarly, C., and Dubno, J. R. (2019). Time from hearing aid candidacy to hearing aid adoption: a longitudinal cohort study. *Ear Hear.* 40, 468–476. doi: 10.1097/AUD.0000000000000641

Song, Z., Jadali, A., Fritzsch, B., and Kwan, K. Y. (2017). NEUROG1 regulates CDK2 to promote proliferation in otic progenitors. *Stem Cell Rep.* 9, 1516–1529. doi: 10.1016/j.stemcr.2017.09.011

Song, Z., Laureano, A. S., Patel, K., Yip, S., Jadali, A., and Kwan, K. Y. (2019). Single-cell fluorescence analysis of pseudotemporal ordered cells provides protein expression dynamics for neuronal differentiation. *Front. Cell Dev. Biol.* 7:87. doi: 10.3389/fcell.2019.00087

Soukup, G. A., Fritzsch, B., Pierce, M. L., Weston, M. D., Jahan, I., McManus, M. T., et al. (2009). Residual microRNA expression dictates the extent of inner ear development in conditional Dicer knockout mice. *Dev. Biol.* 328, 328–341. doi: 10.1016/j.ydbio.2009.01.037

Spongr, V. P., Flood, D. G., Frisina, R. D., and Salvi, R. J. (1997). Quantitative measures of hair cell loss in CBA and C57BL/6 mice throughout their life spans. *J. Acoust. Soc. Am.* 101, 3546–3553. doi: 10.1121/1.418315

Stakhovskaya, O., Hradek, G. T., Snyder, R. L., and Leake, P. A. (2008). Effects of age at onset of deafness and electrical stimulation on the developing cochlear nucleus in cats. *Hear. Res.* 243, 69–77. doi: 10.1016/j.heares.2008.05.007

Stebbings, K., Choi, H., Ravindra, A., Caspary, D., Turner, J., and Llano, D. (2016). Ageing-related changes in GABAergic inhibition in mouse auditory cortex, measured using *in vitro* flavoprotein autofluorescence imaging. *J. Physiol.* 594, 207–221. doi: 10.1113/JP271221

Sun, S., Siebald, C., and Müller, U. (2021). Subtype maturation of spiral ganglion neurons. *Curr. Opin. Otolaryngol. Head Neck Surg.* 29, 391–399. doi: 10.1097/MOO.0000000000000748

Syka, J. (2020). "Age-related changes in the auditory brainstem and inferior colliculus," in *Aging and Hearing. Causes and Consequences. Springer Handbook of Auditory Research Series*, eds Karen S. Helfer, Edward L. Bartlett, Arthur N. Popper, and Richard R. Fay (Berlin: Springer) 72, 67–96.

Tateya, T., Sakamoto, S., Ishidate, F., Hirashima, T., Imayoshi, I., and Kageyama, R. (2019). Three-dimensional live imaging of Atoh1 reveals the dynamics of hair cell induction and organization in the developing cochlea. *Development* 146:dev177881. doi: 10.1242/dev.177881

Taylor, R. R., Jagger, D. J., and Forge, A. (2012). Defining the cellular environment in the organ of Corti following extensive hair cell loss: a basis for future sensory cell replacement in the Cochlea. *PLoS One* 7:e30577. doi: 10.1371/journal.pone.0030577

Tong, L., Strong, M. K., Kaur, T., Juiz, J. M., Oesterle, E. C., Hume, C., et al. (2015). Selective deletion of cochlear hair cells causes rapid age-dependent changes in spiral ganglion and cochlear nucleus neurons. *J. Neurosci.* 35, 7878–7891. doi: 10.1523/JNEUROSCI.2179-14.2015

Ueyama, T., Sakaguchi, H., Nakamura, T., Goto, A., Morioka, S., Shimizu, A., et al. (2014). Maintenance of stereocilia and apical junctional complexes by Cdc42 in cochlear hair cells. *J. Cell Sci.* 127, 2040–2052. doi: 10.1242/jcs.143602

Urness, L. D., Wang, X., Doan, H., Shumway, N., Noyes, C. A., Gutierrez-Magana, E., et al. (2018). Spatial and temporal inhibition of FGFR2b ligands reveals continuous requirements and novel targets in mouse inner ear morphogenesis. *Development* 145:dev170142. doi: 10.1242/dev.170142

van der Valk, W. H., Steinhart, M. R., Zhang, J., and Koehler, K. R. (2021). Building inner ears: recent advances and future challenges for *in vitro* organoid systems. *Cell Death Differ.* 28, 24–34. doi: 10.1038/s41418-020-00678-8

Walters, B. J., Coak, E., Dearman, J., Bailey, G., Yamashita, T., Kuo, B., et al. (2017). *In vivo* interplay between p27Kip1, GATA3, ATOH1 and POU4F3 converts non-sensory cells to hair cells in adult mice. *Cell Rep.* 19, 307–320. doi: 10.1016/j.celrep.2017.03.044

Wang, L., Kempton, J. B., and Brigande, J. V. (2018). Gene therapy in mouse models of deafness and balance dysfunction. *Front. Mol. Neurosci.* 11:300. doi: 10.3389/fnmol.2018.00300

Wang, V. Y., Rose, M. F., and Zoghbi, H. Y. (2005). Math1 expression redefines the rhombic lip derivatives and reveals novel lineages within the brainstem and cerebellum. *Neuron* 48, 31–43. doi: 10.1016/j.neuron.2005.08.024

Wang, H., Turner, J. G., Ling, L., Parrish, J. L., Hughes, L. F., and Caspary, D. M. (2009). Age-related changes in glycine receptor subunit composition and

binding in dorsal cochlear nucleus. *Neuroscience* 160, 227–239. doi: 10.1016/j.neuroscience.2009.01.079

Wang, M., Zhang, C., Lin, S., Wang, Y., Seicol, B. J., Ariss, R. W., et al. (2021). Biased auditory nerve central synaptopathy is associated with age-related hearing loss. *J. Physiol.* 599, 1833–1854. doi: 10.1113/JP281014

White, J. A., Burgess, B. J., Hall, R. D., and Nadol, J. B. (2000). Pattern of degeneration of the spiral ganglion cell and its processes in the C57BL/6J mouse. *Hear. Res.* 141, 12–18. doi: 10.1016/s0378-5955(99)00204-x

Willott, J. F., and Bross, L. S. (1990). Morphology of the octopus cell area of the cochlear nucleus in young and aging C57BL/6J and CBA/J mice. *J. Comp. Neurol.* 300, 61–81. doi: 10.1002/cne.903000106

Willott, J. F., Jackson, L. M., and Hunter, K. P. (1987). Morphometric study of the anteroventral cochlear nucleus of two mouse models of presbycusis. *J. Comp. Neurol.* 260, 472–480. doi: 10.1002/cne.902600312

Wiwatpanit, T., Lorenzen, S. M., Cantú, J. A., Foo, C. Z., Hogan, A. K., Márquez, F., et al. (2018). Trans-differentiation of outer hair cells into inner hair cells in the absence of INSM1. *Nature* 563, 691–695. doi: 10.1038/s41586-018-0570-8

Wu, P.-Z., O'Malley, J. T., de Gruttola, V., and Liberman, M. C. (2021). Primary neural degeneration in noise-exposed human cochleas: correlations with outer hair cell loss and word-discrimination scores. *J. Neurosci.* 41, 4439–4447. doi: 10.1523/JNEUROSCI.3238-20.2021

Xiang, M., Maklad, A., Pirvola, U., and Fritzsch, B. (2003). Brn3c null mutant mice show long-term, incomplete retention of some afferent inner ear innervation. *BMC Neurosci.* 4:2. doi: 10.1186/1471-2202-4-2

Xie, R. (2016). Transmission of auditory sensory information decreases in rate and temporal precision at the endbulb of Held synapse during age-related hearing loss. *J. Neurophysiol.* 116, 2695–2705. doi: 10.1152/jn.00472.2016

Xie, M., and Fussenegger, M. (2018). Designing cell function: assembly of synthetic gene circuits for cell biology applications. *Nat. Rev. Mol. Cell Biol.* 19, 507–525. doi: 10.1038/s41580-018-0024-z

Xie, R., and Manis, P. B. (2017). Synaptic transmission at the endbulb of Held deteriorates during age-related hearing loss. *J. Physiol.* 595, 919–934. doi: 10.1113/JP272683

Xu, J., Li, J., Zhang, T., Jiang, H., Ramakrishnan, A., Fritzsch, B., et al. (2021). Chromatin remodelers and lineage-specific factors interact to target enhancers to establish proneurosensory fate within otic ectoderm. *Proc. Natl. Acad. Sci. U S A* 118:e2025196118. doi: 10.1073/pnas.2025196118

Yamashita, T., Zheng, F., Finkelstein, D., Kellard, Z., Robert, C., Rosencrance, C.D., et al. (2018). High-resolution transcriptional dissection of *in vivo* Atoh1-mediated hair cell conversion in mature cochleae identifies Isl1 as a co-reprogramming factor. *PLoS Genet.* 14:e1007552. doi: 10.1371/journal.pgen.1007552

Yamasoba, T., Lin, F. R., Someya, S., Kashio, A., Sakamoto, T., and Kondo, K. (2013). Current concepts in age-related hearing loss: epidemiology and mechanistic pathways. *Hear. Res.* 303, 30–38. doi: 10.1016/j.heares.2013.01.021

Yamoah, E. N., Li, M., Shah, A., Elliott, K. L., Cheah, K., Xu, P.-X., et al. (2020). Using Sox2 to alleviate the hallmarks of age-related hearing loss. *Ageing Res. Rev.* 59:101042. doi: 10.1016/j.arr.2020.101042

Yang, T., Kersigo, J., Jahan, I., Pan, N., and Fritzsch, B. (2011). The molecular basis of making spiral ganglion neurons and connecting them to hair cells of the organ of Corti. *Hear. Res.* 278, 21–33. doi: 10.1016/j.heares.2011.03.002

Yang, C.-H., Schrepfer, T., and Schacht, J. (2015). Age-related hearing impairment and the triad of acquired hearing loss. *Front. Cell. Neurosci.* 9:276. doi: 10.3389/fncel.2015.00276

Yoshimura, H., Shibata, S. B., Ranum, P. T., Moteki, H., and Smith, R. J. (2019). Targeted allele suppression prevents progressive hearing loss in the mature murine model of human TMC1 deafness. *Mol. Ther.* 27, 681–690. doi: 10.1016/j.ymthe.2018.12.014

Young, E. D., and Oertel, D. (1998). "Cochlear nucleus," in *The Synaptic Organization of the Brain.* ed Gordon M. Shepherd (Oxford Scholarship Online). doi: 10.1093/acprof:oso/9780195159561.003.0004

Zettel, M. L., O'neill, W. E., Trang, T. T., and Frisina, R. D. (2003). The effects of early bilateral deafening on calretinin expression in the dorsal cochlear nucleus of aged CBA/CaJ mice. *Hear. Res* 183, 57–66. doi: 10.1016/s0378-5955(03)00216-8

Zheng, Q. Y., Johnson, K. R., and Erway, L. C. (1999). Assessment of hearing in 80 inbred strains of mice by ABR threshold analyses. *Hear. Res.* 130, 94–107. doi: 10.1016/s0378-5955(99)00003-9

Zhou, H., Q42an, X., Xu, N., Zhang, S., Zhu, G., Zhang, Y., et al. (2020). Disruption of Atg7-dependent autophagy causes electromotility disturbances, outer hair cell loss and deafness in mice. *Cell Death Dis.* 11:913. doi: 10.1038/s41419-020-03110-8

Zhu, C., Cheng, C., Wang, Y., Muhammad, W., Liu, S., Zhu, W., et al. (2018). Loss of ARHGEF6 causes hair cell stereocilia deficits and hearing loss in mice. *Front. Mol. Neurosci.* 11:362. doi: 10.3389/fnmol.2018.00362

Zine, A., Löwenheim, H., and Fritzsch, B. (2014). "Toward translating molecular ear development to generate hair cells from stem cells," in *Adult Stem Cells. Stem Cell Biology and Regenerative Medicine* (New York: Springer), 111–161. doi: 10.1007/978-1-4614-9569-7_6

Zine, A., Messat, Y., and Fritzsch, B. (2021). A human induced pluripotent stem cell-based modular platform to challenge sensorineural hearing loss. *Stem Cells* 39, 697–706. doi: 10.1002/stem.3346

Zou, D., Silvius, D., Fritzsch, B., and Xu, P.-X. (2004). Eya1 and Six1 are essential for early steps of sensory neurogenesis in mammalian cranial placodes. *Development* 131, 5561–5572. doi: 10.1242/dev.01437

Conflict of Interest: The authors declare that the research was conducted in the absence of any commercial or financial relationships that could be construed as a potential conflict of interest.

Publisher's Note: All claims expressed in this article are solely those of the authors and do not necessarily represent those of their affiliated organizations, or those of the publisher, the editors and the reviewers. Any product that may be evaluated in this article, or claim that may be made by its manufacturer, is not guaranteed or endorsed by the publisher.

frontiers | Frontiers in Aging Neuroscience

REVIEW
published: 07 April 2022
doi: 10.3389/fnagi.2022.814463

Exploration on the Mechanism of Ubiquitin Proteasome System in Cerebral Stroke

*Yu-Chao Li[1], Yan Wang[2] and Wei Zou[1,3]**

[1] Heilongjiang University of Chinese Medicine, Harbin, China, [2] School of Traditional Chinese Medicine, Ningxia Medical University, Yinchuan, China, [3] First Affiliated Hospital, Heilongjiang University of Chinese Medicine, Harbin, China

Stroke's secondary damage, such as inflammation, oxidative stress, and mitochondrial dysfunction, are thought to be crucial factors in the disease's progression. Despite the fact that there are numerous treatments for secondary damage following stroke, such as antiplatelet therapy, anticoagulant therapy, surgery, and so on, the results are disappointing and the side effects are numerous. It is critical to develop novel and effective strategies for improving patient prognosis. The ubiquitin proteasome system (UPS) is the hub for the processing and metabolism of a wide range of functional regulatory proteins in cells. It is critical for the maintenance of cell homeostasis. With the advancement of UPS research in recent years, it has been discovered that UPS is engaged in a variety of physiological and pathological processes in the human body. UPS is expected to play a role in the onset and progression of stroke via multiple targets and pathways. This paper explores the method by which UPS participates in the linked pathogenic process following stroke, in order to give a theoretical foundation for further research into UPS and stroke treatment.

Keywords: UPS, stroke, ubiquitination, mitochondrial dysfunction, oxidative stress, inflammation

OPEN ACCESS

Edited by:
Benoit LAURENT,
Université de Sherbrooke, Canada

Reviewed by:
Yomna Badawi,
University of Pittsburgh, United States
Nur M. Kocaturk,
MRC Protein Phosphorylation and Ubiquitylation Unit (MRC), United Kingdom

****Correspondence:***
Wei Zou
weiz2021@126.com

Specialty section:
This article was submitted to Cellular and Molecular Mechanisms of Brain-Aging, a section of the journal Frontiers in Aging Neuroscience

Received: *13 November 2021*
Accepted: *14 March 2022*
Published: *07 April 2022*

Citation:
Li Y-C, Wang Y and Zou W (2022) Exploration on the Mechanism of Ubiquitin Proteasome System in Cerebral Stroke. Front. Aging Neurosci. 14:814463. doi: 10.3389/fnagi.2022.814463

INTRODUCTION

Stroke is a potentially fatal cerebrovascular event defined by brain tissue damage produced by a sudden rupture of cerebral vessels or cessation of cerebral blood supply, resulting in neurological dysfunction, including ischemic and hemorrhagic stroke (Landowski et al., 2020). Stroke has overtaken ischemic heart disease as the second largest cause of death worldwide (Benjamin et al., 2017; Li et al., 2021). According to a comprehensive analysis of Chinese population's health, stroke has become the leading cause of mortality in the country (Zhou et al., 2019). According to current research, the ubiquitin proteasome system (UPS) plays a role in the molecular processes that lead to the occurrence and progression of stroke. UPS is also linked to a number of signaling pathways that cause injuries after stroke.

UBIQUITIN PROTEASOME SYSTEM

In cells, UPS is the primary non-lysosomal route for protein breakdown. This system destroys proteins with basic functions in addition to misfolded or oxidized proteins. Under physiological

and pathological situations, it is a critical mechanism for maintaining protein homeostasis (Kramer et al., 2021). In addition, the system is participated in a variety of cellular functions, including DNA repair (Uckelmann and Sixma, 2017), endocytic trafficking (Hicke, 2001), and immunological response (Bednash and Mallampalli, 2016). UPS is vital in central nervous system disorders because it can clean up aberrant proteins in neurodegenerative diseases including Alzheimer's and Parkinson's disease (Graham and Liu, 2017). At the same time, the system controls the primary risk factors for cerebrovascular disease, such as atherosclerosis (Wilck and Ludwig, 2014), hypertension (Li et al., 2013), hyperlipidemia (Sharpe et al., 2020), type 2 diabetes (Sun-Wang et al., 2021), and so on.

Ubiquitination Process

Ubiquitination is usually mediated by UPS. Ubiquitin, ubiquitin-activating enzyme (E1), ubiquitin-conjugating enzyme (E2), ubiquitin protein ligase (E3), deubiquitinase (DUB), and the proteasome are all important components of the UPS (Kane et al., 2021). Ubiquitin is a tiny peptide with a molecular weight of about 8.5 kDa that consists of 76 amino acids. It has a highly conserved sequence and is found in eukaryotic cells in large quantities. Ubiquitin molecule contains seven lysine residues (K6, K11, K27, K29, K33, K48, K63) and an N-terminal methionine residue (M1), which allow ubiquitin molecules to connect to one another (Kwon and Ciechanover, 2017). Homotypic polyubiquitination modification and heterotypic polyubiquitination modification are two types of ubiquitin-ubiquitination modification (Komander and Rape, 2012). Furthermore, ubiquitin can undergo post-translational modifications such as phosphorylation or acetylation (Yau and Rape, 2016; Ohtake and Tsuchiya, 2017). This complicates the ubiquitination process. Generally, E1 forms a high-energy thiohydroxyester bond between the carboxyl group of ubiquitin's C-terminal glycine and the sulfhydryl side chain of E1's active cysteine under the action of ATP (Ciechanover, 2015). E2 is an intermediate enzyme in ubiquitination reaction, which can bind E1 and E3. E2 enzyme has a highly conserved ubiquitin-conjugating enzyme domain (UBC). On the UBC sequence, there is a cysteine site with symbolic activity, which can accept ubiquitin molecules activated by E1 and form a thioester bond with ubiquitin (Zheng and Shabek, 2017). Subsequently, E2 with activated ubiquitin binds to E3; Finally, E2 transfers the ubiquitin molecule to the substrate by inducing the formation of an isopeptide bond between the C-terminus of ubiquitin and a target lysine of the substrate. E3 specifically recognizes target proteins during ubiquitination (Buetow and Huang, 2016).

E3's function reflects selectivity and efficiency of ubiquitination. Single subunit proteins and multisubunit complexes are two types of E3. There are four families of E3 single subunit proteins that have been identified: the HECT domain family, the RING domain family, the U-box domain family, and the N-recognition family. Cullin-RING and APC/C are the most common multisubunit complexes found in E3 (Zheng and Shabek, 2017). The human genome encodes approximately more than 600 ubiquitin ligases E3. Different E3 enzymes can specifically mediate the formation of different ubiquitin chain types. According to the different types of ubiquitin chain modification, it shows different functions. Polyubiquitination modification mediated by K48 or K11 ubiquitin chain is involved in proteasome degradation. Many E3 enzymes, such as SCF, gp78 and E6AP, can form K48 ubiquitin chains on substrate proteins, thus mediating the degradation of substrate proteins through proteasome (Wang and Pickart, 2005; Gao et al., 2016; Thacker et al., 2020). K11 ubiquitin chain was first considered as a regulator of cell fission, and its abundance increased with the increase of APC/C activity. APC/C, as an E3 enzyme, mediates the substrate Cyclin B1 to form K11 ubiquitin chain, which is finally degraded by proteasome, so as to promote the normal progress of cell mitosis (Song and Rape, 2010). In addition, studies have shown that K11 ubiquitin chain is often difficult to bind to 26S proteasome, but its degradation efficiency will be significantly enhanced when it forms a composite chain with K48 (Grice et al., 2015). Previous studies have shown that linear ubiquitination assembly complex (LUBAC) can modify NEMO by M1 ubiquitin chain to activate NF-κB pathway (Rahighi et al., 2009). This indicates that M1 ubiquitin chain is involved in activation of NF-κB pathway. ITCH and SMURF1 of the HECT family are members of the K29 ubiquitin chain's ubiquitin ligases. SMURF1 has been found to add K29 ubiquitin chain to AXIN in WNT pathway. AXIN modified by K29 ubiquitin chain will not be degraded, but will lose the ability to interact with receptor LRP5/6 of WNT pathway (Fei et al., 2013). ITCH has been reported to catalyze Deltex in the NOTCH pathway to form K29 ubiquitin chain, which enables Deltex to enter the lysosomal pathway (Chastagner et al., 2006). In the process of DNA damage repair, RNF168 will form K27 polyubiquitin chain on histone, and then recruit 53BP1 and BRCA1 to DNA damage site to start the DNA damage repair (Brown and Jackson, 2015; Gatti et al., 2015).

Proteasome

The proteasome is a multi-subunit protease complex that is found in both the cytoplasm and the nucleus. In mammalian cells, it is the primary neutral protein hydrolase. It is ubiquitin-dependent and possesses a variety of protein hydrolase functions. In UPS, the term "proteasome" usually refers to the 26S proteasome. The 20S proteasome and the 19S subcomplex make up the 26S proteasome (Gillette et al., 2008). Before the target proteins enter the 20S proteasome, each 19S sub complex comprises several ATPase active sites and ubiquitin binding sites that can recognize ubiquitinated target proteins, deubiquitinate the target proteins, and open the structural folding of the target proteins (Matyskiela et al., 2013). The 20S proteasome of eukaryotic cells contains two α rings and two β rings, these α rings and β rings together form a cylindrical structure, both α rings or β rings are composed of seven subunits. α rings are found in the outer layer of the 20S protease and are mostly employed for substrate identification; β rings are found in the inner layer and are primarily responsible for substrate degradation (Fricker, 2020). The β1, β2, and β5 of the seven β subunits have proteolytic activities, which are referred to as caspase-like activity, trypsin-like activity, and chymotrypsin-like activity, respectively, enzymolysis of acidic,

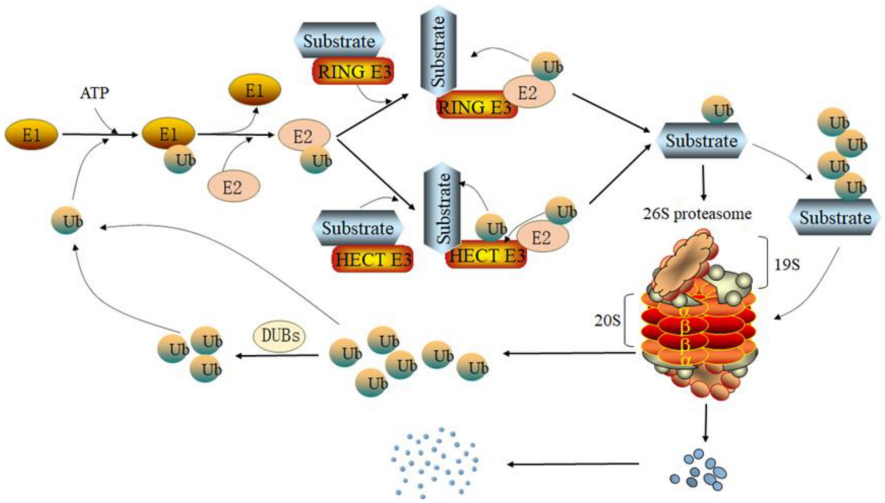

FIGURE 1 | Degradation pathway of the ubiquitin proteasome system (UPS). Under the action of ATP, the ubiquitin activating enzyme E1 forms a high-energy thiohydroxyester bond between the carboxyl group of ubiquitin's C-terminal glycine and the sulfhydryl side chain of E1's active cysteine. Then, ubiquitin-conjugating enzyme E2 receives ubiquitin activated by E1 through a cystine site on its ubiquitin-conjugating enzyme domain (UBC) and forms a thioester bond. Depending on the type of ubiquitin protein ligase E3, E2 can transfer ubiquitin to the substrate directly (RING E3s) or indirectly (HECT E3s) and form an isopeptide between the substrate and ubiquitin. In addition, ubiquitin can itself be the target of the ubiquitination cascade. Finally, the ubiquitinated substrate is degraded by the 26S proteasome. The ubiquitin separated from the substrate will re-enter the ubiquitination cycle.

alkaline, hydrophobic, or aromatic amino acid residues at the carboxyl end (Unno et al., 2002; **Figure 1**).

OCCURRENCE AND DEVELOPMENT OF STROKE

According to the causes, stroke can be classified as hemorrhagic or ischemic, with ischemic stroke accounting for around 87% of all cases (Virani et al., 2021). Due to cerebral ischemia or hemorrhage, the normal blood supply of neurons is destroyed, which leads to a series of pathophysiological reactions and finally to the death of nerve cells. The mechanisms involved in nerve injury include excitotoxicity, mitochondrial dysfunction, free radical disorder, inflammation, apoptosis, necrosis, autophagy and so on. According to analyses based on data from the Global Burden of Disease (GBD) study, modifiable risk factors such as hypertension, obesity, hyperglycemia, hyperlipidemia, atrial fibrillation and renal dysfunction account for 87% of stroke risk, while behavioral risk factors such as smoking, sedentary behavior, and an unhealthy diet account for 47%. Air pollution was found to be responsible for 30% of the global risk of stroke (Collaborators, 2020). In addition, age, gender and race are also associated with stroke (Diseases and Injuries, 2020). The combined action of multiple risk factors leads to pathological changes of cardiovascular and cerebrovascular system, including but not limited to atherosclerosis, arteriolar fat hyalinization and fibrin like necrosis, coronary artery disease, and myocardial injury. These pathological changes provide clues for the occurrence, recurrence, and secondary prevention of stroke.

Although brain tissue makes up only 2% of total body weight, cerebral blood flow accounts for 15% of cardiac output. The aerobic oxidation of glucose provides the majority of the energy required by brain tissue, although the glucose reserve is limited. Though brain oxygen use contributes for 23% of total body oxygen consumption, the oxygen reserve is small (Hyder et al., 2013). For these factors, the brain is extremely vulnerable to ischemia and hypoxia. Following a stroke, brain ischemia, and hypoxia are major concerns. In the ischemic core the major mechanism of cell death is energy failure. Neurons cannot create the ATP needed to supply the ionic pumps that maintain the ionic gradient across the neuronal membrane, primarily the Na^+/K^+ ATPase, without oxygen or glucose. As a result, a substantial amount of Na^+ and Ca^{2+} accumulate in the cytoplasm, causing organelles swelling and degeneration, loss of cell membrane integrity, and ultimately cell necrosis (Lipton, 1999). In the ischemic penumbra, the decrease in blood flow due to collateral blood supply is not enough to lead to rapid energy failure, and neurons still survive for a long time after ischemia and hypoxia. The excessive accumulation of extracellular glutamate is an important factor leading to ischemic penumbra injury (Mazzocchetti et al., 2020). Due to the excessive accumulation of glutamate, the overactivation of subtypes of N-methyl-D-aspartate receptors (NMDARs) leads to cellular calcium overload. Therefore, calcium-dependent proteases are activated, such as calpains, resulting in nerve cell damage (Rami et al., 2000). In addition, some studies have shown that calpains are involved in the activation of Caspase-3, which may be an important mechanism of neuronal apoptosis after stroke (Blomgren et al., 2001). Meanwhile, mitochondrial dysfunction is caused by Ca^{2+} overload which leads to mitochondrial permeability transition pore (mPTP) opening (Zhu et al., 2018). Of note, mitochondrial dysfunction leads to insufficient ATP production, which will further lead to Ca^{2+} accumulation

and form a vicious circle. Nerve cell survival is aided by the removal of defective mitochondria. Mitochondrial autophagy is an important regulatory process for the quality and quantity of mitochondria. According to a report, UPS plays a key function in the regulation of mitochondrial autophagy (Alsayyah et al., 2020). Mitochondria are organelles that operate as oxidative energy centers and are required for cell survival, but aging or damaged mitochondria produce deadly reactive oxygen species (ROS; Liu et al., 2018). ROS are important signaling molecules in oxidative stress. In the pathological manifestations of stroke, relatively excessive ROS will destroy the homeostasis of intracellular environment, resulting in oxidative stress and mitochondrial damage (Sims and Muyderman, 2010). The main defensive response to oxidative and electrophilic stressors is the Keap1-Nrf2 pathway. UPS can strictly regulate the transcription of nuclear factor erythroid2-related factor (Nrf2) through this pathway, thereby affecting the antioxidant process (Baird and Yamamoto, 2020). Whether it is mitochondrial dysfunction or oxidative stress, it will eventually lead to neuronal damage. Inflammation is one of the most prevalent pathological signs following a stroke, and it is induced by a range of factors, including microglia activation (Koh et al., 2018) and cytokine involvement (Xu et al., 2018). Inflammation has the potential to be neurotoxic., which can lead to neuronal death (Liddelow et al., 2017). Hypoxia-inducible factor-1 (HIF-1) comprised by α and β subunits is a protein that regulates the expression of genes that code for erythropoietin (EPO) and vascular endothelial growth factor (VEGF), as well as genes involved in glucose transport and glycolysis, such as glucose transporter-1 (GLUT1), pyruvate dehydrogenase kinase 1 (PDK1), and lactate dehydrogenase A (LDHA; Leu et al., 2019). In the hypoxic state caused by stroke, the oxygen-dependent HIF prolyl hydroxylase domain (PHD) is inactivated, leading to the stabilization of HIF-1α, followed by its translocation into the nucleus, where it forms a heterodimeric complex with HIF-1β. This complex, called HIF-1, interacts with DNA and activates the expression of multiple target genes encoding proteins that help increase the tissue's oxygen supply by boosting erythropoiesis and angiogenesis (Semenza, 2004, 2009). UPS has been implicated in the control of HIF in recent research (Delpeso et al., 2003). Therefore, regulating related pathways and their key proteins through UPS may be an effective solution to protect neurons and prevent cell death during stroke.

REGULATORY MECHANISM OF UBIQUITIN PROTEASOME SYSTEM

NF-κB Pathway and Ubiquitin Proteasome System

NF-κB is a transcription factor family that includes NF-κB1 (P50/p105), NF-κB2 (p52/P100), and three RelA (p65), RelB, and c-Rel (REL) proteins (Caamano and Hunter, 2002). As a hub in signal transduction pathway, NF-κB can regulate the expression of many genes involved in cell inflammation, immune response, cell growth and development (DiDonato et al., 2012). IκB protein is a family of constitutive inhibitors of NF-κB, including IκBα, IκBβ, IκBγ, IκBζ, IκBε, Bcl-3, p100 and p105 (Yamazaki et al., 2001; Chiba et al., 2013). IKK complex consists of IKKα, IKKβ and Nemo, which is the kinase of IκB (Durand and Baldwin, 2017). Under normal conditions, NF-κB and inhibitor IκB binding exists in the cytoplasm in an inactive potential state (Wang et al., 2019).

NF-κB signaling pathway mainly includes classical and non-classical activation pathways (**Figure 2**). In the classical one, IKK complex is activated when cells are stimulated by proinflammatory factors, growth factors, immune receptor ligands and stress response (Fricker, 2020), in which IKKβ (ser177 and ser181) and IKKα (ser176 and ser180) sites in the amino terminal kinase domain are phosphorylated. Due to their activation, serine residues of IκB are phosphorylated (Ling et al., 1998; Delhase et al., 1999). The polyubiquitination mode of IκBα depends on the phosphorylation of two serine residues (ser32 and ser36), while the phosphorylation sites of IκBβ are ser19 and ser23 (Chen, 2012). The phosphorylation of IκB leads to the covalent binding of lysine residues at positions 21 and 22 of its amino terminal to multiple ubiquitin molecules through SCF type E3 ubiquitin ligase complex. This binding changes the spatial conformation of IκB, resulting in its recognition and degradation by ATP dependent 26S proteasome (Chen et al., 1995; Karin and Ben-Neriah, 2000; Caamano and Hunter, 2002). Following depolymerization, the liberated NF-κB dimer is activated by several post-translational modifications before being transported to the nucleus and combining with particular DNA sequences to increase target gene transcription (Zhang et al., 2017). Inflammatory cytokines like TNF-α, IL-2, IL-6, and INF-γ are then produced, reactivating NF-κB and causing inflammatory damage to cell tissues (Mitchell and Carmody, 2018). The activation of non-classical NF-κB pathway depends on receptor activated kinase NIK, which can activate IKKα (Cildir et al., 2016). The phosphorylation of NF-κB2 p100 mediated by activated IKKα leads to its own ubiquitination, which is recognized by proteasome and partially degraded to p52. Finally, p52-RelB heterodimer enters the nucleus to start transcription (Xiao et al., 2001; Sun, 2011). Therefore, NF-κB plays a crucial role in acute and chronic inflammatory illnesses as the center regulating the expression of pro-inflammatory genes in the inflammatory process (Baker et al., 2011).

PINK1/Parkin Pathway and Ubiquitin Proteasome System

The PTEN-induced putative kinase 1(PINK1)/Parkin pathway is one of the most prevalent mechanisms for controlling mitochondrial quality and abundance (Shen et al., 2021). PINK1 is a mitochondrial serine (Ser)/threonine (Thr) kinase with a mitochondrial targeting sequence (MTS), a transmembrane (TM) segment, and a Ser/Thr kinase domain that is nuclear encoded (Eiyama and Okamoto, 2015). PINK1, as a Parkin upstream component, is required for Parkin activation and recruitment to depolarized mitochondria (Miller and Muqit, 2019). Parkin has an N-terminal ubiquitin-like (UBL) domain, three RING domains (RING0, RING1, and RING2), and an in-between RING(IBR) domain that separates RING1 and RING2

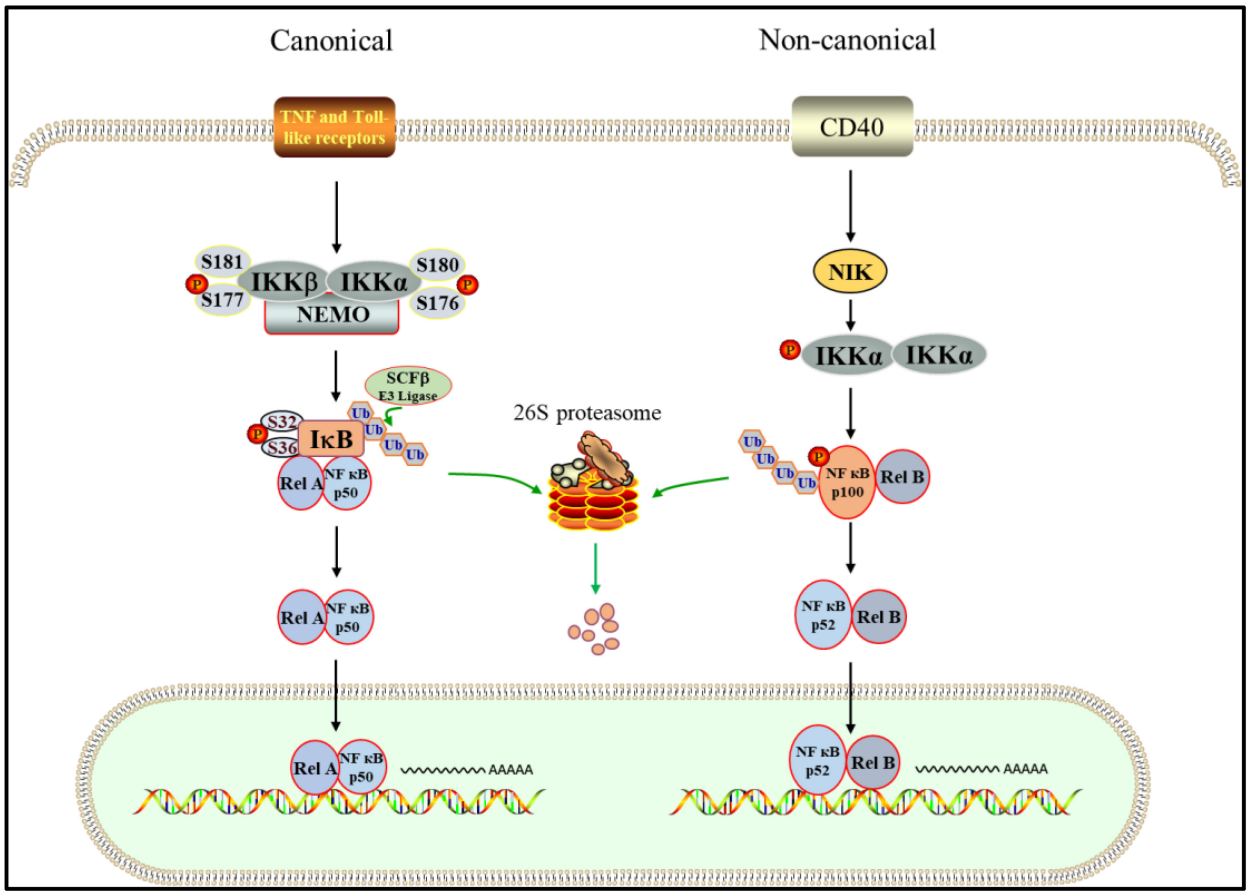

FIGURE 2 | UPS is involved in canonical and non-canonical NF-κB pathway. In the canonical way. After the inflammatory receptor is activated, the activated IKK complex phosphorylates ser32 and ser36 of IκB, which promotes the ubiquitination of IκB mediated by SCFβ. Subsequently, IκB is targeted to the 26S proteasome for proteolysis. NF- κB dimer was released and transferred into the nucleus to start the transcription of target genes. In the non-canonical pattern. IKK is activated by NIK, which leads to phosphorylation of p100. Then, Phosphorylated p100 is degraded by proteasome after ubiquitination, in which p52-RelB heterodimer is produced. Finally, the p52-RelB heterodimer enters the nucleus to start transcription.

as an E3 ligase (Biswas et al., 2020). When the MTS and TM of PINK1 reach the inner mitochondrial membrane under healthy conditions, the transmembrane segment is cleaved in the form of protein hydrolysis by the presenilins-associated rhomboid-like protein (PARL) found in the inner membrane. Cleaved PINK1 is released into the cytoplasm, exposing destabilizing amino acid residues at its N-terminus. E3 ubiquitin ligases (UBR1, UBR2, and UBR4) ubiquitinate them with N-terminal rules and degrade fast by proteasome (Yamano and Youle, 2013; **Figure 3A**). Therefore, the content of PINK1 in cytoplasm is very low and Parkin is not activated (Pickrell and Youle, 2015). When the mitochondrial membrane potential is abnormal, PINK1 avoids PARL-mediated processing and N-end rule-dependent degradation by forming a stable association with the translocase of the outer membrane (TOM) and accumulating on the outer mitochondrial membrane (OMM; Lazarou et al., 2012). PINK1 accumulates on the OMM can activate parkin in two ways. On the one hand, Parkin is activated by PINK1 phosphorylating ser65 in the Parkin UBL domain (Bingol and Sheng, 2016). On the other hand, PINK1 phosphorylates ser65 in ubiquitin, which is coupled with OMM proteins at basic levels. Parkin's affinity for phosphorylated ubiquitin is what causes it to be found in mitochondria. The activated Parkin further binds ubiquitin to the OMM protein, and then ubiquitin is phosphorylated by PINK1 (Bragoszewski et al., 2017; **Figure 3B**). On mitochondria, phospho-ubiquitin produced by PINK1 serves as an autophagy signal, which Parkin amplifies (Lazarou et al., 2015). Subsequently, ubiquitinated OMM protein recruits autophagic adaptor protein SQSTM1/p62 to damaged mitochondria (Geisler et al., 2010), and promotes its degradation through autophagy. There are some negative regulatory mechanisms related to UPS in PINK1/Parkin pathway, which are very important for the stability of mitochondrial autophagy. Ubiquitin-specific protease30 (USP30) is an OMM localized DUB, which antagonizes PINK1/Parkin mediated mitochondrial autophagy by deubiquitination of OMM proteins. The presence of USP30 can maintain the steady state of ubiquitination of OMM protein and prevent excessive mitochondrial autophagy (Tanaka, 2020). Furthermore, UBL exhibits a strong affinity for the Rpn13 subunit of

the 26S proteasome regulatory granules. The proteasome is attracted to mitochondria by this affinity, which increases proteasome degradation of ubiquitinated OMM protein and Parkin (Aguileta et al., 2015).

Keap1-Nrf2 Pathway and Ubiquitin Proteasome System

Nrf2 is the main regulator of redox and metabolic homeostasis. It has seven Nrf2 ECH homologous domains (Neh1-Neh7), and each domain has different functions (Hayes and Dinkova-Kostova, 2014). As the most important regulatory domain of Nrf2, Neh2 includes two motifs, DLG and ETGE, which can regulate the stability and ubiquitination of Nrf2 by binding to other proteins such as Keap1 (Tong et al., 2006). Keap1 is a substrate adaptor protein of Cullin3 (Cul3)-dependent E3 ubiquitin ligase complex, which can be assembled with Cul3 and Rbx1 (ring-box1). Keap1 serves as a substrate adapter, whereas Rbx1 binds to ubiquitin-loaded E2 and Cul3 serves as a scaffold between Keap1 and Rbx1, which can regulate Nrf2 (Tonelli et al., 2018). Keap1 contains three functional domains, including a BTB domain, an IVR and a Kelch or DGR domain (Sajadimajd and Khazaei, 2018). The N-terminal BTB domain of Keap1 can bind Cul3, which is necessary for Keap1 dimerization (Suzuki and Yamamoto, 2015). Under normal conditions, the Neh2 domain of Nrf2 interacts with the Kelch/DGR domain in Keap1 through the mediation of DLG and ETGE motifs. Keap1-Cul3-E3 ubiquitin ligase targets multiple lysine residues located in the Neh2 domain at the N-terminal of Nrf2 and promotes the ubiquitination of Nrf2. The ubiquitinated Nrf2 is transported to the 26S proteasome, where it is degraded (Canning et al., 2015; Karunatilleke et al., 2021; **Figure 4A**). Critical cysteine residues in Keap1, particularly Cys151, operate as sensors of these cellular damages under oxidative stress conditions and become covalently changed by electrophilic molecules or ROS (Zhang and Hannink, 2003). Such changes cause Keap1 to shift conformation, most likely by disrupting the low-affinity link between the Kelch domain and the DLG-motif, resulting in decreased ubiquitylation of Nrf2, inhibiting UPS-mediated degradation and thereby boosting Nrf2 protein levels (Baird et al., 2013). Then Nrf2 translocases to the nucleus and binds to the ARE/EpRE of the target gene through heterodimerization with sMAF protein to induce the expression of a series of cell protective genes, such as NQO1, GST, HMOX1, GCL, GSH, etc. (Kansanen et al., 2013; Fao et al., 2019; **Figure 4B**), so as to reduce or eliminate oxygen free radicals and improve the antioxidant capacity of cells and tissues.

HIF-1 Pathway and Ubiquitin Proteasome System

Hypoxia inducible factor (HIF) is an important transcription factor regulated by the change of oxygen concentration (Wang et al., 1995). It is composed of a α subunit regulated by oxygen concentration and a constitutively expressed β subunit, in which α subunit has three functional forms: HIF-1α, HIF-2α and HIF-3α. HIF is divided into HIF-1, HIF-2 and HIF-3 according to different α subunits. α subunit and β subunit have two important domains: the basic helix-loop-helix (bHLH) and Per-Arnt-Sim (PAS). The bHLH and PAS are required for dimerization between HIF-1α and HIF-1β (Zhang et al., 2011; Shu et al., 2019). HIF-1α is generally expressed in all cells, while HIF-2α and HIF-3α are selectively expressed in some tissues (Majmundar et al., 2010). HIF-1α which has two transactivation domains, N-terminal transactivation domains (N-TAD) and C-terminal transactivation domains (C-TAD), as well as an oxygen-dependent degradation domain (ODDD) that mediates oxygen-regulated stability, is not only the regulatory subunit of HIF-1, but also its active subunit (Ruas et al., 2002). The stability and activity of α subunit are regulated by post-translational modifications such as hydroxylation, ubiquitination, acetylation and phosphorylation. Among them, HIF-1α is mainly regulated by the PHD (Ke and Costa, 2006). Under the normoxic state, the prolyl residues at sites 402 and 564 of HIF-1α are hydroxylated by PHD. Hydroxylated HIF-1α binds to Von Hippel-Lindau (VHL), which together with Elongin C, Elongin B, Cullin-2, and Rbx1, forms the VCB-Cul2 E3 ligase complex. Subsequently, it is ubiquitinated, then recognized by 26S proteasome and degraded (Ohh et al., 2000). Since PHD activity is suppressed during hypoxia, VHL is unable to detect HIF-1α, and hence HIF-1α is not degraded by UPS. Subsequently, accumulated HIF-1α enters the nucleus from the cytoplasm, where it is joined to create a dimer with HIF-1β (Tarhonskaya et al., 2015). In the nucleus, p300/CBP associated factor (PCAF) combines with the C-TAD of HIF-1α to form a complex. The complex combines with the hypoxia response element (HRE) in the promoter region of hypoxia response genes to promote the transcription of hypoxia response gene and cause a series of adaptive responses of cells to hypoxia (Dengler et al., 2014). In addition, HIF-1α is also regulated by the factor inhibiting HIF (FIH; Kaelin and Ratcliffe, 2008). In normoxic environment, FIH hydroxylates the asparagine residue (N803) of HIF-1α to prevent the connection between p300/CBP and C-TAD, thereby reducing the transcriptional activity of HIF-1α (Lando et al., 2002b). Under hypoxia, the hydroxylation of FIH is inhibited, which promotes the interaction between HIF-1α and p300/CBP and leads to the transcription of target genes (Lando et al., 2002a; **Figure 5**).

THE ROLE OF UPS IN SIGNAL PATHWAY AFTER STROKE

UPS Participation in NF-κB Pathway and Stroke

UPS is essential for maintaining protein homeostasis and preventing damaging protein aggregation in cells (Budenholzer et al., 2017). Inflammation is the result of a complicated interplay between soluble substances and cells (Medzhitov, 2008). Inflammatory cell infiltration and activity frequently result in long-term tissue damage (Feehan and Gilroy, 2019). UPS can play an important role in the inflammatory process by regulating a variety of inflammatory regulatory proteins (Goetzke et al., 2021). It was found that inflammatory response widely exists

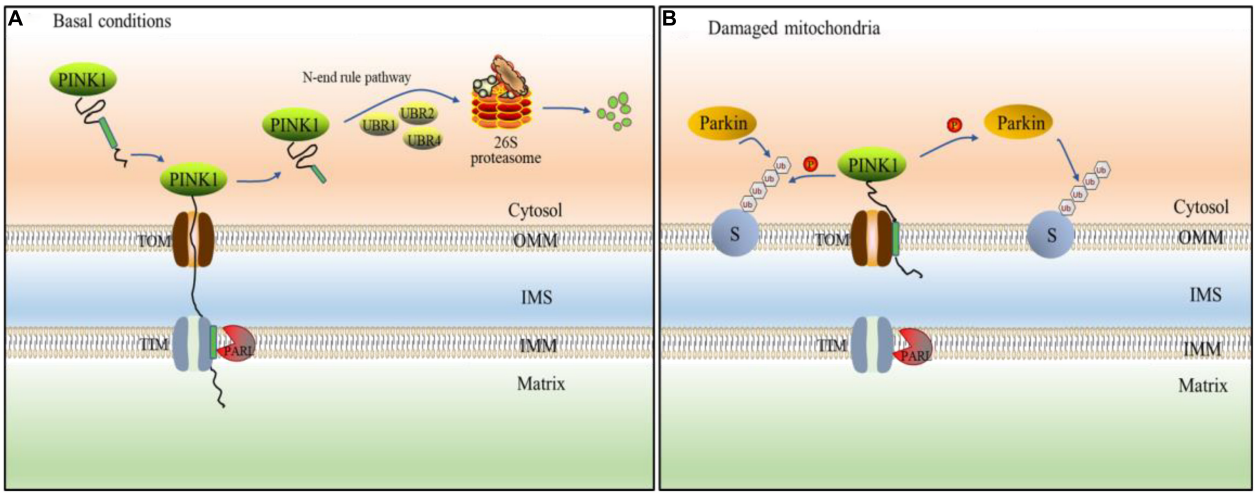

FIGURE 3 | PINK1/Parkin pathway mediates ubiquitination of mitochondria. **(A)** Under basal condition, PINK1 passes through the outer mitochondrial membrane (OMM) to the inner membrane (IMM), and its transmembrane segment is hydrolyzed by presenilins-associated rhomboid-like protein (PARL) protein. The treated PINK1 is released into the cell matrix and mediated proteasome degradation by E3 ubiquitin ligases (UBR1, UBR2, and UBR4). **(B)** When mitochondrial disorder, PINK1 cannot be transported across membranes, so that it cannot be destroyed by PARL. Instead, PINK1 stably binds to the OMM and accumulates on it. Therefore, PINK1 can directly phosphorylate ubiquitin or Parkin. Parkin is recruited by phosphorylated ubiquitin to various mitochondrial substrate proteins(S) in which mitochondrion is ubiquitinated.

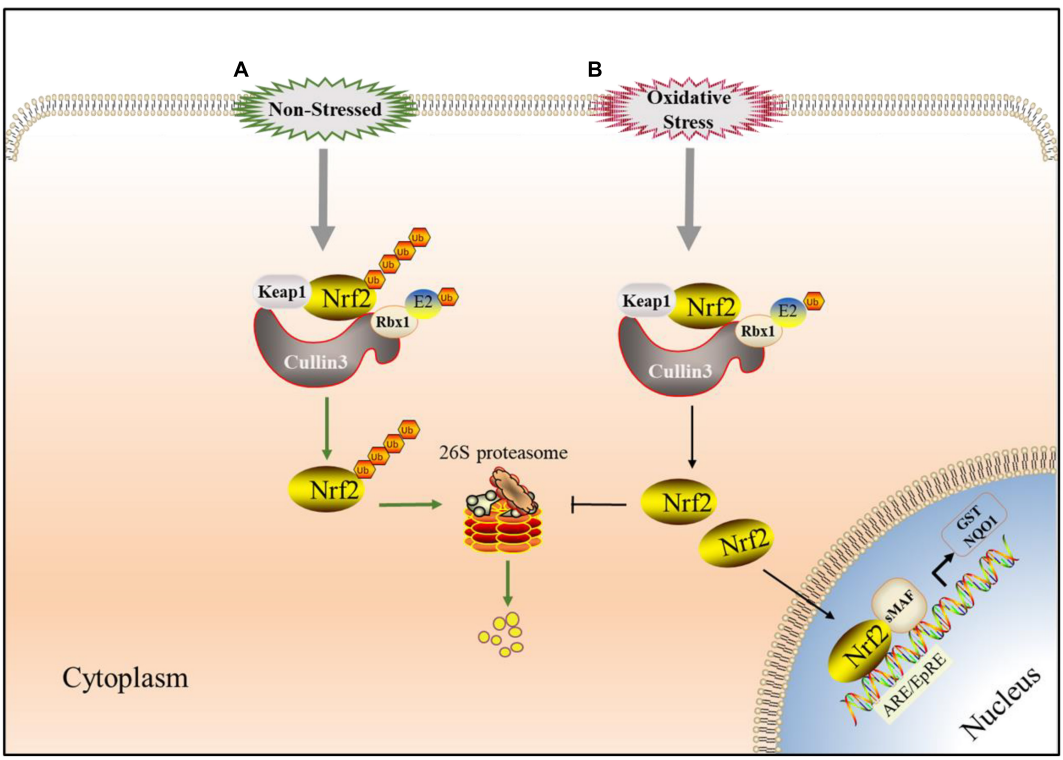

FIGURE 4 | Keap1-Nrf2 signaling pathway involved in UPS. **(A)** Under non-stressed conditions, Nrf2 binds to Keap1 complex which has E3 ligase activity in the cytoplasm. When Nrf2 is ubiquitinated, it is targeted to the 26S proteasome for proteolysis which keep it low in cytoplasm. **(B)** Under oxidative stress conditions, Critical cysteine residues in Keap1 is covalently-modified by electrophilic species or reactive oxygen species (ROS) and Nrf2 avoides Keap1-mediated ubiquitination modification. Then Nrf2 translocated to the nucleus, starts ARE/EpRE transcription through heterodimerization with SMAF protein, and induced the expression of a series of cytoprotective genes.

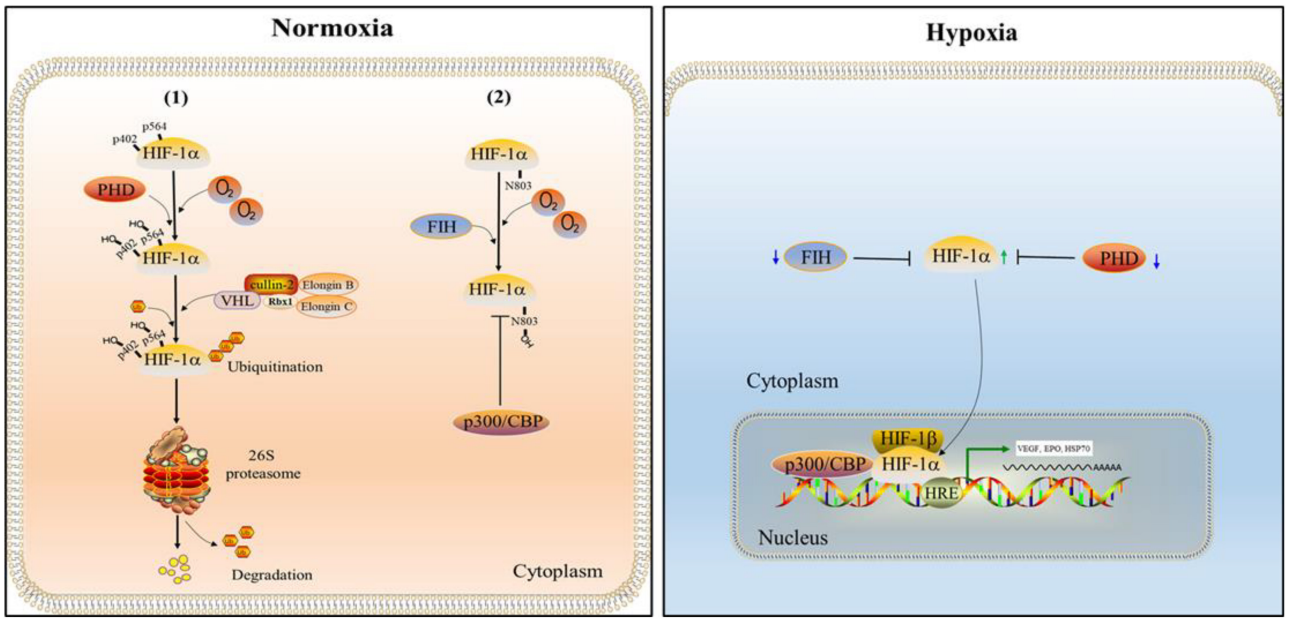

FIGURE 5 | The regulation of HIF-1. Under the normal oxygen condition, the prolyl residues at sites 402 and 564 of HIF-1α are hydroxylated by the prolyl hydroxylase domain (PHD). Subsequently, hydroxylated HIF-1α is ubiquitinated by Von Hippel-Lindau (VHL) and degraded by 26S proteasome. In addition, the asparagine residue (N803) of HIF-1α is hydroxylated by the factor inhibiting HIF (FIH) which inhibits the connection between p300/CBP and C-TAD, thereby reducing the transcriptional activity of HIF-1α. When hypoxia occurs, the activities of FIH and PHD are inhibited. Therefore, HIF-1α can enter the nucleus to form complexes with HIF-1β and p300/CBP, and promote the transcription of hypoxia response genes and cause a series of adaptive responses of cells to hypoxia.

after cerebral ischemia and acute ischemic stroke (Chamorro et al., 2016). It can be seen that inhibiting the activity of NF-κB can reduce the nerve injury after intracerebral hemorrhage or cerebral ischemia (Liu et al., 2019; Shang et al., 2019). In recent years, many studies have reported that the effect of UPS is related to the activation of NF-κB. Intervening UPS can prevent the degradation of IκB and the activity of NF-κB and combine them in cell solute. Ginsenoside Rd treatment can restore IκB expression in the cytoplast after ischemia injury by decreasing proteasome activity, therefore suppressing NF-κB activity and protecting neurons, according to a study (Zhang et al., 2020). Phillips et al. applied proteasome inhibitor PS519 to rats with focal cerebral ischemia and found that PS519 can reduce the inflammatory response by restraining NF-κB and improve the recovery of neurological function in rats with brain injury (Phillips et al., 2000). According to another study, the neuroprotective effect of PS519 may be related to its involvement in the regulation of cell adhesion molecules ICAM-1 and E-selectin, because these two adhesion molecules play a key role in the adhesion and exudation of neutrophils and macrophages across the blood-brain barrier (Berti et al., 2003). These suggest that the effect of proteasome inhibitors on inflammatory response may be multi-channel. Moreover, although early intervention of UPS has a neuroprotective effect on inhibiting NF-κB overexpression at the transcriptional level, the decrease of long-term proteasome activity is related to intracellular protein aggregation, delayed neuronal degeneration, and death (Meller, 2009). It suggested that UPS may played a dual role in neurons after ischemia. Although proteasome inhibitors have been shown to provide protection in cerebral ischemia, other nerve injury problems caused by decreased proteasome activity cannot be ignored (Caldeira et al., 2014). Due to the non-selectivity of most proteasome inhibitors, the application of proteasome inhibitors is limited (Wojcik and Di Napoli, 2004). Chen et al. suggested that selective immunoproteasome inhibitors may be a promising strategy for stroke treatment. They discovered that inhibiting the expression of p65 and reducing infarction volumes in rats may be accomplished by inhibiting the low molecular weight protein 2 (LMP2), a significant catalytic subunit of immunoproteasome (Chen et al., 2015).

PINK1/Parkin and Cerebral Stroke Regulated by UPS

PINK1/Parkin pathway is one of the classical pathways of mitochondrial autophagy. Under normal conditions, UPS forms a strict PINK1 and Parkin regulatory mechanism to maintain the balance of mitochondrial autophagy and prevent mitochondrial damage caused by excessive mitochondrial autophagy (Oshima et al., 2021). In the stroke induced by mitochondrial dysfunction (Youn et al., 2021; Zhou et al., 2021), PINK1/Parkin pathway mediates ubiquitination of dysfunctional mitochondrial OMM protein, and then clears abnormal mitochondria through crosstalk with autophagy (Geisler et al., 2010). In recent years, there has been more and more studies on this mechanism, which to some extent shows that UPS plays an important role in PINK1/Parkin pathway in the process of brain injury in stroke. At present, the researches on the pathway in

stroke mainly focus on its relationship with autophagy, but ignore the role of UPS. In fact, mitochondrial ubiquitination mediated by PINK1/Parkin pathway is the basis of mitochondrial autophagy. Inactive PINK1 cannot activate or recruit Parkin to mitochondria (Narendra et al., 2008; Matsuda et al., 2010). The UPS mechanism can be inhibited to prevent PINK1/Parkin-mediated ubiquitination of OMM proteins (Chan et al., 2011). Furthermore, inhibiting Parkin mitochondrial translocation, lowering Parkin phosphorylation, and lowering the quantity of phosphorylated ubiquitin (pser65 Ub) can all be used to prevent mitochondrial autophagy triggered by various mitochondrial damage causes (Wang et al., 2018a). OMM proteins could be destroyed through an autophagy-independent UPS route, according to Rakovic et al. The bigger OMM proteins MFN2 and TOM70 were only partially ubiquitinated and primarily destroyed by the lysosomal system, whereas the smaller OMM proteins TOM40 and TOM20 were only slightly ubiquitinated and mostly degraded by UPS (Rakovic et al., 2019). It showed that depolarized mitochondrial membrane proteins could be degraded by two different mechanisms: UPS or lysosomal mediated protein hydrolysis. At the same time, the degradation of larger OMM protein affected the stability of OMM, led to its rupture, exposed mitochondrial inner membrane (IMM) to the cytoplasmic environment, and caused drastic changes in IMM structure and morphology, which might eventually lead to the secondary degradation of IMM and matrix protein (Yoshii et al., 2011). In the oxygen-glucose deprivation (OGD) neuronal model, PINK1 knockout mice ($PINK1^{-/-}$) were more sensitive to ischemic injury than control group (Imbriani et al., 2020). Moreover, in traumatic brain injury (TBI), the loss of Parkin would increase the production of ROS, promote oxidative stress and further lead to neuronal death (Mukhida et al., 2005). In a rat model of ischemia, PINK1/Parkin-mediated mitochondrial autophagy may perform a neuroprotective role in hippocampus neurons (Wu et al., 2018). The deletion of either the PINK1 or Parkin genes has been shown to cause aggregated neuronal damage. Increasing the expression of PINK1 and Parkin, on the other hand, could prevent a huge number of nerve cells from dying. Therefore, it is necessary to pay attention to the role of PINK1/Parkin/UPS mechanism in mitochondrial damage after stroke, rather than autophagy.

UPS Control in Stroke and Keap1-Nrf2

Oxidative stress refers to the imbalance of redox balance caused by the production of excessive ROS after the body is stimulated by the outside world, resulting in the damage of cell tissue (Hybertson et al., 2011). Because of its high oxygen consumption and fat content, the brain is prone to oxidative injury. The role of oxidative stress in ischemia-reperfusion brain injury has long been recognized (Chamorro et al., 2016). Nrf2 is the main regulator of endogenous and exogenous stress defense mechanisms in cells and tissues. Its primary role is to activate the antioxidant response and trigger the transcription of a number of genes in order to protect cells from oxidative stress and restore intracellular homeostasis (Villeneuve et al., 2010; Chen and Maltagliati, 2018). That Nrf2 escape from Keap1 repression is the crucial event for Nrf2-mediated activation (Kaspar et al., 2009). Oxidative stress caused by cerebral ischemia or intracerebral hemorrhage affects the conformation of Keap1. Then, Nrf2 dissociates and transfers to the nucleus, binds to ARE, and stimulates the target gene expression of downstream antioxidant enzymes and other cytoprotective proteins (Hu et al., 2016; Jiang et al., 2017). The expression of Nrf2 is highly up-regulated in ischemic brain tissue, according to studies, and a range of Nrf2 inducers exhibit neuroprotective effects following cerebral ischemia (Wang et al., 2018b). Monomethylfumarate, the immediate metabolite of dimethylfumarate (DMF), causes direct alteration of the cysteine 151 of Keap1, which increases the dissociation of Nrf2 and has neuroprotective properties (Linker et al., 2011; Bomprezzi, 2015). Furthermore, in the human neuroblastoma cell line SH-SY5Y, miR-7 can target to limit Keap1 mRNA translation, preventing the degradation of Nrf2 protein, resulting in Nrf2 activation and cytoprotection (Kabaria et al., 2015). Although these reagents need to be further studied in the stroke model, it is undeniable that preventing Nrf2 from being degraded by proteasome through modification or inhibition of Keap1 is a promising measure in the protection of neurons after stroke. According to a report, p62 expression reduced Nrf2 degradation and increased subsequent Nrf2 nuclear accumulation by inactivating Keap1 (Sun et al., 2016). Li et al. found that sestrin2 stimulated angiogenesis to ameliorate brain injury by activating Nrf2 and modulating the interaction between p62 and Keap1, following photothrombotic stroke in rats (Li et al., 2020). In addition, it has been reported that PINK1/Parkin pathway can promote the release of Nrf2 by inhibiting Keap1 (Xiao et al., 2017). Zhang et al. found that mitophagy reduced oxidative stress via Keap1/Nrf2/PHB2 (Prohibitin 2) pathway after subarachnoid hemorrhage in rats (Zhang et al., 2019). A study has shown that Britanin leading to the induction of the Nrf2 pathway ameliorated cerebral ischemia–reperfusion injury by selectively binding to cysteine 151 of Keap1 and inhibiting Keap1-mediated ubiquitylation of Nrf2 (Wu et al., 2017). Obviously, preventing the proteasome degradation of Nrf2 through the regulation of Keap1 is very important for neuroprotection after stroke.

HIF-1 Pathway and Stroke Regulated by UPS

Tissue oxygen content plays crucial roles in maintaining the normal functioning of cells and regulation of their development (Mohyeldin et al., 2010). HIF-1 is an important transcriptional regulator of hypoxia and plays an important role in cerebrovascular diseases (Correia and Moreira, 2010). Accumulating evidence indicates that the induction of HIF-1 provides protection against cerebral ischemic damage (Zhang et al., 2011). HIF-1α is widely expressed in the hypoxic/ischemic brain (Chavez et al., 2000). Mice with neuron-specific reduction of HIF-1α that were subjected to temporary focal cerebral ischemia showed higher tissue damage and a lower survival rate, indicating that HIF-1-mediated responses have an overall positive impact in the ischemic brain (Baranova et al., 2007). HIF-1α has complex effects on the brain, which largely depends on the time-point after hypoxic damage. At the earliest post-ischemic

stage (i.e., within 24 h), HIF-1α accumulation promotes cell death. In contrast, during the later stage (i.e., >4 days), HIF-1α signaling has a pro-survival effect through limitation of the infarct size (Mitroshina et al., 2021). HIF-1α which is an important regulator of hypoxia being regulated by proteasomal degradation (Shi, 2009). There is now overwhelming data suggesting that the UPS contributes to cerebral ischemic injury and proteasome inhibition is a potential treatment option for stroke (Wojcik and Di Napoli, 2004). Growing evidence shows that proteasome inhibitors enhance angioneurogenesis and induces a long-term neuroprotection after cerebral ischemia. Inhibition of immunoproteasome LMP2 was able to enhance angiogenesis and facilitate neurological functional recovery in rats after focal cerebral ischemia/reperfusion. A study highlights an important role for inhibition of LMP2 in promoting angiogenesis events in ischemic stroke, and point to HIF-1α as a key mediator of this response (Chen et al., 2018). The novel proteasome inhibitor BSc2118 protects against cerebral ischemia through HIF1A accumulation and enhanced angioneurogenesis (Doeppner et al., 2012). Although the role of HIF-1α in cerebral ischemia remains complex, the role of HIF-1α as mediator of BSc2118-induced neuroprotection is appealing based on the data present (Yan et al., 2011). Furthermore, a result indicates that 20S proteasomes are involved in HIF-1α degradation in ischemic neurons and that proteasomal inhibition provides more HIF-1α stabilization and neuroprotection than PHD inhibition in cerebral ischemia (Badawi and Shi, 2017).

CONCLUSION AND FUTURE DIRECTIONS

UPS is the main pathway for the degradation of cytosolic, nuclear and transmembrane proteins, and also the main regulator for maintaining neural development, brain structure and function (Park et al., 2020). Neuron is a highly differentiated terminal cell. Various components of UPS widely exist in synapses and participate in the regulation of synaptic function (Tsakiri and Trougakos, 2015). After stroke, due to the destruction of the internal environment of neuron survival, a series of neuron injury events are caused, which eventually leads to the death of nerve cells and the loss of nerve function. In recent years, there have been more and more researches on UPS. It is found that UPS mediated protein degradation is an important mechanism for the body to regulate the level and function of intracellular proteins. The components involved in this biological process mainly include ubiquitin and its related starting enzymes. UPS plays a very important role in maintaining cell homeostasis (Shang and Taylor, 2011). At the same time, UPS is also involved in the pathological process related to nerve injury after stroke (Ge et al., 2007). At present, there are many research results on the physiological and pathological mechanism of stroke. However, the discussion on UPS and stroke is insufficient and there is a lack of literature for reference. Nevertheless, it may still become a new hotspot in basic research and potential clinical application. It should be noted that the aggregation of ubiquitinated proteins is one of the important features after stroke (Luo et al., 2013). UPS is closely related to the pathways of post-stroke related pathological changes such as mitochondrial autophagy, oxidative stress, hypoxia and inflammatory response (Ahmad et al., 2014). To study the role of UPS in PINK1/Parkin, NF-κB, HIF-1α and the regulatory mechanism of Keap1-Nrf2 pathway is of great significance for the clinical treatment and prognosis of stroke patients. At present, there are still many problems that need more experiments to study. From the perspective of maintaining homeostasis, it is necessary to clarify how to moderately activate or inhibit UPS to play a cytoprotective role. The pathological process of stroke is a dynamic process. It is necessary to observe the changes of UPS by stages. Due to the lack of research on the side effects of drugs in experimental animals and the results of clinical trials, the conclusion whether UPS regulating drugs mediate cell protection or cytotoxicity after stroke is still controversial. To explore the relationship between UPS and stroke and its mechanism has great potential to improve the prognosis of stroke patients.

AUTHOR CONTRIBUTIONS

Y-CL wrote the manuscript. WZ and YW proofread the manuscript. All authors read and approved the final manuscript.

FUNDING

This work was supported by the National Natural Science Foundation of China (Grant No. 81774416).

REFERENCES

Aguileta, M. A., Korac, J., Durcan, T. M., Trempe, J.-F., Haber, M., Gehring, K., et al. (2015). The E3 ubiquitin ligase parkin is recruited to the 26 S proteasome via the proteasomal ubiquitin receptor Rpn13. *J. Biol. Chem.* 290, 7492–7505. doi: 10.1074/jbc.M114.614925

Ahmad, M., Dar, N. J., Bhat, Z. S., Hussain, A., Shah, A., Liu, H., et al. (2014). Inflammation in ischemic stroke: mechanisms, consequences and possible drug targets. *CNS Neurol. Disord. Drug Targets* 13, 1378–1396. doi: 10.2174/1871527313666141023094720

Alsayyah, C., Ozturk, O., Cavellini, L., Belgareh-Touze, N., and Cohen, M. M. (2020). The regulation of mitochondrial homeostasis by the ubiquitin proteasome system. *Biochim. Biophys. Acta Bioenerg.* 1861:148302. doi: 10.1016/j.bbabio.2020.148302

Badawi, Y., and Shi, H. (2017). Relative contribution of prolyl hydroxylase-dependent and -independent degradation of HIF-1alpha by proteasomal pathways in cerebral ischemia. *Front. Neurosci.* 11:239. doi: 10.3389/fnins.2017.00239

Baird, L., Llères, D., Swift, S., and Dinkova-Kostova, A. T. (2013). Regulatory flexibility in the Nrf2-mediated stress response is conferred by conformational cycling of the Keap1-Nrf2 protein complex. *Proc. Natl. Acad. Sci. U.S.A* 110, 15259–15264. doi: 10.1073/pnas.1305687110

Baird, L., and Yamamoto, M. (2020). The Molecular mechanisms regulating the KEAP1-NRF2 Pathway. *Mol. Cell Biol.* 40, e99–e20. doi: 10.1128/MCB.00099-20

Baker, R. G., Hayden, M. S., and Ghosh, S. (2011). NF-κB, inflammation, and metabolic disease. *Cell Metab.* 13, 11–22. doi: 10.1016/j.cmet.2010.12.008

Baranova, O., Miranda, L. F., Pichiule, P., Dragatsis, I., Johnson, R. S., and Chavez, J. C. (2007). Neuron-specific inactivation of the hypoxia inducible factor 1 alpha increases brain injury in a mouse model of transient focal cerebral ischemia. *J. Neurosci.* 27, 6320–6332. doi: 10.1523/JNEUROSCI.0449-07.2007

Bednash, J. S., and Mallampalli, R. K. (2016). Regulation of inflammasomes by ubiquitination. *Cell Mol. Immunol.* 13, 722–728. doi: 10.1038/cmi.2016.15

Benjamin, E. J., Blaha, M. J., Chiuve, S. E., Cushman, M., Das, S. R., Deo, R., et al. (2017). Heart disease and stroke statistics-2017 update: a report from the american heart association. *Circulation* 135, e146–e603. doi: 10.1161/CIR.0000000000000485

Berti, R., Williams, A. J., Velarde, L. C., Moffett, J. R., Elliott, P. J., Adams, J., et al. (2003). Effect of the proteasome inhibitor MLN519 on the expression of inflammatory molecules following middle cerebral artery occlusion and reperfusion in the rat. *Neurotox. Res.* 5, 505–514. doi: 10.1007/BF03033160

Bingol, B., and Sheng, M. (2016). Mechanisms of mitophagy: pink1, Parkin, USP30 and beyond. *Free Radic. Biol. Med.* 100, 210–222. doi: 10.1016/j.freeradbiomed.2016.04.015

Biswas, S., Roy, R., Biswas, R., and Bagchi, A. (2020). Structural analysis of the effects of mutations in Ubl domain of parkin leading to parkinson's disease. *Gene* 726:144186. doi: 10.1016/j.gene.2019.144186

Bomprezzi, R. (2015). Dimethyl fumarate in the treatment of relapsing-remitting multiple sclerosis: an overview. *Ther. Adv. Neurol. Disord.* 8, 20–30. doi: 10.1177/1756285614564152

Blomgren, K., Zhu, C., Wang, X., Karlsson, J. O., Leverin, A. L., Bahr, B. A., et al. (2001). Synergistic activation of caspase-3 by m-calpain after neonatal hypoxia-ischemia: a mechanism of "pathological apoptosis"? *J. Biol. Chem.* 276, 10191–10198. doi: 10.1074/jbc.M007807200

Bragoszewski, P., Turek, M., and Chacinska, A. (2017). Control of mitochondrial biogenesis and function by the ubiquitin-proteasome system. *Open Biol.* 7:170007. doi: 10.1098/rsob.170007

Brown, J. S., and Jackson, S. P. (2015). Ubiquitylation, neddylation and the DNA damage response. *Open Biol.* 5:150018. doi: 10.1098/rsob.150018

Budenholzer, L., Cheng, C. L., Li, Y., and Hochstrasser, M. (2017). Proteasome structure and assembly. *J. Mol. Biol.* 429, 3500–3524. doi: 10.1016/j.jmb.2017.05.027

Buetow, L., and Huang, D. T. (2016). Structural insights into the catalysis and regulation of E3 ubiquitin ligases. *Nat. Rev. Mol. Cell Biol.* 17, 626–642. doi: 10.1038/nrm.2016.91

Caamano, J., and Hunter, C. A. (2002). NF-kappaB family of transcription factors: central regulators of innate and adaptive immune functions. *Clin. Microbiol. Rev.* 15, 414–429. doi: 10.1128/CMR.15.3.414-429.2002

Caldeira, M. V., Salazar, I. L., Curcio, M., Canzoniero, L. M., and Duarte, C. B. (2014). Role of the ubiquitin-proteasome system in brain ischemia: friend or foe? *Prog. Neurobiol.* 112, 50–69. doi: 10.1016/j.pneurobio.2013.10.003

Canning, P., Sorrell, F. J., and Bullock, A. N. (2015). Structural basis of Keap1 interactions with Nrf2. *Free Radic. Biol. Med.* 88, 101–107. doi: 10.1016/j.freeradbiomed.2015.05.034

Chamorro, A., Dirnagl, U., Urra, X., and Planas, A. M. (2016). Neuroprotection in acute stroke: targeting excitotoxicity, oxidative and nitrosative stress, and inflammation. *Lancet Neurol.* 15, 869–881. doi: 10.1016/S1474-4422(16)00114-9

Chan, N. C., Salazar, A. M., Pham, A. H., Sweredoski, M. J., Kolawa, N. J., Graham, R. L., et al. (2011). Broad activation of the ubiquitin–proteasome system by parkin is critical for mitophagy. *Hum. Mol. Genet.* 20, 1726–1737. doi: 10.1093/hmg/ddr048

Chastagner, P., Israel, A., and Brou, C. (2006). Itch/AIP4 mediates deltex degradation through the formation of K29-linked polyubiquitin chains. *EMBO Rep.* 7, 1147–1153. doi: 10.1038/sj.embor.7400822

Chavez, J. C., Agani, F., Pichiule, P., and LaMAnnua, J. C. (2000). Expression of hypoxia-inducible factor-1alpha in the brain of rats during chronic hypoxia. *J. Appl. Physiol.* 89, 1937–1942. doi: 10.1152/jappl.2000.89.5.1937

Chen, Q. M., and Maltagliati, A. J. J. P. G. (2018). Nrf2 at the heart of oxidative stress and cardiac protection. *Physiol. Genom.* 50, 77–97. doi: 10.1152/physiolgenomics.00041.2017

Chen, X., Zhang, X., Chen, T., Jiang, X., Wang, X., Lei, H., et al. (2018). Inhibition of immunoproteasome promotes angiogenesis via enhancing hypoxia-inducible factor-1alpha abundance in rats following focal cerebral ischaemia. *Brain Behav. Immun.* 73, 167–179. doi: 10.1016/j.bbi.2018.04.009

Chen, X., Zhang, X., Wang, Y., Lei, H., Su, H., Zeng, J., et al. (2015). Inhibition of immunoproteasome reduces infarction volume and attenuates inflammatory reaction in a rat model of ischemic stroke. *Cell Death Dis.* 6:e1626. doi: 10.1038/cddis.2014.586

Chen, Z., Hagler, J., Palombella, V. J., Melandri, F., Scherer, D., Ballard, D., et al. (1995). Signal-induced site-specific phosphorylation targets I kappa B alpha to the ubiquitin-proteasome pathway. *Genes Dev.* 9, 1586–1597. doi: 10.1101/gad.9.13.1586

Chen, Z. J. (2012). Ubiquitination in signaling to and activation of IKK. *Immunol. Rev.* 246, 95–106. doi: 10.1111/j.1600-065X.2012.01108.x

Chiba, T., Inoko, H., Kimura, M., and Sato, T. (2013). Role of nuclear IκBs in inflammation regulation. *Biomol. Concepts* 4, 187–196. doi: 10.1515/bmc-2012-0039

Ciechanover, A. (2015). The unravelling of the ubiquitin system. *Nat. Rev. Mol. Cell Biol.* 16, 322–324. doi: 10.1038/nrm3982

Cildir, G., Low, K. C., and Tergaonkar, V. (2016). Noncanonical NF-κB signaling in health and disease. *Trends Mol. Med.* 22, 414–429. doi: 10.1016/j.molmed.2016.03.002

Collaborators, G. B. D. R. F. (2020). Global burden of 87 risk factors in 204 countries and territories, 1990-2019: a systematic analysis for the global burden of disease study 2019. *Lancet* 396, 1223–1249. doi: 10.1016/S0140-6736(20)30752-2

Correia, S. C., and Moreira, P. I. (2010). Hypoxia-inducible factor 1: a new hope to counteract neurodegeneration? *J. Neurochem.* 112, 1–12. doi: 10.1111/j.1471-4159.2009.06443.x

Delhase, M., Hayakawa, M., Chen, Y., and Karin, M. J. S. (1999). Positive and negative regulation of IκB kinase activity through IKKβ subunit phosphorylation. *Science* 284, 309–313. doi: 10.1126/science.284.5412.309

Dengler, V. L., Galbraith, M., and Espinosa, J. M. (2014). Transcriptional regulation by hypoxia inducible factors. *Crit. Rev. Biochem. Mol. Biol.* 49, 1–15. doi: 10.3109/10409238.2013.838205

Delpeso, L., Castellanos, M. C., Temes, E., Martin-Puig, S., Cuevas, Y., Olmos, G., et al. (2003). The von Hippel Lindau/hypoxia-inducible factor (HIF) pathway regulates the transcription of the HIF-proline hydroxylase genes in response to low oxygen. *J. Biol. Chem.* 278, 48690–48695. doi: 10.1074/jbc.M308862200

DiDonato, J. A., Mercurio, F., and Karin, M. (2012). NF−κB and the link between inflammation and cancer. *Immunol. Rev.* 246, 379–400. doi: 10.1111/j.1600-065X.2012.01099.x

Diseases, G. B. D., and Injuries, C. (2020). Global burden of 369 diseases and injuries in 204 countries and territories, 1990-2019: a systematic analysis for the global burden of disease study 2019. *Lancet* 396, 1204–1222. doi: 10.1016/S0140-6736(20)30925-9

Doeppner, T. R., Mlynarczuk-Bialy, I., Kuckelkorn, U., Kaltwasser, B., Herz, J., Hasan, M. R., et al. (2012). The novel proteasome inhibitor BSc2118 protects against cerebral ischaemia through HIF1A accumulation and enhanced angioneurogenesis. *Brain* 135, 3282–3297. doi: 10.1093/brain/aws269

Durand, J., and Baldwin, A. S. (2017). Targeting IKK and NF-κB for therapy. *Adv. Protein Chem. Struct. Biol.* 107, 77–115. doi: 10.1016/bs.apcsb.2016.11.006

Eiyama, A., and Okamoto, K. (2015). PINK1/Parkin-mediated mitophagy in mammalian cells. *Curr. Opin. Cell Biol.* 33, 95–101. doi: 10.1016/j.ceb.2015.01.002

Fao, L., Mota, S. I., and Rego, A. C. (2019). Shaping the Nrf2-ARE-related pathways in Alzheimer's and Parkinson's diseases. *Ageing Res. Rev.* 54:100942. doi: 10.1016/j.arr.2019.100942

Feehan, K. T., and Gilroy, D. W. (2019). Is resolution the end of inflammation? *Trends Mol. Med.* 25, 198–214. doi: 10.1016/j.molmed.2019.01.006

Fei, C., Li, Z., Li, C., Chen, Y., Chen, Z., He, X., et al. (2013). Smurf1-mediated Lys29-linked nonproteolytic polyubiquitination of axin negatively regulates Wnt/beta-catenin signaling. *Mol. Cell Biol.* 33, 4095–4105. doi: 10.1128/MCB.00418-13

Fricker, L. D. (2020). Proteasome Inhibitor Drugs. *Annu. Rev. Pharmacol. Toxicol.* 60, 457–476. doi: 10.1146/Annurev-pharmtox-010919-023603

Gao, F., Shang, Y., Liu, W., and Li, W. (2016). The linkage specificity determination of Ube2g2-gp78 mediated polyubiquitination. *Biochem. Biophys. Res. Commun.* 473, 1139–1143. doi: 10.1016/j.bbrc.2016.04.029

Gatti, M., Pinato, S., Maiolica, A., Rocchio, F., Prato, M. G., Aebersold, R., et al. (2015). RNF168 promotes noncanonical K27 ubiquitination to signal DNA damage. *Cell Rep.* 10, 226–238. doi: 10.1016/j.celrep.2014.12.021

Ge, P., Luo, Y., Liu, C. L., and Hu, B. (2007). Protein aggregation and proteasome dysfunction after brain ischemia. *Stroke* 38, 3230–3236. doi: 10.1161/STROKEAHA.107.487108

Geisler, S., Holmström, K. M., Skujat, D., Fiesel, F. C., Rothfuss, O. C., Kahle, P. J., et al. (2010). PINK1/Parkin-mediated mitophagy is dependent on VDAC1 and p62/SQSTM1. *Nat. Cell. Biol.* 12, 119–131. doi: 10.1038/ncb2012

Gillette, T. G., Kumar, B., Thompson, D., Slaughter, C. A., and DeMartino, G. N. (2008). Differential roles of the COOH termini of AAA subunits of PA700 (19 S regulator) in asymmetric assembly and activation of the 26 S proteasome. *J. Biol. Chem.* 283, 31813–31822. doi: 10.1074/jbc.M805935200

Goetzke, C. C., Ebstein, F., and Kallinich, T. (2021). Role of proteasomes in inflammation. *J. Clin. Med.* 10:1783. doi: 10.3390/jcm10081783

Graham, S. H., and Liu, H. (2017). Life and death in the trash heap: the ubiquitin proteasome pathway and UCHL1 in brain aging, neurodegenerative disease and cerebral Ischemia. *Ageing Res. Rev.* 34, 30–38. doi: 10.1016/j.arr.2016.09.011

Grice, G. L., Lobb, I. T., Weekes, M. P., Gygi, S. P., Antrobus, R., and Nathan, J. A. (2015). The proteasome distinguishes between heterotypic and homotypic lysine-11-linked polyubiquitin chains. *Cell Rep.* 12, 545–553. doi: 10.1016/j.celrep.2015.06.061

Hayes, J. D., and Dinkova-Kostova, A. T. (2014). The Nrf2 regulatory network provides an interface between redox and intermediary metabolism. *Trends Biochem. Sci.* 39, 199–218. doi: 10.1016/j.tibs.2014.02.002

Hicke, L. (2001). Protein regulation by monoubiquitin. *Nat. Rev. Mol. Cell Biol.* 2, 195–201. doi: 10.1038/35056583

Hu, X., Tao, C., Gan, Q., Zheng, J., Li, H., and You, C. (2016). Oxidative Stress in intracerebral hemorrhage: sources, mechanisms, and therapeutic targets. *Oxid. Med. Cell Longev.* 2016:3215391. doi: 10.1155/2016/3215391

Hybertson, B. M., Gao, B., Bose, S. K., and McCord, J. M. (2011). Oxidative stress in health and disease: the therapeutic potential of Nrf2 activation. *Mol Aspects Med.* 32, 234–246. doi: 10.1016/j.mam.2011.10.006

Hyder, F., Rothman, D. L., and Bennett, M. R. (2013). Cortical energy demands of signaling and nonsignaling components in brain are conserved across mammalian species and activity levels. *Proc. Natl. Acad. Sci. U.S.A* 110, 3549–3554. doi: 10.1073/pnas.1214912110

Imbriani, P., D'Angelo, V., Platania, P., Di Lazzaro, G., Scalise, S., Salimei, C., et al. (2020). Ischemic injury precipitates neuronal vulnerability in Parkinson's disease: insights from PINK1 mouse model study and clinical retrospective data. *Parkinsonism Relat. Disord.* 74, 57–63. doi: 10.1016/j.parkreldis.2020.04.004

Jiang, S., Deng, C., Lv, J., Fan, C., Hu, W., Di, S., et al. (2017). Nrf2 Weaves an elaborate network of neuroprotection against stroke. *Mol. Neurobiol.* 54, 1440–1455. doi: 10.1007/s12035-016-9707-7

Kabaria, S., Choi, D. C., Chaudhuri, A. D., Jain, M. R., Li, H., and Junn, E. (2015). MicroRNA-7 activates Nrf2 pathway by targeting Keap1 expression. *Free Radic. Biol. Med.* 89, 548–556. doi: 10.1016/j.freeradbiomed.2015.09.010

Kane, E. I., Waters, K. L., and Spratt, D. E. (2021). Intersection of redox chemistry and ubiquitylation: post-translational modifications required for maintaining cellular homeostasis and neuroprotection. *Cells* 10:2121. doi: 10.3390/cells10082121

Kansanen, E., Kuosmanen, S. M., Leinonen, H., and Levonen, A. L. (2013). The Keap1-Nrf2 pathway: mechanisms of activation and dysregulation in cancer. *Redox Biol* 1, 45–49. doi: 10.1016/j.redox.2012.10.001

Karin, M., and Ben-Neriah, Y. (2000). Phosphorylation meets ubiquitination: the control of NF-κB activity. *Annuu. Rev. Immunol.* 18, 621–663. doi: 10.1146/Annuurev.immunol.18.1.621

Karunatilleke, N. C., Fast, C. S., Ngo, V., Brickenden, A., Duennwald, M. L., KonermAnnu, L., et al. (2021). Nrf2, the major regulator of the cellular oxidative stress response, is partially disordered. *Int. J. Mol. Sci.* 22:7434. doi: 10.3390/ijms22147434

Kaspar, J. W., Niture, S. K., and Jaiswal, A. K. (2009). Nrf2:INrf2 (Keap1) signaling in oxidative stress. *Free Radic. Biol. Med.* 47, 1304–1309. doi: 10.1016/j.freeradbiomed.2009.07.035

Kaelin, W. G. Jr., and Ratcliffe, P. J. (2008). Oxygen sensing by metazoans: the central role of the HIF hydroxylase pathway. *Mol. Cell* 30, 393–402. doi: 10.1016/j.molcel.2008.04.009

Ke, Q., and Costa, M. (2006). Hypoxia-inducible factor-1 (HIF-1). *Mol. Pharmacol.* 70, 1469–1480. doi: 10.1124/mol.106.027029

Koh, Y. C., Yang, G., Lai, C. S., Weerawatanakorn, M., and Pan, M. H. (2018). Chemopreventive effects of phytochemicals and medicines on M1/M2 polarized macrophage role in inflammation-related diseases. *Int. J Mol. Sci.* 19:2208. doi: 10.3390/ijms19082208

Komander, D., and Rape, M. (2012). The ubiquitin code. *Annuu. Rev. Biochem.* 81, 203–229. doi: 10.1146/Annuurev-biochem-060310-170328

Kramer, L., Groh, C., and HerrmAnnu, J. M. (2021). The proteasome: friend and foe of mitochondrial biogenesis. *FEBS Lett.* 595, 1223–1238. doi: 10.1002/1873-3468.14010

Kwon, Y. T., and Ciechanover, A. (2017). The Ubiquitin code in the ubiquitin-proteasome system and autophagy. *Trends Biochem. Sci.* 42, 873–886. doi: 10.1016/j.tibs.2017.09.002

Lando, D., Peet, D. J., Whelan, D. A., Gorman, J. J., and Whitelaw, M. L. (2002b). Asparagine hydroxylation of the HIF transactivation domain a hypoxic switch. *Science* 295, 858–861. doi: 10.1126/science.1068592

Lando, D., Peet, D. J., Gorman, J. J., Whelan, D. A., Whitelaw, M. L., and Bruick, R. K. (2002a). FIH-1 is an asparaginyl hydroxylase enzyme that regulates the transcriptional activity of hypoxia-inducible factor. *Genes Dev.* 16, 1466–1471. doi: 10.1101/gad.991402

Landowski, L. M., Niego, B., Sutherland, B. A., Hagemeyer, C. E., and Howells, D. W. (2020). Applications of nanotechnology in the diagnosis and therapy of stroke. *Semin. Thromb. Hemost.* 46, 592–605. doi: 10.1055/s-0039-3399568

Lazarou, M., Jin, S. M., Kane, L. A., and Youle, R. J. (2012). Role of PINK1 binding to the TOM complex and alternate intracellular membranes in recruitment and activation of the E3 ligase Parkin. *Dev. Cell* 22, 320–333. doi: 10.1016/j.devcel.2011.12.014

Lazarou, M., Sliter, D. A., Kane, L. A., Sarraf, S. A., Wang, C., Burman, J. L., et al. (2015). The ubiquitin kinase PINK1 recruits autophagy receptors to induce mitophagy. *Nature* 524, 309–314. doi: 10.1038/nature14893

Leu, T., Schutzhold, V., Fandrey, J., and Ferenz, K. B. (2019). When the brain yearns for oxygen. *Neurosignals* 27, 50–61. doi: 10.33594/000000199

Li, C., Sun, T., and Jiang, C. (2021). Recent advances in nanomedicines for the treatment of ischemic stroke. *Acta Pharm. Sin. B* 11, 1767–1788. doi: 10.1016/j.apsb.2020.11.019

Li, S., Wang, X., Li, Y., Kost, C. K. Jr., and Martin, D. S. (2013). Bortezomib, a proteasome inhibitor, attenuates angiotensin II-induced hypertension and aortic remodeling in rats. *PLoS One* 8:e78564. doi: 10.1371/journal.pone.0078564

Li, Y., Wu, J., Yu, S., Zhu, J., Zhou, Y., Wang, P., et al. (2020). Sestrin2 promotes angiogenesis to alleviate brain injury by activating Nrf2 through regulating the interaction between p62 and Keap1 following photothrombotic stroke in rats. *Brain Res.* 1745:146948. 10.1016/j.brainres.2020.146948

Liddelow, S. A., Guttenplan, K. A., Clarke, L. E., Bennett, F. C., Bohlen, C. J., Schirmer, L., et al. (2017). Neurotoxic reactive astrocytes are induced by activated microglia. *Nature* 541, 481–487. doi: 10.1038/nature21029

Ling, L., Cao, Z., and Goeddel, D. V. (1998). NF-kappaB-inducing kinase activates IKK-alpha by phosphorylation of Ser-176. *Proc. Natl. Acad. Sci. U.S.A* 95, 3792–3797. doi: 10.1073/pnas.95.7.3792

Linker, R. A., Lee, D. H., Ryan, S., van Dam, A. M., Conrad, R., Bista, P., et al. (2011). Fumaric acid esters exert neuroprotective effects in neuroinflammation via activation of the Nrf2 antioxidant pathway. *Brain* 134, 678–692. doi: 10.1093/brain/awq386

Lipton, P. (1999). Ischemic cell death in brain neurons. *Physiol. Rev.* 79, 1431–1568. doi: 10.1152/physrev.1999.79.4.1431

Liu, F., Lu, J., Manaenko, A., Tang, J., and Hu, Q. (2018). Mitochondria in ischemic stroke: new insight and implications. *Aging Dis.* 9, 924–937. doi: 10.14336/AD.2017.1126

Liu, H., Wu, X., Luo, J., Wang, X., Guo, H., Feng, D., et al. (2019). Pterostilbene attenuates astrocytic inflammation and neuronal oxidative injury after ischemia-reperfusion by inhibiting NF-κB phosphorylation. *Front. Immunol.* 10:2408. doi: 10.3389/fimmu.2019.02408

Luo, T., Park, Y., Sun, X., Liu, C., and Hu, B. (2013). Protein misfolding, aggregation, and autophagy after brain ischemia. *Transl. Stroke Res.* 4, 581–588. doi: 10.1007/s12975-013-0299-5

Majmundar, A. J., Wong, W. J., and Simon, M. C. (2010). Hypoxia-inducible factors and the response to hypoxic stress. *Mol. Cell* 40, 294–309. doi: 10.1016/j.molcel.2010.09.022

Matsuda, N., Sato, S., Shiba, K., Okatsu, K., Saisho, K., Gautier, C. A., et al. (2010). PINK1 stabilized by mitochondrial depolarization recruits parkin to damaged mitochondria and activates latent Parkin for mitophagy. *J. Cell Biol.* 189, 211–221. doi: 10.1083/jcb.200910140

Matyskiela, M. E., Lander, G. C., and Martin, A. (2013). Conformational switching of the 26S proteasome enables substrate degradation. *Nat. Struct. Mol. Biol.* 20, 781–788. doi: 10.1038/nsmb.2616

Mazzocchetti, P., Mancini, A., Sciaccaluga, M., Megaro, A., Bellingacci, L., Di Filippo, M., et al. (2020). Low doses of Perampanel protect striatal and hippocampal neurons against in vitro ischemia by reversing the ischemia-induced alteration of AMPA receptor subunit composition. *Neurobiol. Dis.* 140, 104848. doi: 10.1016/j.nbd.2020.104848

Medzhitov, R. (2008). Origin and physiological roles of inflammation. *Nature* 454, 428–435. doi: 10.1038/nature07201

Meller, R. (2009). The role of the ubiquitin proteasome system in ischemia and ischemic tolerance. *Neuroscientist* 15, 243–260. doi: 10.1177/1073858408327809

Miller, S., and Muqit, M. M. K. (2019). Therapeutic approaches to enhance PINK1/Parkin mediated mitophagy for the treatment of Parkinson's disease. *Neurosci. Lett.* 705, 7–13. doi: 10.1016/j.neulet.2019.04.029

Mitchell, J. P., and Carmody, R. (2018). NF-κB and the transcriptional control of inflammation. *Int. Rev. Cell Mol. Biol.* 335, 41–84. doi: 10.1016/bs.ircmb.2017.07.007

Mitroshina, E. V., Savyuk, M. O., Ponimaskin, E., and Vedunova, M. V. (2021). Hypoxia-Inducible Factor (HIF) in Ischemic Stroke and Neurodegenerative Disease. *Front. Cell Dev. Biol.* 9:703084. doi: 10.3389/fcell.2021.703084

Mohyeldin, A., Garzon-Muvdi, T., and Quinones-Hinojosa, A. (2010). Oxygen in stem cell biology: a critical component of the stem cell niche. *Cell Stem Cell* 7, 150–161. doi: 10.1016/j.stem.2010.07.007

Mukhida, K., Kobayashi, N. R., and Mendez, I. (2005). A novel role for parkin in trauma-induced central nervous system secondary injury. *Med. Hypotheses* 64, 1120–1123. doi: 10.1016/j.mehy.2004.12.020

Narendra, D., Tanaka, A., Suen, D.-F., and Youle, R. (2008). Parkin is recruited selectively to impaired mitochondria and promotes their autophagy. *J. Cell Biol.* 183, 795–803. doi: 10.1083/jcb.200809125

Ohh, M., Park, C. W., Ivan, M., Hoffman, M. A., Kim, T. Y., Huang, L. E., et al. (2000). Ubiquitination of hypoxia-inducible factor requires direct binding to the beta-domain of the von Hippel-Lindau protein. *Nat. Cell Biol.* 2, 423–427. doi: 10.1038/35017054

Ohtake, F., and Tsuchiya, H. (2017). The emerging complexity of ubiquitin architecture. *J. Biochem.* 161, 125–133. doi: 10.1093/jb/mvw088

Oshima, Y., Verhoeven, N., Cartier, E., and Karbowski, M. (2021). The OMM-severed and IMM-ubiquitinated mitochondria are intermediates of mitochondrial proteotoxicity-induced autophagy in PRKN/parkin-deficient cells. *Autophagy* 17, 3884–3886. doi: 10.1080/15548627.2021.1964887

Park, J., Cho, J., and Song, E. (2020). Ubiquitin–proteasome system (UPS) as a target for anticancer treatment. *Arch. Pharm. Res.* 43, 1144–1161. doi: 10.1007/s12272-020-01281-8

Phillips, J. B., Williams, A. J., Adams, J., Elliott, P. J., and Tortella, F. C. J. S. (2000). Proteasome inhibitor PS519 reduces infarction and attenuates leukocyte infiltration in a rat model of focal cerebral ischemia. *Stroke* 31, 1686–1693. doi: 10.1161/01.str.31.7.1686

Pickrell, A. M., and Youle, R. J. (2015). The roles of PINK1, parkin, and mitochondrial fidelity in Parkinson's disease. *Neuron* 85, 257–273. doi: 10.1016/j.neuron.2014.12.007

Rahighi, S., Ikeda, F., Kawasaki, M., Akutsu, M., Suzuki, N., Kato, R., et al. (2009). Specific recognition of linear ubiquitin chains by NEMO is important for NF-kappaB activation. *Cell* 136, 1098–1109. doi: 10.1016/j.cell.2009.03.007

Rakovic, A., Ziegler, J., Mårtensson, C. U., Prasuhn, J., Shurkewitsch, K., König, P., et al. (2019). PINK1-dependent mitophagy is driven by the UPS and can occur independently of LC3 conversion. *Cell Death Differ.* 26, 1428–1441. doi: 10.1038/s41418-018-0219-z

Rami, A., Agarwal, R., Botez, G., and Winckler, J. (2000). mu-Calpain activation, DNA fragmentation, and synergistic effects of caspase and calpain inhibitors in protecting hippocampal neurons from ischemic damage. *Brain Res.* 866, 299–312. doi: 10.1016/s0006-8993(00)02301-5

Ruas, J. L., Poellinger, L., and Pereira, T. (2002). Functional analysis of hypoxia-inducible factor-1 alpha-mediated transactivation. Identification of amino acid residues critical for transcriptional activation and/or interaction with CREB-binding protein. *J. Biol. Chem.* 277, 38723–38730. doi: 10.1074/jbc.M205051200

Sajadimajd, S., and Khazaei, M. (2018). Oxidative stress and cancer: the Role of Nrf2. *Curr. Cancer Drug Targets* 18, 538–557. doi: 10.2174/1568009617666171002144228

Semenza, G. L. (2004). Hydroxylation of HIF-1: oxygen sensing at the molecular level. *Physiology (Bethesda)* 19, 176–182. doi: 10.1152/physiol.00001.2004

Semenza, G. L. (2009). Regulation of oxygen homeostasis by hypoxia-inducible factor 1. *Physiology (Bethesda)* 24, 97–106. doi: 10.1152/physiol.00045.2008

Shang, F., and Taylor, A. (2011). Ubiquitin-proteasome pathway and cellular responses to oxidative stress. *Free Radic. Biol. Med.* 51, 5–16. doi: 10.1016/j.freeradbiomed.2011.03.031

Shang, Y., Dai, S., Chen, X., Wen, W., and Liu, X. J. C. C. (2019). MicroRNA-93 regulates the neurological function, cerebral edema and neuronal apoptosis of rats with intracerebral hemorrhage through TLR4/NF-κB signaling pathway. *Cell Cycle* 18, 3160–3176. doi: 10.1080/15384101.2019.1670509

Sharpe, L. J., Coates, H. W., and Brown, A. J. (2020). Post-translational control of the long and winding road to cholesterol. *J. Biol. Chem.* 295, 17549–17559. doi: 10.1074/jbc.REV120.010723

Shen, J. L., Fortier, T. M., Wang, R., and Baehrecke, E. H. (2021). Vps13D functions in a Pink1-dependent and Parkin-independent mitophagy pathway. *J. Cell Biol.* 220, e202104073. doi: 10.1083/jcb.202104073

Shi, H. (2009). Hypoxia inducible factor 1 as a therapeutic target in ischemic stroke. *Curr. Med. Chem.* 16, 4593–4600. doi: 10.2174/092986709789760779

Shu, S., Wang, Y., Zheng, M., Liu, Z., Cai, J., Tang, C., et al. (2019). Hypoxia and hypoxia-inducible factors in kidney injury and repair. *Cells* 8:207. doi: 10.3390/cells8030207

Sims, N. R., and Muyderman, H. (2010). Mitochondria, oxidative metabolism and cell death in stroke. *Biochim. Biophys. Acta* 1802, 80–91. doi: 10.1016/j.bbadis.2009.09.003

Song, L., and Rape, M. (2010). Regulated degradation of spindle assembly factors by the anaphase-promoting complex. *Mol. Cell* 38, 369–382. doi: 10.1016/j.molcel.2010.02.038

Sun, X., Ou, Z., Chen, R., Niu, X., Chen, D., Kang, R., et al. (2016). Activation of the p62-Keap1-NRF2 pathway protects against ferroptosis in hepatocellular carcinoma cells. *Hepatology* 63, 173–184. doi: 10.1002/hep.28251

Sun-Wang, J. L., Yarritu-Gallego, A., Ivanova, S., and Zorzano, A. (2021). The ubiquitin-proteasome system and autophagy: self-digestion for metabolic health. *Trends Endocrinol. Metab.* 32, 594–608. doi: 10.1016/j.tem.2021.04.015

Sun, S.-C. (2011). Non-canonical NF-κB signaling pathway. *Cell Res.* 21, 71–85. doi: 10.1038/cr.2010.177

Suzuki, T., and Yamamoto, M. (2015). Molecular basis of the Keap1-Nrf2 system. *Free Radic. Biol. Med.* 88, 93–100. doi: 10.1016/j.freeradbiomed.2015.06.006

Tanaka, K. (2020). The PINK1-Parkin axis: an overview. *Neurosci. Res.* 159, 9–15. doi: 10.1016/j.neures.2020.01.006

Tarhonskaya, H., Hardy, A. P., Howe, E. A., Loik, N. D., Kramer, H. B., McCullagh, J. S., et al. (2015). Kinetic investigations of the role of factor inhibiting hypoxia-inducible factor (FIH) as an oxygen sensor. *J. Biol. Chem.* 290, 19726–19742. doi: 10.1074/jbc.M115.653014

Thacker, G., Mishra, M., Sharma, A., Singh, A. K., Sanyal, S., and Trivedi, A. K. (2020). E3 ligase SCF(SKP2) ubiquitinates and degrades tumor suppressor C/EBPalpha in acute myeloid leukemia. *Life Sci.* 257:118041. doi: 10.1016/j.lfs.2020.118041

Tonelli, C., Chio, I. I. C., and Tuveson, D. A. (2018). Transcriptional regulation by Nrf2. *Antioxid. Redox Signal.* 29, 1727–1745. 10.1089/ars.2017.7342

Tong, K. I., Katoh, Y., Kusunoki, H., Itoh, K., Tanaka, T., Yamamoto, M. J. M., et al. (2006). Keap1 recruits Neh2 through binding to ETGE and DLG motifs: characterization of the two-site molecular recognition model. *Mol. Cell Biol.* 26, 2887–2900. doi: 10.1128/MCB.26.8.2887-2900.2006

Tsakiri, E. N., and Trougakos, I. P. (2015). The amazing ubiquitin-proteasome system: structural components and implication in aging. *Int. Rev. Cell Mol. Biol.* 314, 171–237. doi: 10.1016/bs.ircmb.2014.09.002

Uckelmann, M., and Sixma, T. K. (2017). Histone ubiquitination in the DNA damage response. *DNA Repair (Amst)* 56, 92–101. doi: 10.1016/j.dnarep.2017.06.011

Unno, M., Mizushima, T., Morimoto, Y., Tomisugi, Y., Tanaka, K., Yasuoka, N., et al. (2002). The structure of the mammalian 20S proteasome at 2.75 a resolution. *Structure* 10, 609–618. doi: 10.1016/s0969-2126(02)00748-7

Villeneuve, N. F., Lau, A., and Zhang, D. D. (2010). Regulation of the Nrf2–Keap1 antioxidant response by the ubiquitin proteasome system: an insight into cullin-ring ubiquitin ligases. *Antioxid. Redox Signal.* 13, 1699–1712. doi: 10.1089/ars.2010.3211

Virani, S. S., Alonso, A., Aparicio, H. J., Benjamin, E. J., Bittencourt, M. S., Callaway, C. W., et al. (2021). heart disease and stroke statistics-2021 update: a report from the american heart association. *Circulation* 143, e254–e743. doi: 10.1161/CIR.0000000000000950

Wang, G. L., Jiang, B. H., Rue, E. A., and Semenza, G. L. (1995). Hypoxia-inducible factor 1 is a basic-helix-loop-helix-PAS heterodimer regulated by cellular O2 tension. *Proc. Natl. Acad. Sci. U.S.A* 92, 5510–5514. doi: 10.1073/pnas.92.12.5510

Wang, L., Cho, Y.-L., Tang, Y., Wang, J., Park, J.-E., Wu, Y., et al. (2018a). PTEN-L is a novel protein phosphatase for ubiquitin dephosphorylation to inhibit PINK1–Parkin-mediated mitophagy. *Cell Res.* 28, 787–802. doi: 10.1038/s41422-018-0056-0

Wang, M., and Pickart, C. M. (2005). Different HECT domain ubiquitin ligases employ distinct mechanisms of polyubiquitin chain synthesis. *EMBO J.* 24, 4324–4333. doi: 10.1038/sj.emboj.7600895

Wang, Y., Huang, Y., Xu, Y., Ruan, W., Wang, H., Zhang, Y., et al. (2018b). A dual AMPK/Nrf2 activator reduces brain inflammation after stroke by enhancing microglia M2 polarization. *Antioxid. Redox Signal.* 28, 141–163. doi: 10.1089/ars.2017.7003

Wang, Y., Wang, L., Wen, X., Hao, D., Zhang, N., He, G., et al. (2019). NF-κB signaling in skin aging. *Mech. Ageing Dev.* 184:111160. doi: 10.1016/j.mad.2019.111160

Wilck, N., and Ludwig, A. (2014). Targeting the ubiquitin-proteasome system in atherosclerosis: status quo, challenges, and perspectives. *Antioxid. Redox Signal.* 21, 2344–2363. doi: 10.1089/ars.2013.5805

Wojcik, C., and Di Napoli, M. (2004). Ubiquitin-proteasome system and proteasome inhibition: new strategies in stroke therapy. *Stroke* 35, 1506–1518. doi: 10.1161/01.STR.0000126891.93919.4e

Wu, G., Zhu, L., Yuan, X., Chen, H., Xiong, R., Zhang, S., et al. (2017). Britanin ameliorates cerebral ischemia-reperfusion injury by inducing the Nrf2 protective pathway. *Antioxid. Redox Signal.* 27, 754–768.

Wu, X., Li, X., Liu, Y., Yuan, N., Li, C., Kang, Z., et al. (2018). Hydrogen exerts neuroprotective effects on OGD/R damaged neurons in rat hippocampal by protecting mitochondrial function via regulating mitophagy mediated by PINK1/Parkin signaling pathway. *Brain Res.* 1698, 89–98. doi: 10.1016/j.brainres.2018.06.028

Xiao, G., Harhaj, E. W., and Sun, S. C. (2001). NF-kappaB-inducing kinase regulates the processing of NF-kappaB2 p100. *Mol. Cell* 7, 401–409. doi: 10.1016/s1097-2765(01)00187-3

Xiao, L., Xu, X., Zhang, F., Wang, M., Xu, Y., Tang, D., et al. (2017). The mitochondria-targeted antioxidant MitoQ ameliorated tubular injury mediated by mitophagy in diabetic kidney disease via Nrf2/PINK1. *Redox Biol.* 11, 297–311. doi: 10.1016/j.redox.2016.12.022

Xu, C., Ge, H., Wang, T., Qin, J., Liu, D., Liu, Y., et al. (2018). Increased expression of T cell immunoglobulin and mucin domain 3 on CD14+ monocytes is associated with systemic inflammatory reaction and brain injury in patients with spontaneous intracerebral hemorrhage. *J. Stroke Cerebrovasc. Dis.* 27, 1226–1236. doi: 10.1016/j.jstrokecerebrovasdis.2017.11.041

Yamano, K., and Youle, R. (2013). PINK1 is degraded through the N-end rule pathway. *Autophagy* 9, 1758–1769. doi: 10.4161/auto.24633

Yamazaki, S., Muta, T., and Takeshige, K. (2001). A novel IkappaB protein, IkappaB-zeta, induced by proinflammatory stimuli, negatively regulates nuclear factor-kappaB in the nuclei. *J. Biol. Chem.* 276, 27657–27662. doi: 10.1074/jbc.M103426200

Yan, J., Zhou, B., Taheri, S., and Shi, H. (2011). Differential effects of HIF-1 inhibition by YC-1 on the overall outcome and blood-brain barrier damage in a rat model of ischemic stroke. *PLoS One* 6:e27798. doi: 10.1371/journal.pone.0027798

Yau, R., and Rape, M. (2016). The increasing complexity of the ubiquitin code. *Nat. Cell Biol.* 18, 579–586. doi: 10.1038/ncb3358

Yoshii, S. R., Kishi, C., Ishihara, N., and Mizushima, N. (2011). Parkin mediates proteasome-dependent protein degradation and rupture of the outer mitochondrial membrane. *J. Biol. Chem.* 286, 19630–19640. doi: 10.1074/jbc.M110.209338

Youn, D. H., Kim, Y., Kim, B. J., Jeong, M. S., Lee, J., Rhim, J. K., et al. (2021). Mitochondrial dysfunction associated with autophagy and mitophagy in cerebrospinal fluid cells of patients with delayed cerebral ischemia following subarachnoid hemorrhage. *Sci. Rep.* 11:16512. doi: 10.1038/s41598-021-96092-2

Zhang, D. D., and Hannink, M. (2003). Distinct cysteine residues in Keap1 are required for Keap1-dependent ubiquitination of Nrf2 and for stabilization of Nrf2 by chemopreventive agents and oxidative stress. *Mol. Cell. Biol.* 23, 8137–8151. doi: 10.1128/MCB.23.22.8137-8151.2003

Zhang, Q., Lenardo, M. J., and Baltimore, D. J. C. (2017). 30 years of NF-κB: a blossoming of relevance to human pathobiology. *Cell* 168, 37–57. doi: 10.1016/j.cell.2016.12.012

Zhang, T., Wu, P., Budbazar, E., Zhu, Q., Sun, C., Mo, J., et al. (2019). Mitophagy reduces oxidative stress via Keap1 (Kelch-Like epichlorohydrin-associated protein 1)/Nrf2 (Nuclear Factor-E2-Related Factor 2)/PHB2 (Prohibitin 2) pathway after subarachnoid hemorrhage in rats. *Stroke* 50, 978–988. doi: 10.1161/STROKEAHA.118.021590

Zhang, X., Liu, X., Hu, G., Zhang, G., Zhao, G., and Shi, M. (2020). Ginsenoside Rd attenuates blood-brain barrier damage by suppressing proteasome-mediated signaling after transient forebrain ischemia. *Neuroreport* 31, 466–472. doi: 10.1097/WNR.0000000000001426

Zhang, Z., Yan, J., Chang, Y., ShiDu Yan, S., and Shi, H. (2011). Hypoxia inducible factor-1 as a target for neurodegenerative diseases. *Curr. Med. Chem.* 18, 4335–4343. doi: 10.2174/092986711797200426

Zheng, N., and Shabek, N. (2017). Ubiquitin ligases: structure, function, and regulation. *Annu. Rev. Biochem.* 86, 129–157. doi: 10.1146/Annurev-biochem-060815-014922

Zhou, M., Wang, H., Zeng, X., Yin, P., Zhu, J., Chen, W., et al. (2019). Mortality, morbidity, and risk factors in China and its provinces, 1990-2017: a systematic analysis for the global burden of disease study 2017. *Lancet* 394, 1145–1158. doi: 10.1016/S0140-6736(19)30427-1

Zhou, X., Chen, H., Wang, L., Lenahan, C., Lian, L., Ou, Y., et al. (2021). Mitochondrial dynamics: a potential therapeutic target for ischemic stroke. *Front. Aging Neurosci.* 13:721428. doi: 10.3389/fnagi.2021.721428

Zhu, P., Hu, S., Jin, Q., Li, D., Tian, F., Toan, S., et al. (2018). Ripk3 promotes ER stress-induced necroptosis in cardiac IR injury: a mechanism involving calcium overload/XO/ROS/mPTP pathway. *Redox Biol.* 16, 157–168. doi: 10.1016/j.redox.2018.02.019

Conflict of Interest: The authors declare that the research was conducted in the absence of any commercial or financial relationships that could be construed as a potential conflict of interest.

Publisher's Note: All claims expressed in this article are solely those of the authors and do not necessarily represent those of their affiliated organizations, or those of the publisher, the editors and the reviewers. Any product that may be evaluated in this article, or claim that may be made by its manufacturer, is not guaranteed or endorsed by the publisher.

frontiers | Frontiers in Aging Neuroscience

ORIGINAL RESEARCH
published: 02 June 2022
doi: 10.3389/fnagi.2022.851711

Uric Acid Enhances Neurogenesis in a Parkinsonian Model by Remodeling Mitochondria

*Ji Eun Lee[1], Yu Jin Shin[1], Yi Seul Kim[1], Ha Na Kim[1], Dong Yeol Kim[1], Seok Jong Chung[2], Han Soo Yoo[1], Jin Young Shin[1,3] and Phil Hyu Lee[1,3]**

[1] Department of Neurology, Yonsei University College of Medicine, Seoul, South Korea, [2] Department of Neurology, Yongin Severance Hospital, Yonsei University Health System, Yongin, South Korea, [3] Severance Biomedical Science Institute, Yonsei University, Seoul, South Korea

Background: Adult neurogenesis is the process of generating new neurons to enter neural circuits and differentiate into functional neurons. However, it is significantly reduced in Parkinson's disease (PD). Uric acid (UA), a natural antioxidant, has neuroprotective properties in patients with PD. This study aimed to investigate whether UA would enhance neurogenesis in PD.

Methods: We evaluated whether elevating serum UA levels in a 1-methyl-4-phenyl-1,2,3,6-tetrahydropyridine (MPTP)-induced parkinsonian mouse model would restore neurogenesis in the subventricular zone (SVZ). For a cellular model, we primary cultured neural precursor cells (NPCs) from post-natal day 1 rat and evaluated whether UA treatment promoted cell proliferation against 1-methyl-4-phenylpyridinium (MPP^+).

Results: Uric acid enhanced neurogenesis in both *in vivo* and *in vitro* parkinsonian model. UA-elevating therapy significantly increased the number of bromodeoxyuridine (BrdU)-positive cells in the SVZ of PD animals as compared to PD mice with normal UA levels. In a cellular model, UA treatment increased the expression of Ki-67. In the process of modulating neurogenesis, UA elevation up-regulated the expression of mitochondrial fusion markers.

Conclusion: In MPTP-induced parkinsonian model, UA probably enhanced neurogenesis *via* regulating mitochondrial dynamics, promoting fusion machinery, and inhibiting fission process.

Keywords: uric acid, neurogenesis, Parkinson's disease, mitochondrial dynamics, neural precursor cell

OPEN ACCESS

Edited by:
Benoit Laurent,
Université de Sherbrooke, Canada

Reviewed by:
Jannik Prasuhn,
University of Lübeck, Germany
Marco Tulio Nunez,
University of Chile, Chile
Vanessa A. Morais,
Universidade de Lisboa, Portugal
Xinwen Zhang,
China Medical University, China

****Correspondence:***
Phil Hyu Lee
phlee@yuhs.ac

Specialty section:
This article was submitted to Parkinson's Disease and Aging-related Movement Disorders, a section of the journal Frontiers in Aging Neuroscience

Received: *10 January 2022*
Accepted: *06 May 2022*
Published: *02 June 2022*

Citation:
Lee JE, Shin YJ, Kim YS, Kim HN, Kim DY, Chung SJ, Yoo HS, Shin JY and Lee PH (2022) Uric Acid Enhances Neurogenesis in a Parkinsonian Model by Remodeling Mitochondria. Front. Aging Neurosci. 14:851711. doi: 10.3389/fnagi.2022.851711

INTRODUCTION

Neurogenesis is the ability of the brain to produce neurons and strengthen existing connections between neuronal cells across the lifespan. Remarkably, the brain continually generates new neurons even after embryonic development. Under normal physiology, new neurons are generated from neural stem cells (NSCs) of the subventricular zone (SVZ) or subgranular zone, which then migrate to the neurogenesis niche, enter neural circuits, and differentiate into functional neurons (Berdugo-Vega et al., 2020). This process is known to be involved in various brain functions such as

memory formation, motor control, neuronal plasticity, and endogenous recovery. Ample evidence has demonstrated that patients with neurodegenerative diseases such as Alzheimer's disease, Parkinson's disease (PD), and Huntington's disease show deficient neurogenesis compared to healthy controls (Gil-Mohapel et al., 2011; Winner and Winkler, 2015; Scopa et al., 2020). Gradual loss of neuronal populations and diseased neurons disrupt synaptic transmission, cell renewal, and putative function in neurodegenerative diseases (Luo and O'Leary, 2005). Specifically, SVZ is under control of dopaminergic afferents from the substantia nigra (SN) (Hoglinger et al., 2004). In parkinsonian environment, dopaminergic deafferentation results in decreased proliferation in SVZ, reducing population of neural stem cell which will differentiate into dopaminergic neurons (Marxreiter et al., 2013). Thus, restoring adult neurogenesis is considered to be one of the important strategies for treating patients suffering from neurodegenerative diseases (Geraerts et al., 2007).

Parkinson's disease is characterized by the selective loss of dopaminergic neurons in the (SN) and the degeneration of projecting nerve fibers to the striatum, leading to parkinsonian motor symptoms such as bradykinesia, rigidity, and tremor (Jankovic, 2008). Among the multiple factors underlying PD pathogenesis, oxidative stress plays a key role in PD pathology *via* disrupting the electron transport chain and subsequent electron leakage from donor redox to molecular oxygen (Hwang, 2013). Moreover, oxidative stress is intertwined with other mechanisms implicated in PD, including protein misfolding and aggregation, mitochondrial dysfunction, and apoptosis (Picca et al., 2020). Uric acid (UA), purine metabolite, is a powerful antioxidant, present intracellularly and in all body fluids. It not only scavenges reactive oxygen species (ROS) but also blocks the reaction of superoxide anion with nitric oxide that can injure cells by nitrosylating the tyrosine residues of proteins, and prevents extracellular superoxide dismutase degradation (Squadrito et al., 2000). Several epidemiological studies reported that UA has neuroprotective properties against PD, showing that PD patients with higher UA have reduced risk of PD incidence as well as slower disease progression (Wen et al., 2017; Tana et al., 2018). Additionally, the beneficial effects of UA have been observed in other neurodegenerative diseases, such as amyotrophic lateral sclerosis (Bakshi et al., 2018), Alzheimer's disease (Scheepers et al., 2019), Huntington's disease (Auinger et al., 2010), or other disorders (Li et al., 2018; Ya et al., 2018). These studies imply that in addition to antioxidant properties, UA may have another pathway to exerting neuroprotective effects against neurodegenerative conditions.

Emerging evidence indicates that mitochondria are central regulators of NSC fate decisions and are crucial for adult neurogenesis (Beckervordersandforth, 2017). NSCs are not only dependent on generation of mitochondrial metabolites (Zheng et al., 2018), but are also dependent on changes in mitochondrial morphology and metabolic properties across various stages of differentiation (Khacho et al., 2016). Mitochondrial malfunction makes stem cells vulnerable to oxidative stress, which in turn accelerates NSC death, resulting in reduced neurogenesis (Khacho et al., 2017). As mitochondria are dynamic organelles that change their size and morphology actively, the processes of fission and fusion oppose each other and allow the mitochondria to constantly remodel themselves depending on their environment (Hollenbeck and Saxton, 2005; Okamoto and Shaw, 2005). A recent study found that adult neurogenesis in the hippocampus is critically dependent on mitochondrial complex function in mice and NSCs isolated from mice with malfunctioning mitochondria (Beckervordersandforth et al., 2017). Indeed, mitochondrial dynamics may have an important role in neurogenesis *via* maintaining a functional mitochondrial network during biogenesis (Flippo and Strack, 2017; Khacho and Slack, 2018; Arrázola et al., 2019). In this study, we hypothesized that UA would enhance neurogenesis by controlling mitochondrial dynamics in PD. To do this, we evaluated whether high levels of UA increase neurogenic activity in primary cultured neural precursor cells (NPCs) and SVZ of 1-methyl-4-phenyl-1,2,3,6-tetrahydropyridine (MPTP)-treated animals. In addition, we examined possible role of mitochondrial dynamics in UA-mediated modulation of neurogenesis in PD models.

MATERIALS AND METHODS

Parkinsonian Animal Model and Drugs Administration

All procedures were performed in accordance with the Laboratory Animals Welfare Act, the Guide for the Care and Use of Laboratory Animals and the Guidelines and Policies. The rodent experiment was approved by IACUC (Institutional Animal Care and Use Committee) in the Yonsei University Health System. ARRIVE guidelines were followed.[1] Male C57BL/6J mice (4 weeks old) were acclimated in a climate-controlled room with a constant 12 h light/dark cycle (12 h on, 12 h off) for a week prior to the initiation of drug administration. At 5 weeks of age, the mice were randomly divided into three groups: control group, MPTP PD group, and MPTP PD + UA treatment group. To elevate serum UA levels, the UA treatment group received an i.p injection of KOx (Sigma, 500 mg/kg) and IMP (Sigma, 500 mg/kg) daily for 2 weeks while others received normal saline. To construct parkinsonian model, the mice (except for those in the control group) received a sub-acute injection of MPTP freshly dissolved in 20% DMSO/80% normal saline (25 mg/kg) by i.p injection (Sigma, St. Louis, MO, United States) for 5 days. After 72 h had passed since the last MPTP injection, the UA groups received 4 weeks of UA injections. During drug administration period, the control group mice received same volume of saline i.p injection. Four days prior to last UA injection, all animals received a bromodeoxyuridine (BrdU) injection (Sigma, 100 mg/kg) daily on five consecutive days.

Preparation of Serum and Brain Tissue

At the end of the experimental period, mice were deeply anesthetized with isoflurane and their blood and brains were collected. Mouse blood was collected from the abdominal aorta. To evaluate whether serum UA levels were elevated by injection of KOx and IMP, mouse blood samples were collected in SST

[1] http://arriveguidelines.org

tubes (BD Diagnostic Systems, Sparks, MD, United States), and serum and blood cells were separated by centrifugation (2000 × *g* for 20 min). The isolated serum samples were rapidly frozen and stored at −20°C until analyzed. For immunohistochemistry, the mice were perfused with 4% paraformaldehyde. Brains were harvested from the skulls, post-fixed overnight in 4% paraformaldehyde, and stored in 30% sucrose solution for 1–2 days at 4°C until they sank. Finally, 25-μm coronal sections were obtained using cryostat. The sections were stored in tissue storage solution (30% glycerol, 30% ethylene glycol, 30% distilled water, 10% 0.2 M PB) at 4°C until required (Na Kim et al., 2017).

Neural Precursor Cell Primary Culture and Identification

Neural precursor cells were isolated from a postnatal day-1 Sprague-Dawley rat. Offspring of rats were decapitated under halothane anesthesia. Brain tissue was taken from the rat and a wedge of tissue was microdissected from the portion of the lateral ventricle that included the anterior part of the SVZ. The tissues were incubated in Hank's balanced salt solution (HBSS) for 10 min and trypsin for 3 min at room temperature. NPCs were dissociated into single cells by pipetting, and Dulbecco's modified eagle medium (DMEM) supplementation with 10% fetal bovine serum (FBS; Hyclone) and 1% penicillin/streptomycin (P/S; Hyclone) was added to inhibit trypsin function. Cells were plated in 100-mm plastic culture dishes and cultivated in low glucose DMEM in a humidified incubator at 37°C under 5% CO_2. After 24 h, non-adherent cells were removed by changing media. To identify characteristics of NPCs, total RNA was extracted from the NPCs using Trizol reagent (Lugen Sci, Korea) according to the manufacturer's instructions. RNA concentration was measured by absorption at 260 nm using NanoDrop Lite Spectrophotometer (Thermo Scientific, Wilmington, DE, United States) and an equal amount of RNA (approximately 1 ug) in each experiment was reverse transcribed. The PCR reaction was performed using 10 pmol each of the primers for NES (forward 5′-GGCCACAGTGCCTAGTTCTT-3′, reverse 5′-GTTCCCAGATTTGCCCCTCA), SOX2 (forward 5′-TAAGTACACGCTTCCCGGAG-3′, reverse 5′-CATCATGC TGTAGCTGCCGT-3′), DCX (forward 5′-TCACAGCATCT CCACCCAAC-3′, reverse 5′-ATGCCTGCAAGGTTCTGGTT-3′), MSI1 (forward 5′-CGGAGAGCACAGCCTAAGAT-3′, reverse 5′-TCGAACGTGACAAACCCGAA-3′), and GFAP (forward 5′-ACGAGGCTAATGACTATCGC-3′, reverse 5′-GTT TCTCGGATCTGGAGGTT-3′). After an initial denaturation at 95°C for 10 min, 30 cycles of PCR were performed, consisting of denaturation at 95°C for 20 s, annealing at 60°C for 30 s, extension at 72°C for 60 s followed by a final extension at 72°C for 5 min. The PCR products were separated by electrophoresis on 1.5% agarose gel and stained with Noble View (Noble Bio). Gels were examined under UV illumination Gel doc (MiniBISpro, DNR).

Neural Precursor Cell Treatment

Identified NPCs (positive for NES, sox2, DCX, and MSI1, but negative for GFAP and CD11b) were seeded in 96-well cell culture plates (SPL) at a density of 0.5×10^4/well. Plates were incubated at 37°C for 72 h to allow cells to be attached. Solution of MPP^+ and UA were prepared in advance. MPP^+ (sigma) was dissolved in distilled water to a final concentration of 100 mM stock. After stabilization, each well was randomly divided into three groups as follows: control group, MPP^+ group, MPP^+/UA group. MPP^+/UA group cells were treated with 150 μM of UA while others were just changed media. After 24 h, the MPP^+ group was treated with 150 μM of MPP^+ and the UA group was treated with 150 μM of MPP^+ and UA mixture. Plates were incubated in a cell incubator for 72 h. 150 μM of MPP^+ was treated to the MPP^+ group cells and the MPP^+ and UA mixture were treated to both UA groups. Plates were incubated in a cell incubator for an additional 72 h.

Cell Viability Analysis

Cell viability was measured by MTS cell proliferation assay (promega). According to the assay manufacturer's instructions, right before the measurement time, MTS and PMS were mixed in a 1 ml:50 μl ratio and incubated for 10 min. Then, 20 μl of mix was added to each well. The plates were incubated at 37°C for 1 h, and we measured the absorbance at 490 nm using a 96-well plate reader. Cell viability values were expressed as experimental group/average of control group × 100 = viability percentage. All experiments were repeated at least three times.

Measurements of Serum Uric Acid Level

Serum UA levels were measured using an Amplex Red Uric Acid/Uricase Assay Kit (Molecular Probes, Eugene, OR, United States) according to the manufacturer's instructions. Each serum samples were 1/10 diluted for measurement. Briefly, uricase catalyzes the conversion of UA to allantoin, H_2O_2, and CO_2. Under the presence of horseradish peroxidase, H_2O_2 reacts stochiometrically with Amplex Red reagent to generate the red-fluorescent oxidation product, resorufin, which is measured using excitation at 540 nm and detection at 590 nm.

Measurements of Reactive Oxygen Species Level

The level of intracellular ROS in NPCs was measured using 2′,7′-Dichlorofluorescin diacetate (DCFDA), DCFDA Cellular ROS Detection Assay Kit (ab113851, Abcam, United Kingdom). This reagent diffuses into the cell, which goes through deacetylation and oxidization by cellular enzymes into 2′,7′-dichlorofluorescein (DCF). According to manufacturer's protocol, cells were seeded at 1×10^4 cells/well in 96-well plate. When chemical treatment was done, cells were washed twice with 1X buffer. Washed cells were incubated with 25 μM DCFDA solution for 45 min at 37°C. Then, DCFDA solution was removed, cells were washed with buffer again, and the level of ROS was measured using excitation at 485 nm and detection at 535 nm.

Immunohistochemistry

When drug administration was done in the animal model, brain tissue was immunostained with anti-BrdU and TH antibodies

(1:500, Sigma, St. Louis, MO, United States) in SVZ and SN respectively to investigate newborn neurons and dopaminergic neurons, which we interpret as the degree of neurogenesis and as confirmation of the MPTP parkinsonian model. First, brain tissues were frozen with O.C.T. compound (Sakura Finetek) and 25-um coronal sections were obtained using cryostat. Sections were immunostained using immunofluorescence analysis or 3,3-diaminobenzidine (DAB) method. For BrdU detection, the slides were washed three times in PBS, incubated with 50% formamide in 2X SSC DW (standard saline citrate distilled water) for 2 h at 65°C for antigen retrieval, and rinsed three times in 2X SSC DW. After rinsing, the slides were incubated with 2 N HCl in DW for 30 min at 37°C to denature DNA and rinsed three times in PBS. They were incubated in borate buffer (0.1 M, pH-8.5) to neutralize the acidic medium and then blocked in 3% H_2O_2 to remove endogenous peroxidase for 10 min. To reduce non-specific binding, slides were blocked with 1% BSA in PBST for 2 h at room temperature and incubated with primary antibody, mouse anti-BrdU (1:500, Thermofisher Scientific, Waltham, MA, United States) for overnight at 4°C. As secondary antibodies, 1:200 dilutions of biotinylated in blocking solution which was visualized with 0.05% diaminobenzidine (DAB, Dako, Carpinteria, CA, United States). Immunofluorescence labeling was carried out by incubating tissue slides in donkey anti-mouse IgG and goat anti-rabbit IgG (both Alexa Fluor-488, green and Alexa Fluor-555, red) secondary antibodies (1:200, invitrogen). The cell nuclei were counterstained with 4′,6-diamidino-2-phenylindole (DAPI; 1:2000 dilution, invitrogen). The brain tissue was dried and stained with Mayer's hematoxylin (Muto Pure Chemicals Ltd., Tokyo, Japan). The immunostained tissues were analyzed using bright-field microscopy and immunofluorescence images were viewed with a Zeiss LSM 700 confocal microscope (Carl Zeiss, Berlin, Germany) (Oh et al., 2015).

Quantitative Real-Time PCR

Total RNA was isolated from NPCs using Trizol reagent (Lugen Scei, Korea) according to manufacturer's instructions. An equal amount of RNA (approximately 1 ug) in each experiment was reverse transcribed using an cDNA synthesis premix (Applied Biosystems, Promega, Madison, WI, United States). A master mix of the following reaction components was prepared to the indicated end-concentration: 12.5 μl of 2X SYBR green buffer (Promega, United States), 2 μl of forward and reverse primer (10 pM), and 2 μl DNA template (100 ng). Amplification conditions were as follows: initial denaturation at 95°C for 2 min, followed by 40 amplification cycles of 95°C for 15 s and 60°C for 1 min to anneal and extend, respectively. Quantitative PCR experiments were performed using Applied Biosystems (Thermofisher Scientific, Waltham, MA, United States). The quantitative real-time PCR reaction was performed using 10 pmol each of the primers for rat PGC1-α (forward 5′-GGACATGTGCAGCCAAGACT-3′, reverse 5′-TCGAATATGTTCGCGGGCTC), FIS1 (forward 5′-CGTGCTTTCTGTAACGCCTG-3′, reverse 5′-CTACAGGCA CTTTGGGGGTT-3′), MFN2 (forward 5′-AAGAGCTCAG GGGACGGTAT-3′, reverse 5′-GCAAGGTGAGCCTTACAG GT-3′), and TFAM (forward 5′-GTGATCTCATCCGTCG CAGT-3′, reverse 5′-CATTCAGTGGGCAGAAGTCCA-3′) (Kim et al., 2021).

MitoTracker Staining

To visualize mitochondria, MitoTrackerRed CMXRos (Invitrogen, Camarillo, CA, United States) was diluted in NPC cell culture media to a final concentration of 50 nM according to manufacturer's instructions. The cells were incubated under normal culture conditions for 30 min, fixed with 1:1 ratio of methanol and acetone for 5 min at −20°C, and permeabilized with 0.1% triton X-100 in PBS. All NPCs were counter stained for nuclei using DAPI (blue), and then visualized by a Zeiss LSM 700 confocal microscope (Carl Zeiss, Berlin, Germany) and Zen imaging software. All cells were imaged using identical exposure times and laser power settings.

Electron Microscope Analysis

Primary cultured NPCs were fixed with 2% glutaraldehyde - paraformaldehyde in 0.1 M PB (pH 7.4) for 12 h and then washed twice for 30 min in 0.1 M PB. They were post-fixed with 1% OsO4 dissolved in 0.1 M PB for 2 h and dehydrated in an ascending gradual series (50–100%) of ethanol and infiltrated with propylene oxide. Specimens were embedded using a Poly/Bed 812 kit (Polysciences). After pure fresh resin embedding and polymerization at 65°C in an electron microscope oven (TD-700, DOSAKA) for 24 h, 200 nm-thick sections were initially cut and stained with toluidine blue for light microscopy. Thin sections (80 nm) were double stained with 3% uranyl acetate and lead citrate for contrast staining. The sections were cut using a Leica electron microscope (EM) UC7 Ultra-microtome (Leica Microsystems). All of the thin sections were observed by transmission electron microscopy (TEM) (JEM-1011, JEOL) at an acceleration voltage of 80 kV.

Mitochondrial Morphology Assessment

To quantify mitochondrial morphology, mitochondrial tubule length was measured. Mitochondrial tubule of 5 μm or more was determined as tubular. Mitochondria tubule between 0.5 and 5 μm but none more than 5 μm was determined as intermediate. None of more than 0.5 μm determined as fragmented. If more than 75% mitochondria were tubular a cell was judged to have tubular form. If cells presented mitochondria with mixed morphologies, they were classified as intermediate. If none of mitochondria were more than 0.5 μm, they were determined as fragmented (Duvezin-Caubet et al., 2006). For the TEM analysis, mitochondria with intact membrane and matrix were considered as normal while mitochondria with broken membrane and abnormal morphology with large vacuole area (over 20% of the total organelle) were determined as swollen (Xiong et al., 2016). We also analyzed mitochondrial network using Mitochondrial Network Analysis (MiNA) toolset. Mitotracker images were pre-processed using unsharp mask and skeletonized to visualize mitochondrial wireframe using Image J. The skeletonized feature was measured and analyzed by MiNA (Valente et al., 2017).

Western Blotting Analysis

When animal drug administration was over, five animals in each group were fixed with paraformaldehyde while other five animals'

brain tissue was dissected under a microscope. The portion of the lateral ventricle that included the SVZ was dissected and dissolved in ice-cold RIPA buffer (50 mM Tris-HCl, pH 7.5, with 150 mM sodium chloride, 1% triton X-100, 1% sodium deoxycholate, 0.1% SDS, 2 mM EDTA sterile solution; Lugen Sci, Korea) plus protease inhibitor cocktail (Sigma). The lysates were centrifuged at 4°C for 20 min (14,000 g), and supernatants were transferred to fresh tubes. Briefly, 30 ug of protein was separated by SDS-gel electrophoresis and transferred to hydrophobic polyvinylidene difluoride (PVDF) membranes (GE Healthcare, Little Chalfont, United Kingdom). DLP1 analysis was performed in non-reducing condition. The membranes were blocked in 5% skim milk in PBST. Membranes were probed with the following primary antibodies: mouse anti-MFN1 (Abcam), rabbit anti-MFN2 (Epitomics), mouse anti-OPA1 (BD biosciences), rabbit anti-FIS1 (Abnova), mouse anti-Dlp1 (BD biosciences), mouse anti-NES (Millipore), and mouse anti-Actin (santacruz). As secondary antibodies, 1:5000 dilutions of horseradish peroxidase-conjugated goat anti-rabbit antibody (Solarbio) and anti-mouse antibody (Solarbio) were used. Antigen–antibody complexes were visualized with ECL solution (GenDEPOT). For quantitative analysis, immunoblotting band densities were measured by image J (Kim et al., 2021).

Stereological Cell Counts

To determine the number of BrdU- and TH-positive cells in the granule cell layer of mouse brains, an average of five sections per mouse were counted, and each experimental group consisted of

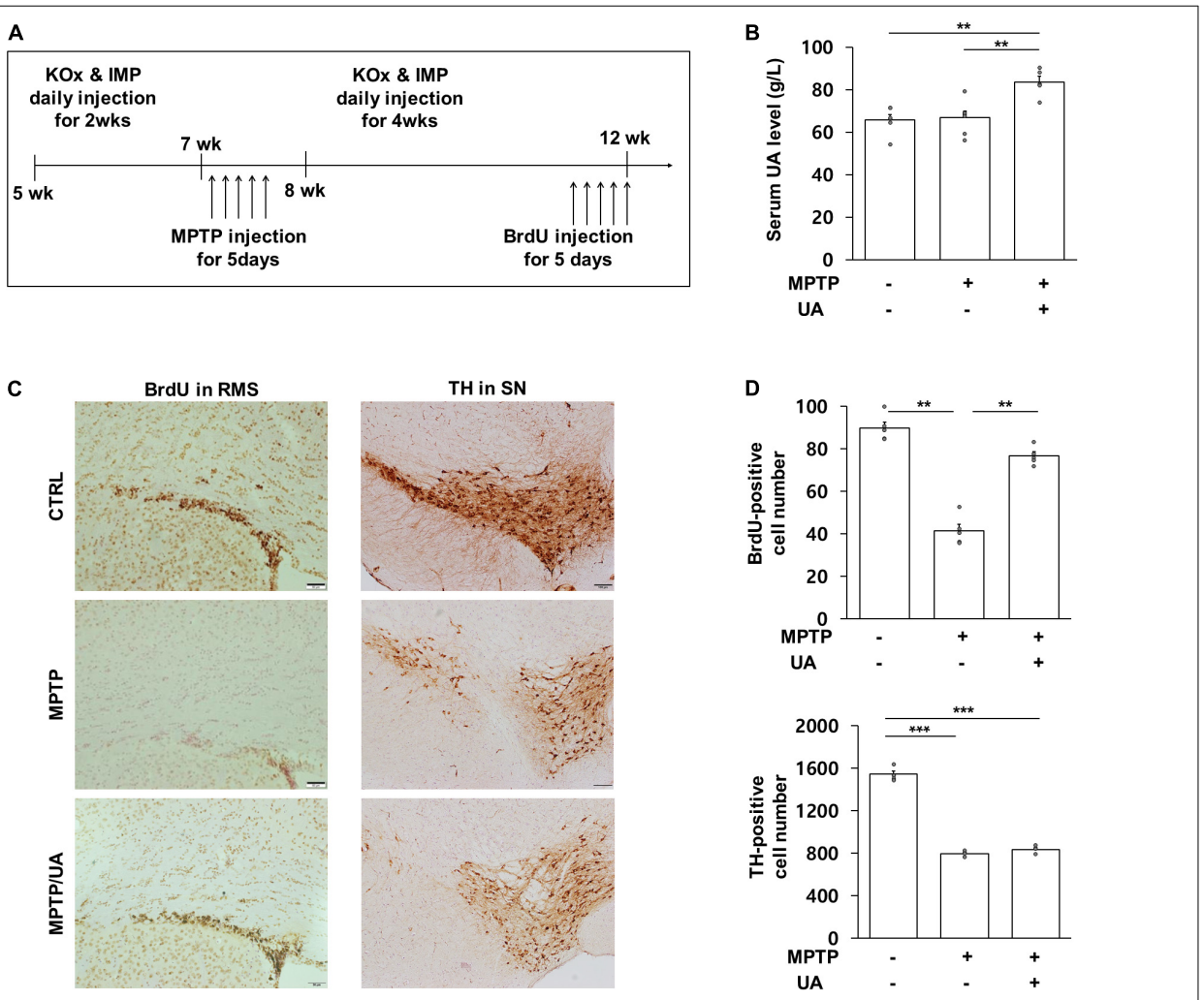

FIGURE 1 | UA elevation increased the number of BrdU-positive cells in the SVZ of a MPTP-induced PD animal model. **(A)** Animal experimental schedule design. **(B)** Serum UA levels were significantly higher in mice that received IMP with KOx as compared to control and MPTP-treated mice (n = 8 per group). **(C,D)** The number of BrdU-positive cells in SVZ at 12 weeks. PD mice with high serum UA levels showed considerably more BrdU-positive cells as compared to PD mice with normal serum UA levels (n = 5 per group). The number of TH-positive cells in the SN at 12 weeks. Both PD mice with high and normal UA levels revealed a significant reduction in the number of TH-positive cells compared to the control group. There was no statistically significant difference between PD mice with high serum UA levels and those with normal levels (n = 5 per group). Differences among the conditions were evaluated by ANOVA with a Bonferroni correction for multiple comparison. The data are presented as mean ± SE. $^{**}p < 0.01$ and $^{***}p < 0.001$.

five mice. BrdU-positive cells were counted in the lateral wall of the SVZ and rostral migratory stream. TH-positive cells were counted in the SN region. Unbiased stereological estimations of the total number of stained cells in each region were made using an optical fractionator. This sampling technique is not affected by tissue volume changes and does not require reference volume determinations. The sections used for counting covered the entire SN from the rostral tip of the pars compacta back to the caudal end of the pars reticulate and the lateral wall of the SVZ including RMS. This generally yielded five sections in a series. A counting frame (60%, 36,650 μm^2) was randomly placed onto the first counting area and systematically moved through all counting areas until the entire delineated area was complete. Actual counting was performed using a 40 x object. The total number of stained cells was calculated according to the optical fractionator formula.

Statistical Analysis

After verification of normality distribution, mean differences between experimental groups were determined by one-way analysis of variance (ANOVA) followed by a Bonferroni *post-hoc* test. Differences were considered statistically significant at $p < 0.05$. Statistical analysis was performed using the software SPSS v. 25 (Yonsei University, Seoul, Korea).

RESULTS

Uric Acid-Elevating Therapy Increased Neurogenesis in the Subventricular Zone of MPTP-Induced Parkinson's Disease Animal Model

To determine the effect UA elevation on neurogenesis in an MPTP-induced parkinsonian model, the mice were treated with mixture of KOx and IMP before MPTP treatment *via* the intraperitoneal route. The *in vivo* study design is illustrated in **Figure 1A**. Two weeks of KOx injection (500 mg/kg) slightly but not significantly raised the level of serum UA (88.3 g/L vs. 85.8 g/L). However, 2 weeks of co-treatment of IMP (500 mg/kg) with KOx (500 mg/kg) led to a significant increase in the level of UA (76.4 g/L) relative to baseline (63.1 g/L, $p = 0.006$, **Figure 1B**). To investigate whether UA-elevating therapy modulated neurogenesis, new born cells in the SVZ of MPTP-treated mice received IMP with KOx were immunostained with BrdU, a commonly used marker for neurogenesis (Kuhn et al., 2016). Compared to the control group, the number of BrdU-positive cells in ependymal and rostral migratory stream (RMS) was significantly reduced in the MPTP-treated mice by 46.2% ($p = 0.001$, **Figures 1C,D**). Compared to MPTP-only-treated mice, PD mice received co-treatment of IMP with KOx exhibited a significant increase in the number of BrdU-positive cells, restoring up to 85.3% ($p = 0.006$, **Figures 1C,D**). However, only post injection of IMP with KOx in MPTP-treated mice did not increase the number of BrdU-positive cells (**Supplementary Figure 1**). Next, as dopaminergic neurons can modulate neurogenic activity *via* dopaminergic receptors in the SVZ, we determined whether UA elevation in MPTP-treated mice would lead to a difference in the density of nigral dopaminergic neurons. As expected, the number of TH (tyrosine hydroxylase)-positive cells in the SN was reduced to 51.5% in MPTP-treated animals compared to the control group ($p < 0.01$, **Figures 1C,D**). However, the number of TH-positive cells in PD mice co-treated with IMP and KOx was not statistically different from the MPTP-only-treated group. In addition, we investigated neurogenesis in hippocampal dentate gyrus (DG). MPTP induced PD mice showed decreased number of BrdU positive cells in DG by 19.1% compared to the control group ($p < 0.001$). Compared to MPTP-treated mice, PD mice received UA elevating therapy showed significantly increased number of BrdU-positive cells ($p < 0.001$, **Supplementary Figures 2A,B**). These data indicate that UA-elevating therapy promotes neurogenic activity in MPTP-induced parkinsonian animals without modulating the nigrostriatal dopaminergic system.

Uric Acid Treatment Exerted a Neuroprotective Effect and Enhanced Proliferation Against MPP^+ in Primary Cultured Neural Precursor Cells From the Subventricular Zone

Primary cultured NPCs were positive for NES (nestin), SOX2 (SRY-box transcription factor2), DCX (doublecortin), and MSI1 (musashi RNA binding protein 1), but negative for GFAP (glial fibrillary acidic protein) (**Supplementary Figure 3A**). To determine the purity of cultured NPCs, cells were stained with NES and GFAP. All DAPI positive cells were co-localized with NES, but not GFAP and NeuN (**Supplementary Figure 3B**). To examine the effect of UA on cell survival followed by MPP^+ treatment, primary cultured NPCs were treated with MPP^+ at various concentrations for 72 h. MPP^+ treatment with a concentration of 150 μM or more markedly decreased cell viability of NPCs in a dose-dependent manner (**Figure 2A**). However, UA treatment at various concentrations did not result in decreased viability of NPCs (**Figure 2B**). Next, we examined if UA treatment exhibited a neuroprotective effect against MPP^+-induced cytotoxicity in NPCs. Similar to *in vivo* data, UA treatment in MPP^+-treated NPCs exerted a prosurvival effect, restoring cell viability up to 90.1% compared to the MPP^+-treated group ($p = 0.049$, **Figure 2C**). On evaluating proliferation of NPCs, the mRNA expression level of Ki-67 was significantly decreased in MPP^+-treated NPCs, whereas UA treatment markedly increased the level of Ki-67 relative to the MPP^+ treatment group ($p = 0.026$, **Figure 2D**). Similarly, UA treatment significantly increased the protein level of Ki-67 compared to the MPP^+ treatment group (**Figures 2F,G**). To determine that detected Ki-67 in western blot and real-time PCR is solely from NPCs, we stained NPCs with NES and Ki-67. The immunofluorescence staining data shows that Ki-67 is co-localized with NES (**Supplementary Figure 4**). We also measured intracellular ROS level in NPCs. As expected, MPP^+ treatment increased ROS level compared to controls ($p = 0.023$, **Figure 2E**). However, when UA was treated prior to MPP^+ treatment for 24 h, it significantly scavenged

excessive ROS, restoring back to control level (p = 0.047, **Figure 2E**). These data suggest that UA not only increased the survival of NPCs against MPP^+ toxicity, but also enhanced proliferation *in vitro*. Next, the modulatory mechanism of UA on neurogenic activity was further studied in mitochondrial dynamics. To analyze mitochondrial morphology, we performed immunofluorescence staining using mitotracker. MPP^+-treated NPCs displayed many more fragmented mitochondria over 78% rather than tubular shape. On contrast, UA treated NPCs exhibited more interconnected, elongated and filamentous mitochondria similar to those of naïve NPCs. About 18% of UA treated NPCs showed fragmented mitochondria (**Figure 2H**). We also confirmed the effect of UA on mitochondrial network morphology using MiNA. UA treated NPCs showed lower number of individuals (puncta), longer branch length, and lower branch number per network compared to the MPP+ treatment group (**Figure 2I**).

Uric Acid Treatment Rescued the Abnormal Mitochondrial Phenotype Observed in Primary Cultured Neural Precursor Cells by Modulating Mitochondrial Dynamics

To investigate the mitochondrial dynamics modulatory mechanism in detail, mitochondrial dynamics-related genes were measured with quantitative real-time PCR analysis. The expression level of mitochondrial fusion marker, MFN1 (mitofusin 1), MFN2 (mitofusin 2), and OPA1 (mitochondrial dynamin like GTPase) was significantly decreased in NPCs following MPP^+ treatment as compared to the control group (p = 0.000, p = 0.046, p = 0.048), whereas UA treatment restored them in MPP^+-treated NPCs (p = 0.023, p = 0.01, p = 0.002, **Figures 3A–C**). Conversely, expression level of FIS1 (mitochondrial fission 1) was markedly increased in NPCs approximately two- and three-fold following MPP^+ treatment, repectively (p = 0.021); however, UA treatment counteracted them in MPP^+-treated NPCs (**Figure 3D**). Under MPP^+ treatment, mitochondrial master regulator, PGC-1α (PPARG coactivator 1 alpha), tended to decrease in NPCs but did not reach statistical significance (p = 0.406), whereas UA treatment significantly upregulated the expression of PGC-1α compared to the only-MPP^+-treated group (p = 0.029, **Figure 3E**). In addition, UA treatment in MPP^+-treated NPCs significantly increased the expression of mitochondrial transcription factor, TFAM (transcription factor A, mitochondrial) (p = 0.001) relative to the MPP^+-treated group (p = 0.001, **Figure 3F**). Additionally, we measured protein level of DLP1 (GTPase Dynamin-related protein 1) tetramer and monomer form to investigate whether Dlp1 was hyperactivated. Both tetramer and monomer form of DLP1 was increased in MPP^+ treated NPCs (p = 0.007, p = 0.006), while UA treatment counteracted it (p = 0.043, p = 0.019, **Figures 3G,H**). These data indicate that UA has scavenged MPP^+ toxins by modulating mitochondrial dynamics. Next, we evaluated the changes of actual mitochondrial morphology using TEM analysis. Mitochondrial morphology was preserved in control NPCs, with well-formed cristae and undisrupted mitochondria membranes. However, mitochondria following MPP^+ treatment were filled with discontinuous cristae, electron-dense structures, and damaged double-membranes. Additionally, mitochondria in MPP^+-treated NPCs exhibited swollen bodies (**Figure 3I**). The number of normal and swollen mitochondria was counted in restricted area and presented in graph (**Figure 3J**). These data suggest that treatment of MPP^+ leads to mitochondrial damage, possibly triggering fission process and/or inhibiting fusion process. However, UA treatment successfully returned mitochondrial morphology to a healthy form, similar to those of naïve NPCs, through a possible rescue of mitochondrial dynamics balance of fusion and fission processes.

Parkinson's Disease Mice With Elevated Serum Uric Acid Levels Showed Increased BrdU-Positive Cell Numbers Through Modulation of Mitochondrial Dynamics Key Actors

Next, mitochondrial dynamics-related proteins were analyzed to investigate whether UA elevation could modulate mitochondrial dynamics in the SVZ of MPTP-treated animals. The protein expression of mitochondrial fusion marker, MFN1 (mitofusin 1), was significantly decreased in MPTP-treated animals as compared to control mice (p = 0.001, **Figure 4A**), and another marker, MFN2, was slightly decreased in the parkinsonian model as compared to healthy mice (p = 0.054, **Figure 4B**). The expression of the OPA1 (OPA1 mitochondrial dynamin like GTPase) tended to decrease in MPTP-treated mice relative to control mice (p = 0.031, **Figure 4C**). However, UA elevation in MPTP-treated animals led to an increase in the expression of MFN1 (p = 0.001), MFN2 (p = 0.005), and OPA1 (p = 0.000) as compared to the MPTP-only-treated group (**Figures 4A–C**). To determine whether DLP1 (GTPase Dynamin-related protein 1), mitochondrial fission-related protein, was activated, we measured the expression level of DLP1 tetramer form. The level of DLP1 tetramer form was significantly increased in MPTP-treated animals compared to control animals, which was down-regulated after UA elevating therapy (p = 0.000, **Figure 4D**). However, there was no significant difference in monomer form among three groups. Another fission regulator, FIS1, was down-regulated with UA-elevating therapy compared to the control and MPTP groups (p = 0.000, **Figure 4E**). Meanwhile, UA elevation in MPTP-treated animals led to a significant increase in expression of Dlp1 and FIS1 (p = 0.029 and 0.000, respectively) compared to the MPTP-only-treated group (**Figures 4D,E**). Finally, UA elevation led to a significant increase in expression of NES in the SVZ of MPTP-treated animals (p = 0.021, **Figure 4F**).

DISCUSSION

This study aimed to investigate whether elevation of serum UA levels modulate neurogenic activity in a parkinsonian model. The major findings of present study are (1) UA elevation in MPTP-induced PD mice led to an increased number

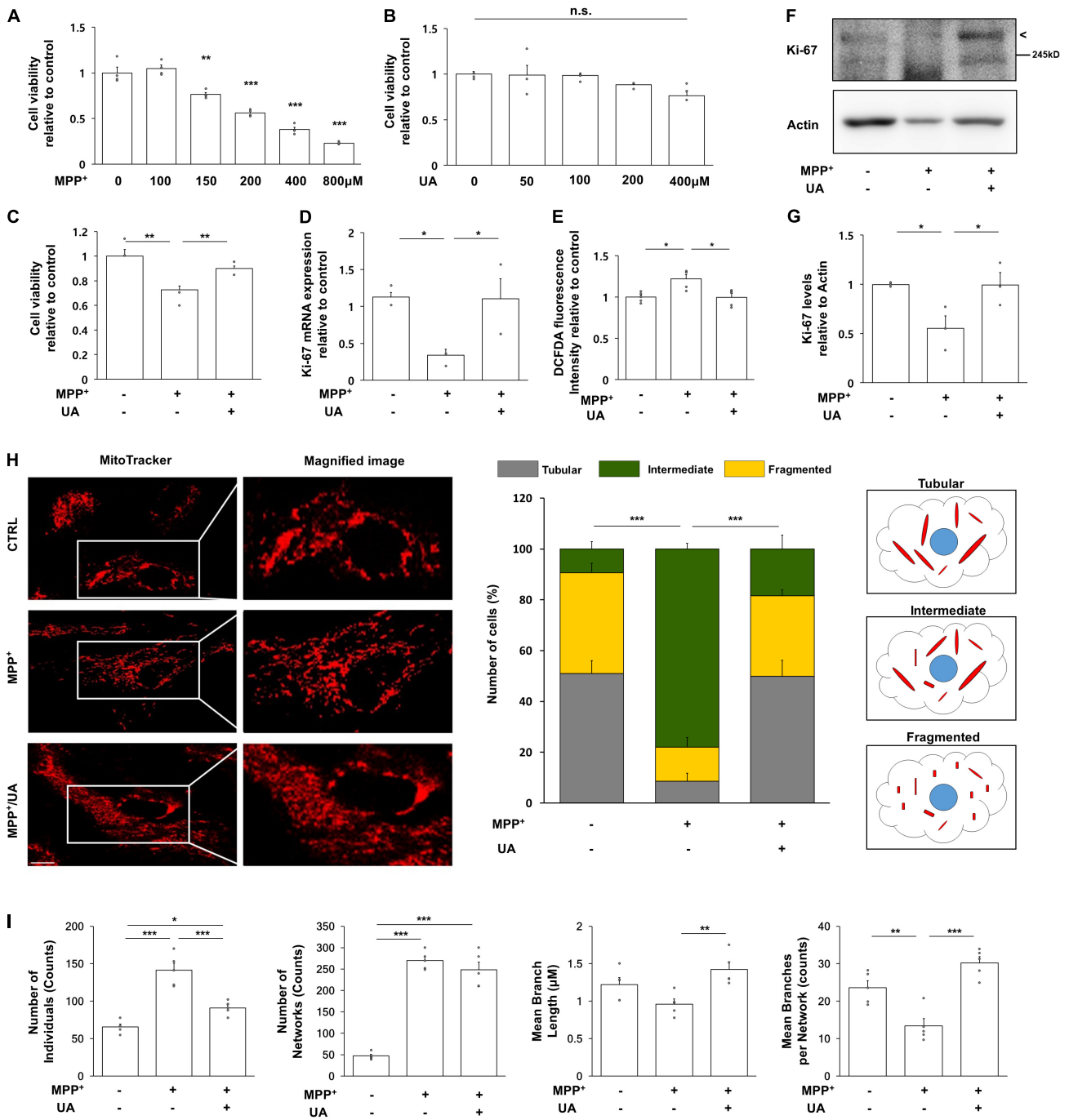

FIGURE 2 | UA treatment exerted neuroprotective effect and promoted proliferation in primary cultured NPCs. **(A)** MTS analysis in MPP^+-treated NPCs with a concentration of 100, 150, 200, 400, and 800 μM. 150 μM of MPP^+ treatment induced about 56% of viability on NPCs (n = 4 per group). **(B)** MTS analysis in UA-treated NPCs with a concentration of 50, 100, 200, and 400 μM. UA treatment did not induce statistically significant cell death up to 400 μM (n = 4 per group). **(C)** MTS analysis in MPP^+ treated or MPP^+ with UA-treated NPCs at a 150 μM concentration of UA for 24 h and MPP^+ for 72 h with UA co-treatment. UA exerted a neuroprotective effect on NPCs by restoring cell viability up to 90% compared to control (n = 4 per group). **(D)** Quantitative RT-PCR for proliferation marker, Ki-67. The expression level of Ki-67 was reduced to 41.6%; however, UA restored it to 92.2% compared to control. **(E)** Intracellular ROS as measured by DCFDA assay after MPP^+ and UA treatment. MPP^+-induced ROS was scavenged by UA pre-treatment. **(F)** Western blot for proliferation marker, Ki67 in MPP^+ and UA-treated NPCs. **(G)** Quantification graph of Ki-67 western blot analysis. **(H)** Immunofluorescent labeling for mitotracker. MPP^+-treated NPCs showed fragmented mitochondrial morphology, whereas UA treatment restored them similar to those of controls. **(I)** Mitochondrial network analysis using MiNA. UA treated NPCs showed lower number of individuals (puncta), longer branch length, and lower branch number per network compared to the MPP^+ treatment group. Each five images per group were analyzed. Scale bar: 10 μm. Differences among the conditions were evaluated by ANOVA with a Bonferroni correction for multiple comparison. The data are presented as the mean ± SE. $^*p < 0.05$, $^{**}p < 0.01$, and $^{***}p < 0.001$.

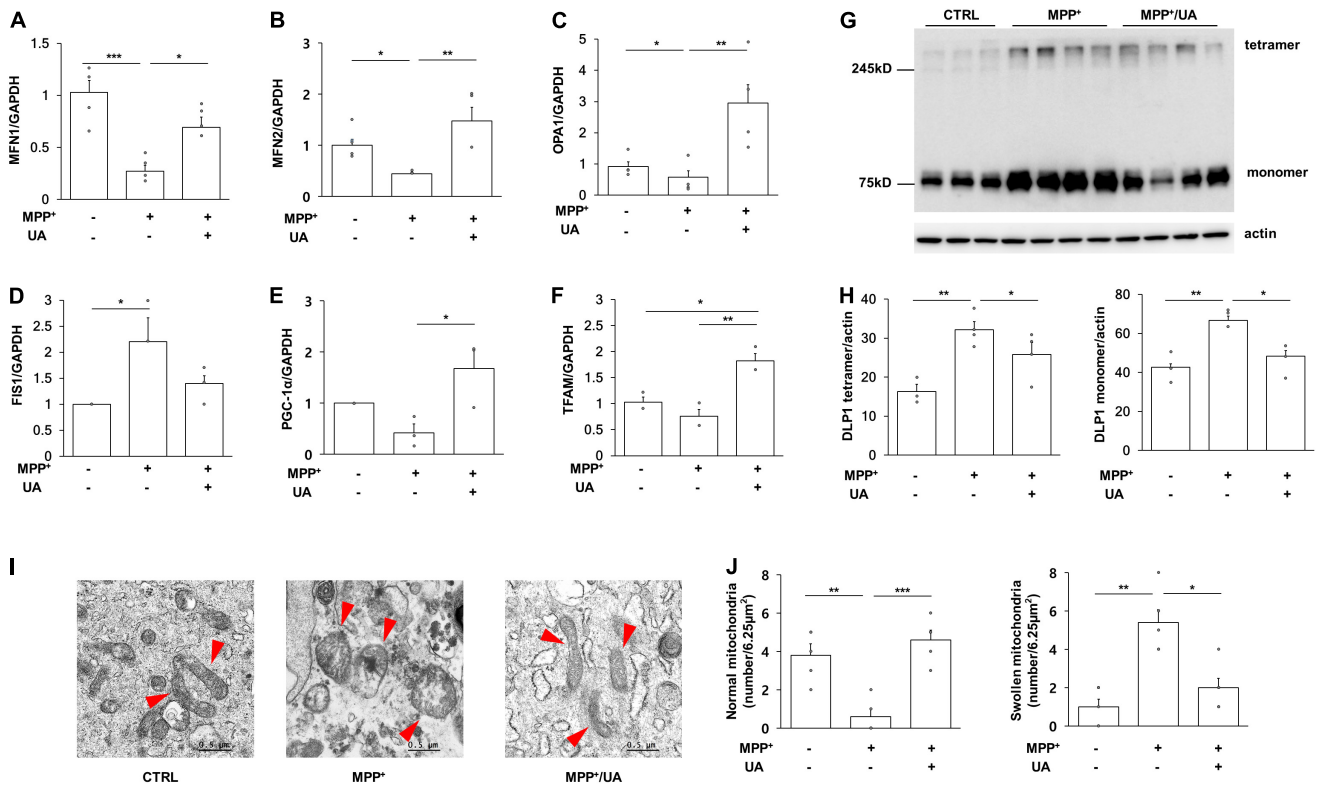

FIGURE 3 | UA treatment rescued the mitochondrial phenotype *via* modulating mitochondrial dynamics in NPCs. **(A)** Quantitative RT-PCR for mitochondrial fusion marker, MFN1. **(B)** Quantitative RT-PCR for mitochondrial fusion marker, MFN2. **(C)** Quantitative RT-PCR for mitochondrial fission marker, OPA1. **(D)** Quantitative RT-PCR for mitochondrial fission marker, FIS1. **(E)** Quantitative RT-PCR for mitochondria master regulator, PGC-1α. **(F)** Quantitative RT-PCR for mitochondrial transcription factor TFAM. MPP^+ treatment led to a significant decrease in the expression level of MFN1, MFN2, PGC-1α, and TFAM and UA treatment has restored it. On the contrary, the expression level of FIS1 and OPA1 was increased when exposed to MPP^+-, and UA treatment restored it (n = 5 per group). **(G,H)** Western blot for mitochondrial fission regulator Dlp1 tetramer and monomer form. Both tetramer and monomer form were increased with MPP^+ treatment, which was rescued by UA (n = 3 for CTRL group, n = 4 for MPP^+ and MPP^+/UA group). **(I)** TEM analysis revealed that MPP^+ treatment induced severe abnormal morphology of mitochondria with a swollen body and fragmented phenotype. However, UA treatment returned mitochondria morphology to a similar state as control NPCs. The arrows indicate mitochondria. **(J)** MPP^+ treated NPCs showed reduced normal mitochondria and increased swollen mitochondria, however, UA treatment rescued it. Differences among the conditions were evaluated by ANOVA with a Bonferroni correction for multiple comparison. The data are presented as mean ± SE. $^*p < 0.05$, $^{**}p < 0.01$, and $^{***}p < 0.001$.

of BrdU-positive cells in the SVZ including RMS and DG compared to MPTP-only-treated mice. (2) UA treatment exerted a prosurvival effect, restoring viability and proliferation of NPCs against MPP^+ treatment. (3) In the process of modulating neurogenesis, our *in vitro and in vivo* data demonstrated that UA elevation regulated mitochondrial dynamics *via* promoting fusion machinery. The results suggest that UA enhances neurogenic activity in the SVZ of a parkinsonian model by modulating mitochondrial dynamics.

Although the underlying molecular mechanisms of the altered neurogenesis in PD remain unknown, neurochemical deficits of dopamine (Mishra et al., 2019b), indirect effects of growth factor release, and α-synuclein accumulation in NPCs of the SVZ *via* the disease process may influence neurogenic activity (Winner et al., 2012). Several studies have demonstrated the effect of α-synuclein in the hippocampus and SVZ of transgenic animal models and murine embryonic stem cells (Winner et al., 2004, 2008; Crews et al., 2008; Kohl et al., 2012). In addition, recent evidence has demonstrated that mitochondrial dysfunction and inappropriate regulation of mitochondrial dynamics have detrimental effects on neurogenesis in the embryonic as well as adult brain. During neurogenesis, mitochondrial dysfunction resulting from deletion of the mitochondrial oxidoreductase protein AIF within the early NSC population disrupted the neurogenic pathway completely, including self-renewal capacity of NSC and proliferation and differentiation of NPCs (Khacho et al., 2017). Likewise, disruption of mitochondrial function by loss of the mitochondrial transcription factor, TFAM, when restricted to the adult NSC population, leads to impairment in adult neurogenesis. During embryonic neurogenesis, mitochondrial dynamics seem to play an important role in the stem cell decision-making process enhanced mitochondrial fusion promotes NSC self-renewal, while mitochondrial fragmentation initiates the commitment of NSC to neuronal differentiation and neuronal maturation (Khacho and Slack, 2018). A recent study reported that inhibition of mitochondrial fission improved mitochondrial dynamics and stimulated hippocampal neurogenesis in Down syndrome animal model (Valenti et al., 2017). Therefore, maintenance of proper

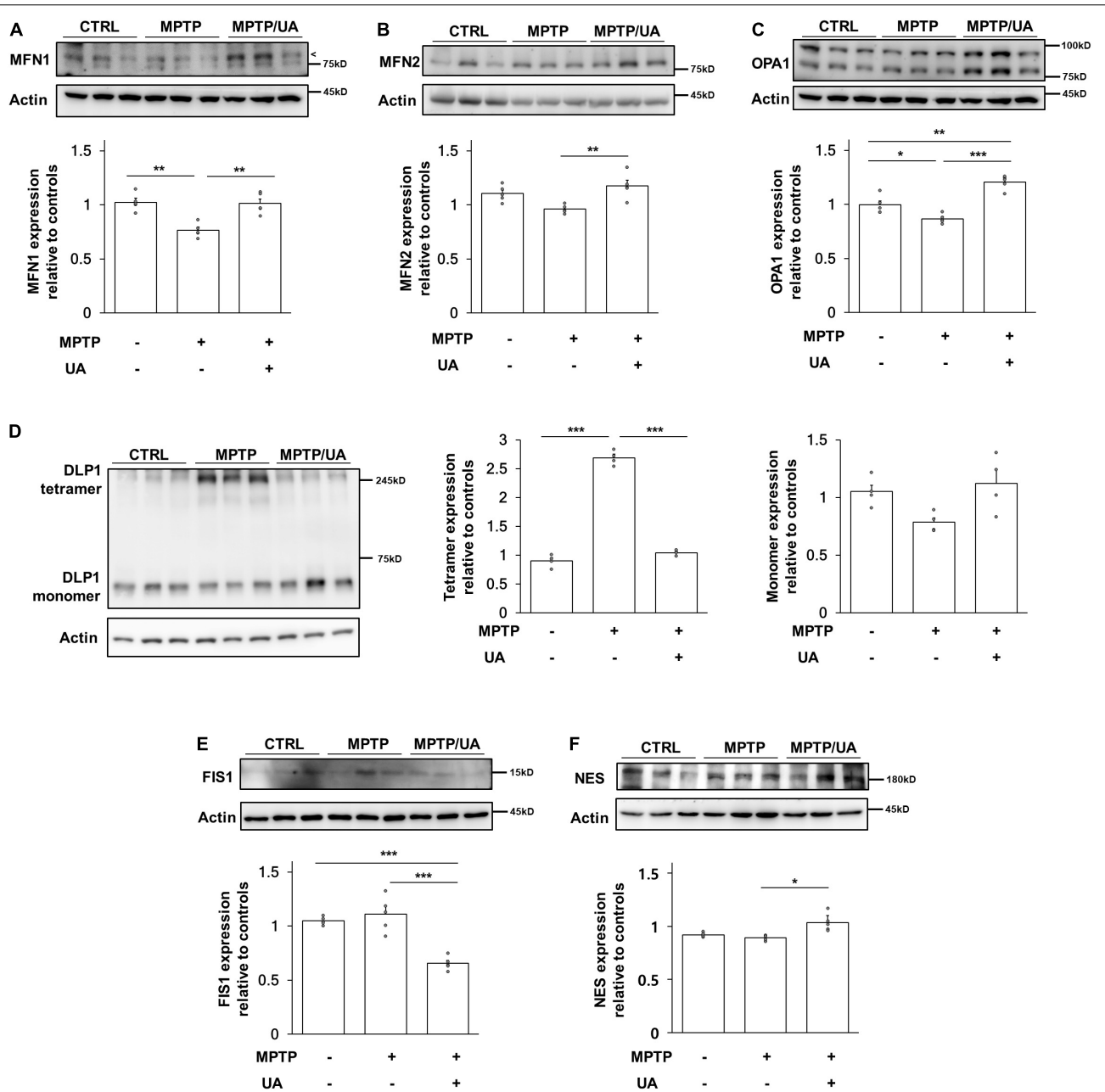

FIGURE 4 | PD mice with high serum UA level showed modulated mitochondrial dynamics. **(A)** Western blot for mitochondrial fusion marker, MFN1. **(B)** Western blot for mitochondrial fusion marker, MFN2. **(C)** Western blot for mitochondrial fusion marker, OPA1. The expression levels of MFN1, MFN2, and OPA1 were decreased in PD mice and upregulated in UA-elevated PD mice (n = 5 per group). **(D)** Western blot for mitochondrial fission regulator Dlp1 tetramer and monomer form. **(E)** Western blot for mitochondrial fission marker, FIS1. The expression level of Dlp1 tetramer form and FIS1 were increased in PD mice and significantly suppressed in PD mice with high serum UA levels (n = 5 per group). **(F)** Western blot for neural stem cell marker, NES. The expression levels of NES were significantly increased in UA-elevated PD mice compared to control or PD mice with normal UA levels (n = 5 per group). Differences among the conditions were evaluated by ANOVA with a Bonferroni correction for multiple comparison. The data are presented as mean ± SE. *$p < 0.05$, **$p < 0.01$, and ***$p < 0.001$.

mitochondrial dynamics would be an important strategy to modulate neurogenic activity in PD.

The present study has demonstrated that UA elevation in MPTP-induced PD mice led to an increased number of BrdU-positive cells in the SVZ compared to MPTP- only-treated mice, restoring up to 85% of neurogenic activity compared to the control mice. In a cellular model using primary culture of NPCs, UA treatment exerted a prosurvival effect, restoring cell viability of NPCs against MPP^+ treatment and led to increased proliferation markers. As impairment in neurogenesis is known to be a critical factor in neurodegenerative diseases including PD, modulating it could be an effective strategy in disease-modifying

treatment. Accumulating clinical data have also reported an association between high serum UA levels and lower likelihood of developing PD (de Lau et al., 2005). Furthermore, we found that the hippocampal neurogenesis was also enhanced with UA-elevating therapy. Previous studies have demonstrated that UA decreases the risk of dementia in general population mice (Euser et al., 2009) and improves cognitive performance in PD mice through the Nrf2-ARE signaling pathway (Huang et al., 2017). Hence, it is possible that UA could improve cognitive function through modulation of hippocampal neurogenesis. A further research is warranted to investigate whether UA would be helpful in AD models by modulating hippocampal neurogenic activity.

Interestingly, we have demonstrated that UA may modulate neurogenesis by remodeling mitochondria. Mitochondria are dynamic organelles that constantly change their size and morphology in response to the environment in the machinery of fission and fusion. In mammals, MFN1, MFN2, and OPA1 are responsible for mitochondrial fusion, while Dlp1 and FIS1 are required for mitochondrial fission. Fission is a process of breaking apart into smaller fragments, which is important for segregating dysfunctional mitochondria from healthy counterparts (Ni et al., 2015). Therefore, this process plays an important role in quality control of maintaining healthy mitochondria, further sustaining healthy neurons that require considerable energy. In the process of neurogenesis, a critical amount of ATP is required to facilitate cytoskeletal rearrangement, neuronal sprouting, and organelle transport. Being a primary source of cellular ATP, healthy mitochondrial function is necessary for the brain to perform neurogenesis effectively. We also demonstrated that UA up-regulated mitochondrial biogenesis-related genes including PGC-1α and TFAM. According to previous study, PGC-1α guarantees the production of healthy mitochondria and a correct equilibrium between mitophagy and mitochondrial biogenesis, thus blocking excessive ROS (Baldelli et al., 2014). In terms of the association between oxidative stress and neurogenesis, several studies have highlighted the fact that oxidative stress load directly affects cellular states by modulating the redox state of NSCs or NPCs, given that adult neurogenesis is a high-energy-consuming process, and thus, leads to ROS accumulation (Yuan et al., 2015). MPTP, the neurotoxin widely known to induce PD models, is highly lipophilic, and so it can rapidly cross the blood brain barrier after systemic administration. MPTP is metabolized within the brain to active toxin MPP^+ by monoamine oxidase, resulting in mitochondrial complex I dysfunction and impaired mitochondrial homeostasis (Kopin, 1987). Mitochondrial malfunction, already problematic in the process of PD, makes stem cells vulnerable to oxidative stress, which in turn accelerates impairment of neurogenesis. Moreover, emerging data from human and animal models of PD have reported that α-synuclein has an important role in the control of neuronal mitochondrial dynamic processes (Banerjee et al., 2010; Melo et al., 2018), suggesting a strong candidate for a pathogenic mechanism underpinning PD pathogenesis beyond mitochondrial biogenesis, a well-known factor. Therefore, UA, having potent antioxidant properties, would defend mitochondrial homeostasis and dynamics against MPTP-induced oxidative stress, which can lead to maintenance of neurogenic activity in the SVZ of PD models. There are several other neurotoxins inducing PD experimental model. Rotenone is reported to cause excessive mitochondrial fission, resulting disrupted mitochondrial dynamics (Peng et al., 2016) and 6-hydroxydopamine (6-OHDA) promoted mitochondrial fission process, elevating Drp-1 level (Galindo et al., 2012). Also rats who received surgical injection of human alpha-synuclein showed increased mitochondrial fission (Park et al., 2020). As our study described mitochondrial dynamics regulation as a mechanism underlying enhanced neurogenesis, it is plausible that UA could work in other PD models as well. Given that the precise mechanism of mitochondrial dynamics by UA is still elusive, future study focusing on down signaling pathways of UA-associated mitochondrial remodeling is warranted. Accordingly, our data provide additional evidence that modulation of neurogenic activity *via* modulating mitochondrial dynamics by a UA-elevating strategy may be an intriguing mechanism in the development of disease modifying treatment of PD.

Recent studies have suggested the important role of dopaminergic modulation in the neurogenic activity of the SVZ by demonstrating that NPCs in the SVZ express dopaminergic receptors and dopaminergic innervation from the SN in a 6-OHDA-induced PD rat model (Hoglinger et al., 2004; Mishra et al., 2019a). Specifically, dopamine agonists augment neurogenesis in animal models of PD (Winner et al., 2009), and chronic use of levodopa has a positive effect on the number of NSCs in the SVZ of patients with PD (O'Sullivan et al., 2011). Based on these previous data, the present study evaluated the density of nigral dopaminergic neurons between MPTP-induced PD animals with and without UA-elevating therapy to exclude the direct effect of nigral dopamine on neurogenesis in the SVZ. However, there was no significant change in nigral dopaminergic density between groups, suggesting that the modulating effect of UA on neurogenesis in NPCs of the SVZ may reflect a primary effect of UA itself rather than an indirect effect of dopaminergic medication.

This study has several limitations to extend clinical implications. First, although neuroprotective effect of UA in PD incidence and progression seems to be sex-dependent (O'Reilly et al., 2010), the present study examined effect of UA elevation on neurogenic activity only in male PD mice. Further study of UA-mediated neurogenic activity in female animals is also necessary. Second, although serum UA levels increased following injection of IMP with KOx, post-treatment after MPTP induction without pre-treatment prior to MPTP induction did not lead to a significant increase in neurogenesis. In both an animal and cellular model, pre-treatment of UA enhanced neurogenesis and exerted prosurvival effect of NPCs. Regarding these data, neurogenic modulation of UA seems to be effective in the premotor stage of PD; however, this issue should be investigated in future studies. Third, we could not provide mitochondrial morphology in animal tissue, which may limit the role of UA in mitochondrial dynamics. Finally, when UA is elevated beyond the normal range, it increases risk of gout and cardiovascular diseases. This issue requires further study to

determine the appropriate UA level exerting beneficial effects in parkinsonian disorder.

CONCLUSION

In summary, this study demonstrates that UA elevation can enhance neurogenic activity in the NPCs of the SVZ in parkinsonian animal and cellular models by modulating mitochondrial dynamics.

DATA AVAILABILITY STATEMENT

The original contributions presented in the study are included in the article/**Supplementary Material**, further inquiries can be directed to the corresponding author.

ETHICS STATEMENT

All procedures were performed in accordance with the Laboratory Animals Welfare Act, the Guide for the Care and Use of Laboratory Animals and the Guidelines and Policies. The rodent experiment was approved by IACUC (Institutional Animal Care and Use Committee) in the Yonsei University Health System. ARRIVE guidelines were followed (http://arriveguidelines.org).

AUTHOR CONTRIBUTIONS

JL contributed to study design, draft, performing experiments, and revise the manuscript and figures. YS, YK, HK, and DK contributed to analysis of data, verifying the underlying data, and interpretation of results. SC and HY contributed to interpretation of results. JS contributed to conception, study design, analysis of data, and interpretation of results. PL contributed to conception, study design, revise the manuscript and figures, supervision, and funding acquisition. All authors edited and approved the manuscript.

FUNDING

This research was supported by the Basic Science Research Program through the National Research Foundation of Korea (NRF) funded by the Ministry of Science, ICT and Future Planning (Grant Number: NRF-2019R1A2C2085462), and the Brain Korea 21 PLUS Project for Medical Science, Yonsei University.

SUPPLEMENTARY MATERIAL

The Supplementary Material for this article can be found online at: https://www.frontiersin.org/articles/10.3389/fnagi.2022.851711/full#supplementary-material

REFERENCES

Arrázola, M. S., Andraini, T., Szelechowski, M., Mouledous, L., Arnauné-Pelloquin, L., Davezac, N., et al. (2019). Mitochondria in Developmental and Adult Neurogenesis. *Neurotox Res.* 36, 257–267. doi: 10.1007/s12640-018-9942-y

Auinger, P., Kieburtz, K., and McDermott, M. P. (2010). The relationship between uric acid levels and Huntington's disease progression. *Move. Dis.* 25, 224–228. doi: 10.1002/mds.22907

Bakshi, R., Xu, Y., Mueller, K. A., Chen, X., Granucci, E., Paganoni, S., et al. (2018). Urate mitigates oxidative stress and motor neuron toxicity of astrocytes derived from ALS-linked SOD1(G93A) mutant mice. *Mol. Cell. Neurosci.* 92, 12–16. doi: 10.1016/j.mcn.2018.06.002

Baldelli, S., Aquilano, K., and Ciriolo, M. R. (2014). PGC-1alpha buffers ROS-mediated removal of mitochondria during myogenesis. *Cell Death Dis.* 5:e1515. doi: 10.1038/cddis.2014.458

Banerjee, K., Sinha, M., Pham Cle, L., Jana, S., Chanda, D., Cappai, R., et al. (2010). Alpha-synuclein induced membrane depolarization and loss of phosphorylation capacity of isolated rat brain mitochondria: implications in Parkinson's disease. *FEBS Lett.* 584, 1571–1576. doi: 10.1016/j.febslet.2010.03.012

Beckervordersandforth, R. (2017). Mitochondrial Metabolism-Mediated Regulation of Adult Neurogenesis. *Brain plasticity* 3, 73–87. doi: 10.3233/bpl-170044

Beckervordersandforth, R., Ebert, B., Schäffner, I., Moss, J., Fiebig, C., and Shin, J. (2017). Role of Mitochondrial Metabolism in the Control of Early Lineage Progression and Aging Phenotypes in Adult Hippocampal Neurogenesis. *Neuron* 93, 560.e–573.e. doi: 10.1016/j.neuron.2016.12.017

Berdugo-Vega, G., Arias-Gil, G., Lopez-Fernandez, A., Artegiani, B., Wasielewska, J. M., Lee, C. C., et al. (2020). Increasing neurogenesis refines hippocampal activity rejuvenating navigational learning strategies and contextual memory throughout life. *Nat. Commun.* 11:135. doi: 10.1038/s41467-019-14026-z

Crews, L., Mizuno, H., Desplats, P., Rockenstein, E., Adame, A., Patrick, C., et al. (2008). Alpha-synuclein alters Notch-1 expression and neurogenesis in mouse embryonic stem cells and in the hippocampus of transgenic mice. *J. Neurosci.* 28, 4250–4260. doi: 10.1523/JNEUROSCI.0066-08.2008

de Lau, L. M., Koudstaal, P. J., Hofman, A., and Breteler, M. M. (2005). Serum uric acid levels and the risk of Parkinson disease. *Ann. Neurol.* 58, 797–800. doi: 10.1002/ana.20663

Duvezin-Caubet, S., Jagasia, R., Wagener, J., Hofmann, S., Trifunovic, A., Hansson, A., et al. (2006). Proteolytic processing of OPA1 links mitochondrial dysfunction to alterations in mitochondrial morphology. *J. Biol. Chem.* 281, 37972–37979. doi: 10.1074/jbc.M606059200

Euser, S. M., Hofman, A., Westendorp, R. G., and Breteler, M. M. (2009). Serum uric acid and cognitive function and dementia. *Brain* 132, 377–382. doi: 10.1093/brain/awn316

Flippo, K. H., and Strack, S. (2017). Mitochondrial dynamics in neuronal injury, development and plasticity. *J. Cell Sci.* 130, 671–681. doi: 10.1242/jcs.171017

Galindo, M. F., Solesio, M. E., Atienzar-Aroca, S., Zamora, M. J., and Jordan Bueso, J. (2012). Mitochondrial dynamics and mitophagy in the 6-hydroxydopamine preclinical model of Parkinson's disease. *Park. Dis.* 2012:131058. doi: 10.1155/2012/131058

Geraerts, M., Krylyshkina, O., Debyser, Z., and Baekelandt, V. (2007). Concise review: therapeutic strategies for Parkinson disease based on the modulation of adult neurogenesis. *Stem Cells* 25, 263–270. doi: 10.1634/stemcells.2006-0364

Gil-Mohapel, J., Simpson, J. M., Ghilan, M., and Christie, B. R. (2011). Neurogenesis in Huntington's disease: can studying adult neurogenesis lead to the development of new therapeutic strategies? *Brain Res.* 1406, 84–105. doi: 10.1016/j.brainres.2011.06.040

Hoglinger, G. U., Rizk, P., Muriel, M. P., Duyckaerts, C., Oertel, W. H., Caille, I., et al. (2004). Dopamine depletion impairs precursor cell proliferation in Parkinson disease. *Nat. Neurosci.* 7, 726–735. doi: 10.1038/nn1265

Hollenbeck, P. J., and Saxton, W. M. (2005). The axonal transport of mitochondria. *J. Cell Sci.* 118, 5411–5419. doi: 10.1242/jcs.02745

Huang, T. T., Hao, D. L., Wu, B. N., Mao, L. L., and Zhang, J. (2017). Uric acid demonstrates neuroprotective effect on Parkinson's disease mice through Nrf2-ARE signaling pathway. *Biochem. Biophys. Res. Commun.* 493, 1443–1449. doi: 10.1016/j.bbrc.2017.10.004

Hwang, O. (2013). Role of oxidative stress in Parkinson's disease. *Exp. Neurobiol.* 22, 11–17. doi: 10.5607/en.2013.22.1.11

Jankovic, J. (2008). Parkinson's disease and movement disorders: moving forward. *Lancet. Neurol.* 7, 9–11. doi: 10.1016/s1474-4422(07)70302-2

Khacho, M., Clark, A., Svoboda, D. S., Azzi, J., MacLaurin, J. G., Meghaizel, C., et al. (2016). Mitochondrial Dynamics Impacts Stem Cell Identity and Fate Decisions by Regulating a Nuclear Transcriptional Program. *Cell Stem cell* 19, 232–247. doi: 10.1016/j.stem.2016.04.015

Khacho, M., Clark, A., Svoboda, D. S., MacLaurin, J. G., Lagace, D. C., Park, D. S., et al. (2017). Mitochondrial dysfunction underlies cognitive defects as a result of neural stem cell depletion and impaired neurogenesis. *Hum. Mol. Gen.* 26, 3327–3341. doi: 10.1093/hmg/ddx217

Khacho, M., and Slack, R. S. (2018). Mitochondrial dynamics in the regulation of neurogenesis: From development to the adult brain. *Dev. Dyn.*247, 47–53. doi: 10.1002/dvdy.24538

Kim, H. N., Shin, J. Y., Kim, D. Y., Lee, J. E., and Lee, P. H. (2021). Priming mesenchymal stem cells with uric acid enhances neuroprotective properties in parkinsonian models. *J. Tissue Eng.* 12:20417314211004816. doi: 10.1177/20417314211004816

Kohl, Z., Winner, B., Ubhi, K., Rockenstein, E., Mante, M., Münch, M., et al. (2012). Fluoxetine rescues impaired hippocampal neurogenesis in a transgenic A53T synuclein mouse model. *Eur. J. Neurosci.* 35, 10–19. doi: 10.1111/j.1460-9568.2011.07933.x

Kopin, I. J. (1987). MPTP: an industrial chemical and contaminant of illicit narcotics stimulates a new era in research on Parkinson's disease. *Environ. Health Perspect.* 75, 45–51. doi: 10.1289/ehp.877545

Kuhn, H. G., Eisch, A. J., Spalding, K., and Peterson, D. A. (2016). Detection and Phenotypic Characterization of Adult Neurogenesis. *Cold Spring Harbor Perspect. Biol.* 8:a025981. doi: 10.1101/cshperspect.a025981

Li, X., Jia, S., Zhou, Z., Jin, Y., Zhang, X., Hou, C., et al. (2018). Effect of serum uric acid on cognition in patients with idiopathic REM sleep behavior disorder. *J. Neural Trans.* 125, 1805–1812. doi: 10.1007/s00702-018-1935-8

Luo, L., and O'Leary, D. D. (2005). Axon retraction and degeneration in development and disease. *Ann. Rev. Neurosci.* 28, 127–156. doi: 10.1146/annurev.neuro.28.061604.135632

Marxreiter, F., Regensburger, M., and Winkler, J. (2013). Adult neurogenesis in Parkinson's disease. *Cell Mol. Life Sci.* 70, 459–473. doi: 10.1007/s00018-012-1062-x

Melo, T. Q., Copray, S., and Ferrari, M. F. R. (2018). Alpha-Synuclein Toxicity on Protein Quality Control. Mitochondria and Endoplasmic Reticulum. *Neurochem. Res.* 43, 2212–2223. doi: 10.1007/s11064-018-2673-x

Mishra, A., Singh, S., Tiwari, V., Chaturvedi, S., Wahajuddin, M., and Shukla, S. (2019a). Dopamine receptor activation mitigates mitochondrial dysfunction and oxidative stress to enhance dopaminergic neurogenesis in 6-OHDA lesioned rats: A role of Wnt signalling. *Neurochem. Int.* 129:104463. doi: 10.1016/j.neuint.2019.104463

Mishra, A., Singh, S., Tiwari, V., Parul, and Shukla, S. (2019b). Dopamine D1 receptor activation improves adult hippocampal neurogenesis and exerts anxiolytic and antidepressant-like effect via activation of Wnt/beta-catenin pathways in rat model of Parkinson's disease. *Neurochem. Int.* 122, 170–186. doi: 10.1016/j.neuint.2018.11.020

Na Kim, H., Yeol Kim, D., Hee, Oh, S., Sook Kim, H., Suk Kim, K., et al. (2017). Feasibility and Efficacy of Intra-Arterial Administration of Mesenchymal Stem Cells in an Animal Model of Double Toxin-Induced Multiple System Atrophy. *Stem Cells Transl. Med.* 6, 1424–1433. doi: 10.1002/sctm.16-0438

Ni, H. M., Williams, J. A., and Ding, W. X. (2015). Mitochondrial dynamics and mitochondrial quality control. *Redox Biol.* 4, 6–13. doi: 10.1016/j.redox.2014.11.006

Oh, S. H., Kim, H. N., Park, H. J., Shin, J. Y., and Lee, P. H. (2015). Mesenchymal Stem Cells Increase Hippocampal Neurogenesis and Neuronal Differentiation by Enhancing the Wnt Signaling Pathway in an Alzheimer's Disease Model. *Cell Transplant.* 24, 1097–1109. doi: 10.3727/096368914x679237

Okamoto, K., and Shaw, J. M. (2005). Mitochondrial morphology and dynamics in yeast and multicellular eukaryotes. *Ann. Rev. Gen.* 39, 503–536. doi: 10.1146/annurev.genet.38.072902.093019

O'Reilly, E. J., Gao, X., Weisskopf, M. G., Chen, H., Schwarzschild, M. A., Spiegelman, D., et al. (2010). Plasma urate and Parkinson's disease in women. *Am. J. Epidemiol.* 172, 666–670. doi: 10.1093/aje/kwq195

O'Sullivan, S. S., Johnson, M., Williams, D. R., Revesz, T., Holton, J. L., Lees, A. J., et al. (2011). The effect of drug treatment on neurogenesis in Parkinson's disease. *Move. Dis* 26, 45–50. doi: 10.1002/mds.23340

Park, J. H., Burgess, J. D., Faroqi, A. H., DeMeo, N. N., Fiesel, F. C., Springer, W., et al. (2020). Alpha-synuclein-induced mitochondrial dysfunction is mediated via a sirtuin 3-dependent pathway. *Mol. Neurodegener.* 15:5. doi: 10.1186/s13024-019-0349-x

Peng, K., Tao, Y., Zhang, J., Wang, J., Ye, F., Dan, G., et al. (2016). Resveratrol Regulates Mitochondrial Biogenesis and Fission/Fusion to Attenuate Rotenone-Induced Neurotoxicity. *Oxid Med. Cell Longev.* 2016:6705621. doi: 10.1155/2016/6705621

Picca, A., Calvani, R., Coelho-Junior, H. J., Landi, F., Bernabei, R., and Marzetti, E. (2020). Mitochondrial Dysfunction, Oxidative Stress, and Neuroinflammation: Intertwined Roads to Neurodegeneration. *Antioxidants* 9:647 doi: 10.3390/antiox9080647

Scheepers, L., Jacobsson, L. T. H., Kern, S., Johansson, L., Dehlin, M., and Skoog, I. (2019). Urate and risk of Alzheimer's disease and vascular dementia: A population-based study. *Alzheimers Dement* 15, 754–763. doi: 10.1016/j.jalz.2019.01.014

Scopa, C., Marrocco, F., Latina, V., Ruggeri, F., Corvaglia, V., La Regina, F., et al. (2020). Impaired adult neurogenesis is an early event in Alzheimer's disease neurodegeneration, mediated by intracellular Abeta oligomers. *Cell Death Differ.* 27, 934–948. doi: 10.1038/s41418-019-0409-3

Squadrito, G. L., Cueto, R., Splenser, A. E., Valavanidis, A., Zhang, H., Uppu, R. M., et al. (2000). Reaction of uric acid with peroxynitrite and implications for the mechanism of neuroprotection by uric acid. *Arch. Biochem. Biophys.* 376, 333–337. doi: 10.1006/abbi.2000.1721

Tana, C., Ticinesi, A., Prati, B., Nouvenne, A., and Meschi, T. (2018). Uric Acid and Cognitive Function in Older Individuals. *Nutrients* 10:975 doi: 10.3390/nu10080975

Valente, A. J., Maddalena, L. A., Robb, E. L., Moradi, F., and Stuart, J. A. (2017). A simple ImageJ macro tool for analyzing mitochondrial network morphology in mammalian cell culture. *Acta Histochem.* 119, 315–326. doi: 10.1016/j.acthis.2017.03.001

Valenti, D., Rossi, L., Marzulli, D., Bellomo, F., De Rasmo, D., Signorile, A., et al. (2017). Inhibition of Drp1-mediated mitochondrial fission improves mitochondrial dynamics and bioenergetics stimulating neurogenesis in hippocampal progenitor cells from a Down syndrome mouse model. *Biochim. Biophys. Acta Mol. Basis Dis.* 1863, 3117–3127. doi: 10.1016/j.bbadis.2017.09.014

Wen, M., Zhou, B., Chen, Y. H., Ma, Z. L., Gou, Y., Zhang, C. L., et al. (2017). Serum uric acid levels in patients with Parkinson's disease: A meta-analysis. *PloS One* 12:e0173731. doi: 10.1371/journal.pone.0173731

Winner, B., Desplats, P., Hagl, C., Klucken, J., Aigner, R., Ploetz, S., et al. (2009). Dopamine receptor activation promotes adult neurogenesis in an acute Parkinson model. *Exp. Neurol.* 219, 543–552. doi: 10.1016/j.expneurol.2009.07.013

Winner, B., Lie, D. C., Rockenstein, E., Aigner, R., Aigner, L., Masliah, E., et al. (2004). Human wild-type alpha-synuclein impairs neurogenesis. *J. Neuropathol. Exp. Neurol.* 63, 1155–1166. doi: 10.1093/jnen/63.11.1155

Winner, B., Regensburger, M., Schreglmann, S., Boyer, L., Prots, I., Rockenstein, E., et al. (2012). Role of alpha-synuclein in adult neurogenesis and neuronal maturation in the dentate gyrus. *J. Neurosci.* 32, 16906–16916. doi: 10.1523/JNEUROSCI.2723-12.2012

Winner, B., Rockenstein, E., Lie, D. C., Aigner, R., Mante, M., Bogdahn, U., et al. (2008). Mutant alpha-synuclein exacerbates age-related decrease of neurogenesis. *Neurobiol. Aging* 29, 913–925. doi: 10.1016/j.neurobiolaging.2006.12.016

Winner, B., and Winkler, J. (2015). Adult neurogenesis in neurodegenerative diseases. *Cold Spring Harbor Perspect. Biol.* 7:a021287. doi: 10.1101/cshperspect.a021287

Xiong, Z. M., Choi, J. Y., Wang, K., Zhang, H., Tariq, Z., Wu, D., et al. (2016). Methylene blue alleviates nuclear and mitochondrial abnormalities in progeria. *Aging Cell* 15, 279–290. doi: 10.1111/acel.12434

Ya, B. L., Liu, Q., Li, H. F., Cheng, H. J., Yu, T., Chen, L., et al. (2018). Uric Acid Protects against Focal Cerebral Ischemia/Reperfusion-Induced Oxidative Stress via Activating Nrf2 and Regulating Neurotrophic Factor Expression. *Oxidative Med. Cellul. longevity* 2018:6069150. doi: 10.1155/2018/6069150

Yuan, T. F., Gu, S., Shan, C., Marchado, S., and Arias-Carrion, O. (2015). Oxidative Stress and Adult Neurogenesis. *Stem Cell Rev. Rep*. 11, 706–709. doi: 10.1007/s12015-015-9603-y

Zheng, H., Yu, W. M., Shen, J., Kang, S., Hambardzumyan, D., Li, J. Y., et al. (2018). Mitochondrial oxidation of the carbohydrate fuel is required for neural precursor/stem cell function and postnatal cerebellar development. *Sci. Adv.* 4:eaat2681. doi: 10.1126/sciadv.aat2681

Conflict of Interest: The authors declare that the research was conducted in the absence of any commercial or financial relationships that could be construed as a potential conflict of interest.

Advantages of publishing in Frontiers

OPEN ACCESS
Articles are free to read for greatest visibility and readership

FAST PUBLICATION
Around 90 days from submission to decision

HIGH QUALITY PEER-REVIEW
Rigorous, collaborative, and constructive peer-review

TRANSPARENT PEER-REVIEW
Editors and reviewers acknowledged by name on published articles

Frontiers
Avenue du Tribunal-Fédéral 34
1005 Lausanne | Switzerland

Visit us: www.frontiersin.org
Contact us: frontiersin.org/about/contact

REPRODUCIBILITY OF RESEARCH
Support open data and methods to enhance research reproducibility

DIGITAL PUBLISHING
Articles designed for optimal readership across devices

FOLLOW US
@frontiersin

IMPACT METRICS
Advanced article metrics track visibility across digital media

EXTENSIVE PROMOTION
Marketing and promotion of impactful research

LOOP RESEARCH NETWORK
Our network increases your article's readership